UNIVERSITAT DE BARCELONA

Tree-ring networks at multiple geographical scales: patterns of coordinated ecological responses to global warming

Xarxes d'anells de creixement en arbres a escales geogràfiques múltiples: patrons de respostes ecològiques coordinades en front a l'escalfament global

Tatiana A. Shestakova

TREE-RING NETWORKS AT MULTIPLE GEOGRAPHICAL SCALES: PATTERNS OF COORDINATED ECOLOGICAL RESPONSES TO GLOBAL WARMING

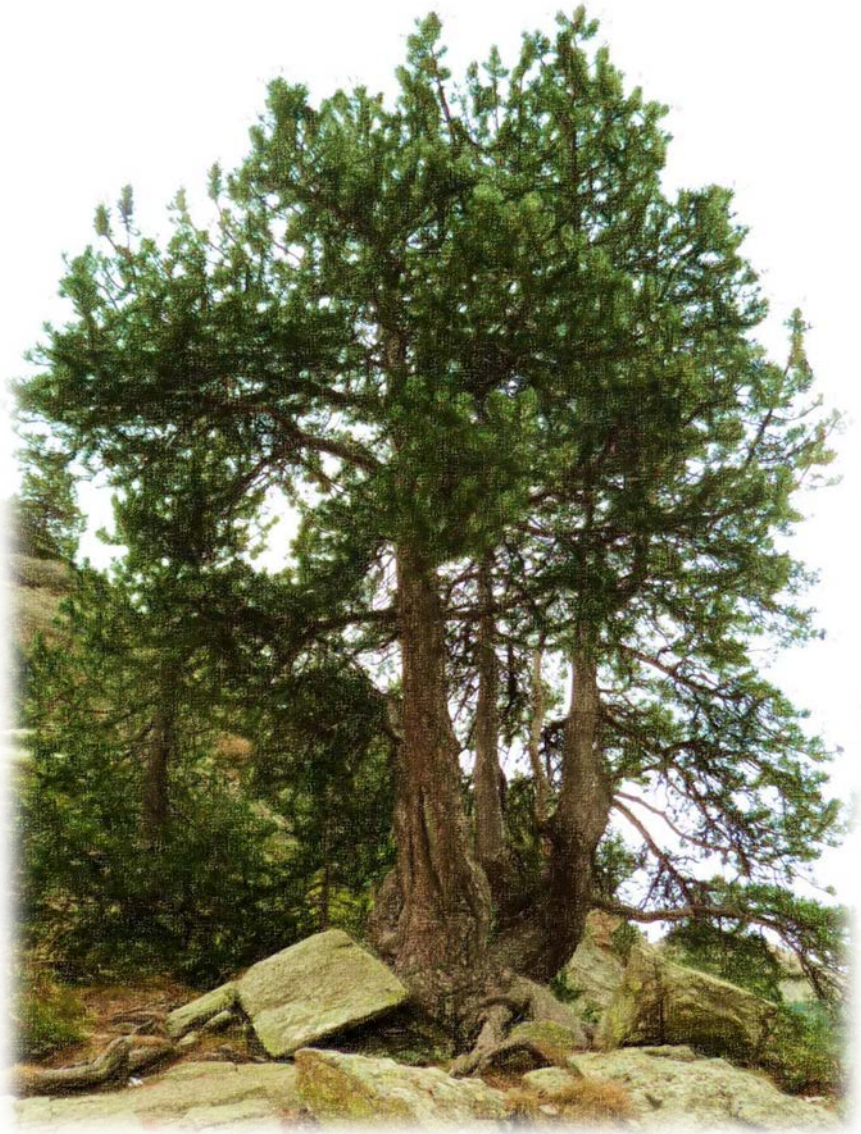

Tatiana A. Shestakova

Tatiana A. Shestakova (2016)
Doctoral thesis "Tree-ring networks at multiple geographical scales: patterns of coordinated ecological responses to global warming"
Doctoral program "Essential and Applied Ecology"
Dept. Evolutionary Biology, Ecology and Environmental Sciences
Faculty of Biology, University of Barcelona
The author has received a 3-year scholarship from the European Commission in the frame of the program Erasmus Mundus Action 2: ERANET-MUNDUS (Grant agreement 20112573)
Cover image and design by T.A. Shestakova

UNIVERSITAT DE BARCELONA

TESI DOCTORAL

Universitat de Barcelona, Facultat de Biologia
Departament de Biologia Evolutiva, Ecologia i Ciències Ambientals
Programa de Doctorat en Ecologia Fonamental i Aplicada

TREE-RING NETWORKS AT MULTIPLE GEOGRAPHICAL SCALES: PATTERNS OF COORDINATED ECOLOGICAL RESPONSES TO GLOBAL WARMING

XARXES D'ANELLS DE CREIXEMENT EN ARBRES A ESCALES GEOGRÀFIQUES MÚLTIPLES: PATRONS DE RESPOSTES ECOLÒGIQUES COORDINADES EN FRONT A L'ESCALFAMENT GLOBAL

Memòria presentada per Tatiana A. Shestakova per optar al
Grau de Doctora per la Universitat de Barcelona

Tatiana A. Shestakova
Dept. Biologia Evolutiva, Ecologia i Ciències Ambientals
Universitat de Barcelona

Vist-i-plau dels directors de la tesi:

Dra. Emilia Gutiérrez Merino
Dept. Biologia Evolutiva,
Ecologia i Ciències Ambientals
Universitat de Barcelona

Dr. Jordi Voltas Velasco
Dept. Producció Vegetal i Ciència Forestal
Universitat de Lleida

Barcelona, Novembre de 2016

To my family and friends

Without their love, support, and encouragement,
This project would never have seen the light of day

Hasta que no aprendamos a leer en los árboles,
Seguiremos leyendo en los libros

(El Bosque Habitado, RNE)

Contents

Summary

Forest biomes are major reserves for terrestrial carbon and thus small shifts in the carbon balance of forests could have a large impact on the global carbon cycle. In spite of unambiguous evidence pointing to climate warming as modern factor increasing the risk of regional forest vulnerability, many uncertainties still remain preventing accurate predictions of forest productivity under future climate change. Improving our understanding of the diversity in tree performance at varying spatiotemporal scales must provide insights on the environmental responses of forests and their function as carbon holders in the coming years. To this end, we proposed a new conceptual framework to investigate tree-ring records by grouping chronologies into potentially homogeneous subsets based on mixed modeling principles, as illustrated for a *Quercus* spp. dataset from the northeastern Iberian Peninsula. Accordingly, we assessed spatiotemporal patterns of signal strength of tree-ring assemblages across environmental gradients and at multiple geographical scales. We used long-term tree ring-width (TRW) records to assess changes in the temporal coherence of radial growth in multispecies dendrochronological networks. In combination with stable isotope records (carbon isotope discrimination, $\Delta^{13}C$; oxygen isotope composition, $\delta^{18}O$) we characterized the physiological drivers of tree productivity under varying environmental conditions. Finally, we investigated shifts in climate sensitivity of tree growth and performance in response to warming-induced heat and drought effects. We found significant spatial autocorrelations for TRW, $\Delta^{13}C$ and $\delta^{18}O$ spreading over sites separated up to 1,000 km in Eurasia. However, growth synchrony was not uniform continent-wide, increasing along a latitudinal gradient and, thus, reflecting the extent of environmental coherence in the dominant climatic drivers of regional tree growth (i.e., rainfall patterns at mid latitudes *vs.* temperature patterns at high latitudes). Also, there were geographically-structured relationships between ring-width and either $\Delta^{13}C$ (decreasing northwards and upwards) and $\delta^{18}O$ (increasing northwards). These results pointed to limited CO_2 diffusion impairing carbon uptake as main mechanism controlling the temporal coherence of forest growth signals at latitudes below 50°N in Europe and altitudes below ~1,600 m a.s.l. in Western Mediterranean. Notably, our results showed an increasing influence of climate on the spatial variability of tree growth over the twentieth century, ultimately leading to enhanced temporal coherence in ring-width records (spatial synchrony) along the local–continental continuum in most European forests (except Fennoscandia) and also in central Siberia. Growth-climate analyses highlighted coherent shifts in vegetative activity towards more favorable periods depending on site location through an advanced onset of growth in the early season and temperature effects in summer (e.g., strengthening of drought-induced growth limitations in Mediterranean forests and relaxation of cold constraints in boreal forests). Increase in growth synchrony together with a tighter relationship between ring-width and $\Delta^{13}C$ over the twentieth century suggested increasing drought effects on growth patterns in southern and central European forests and

also in mountain Mediterranean forests. Particularly, our results indicated that warming-induced drought stress is spreading upwards in Mediterranean forests and northwards in temperate forests, overriding taxonomic imprints and local drivers of tree growth. However, uppermost and northernmost forests exhibited a diverging reaction to warming, which highlights the complexities of changing climate effects on peripheral forest populations, hence requiring further examination. Collectively, we demonstrated that broad-scale climatic variation influence ecophysiological traits in both conifers and hardwoods in ways that have previously gone unrecognized, which may help to understand the ecological implications of ecosystem functioning and make better predictions on future forest responses to the ongoing global warming. The evidence for substantial altitudinal and latitudinal variation in tree growth dependencies on leaf-level physiology could be valuable to forecast the extent by which future forests may progressively shift from temperature- to moisture-sensitive growth.

Key words: climate warming, dendroecology, environmental gradients, mixed modelling, spatial synchrony, tree physiology, tree rings

Resumen

Los biomas forestales son importantes reservas de carbono terrestre y, por tanto, pequeños cambios en el balance de carbono de los bosques pueden producir un gran impacto en el ciclo global del mismo. A pesar de la evidencia actual que señala al cambio climático como factor de incremento de la vulnerabilidad de los bosques a escala regional, todavía existen hoy en día muchas incertezas que impiden predecir con precisión futuros cambios en productividad de los bosques en respuesta al cambio global. Una mejor comprensión de la diversidad de comportamiento de los árboles a diversas escalas espaciotemporales debe proporcionar pistas sobre las respuestas de éstos frente al medio y su función como sumideros de carbono en los años venideros. Con este fin, se propone un nuevo marco conceptual para investigar registros de anillos de crecimiento mediante la agrupación de cronologías en conjuntos potencialmente homogéneos utilizando principios de modelos mixtos, como se ilustra para el caso de *Quercus* spp. en el noreste de la Península Ibérica. Así, se han caracterizado patrones espaciotemporales de intensidad de señal en ensambles de anillos de crecimiento a lo largo de gradientes ambientales y a escalas geográficas variadas. Se han utilizado series de anchura de anillos (TRW) para determinar cambios en la coherencia temporal del crecimiento radial en redes dendrocronológicas multiespecíficas. En combinación con registros isotópicos (discriminación isotópica del carbono, $\Delta^{13}C$; composición isotópica del oxígeno, $\delta^{18}O$), se han estudiado los controladores fisiológicos de la productividad bajo circunstancias ambientales variables. Finalmente, se han investigado los cambios en sensibilidad climática del crecimiento y comportamiento en respuesta a elevadas temperaturas y sequía consecuencia del calentamiento global. Se hallaron autocorrelaciones espaciales relevantes para TRW, $\Delta^{13}C$ y $\delta^{18}O$ entre bosques separados hasta 1000 km en Eurasia. Sin embargo, la sincronía en el crecimiento anual no resultó uniforme a lo largo del continente, incrementando de acuerdo a un gradiente latitudinal y reflejando, de este modo, la importancia de los factores climáticos dominantes sobre el crecimiento regional de los árboles (p. ej. patrón de precipitaciones en latitudes medias *vs.* patrón de temperaturas en latitudes altas). Igualmente, se observaron relaciones geográficamente estructuradas entre el grosor de los anillos y $\Delta^{13}C$ (disminuyendo hacia el norte y hacia cotas altas) o $\delta^{18}O$ (incrementando hacia el norte). Estos resultados apuntan hacia una limitación en la difusión del CO_2 restringiendo la fijación de carbono atmosférico como principal mecanismo de control de la coherencia temporal de los registros de crecimiento en latitudes inferiores a 50°N en Europa y altitudes por debajo de ~1,600 m en el oeste mediterráneo. Especialmente, los resultados mostraron una influencia creciente del clima sobre la variabilidad espacial del crecimiento de los árboles en el siglo XX, conduciendo en última instancia a un aumento de la coherencia temporal de los registros de anchura de anillo (sincronía espacial) a lo largo del continuo local-continental en la mayoría de bosques europeos (con la excepción de Fennoscandia) y también en Siberia central. El análisis de las relaciones crecimiento-clima

destacó la presencia de cambios coherentes en la actividad vegetativa hacia periodos más favorables (dependientes de la localización) que se concretan en un inicio avanzado del crecimiento unido al efecto de las temperaturas en verano (p. ej., refuerzo de la limitación del crecimiento por sequía en bosques mediterráneos y relajación de limitaciones por frío en bosques boreales). El incremento en crecimiento sincrónico conjuntamente con la relación más estrecha entre anchura de anillo y $\Delta^{13}C$ a lo largo del siglo XX sugiere un aumento de los efectos negativos de la sequía sobre el crecimiento en el sur y centro de Europa así como en bosques mediterráneos de montaña. En particular, los resultados de la presente tesis indican que la sequía inducida por el calentamiento global se extiende hacia cotas altas en bosques mediterráneos y hacia el norte en bosques templados, encubriendo diferencias taxonómicas y factores locales relacionados con el crecimiento de los árboles. Sin embargo, los bosques situados a cotas altitudinales más elevadas o en latitudes más septentrionales de Europa exhibieron reacciones ciertamente divergentes frente al calentamiento global, lo que enfatiza la complejidad de los efectos cambiantes del clima sobre las poblaciones forestales periféricas y la necesidad de prestar mayor atención a dicho fenómeno. Colectivamente, se ha evidenciado que la variación climática a escala amplia influencia el comportamiento ecofisiológico en coníferas y angiospermas de forma desconocida hasta la fecha, lo que debería ayudar a comprender las implicaciones sobre el funcionamiento de los ecosistemas y así realizar predicciones más fiables de la respuesta futura de los bosques frente al calentamiento global. La evidencia de variación sustancial (altitudinal y latitudinal) en la dependencia del crecimiento de procesos fisiológicos a nivel de hoja será de gran utilidad para predecir el alcance de cambios progresivos en la sensibilidad climática de los bosques europeos, que están permutando su comportamiento desde una restricción por bajas temperaturas a una limitación generalizada por sequía.

Palabras clave: anillos de crecimiento, calentamiento climático, dendroecología, fisiología de árboles, gradientes ambientales, modelos mixtos, sincronía espacial

Resum

Els biomes forestals representen importants reserves de carboni terrestre i, conseqüentment, petits canvis en el balanç de carboni dels boscos poden produir un gran impacte en el cicle global del mateix. Tot i que l'evidència actual assenyala al canvi climàtic com a factor d'increment de la vulnerabilitat dels boscos a escala regional, existeixen encara moltes incerteses que impedeixen predir amb precisió futurs canvis en productivitat dels boscos en resposta al canvi global. Una millor comprensió de la diversitat de comportament dels arbres a diverses escales espaciotemporals ha de proporcionar pistes en relació a les respostes d'aquests front al medi i la seva funció com embornals de carboni en els propers anys. Amb aquesta finalitat es proposa un nou marc conceptual per investigar registres d'anells de creixement mitjançant l'agrupació de cronologies en conjunts potencialment homogenis utilitzant principis de models mixtes, com queda il·lustrat pel cas de *Quercus* spp. en el nord-est de la Península Ibèrica. Així, s'han caracteritzat patrons espaciotemporals d'intensitat de senyal en conjunts d'anells de creixement al llarg de gradients ambientals i a escales geogràfiques variades. S'han utilitzat sèries d'amplada d'anells (TRW) per determinar canvis en la coherència temporal del creixement radial en xarxes dendrocronològiques multiespecífiques. En combinació amb registres isotòpics (discriminació isotòpica del carboni, $\Delta^{13}C$; composició isotòpica de l'oxigen, $\delta^{18}O$), s'han estudiat els factors fisiològics controladors de la productivitat sota circumstàncies ambientals diverses. Finalment, s'han investigat els canvis en sensibilitat climàtica del creixement i comportament en resposta a elevades temperatures i sequera conseqüència de l'escalfament global. Es van trobar autocorrelacions espacials rellevants per TRW, $\Delta^{13}C$ i $\delta^{18}O$ entre boscos allunyats fins a 1000 km a Euràsia. No obstant, la sincronia en el creixement anual no va ser uniforme al llarg del continent, incrementant d'acord a un gradient latitudinal i reflectint, d'aquesta forma, la importància dels factors climàtics dominants sobre el creixement regional dels arbres (p. ex. patró de precipitacions en latituds mitjanes *vs.* patró de temperatures en latituds elevades). Igualment, es van observar relacions geogràficament estructurades entre el gruix dels anells i $\Delta^{13}C$ (disminuint en direcció nord i cap a cotes elevades) o $\delta^{18}O$ (incrementant en direcció nord). Aquests resultats apunten cap a una limitació en la difusió del CO_2 restringint la fixació de carboni atmosfèric com a principal mecanisme de control de la coherència temporal dels registres de creixement en latituds inferiors a 50°N a Europa i altituds per sota de ~1,600 m a l'oest mediterrani. Especialment, els resultats mostraren una influència creixent del clima sobre la variabilitat espacial del creixement dels arbres en el segle XX, conduint en darrer terme a un augment de la coherència temporal dels registres d'amplada d'anell (sincronia espacial) al llarg del continu local-continental a la major part de boscos europeus (amb l'excepció de Fennoscandia) i també a Sibèria central. L'anàlisi de les relacions creixement-clima destacà la presència de canvis coherents en l'activitat vegetativa cap a períodes més favorables (dependents de la localització) que es concretaren en un inici avançat

del creixement unit a l'efecte de les temperatures a l'estiu (p. ex., reforçament de la limitació del creixement per sequera en boscos mediterranis i relaxació de les limitacions per fred en boscos boreals). L'increment en creixement sincrònic conjuntament amb la relació més estreta entre amplada d'anell i $\Delta^{13}C$ al llarg del segle XX suggereixen un augment dels efectes negatius de la sequera sobre el creixement al sud i centre d'Europa així com en boscos mediterranis de muntanya. En particular, els resultats de la present tesis doctoral indiquen que la sequera induïda per l'escalfament global se estén cap a cotes elevades en boscos mediterranis i cap al nord en boscos temperats, emmascarant diferències taxonòmiques i factors locals relacionats amb el creixement dels arbres. No obstant, els boscos situats a cotes altitudinals més elevades o en latituds més septentrionals d'Europa varen exhibir una reacció divergent a l'escalfament global, el que emfatitza la complexitat dels efectes canviants del clima sobre les poblacions forestals perifèriques i la necessitat de prestar més atenció a aquest fenomen. Col·lectivament, s'ha evidenciat que la variació climàtica a escala àmplia influencia el comportament ecofisiològic en coníferes i angiospermes de forma desconeguda fins ara, el que hauria de resultar útil per comprendre les implicacions sobre el funcionament dels ecosistemes i així realitzar prediccions més fiables de la resposta futura dels boscos en front a l'escalfament global. L'evidència de variació substancial (altitudinal i latitudinal) en la dependència del creixement de processos fisiològics a nivell de fulla ha de resultar força útil per a predir l'abats de canvis progressius en la sensibilitat climàtica dels boscos europeus, que estan modificant el seu comportament des d'una restricció per baixes temperatures a una limitació generalitzada per sequera.

Paraules clau: anells de creixement, dendroecologia, escalfament climàtic, fisiologia d'arbres, gradients ambientals, models mixtes, sincronia espacial

Report by thesis supervisors

Dr. Emilia Gutiérrez Merino (UB) and Dr. Jordi Voltas Velasco (UdL), supervisors of the Doctoral thesis entitled "***Tree-ring networks at multiple geographical scales: patterns of coordinated ecological responses to global warming***",

INFORM

That the research studies presented in this dissertation have been carried out by Tatiana A. Shestakova as part of her doctoral project and have been organized in four chapters (Chapters 2–5 of this document). Below, we detail the publication status of each chapter and indicate the impact factor of the journals where they have been published or submitted (data according to ISI Journal Citation Reports®).

Chapter 2

Title: "Unravelling spatiotemporal tree-ring signals in Mediterranean oaks: a variance–covariance modelling approach of carbon and oxygen isotope ratios"
Authors: **Shestakova TA**, Aguilera M, Ferrio JP, Gutiérrez E, Voltas J
Research paper published in *Tree Physiology* **34**:819–838 (2014).
Doi: 10.1093/treephys/tpu037
Impact factor: 3.655 (2014). Q1 Forestry (3/65)

Chapter 3

Title: "Forests synchronize their growth in contrasting Eurasian regions in response to climate warming"
Authors: **Shestakova TA**, Gutiérrez E, Kirdyanov AV, Camarero JJ, Génova M, Knorre AA, Linares JC, Resco de Dios V, Sánchez-Salguero R, Voltas J
Research paper published in *Proceedings of the National Academy of Sciences of the United States of America* **113**:662–667 (2016).
Doi: 10.1073/pnas.1514717113
Imact factor: 9.423 (2015). Q1 Multidisciplinary Sciences (4/63)

Chapter 4

Title: "Increasing drought effects on five European pines modulate Δ^{13}C-growth coupling along a Mediterranean altitudinal gradient"
Authors: **Shestakova TA**, Camarero JJ, Ferrio JP, Knorre AA, Gutiérrez E, Voltas J
Manuscript submitted to *Functional Ecology* (May 2016)
Impact factor: 5.210 (2015). Q1 Ecology (15/149)

Chapter 5

Title: "Physiological drivers of twentieth-century forest growth in Europe"
Authors: **Shestakova TA**, Voltas J, Saurer M, Gutiérrez E, *et al.*
Manuscript in preparation

The PhD candidate has been the main author of the research studies listed above and has led all tasks regarding them such as conceiving the research objectives, designing the studies, analysing the data, interpreting the results, writing the manuscripts, reviewing and editing them during the publication process.

On behalf of all the co-authors, we also

CERTIFY

That none of the information presented in this dissertation will be used to elaborate other doctoral thesis.

Barcelona, November 2016

Dr. Emilia Gutiérrez Merino
Dept. Evolutionary Biology, Ecology and Environmental Sciences
University of Barcelona

Dr. Jordi Voltas Velasco
Dept. Crop and Forest Sciences
University of Lleida

CHAPTER 1

General Introduction & Objectives

General Introduction

Overview

There is no longer any doubt that human activities have dramatically altered the natural environment, including climate system (Steffen *et al.* 2011; Lewis & Maslin 2015). Fossil fuel combustion, deforestation and extensive land use change have caused a sharp increase in greenhouse gases in the atmosphere and pushed surface air temperature to rise (IPCC 2013). Current carbon dioxide (CO_2) concentration – the primary driver of climate warming – has surpassed the 400 ppm milestone (Dlugokencky & Tans 2016), which is about 40% higher than preindustrial levels (Olivier *et al.* 2013). With such steady increase in CO_2 emissions being added daily, too much heat is now trapped in the atmosphere which, in turn, induces substantial changes in the frequency, intensity and spatial extent of extreme weather events such as drought, heat/cold waves, heavy precipitation, *etc.* (Fischer & Knutti 2015). An additional two-fold increase in CO_2 concentrations projected within this century (IPCC 2007) is expected to further warm the planet and lead to cataclysmic instability in the climate system (IPCC 2013).

Because of their role in climate feedback processes, forest ecosystems are increasingly recognized as relevant sinks of carbon to mitigate the adverse impacts of climate change (Bonan 2008). Covering one-third of the land surface, forests contain an important stock of carbon (C) in the biosphere (*ca.* 45% of terrestrial carbon) and, hence, contribute significantly to the regulation of the global C cycle (Pan *et al.* 2011). Secondary growth is the dominant sink in natural forests owing to the ability of trees to absorb and lock up large amounts of carbon in their wood by adding new growth layers every year. However, the decrease in efficiency of carbon fixation capacity under stress conditions is alarming (Ciais *et al.* 2005; Silva *et al.* 2010; Zhao & Running 2010) because the long life-span of trees does not allow for rapid adaptation to environmental changes (Lindner *et al.* 2010). Thus, there is an urgent need for in-depth understanding of the sensitivity and long-term responses of forests to climate change.

Research on the possible impacts of global warming on forests started in the early 1990s, shortly after the first concerns about the implications of anthropogenic activities on the natural environment were raised (e.g., Kräuchi 1993). Since then, assessments of climate change, its impacts and subsequent consequences to forest stands have been the focus of continuous research efforts (Bonan 2008). Much uncertainty, however, remains in the combined impact of climate change drivers on tree growth and, thus, in the carbon budgets of forests (Litton *et al.* 2007; Silva *et al.* 2010; Nabuurs *et al.* 2014). For example, atmospheric CO_2 enrichment can increase photosynthetic rates (Gunderson & Wullschleger 1994) and water-use efficiency of trees (Keenan *et al.* 2013). Concurrent increases in nitrogen deposition may further stimulate growth (Thomas *et al.* 2010), but growth acceleration might be diminished by accompanied changes in light availability (Stine & Huybers 2014). Similarly,

the effect of high temperatures on trees may distinctly vary throughout the year. On the one hand, warmer winters and an earlier start of growing season are expected to promote tree growth owing to an advancement of spring phenology (Menzel *et al.* 2006). This positive effect, however, may be largely offset by higher summer temperatures and enhanced drought and/or heat stress (Allen *et al.* 2010, 2015; Anderegg *et al.* 2013; Williams *et al.* 2013). Due to interactions between several forcing factors acting simultaneously and complex tree physiology processes, the resultant ecological impacts of climate change are highly dubious and may vary considerably depending on tree species and local site conditions (Vila *et al.* 2008; Way & Oren 2010; Gazol *et al.* 2015).

To date, numerous studies have addressed climate change impacts with varying research methods; yet, dendroecological approach offers a unique possibility to infer and quantify long-term trends in forest responses to environmental forcing (Babst *et al.* 2014). Tree-ring analysis has been shown to be a powerful tool to provide insights into a diverse array of questions related to climate change processes including impacts of rising atmospheric CO_2 concentrations (e.g., Peñuelas *et al.* 2011), nutrient limitation and deposition (e.g., Hietz *et al.* 2011), anthropogenic aerosol emissions (e.g., Stine & Huybers 2014), carbon sink dynamics (e.g., Richardson *et al.* 2010) and climate response (e.g., Williams *et al.* 2013). Particularly, many studies have reported a widespread drift in the ecophysiological response of tree growth to climate over the twentieth century (e.g., Andreu *et al.* 2007; D'Arrigo *et al.* 2008; Carrer 2011). This alteration of growth reaction has been essentially attributed to the effects of drought and heat stress on tree physiology, which may coincide among co-existing species and lead to a high risk of population extinction at local, regional and global scales (Allen *et al.* 2010, 2015; Anderegg *et al.* 2013; Williams *et al.* 2013). Understanding tree growth responses at various spatiotemporal scales and among different species will substantially improve our ability to predict the potential ecological impacts of climate change on forest ecosystems in the near and long-term future.

From tree rings to dendroecology

Tree growth is one of the key processes that need to be assessed at a global scale to understand and quantify the short- to long-term impacts of environmental changes on terrestrial ecosystems (Fritts & Swetman 1989). Tree rings are a direct measure of stem growth, which represents the principal above-ground carbon accumulation pool (Pan *et al.* 2011). The total amount of carbon stored in trees depends on the balance of C input via photosynthesis and C output via respiration. Since the energy costs associated with tree growth and maintenance of living material are high, much of the assimilated carbon is released back to the atmosphere as a product of metabolism. The remaining C is allocated to leaf, twigs, stems and root biomass. Ultimately the fixed carbon is partly lost through litter decomposition associated with short-lived components, with only a proportion of total C stock being retained in the longer term as wood. Accordingly, temporal dynamics of radial

growth reflects annual carbon gain of a tree (i.e., biosynthesis) which, in turn, is predominantly driven by environmental conditions prevailing during vegetative growth.

Trees form distinct annual rings whenever there is seasonality in environmental factors triggering growth spurts and dormant periods which, in turn, may serve as top-notch biological indicators of past environmental variability over their entire life span (Fritts 2001). If growing conditions of a given year are favorable, enough photosynthate is produced for growth, maintenance and storage requirements. Eventually, an excess of photosynthate is allocated to secondary growth which can be measured as an increase in stem diameter. Therefore, minor changes in the thickness of tree rings provide evidence of good or poor growing years as reflected by wide and narrow rings, respectively.

Environmental information stored in tree rings can be retrieved and analyzed using well-established dendrochronological techniques. Dendrochronology has applications in many different fields of science allowing studies of natural phenomena whenever they could be adequately tracked by tree-ring records (Fritts 2001). Because trees are an important functional feature of many terrestrial ecosystems, they are silent witnesses of a wide range of ecological processes and can provide insight into interannual climate fluctuations (high-frequency signals) as well as record long-term and more subtle environmental and management changes (low-frequency signals) as far back as thousands of years.

Despite being a relatively young discipline (Fritts & Swetman 1989), dendroecology is one of the well-developed branches of dendrosciences. Since the first studies in the 1960s (e.g., Fritts 1965, 1971), there has been an exponential increase in number of publications on this topic worldwide. Owing to the great potential of tree rings to register manifold environmental signals, dendroecological studies that primarily focused on endogenous stand or community dynamics (e.g., Clark *et al.* 1975; Lorimer 1985; Kneeshaw & Bergeron 1998) have rapidly expanded beyond established disciplinary boundaries. The method has proven to be a valuable tool for investigating tree growth responses to an entire spectrum of natural and human-mediated disturbances (e.g., Fonti *et al.* 2006; Büntgen *et al.* 2009; Christopoulou *et al.* 2013; Altman *et al.* 2015). However, implications of climate change on forest dynamics is probably one of the hottest research topic in today's discussions among international scientific community.

Tree rings and climate

Forest trees are exposed throughout their lifetime to a great heterogeneity of environmental stressors with varying strength and duration. In regions where tree growth is primarily limited by a similar set of environmental factors, these are most likely recorded in ring-width sequences (Fritts 2001). Since tree species are associated with specific ranges of temperature and moisture regimes (i.e., species' distribution), climate is generally accepted as a major environmental constraint controlling tree growth across wide geographical areas. This holds particularly true for tree populations growing near the margins of a geographical

range (i.e., latitudinal or altitudinal distribution limits) where tree-ring variability predominantly reflects climatic forcing (Fritts 2001). For example, in cold areas where tree growth is mainly temperature-sensitive (i.e., high latitudes and altitudes), radial growth reflects temperature variations, whereas growth rates in arid and semiarid areas, primarily constrained by water availability, mirror changes in precipitation.

Although climate restrictions tend to strengthen climate-growth relationships resulting in enhanced common ring-width signals in an area, stand-level growth may reveal complex and highly variable microsite conditions (e.g., topography, soil properties, disturbances and nutrient availability). Ontogenetic growth patterns influenced by a variety of other factors, such as different sizes, ages, competition, species and successional trajectories, may further complicate the interpretation of tree-ring signals. In order to reduce undesirable growth variability at tree level and to enhance common climatic signals, individual ring-width series undergo standardization. This procedure involves fitting a time function to the tree-ring series, and then dividing each ring-width value by the corresponding curve value to generate a series of growth indices with constant mean (i.e., stationary series). Thus, standardization removes differences in growth rates between samples and allows them to be combined into a site chronology.

To assess the 'quality' of the resultant tree-ring chronology and to characterize the strength of the common growth signal within a stand, a number of descriptive statistics are commonly used in dendrochronology (Wigley *et al.* 1984; Briffa & Jones 1990). These includes the **mean inter-series correlation** (*Rbar*), which is a measure of the common stand-level signal recorded for a site; the **expressed population signal** (*EPS*), which estimates the level of coherence of the constructed chronology; and the **signal-to-noise ratio** (*SNR*), which is an indicator of the strength of the observed common signal among trees in the chronology (Cook & Kairiukstis 1990).

Rbar is a basic statistic to examine the general year-to-year agreement between ring-width variations of different trees at a stand level (i.e., signal strength). It is calculated as the mean of all pairwise correlations between tree-ring series within a chronology and indicates the amount of common variance that may be attributed to environmental (i.e., climatic) forcing on tree growth. *EPS* reflects the degree to which the chronology represents a hypothetical chronology based on an infinite number of samples and is calculated from the mean inter-series correlation (*Rbar*) and the number of tree-ring series included in the calculation (*n*) as follows (Wigley *et al.* 1984):

$$EPS = \frac{n \times \overline{Rbar}}{n \times \overline{Rbar} + (1 - \overline{Rbar})} \qquad (1.1)$$

To ensure a robust mean chronology, an *EPS* value of 0.85 is commonly accepted as a reasonable threshold for chronology reliability (Wigley *et al.* 1984). Further, the relationship

between the desired (signal) and undesired (noise) information recorded in the tree-ring chronology is expressed as the signal-to-noise ratio (*SNR*; Fritts 2001):

$$SNR = \frac{n \times \overline{Rbar}}{1 - \overline{Rbar}} \approx \frac{signal}{noise} \quad (1.2)$$

High *EPS* and *SNR* values indicate that the dataset contains a strong common signal and may be used as a proxy to infer the dominant environmental forcing on tree growth. As both statistics are sensitive to sample size, the common signal may be reinforced by increasing the number of tree-ring series used for chronology building.

Stable isotopes in tree rings: theoretical background

Although tree ring-width chronologies provide some of the best high-resolution ecological datasets available, there are a number of limitations that restrict their potential. One of the most prominent constraints is that ring-width archives may show limited sensitiveness to climate conditions and, accordingly, they are preferentially developed for sites where a single climate factor largely limits tree-ring formation (i.e., peripheral populations) (e.g., Briffa *et al.* 2002; Cook *et al.* 2004;). Indeed, tree populations located between the ecological "extremes" of distribution ranges (e.g., most of central Europe) may exhibit complex tree-ring patterns responding to both miscellaneous climatic and other environmental factors and, hence, no simple growth-climate relationship can be identified (e.g., Gagen *et al.* 2004; Hartl-Meier *et al.* 2014). By using stable isotopes it may be possible to exploit the great advantages of tree-ring chronologies whilst avoiding some of the problems associated with ring-width properties, as they are usually more sensitive to environmental variables than tree-ring width (e.g., McCarroll & Loader 2004; Leavitt *et al.* 2010; Cernusak & English 2015).

The two main elements in wood, carbon (C) and oxygen (O), have more than one naturally occurring stable (non-radioactive) isotope. These isotopes have almost identical chemical properties but the difference in mass allows physical, chemical and biological processes to discriminate against the heavier one, thereby imparting an environmental signal. Because of the very small absolute abundances of each isotope in plant tissues (Ehleringer & Rundel 1989), the stable isotope composition is expressed by convention relative to an international standard. Relative abundances can then be discussed more precisely than absolute isotope abundance ratios. This has led to the widely used "delta-notation" (McKinney *et al.* 1950), which expresses the isotope values as a ratio of heavy to light isotope (R_{sample}) in the delta notation as:

$$\delta^{xx}E = \left(\frac{R_{sample}}{R_{standard}} - 1 \right) \times 1{,}000‰ \quad (1.3)$$

where *E* is the element of interest (e.g., C, O), *xx* is the atomic mass of the heavier isotope in the ratio and *R* is the absolute ratio of *E* (R_{sample}; e.g., $^{13}C/^{12}C$) relative to an international standard ($R_{standard}$; e.g., VPDB for carbon and VSMOW for oxygen; Hayes 1983). A positive value means therefore that the sample contains more of the heavier isotope than the given standard; a negative value means that the sample contains less of the heavier isotope than the standard.

Carbon stable isotopes in tree rings

The carbon isotope composition of plant tissues is determined by the isotopic composition of CO_2 in the atmosphere, which is increasingly being depleted in ^{13}C due to the synergetic effect of deforestation and fossil-fuel combustion (Keeling *et al.* 1979). Plants naturally discriminate between ^{12}C and ^{13}C isotopes during CO_2 fixation by photosynthesis, which results in ^{13}C depletion of plant organic matter relative to atmospheric CO_2 (Farquhar *et al.* 1989). The discrimination (Δ) occurring in the incorporation of source (CO_2) into product (plant biomass) can be defined as:

$$\Delta^{13}C_{plant} = \frac{\delta^{13}C_{CO_2} - \delta^{13}C_{plant}}{1 + \delta^{13}C_{plant}/1{,}000} \quad (1.4)$$

The advantage of reporting $\Delta^{13}C_{plant}$ is that it directly expresses the consequences of biological processes, whereas $\Delta^{13}C_{plant}$ is the result of both source isotopic composition and carbon isotope discrimination (Farquhar *et al.* 1989). The magnitude of carbon isotope discrimination by plants depends on both physical and biochemical processes during CO_2 uptake. The most important are diffusion of CO_2 through stomata (*a*, –4.4‰) and enzymatic discrimination during CO_2 fixation (*b*, –27.0‰). The interplay between these fractionation factors and the resulting isotopic ratio of the carbon fixed by the plant could be described by a simplified model (Farquhar *et al.* 1982):

$$\Delta^{13}C_{plant} = a + (b - a) \times \frac{c_i}{c_a} \quad (1.5)$$

where *a* and *b* are the fractionation factors as stated above, and c_i/c_a is the ratio of intercellular to ambient CO_2 concentrations. The fractionations occurring during diffusion and carboxylation are continuous and additive. If photosynthesis consumes CO_2 faster than it can be replaced by stomatal conductance, the relative pool of $^{12}CO_2$ would decrease, resulting in a decrease in fractionation against ^{13}C and an enriched ^{13}C value. Any change in the assimilation rate will therefore influence c_i. Similarly, a change in stomatal conductance will affect the rate at which the internal CO_2 can be replaced. If stomatal conductance is low and little CO_2 enters the leaf, c_i approaches 0 and the "fractionation due to diffusion" (*a*) more

strongly determines the $\Delta^{13}C_{plant}$. If stomatal conductance is high and CO_2 can exchange unhampered, $c_i \approx c_a$ so that ^{13}C is more strongly determined by the "fractionation due to carboxylation" (*b*). In fact, the isotopic discrimination is situated somewhere in between these two extremes resulting in $\Delta^{13}C_{plant}$ values around 20‰ for C3 plants (Farquhar *et al.* 1982).

The climate factors that could potentially be imprinted in tree-ring $\Delta^{13}C$ series are thus those that influence stomatal conductance and photosynthetic rate, with the dominant control being determined by tree species, location and the prevailing climatic regime (McCarroll & Loader 2004). In dry environments or where shallow rooted trees are growing on well-drained soils, stomatal conductance will tend to dominate, giving strong correlations between $\Delta^{13}C$ and relative humidity and soil moisture. In contrast, photosynthetic rate is likely to be the dominant control on carbon isotopic signature in tree rings in moist environments, resulting in strong correlations with sunlight and temperature (McCarroll & Loader 2004).

Oxygen stable isotopes in tree rings

Atmospheric precipitation is the main source of oxygen atoms in the annual growth rings of trees (Rozanski *et al.* 1992). However, the precipitation signal in soil can be damped, lagged or even masked depending on a number of environmental factors, to a large degree on the condensation temperature of droplets in the atmosphere and further effects such as the evaporative enrichment of soil water or the influence of groundwater (Ehleringer & Dawson 1992). When a tree takes up water from the soil through the roots, it is assumed that no fractionation occurs during water transport to the leaf (Dawson & Ehleringer 1991). In the leaf, enrichment in ^{18}O happens during transpiration as $H_2{}^{16}O$ evaporates to the atmosphere more readily than $H_2{}^{18}O$ (Dongmann *et al.* 1974). The extent of ^{18}O enrichment of leaf water above source water at the sites of evaporation ($\delta^{18}O_e$) is given by a Craig–Gordon model:

$$\delta^{18}O_e = \delta^{18}O_t + \varepsilon^* + \varepsilon_k + (\delta^{18}O_v - \delta^{18}O_t - \varepsilon_k) \times \frac{e_a}{e_i} \qquad (1.6)$$

where $\delta^{18}O_e$ is the isotope ratio of transpiration water, ε^* is the equilibrium fractionation between liquid water and vapor, ε_k is the kinetic fractionation during diffusion of water vapor through the stomata to the atmosphere, $\delta^{18}O_v$ is the isotopic difference of atmospheric water vapor compared with source water, and e_a/e_i is the ratio of atmosphere to intercellular vapor pressures (Craig & Gordon 1965; Dongmann *et al.* 1974; Farquhar & Lloyd 1993). This evaporative enrichment of water is, thus, governed by the bidirectional exchange of water vapor between the leaf and the ambient air, and so is affected by the vapor pressure deficit of the air and the isotopic composition of the water vapor (Craig & Gordon 1965).

Average lamina leaf water is, however, expected to be less enriched than the water at the evaporative sites due to the isotopic gradient of water in a leaf (e.g., Cuntz *et al.* 2007). Indeed, the isotopic composition of lamina leaf water ($\delta^{18}O_l$) is determined by the balance between two water fluxes in opposite directions: advection of non-enriched xylem (source) water to the evaporative sites and back-diffusion of enriched water at the evaporative sites to the xylem (Péclet effect; Farquhar & Lloyd 1993). Following Eq. (1.6) the evaporative enrichment can be expanded to the whole leaf lamina by considering the relative effects of convective and diffusive flows (e.g., Sternberg 2009):

$$\delta^{18}O_l = (1-a)\times\delta^{18}O_t + a\times\delta^{18}O_e \qquad (1.7)$$

where a is the fraction of enriched water in the leaf which is adjusted to take into account the Péclet effect (ϱ) as follows $(1-e^{-\varrho})/\varrho$ (Farquhar & Lloyd 1993). To reconcile the differences between the observed and Craig–Gordon predicted isotopic ratios, the fraction of xylem water (i.e., [1–a]) should vary between 25% and 50% of total leaf water (Leaney *et al.* 1985; Walker *et al.* 1989), which, however, reflects a continuous gradient, not a discrete compartment. This gradient is dynamic and subject to change depending on the transpiration rate of the leaf (Farquhar & Lloyd 1993). The greater the transpiration, the greater the Péclet effect, which reduces the contribution of enriched water (a) and, hence, lowers the $\delta^{18}O$ value of lamina leaf water.

The isotopic signal of leaf water is next carried into the signature of newly produced assimilates. During carbon fixation, one oxygen atom is directly incorporated into organic matter from water, and two derived from CO_2. As the $\delta^{18}O$ value of CO_2 equilibrated with water is ~40‰ higher than that of the water it equilibrated with, it results in carbonyl oxygen being ~27‰ more enriched than the lamina water (Sternberg & DeNiro 1983). This fractionation is constant and has been confirmed for cellulose (e.g., Yakir & DeNiro 1990), leaf soluble organic matter (e.g., Barnard *et al.* 2007) and phloem sap sucrose (e.g., Cernusak *et al.* 2003; Gessler *et al.* 2007). However the physiological mechanisms of isotope fractionation in downstream metabolic processes remain fragmentary (Farquhar *et al.* 1998; Sternberg 2009; Gessler *et al.* 2014), there are indicators that the initial oxygen isotope signal of the photosynthates might be altered during phloem loading and transport to plant sinks (Gessler *et al.* 2013; Treydte *et al.* 2014). Finally, an additional oxygen exchange occurs between sugars and non-enriched xylem water during cellulose biosynthesis in the tree ring (Sternberg *et al.* 2006). The proportion of organic oxygen effectively exchanging with reaction water has been estimated to vary between 36% and 42% (Roden & Ehleringer 1999; Cernusak *et al.* 2005).

As could be seen, the interpretation of $\delta^{18}O$ variability in tree rings is not as direct as that of $\Delta^{13}C$ and involves several fractionation processes (Farquhar *et al.* 1998; Sternberg 2009; Treydte *et al.* 2014; Gessler *et al.* 2014). Owing to the partial exchange of organic oxygen with xylem water, isotope composition of wood constituents is largely determined by isotope composition of source water (i.e., precipitation) and evaporative effects on leaf water

enrichment (Roden *et al.* 2000; McCarroll & Loader 2004; Treydte *et al.* 2014). Meteoric water $\delta^{18}O$ reflects temperature signal at which condensation takes place with higher temperature resulting in relatively more positive (enriched) isotope signal in precipitation (Dansgaard 1964). On the other hand, leaf enrichment is primarily driven by leaf to air vapor pressure deficit (ratio e_a/e_i in Eq. [1.6]), which is controlled by air humidity (McCarroll & Loader 2004). Low relative humidity leads to reduced stomatal conductance which increases enrichment of leaf water and ultimately of the assimilated sugars. In addition, since $\delta^{18}O$ variation in tree rings is not influenced by photosynthetic rate, a dual isotope approach (i.e., simultaneous measurements of $\delta^{18}O$ and $\Delta^{13}C$) offers insights into the interplay between stomatal control of water losses and photosynthesis by inferring stomatal behavior (e.g., Scheidegger *et al.* 2000; Barbour *et al.* 2002; Ripullone *et al.* 2009; Barnard *et al.* 2012).

Concept of synchrony in ecology

Temporal changes in time-varying characteristics of geographically disjunct populations often exhibit correlated fluctuations, a phenomenon known as spatial synchrony (Liebhold *et al.* 2004). Biological synchrony is a ubiquitous yet highly diverse phenomenon which may be observed in a wide range of natural systems including forests (e.g., Koenig & Knops 1998). The classical explanation for growth adjustment among distant stands is that regionally correlated climatic forces engender population synchronization across vast geographical areas (i.e., the Moran effect; Moran 1953). Indeed, Koenig (2002) has demonstrated that climatic factors such as temperature and precipitation vary in the same direction on a large spatial scale and thus can cause synchronized dynamics (e.g., radial growth) between spatially separated populations (Haydon & Steen 1997).

According to ecological theory populations whose dynamics are entrained by environmental correlation face increased extinction risk under rapidly changing climate conditions. The existence of synchrony among nearby populations is particularly significant to such systems because the more spatially synchronous a metapopulation is, the shorter its expected persistence time in face of new emerging threats such as drought or heat stress (Heino *et al.* 1997; Amritkar & Rangarajan 2006; Ruokolainen & Fowler 2008). The reason for this is straightforward: if all subpopulations fluctuate in concord, then the extinction probability for the whole population increases as all the subpopulations are expected to suffer the same fate simultaneously. On the other hand, if spatial synchrony is low, some subpopulations are likely to persist and serve to re-establish extinct subpopulations. Thus, estimation of the degree of synchronous population dynamics in time and space is highly relevant to study the ecological consequences of climate change.

Considerable effort has been devoted recently to extensively document the responses of forest populations to climate variability from local to global scales. Obviously, the manifold ways in which climate may affect forest dynamics are indeed complex. Whereas the ability of trees to cope with short-term disturbances (e.g., drought) is related to phenotypic

plasticity and long-term changes (e.g., gradual increase in the duration and severity of dry spells) to the adaptation process, both ultimately lead to population level changes in growth dynamics. If the former may vary among species or functional groups, the latter is probable to superimpose on taxonomic differences and trigger change in climate-driven population synchrony. Since large-scale climate patterns often affect different geographic regions in a different manner, the ecological repercussions of climatic change may vary among distinct ecoregions or biomes (Allen *et al.* 2015).

Despite a surge of interest in spatial synchrony, limited attention has been given to the issue of how synchrony of population dynamics should be measured and tested. Many studies have attempted to infer mechanisms indirectly via the analysis of population time series (Royama 1981; Turchin 1990; Kendall *et al.* 1999). These studies characterize temporal patterns (e.g., through Principle Component Analysis) and use this information to infer the relative role of biotic and abiotic forces in temporal dynamics. More recent flurry of studies on population synchrony may be seen as advancing this line of inquiry to include spatial dynamics. Techniques such as Mantel correlograms (Oden & Sokal 1986) and modified correlograms (Koenig & Knops 1998) have been extensively employed to describe the relationship between synchrony and distance between sampling locations (reviewed in Bjørnstad *et al.* 1999; Koenig 1999). However, population dynamics is a complex phenomenon which may exhibit spatial variations in different time periods, although the majority of existing research is focused on only one domain (temporal or spatial) and does not consider the other. Climate change and its spatial heterogeneity further complicate the evaluation and future prediction of changes in population trajectories. In this context, there is an urgent need for new statistical tools and systematic approaches to analyze synchrony patterns in population dynamics over time and across space simultaneously.

A new modelling framework in dendrochronology

Traditionally, dendroecologists have used the Analysis of Variance (ANOVA) to estimate common forcing (or "signal") within groups of standardized tree-ring series (or chronologies) by quantifying the variability shared by a number of trees (or sites) (Fritts 2001; Wigley *et al.* 1984; Briffa & Jones 1990). However, the standard ANOVA approach has some weaknesses when applied to longitudinal data (Piepho *et al.* 2004), for example tree-ring datasets. Particularly, it has limited competence to account for complex data structures, non-independent observations and missing values, to name a few, that are essential characteristics of dendroecological archives. Alternatively, mixed modelling provides the very flexible framework to accomplish these tasks.

The fundamental advantage of mixed models is that they are able to deal with multiple sources of variation of different nature by including simultaneously fixed and random effects. For instance, when testing the effect of an explanatory variable x (e.g., site-specific

chronology) that is measured sequentially following a serial ordering (e.g., across years) on a trait of interest *y* (e.g., ring-width), the serial effect (year factor) can be assumed to behave like a random sample and so is regarded as random. Unlike fixed effects, random terms allow broadening the inference space beyond the observed levels and, in case the year factor is taken as random, this decision provides inferences about the entire population of years owing to the estimation of the inter-annual variance for *y* that underlies the set of tree-ring chronologies. An important feature of this setting is that the serial ordering of observations on the same unit *x* may give rise to correlations, which need to be accounted for in statistical analysis. In this framework, additional random effects can be fitted if other sources of non-independence between observations are suspected (e.g., taxonomic affiliation, geographic vicinity), and for each random effect a corresponding component of the total variance can be estimated. In other words, the use of mixed models permits to partition the overall variability by accounting for repeated measurements and the presence of natural grouping in the dataset.

Linear mixed models in dendrochronology are extensions of traditional fixed effects models in which a time factor (e.g., year) is included as repeated factor *x* for a trait of interest *y*. The theoretical basis for the application of mixed models in dendrosciences was already sketched by Wigley *et al.* (1984). Following our example, if we simply express the year factor (random) relative to the population mean (fixed), the resulting model can be written as follows:

$$y = \mu + a_j + \varepsilon_{ij} \tag{1.8}$$

where *y* is the vector of measurements of the study variable, μ is the intercept (the population mean), α_j is a random effect (i.e., effect of the j^{th} year relative to mean) and ε_{ij} is the residual term (i.e., deviation of the i^{th} chronology in the j^{th} year). Here, we assume that observations made in the same year are not independent so covariation arises among chronologies which originates from common forcing mechanisms.

It often may be of interest to characterize the strength of common signal underlying a particular set of chronologies (i = 1, N). In the same way as time series of tree-ring features are frequently analyzed together to assess variability common to all trees at a site (Wigley *et al.* 1984), at a broader scale we can obtain unbiased estimates of the average correlation $\bar{\rho}$ over pairs of chronologies, excluding the N pairs $i = i^*$ for which $\varrho = 1$, as follows:

$$\bar{\rho} = \frac{\sigma_Y^2}{\sigma_Y^2 + \sigma_e^2} \tag{1.9}$$

where σ_Y^2 refers to the variance of year effects and σ_e^2 stands for the residual variance. The above expression estimates the mean inter-chronology correlation over the whole set of *N*

chronologies, which we refer to as intraclass correlation, common signal strength or spatial synchrony.

However, we may suppose that there are other (partially shared or independent) sources of similarities among records. This may include intrinsic variables (e.g., taxonomy) and extrinsic variables (e.g., locality). If we hypothesize that such effects are important, then the random model (8) can be expanded to an alternative mixed model by adding a new fixed effect β_r (r = 1 to n). In this case, the estimators can be defined in terms of the following model:

$$y = \mu + \beta_r + a_{jr} + \varepsilon_{ijr} \tag{1.10}$$

where β_r is the fixed part of the model (i.e., expected mean value in the r^{th} group), α_{jr} is a random effect (i.e., effect of the j^{th} year in the r^{th} group) and ε_{ijr} is the residual term (i.e., deviation of the i^{th} chronology in the j^{th} year within the r^{th} group). According to the theory of survey sampling (Kish 1965), the stratification improves the accuracy of parameter estimates, provided there is heterogeneity between groups as defined by the factor(s) under evaluation. Gain in accuracy is largest in the one (but hypothetical) extreme case that all heterogeneity in a_j occurs between groups, while there is complete homogeneity in a_j within groups. On the other hand, in the other extreme case denoting that all heterogeneity occurs within groups and none among groups, stratification would be no longer beneficial.

When two or more groups are successfully defined following the theory of survey sampling, mixed modeling allows for the estimation of the intraclass correlations as defined in Eq. (1.9) either at the intragroup or intergroup level. The underlying idea is to split the mean correlation estimated between all possible pairs of chronologies drawn from the whole dataset into: (*i*) a mean correlation between pairs of chronologies for every group; and (*ii*) a mean correlation between pairs of chronologies for pairs of groups. Thus, it can be demonstrated (Chapter 2 of this thesis) that the correlation between chronologies belonging to group r becomes:

$$\overline{\rho_r} = \frac{\sigma^2_{Y_r}}{\sigma^2_{Y_r} + \sigma^2_e} \tag{1.11}$$

Conversely, the correlation of chronologies belonging to groups r and r^* is:

$$\overline{\rho_{rr^*}} = \frac{\sigma^2_{Y_{rr^*}}}{\sqrt{(\sigma^2_{Y_r} + \sigma^2_e) \times (\sigma^2_{Y_{r^*}} + \sigma^2_e)}} \tag{1.12}$$

Mixed models also allow flexible modelling of complex intra- and inter-group and autocorrelation structures. Successful modelling of variance-covariance structures will provide valid statistical inferences for the fixed effects of the mixed model (Eq. 1.10). For

model selection procedure, a likelihood ratio test (Jennrich & Schluchter 1986) can be used in the case of nested models (i.e., a new model being obtained by adding new random terms into the current model) or, alternatively, Akaike's Information Criterion (AIC) and Bayesian Criterion (BIC) (Wolfinger 1996) in case of either nested or non-nested models (e.g., differing in their fixed part).

Dendrochronological archives may consist of multiple traits measured simultaneously in the same tree-ring (e.g., ring-width, isotopic records) across years. If so, one can make useful inferences about the inter-trait relationship without explicit knowledge of the underlying mechanisms involved in such relationship. This, in turn, can provide effective ecological insights and help prioritize likely causal relationships. This relationship may contain three different causes of association: temporal (due to year effects), spatial (due to mean differences among trees [chronologies]) and residual (quantifying the specificity of temporal variability at the tree [chronology] level). For a pair of traits z and w, the relationship between them may be estimated by calculating a correlation of year effects (r_Y) as follows (Chapter 4 of this thesis):

$$r_Y = \frac{COV_{Y_{zw}}}{\sqrt{V_{Y_z}^2 \times V_{Y_w}^2}} \tag{1.13}$$

where $COV_{Y_{zw}}$ is the year covariance between z and w, and V_{Y_z} and V_{Y_w} are the corresponding year variances for the two traits. The temporal association (or correlation of year effects) represents how similarly two traits covariate across years. It is also possible to estimate a residual association, which quantifies how consistent the interaction between time and tree (chronology) effects is across traits. It must be noted that the spatial association is usually obscured in dendrochronology as time-series (trees or chronologies) are usually detrended or indexed prior to statistical analysis, meaning that they take essentially the same mean value.

Thesis structure

This research aims at expanding current knowledge on the ecological footprints of global warming on tree growth and performance at varying spatiotemporal scales. To this end, the Thesis document has been divided into four chapters which are based on a common conceptual framework and follow a logical sequence.

First, a novel *ad-hoc* approach based on mixed modeling principles has been proposed in order to aid disentangling the effects of climate on tree functioning (Chapter 2). For this purpose, the spatiotemporal patterns of signal strength of carbon isotope discrimination ($\Delta^{13}C$) and oxygen isotope composition ($\delta^{18}O$) have been investigated for deciduous and

evergreen oaks co-occurring in Mediterranean forests along an aridity gradient in Northeastern Iberian Peninsula (Spain).

Second, the spatial synchrony patterns of a network of tree-ring width chronologies made up of different conifers originated from two distant regions with very contrasting climate conditions, central Siberia (Russia) and the Iberian Peninsula (Spain), have been explored (Chapter 3). This has been done in order to gain understanding of global change effects on tree growth and dynamics at subcontinental scales. The magnitude of common information shared by ring-width chronologies and its evolution over the twentieth century have been investigated through the use of a variance-covariance mixed modelling framework developed in the previous step (Chapter 2).

Chapter 4 has aimed at assessing whether recent warming is modifying the ecophysiological performance of co-existing European pines and how changes in performance (in terms of radial growth and carbon isotope discrimination, $\Delta^{13}C$) are spatially structured along a Mediterranean altitudinal gradient (eastern Iberian Peninsula, Spain). To this end, the inter-relationship between ring-width and $\Delta^{13}C$ has been assessed throughout the second half of the twentieth century. To take into account the information available on different traits, the mixed modelling framework outlined in Chapter 2 has been extended to a multiple trait analysis.

Finally, the spatial structure and ecophysiological drivers of tree growth have been assessed across European forests during the twentieth century (Chapter 5). For this purpose, functional drivers of tree productivity (as inferred through $\Delta^{13}C$ and $\delta^{18}O$) have been investigated for conifers (*Cedrus*, *Pinus*) and hardwoods (*Quercus*) across a wide latitudinal gradient spanning from northern Africa to Fennoscandia (European tree-ring network ISONET; EVK2-CT-2002-00147) using the mixed modelling framework defined in Chapters 2 and 4.

This Doctoral Thesis has been conceived as a whole; however, chapters 2–5 has been written as separate paper for publication in scientific journals. As a result, the chapters can be read independently from each other, although a certain level of repetition may occur. Conclusions from individual chapters are presented at the end of chapters. Chapters 2 and 3 have already been published, but format has been unified in order to keep it consistent throughout the document. References have been unified in a single list at the end of the document.

Objectives

The general goal of this Thesis is to ascertain and characterize the complex patterns of tree-ring signals that are present across multiple spatiotemporal scales (local, regional, continental) and how these patterns are modified by recent climate warming. The specific objectives of each chapter are:

Chapter 2

The primary research interest of this chapter is to introduce a new conceptual framework for interpreting the variability and common signal strength existing in dendrochronological networks based on mixed modeling principles. To this end, we investigate stable carbon and oxygen isotope ratios in tree rings over the past 20 years for deciduous and evergreen *Quercus* species co-occurring in mixed Mediterranean forests along an aridity gradient. We hypothesized that contrasting strategies in response to drought in evergreen (*Q. ilex*) and deciduous (*Q. faginea*, *Q. humilis* and *Q. petraea*) oaks would lead to a differential spatiotemporal sensitivity to changes in water availability, which could be tracked by means of carbon and oxygen isotope analysis in wood constituents. The specific objectives of this study are:

i. to evaluate spatiotemporal patterns of common signal strength of stable carbon ($\Delta^{13}C$) and oxygen ($\delta^{18}O$) isotope ratios in tree rings for co-occurring *Quercus* species along the aridity gradient.

ii. to assess climate drivers of isotope variability for functional groups with contrasting strategies in response to drought (drought tolerance *vs.* drought avoidance) at both spatial and temporal levels.

Chapter 3

The main goal of this chapter is to interpret forest reactions to climate warming and increased climate variability at large spatial scales through a mixed-modeling approach. For this purpose, we analyze a comprehensive network of ring-width chronologies from six different conifer species spanning the past 120 years across two climatically contrasting Eurasian biomes: boreal forests in central Siberia and Mediterranean forests in Spain. We hypothesized that climate change triggers more synchronous tree growth at subcontinental scales owing to an amplified climatic control of growth, e.g., through higher temperatures in Siberia and decreased water availability in Spain. The specific objectives of this study are:

i. to evaluate temporal trends in growth synchrony patterns in two distant regions (central Siberia *vs.* Iberian Peninsula).

ii. to check if the patterns of synchrony are region- and/or species-specific.

iii. to assess the nature and strength of climate factors driven the synchrony among trees growing under different climatic influences (low temperature *vs.* drought stress).

Chapter 4

In Chapter 4, we analyse the response patterns to climate of five widely distributed European pines (*Pinus halepensis*, *P. nigra*, *P. pinaster*, *P. sylvestris* and *P. uncinata*) along an altitudinal gradient in the Gúdar range (eastern Spain). We hypothesized that increased regional drought stress is homogenizing climate responses over the twentieth century in trees by modulating leaf-level gas exchange processes, which superimposes on species-specific and local drivers of performance, hence resulting in more synchronous growth across species and elevations. The specific objectives of this study are:

i. to evaluate temporal trends in synchrony patterns of tree growth and its dependence on leaf-level gas exchange processes along the altitudinal gradient.

ii. to assess biogeographical interactions underlying tree growth dynamics by characterizing spatial patterns of forest responses to climate instability.

Chapter 5

Chapter 5 aims at understanding spatiotemporal patterns of tree growth and physiological responses to environmental changes at continental level through the joint analysis of ring-width and stable isotopes. To this end, we use a pan-European and North Africa tree-ring network comprising conifers (*Cedrus*, *Pinus*) and hardwoods (*Quercus*) and spanning the twentieth century. We hypothesised that the temporal coherence in radial growth patterns is linked to changes in the environmental drivers of tree performance across European forests, which in turn influences the relevance of carbon assimilation or stomatal conductance determining tree water and carbon economies. The specific objectives of this study are:

i. to characterize the spatial organization of growth synchrony patterns in European forests.

ii. to evaluate the relationships between ring-width and stable isotope signals under varying environmental conditions, hence tracking the importance of photosynthesis and stomatal conductance as drivers of tree productivity.

iii. to assess whether the control of water losses as determinant of tree growth is spreading northwards as a consequence of climate change, hence increasing the spatial synchrony in growth patterns across Europe.

CHAPTER 2

Unravelling spatiotemporal tree-ring signals in Mediterranean oaks: a variance–covariance modelling approach of carbon and oxygen isotope ratios

Tree Physiology **34:**819–838 (2014)
Doi: 10.1093/treephys/tpu037

Unravelling spatiotemporal tree-ring signals in Mediterranean oaks: a variance–covariance modelling approach of carbon and oxygen isotope ratios

Shestakova TA, Aguilera M, Ferrio JP, Gutiérrez E, Voltas J

Tree Physiology **34:**819–838 (2014)

Abstract

Identifying how physiological responses are structured across environmental gradients is critical to understanding in what manner ecological factors determine tree performance. Here, we investigated the spatiotemporal patterns of signal strength of carbon isotope discrimination ($\Delta^{13}C$) and oxygen isotope composition ($\delta^{18}O$) for three deciduous oaks (*Quercus faginea* (Lam.), *Q. humilis* Mill. and *Q. petraea* (Matt.) Liebl.) and one evergreen oak (*Q. ilex* L.) co-occurring in Mediterranean forests along an aridity gradient. We hypothesized that contrasting strategies in response to drought would lead to differential climate sensitivities between functional groups. Such differential sensitivities could result in a contrasting imprint on stable isotopes, depending on whether the spatial or temporal organization of tree-ring signals was analysed. To test these hypotheses, we proposed a mixed modelling framework to group isotopic records into potentially homogeneous subsets according to taxonomic or geographical criteria. To this end, carbon and oxygen isotopes were modelled through different variance–covariance structures for the variability among years (at the temporal level) or sites (at the spatial level). Signal-strength parameters were estimated from the outcome of selected models. We found striking differences between deciduous and evergreen oaks in the organization of their temporal and spatial signals. Therefore, the relationships with climate were examined independently for each functional group. While *Q. ilex* exhibited a large spatial dependence of isotopic signals on the temperature regime, deciduous oaks showed a greater dependence on precipitation, confirming their higher susceptibility to drought. Such contrasting responses to drought among oak types were also observed at the temporal level (interannual variability), with stronger associations with growing-season water availability in deciduous oaks. Thus, our results indicate that Mediterranean deciduous and evergreen oaks constitute two clearly differentiated functional groups in terms of their carbon and water economies, despite co-existing in a wide range of environments. In contrast, deciduous oaks form a rather homogeneous group in terms of climate sensitivity.

Introduction

Oak species occurring in the Mediterranean are adapted to varying degrees to a double climatic stress, drought in summer and cold in winter (Mitrakos 1980; Terradas & Savé 1992; Larcher 2000). Representatives of three contrasting phytoclimatic categories (Mediterranean, transitional nemoro-Mediterranean and nemoral) are found in this region that, according to features of their leaf and water relationships, form different functional groups (Corcuera *et al.* 2002).

The Mediterranean evergreen *Quercus ilex* L. is characteristic of the landscapes dominant in vast areas of the western Mediterranean basin (Barbero *et al.* 1992). It grows often in co-existence with winter deciduous oaks in a wide range of climates and soils: from Mediterranean-continental environments, together with *Quercus faginea* (Lam.) (Mediavilla & Escudero 2010), to the sub-Mediterranean stages, where it can form mixed forests with *Quercus humilis* Mill. (syn. *Quercus pubescens* Willd.) and *Quercus petraea* (Matt.) Liebl. (Sánchez de Dios *et al.* 2009). The nemoro-Mediterranean *Q. faginea* is a relatively drought-tolerant species widely distributed in the Iberian Peninsula and North Africa, preferentially on basic soils (Loidi & Herrera 1990; Mediavilla & Escudero 2010). The nemoro-Mediterranean *Q. humilis* and the nemoral Eurosiberian *Q. petraea* are mainly found throughout eastern and central Europe, reaching their south-western range limit in the north of the Iberian Peninsula. However, *Q. petraea* is rather sensitive to water shortage, while *Q. humilis* may grow under drier conditions, being often found in sub-Mediterranean environments (see, e.g., Epron & Dreyer 1990; Arend *et al.* 2011). These three deciduous oaks partially overlap along a gradient of increasing humidity in north-eastern Spain, with *Q. faginea* inhabiting the driest, continental areas, followed successively by *Q. humilis* and *Q. petraea*, which occupy the wettest zones. In turn, they co-exist with *Q. ilex* along the entire humidity gradient.

Mediterranean deciduous and evergreen oaks differ considerably in ecophysiological properties, which determine their ability to cope with climatic stressors and, ultimately, define their distribution ranges and ecological fitness (Sánchez de Dios *et al.* 2009). Evergreen oaks usually show, among other properties, an extended vegetative period (Damesin *et al.* 1997), sclerophylly (Richards & Lamont 1996), higher turgor pressure (Corcuera *et al.* 2002), lower hydraulic conductance (Tognetti *et al.* 1998), higher stomatal limitation to photosynthesis (Juárez-López *et al.* 2008) and lower susceptibility to photoinhibition (Epron & Dreyer 1990) compared with deciduous oaks, which favour *Q. ilex* in dry years. Besides, deciduous oaks also differ in several features related to water and carbon economies, which help to explain their different distribution. For instance, the nemoral *Q. petraea* tends to maintain turgor pressure at the expense of more water losses than the nemoro-Mediterranean *Q. faginea* and *Q. humilis*, hence performing worse under drought (Corcuera *et al.* 2002).

The dendrochronological archive of carbon and oxygen stable isotopes simultaneously tracks the balance between assimilation rate and stomatal conductance (or intrinsic water-use efficiency; Farquhar & Richards 1984). In turn, it provides indirectly

environmental information relevant to plant functioning with varying temporal resolution. The rising interest in the spatial and temporal dependence of climate processes has resulted in an explosion of tree-ring isotope networks worldwide (Treydte *et al.* 2007; Gagen *et al.* 2008; Leavitt *et al.* 2010; Saurer *et al.* 2012). Although it is not yet well understood to what degree carbon or oxygen isotope signals of tree rings vary under different climate conditions, there are indications that combining records from different species and sites may enhance the potential of isotope studies for inferring environmental drivers of tree performance (Saurer *et al.* 2008; Li *et al.* 2011). On the other hand, this potential is likely to be counterbalanced, to a variable extent, by differences in ecophysiological properties among species. For example, contrasting physiological responses between co-existing oaks in the Mediterranean region (e.g., Tognetti *et al.* 1998; Corcuera *et al.* 2002) may cause a differential reaction to environmental conditions that could imprint on the stable isotope signal of tree rings. When facing this issue, the problem of disentangling the spatial and temporal patterns of tree-ring signals needs to be confronted. Indeed, the environmental drivers of changes in stable isotopes may not necessarily coincide at the temporal (e.g., interannual fluctuations) and spatial (e.g., intersite variability) levels. Very few studies have attempted to address this question (e.g., Treydte *et al.* 2007).

The conventional approach of investigating the magnitude of common information shared by tree-ring records relies on the application of classical analysis of variance (ANOVA) principles (Fritts 2001; Wigley *et al.* 1984). For this purpose, a two-stage hierarchical scheme of analysis is commonly used in which several trees are first sampled at the stand level. Then, the trees are averaged into an annually resolved chronology, with a set of chronologies for a particular region being subsequently analysed (e.g., Hemming *et al.* 1998; Saurer *et al.* 2008). However, the underlying statistical model is of the mixed type because it may include several effects representing different random sources of variation, e.g., those associated with measurements repeated in time (Jennrich & Schluchter 1986). Quite surprisingly, the use of mixed models in dendrochronology does not seem to have reached the level it warrants (but see, e.g., Martínez-Vilalta *et al.* 2008; Lapointe-Garant *et al.* 2010; Linares & Tiscar 2010, 2011). The primary reasons may be twofold: first, they are computationally demanding, being beyond reach until recently; second, the presentation of the methodology in specialized manuals is often biased towards the theoretical side, which makes mixed models challenging for a wide audience.

Often, it may be of interest to stratify a set of chronologies into potentially more homogeneous subsets (e.g., McCarroll & Pawellek 2001). By applying different grouping criteria, stratification may allow unveiling of factors responsible for enhanced common signal strength (or temporal coherence) among chronologies. These factors may be related to the taxonomic affiliation of chronologies or to their assignment to particular sites or regions, among others. The adopted grouping strategy may be readily embedded in a mixed-model framework, where time is a random factor and chronologies (and their grouping) are fixed. A

variant of this approach arises if emphasis is placed on the spatial interpretation of the signal strength stored in a set of trees (e.g., for variability between sites across years) rather than at the temporal (e.g., for variability between years) level (or spatial coherence).

At the temporal level, the interest lies in interpreting common temporal information stored in tree-ring chronologies; at the spatial level, the aim is the exploration of the spatial variability in tree-ring signals (e.g., Leavitt *et al.* 2007; del Castillo *et al.* 2013). In this last case, it may be more informative to group individual tree records (e.g., pooled rings representing a number of years) according to taxonomic criteria in a similar way than to group chronologies. A fundamental advantage of mixed modelling is that all available data are used when assigning chronologies (at the temporal level) or tree records (at the spatial level) to groups, thus allowing for the quantification of common signals at the intra- and intergroup classes.

This study aimed at interpreting the variability and common signal strength of stable carbon and oxygen isotope ratios in tree rings for deciduous and evergreen *Quercus* species co-occurring in mixed Mediterranean forests. Here, we hypothesized that contrasting strategies in response to drought in Mediterranean evergreen (*Q. ilex*), nemoro-Mediterranean deciduous (*Q. faginea and Q. humilis*) and nemoral deciduous (*Q. petraea*) oaks would lead to a differential sensitivity to changes in water availability, and that this could be tracked by means of carbon and oxygen isotope analysis in tree rings. In turn, such differential sensitivity could imprint on stable isotopes in a contrasting manner, depending on whether the spatial or temporal organization of tree-ring signals was analysed.

To test these hypotheses, we compared the responses of these species using a tree-ring isotope network consisting of 24 sites (21 new and three already published) scattered across an aridity gradient in the north-eastern Iberian Peninsula covering an area of ~25,000 km². For some sites, annually resolved chronologies for stable isotopes were available, which allowed investigation of how temporal signals were structured according to taxonomic or geographical criteria for grouping chronologies and which climate drivers were involved in the observed responses. Alternatively, sites where the evergreen *Q. ilex* co-existed with deciduous oaks were investigated to identify potentially contrasting spatial signals between functional types and their driving climate factors across an aridity gradient in the Mediterranean. To this end, we proposed a new conceptual framework by which the patterns of tree-ring signals were investigated through mixed modelling.

Materials & methods

Materials

Study area and sampling strategy

The study was conducted in natural mixed-oak (*Quercus* spp.) forest stands located in the north-eastern Iberian Peninsula, western Mediterranean basin, between latitudes 41°11'N and 42°25'N and longitudes 0°39'E and 2°45'E (Fig. 2.1). Different combinations of one

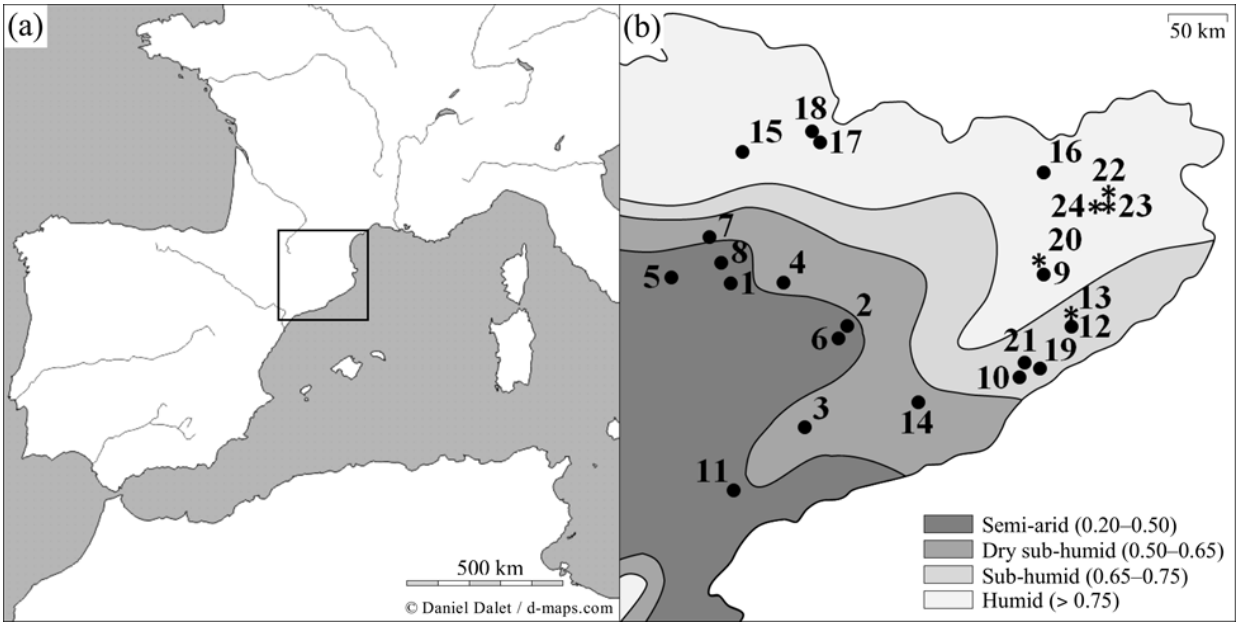

Figure 2.1. Study area **(a)** and geographical distribution of sampling sites **(b)**. For reference, a contour map of the main bioclimatic regions in the studied area according to the UNESCO aridity index (total precipitation/Penman–Monteith evapotranspirative demand) is presented. Site numbering is according to Table 2.1. Asterisks identify sampling sites with availability of annually resolved chronologies for analysis at the temporal level.

deciduous (either *Q. faginea*, *Q. humilis* or *Q. petraea*) and one evergreen (*Q. ilex*) oak species were present at each site, except for three sites (named Banyoles) in which either a single species or two deciduous co-occurring species were available (Table 2.1).

The study area is characterized by a complex topography and the interaction of African subtropical, North Atlantic and Mediterranean climate systems (Rodó *et al.* 1997), with cold wet winters and a period of summer drought that occurs every year. The mean annual precipitation varies from 498 to 998 mm among the study sites (Table 2.1), with summer (June to August) precipitation ranging from 102 to 316 mm. The average annual temperature ranges from 8.4 to 15.6°C (Table 2.1), with an average minimum temperature of –0.1°C in January for the coldest site and an average maximum temperature of 28.5°C in July for the warmest site (Digital Climatic Atlas of the Iberian Peninsula, available at http://www.opengis.uab.es/wms/iberia/mms/index.htm; Ninyerola *et al.* 2005).

Wood cores of *Q. faginea*, *Q. humilis*, *Q. ilex* and *Q. petraea* were collected using a 5-mm-diameter increment borer in 2009. As a sampling strategy, a representative set of 21 sites encompassing the natural biogeographical range of conditions where deciduous and evergreen Mediterranean oaks co-occur in mature forest stands in the region were identified based on information of the Ecological Forest Inventory of Catalonia. These ranged from humid, relatively mild territories near the Mediterranean coastal strip having a

Table 2.1. Main biogeographical variables and carbon ($\Delta^{13}C$) and oxygen ($\delta^{18}O$) stable isotopes (means ± SD) of sampling sites.

Id	Site	Species combination	Lat	Lon	Alt (m a.s.l)	*T* (ºC)	*P* (mm)	$\Delta^{13}C$ (‰)		$\delta^{18}O$ (‰)	
								Species 1	Species 2	Species 1	Species 2
1	Alos de Balaguer	*Q. ilex*/*Q. faginea*	41º54'N	0º56'E	429	13.2	622	17.75 ± 0.57	17.85 ± 1.13	33.09 ± 0.50	32.11 ± 0.17
2	Calonge de Segarra	*Q. ilex*/*Q. faginea*	41º44'N	1º28'E	680	12.2	537	17.39 ± 0.57	16.21 ± 1.31	32.56 ± 0.98	31.56 ± 0.88
3	Figuerola del Camp	*Q. ilex*/*Q. faginea*	41º23'N	1º15'E	628	12.8	645	17.14 ± 0.83	18.15 ± 1.15	31.82 ± 0.28	31.64 ± 0.40
4	Oliola	*Q. ilex*/*Q. faginea*	41º54'N	1º11'E	407	13.2	498	16.23 ± 0.74	16.46 ± 0.50	33.26 ± 0.58	32.23 ± 0.41
5	Os de Balaguer	*Q. ilex*/*Q. faginea*	41º56'N	0º39'E	668	12.0	669	17.36 ± 0.53	16.32 ± 0.68	32.43 ± 0.30	31.67 ± 0.36
6	Pujalt	*Q. ilex*/*Q. faginea*	41º42'N	1º26'E	696	12.2	544	15.90 ± 0.89	16.52 ± 0.61	32.70 ± 1.10	32.00 ± 0.92
7	Sant Esteve de la Sarga	*Q. ilex*/*Q. faginea*	42º04'N	0º50'E	745	11.4	505	17.50 ± 0.51	16.99 ± 0.47	33.57 ± 0.30	32.04 ± 0.56
8	Camarasa	*Q. ilex*/*Q. humilis*	41º59'N	0º53'E	737	11.6	558	17.41 ± 0.66	16.70 ± 0.60	32.73 ± 0.88	31.52 ± 0.37
9	Espinelves	*Q. ilex*/*Q. humilis*	41º52'N	2º25'E	793	11.3	816	16.87 ± 0.83	17.38 ± 0.69	31.42 ± 0.25	31.14 ± 0.52
10	Montornès del Vallès	*Q. ilex*/*Q. humilis*	41º32'N	2º17'E	296	14.3	634	16.22 ± 0.73	16.99 ± 0.51	32.07 ± 0.55	31.33 ± 0.50
11	Pradell de la Teixeta	*Q. ilex*/*Q. humilis*	41º10'N	0º54'E	527	13.0	568	17.39 ± 0.95	18.09 ± 0.83	31.61 ± 0.07	31.12 ± 0.87
12	Sant Celoni I	*Q. ilex*/*Q. humilis*	41º42'N	2º32'E	252	14.2	717	16.71 ± 0.58	17.33 ± 1.16	32.27 ± 0.28	32.29 ± 0.24
13	Sant Celoni II[1]	*Q. ilex*/*Q. humilis*	41º43'N	2º32'E	128	15.2	825	17.51 ± 0.47	17.81 ± 0.77	32.42 ± 0.60	32.13 ± 0.50
14	Sant Sadurní d'Anoia	*Q. ilex*/*Q. humilis*	41º27'N	1º47'E	147	15.6	564	15.95 ± 1.29	17.34 ± 0.99	33.46 ± 0.70	32.74 ± 0.24
15	Baix Pallars	*Q. ilex*/*Q. petraea*	42º22'N	1º01'E	1140	9.3	998	17.45 ± 0.65	17.01 ± 0.72	32.66 ± 0.75	32.03 ± 0.63
16	La Vall de Bianya	*Q. ilex*/*Q. petraea*	42º14'N	2º27'E	436	13.0	928	17.31 ± 0.75	17.68 ± 0.82	31.47 ± 0.25	31.38 ± 0.49
17	Montferrer i Castellbò I	*Q. ilex*/*Q. petraea*	42º24'N	1º22'E	1254	8.6	737	17.37 ± 0.43	16.43 ± 0.57	32.67 ± 0.71	31.4 ± 0.12
18	Montferrer i Castellbò II	*Q. ilex*/*Q. petraea*	42º25'N	1º22'E	1300	8.4	799	16.91 ± 0.50	16.58 ± 0.61	32.45 ± 0.48	31.79 ± 0.24
19	Òrrius	*Q. ilex*/*Q. petraea*	41º33'N	2º21'E	371	13.8	718	17.51 ± 0.70	17.79 ± 0.86	32.28 ± 0.21	31.52 ± 0.67
20	Sant Sadurní d'Osormort[1]	*Q. ilex*/*Q. petraea*	41º55'N	2º24'E	626	12.1	787	16.77 ± 0.63	17.74 ± 0.69	32.36 ± 0.44	31.57 ± 0.50
21	Vilanova del Vallès	*Q. ilex*/*Q. petraea*	41º33'N	2º18'E	108	15.2	639	17.22 ± 0.77	17.78 ± 1.17	32.92 ± 0.33	32.77 ± 0.68
22	Banyoles (low altitude)[2]	*Q. humilis*/*Q. petraea*	42º09'N	2º45'E	231	14.0	877	17.32 ± 0.65	17.95 ± 0.54	31.84 ± 0.70	30.87 ± 1.81
23	Banyoles (medium altitude)**	*Q. humilis*/*Q. petraea*	42º06'N	2º43'E	310	13.5	937	18.26 ± 0.43	18.44 ± 1.06	27.64 ± 0.84	29.43 ± 1.78
24	Banyoles (high altitude)[2]	*Q. humilis*/—	42º06'N	2º42'E	423	13.1	966	18.11 ± 0.56	—	26.61 ± 0.75	—

[1]Sites used for analysis at the temporal and spatial levels.
[2]Sites used only for analysis at the temporal level.
Lat, latitude; Lon, longitude; Alt, altitude; a.s.l., above sea level; *T*, temperature; *P*, precipitation.

nemoro-Mediterranean vegetation to contact areas between the Mediterranean and Eurosiberian regions, with recurrent presence of winter frosts and characterized by sub-Mediterranean taxa (Rivas-Martínez 1982).

For each of the three deciduous species (*Q. faginea*, *Q. humilis* and *Q. petraea*), seven sites were chosen in which the deciduous oak was found co-occurring with the evergreen holm oak (*Q. ilex*; Table 2.1). Mean values of altitude, temperature and precipitation for the sampling sites of each deciduous species in combination with *Q. ilex* were 608 m above sea level (a.s.l.), 12.4°C and 574 mm for *Q. faginea*, 411 m a.s.l., 13.6°C and 669 mm for *Q. humilis*, and 748 m a.s.l., 11.5°C and 801 mm for *Q. petraea*. The selection preserved the original range of variation in thermal and precipitation regimes for each species, while avoiding a strong dependence between both bioclimatic indicators for the complete set of sites (correlation between mean annual precipitation and average annual temperature, $r = 0.36$; $P = 0.11$). In this way, we aimed at reducing potential confounding effects in the interpretation of climate-driven variability in the studied traits.

For each species combination, five nearest-neighbour pairs of mature, dominant and healthy trees of a similar size (one deciduous and one evergreen), growing within a radius of 4 m and far from water sources other than precipitation (e.g., springs, gullies, ravines, etc.), were selected at each site. As a result, 35 trees of each deciduous oak (*Q. faginea*, *Q. humilis* and *Q. petraea*) and 105 *Q. ilex* trees were sampled in May–July 2009 (diameters at breast height of 22.0 ± 3.5, 22.6 ± 6.2, 21.0 ± 3.8 and 21.4 ± 4.7 cm, respectively; mean ± standard deviation [SD]). Two cores were taken from the south side of each tree. One core was used for tree-ring dating and the other for subsequent isotope analyses. This sampling scheme was employed to identify potentially contrasting spatial signals in stable isotopes between deciduous and evergreen oaks. The exploration of spatial patterns in stable isotopes was investigated using 20-year pooled tree-ring samples spanning the period 1989–2008 (see the next sections).

In addition, the temporal variability in stable isotopes was explored through annually resolved chronologies in three selected sites representing every species combination (one of the deciduous oak species co-occurring with the evergreen *Q. ilex*), from which additional cores of five trees per species were taken in April 2010. These sites were representative of the average precipitation and temperature conditions in which the above-mentioned tree species combinations were found along the ecological transect. They were complemented by data compiled from a previous study (Aguilera *et al.* 2011) in which co-occurring *Q. humilis* and *Q. petraea* trees were sampled near Banyoles lake, NE Spain (42°07'N, 2°45'E) in May 2006. In this study, three sites were chosen following an altitudinal gradient, and the criteria for tree selection and the sampling protocol were the same as specified above. However, for the highest elevation site (423 m a.s.l.), only *Q. humilis* individuals were available, while at the medium (310 m a.s.l.) and low (231 m a.s.l.) elevation sites, only two and four trees of *Q. petraea*, respectively, were found having the required features. As a result, a total of 15 trees of *Q. humilis* and six trees of *Q. petraea*, with mean diameters at breast height of 19.8 ± 2.9 and

19.1 ± 2.9 cm, respectively, were sampled. Altogether, a set of 24 sampling sites were used to investigate the spatiotemporal patterns of variability in stable isotopes, with the following representation of species (Table 2.1): *Q. faginea* (seven sites), *Q. humilis* (10 sites), *Q. ilex* (21 sites) and *Q. petraea* (nine sites).

Sample preparation and tree-ring dating

All samples were oven-dried at 60°C for 48 h and one core per tree was sanded with sandpapers of progressively finer grain until tree rings were clearly visible. The remaining core of every tree was kept intact for isotope analyses. Tree rings were visually cross-dated using a binocular microscope coupled to a PC with the image processing program ImageJ (ImageJ v. 1.42, available at http://rsb.info.nih.gov/ij). The COFECHA program (Holmes 1983) was used to evaluate the visual cross-dating for samples requiring annual resolution (originating from three selected sites of the biogeographical transect, in addition to those reported in Aguilera *et al.* 2011). Each individual tree-ring width series showed a decreasing growth trend, which was removed by fitting a straight line and keeping the residuals obtained by the difference of this linear fit. The residuals were subjected to autoregressive modelling to remove the first-order autocorrelation. Annually resolved isotope chronologies were produced by pooling dated growth rings from about five trees prior to the isotopic analyses.

A prerequisite for pooling was availability of tree-ring series reflecting consistent ring-width variation common to all trees. For this purpose, the quality of the average chronology for every site–species combination was examined by calculating the mean interseries correlation ($\hat{a}$), the signal-to-noise ratio (SNR) and the expressed population signal (EPS) statistics according to Wigley *et al.* (1984). Three site–species chronologies (Oliola, for both *Q. faginea* and *Q. ilex*, and Sant Sadurní d'Osormort, for *Q. ilex*) had low values of $\hat{a}$, SNR and EPS, indicating a poor cross-dating for ring width. This could be due either to the influence of local factors such as micro-topography and competition (bearing in mind the limited amount of sampled trees) or to difficulties in the identification of rings in diffuse-porous species such as *Q. ilex* (Cherubini *et al.* 2003). These chronologies were therefore excluded from the analysis of isotope patterns at the temporal level. Finally, a total of eight chronologies were used (four chronologies of *Q. humilis*, three of *Q. petraea* and one of *Q. ilex*), which had the following average quality: $\hat{a} = 0.49 \pm 0.02$, SNR = 4.89 ± 0.20, EPS = 0.83 ± 0.03 (mean ± SD; $n = 5$ trees per chronology).

Stable isotope analyses

A core fragment containing rings that spanned the period 1989–2008 (20 years) was selected for every tree sampled in 2009. The 20-year wood fragments were split from the original cores using a scalpel. They were used to characterize the spatial pattern of isotope signals along the biogeographical gradient. In addition, eight annually resolved isotope chronologies (see the previous section) were available for a period of 20 years (1986–2005 for

the series reported in Aguilera *et al.* 2011; 1989–2008 for the series obtained in this study). Every 20-year wood fragment corresponding to a particular tree, site and species or, alternatively, every set of rings of the same year from about five trees were purified to a-cellulose with a modification of the method of Leavitt & Danzer (1993) for the removal of extractives and lignin, as detailed in Ferrio & Voltas (2005). Sodium hydroxide was used to obtain a-cellulose (Loader *et al.* 1997), which was homogenized to a fine powder with a ball mixer mill (Retsch MM301, Haan, Germany).

For carbon isotope analysis, 0.30–0.40 mg of dry a-cellulose was weighed into tin foil capsules and combusted using a Flash EA-1112 elemental analyser (Thermo Fisher Scientific Inc., MA, USA) interfaced with a Finnigan MAT Delta C isotope ratio mass spectrometer (Thermo Fisher Scientific Inc.). For oxygen isotope analysis, 0.30–0.40 mg of dry a-cellulose was weighed into silver foil capsules and combusted using a Carlo Erba 1108 elemental analyser (Carlo Erba Instruments Ltd., Milan, Italy) interfaced with a Finnigan Deltaplus XP isotope ratio mass spectrometer (Thermo Fisher Scientific Inc.). Isotope ratios were expressed as per mil deviations using the d notation relative to Vienna Pee Dee Belemnite standard (for carbon) and Vienna Standard Mean Ocean Water (for oxygen) standards. The accuracy of the analyses (SD of working standards) was 0.06‰ ($\delta^{13}C$) and 0.25‰ ($\delta^{18}O$).

To account for changes in $\delta^{13}C$ of atmospheric CO_2 ($\delta^{13}C_{air}$), we calculated carbon isotope discrimination in cellulose ($\Delta^{13}C$) from $\delta^{13}C_{air}$ and α-cellulose $\delta^{13}C$ ($\delta^{13}C$), as described by Farquhar & Richards (1984):

$$\Delta^{13}C = \frac{\delta^{13}C_{air} - \delta^{13}C}{1 + \delta^{13}C} \qquad (2.1)$$

$\delta^{13}C_{air}$ was inferred by interpolating a range of data from Antarctic ice-core records, together with modern data from two Antarctic stations (Halley Bay and Palmer Station) of the CU-INSTAAR/NOAA-CMDL network for atmospheric CO_2 measurements, as first described in Ferrio *et al.* (2005); smoothed $\delta^{13}C_{atm}$ curve from 16,100 BCE to 2010, available at http://web.udl.es/usuaris/x3845331/ AIRCO2_LOESS.xls). According to these records, the $\delta^{13}C_{air}$ value applied to extant α-cellulose samples varied between −8.21 and −7.60‰.

The isotope chronologies (either $\Delta^{13}C$ or $\delta^{18}O$) exhibiting a linear trend over time were detrended by fitting a straight line and keeping the residuals of these linear fits as input for mixed modelling. There were three chronologies for $\Delta^{13}C$ (the two chronologies from Sant Celoni II, with negative trends, and one chronology of *Q. petraea* from Banyoles of medium altitude, with a positive trend) and two for $\delta^{18}O$ (one chronology of *Q. petraea* from Banyoles of low altitude, with a positive trend, and one chronology of *Q. petraea* from Banyoles of medium altitude, with a negative trend). For the rest of the chronologies, which did not show significant trends over time, each individual record was corrected by subtracting from the average value of its corresponding chronology in order to also obtain residual

chronologies for mixed modelling. Therefore, mixed modelling focused on the analysis of interannual variability in isotopic signals.

Strategy for grouping isotopic records at spatial and temporal levels

We checked several grouping structures. At the temporal level, two different grouping strategies were tested: (*i*) a taxonomy-based strategy, by which chronologies from the same species were considered as a single group; and (*ii*) a site-based strategy, by which chronologies from the same site, irrespective of the species, were considered as a single group. In the first case, two groups were formed: *Q. humilis* (consisting of four chronologies) and *Q. petraea* (consisting of three chronologies). In the second, three groups emerged corresponding to three different sites: (*i*) Banyoles of low elevation (including *Q. humilis* and *Q. petraea*); (*ii*) Banyoles of medium elevation (including *Q. humilis* and *Q. petraea*); and (*iii*) Sant Celoni (including *Q. humilis* and *Q. ilex*). It is important to stress that each grouping strategy involved a particular set of chronologies, although five chronologies were used in both analyses.

At the spatial level, 10 oaks from each of the 21 available sites (and represented by their 20-year isotope averages) were classified into two groups, deciduous and evergreen. This meant that oaks from the three deciduous species formed a single group across the biogeographical transect that was tested for coherence of its isotope signals against the group formed by the evergreen oaks (*Q. ilex*).

Meteorological data

Estimates of monthly mean temperatures (minimum, mean and maximum) and total precipitation for each site were obtained from the Digital Climatic Atlas of the Iberian Peninsula (Ninyerola *et al.* 2005), which provides averages for the period 1950–1999 with a spatial resolution of 200 m. These records were used to infer the climatic sensitivity of isotopic signals across the biogeographical transect (i.e., at the spatial level). Annual meteorological records (monthly averages for minimum, mean and maximum temperature, and total monthly precipitation) covering the studied period were supplied by the Spanish National Meteorological Agency for the five sites in which annually resolved tree-ring chronologies were available. They were used to ascertain the relationships of tree-ring isotopes with climate at the temporal level. The records originated from the nearest meteorological station to each sampling point, located <15 km from the study sites. Wherever the altitude of the sampling site differed from that of the meteorological station, we applied the following correction (Gandullo 1994): for temperature, a decrease of 0.6°C per 100 m; for precipitation, an 8% increment per 100 m, except for July and August, when precipitation is mostly convective and not related to altitude. Climate records and isotope data were compared using simple correlations at both spatial and temporal levels.

Statistical analysis

In dendroclimatology and dendroecology, time series of tree-ring features are averaged to produce 'chronologies' that reflect variability common to all trees at a particular site (Wigley *et al.* 1984). A particular set of chronologies ($i = 1, N$) can thereafter be analysed together to characterize the strength of their common signal. Suppose that W_{ij} is the jth observation (i.e., year) of a parameter W_i, and that each W_i reflects some controlling process by a particular tree-ring feature (i.e., carbon or oxygen stable isotope ratios) that may be obscured by noise that depends on both i and j. The estimators can be defined in terms of the following random model (random variables are shown underlined in this paper):

$$\underline{W}_{ij} = \underline{Y}_j + \underline{e}_{ij} \tag{2.2}$$

where $\underline{Y}_j$ is a random time effect of the jth year and $\underline{e}_{ij}$ is a random deviation of the ith chronology in the jth year. Here, we assume that the year effects behave as if they came from a normal distribution with mean zero and variance σ^2_y. This means that observations made in the same year have a covariance, and so they are not independent. To quantify how strongly the chronologies ($i = 1, N$) are correlated, let us now consider the values that two chronologies, i and i^*, can attain for a particular year, j. The covariance between observations is:

$$\begin{aligned} &\mathrm{cov}(\underline{W}_{ij}, \underline{W}_{i^*j}) = \mathrm{cov}(\underline{Y}_j + \underline{e}_{ij}, \underline{Y}_j + \underline{e}_{i^*j}) = \\ &= \mathrm{cov}(\underline{Y}_j, \underline{Y}_j) + \mathrm{cov}(\underline{e}_{ij}, \underline{e}_{i^*j}) = Var(\underline{Y}) = \sigma^2_Y \end{aligned} \tag{2.3}$$

Here, a typical, but not obligatory, assumption in mixed modelling is to take the random effects belonging to different random terms, in our case $\underline{Y}_j$ and $\underline{e}_{ij}$, as independent of each other (Demidenko 2004). This assumption may not necessarily hold for longitudinal data, and can be avoided by allowing for correlation of random effects in Eq. (2.3). However, the consequences of incorporating such correlation, disregarding parsimony, would need a detailed examination.

Likewise, the variance of chronology i is:

$$Var(\underline{W}_i) = Var(\underline{Y} + \underline{e}_i) = Var(\underline{Y}) + Var(\underline{e}_i) = \sigma^2_Y + \sigma^2_e \tag{2.4}$$

The intraclass correlation (or reproducibility of observations by chronologies i and i^*) then becomes:

$$\rho(\underline{W}_i, \underline{W}_{i^*}) = \frac{\mathrm{cov}(\underline{W}_i, \underline{W}_{i^*})}{\sqrt{Var(\underline{W}_i) \times Var(\underline{W}_{i^*})}} = \frac{\sigma^2_Y}{\sigma^2_Y + \sigma^2_e} \tag{2.5}$$

If the whole set of N chronologies is analysed together, this parameter becomes the average correlation over all possible pairs of chronologies, excluding the N pairs $I = i^*$ for which $r_{ii^*} = 1$. This correlation is closely related to the mean interseries correlation parameter

defined at the intrasite level, $\hat{a}$, which is widely used in dendroclimatology and dendroecology (Wigley *et al.* 1984). We will refer to it as the mean interchronology correlation, $\hat{a}_C$. It estimates the strength of the common signal underlying the set of N chronologies. Unlike the classical ANOVA approach, mixed modelling is capable of dealing with partially overlapping chronologies, so unbalancedness is not a concern here if we consider the missing-data pattern as being completely random (see Little & Rubin 2002 for details).

A natural variant of the model (Eq. [2.2]) arises if a set of trees ($i = 1, N$) is used across a number of sites to characterize the strength of tree-ring signals at the spatial level (signals are represented here by 20-year pooled isotopic values). In this case, $\underline{W_{ij}}$ is the observation corresponding to the jth site of a parameter $\underline{W_i}$, but now the ith tree is nested to the jth site from where it originates. The model remains the same as in Eq. (2.2), but now $\underline{Y_j}$ represents a random site effect of the jth site, and $\underline{e_{ij}}$ is a random deviation of the ith tree of the jth site. We assume that the site effects behave as if they came from a normal distribution with mean zero and variance σ^2_S, so the intraclass correlation (Eq. [2.5]) still holds true by replacing σ^2_Y by σ^2_S. Such an alternative intraclass correlation will be referred to as spatial signal strength, $\hat{a}_S$. In this case, it estimates the strength of the common signal underlying a set of N trees that vary from site to site.

Mixed modelling for grouping chronologies (analysis of temporal variability)

In order to search for contributing causes of enhanced common variance for isotope signals among chronologies, these were grouped considering the two above-mentioned criteria: (*i*) taxonomy (with two groups, *Q. humilis* and *Q. petraea*); and (*ii*) species co-occurrence (with three groups corresponding to each one of three sites). If a random sample of chronologies is used for trait testing in each group, the resulting data may be regarded as a random stratified sample, with strata corresponding to groups. According to the theory of survey sampling (Kish 1965), stratification is beneficial (i.e., it improves the accuracy of parameter estimates), provided there is heterogeneity between groups as defined by the factor(s) under evaluation.

Now the estimators can be defined in terms of the following mixed model:

$$\underline{W}_{ijr} = \mu_r + \underline{Y}_{jr} + \underline{e}_{ijr} \qquad (2.6)$$

where μ_r is the expected value in the rth group (if the chronologies are detrended or indexed, as in this study, this term vanishes but can be saved for further analysis), $\underline{Y_{jr}}$ is a random time effect of the jth year in the rth group and $\underline{e_{ijr}}$ is a random deviation of the ith chronology in the jth year within the rth group. The random deviation can be further partitioned as:

$$\underline{e}_{ijr} = \underline{p}_{i(r)} + \underline{f}_{ij(r)} \qquad (2.7)$$

where $\underline{p_{i(r)}}$ is a random effect of the *i*th chronology nested within the *r*th group and $\underline{f_{ji(r)}}$ is a year-specific deviation. Both effects appearing in $\underline{e_{jir}}$ are assumed to be independent homoscedastic normal deviates with zero means; in particular, if the chronologies are detrended or indexed then the term $\underline{p_{i(r)}}$ has null variability (i.e., all chronologies share the same mean value).
In turn, the year effect may be further partitioned as:

$$\underline{Y}_{jr} = \underline{Y}_{j} + \underline{(YR)}_{jr} \qquad (2.8)$$

where $\underline{Y_j}$ is a main effect for the *j*th year and $\underline{(YR)_{jr}}$ is the *jr*th year × group interaction, assuming that $\underline{Y_j}$ and $\underline{(YR)_{jr}}$ are independent homoscedastic normal deviates. This model corresponds to the standard ANOVA partition accommodating between- and within-group variability and has the so-called compound symmetry variance–covariance (VCOV) structure (model M_1) for the variability among years:

M_1: *compound symmetry*

$$\mathrm{cov}(\underline{Y}_{jr};\underline{Y}_{jr^*}) = \sigma^2_{Y+YR} \quad , \quad \text{when } r = r^*,$$
$$\text{otherwise } \mathrm{cov}(\underline{Y}_{jr};\underline{Y}_{jr^*}) = \sigma^2_{Y}$$

Under the compound symmetry model, year variances are the same in each group, with $\sigma^2_{\mathrm{Y+YR}} = \sigma^2_{\mathrm{Y}} + \sigma^2_{\mathrm{YR}}$, and year covariances (and correlations) are the same for each pair of groups. While this assumption may be adequate in some circumstances, a range of alternative assumptions can be covered by other VCOV structures. In some cases, there may be heterogeneity of year variance between groups although the property of constant correlation (ϱ) across all pairs of groups may still hold true (model M_2), provided there is null residual variance associated with the values of $\underline{f_{ji(r)}}$ in Eq. (2.7):

M_2: *heterogeneous compound symmetry*

$$\mathrm{cov}(\underline{Y}_{jr};\underline{Y}_{jr^*}) = \sigma^2_{Y_r} \quad , \quad \text{when } r = r^*,$$
$$\text{otherwise } \mathrm{cov}(\underline{Y}_{jr};\underline{Y}_{jr^*}) = \sigma_{Y_r} \times \sigma_{Y_{r^*}} \times \rho$$

Alternatively, we may assign each group its own year variance and each pair of groups its own year covariance (model M_3):

M_3: *unstructured (full model)*

$$\mathrm{cov}(\underline{Y}_{jr};\underline{Y}_{jr^*}) = \sigma^2_{Y_r} \quad , \quad \text{when } r = r^*,$$
$$\text{otherwise } \mathrm{cov}(\underline{Y}_{jr};\underline{Y}_{jr^*}) = \sigma^2_{Y_{rr^*}}$$

Under the unstructured model, all causes of year × group interaction (i.e., year heterogeneity across groups and deviations from equal year correlations between groups) are allowed.

Two simple variants of M_1 can act as a baseline against which to compare the more refined modelling alternatives shown before:

M_4: *banded main diagonal (narrow evaluation)*

$$\text{cov}(\underline{Y}_{jr}; \underline{Y}_{jr^*}) = \sigma^2_{YR} \quad , \quad \text{when } r = r^*,$$
$$\text{otherwise } \text{cov}(\underline{Y}_{jr}; \underline{Y}_{jr^*}) = 0$$

Model M_4 constrains the covariance (and correlation) between groups to zero, thus testing for a lack of common signal between chronologies belonging to different groups.

M_5: *Null model (broad evaluation)*

$$\text{cov}(\underline{Y}_{jr}; \underline{Y}_{jr^*}) = \sigma^2_{Y} \quad , \quad \text{when } r = r^* \text{ or } r \neq r^*,$$

Under the null model M_5, we simply ignore the existence of groups so year variance and covariances have the same value. This model is useful for testing the adequacy of grouping chronologies into different classes as for models M_1–M_4.

Alternative VCOV structures can also be fitted, but here we stuck to the aforementioned models as the number of groups tested in this work was quite limited (two to three), and thus additional extensions of the standard ANOVA partition (Eq. [2.8]) were deemed unnecessary. In turn, models M_1–M_5 can be enhanced in two ways: (*i*) by allowing the residual variance associated with $\underline{f_{ji(r)}}$ to vary among groups; and (*ii*) by assuming a steady decay in correlation with increasing time between observations (i.e., accounting for non-independence of random deviates $\underline{f_{ji(r)}}$ of Eq. [2.7]). The former represents a heteroscedastic variant of models M_1–M_4 (model M_5 has no definition of groups). Homogeneity of residual variance is a main assumption of standard ANOVA, and conclusions on year × group interactions may not be appropriate if this assumption is not fulfilled. For the latter, we used an autoregressive model of order 1, with one extra correlation parameter in addition to the residual variance associated with $\underline{f_{ji(r)}}$ in Eq. (2.7). The correlation between records from a particular chronology *i* in years *j* and *j** is $\varrho^{|j-j^*|}$ as $|\varrho| < 1$. The heteroscedastic variants of models M_1–M_4 were also tested for independent autoregressive structures at the group level, in association with the random deviates $\underline{f_{ji(r)}}$ in Eq. (2.7). A detailed list of the different models is given in Table 2.2.

Mixed modelling for grouping trees (analysis of spatial variability)

At the site level, we grouped trees into two classes (evergreen and deciduous), extending this classification to a number of *J* sites. Similar to the previous case of chronology

Table 2.2. Description of the models used for interpreting temporal and spatial patterns in isotope records according to the assignment of chronologies (for analysis at the temporal level) or trees within a site (for analysis at the spatial level) to pre-defined groups.

	Model and interpretation	Covariance structure	Variances	Covariances	Correlations	Residual variance[1]
M_1	Homogeneity of year (temporal) or site (spatial) variances and covariances across groups	Compound symmetry	Homogeneous	Homogeneous	Homogeneous[2]	Homoscedastic / heteroscedastic
M_2	Different variances but equal year (temporal) or site (spatial) correlation between all group pairs[3]	Heterogeneous compound symmetry	Heterogeneous	Heterogeneous	Homogeneous[3]	Homoscedastic / heteroscedastic
M_3	Full model (different variances and covariances). All causes of year × group (temporal) or site × group (spatial) interaction are allowed	Unstructured	Heterogeneous	Heterogeneous	Heterogeneous	Homoscedastic / heteroscedastic
M_4	Lack of common signal between groups	Banded main diagonal	Heterogeneous	Zero	Zero	Homoscedastic / heteroscedastic
M_5	Null model. Broad evaluation ignoring groups	None	Single	-	-	Homoscedastic

[1]Autoregressive structures at the group level were also tested, accounting for non-independence of temporal (year) random deviates.
[2]If homoscedastic residual variance.
[3]If null residual variance.

grouping, we aimed at searching for contributing causes of enhanced common variance, but focusing on the organization of spatial rather than temporal isotope signals. Equations (2.5) and (2.7) are equally valid after replacing the year effect by a site effect *j*, and the chronology effect by a tree effect *i*. In turn, model residuals (as for Eq. [2.7]) appear from the deviation of the *i*th tree within the *rj*th group × site interaction. The heteroscedastic variants of models M_1–M_4 were also tested at the spatial level.

Model selection

In mixed modelling, it is important to choose a random structure that combines sufficient flexibility with parsimony in the number of VCOV parameters. The adequacy of different VCOV models can be compared by computing the restricted log-likelihood for each model and deriving criteria such as Akaike's information criterion (AIC) and the Bayesian information criterion (BIC). Both involve a penalty for the number of parameters in the VCOV structure, which favours parsimonious models, but BIC generally penalizes a large number of parameters more strongly than does AIC (however, Barnett *et al.* (2010) have demonstrated that AIC may over-penalize the covariance parameters for complex structures). Both statistics are in the smaller-is-better form. We considered models with substantial support to be those in which the difference of either AIC or BIC between models was <2 (Raftery 1996; Burnham & Anderson 2002). This difference corresponds to the information loss experienced when using an alternative model instead of the best-fit model for inference (Burnham & Anderson 2002).

Estimation of signal-strength parameters

The intraclass correlation defined in Eq. (2.) quantifies the degree to which the values of *N* chronologies (or trees) contain a common temporal (or spatial) signal. Models M_1–M_4 allow for the estimation of intraclass correlations either at the intragroup or intergroup level. The underlying idea is to split the mean correlation estimated between all possible pairs of chronologies (trees) drawn from the whole dataset as in Eq. (2.5) into: (*i*) a mean correlation between pairs of chronologies (trees) for every group; and (*ii*) a mean correlation between pairs of chronologies (trees) for pairs of groups. For the more general M_3 (unstructured) model, the correlation of pairs of chronologies (trees) *i* and *i** belonging to group *r* becomes:

$$\rho(\underline{W}_i, \underline{W}_{i*}) = \frac{\mathrm{cov}(\underline{W}_i, \underline{W}_{i*})}{\sqrt{\mathrm{Var}(\underline{W}_i) \times \mathrm{Var}(\underline{W}_{i*})}} = \frac{\sigma^2_{Y_r}}{\sigma^2_{Y_r} + \sigma^2_e} \qquad (2.9)$$

Conversely, the correlation of pairs of chronologies (trees) *i* and *i** belonging to groups *r* and *r** is:

$$\rho(\underline{W}_i,\underline{W}_{i*}) = \frac{\mathrm{cov}(\underline{W}_i,\underline{W}_{i*})}{\sqrt{\mathrm{Var}(\underline{W}_i)\times \mathrm{Var}(\underline{W}_{i*})}} = \frac{\sigma^2_{Y_{rr*}}}{\sqrt{(\sigma^2_{Y_r}+\sigma^2_e)\times(\sigma^2_{Y_{r*}}+\sigma^2_e)}} \qquad (2.10)$$

Similar to Eq. (2.5), if the whole set of *N* chronologies (trees) is analysed together, these parameters become mean correlations over all possible pairs of chronologies ($\hat{a}_C$) or trees ($\hat{a}_S$) at the intragroup or intergroup level, respectively. Alternative mean correlation expressions for models M_1, M_2 or M_4 can be obtained by applying their corresponding variance–covariance structures to Eq. (2.5). Note that the mean correlation estimates for M_5 (broad evaluation model) correspond to that defined by Eq. (2.5). The EPS, which quantifies how well a chronology based on a finite number of trees represents the hypothetical perfect or true chronology, can be generalized from these estimates at either the temporal or spatial level following Wigley *et al.* (1984):

$$EPS \approx \frac{N\hat{a}}{1+(N-1)\hat{a}} \qquad (2.11)$$

where *N* is the number of chronologies (trees) and $\hat{a}$ is the mean correlation at the temporal ($\hat{a}_C$) or spatial ($\hat{a}_S$) level.

All analyses were performed with the MIXED procedure of SAS/STAT (ver. 9.3, SAS, Inc., Cary, NC, USA) using restricted maximum likelihood (REML) for estimation of variance components. The covariance structure for groups was specified using the RANDOM statement and the autoregressive structure was fitted using the REPEATED statement. Heterogeneity of residual variances across groups was implemented with the GROUP option of the REPEATED statement.

Results

Sources of variability in stable isotopes

$\Delta^{13}C$ in *Q. ilex* varied among sites from 16.2 to 18.2‰ (Table 2.1). For the deciduous oaks co-occurring with *Q. ilex*, $\Delta^{13}C$ ranged from 15.9 to 17.8‰ in *Q. faginea*, from 16.0 to 17.5‰ in *Q. humilis*, and from 16.8 to 17.5‰ in *Q. petraea* (Table 2.1). $\delta^{18}O$ in *Q. ilex* varied among sites from 31.1 to 32.8‰ (Table 2.1). For the deciduous oaks, $\delta^{18}O$ ranged from 31.8 to 33.6‰ in *Q. faginea*, from 31.4 to 33.5‰ in *Q. humilis*, and from 31.5 to 32.9‰ in *Q. petraea* (Table 2.1). For *Q. humilis* and *Q. petraea*, the range of variability in both isotopes increased considerably after the Banyoles sites (used only for analysis at the temporal level) were included in the dataset (sites 22, 23 and 24, Table 2.1; Fig. 2.2). The mean $\Delta^{13}C$ site values for deciduous and evergreen oak combinations were 17.0 and 17.1‰ for *Q. ilex* and *Q. faginea*, 17.4 and 16.9‰ for *Q. ilex* and *Q. humilis*, and 17.3 and 17.3‰ for *Q. ilex* and *Q. petraea*, respectively. The mean $\delta^{18}O$ values were 31.9 and 32.8‰ for *Q. ilex* and *Q. faginea*, 31.8 and

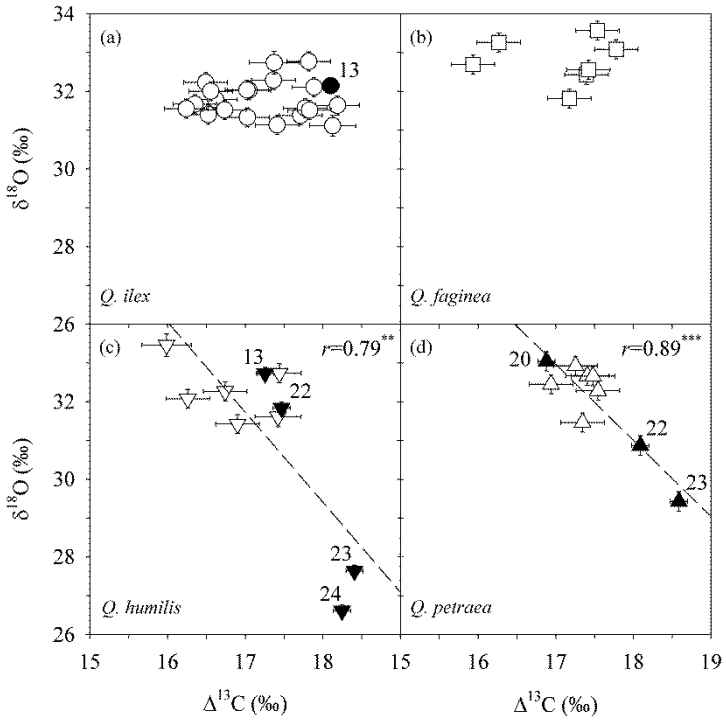

Figure 2.2. Relationships between carbon isotope discrimination ($\Delta^{13}C$) and oxygen isotope composition ($\delta^{18}O$) at the site level for **(a)** *Q. ilex*, **(b)** *Q. faginea*, **(c)** *Q. humilis* and **(d)** *Q. petraea*. Error bars indicate standard errors. Filled symbols identify sites with annually resolved chronologies for the analysis of temporal trends in both isotopes. Site numbering is according to Table 2.1.

32.3‰ for *Q. ilex* and *Q. humilis*, and 31.8 and 32.4‰ for *Q. ilex* and *Q. petraea*, respectively. Differences between species were significant for $\Delta^{13}C$ (but only for the *Q. ilex*–*Q. humilis* combination) and for $\delta^{18}O$ (for all combinations).

Relationships between $\Delta^{13}C$ and $\delta^{18}O$ were not significant regardless of the species only if sites where evergreen and deciduous oaks co-occurred were considered. However, they became significant (negative) for *Q. humilis* and *Q. petraea* after including Banyoles (sites 22, 23 and 24; Fig. 2.2). For chronologies, the association between both isotopes was usually significant (negative), except for *Q. humilis* in Banyoles (a low-altitude site) and for *Q. ilex* in Sant Celoni (results not shown).

Model selection at the temporal level (grouping of chronologies)

The $\Delta^{13}C$ and $\delta^{18}O$ residuals that appeared after linear detrending of chronologies or, otherwise, simply differencing from the mean are displayed in Fig. 2.3. The common signal of the eight chronologies seemed much larger for $\Delta^{13}C$ than for $\delta^{18}O$. This visual assessment was checked against mixed modelling results by using the above-mentioned grouping strategies: taxonomy- and site-based. Table 2.3 shows the log-likelihood statistics for various VCOV structures. The AIC and BIC criteria applied to $\Delta^{13}C$ pointed to the inadequacy of complex VCOV models to describe properly a taxonomy-based grouping of chronologies (with groups *Q. humilis* and *Q. petraea*). In fact, the null model M_5, which simply ignores the presence of groups, obtained better support (i.e., smaller AIC and BIC values), suggesting

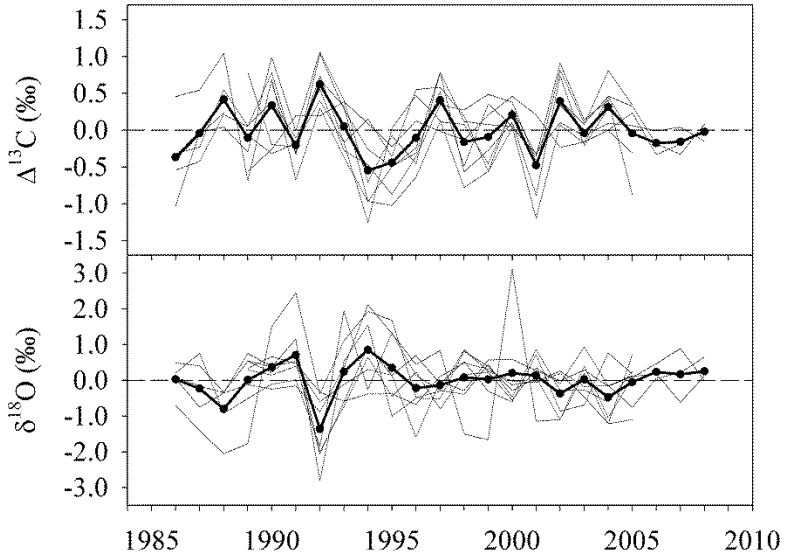

Figure 2.3. Isotope values indexed (residuals) by linear detrending or by subtracting from the mean of each chronology (above: $\Delta^{13}C$; below: $\delta^{18}O$). Eight chronologies were available: four for *Q. humilis*, three for *Q. petraea* and one for *Q. ilex*. The black line represents the mean chronology.

that common temporal patterns in $\Delta^{13}C$ were independent of taxonomic affiliation of deciduous oaks. Conversely, the M_1 (compound symmetry) model with heteroscedastic error variances was clearly favoured for $\delta^{18}O$. In this case, the $\delta^{18}O$ signal across years was species dependent, since the magnitude of residual variation (random deviations $f_{ij(r)}$ in Eq. [2.7]) was distinct for each species. A correction for serial autocorrelation was unnecessary for both isotopes.

The alternative, site-based classification of chronologies yielded different results for $\Delta^{13}C$ (Table 2.3). Here, the M_2 (heterogeneous compound symmetry) model provided the best fit, together with the heteroscedastic M_2 model. We favoured parsimony in the number of VCOV parameters; thus, M_2 was the model of choice. For $\delta^{18}O$, the M_1 heteroscedastic model was again the selected model, being slightly favoured over the M_2 heteroscedastic model (Table 2.3). The preferred models for both isotopes benefited in this case from site-specific serial autocorrelation corrections, as suggested by decreases in AIC and BIC (results not shown).

Model selection at the spatial level (grouping of trees)

Oaks were grouped into two groups at the site level (deciduous and evergreen). This classification was extended to the total available number of sites (21). As three deciduous species were available, we checked for possible differences in their mean isotopic values (consisting of 20-year pooled tree rings) that could eventually inflate the common signal of

Table 2.3. Model comparison for oak chronologies according to AIC and BIC. The model of choice for each grouping and isotope is shown in bold.

Model	$\Delta^{13}C$			$\delta^{18}O$		
	Parameters	AIC *(smaller is better)*	BIC	Parameters	AIC *(smaller is better)*	BIC
Species grouping						
M_1	3	164.8	168.2	3	362.1	365.5
M_1 (heteroscedastic)	4	166.7	171.3	**4**	**342.9**	**346.3**
M_3	4	164.0	168.6	4	358.2	362.8
M_3 (heteroscedastic)	5	166.0	171.7	5	346.1	351.8
M_4	3	177.6	181.0	3	361.7	365.1
M_4 (heteroscedastic)	4	179.6	184.1	4	349.6	354.2
M_5	**2**	**162.9**	**165.2**	2	360.6	362.8
Site grouping						
M_1	3	138.5	141.9	3	306.9	309.2
M_1 (heteroscedastic)	5	136.1	141.8	**5**	**285.9**	**291.6**
M_2	**5**	**119.5**	**124.0**	5	307.3	312.9
M_2 (heteroscedastic)	7	118.7	125.5	7	286.8	293.6
M_3	7	122.9	129.7	7	305.6	312.4
M_3 (heteroscedastic)	9	123.5	133.7	9	288.9	299.1
M_4	4	135.5	138.9	4	306.0	309.4
M_4 (heteroscedastic)	6	136.0	142.8	6	289.3	296.1
M_5	2	138.2	140.4	2	306.9	309.2

trees for this group along the aridity transect. There were no significant differences between species for $\Delta^{13}C$ or $\delta^{18}O$, hence avoiding a correction for shifts in mean isotopic values. Table 2.4 shows the log-likelihood statistics for VCOV models. The AIC and BIC criteria applied to $\Delta^{13}C$ pointed to M_1 (compound symmetry) as the best explanatory model for differences in signal strength between groups. Although other models seemed also satisfactory (particularly the heteroscedastic M_1), we favoured parsimony in the number of VCOV parameters. In turn, M_4 (banded main diagonal) was the selected model for $\delta^{18}O$, being slightly favoured over M_3 (unstructured; Table 2.4). This model suggested a lack of relationship (i.e., lack of covariance) between $\delta^{18}O$ signals stored in deciduous and evergreen oaks.

Outcome of mixed models

Restricted maximum likelihood estimates of variance/covariance components under the the selected models are given in Table 2.5. The analysis of temporal signals indicated that

Table 2.4. Model comparison for spatial records based on taxonomic grouping according to AIC and BIC. The model of choice for each grouping and isotope is shown in bold.

Model	$\Delta^{13}C$			$\delta^{18}O$		
	Parameters	AIC *(smaller is better)*	BIC *(smaller is better)*	Parameters	AIC *(smaller is better)*	BIC *(smaller is better)*
M_1	**3**	**521.6**	**524.8**	3	423.2	425.4
M_1 (heterocedastic)	4	520.7	524.9	4	422.9	427.0
M_3	4	523.1	527.2	4	420.9	425.0
M_3 (heterocedastic)	5	522.5	527.8	5	422.6	427.8
M_4	3	522.6	525.8	**3**	**420.7**	**423.9**
M_4 (heterocedastic)	4	522.1	526.3	4	422.5	426.7
M_5	2	524.9	526.9	2	454.4	456.5

taxonomy-based grouping was inadequate for identifying contrasting changes in $\Delta^{13}C$ of *Q. humilis* and *Q. petraea* over years. Thus, year and residual variances common to all chronologies were estimated (null model M_5). These estimates produced a mean interchronology correlation ($\hat{a}_C$) of 0.44 and an EPS of 0.85. In the case of $\delta^{18}O$, the compound symmetry (M_1) model with heteroscedastic residuals gave a threefold higher residual variance for *Q. petraea* than for *Q. humilis*. Accordingly, *Q. humilis* had substantially higher $\hat{a}_C$ and EPS values than *Q. petraea*, although these values were lower than those for $\Delta^{13}C$. The intergroup mean correlation, $\hat{a}_C$, was higher than the intragroup estimate for *Q. petraea*, which pointed to a weak signal shared by the chronologies of this species.

A site-based grouping of chronologies identified the M_2 (heterogeneous compound symmetry) model, with different variances for each group, as the model of choice for $\Delta^{13}C$. The largest common variance corresponded to the group of chronologies originating from the low-altitude Banyoles site; hence, it provided the highest $\hat{a}_C$ and EPS values (Table 2.5). Also, the medium-altitude Banyoles site had relatively high $\hat{a}_C$ and EPS values. Chronologies of these sites corresponded to deciduous *Q. humilis* and *Q. petraea* and, in fact, the combined $\hat{a}_C$ of both sites was also very high (0.60), indicating a strong coherence associated with geographical proximity. On the other hand, the synchronicity between chronologies in Sant Celoni II was very weak, in clear disagreement with the Banyoles results. In Sant Celoni II, evergreen (*Q. ilex*) and deciduous (*Q. humilis*) oaks were represented, and genetic differences producing contrasting $\Delta^{13}C$ values could be involved. For $\delta^{18}O$, the compound symmetry (M_1) model with heteroscedastic residuals provided very contrasting residual variances (low for Sant Celoni II, high for Banyoles sites). They translated into very different $\hat{a}_C$ and EPS values, with a relatively high synchronicity between chronologies of Sant Celoni II, an opposite trend to that observed for $\Delta^{13}C$. Overall, signal-strength parameters ($\hat{a}_C$ and EPS) were higher for $\Delta^{13}C$ than for $\delta^{18}O$, regardless of the grouping structure used for estimating VCOV parameters.

Table 2.5. Outcome of mixed-model analyses, including variance/covariance parameters, first-order autocorrelation AC(1) (for annually resolved chronologies) and related statistics: mean interseries correlation ($\hat{a}_C$) or spatial signal strength ($\hat{a}_S$), number of series (Nr) and EPS.

Chronologies	$\Delta^{13}C$						$\delta^{18}O$					
	Variance / covariance	Residual variance	AC(1)	$\hat{a}_C$ / $\hat{a}_S$	Nr[1]	EPS	Variance / covariance	Residual variance	AC(1)	$\hat{a}_C$ / $\hat{a}_S$	Nr[1]	EPS
Species grouping												
Quercus humilis	0.107	0.136	—	0.439	7 (7)	0.85	0.150	0.323	—	0.317	4 (12)	0.65
Quercus petraea							0.150	1.063	—	0.124	3 (>20)	0.30
Q. humilis / *Q. petraea*							0.150			0.198		
Site grouping												
Banyoles, medium altitude (BM)	0.133	0.105	0.308	0.559	2 (5)	0.72	0.092	0.923	–0.211	0.091	2 (>20)	0.17
Banyoles, low altitude (BL)	0.190	0.105	0.308	0.644	2 (4)	0.78	0.092	0.810	0.161	0.102	2 (>20)	0.19
Sant Celoni II (SC)	0.002	0.105	0.308	0.018	2 (>20)	0.04	0.092	0.138	0.213	0.401	2 (9)	0.57
BM / BL	0.159			0.600			0.048			0.050		
BM / SC	0.016			0.100			0.048			0.100		
BL / SC	0.019			0.108			0.048			0.106		
Spatial records												
Quercus spp. (deciduous)	0.215	0.595	—	0.266	5 (16)	0.64	0.191	0.307	—	0.384	5 (9)	0.76
Quercus ilex	0.215	0.595	—	0.266	5 (16)	0.64	0.494	0.307	—	0.617	5 (5)	0.89
Quercus spp. / *Quercus ilex*	0.091			0.112			0			0		

[1]Number of series required to reach EPS ≥ 0.85 is given in parentheses.

The analysis of spatial signals provided REML estimates of variance/covariance parameters, as shown in Table 2.4. For $\Delta^{13}C$, the compound symmetry M_1 model pointed to a similar signal strength of deciduous and evergreen oaks across sites. However, the site variance was low compared with the residual variance and, therefore, $\hat{a}_S$ values were <0.3. According to dendrochronology standards, about 16 trees per site would be necessary to achieve an EPS of good quality (i.e., ≥0.85), although this parameter should be interpreted flexibly in the context of typifying spatial signals. In any case, the common signal strength between deciduous and evergreen oaks was much weaker ($\hat{a}_S$ = 0.112). For $\delta^{18}O$, the narrow evaluation (M_4) model pointed to the lack of a common spatial signal between deciduous and evergreen oaks. Evergreen and deciduous oaks therefore bore totally unrelated information. However, the spatial signal ($\hat{a}_S$) in $\delta^{18}O$ for a given species was higher than that for $\Delta^{13}C$ (particularly for *Q. ilex*), which provided EPS values close to or higher than 0.85.

Relationships with climate

The outcome of the selected VCOV structures provided a guideline for investigating the influence of climate factors on isotope ratios. For $\Delta^{13}C$, the deciduous oak chronologies shared a strong signal that was unrelated to that of *Q. ilex*. Accordingly, the relationships of stable isotopes with climate were assessed separately for these two groups, which showed distinct monthly sensitivities to climate (Fig. 2.4). In particular, maximum temperatures in July were significantly related (negatively) to $\Delta^{13}C$ in deciduous oaks, while a significant negative relationship between $\Delta^{13}C$ and minimum temperatures of November of the previous year was detected for *Q. ilex*. There were also positive relationships between $\Delta^{13}C$ and either June precipitation (for deciduous oaks) or September precipitation (for *Q. ilex*), and negative relationships between $\Delta^{13}C$ and precipitation of both November of the previous year and August (for *Q. ilex*).

For $\delta^{18}O$, the signal shared by *Q. petraea* chronologies was negligible, while Sant Celoni chronologies (*Q. ilex* and *Q. humilis*) on one hand, and *Q. humilis* chronologies from Banyoles sites on the other hand, had relatively high common signals. Based on these results, relationships with climate were assessed separately for the latter two groups only (Fig. 2.4). For Sant Celoni, $\delta^{18}O$ was related (positively) to September temperatures, whereas there was a strong negative relationship between $\delta^{18}O$ and June precipitation for Banyoles.

At the spatial level, mixed modelling reported contrasting patterns of geographical variation for both $\Delta^{13}C$ and $\delta^{18}O$ between evergreen (*Q. ilex*) and deciduous oaks along the aridity transect. Therefore, relationships with temperature and precipitation were obtained independently for each taxonomic group (Fig. 2.5). For $\Delta^{13}C$, *Q. ilex* showed a strong spatial temperature signal, since temperature–$\Delta^{13}C$ associations were positive and mostly significant throughout the year (with the exception of maximum temperature during spring and summer). Also, *Q. ilex* showed positive relationships between $\Delta^{13}C$ and both March and September–October precipitation. Conversely, deciduous oaks were spatially sensitive only

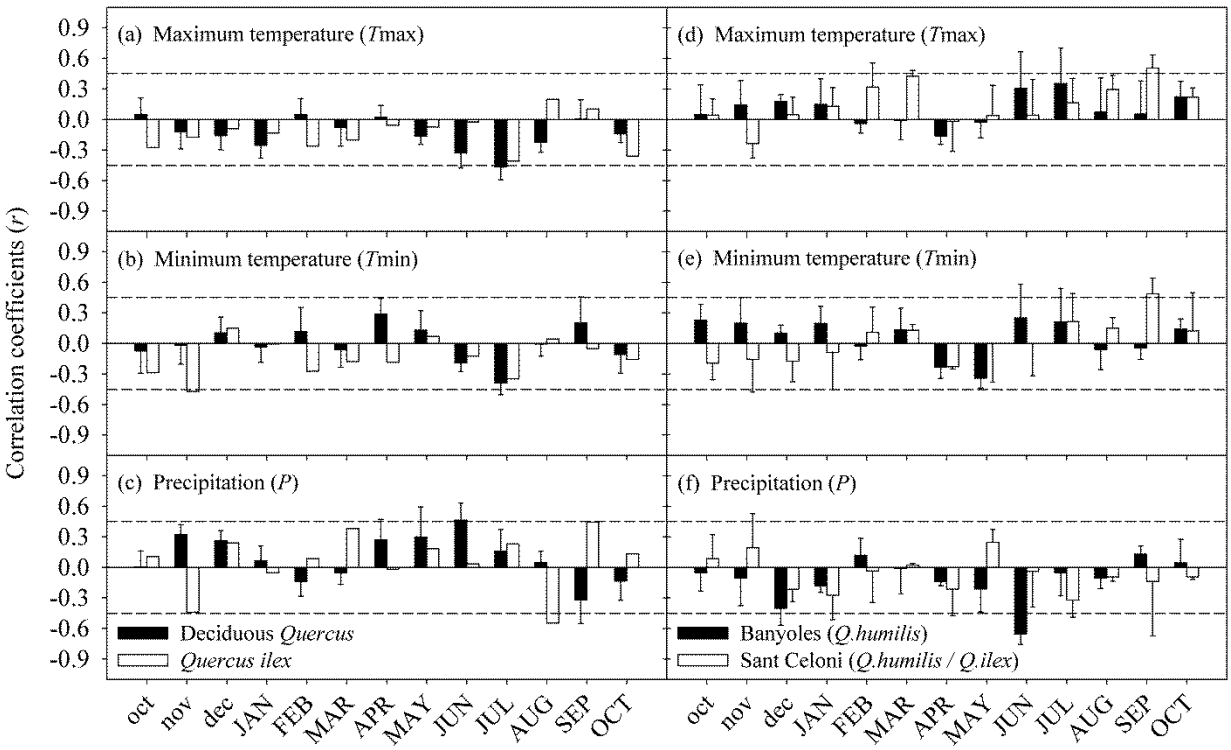

Figure 2.4. Mean (±SD) correlation coefficients calculated between carbon ($\Delta^{13}C$) **(a–c)** and oxygen ($\delta^{18}O$) stable isotope chronologies **(d–f)** and monthly climate variables (maximum and minimum temperature, precipitation). The horizontal lines indicate the threshold for correlations significant at $P \leq 0.05$ ($n = 20$ years). Lower case indicates months of the year prior to tree growth; upper case indicates current-year months. For $\Delta^{13}C$, the number of chronologies involved in the correlation analysis was seven (for deciduous oaks) and one (for *Q. ilex*). For $\delta^{18}O$, the number of chronologies involved in the analysis was three (for *Q. humilis* at Banyoles sites) and two (for *Q. humilis* and *Q. ilex* at the Sant Celoni II site).

to precipitation, with positive relationships with $\Delta^{13}C$ in spring (April–May). For $\delta^{18}O$, *Q. ilex* also showed a strong spatial signal of temperature (especially with maximum temperature), with positive relationships for most of the year (except for winter). Conversely, the deciduous oaks showed a positive (significant) relationship with maximum temperature only for July. *Q. ilex* also displayed a negative spatial relationship between $\delta^{18}O$ and May precipitation, whereas the deciduous oaks were overall more sensitive to precipitation, with negative relationships with $\delta^{18}O$ in autumn, winter and early spring.

Discussion

Mixed models unravel the complexities of tree-ring signals in stable isotopes

The interpretation of complex temporal patterns in tree-ring records has traditionally

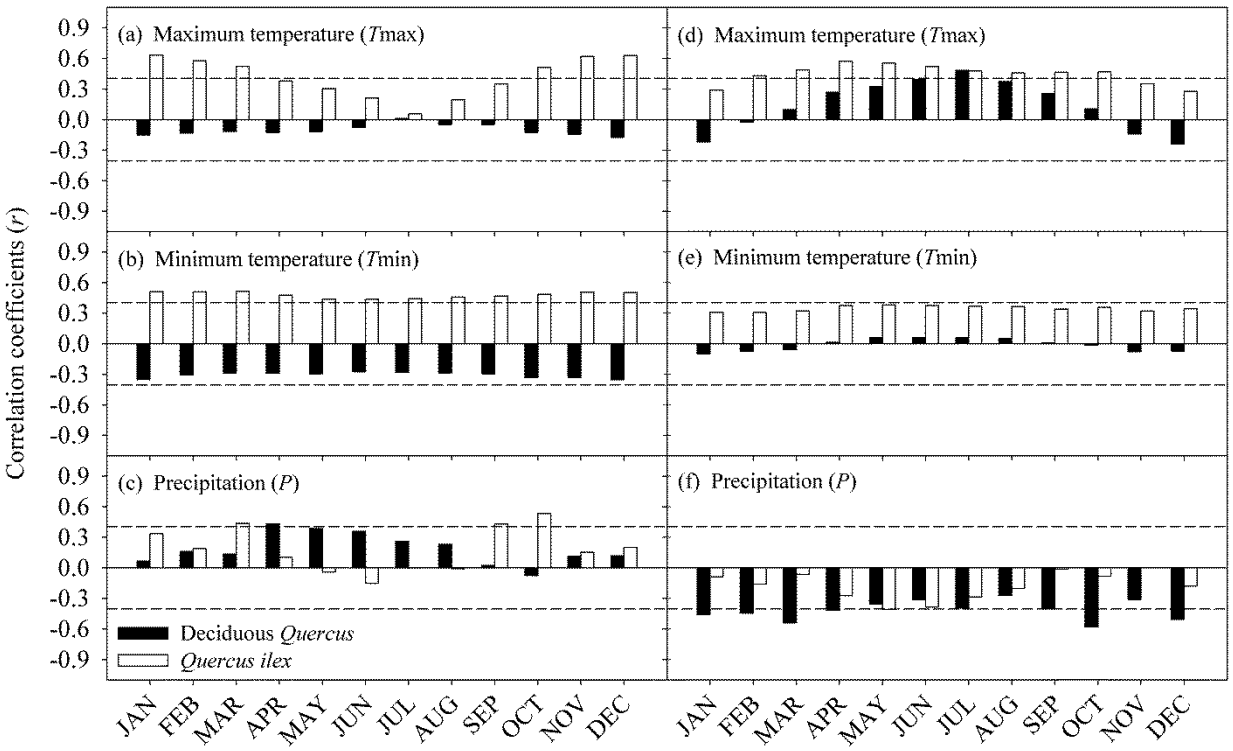

Figure 2.5. Correlation coefficients calculated between carbon ($\Delta^{13}C$) **(a–c)** and oxygen ($\delta^{18}O$) spatial records **(d–f)** and monthly meteorological parameters (maximum and minimum temperature, precipitation). The horizontal lines indicate the threshold for correlations significant at $P \leq 0.05$ (n = 21 sites for both deciduous *Quercus* and *Q. ilex*).

relied on the application of the 'mean correlation technique' (Wigley *et al.* 1984; Briffa & Jones 1990), which uses the mean correlation calculated between all possible pairs of chronologies drawn from a group to quantify their common signal. In turn, between-group signals can be obtained by calculating the mean correlation derived from all possible between-group pairs of chronologies. Examples involving dendro-isotope data can be found in McCarroll & Pawellek (1998), Saurer *et al.* (2008) and Esper *et al.* (2010a).

Overall, this scheme is roughly equivalent to our unstructured mixed model (M3) for the variability among years, but other less complex settings may describe the relationships between chronologies more plausibly. In fact, in mixed modelling the model of choice depends on the particular structure and statistical properties of the dataset. This approach of analysing coherence in tree-ring networks can be regarded as complementary to multivariate methods such as principal component or cluster analysis, which allow for the identification of homogeneous subsets of chronologies (Treydte *et al.* 2007) but without testing on possible processes underlying patterns of signal strength. Conversely, the REML analysis, grounded on the mixed-model theory, allows estimating common signals in tree-ring records by testing for different group and error covariance structures required for characterizing the

correlations in the dataset. Another major advantage over multivariate techniques is that mixed modelling is capable of dealing with unbalanced datasets (e.g., partially overlapping chronologies) in a straightforward manner.

Mixed modelling of temporal tree-ring patterns pointed to the suitability of the simple compound symmetry structure (M_1) for explaining variability in $\delta^{18}O$, but only after allowing for heterogeneity of residual variances, either at the species or site level. Conversely, alternative models fitted $\Delta^{13}C$ chronologies better: a heterogeneous compound symmetry structure (M_2) for site-based grouping and the simplest broad evaluation structure (M_5) identified for taxonomy-based grouping. Such an array of selected models highlights the need to understand the complexities in the data in testing and characterizing the nature of common signals shared by a set of chronologies.

The flexibility of mixed models proved equally useful for the investigation of spatial signals stored in tree-ring isotopes. Traditionally, these signals have been considered to be essentially independent among species (Ferrio *et al.* 2003; Leavitt *et al.* 2010). Here, the model for independence of $\delta^{18}O$ signals between evergreen and deciduous oaks (M_4) was slightly favoured over alternative variance–covariance structures. This was not the case for $\Delta^{13}C$ records, which showed a common (albeit low) spatial signal shared by both groups, as suggested by the preferred compound symmetry (M_1) model. This contrasting choice of models was somewhat anticipated by the lack of spatial associations observed between $\Delta^{13}C$ and $\delta^{18}O$ at the species level (if the more humid Banyoles sites, where *Q. ilex* was absent, were excluded from the correlation analysis; *cf.* Fig. 2.2), suggesting that the physiological drivers of carbon and oxygen isotopes did not coincide along the aridity transect.

Structure and strength of spatiotemporal isotope signals in Mediterranean oaks

The high temporal $\Delta^{13}C$ signal strength for deciduous oaks (the nemoro-Mediterranean *Q. humilis* and the nemoral *Q. petraea*) was the consequence of a strong interannual coherence between chronologies, irrespective of taxonomy or site. In other words, the correlation between chronologies of co-occurring deciduous oaks was similar to the intersite correlation for chronologies of the same or different species. Thus, the combination of chronologies across sites gave EPS values of acceptable statistical quality (0.85; $n = 7$). Similar results have been reported at temperate (Hemming *et al.* 1998; Saurer *et al.* 2008) and high-latitude sites (McCarroll & Pawellek 1998) by combining chronologies from different sets of species. Conversely, the only available Q. ilex chronology was unrelated to any other chronology, either from the same site or from other sites. This realization points out that Mediterranean deciduous and evergreen oaks constitute two clearly differentiated functional groups, despite co-existing along a wide range of environments (Damesin *et al.* 1998; Mediavilla & Escudero 2010).

On the contrary, the annually resolved $\delta^{18}O$ chronologies showed much less similarity to each other compared with that for $\Delta^{13}C$, despite the presence of significant (negative)

interannual correlations between both isotopes. Nevertheless, both taxonomic (for *Q. humilis*) and site imprints (for Sant Celoni II; the most xeric site with available chronologies) were detected for $\delta^{18}O$, although EPS values were always lower than for $\Delta^{13}C$. Saurer *et al.* (2008) also reported more robust signals for $\Delta^{13}C$ than for $\delta^{18}O$ across temperate sites from Switzerland. Carbon and oxygen stable isotopes are partially linked through effects at the leaf level that are mediated through variation in stomatal conductance related to moisture conditions (precipitation and relative humidity; Scheidegger *et al.* 2000). However, different sources and fractionation processes may override, to varying degrees, the presence of co-ordinated isotopic signals (Saurer *et al.* 2003; Roden & Farquhar 2012). Altogether, these results point to the existence of more complex drivers of temporal $\delta^{18}O$ signals in Mediterranean oaks compared with $\Delta^{13}C$.

In clear contrast to the aforementioned temporal patterns, the examination of spatial signals through mixed modelling indicated a stronger coherence at the species level (i.e., higher $\hat{a}_S$ and EPS statistics) in $\delta^{18}O$ variation between trees across sites compared with $\Delta^{13}C$. This suggests that temporal and spatial variability in external factors (e.g., climate forcing) have a different impact on tree-ring $\Delta^{13}C$ (with higher temporal coherence) and $\delta^{18}O$ (with higher spatial coherence) in either deciduous or evergreen Mediterranean oaks.

In water-limited environments, $\Delta^{13}C$ in tree rings can be mostly explained by the stomatal regulation of CO_2 fluxes into the leaf, integrating any environmental variable related to stomatal conductance (Warren *et al.* 2001; Ferrio *et al.* 2003; Gessler *et al.* 2009). However, it is also affected by changes in photosynthetic activity derived from irradiance, nutritional stresses or phenology when water becomes non-limiting (Yakir & Israeli 1995; Livingston *et al.* 1998; Ferrio *et al.* 2003). On the other hand, the signal of $\delta^{18}O$ in tree rings is primarily defined by leaf-level processes, being responsive to stomatal conductance, but not to photosynthetic activity (Farquhar & Lloyd 1993; Yakir & Israeli 1995). Since $\delta^{18}O$ is not sensitive to photosynthetic activity, it has the potential to discriminate between both sources of variation in $\Delta^{13}C$ (Yakir & Israeli 1995; Scheidegger *et al.* 2000).

However, this dual-isotope model, which has proved to be useful for interpreting tree-ring records, is not always applicable. On one hand, the leaf-level signal of $\delta^{18}O$ responds to variations in relative humidity in a way that is partly independent of stomatal conductance (Roden & Farquhar 2012). On the other hand, the $\delta^{18}O$ of tree-ring cellulose also reflects variability in source water, to a degree that could be variable during the growing season (Offermann *et al.* 2011; Sarris *et al.* 2013). The presence of a source-water signature in the $\delta^{18}O$ of wood could explain the strong site-specific signal found in this study (Radoglou 1996; David *et al.* 2007; Mediavilla & Escudero 2010), but this geographical imprint can be modulated by interspecific differences in water uptake (see, e.g., Moreno-Gutiérrez *et al.* 2012), as also suggested by the contrasting $\delta^{18}O$ patterns observed between deciduous and evergreen oaks.

Below-ground niche segregation, as a means of reducing competition for water resources, might facilitate the co-existence of evergreen and deciduous oaks, as has been described in other Mediterranean mixed stands (see, e.g., David *et al.* 2007; Klein *et al.* 2013), but this possibility needs further examination. Yet, it is somewhat surprising that the relatively low range of intraspecific variation found in $\delta^{18}O$ across sites (<2‰) led to a more consistent spatial signal (i.e., higher $\hat{a}_S$) for both evergreen and deciduous oaks than that associated with $\Delta^{13}C$. In fact, $\Delta^{13}C$ showed a high intraspecific variation across sites, representing a near 20% divergence among extreme sites in intrinsic water-use efficiency (Farquhar & Richards 1984).

Such a relatively low spatial coherence of tree-ring $\Delta^{13}C$ records at the species level does not seem to preclude the use of spatially explicit models of carbon isotope distribution to infer climatic trends (e.g., Leavitt *et al.* 2007), provided the assumption of a common climatic signal based on customary thresholds (i.e., SNR, EPS) is relaxed. These models have also involved Mediterranean oaks such as the evergreen *Q. ilex* (Aguilera *et al.* 2009; del Castillo *et al.* 2013). Overall, spatiotemporal changes in both isotopes seemed strongly dependent on the particular functional imprints of evergreen and deciduous oaks. This is not as clearly observed in temperate regions, where the coherence of spatiotemporal signals seems fairly species independent (e.g., Hemming *et al.* 1998; Saurer *et al.* 2012). Altogether, the outcome of the selected VCOV structures suggested investigating the influence of climate factors on stable isotope ratios separately for evergreen and deciduous oaks.

Climate drivers of temporal variation in stable isotopes

The EPS statistic of $\Delta^{13}C$ of deciduous oaks was in the range of previously reported individual chronologies made up of four to six trees (e.g., 0.80–0.90, Gagen *et al.* 2004; 0.90; Kirdyanov *et al.* 2008). This result is noteworthy since it was obtained by combining chronologies of limited length (20 years) from different sites and oak species (*Q. humilis* and *Q. petraea*). It suggests a strong climate signal driving changes in $\Delta^{13}C$. In particular, $\Delta^{13}C$ was positively related to precipitation of early summer (June). It is known that the phenological activity of Mediterranean deciduous oaks during summer is almost ceased compared with that of the evergreen *Q. ilex* (Montserrat-Martí *et al.* 2009). Thus, a rainy late spring–early summer may entail optimal conditions for secondary growth imprinting on tree-ring $\Delta^{13}C$.

Conversely, high temperatures in July are likely to reduce stomatal conductance, leading to a decrease in $\Delta^{13}C$ and increased water-use efficiency. These relationships with climate elements determining water availability agree with the effect of water status on $\Delta^{13}C$ reported for other species in drought-prone environments (Damesin *et al.* 1997; Warren *et al.* 2001; Ferrio *et al.* 2003; Battipaglia *et al.* 2010). Also, these associations with both precipitation and temperature are in line with the negative correlation between $\delta^{18}O$ and precipitation observed in June, in agreement with earlier works reporting similar relationships for deciduous oaks (Raffalli-Delerce *et al.* 2004; Loader *et al.* 2008).

In the present study, the low relative humidity of summer (typical of the Mediterranean climate), linked to low precipitation and high temperatures, would cause an increase in leaf water enrichment, which is not only reflected in $\delta^{18}O$, but also in $\Delta^{13}C$ (Roden *et al.* 2000; McCarroll & Loader 2004). Altogether, our results confirm the existence of shared temporal responses to climate in two deciduous oaks, *Q. humilis* and *Q. petraea*, which can be found under relatively humid sub-Mediterranean conditions.

On the other hand, climate variables imprinting on $\Delta^{13}C$ for *Q. ilex* were basically unrelated to those for deciduous oaks, with the exception of July temperatures. March precipitation and September precipitation, especially, were associated with high $\Delta^{13}C$. This result indicates a temporal agreement of $\Delta^{13}C$ signals with the bimodal pattern of secondary growth in *Q. ilex* (Gutiérrez *et al.* 2011) and the two peaks of precipitation (early spring and early summer) in the western Mediterranean, which supports the dependence of *Q. ilex*, a deep-rooted species with very effective water uptake, on the seasonal recharge of groundwater reservoirs (Ferrio *et al.* 2003; Aguilera *et al.* 2009; Klein *et al.* 2013). In this regard, the imprint of March and September temperatures on $\delta^{18}O$ through leaf water enrichment processes also highlights such a pattern of wood deposition in this species.

The negative association between $\Delta^{13}C$ and August precipitation could be explained by the early restitution of secondary growth in wet but still warm late summers (Gutiérrez *et al.* 2011), which could imprint wood with low $\Delta^{13}C$ values. Finally, negative associations with precipitation and minimum temperature of November of the previous year might suggest mobilization of carbohydrate reserves synthesized in autumns with very favourable (warm and wet) conditions for tree functioning, one of the most active periods for evergreen oaks (Mediavilla & Escudero 2010; Klein *et al.* 2013). Indeed, low $\Delta^{13}C$ of current-year wood has been associated with mobilization of previous-year starch reserves (Kozlowski *et al.* 1991), which are relatively more ^{13}C-enriched than freshly produced assimilates for wood production (Helle & Schleser 2004).

Climate drivers of spatial variation in stable isotopes

The evergreen *Q. ilex* showed a strong spatial dependence on temperature for both isotopes that was linked to the double climate stress typical of Mediterranean environments (summer drought and winter cold). Limitations exerted by low temperatures on the effective vegetative period at cold (i.e., continental) sites are reflected in low $\Delta^{13}C$ values, since trees are obliged to concentrate their photosynthetic activity in warmer and more drought-prone months. Besides, high temperatures associated with high evaporative demand and water stress, especially in spring–summer, are reflected in high $\delta^{18}O$ records. Such a temperature imprint on carbon and oxygen stable isotopes is more clearly observed in the spatial signal recorded along the aridity transect than in the annually resolved chronologies, probably because the latter originate from coastal, mild sites lacking a strong influence of winter cold.

On the other hand, spatial associations with precipitation (basically for $\Delta^{13}C$) were restricted to months of groundwater recharge (autumn and late winter), which again is consistent with the assumption that *Q. ilex* relies mostly on groundwater to thrive in drought-prone environments (Ferrio *et al.* 2003; Aguilera *et al.* 2009; Klein *et al.* 2013). In addition to using groundwater during summer, the strong response to autumn–winter precipitation could be due to the fact that *Q. ilex* can be particularly active during this period, taking advantage of increased water availability, as long as temperatures are still warm (Radoglou 1996; Mediavilla & Escudero 2010; Klein *et al.* 2013).

Climate drivers of variability in stable isotopes for deciduous oaks were different: they showed more consistent responses to precipitation, not only across the aridity transect, but also at the temporal (interannual) scale (see above). For $\Delta^{13}C$, there was a lagged response to early-season precipitation in deciduous oaks compared with *Q. ilex*, hence reflecting phenological differences in the onset of cambium activity (Liphschitz & Lev-Yadun 1986). For $\delta^{18}O$, a strong negative effect of the amount of soil recharge (autumn and winter) was observed along the transect. This might be associated with partly different strategies of water uptake between deciduous and evergreen oaks, pointing to a stronger reliance on groundwater in deciduous species, since they have fewer alternative mechanisms to cope with drought (Damesin *et al.* 1998; David *et al.* 2007). Whereas for deciduous oaks autumn conditions mainly have an indirect effect (through groundwater recharge) on the signature of wood formed in the following year, in the case of evergreen oaks the extension of radial growth over autumn–winter (Gutiérrez *et al.* 2011) also causes a (direct) response to climate drivers during this period.

Conclusions

This paper provides new information on the ecophysiological performance of Mediterranean oaks using spatiotemporal isotope signals stored in tree rings. Through mixed modelling, we unveiled large differences between deciduous and evergreen *Quercus* species in the organization of their temporal and spatial isotope signals. Climate factors impacted differentially on isotope records at both taxonomic and geographical levels, most likely through contrasting interspecific physiological adaptations and phenotypic plasticity linked to phenology and wood growth (Cherubini *et al.* 2003; De Micco *et al.* 2008; Montserrat-Martí *et al.* 2009

On one hand, the evergreen *Q. ilex* exhibited a clear spatial dependence of isotopic signals on the temperature regime, likely related to the effective length of its vegetative period in autumn–winter and the incidence of drought in summer. On the other hand, the water and carbon economies of deciduous oaks (*Q. faginea*, *Q. humilis* and *Q. petraea*) showed a more marked dependence on precipitation along the aridity transect, confirming their higher susceptibility to drought in the western Mediterranean. Such contrasting responses to drought among deciduous and evergreen oaks were also observed at an interannual scale,

with stronger associations with growing-season water availability in deciduous oaks than in the evergreen *Q. ilex*. The latter, in contrast, was found to rely mainly on the seasonal recharge of groundwater reservoirs. Conversely, the nemoro-Mediterranean *Q. humilis* and the nemoral *Q. petraea* deciduous oaks, co-occurring under relatively humid sub-Mediterranean conditions, shared common temporal responses to climate, showing a similar sensitivity to changes in water availability.

CHAPTER 3

Forests synchronize their growth in contrasting Eurasian regions in response to climate warming

Proceedings of the National Academy of Sciences of the United States of America **113**:662–667 (2016)
Doi: 10.1073/pnas.1514717113

Forests synchronize their growth in contrasting Eurasian regions in response to climate warming

Shestakova TA, Gutiérrez E, Kirdyanov AV, Camarero JJ, Génova M, Knorre AA, Linares JC, Resco de Dios V, Sánchez-Salguero R, Voltas J

Proc Natl Acad Sci USA **113**:662–667 (2016)

Abstract

Forests play a key role in the carbon balance of terrestrial ecosystems. One of the main uncertainties in global change predictions lies in how the spatiotemporal dynamics of forest productivity will be affected by climate warming. Here we show an increasing influence of climate on the spatial variability of tree growth during the last 120 years, ultimately leading to unprecedented temporal coherence in ring-width records over wide geographical scales (spatial synchrony). Synchrony in growth patterns across cold-constrained (central Siberia) and drought-constrained (Spain) Eurasian conifer forests have peaked in the early twenty-first century at subcontinental scales (~1,000 km). Such enhanced synchrony is similar to that observed in trees co-occurring within a stand. In boreal forests, the combined effects of recent warming and increasing intensity of climate extremes are enhancing synchrony through an earlier start of wood formation and a stronger impact of year-to-year fluctuations of growing-season temperatures on growth. In Mediterranean forests, the impact of warming on synchrony is related mainly to an advanced onset of growth and the strengthening of drought-induced growth limitations. Spatial patterns of enhanced synchrony represent early warning signals of climate change impacts on forest ecosystems at subcontinental scales.

Introduction

Understanding how climate change affects forests across multiple spatiotemporal scales is important for anticipating its impacts on terrestrial ecosystems. Increases in atmospheric CO_2 concentration and shifts in phenology (Menzel *et al.* 2006; IPCC 2013; Reyes-Fox *et al.* 2014) could favor tree growth by enhancing photosynthesis and extending the effective growing period, respectively (McMahon *et al.* 2010). Conversely, recent warming could increase respiration rates and, together with increasing heat and drought stresses, exert negative impacts on forest productivity (Silva *et al.* 2010; Williams *et al.* 2013). Given the uncertainty as to what extent enhanced carbon uptake could be offset by the detrimental effects of warming on tree performance, the actual consequences of climate change on forest carbon cycling remain under debate. Notably, climate change has a stronger impact on forests constrained by climatic stressors, such as suboptimal temperatures or water shortage (Hampe & Petit 2005). As high-resolution repositories of biological responses to the environment, dendrochronological archives can be used to monitor this impact (Fritts 2001).

The concept of spatial synchrony in tree growth refers to the extent of coincident changes in ring-width patterns among geographically disjunct tree populations (Liebhold *et al.* 2004). Climatic restrictions tend to strengthen growth–climate relationships, resulting in enhanced common ring-width signals (i.e., more synchronous tree growth). Thus, regional bioclimatic patterns can be delineated by identifying groups of trees whose growth is synchronously driven by certain climatic constraints (Wettstein *et al.* 2011; Babst *et al.* 2013). Previous synthesis studies have provided evidence for globally coherent multispecies responses to climate change in natural systems, including forests, with a focus on the role of increasingly warmer temperatures (Walther *et al.* 2002; Parmesan & Yohe 2003). Indeed, climate has changed markedly over the last decades, prompting an array of physiological reactions in trees that could strengthen growth–climate relationships, thereby enhancing spatial synchrony. Such tree responses may be linked to global shifts in the timing of plant activity (Menzel *et al.* 2006), drought stress in mid latitudes (Macias *et al.* 2006; Williams *et al.* 2013), or an uncoupling of air and soil thermal regimes in the early growing season (Vaganov *et al.* 1999) and direct heat stress (Lloyd & Bunn 2007) in high latitudes, among other factors. Changing tree growth patterns associated with enhanced synchrony in response to warming have been reported at small geographical scales (<150 km) (Tardif *et al.* 2003; Latte *et al.* 2015; but see Andreu *et al.* 2007); however, an extended examination of synchrony patterns is currently lacking for large (i.e., subcontinental) areas.

To determine whether climate warming and increased variability (IPCC 2013) lead to more synchronous tree growth, we examined changes in spatial synchrony over the last 120 years across subcontinental areas by using a comprehensive network of 93 ring-width chronologies from six different conifer species across two climatically contrasting Eurasian biomes: boreal forests in central Siberia (n = 45 chronologies) and Mediterranean forests in Spain (n = 48 chronologies) (*SI Appendix*, Fig. S1 and Table S1). Central Siberia has a severe

continental climate with a prolonged cold season, large intra-annual temperature variations, and moderate precipitation. Spain is dominated by a typical Mediterranean climate, with mild (coast) to cool (inland) wet winters and summer droughts. Thus, temperature exerts the main climatic control over productivity in boreal forests, whereas Mediterranean forests are primarily water-limited (*SI Appendix*, section 1*A*).

Temporal changes in spatial synchrony (hereinafter, $\hat{a}_C$) are quantified using a novel mixed model framework (Shestakova *et al.* 2014). This methodology has two fundamental advantages for dendroscience (Little & Rubin 2002) over other alternative approaches useful for interpreting population dynamics in ecology (Koenig & Knops 1998) or patterns of environmental synchrony (Jones *et al.* 1997): (*i*) it is capable of dealing with partially overlapping chronologies, yielding valid inferences of spatial synchrony for large areas in which ring-width data are available but covering different time periods, and (*ii*) it is highly flexible to fit general statistical structures for subdivided groups of chronologies, opening new avenues for stratification of a target region. We hypothesized that climate warming (IPCC 2013) triggers more synchronous tree growth at subcontinental scales owing to an amplified climatic control of growth, e.g., through higher temperatures in Siberia and decreased water availability in Spain. Our objective was to interpret forest reactions to warming through an alternative approach to model-based assessment or field experimentation. Specifically, this study asked the following questions: (*i*) is spatial synchrony of tree growth increasing across terrestrial biomes and if so, at what pace?; (*ii*) how are synchrony patterns related to intraspecific and interspecific responses to climate warming?; and (*iii*) what are the main climate factors underlying more synchronous forest growth? In ecological theory, it is widely accepted that spatial synchrony influences metapopulation persistence and the likelihood of species extinction (Earn *et al.* 2000). As forests are becoming more prone to widespread mortality (Allen *et al.* 2015), interpreting long-term synchrony patterns of tree growth may be relevant to identifying broad-scale threshold responses to climate change.

Materials & methods

Tree-ring indices and absolute growth trends

Site chronologies of tree-ring indices were obtained by cross-dating the tree-ring width (TRW) series (*SI Appendix*, section 1*B*) and posterior detrending and autocorrelation removal with the Friedman supersmoother spline and autoregressive modeling (Friedman 1984). This procedure eliminates the juvenile growth trend and generates stationary (mean = 1) and residual TRW chronologies of dimensionless indices that preserve a common variance encompassing interannual time scales (high frequency variability potentially related to climate). The adequacy of sample size for capturing the hypothetical population signal was assessed by the expressed population signal (*EPS*), with a threshold value of 0.85 used to

identify the "critical year" at which the site chronology became reliable (Wigley *et al.* 1984). The study period was 1890–2009, i.e., the period when the impact of climate change on tree performance became noticeable (Pretzsch *et al.* 2014). The common time spans across chronologies were 1924–1990 in central Siberia and 1950–1988 in Spain.

Temporal trends in tree growth were characterized by the estimation of growth rate changes using raw TRW records. To this end, the slope of the linear regression of TRW on time was calculated for each chronology for successive 30-year periods lagged by five years. The slopes were then averaged for a particular region (or species) and for each period, and a simple linear function was fitted after visual inspection. The slope of this function was interpreted as rate of regional (species) growth change. Comparison of growth rates between regions (species) was performed through ANOVA heterogeneity of slopes.

Mixed modelling

To investigate spatial synchrony patterns in indexed chronologies, we made extensive use of variance-covariance (VCOV) mixed modeling (Shestakova *et al.* 2014) (*SI Appendix*, section 1*C*). To this end, chronologies were grouped into potentially homogeneous subsets (Shestakova *et al.* 2014). First, two groups were formed corresponding to each region. Next, chronologies were classified at the regional level into three groups according to membership in a particular species. A number of VCOV models accommodating between-and within-group variability were tested (*SI Appendix*, section 1*C*) and compared using Akaike and Bayesian information criteria, which favor parsimonious models (Burnham & Anderson 2002). Then estimates of spatial synchrony (or mean interchronology correlation, $\hat{a}_C$) were derived for chronologies belonging to either the same region (species) or different regions (pairs of species) through the best VCOV model (*SI Appendix*, section 1*D* and Tables S2 and S3). The parameter $\hat{a}_C$ is related to the mean interseries correlation defined at the intrasite level in dendroscience (Wigley *et al.* 1984). In both cases, VCOV structures were tested for successive 30-year periods lagged by five years. The 30-year duration was established by plotting the SE of $\hat{a}_C$ against segments of varying duration (from 10 to 50 years) for each region. The segment length corresponding to the inflection point of the curves was selected as a balance between number of years and precision achieved (*SI Appendix*, Fig. S12).

Development of regional and species master chronologies

We estimated TRW indices at the regional and species levels by best linear unbiased prediction (BLUP), thus obtaining regional and species master chronologies underlying the network of site chronologies (*SI Appendix*, section 1*E*). BLUP estimates were derived from the best VCOV model fitted to the whole study period using either a regional or a species classification as grouping criterion. BLUPs were used as input for climate analysis.

Spatial patterns in synchrony

To assess how far the spatial patterns in forest synchrony extend, we calculated the geographical distance between pairs of chronologies, which were used (*i*) to obtain correlograms (Koenig & Knops 1998) testing for significant correlations between chronologies located within ranges of 300 km apart (*SI Appendix*, section 1*F*) and (*ii*) to regress correlations between pairs of chronologies on distances. The linear regressions were calculated at the species level for the periods 1890–1949 and 1950–2009, and their slopes were tested through ANOVA heterogeneity of slopes. Regression slopes were interpreted as indicators of spatial synchrony.

Relationships with climate

We quantified the effects of temperature, precipitation, and SPEI (Vicente-Serrano *et al.* 2010) on the interannual variability of TRW indices through bootstrapping correlations and response function analyses (Fritts 2001) relating regional and species master chronologies to monthly climatic data (*SI Appendix*, section 1*G*). We analyzed growth–climate relationships from the previous October to the current September, i.e., the year of tree-ring formation. In addition, we obtained correlograms for temperature and precipitation testing for significant correlations between sites located within 300 km apart (*SI Appendix*, section 1*F*) (Koenig & Knops 1998). We also performed cross-correlation analyses to test for causality of synchrony patterns in relevant climate factors as drivers of forest synchrony over progressively larger distances (*SI Appendix*, section 1*F*) (Koenig & Knops 1998).

We assessed the influence of climate change on regional synchrony through a two-step procedure. First, we performed a moving correlation analysis involving regional chronologies and monthly climate factors for successive 30-year periods lagged by five years and then related changes in temporal dependence of growth on climate (i.e., r values of the moving correlation analysis) to variations in $\hat{a}_C$ over time through simple correlations. Second, we examined a possible role of climate variability in explaining changes in synchrony. To this end, we calculated the SD for monthly climate factors of successive 30-year periods lagged by five years. We also investigated the relationships between the SD of climate variables and $\hat{a}_C$ through simple correlations. The analyses of both climate trends and variability determining synchrony was restricted to the subset of climate factors showing a significant impact on growth for the entire period 1930–2009, as a prerequisite for identifying climate drivers of $\hat{a}_C$ fluctuations. To determine the predictive ability of climate factors and their variability on the explanation of synchrony patterns, we built linear stepwise models at the regional level using the r values of the moving correlation analysis (step 1) and the SD changes over time (step 2) as independent variables, with a threshold value of $P = 0.15$ as the criterion for the inclusion or removal of variables.

Results & Discussion

Increases in synchrony and absolute growth trends: regional patterns

Synchrony trends show that $\hat{a}_C$ has increased during the period 1890–2009 in both study regions (Fig. 3.1 *A* and *B*), but at a twofold higher pace in Siberia than in Spain (b = 0.002 y^{-1} *vs.* 0.001 y^{-1}). Whereas the increasing trend is steady over time for Spain, $\hat{a}_C$ has experienced larger fluctuations for Siberia, with an abrupt rise observed in the last three decades. Overall, $\hat{a}_C$ values were significantly higher after 1950 compared with the first half of the twentieth century (P = 0.002 for Siberia and P < 0.001 for Spain, one-tailed Student's *t*-test), reaching unmatched values after the 1970s in both regions.

Notably, peaks in spatial synchrony were reached in the early twenty-first century (Fig. 3.1 *A* and *B*). This finding suggests a progressive influence of external forcing mechanisms impacting tree performance through vast geographical areas and overriding local drivers of growth (e.g., topography, nutrient availability, tree competition, management). Regional

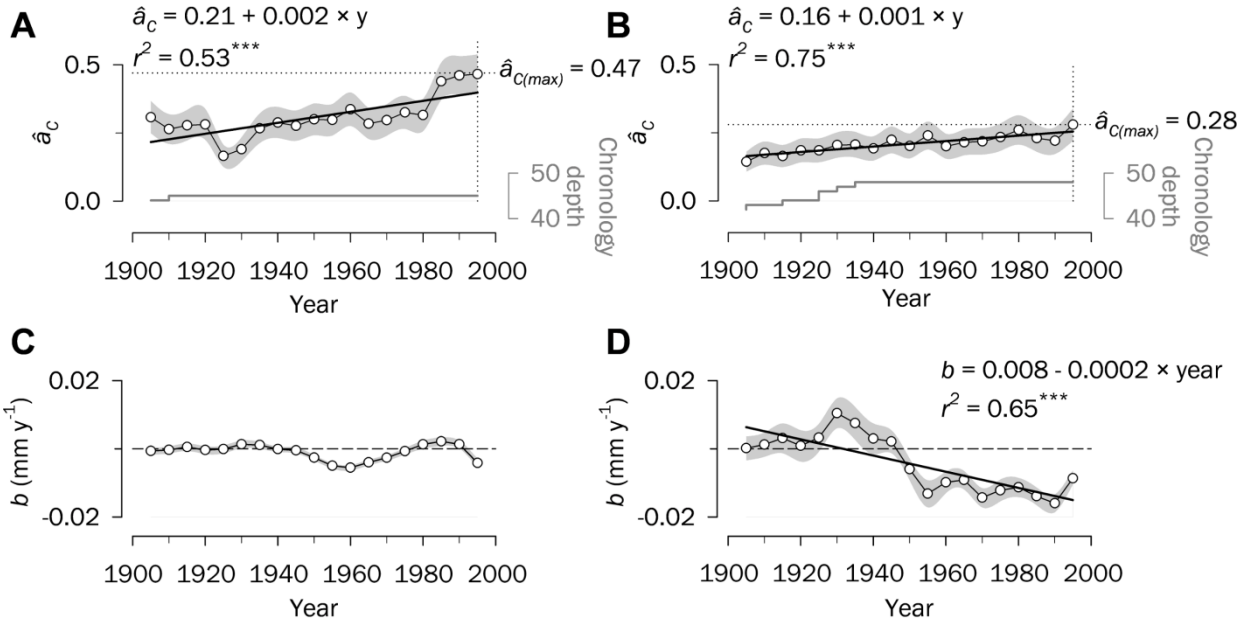

Figure 3.1. Synchrony patterns and changes in absolute growth for the period 1890–2009. **(*A, B*)** Spatial synchrony, $\hat{a}_C$, estimated for central Siberia (*A*) and Spain (*B*) using ring-width chronologies for successive 30-year periods lagged by five years. The dotted lines indicate $\hat{a}_C$ maxima over the study period. Gray lines represent the number of chronologies with an *EPS* > 0.85 (i.e., chronology depth). **(*C, D*)** Temporal trends in the slope (b) of growth in central Siberia (*C*) and Spain (*D*) estimated based on raw ring-width data for the same time intervals used for synchrony. The dashed lines indicate no change in growth rate over the study period. Significant linear trends over time are depicted as black lines (***P < 0.001). Shaded areas denote SEs. Values on the x-axes correspond to the middle years of 30-year moving intervals.

forest synchrony is currently reaching values comparable to the mean synchrony between co-occurring trees within a stand (mean ± SE, Spain: $\hat{a}_C$ = 0.28 ± 0.06 [region] *vs.* 0.40 ± 0.13 [stand]; Siberia: $\hat{a}_C$ = 0.47 ± 0.07 [region] *vs.* 0.49 ± 0.10 [stand]). The lower mean $\hat{a}_C$ in Spain over the study period (0.21 ± 0.02 *vs.* 0.32 ± 0.03 in Siberia) contrasts with the lower average distance between stands in Spain compared with Siberia (mean ± SD, 346 ± 195 km *vs.* 575 ± 331 km) (*SI Appendix*, Fig. S1). In any case, synchrony patterns in Siberia and Spain are statistically independent (*SI Appendix*, Tables S2 and S3), indicating that the increasing synchrony in tree growth is a widespread ecological phenomenon, although regionally dependent. Synchrony estimates could be sensitive to the number of available chronologies, a number that has decreased progressively in the most recent years (*SI Appendix*, Table S1); however, there is a close agreement in $\hat{a}_C$ between the complete set of chronologies and a subset that extends beyond the year 2000 (Siberia, r = 0.90; Spain, r = 0.87; $P < 0.001$ in both cases). An analysis of anomalously wide or narrow rings (i.e., "pointer years"), originating from extreme external events (Babst *et al.* 2012), is in agreement with the absolute peaks in synchrony seen in both regions at the turn of this century (*SI Appendix*, section 2*A* and Fig. S2).

To further explore how increasing synchrony is related to regional growth patterns, we used raw ring-width records and assessed shifts in growth rates over time. We noted differential paces of tree growth in Siberia and Spain for the period 1890–2009. A clear growth slowdown was seen in Spain (b = –0.00024 mm y^{-2}), but no significant trend appeared in Siberia (Fig. 3.1 *C* and *D*). Such temporal changes could be affected by variations in the population age/size structure (mean ± SD chronology length, 303 ± 82 years for Siberia and 247 ± 129 years for Spain). To check for age-independent growth declines, we assessed growth dynamics only for old-growth forest stands (>200 years old; n = 43 chronologies for Siberia, n = 30 chronologies for Spain). This approach minimizes the temporary dynamics associated with stand development and succession. We observed a good agreement when comparing the results from this subset with the growth patterns found for the complete dataset (r = 0.99, $P < 0.001$ for Siberia; r = 0.87, $P < 0.001$ for Spain; slowdown for Spain, b = –0.00014 mm y^{-2}), indicating that age-dependent declines cannot explain temporal changes in growth. The growth reduction in Mediterranean forests may be caused by increasing water limitations (Williams *et al.* 2013), but the lack of a positive growth response to warming in boreal forests is puzzling. Various hypotheses have been proposed to explain this phenomenon (D'Arrigo *et al.* 2008), but temperature-induced drought or direct heat stress are plausible constraints of forest productivity in high latitudes (Lloyd & Bunn 2007).

Increases in synchrony and absolute growth trends: taxonomic patterns

At the species level, $\hat{a}_C$ values peaked at the turn of this century in most cases (Fig. 3.2). Overall, species-specific changes in synchrony were in good agreement with regional trends, although *Larix gmelinii* in Siberia and *Pinus sylvestris* in Spain exhibited less obvious (but

also significant) increments in $\hat{a}_C$ over the past 120 years. Notably, the spatial synchrony between pairs of species also increased with time (Fig. 3.2); however, $\hat{a}_C$ values across species pairs tended to be lower than those for individual species, indicating that although interspecific variability in growth responses certainly exists and is important (e.g., deciduous *vs.* evergreen conifers in Siberia), the strength of these interspecific differences is diminishing with time, resulting in more synchronous tree growth.

Boreal forests in Siberia, limited mainly by low temperatures (Vaganov *et al.* 1999; Lloyd & Bunn 2007), show high synchrony irrespective of species. In contrast, the primarily water-limited forests in Spain (Macias *et al.* 2006; Andreu *et al.* 2007) have lower synchrony. It is likely that temperature exerts a greater influence than precipitation on the spatial signals imprinted in tree rings (Wettstein *et al.* 2011), owing to the greater spatial homogeneity of temperature in Siberia compared with the more complex rainfall pattern countrywide in Spain (*SI Appendix*, Fig. S3). In fact, *Abies alba* has the largest $\hat{a}_C$ values among the three Spanish species, which could be explained by its limited spatial distribution and narrow niche amplitude at mesic sites in northeastern Spain (mean ± SD distance between stands, 124 ± 68 km) (*SI Appendix*, Fig. S1).

To further test for spatial consistency in synchrony patterns (Koenig & Knops 1998), we examined how the correlations between pairs of chronologies vary with distance among

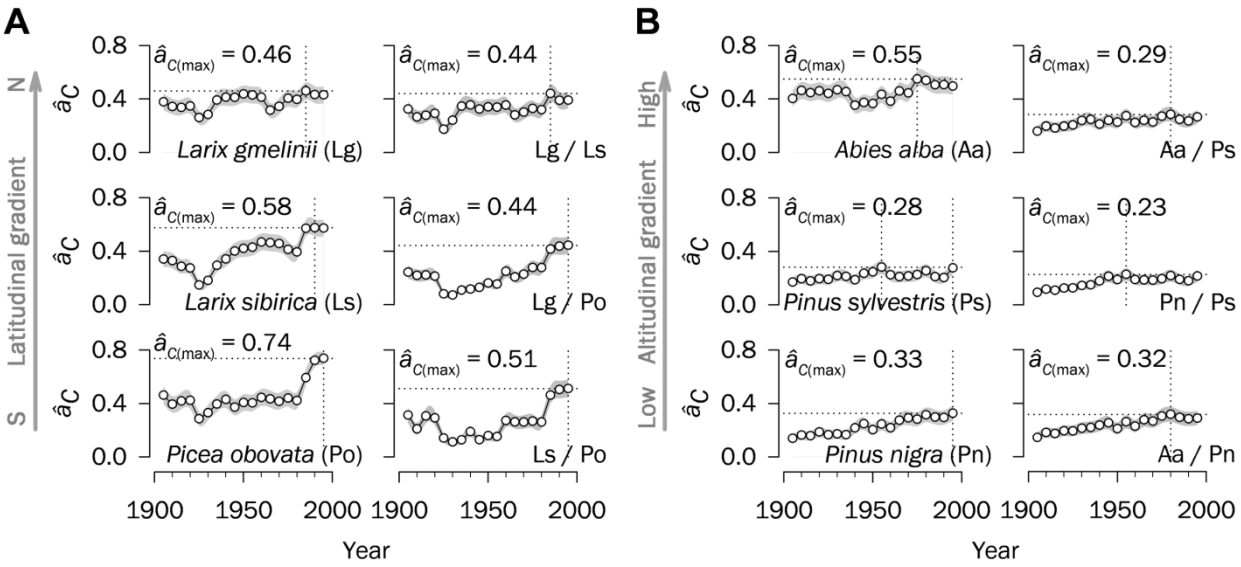

Figure 3.2. Temporal trends in spatial synchrony for single and paired species for central Siberia **(*A*)** and Spain **(*B*)**. Synchrony estimates ($\hat{a}_C$) in single species (first and third columns) and species pairs (second and fourth columns) are calculated based on ring-width chronologies using successive 30-year periods lagged by five years. The dotted lines indicate $\hat{a}_C$ maxima over the study period in each case. SEs are shown as shaded areas. Values on the *x*-axes correspond to the middle years of 30-year moving intervals.

forest stands. The spatial synchrony spread over distances >900 km in Siberia and >600 km in Spain (*SI Appendix*, Fig. S3). More importantly, synchrony was higher in the second half of the twentieth century than in the first half for all species and regions at most distances (*SI Appendix*, Fig. S4). The intercept (but not the slope) of the linear relationship between *r* values and distances increased for all evergreen conifers. *Larix* spp. demonstrated significant slope changes, indicating that greater synchrony occurred after 1950 than before 1950 proportionally with distance. Taken together, our results suggest that external forcing factors superimpose on species-specific and local controls, triggering more synchronous tree growth.

We also investigated shifts in absolute growth trends over time at the species level (*SI Appendix*, Fig. S5). We found a growth slowdown for all species in Spain, but a steady growth rate in Siberia. Notably, growth fluctuations in Siberia became more consistent across species after the 1950s (mean correlation of growth trends between pairs of species before 1950, $r = -0.41$; after 1950, $r = 0.53$). A gradual growth decline in Spain, reflecting increasingly limiting conditions over time, and a more systematic pattern of growth changes in Siberia from 1950 onward seems to concur with the rise in synchrony observed at different regional paces (sustained in Spain, abrupt in the last decades in Siberia) over the last 120 years.

Processes driving increases in synchrony

Increases in synchrony are usually attributed to the influence of climate on tree growth, given that no other environmental driver is likely to act on the same range in time and space (Fritts 2001); however, other global drivers also might trigger the observed increase in synchrony through their effect on growth. First, increasing atmospheric CO_2 concentrations can be expected to augment water-use efficiency, thereby boosting forest productivity (McMahon *et al.* 2010). Second, nitrogen deposition could further increase growth through higher rates of carbon sequestration in sites with unfertile or poorly developed soils (Thomas *et al.* 2010). Third, a decrease in solar radiation caused by anthropogenic aerosol emissions from 1950 (global dimming; Liepert 2002) may counteract the effect of CO_2 fertilisation or rising N deposition, negatively impacting photosynthesis, especially in high latitudes (Stine & Huybers 2014). Fourth, changes in stand structure due to rural abandonment, limited forest management, and encroachment usually increase competition for resources and could reduce tree growth (Linares *et al.* 2010). A detailed examination of these drivers (*SI Appendix*, section 2*B*) led us to discard them as major causes of growth synchrony as opposed to climate.

We then examined whether enhanced synchrony is driven by regional climate trends. Although the Earth's surface has experienced conspicuous warming in the last century, the pace of temperature changes differs regionally (IPCC 2013). Interestingly, the steady increase in synchrony among Spanish forests seems in line with the gradual warming observed over the twentieth century. In turn, temperatures at high Eurasian latitudes have shown a consistent upward trend since the 1970s, which coincides with the steep increase in synchrony observed in Siberia (*SI Appendix*, Fig. S6).

Our analyses of climatic factors causing changes in growth and of climate drivers underlying *âC* fluctuations were restricted to data collected after 1930, in concert with the availability of reliable instrumental records (Esper *et al.* 2010b). Despite species-specific ecological features, the main climate variables related to growth were regionally consistent across taxa (Fig. 3.3). As expected, we found strong positive associations between growth and June–July temperatures in Siberia (i.e., cold-limited growth) (Vaganov *et al.* 1999; Knorre *et al.* 2006) and between May–July precipitation and the Standardized Precipitation Evapotranspiration Index (SPEI) in Spain (i.e., drought-constrained growth) (Andreu *et al.* 2007). Moreover, growth was correlated with early spring (April) temperatures in Siberia (negatively) and with late winter (February) temperatures in Spain (positively) (Fig. 3.3). Such contrasting regional responses to temperature in the early growing season may be a consequence of varying physiological processes underlying the mechanisms of dormancy breaking. After chilling requirements are met in winter, cambial reactivation can occur earlier

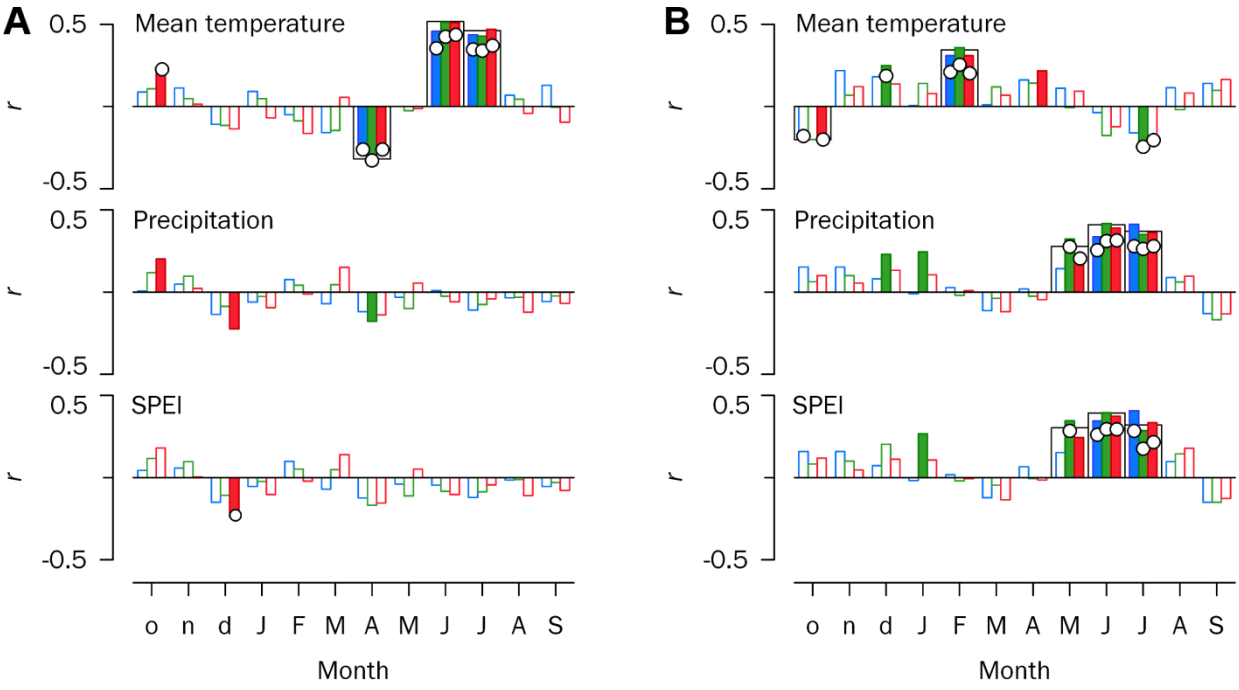

Figure 3.3. Growth–climate relationships at the species and regional levels for central Siberia **(*A*)** and Spain **(*B*)**. Tree growth responses to climate are based on bootstrapped correlations (indicated by bars) and response function partial regression coefficients between tree-ring indices for species or regions and monthly mean temperature, precipitation, and SPEI for the period 1930–2009. Significant correlation and partial regression coefficients ($P < 0.05$) are indicated by filled bars and white circles, respectively. Species are represented in blue (*Larix gmelinii*, *Abies alba*), green (*Larix sibirica*, *Pinus nigra*), and red (*Picea obovata*, *Pinus sylvestris*). Wide bars denote significant relationships at the regional level. Lowercase and uppercase letters on the *x*-axes correspond to the years before and during tree-ring formation, respectively.

in Siberia under higher April temperatures (Oquist & Huner 2003), hastening the onset of xylogenesis (Linkosalo 1999); however, newly formed tissues can be damaged if followed by severe frosts (Knorre *et al.* 2006), causing hydraulic dysfunction (i.e., freeze–thaw events) (Voltas *et al.* 2013). A warm spring also may activate the photosynthetic machinery in crowns that are functionally uncoupled from roots (Linkosalo 1999), and sudden early-spring temperature drops may impair photosynthesis in boreal evergreen conifers (Heide 1993). These mechanisms may restrict radial growth in high latitudes (Panyushkina *et al.* 1996). In contrast, in Mediterranean environments, early cambial reactivation triggered by warm winters usually increases carbon uptake and enhances wood formation (Bigelow *et al.* 2014).

We characterized the spatial structures of these growth–climate relationships through cross-correlation analyses. The spatial association was significant for most climate factors at sites >900 km apart in Siberia and >600 km apart in Spain (*SI Appendix*, Fig. S7), confirming the existence of consistent subcontinental forest responses to climate (Babst *et al.* 2013). This result identifies climate as a primary mechanism of synchrony in our tree-ring network, and suggests that increases in forest synchrony could be driven by concomitant increases in regional climate synchrony. We found that this actually was not the case, however (*SI Appendix*, section 2*C* and Fig. S8).

Alternatively, we evaluated whether enhanced synchrony is related to climate trends and variability. For this purpose, we first assessed regional changes in growth–climate relationships through moving correlations. Most relevant changes span the period from the onset of the growing season through early summer, matching the period of early wood formation. For Siberia, the negative dependence of growth on warmer April temperature increased over time (Fig. 3.4*A*); for Spain, high February temperatures and high May–June precipitation and SPEI became more important for growth (Fig. 3.5). In this regard, we found that $\hat{a}_C$ values were significantly associated with the correlation coefficients of the varying relationship between growth and early growing season temperature. Notably, this association was negative for April in Siberia (Fig. 3.4*A*) and positive for February in Spain (Fig. 3.5), indicating divergent regional growth dynamics. In both cases, we interpret this result as a sign of earlier cambial reactivation promoting more synchronous growth over time. Rising temperatures may induce earlier cambial reactivation (Begum *et al.* 2013), resulting in both a higher rate of xylem cell production and a longer duration of cambial growth, which in principle should increase ring width (Rossi *et al.* 2014). This was not the case for Siberia, however, where an earlier onset of cambial activity may be associated with an increased risk of frost damage to the cambium (Begum *et al.* 2013). In this region, tree growth has remained limited by low summer temperatures (Fig. 3.4*A* and *SI Appendix*, Fig. S9), exerting growth desynchronization in June (Fig. 3.4*A*), but this constraint has decreased after the 1970s because of the positive warming trend (*SI Appendix*, Fig. S6). This effect is counterbalanced by a reinforcement of the negative impact of high April temperatures on growth as a driver of synchrony (Fig. 3.4*A*). In Spain we also observed a diminishing growth dependence on July

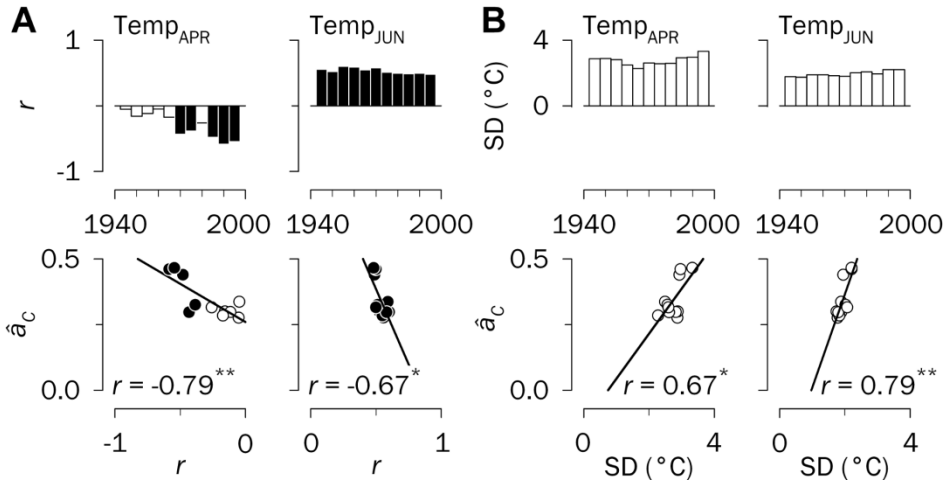

Figure 3.4. Climate factors underlying changes in synchrony in central Siberia, 1930–2009. (*Upper panel*) Moving correlation analyses (*r* values) between regional tree-ring indices and April and June mean temperatures (Temp) **(*A*)** and standard deviations (SD) of April and June mean temperatures **(*B*)** displayed in bar diagrams for successive 30-year periods lagged by five years. Significant correlations are indicated by filled bars in *A* ($P < 0.05$). (*Lower panel*) Relationships between synchrony estimates ($\hat{a}_C$) and *r* values *(A)* and SD of climate variables *(B)* presented in scatterplots. Only monthly climate factors significantly correlated with $\hat{a}_C$ are displayed ($^{*}P < 0.05$; $^{**}P < 0.01$). The filled circles correspond to the periods with significant growth–climate relationships, as indicated by the moving correlation analyses. Years displayed on the x-axes correspond to the middle years of 30-year moving intervals.

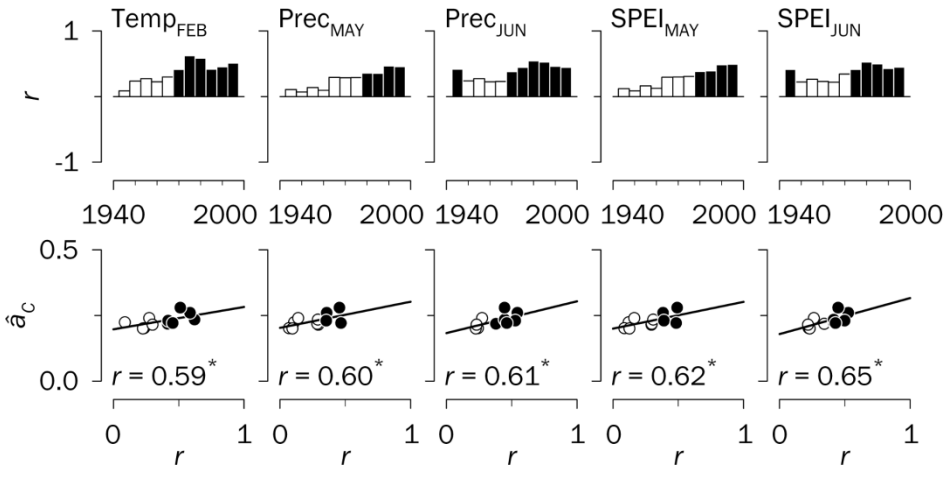

Figure 3.5. Climate factors underlying changes in synchrony in Spain, 1930–2009. (*Upper panel*) Moving correlation analyses (*r* values) between regional tree-ring indices and February mean temperatures (Temp), and May and June precipitation (Prec) and SPEI in May and June displayed in bar diagrams for successive 30-year periods lagged by five years. (*Lower panel*) Relationships between synchrony estimates ($\hat{a}_C$) and *r* values presented in scatterplots. More details are provided in Fig. 3.4.

precipitation and SPEI (*SI Appendix*, Fig. S10) (Andreu *et al.* 2007), which suggests reduced cambial activity in summer (Voltas *et al.* 2013) in response to warming-induced drought (*SI Appendix*, Fig. S11) and a growth shift toward spring (May–June) (Fig. 3.5), thereby enhancing synchrony.

Synchrony patterns might not be linked exclusively to long-term climate trends, but also to changes in climate extremes over time (Babst *et al.* 2012), as suggested by the reported independence of spatial correlations of record-breaking monthly temperature time series from those of the temperatures themselves (Kostinski & Anderson 2014). In general, significant linear trends in climate variability (i.e., standard deviations of monthly climate factors; *SI Appendix*, Fig. S11) were observed for relevant growth periods (Fig. 3.3). We found that a more synchronous growth pattern in Siberia was related to a larger temperature variability in April and June (Fig. 3.4*B*), but not in peak summer (July) (*SI Appendix*, Fig. S9). In contrast, climate variability was unrelated to changes in synchrony in Spain (*SI Appendix*, Fig. S10).

Finally, we explored the complementarity of climate trends and variability in explaining regional synchrony through stepwise linear regression (Table 3.1). Initially, the impact of climate trends on synchrony was considered using the subset of monthly climate factors whose temporal relationships with growth exhibit a significant association with $\hat{a}_C$ values (Figs. 3.4*A* and 5). These models provide a good explanation of synchrony changes (especially for Spain), identifying recent warming as a significant driver of synchrony across the studied Eurasian forests; however, when climate variability is also considered (Fig. 3.4*B*), the model fitting is further improved in Siberia, up to r^2 values similar to those for Spain. In fact, climate variability for April and June in Siberia and climate trends for February temperature and June water availability (precipitation and SPEI) in Spain explain 75% of the observed regional synchrony patterns. Unraveling the exact effects of climate warming and extremes on forest synchrony would require both a greater spatial saturation of site chronologies and more detailed instrumental records covering large geographic areas.

This study illustrates how early signals of climate change impacts on forests can be traced back through the interpretation of synchrony patterns stored in tree rings. Here we demonstrate that climate change is modulating spatial synchrony in forest growth over disparate Eurasian regions, increasing the strength of the common signal shared by trees under warmer conditions to levels comparable to the mean synchrony between co-occurring trees within a stand. Even reporting on different *Pinaceae*, including evergreen and deciduous conifers, our results are consistent across species. The mechanisms behind this pattern require further examination, but they seem to be dependent on the increasing importance of regional-scale climate signals in tree rings overriding local growth drivers. The observed enhanced synchrony may anticipate declines in tree vigor and growth that are critical for the functioning and maintenance of forest ecosystem services under a warmer future climate.

Table 3.1. Multiple linear stepwise regressions explaining synchrony ($\hat{a}_C$) patterns from changing growth–climate relationships (correlation coefficients; *r*) and climate variability (standard deviations of climate factors; SD) over 1930–2009.

Synchrony	Initial variable	Initial r^2	Initial MSE	Final stepwise model	Final r^2	Final MSE
Siberia	*Correlation with climate factors* (rTmean$_{APR}$, rTmean$_{JUN}$)					
	rTmean$_{APR}$	0.63**	0.020	$\hat{a}_C = 0.26 - 0.29\ r\text{Tmean}_{APR}$	0.63**	0.020
	Correlation with climate factors and variability (rTmean$_{APR}$, rTmean$_{JUN}$, *SD*Tmean$_{APR}$, *SD*Tmean$_{JUN}$)					
	*SD*Tmean$_{JUN}$	0.63**	0.020	$\hat{a}_C = -0.47 + 0.28\ SD\text{Tmean}_{JUN} + 0.10\ SD\text{Tmean}_{APR}$	0.75***	0.013
Spain	*Correlation with climate factors* (rTmean$_{FEB}$, rPrec$_{MAY}$, rPrec$_{JUN}$, rSPEI$_{MAY}$, rSPEI$_{JUN}$)					
	rSPEI$_{JUN}$	0.43*	0.003	$\hat{a}_C = 0.18 + 1.03\ r\text{SPEI}_{JUN} - 0.93\ r\text{Prec}_{JUN} + 0.08\ r\text{Tmean}_{FEB}$	0.75***	0.002

Codes for the variables are as in Figs. 3.4 and 3.5 (*Upper*) for Siberia and Spain, respectively. MSE, mean squared error.
*$P < 0.05$; **$P < 0.01$; ***$P < 0.001$.

SUPPORTING INFORMATION (SI Appendix)

Supplementary text

1. Materials & methods

A: Study area

The main environmental factors differentiating central Siberia (Russia) and Spain are temperature and moisture regimes. Central Siberia has a severe continental climate with a prolonged cold season, a large difference between summer and winter temperatures, and a moderate precipitation. Spain is dominated by a typical Mediterranean climate with mild (coast) to cool (inland) wet winters and a summer drought. Tree species occurring in the Mediterranean are adapted to varying degrees to reduced water availability during the growing period (particularly in summer), and tree growth at high latitudes in Eurasia is mainly limited by low temperatures and a very short vegetative period in summer.

The central Siberian region is located in the permafrost zone of the northwestern part of the Central Siberian Plateau (Krasnoyarsk krai, Russia) and extends from the Lower Tunguska River in the south upwards along a latitudinal gradient to the North Siberian Lowland in the north (61°33'–72°30'N, 84°30'–104°15'E) (Fig. S3.1). It covers an approximate area of 700,000 km². The landscape is diverse, with low-altitude plains and high mountain ranges (e.g., the Putorana mountains), and undergoes frequent extreme weather fluctuations. The average annual temperature for the region is –9.9°C, with January being the coldest (–31.1°C) and July the warmest month (+14.0°C) (reference period: 1930 to 2009, CRU TS3.10 dataset; Harris *et al.* 2014). Following a latitudinal gradient, the transition to above-zero mean daily temperatures takes usually place during the second half of May, and to below-zero temperatures from late September through mid-October. The snow cover is formed at this period and lies in the region for about eight months. The mean annual precipitation is 450 mm, with about 40% occurring during summer (June to August) as rain events. The vegetation types can be classified according to three latitudinal subzones that follow a north to south temperature gradient (forest-tundra, northern taiga and middle taiga), with conifers as dominant tree species (Tchebakova *et al.* 2014). *Larix gmelinii* is the northernmost conifer species of the region, while *Larix sibirica* and *Picea obovata* can be mainly found in the southern and western parts of the study area. The study sites, as representative of most forest trees growing in the region, range in elevation from 10 to 590 m a.s.l.

Sites located in Spain embrace mainly the southern and northern edges of the Iberian Peninsula, although some additional sites from the Spanish central plateau are also included (37°04'–43°04'N, 5°15'W–2°26'E) (Fig. S3.1). The study area covers 330,000 km² approximately. The region is characterized by a complex topography, ranging from the coastal plains to the slopes of various mountain ranges, and the interaction of African

subtropical, Mediterranean, and North Atlantic climate systems (Rodó *et al.* 1997). This variety in biogeographical conditions leads to a diverse assortment of forest systems covering a wide range of climates with strong influence of the Mediterranean climate, including semiarid conditions in the south-east, and cooler and more continental and humid conditions in the north. This latitudinal gradient approximately coincides with both increasing precipitation and decreasing temperature gradients (Sánchez-Salguero *et al.* 2015). The mean annual temperature is +12.9°C, ranging from +5.0°C in January to +22.1°C in July (reference period: 1930 to 2009, CRU TS 3.10 dataset; Harris *et al.* 2014). Mean annual precipitation in the region is about 600 mm, but it varies considerably between the studied sites, from 500 mm to more than 1400 mm. Forests are mainly situated in mountain zones along a pronounced altitudinal gradient (700–2,390 m a.s.l.), ranging from warm sub-Mediterranean conditions in low-elevation sites to cold conditions upwards. The ubiquitous *Pinus nigra* subsp. *salzmannii* (Dunal) Franco and *Pinus sylvestris* L. are distributed across the study area, whereas *Abies alba* Mill. is only present in the north-eastern Iberian Peninsula (Pyrenees). The moisture regime is strongly bimodal, with precipitation concentrated in spring (March to May) and autumn (September to November) and presence of a dry summer (<20% of annual precipitation).

B: Tree-ring network

We compiled a network of 93 annually resolved long-term tree-ring width (TRW) chronologies originating from conifer forests located in central Siberia, Russia (n = 45 sites) and Spain (n = 48 sites). These two Eurasian regions are representative of contrasting conditions in terms of temperature and moisture regimes (*SI Text*, section 1*A*). The chronologies were selected as representative of the range of climatic and biogeographical conditions of each region (Table S3.1, Fig. S3.1). In central Siberia, *Larix gmelinii* (Rupr.) Rupr. and *Larix sibirica* Ledeb. were represented by 19 and 13 chronologies, respectively, and *Picea obovata* Ledeb. by 13 chronologies. In Spain, *Pinus nigra* subsp. *salzmannii* (Dunal) Franco and *Pinus sylvestris* L. were represented by 18 and 20 chronologies, respectively, and *Abies alba* Mill. by 10 chronologies. These chronologies were chosen in accordance with the current species distribution ranges. Each chronology consisted of a time series of annual indices derived from TRW measurements on a number of tree increment cores (Table S3.1). Core collection, transportation and preprocessing followed standard dendrochronological techniques (Cook & Kairiukstis 1990). Altogether, data for a total of 663 trees (1021 radii) in central Siberia and 801 trees (1647 radii) in Spain were used.

C: Mixed modelling

We analysed a particular set of indexed tree-ring chronologies ($I = 1, N$) to characterise the strength of their common signal for ring-width. Let us define W_{ij} as the tree-ring index (TRI) achieved by the jth year of the ith chronology. The estimators can be

defined in terms of the following random model (Shestakova *et al.* 2014) (random variables are shown underlined):

$$\underline{W}_{ij} = \underline{Y}_j + \underline{e}_{ij} \quad \text{(S3.1)}$$

where $\underline{Y}_j$ is a random effect of the *j*th year, and $\underline{e}_{ij}$ is a random deviation of the *i*th chronology in the *j*th year. Here we assume that the levels of the factor 'year' come from a random sample of all possible years and, hence, the year effect is defined as random. To quantify the association between a pair of chronologies *i* and *i**, the intraclass correlation (or reproducibility of TRI observations by chronologies *i* and *i**) can be calculated as follows (Shestakova *et al.* 2014):

$$\rho(\underline{W}_i, \underline{W}_{i*}) = \frac{\mathrm{cov}(\underline{W}_i, \underline{W}_{i*})}{\sqrt{Var(\underline{W}_i) \times Var(\underline{W}_{i*})}} = \frac{\sigma_Y^2}{\sigma_Y^2 + \sigma_e^2} \quad \text{(S3.2)}$$

where σ^2_y refers to the variance of year effects and σ^2_e stands for the residual variance. The parameter ϱ becomes the average correlation for TRI over all possible pairs of chronologies provided the whole set of *N* chronologies is analysed together, but excluding the *N* pairs $i = i^*$ for which $\rho(\underline{W}_i, \underline{W}_{i*}) = 1$. It estimates the strength of the common signal for TRI underlying the set of *N* chronologies. We refer to it as the mean inter-chronology correlation or spatial synchrony, $\hat{a}_C$.

We have grouped the available tree-ring chronologies into subsets representing: (*i*) different Eurasian regions and (*ii*) different species within a particular Eurasian region. To this purpose, the following mixed model characterizing synchrony patterns at the between- and within-group levels is used:

$$\underline{W}_{ijr} = \mu_r + \underline{Y}_{jr} + \underline{e}_{ijr} \quad \text{(S3.3)}$$

where μ_r is the expected mean value in the *r*th group (since chronologies are indexed, this term is approximately equal to unity), $\underline{Y}_{jr}$ is a random effect of the *j*th year in the *r*th group, and $\underline{e}_{ijr}$ is a random deviation of the *i*th chronology in the *j*th year within the *r*th group.

In turn, the year effect may be further partitioned as:

$$\underline{Y}_{jr} = \underline{Y}_j + \underline{(YR)}_{jr} \quad \text{(S3.4)}$$

where $\underline{Y}_j$ is a main effect for the *j*th year and $\underline{(YR)}_{jr}$ is the *jr*th year × group interaction, assuming that $\underline{Y}_j$ and $\underline{(YR)}_{jr}$ are independent homoscedastic normal deviates. This model corresponds to the standard analysis of variance (ANOVA) partition accommodating between- and within-group variability, and has the so-called *compound symmetry* variance-covariance (VCOV) structure for variability among years:

$\mathrm{cov}(\underline{Y}_{jr};\underline{Y}_{jr^*}) = \sigma^2_{Y+YR}$, when $r = r^*$,

otherwise $\mathrm{cov}(\underline{Y}_{jr};\underline{Y}_{jr^*}) = \sigma^2_{Y}$

In the *compound symmetry* structure (S_1) year variances are the same in each group, with $\sigma^2_{Y+YR} = \sigma^2_{Y} + \sigma^2_{YR}$, and year covariances (and correlations) are the same for each pair of groups. However, alternative VCOV structures that cover a range of assumptions may describe the data better in accordance with the properties of the grouped chronologies (which are based here on regional or taxonomic criteria).

In the *heterogeneous compound symmetry* structure (S_2) there may be heterogeneity of year variance between groups, although the property of constant correlation (ϱ) across all pairs of groups may still hold true:

$\mathrm{cov}(\underline{Y}_{jr};\underline{Y}_{jr^*}) = \sigma^2_{Y_r}$, when $r = r^*$,

otherwise $\mathrm{cov}(\underline{Y}_{jr};\underline{Y}_{jr^*}) = \sigma_{Y_r} \times \sigma_{Y_{r^*}} \times \rho$

In the *factor-analytic* structure (S_3) λ_r is a group-specific multiplicative parameter and σ^2_d is a residual variance common to all groups:

$\mathrm{cov}(\underline{Y}_{jr};\underline{Y}_{jr^*}) = \lambda_r \lambda_{r^*} + \sigma^2_d$, when $r = r^*$,

otherwise $\mathrm{cov}(\underline{Y}_{jr};\underline{Y}_{jr^*}) = \lambda_r \lambda_{r^*}$

This is a simplified, but almost as flexible, variant of the unstructured model (defined below) in which information is gathered from correlated chronologies through (factor-analytic) correlation of year by chronology effects.

In the *unstructured* (or full) structure (S_4) each group has its own year variance and each pair of groups its own year covariance:

$\mathrm{cov}(\underline{Y}_{jr};\underline{Y}_{jr^*}) = \sigma^2_{Y_r}$, when $r = r^*$,

otherwise $\mathrm{cov}(\underline{Y}_{jr};\underline{Y}_{jr^*}) = \sigma^2_{Y_{rr^*}}$

Two simple variants of the compound symmetry structure act as a baseline against which to compare the more refined modelling alternatives shown before (Shestakova *et al.* 2014).

The *banded main diagonal* (or narrow evaluation) structure (S_5) constrains the covariance (and correlation) between groups to zero, thus testing for a lack of common signal between chronologies belonging to different groups:

$\text{cov}(\underline{Y}_{jr};\underline{Y}_{jr*}) = \sigma^2_{Y_r}$, when $r = r^*$,

otherwise $\text{cov}(\underline{Y}_{jr};\underline{Y}_{jr*}) = 0$

In the *null* (or broad evaluation) structure (S_6) the existence of groups is simply ignored so year variance and covariances have the same value:

$\text{cov}(\underline{Y}_{jr};\underline{Y}_{jr*}) = \sigma^2_{Y}$, when $r = r^*$ or $r \neq r^*$,

This last structure is useful for testing the adequacy of grouping chronologies into different classes as for the previous models.

In turn, these structures can be enhanced by allowing the residual variance associated with $\underline{\underline{e}}_{ijr}$ to vary among groups, hence producing heteroscedastic variants, except for the null model in which no groups are defined. A summary of the properties and interpretation of these structures can be found in Table S3.2.

The estimation of signal strength parameters for selected structures is grounded on the intra-class correlation expression as defined in Eq. (S3.2), which quantifies the degree to which the values of *N* chronologies contain a common temporal signal (i.e., synchrony). The structures defined so far allow estimation of the intra-class correlation either at the intra-group or inter-group levels (except for the null model S_6 in which no groups are defined). Hence the mean correlation estimated between all possible pairs of chronologies drawn from the whole dataset as in Eq. (S3.2) is split into: (*i*) a mean correlation between pairs of chronologies for every group; and (*ii*) a mean correlation between pairs of chronologies for pairs of groups. For the more general unstructured model (S_4), the correlation of pairs of chronologies *i* and *i** belonging to group *r* becomes:

$$\rho(\underline{W}_i,\underline{W}_{i*}) = \frac{\text{cov}(\underline{W}_i,\underline{W}_{i*})}{\sqrt{Var(\underline{W}_i) \times Var(\underline{W}_{i*})}} = \frac{\sigma^2_{Y_r}}{\sigma^2_{Y_r} + \sigma^2_e} \qquad \text{(S3.5)}$$

Besides, the correlation of pairs of chronologies *i* and *i** belonging to groups *r* and *r** is:

$$\rho(\underline{W}_i,\underline{W}_{i*}) = \frac{\text{cov}(\underline{W}_i,\underline{W}_{i*})}{\sqrt{Var(\underline{W}_i) \times Var(\underline{W}_{i*})}} = \frac{\sigma^2_{Y_{rr*}}}{\sqrt{(\sigma^2_{Y_r} + \sigma^2_e) \times (\sigma^2_{Y_{r*}} + \sigma^2_e)}} \qquad \text{(S3.6)}$$

If the whole set of *N* chronologies is analysed together, then these parameters become mean correlations over all possible pairs of chronologies (synchrony, $\hat{a}_C$) at the intra-group or inter-group level, respectively (Wigley *et al.* 1984; Shestakova *et al.* 2014). Alternative mean correlation expressions for other models can be obtained by applying their corresponding VCOV structures to Eq. (S3.3). The Expressed Population Signal (EPS), which quantifies

how well a chronology based on a finite number of trees represents the hypothetical perfect or true chronology, can be generalised from these estimates (Wigley *et al.* 1984):

$$EPS \approx \frac{N \times \hat{a}_C}{1 + (N-1) \times \hat{a}_C} \quad \text{(S3.7)}$$

where N is the number of chronologies at either the intra-group or inter-group levels.

Standard errors for the mean inter-chronology correlation can be estimated as follows (Visscher 1998):

$$SE(\hat{a}_C) \approx \sqrt{\frac{2 \times \hat{a}_C^2 \times (1-\hat{a}_C)^2}{d.f.}} \quad \text{(S3.8)}$$

where *d.f.* are the degrees of freedom from the mean inter-chronology correlation (i.e., number of years).

All analyses were performed with the MIXED procedure of SAS/STAT software (ver. 9.3, SAS Inc., Cary, NC, USA) using restricted maximum likelihood (REML) for estimation of variance components. Further details on the methodological background and on model fitting procedures can be found in (Shestakova *et al.* 2014).

D: Evaluation of changes in synchrony over time

The evolution of changes in $\hat{a}_C$ was studied for successive 30-year segments lagged by five years (Fig. S3.12). The inter-regional evaluation of $\hat{a}_C$ comprised two groups (Siberia and Spain), whereas the inter-specific evaluation comprised three groups (species) at each region. In the former case, this means that both the heterogeneous compound symmetry and the factor-analytic model provided equivalent results to those of the unstructured model, as the number of parameters to be estimated is three in all cases. It must be taken into account that chronologies do not overlap perfectly until the beginning of the twentieth century and, as expected, the number of series increases over time as younger trees are progressively available for building the site chronologies. Although mixed modelling is capable of dealing with unbalanced datasets (e.g., partially overlapping chronologies) provided the missing-data pattern is considered at random (Little & Rubin 2002), the reliability of every chronology in terms of its temporal signal has to be warranted to some extent. In this regard, we adopted as criterion for the year of inclusion of a chronology in the VCOV analysis the year at which its EPS becomes ≥0.85. The regional trends in synchrony (as reported in Fig. 3.1 *A* and *B*) were mostly insensitive to the progressive inclusion of chronologies for two decades in Siberia (with 3 chronologies progressively incorporated) and four decades in Spain (with 10 chronologies progressively incorporated) starting in 1890 (Table S3.1) (correlation coefficient between $\hat{a}_C$ values for the complete set of chronologies and a subset covering the whole study period: $r = 0.99$, $P < 0.001$ for Siberia; $r = 0.94$, $P < 0.001$ for Spain).

E: Best linear unbiased prediction of tree-ring width indices

The best linear unbiased prediction (BLUP) method was developed for estimation of breeding values in animals and it is currently applied in many areas of research through mixed modelling (Henderson 1984). However, its application to dendrochronology remains untested to the best of our knowledge.

Best linear unbiased prediction (BLUP) increases accuracy of tree-ring width indices (TRI) relative to ordinary least squares (OLS) methods (i.e., standard ANOVA) and maximizes, under certain rather general assumptions, the correlation between true and predicted TRI values associated to the random year effect (Piepho & Möhring 2005). For this purpose, the predictors of random year effects (i.e., TRI defined as $\underline{Y_{jr}}$ in Eq. [S3.3]) are shrunken towards zero compared with OLS estimates (Searle *et al.* 2006). For a balanced (i.e., perfectly overlapping) network of chronologies, the impact of shrinkage across years is constant and the shrinkage factor equals the synchrony estimate ($\hat{a}_C$) (or reproducibility of year effects by a set of chronologies), as defined in (Searle *et al.* 2006). However, for unbalanced datasets (this study) BLUP and OLS are not exactly proportional, with under-represented years having predictors more severely shrunken towards zero.

F: Evaluation of the geographic extent of forest and climate synchrony

To evaluate the geographic extent of forest and climate synchrony, spatial autocorrelation was analyzed using a modified correlogram procedure (Koenig & Knops 1998). To this end, tree-ring width indices and climate factors (mean temperature and total precipitation) were used. Site climate series were obtained through bilinear interpolation of the four nearest CRU TS 3.10 grid (0.5° × 0.5°) point values using an inverse distance squared weighting. The resulting series were finally standardized by fitting a straight line and keeping the residuals of these linear fits in order to ensure that results were due to regional processes rather than to long-term trends (e.g., global warming). For statistical analyses, four distance classes were defined depending on geographical distance between sites: <300 km, 300–600 km, 600–900 km, and ≥900 km.

We also evaluated spatial patterns of growth-climate relationships by using cross-correlation analyses (Koenig & Knops 1998). These analyses involved tree-ring width indices and monthly climate factors showing a significant impact on growth for the entire period (1930 to 2009). In both cases (autocorrelation and cross-correlation analyses) the mean *r* value and its statistical significance (*P*) within each distance category was estimated from 1000 randomization trials as described in (Koenig & Knops 1998). All analyses were performed with the non-centred (cross-) correlogram function (correlog.nc) in the package ncf ver. 1.1-5 in R software (ver. 3.2.2, R Foundation for Statistical Computing, Vienna, Austria).

G: Meteorological data and regional climate time series

Monthly mean temperature, precipitation and the Standardized Precipitation Evapotranspiration Index (SPEI) were used for climate analyses. Estimates of monthly temperature and precipitation were obtained from the high-resolution CRU TS 3.10 dataset (http://badc.nerc.ac.uk/data/cru/) available on a 0.5° × 0.5° grid-box basis (Harris *et al.* 2014). The SPEI was obtained from the Global SPEI database (http://sac.csic.es/spei/), which is based on monthly precipitation and potential evapotranspiration available at the CRU TS 3.22 dataset (Vicente-Serrano *et al.* 2010). For each climate variable data were averaged over each region as covered by the network of chronologies in order to create monthly-resolved regional climate time series, hence resulting in regional climate trends (Figs. S3.6 and S3.11). Regional series were then used to assess the relationships between climate and both TRI and synchrony through correlation and response functions. The significance of function parameters was estimated by drawing 1,000 bootstrapped samples with replacement from the initial data set. All climate analyses were performed with the dcc function in the package bootRes ver. 1.2.3 in R software (ver. 3.2.2, R Foundation for Statistical Computing, Vienna, Austria).

2. Additional analyses

A: Pointer years: regional patterns

Extreme external events originate anomalously wide or narrow rings (i.e., "pointer years"), hence being potent drivers of spatial synchrony. To test for the frequency of regional pointer years we use best linear unbiased predictors (BLUPs) of tree-ring width indices derived from mixed modelling (*SI Text*, section 1*E*). Growth anomalies are tagged as those years having BLUPs deviating > ±1SD from the mean. The threshold of ±1.96SD is also used to highlight extraordinary growth reactions at the regional scale. Overall, we find slightly more years with growth anomalies in Siberia (32%) than in Spain (28%) (Fig. S3.2). We also detect more extreme growth anomalies after 1950 in both regions. Hence, the frequency of pointer years has increased from 27% (period 1890–1949) to 37% (1950–2009) in Siberia and from 17% to 40% in Spain. In addition, three pointer years with exceptionally low growth (i.e., deviating over –1.96 SD from the average index) are found in both Siberia and Spain after 1985 (Fig. S3.2). A higher incidence of growth extremes present in the last decades is in agreement with the absolute peaks in synchrony found in both regions at the turn of this century.

B: Attribution analysis: Discarding non-climatic factors as drivers of increased synchrony in forest growth

Two major reasons lead us to reject a CO_2 fertilization effect as the main cause of increased regional synchrony. First, the distinct pace of synchrony changes in Siberia and

Spain is barely compatible with the expected uniform effect of atmospheric CO_2 increasing carbon uptake in temperate and boreal biomes (Fig. 3.1). Second, we did not detect any enhancement of absolute radial growth over time that may underlie the rise in spatial synchrony observed in both regions. Because of such non-positive growth trends, the effect of N deposition as fundamental driver of synchrony, either alone or in conjunction with the increase in atmospheric CO_2 concentration, can also be discarded. Also N deposition is a phenomenon acting at regional scales that should not lead to more homogeneous forest growth across large areas with contrasting N deposition rates. On the other hand, a potential effect of global dimming in boreal forests limited by incoming radiation cannot be neglected, although the lack of growth suppression observed for Siberia and the small impact of global dimming previously reported for radial growth (unlike for wood density) (Stine & Huybers 2014) points to its limited role as trigger of synchrony. Finally, changes in land use and management practices might affect mainly Spanish forests (Linares *et al.* 2010), which display marked use legacies, whereas historical anthropogenic disturbances are negligible in Siberia (Potapov *et al.* 2008). However, the selected Spanish chronologies originate mostly from undisturbed forests composed by old trees, which suggest a reduced influence of stand dynamics on synchrony patterns.

C: Attribution analysis: Discarding the Moran effect as a driver of increased synchrony in forest growth

In order to examine whether the observed increase in regional forest synchrony was driven by more homogeneous climate signals over time (i.e., enhanced 'Moran effect' (Moran 1953; Ranta *et al.* 1997; Pena-Angulo *et al.* 2015), we obtained temporal changes in synchrony patterns of mean annual temperature and annual precipitation for Siberia and Spain. To this end, we used the CRU TS 3.10 dataset using the interpolation scheme outlined in *SI Text*, section 1*F*, and applied the methodology described for tree-ring width records in *SI Text*, section 1*C*. Environmental synchrony patterns are not significantly related to those of forest growth (Fig. S3.8), except for growth *vs.* precipitation in Siberia. However, even in this last case we interpret that such correlation does not imply causation (that increasing rainfall synchrony leads to increased growth synchrony) because of two reasons: (*i*) precipitation, unlike temperature, is not consistently related to growth in Siberia (Fig. 3.3), and (*ii*) for forest growth to be synchronized by an exogenous factor ('Moran effect'), the spatial autocorrelation in the putative environmental factor (precipitation) must extend, in principle, over greater distances that that of the outcome of the cause (forest growth) (Grenfell *et al.* 1998, 2000); however, the spatial autocorrelation of forest growth in Siberia is higher between geographically distant sites (>600 km) as compared with precipitation (Fig. S3.3). Altogether, both considerations lead us to reject an enhanced Moran effect involving precipitation as driver of increased regional synchrony among boreal forests.

Supplementary tables

Table S3.1. Tree-ring sampling sites: geographic features *(A)* and chronology characteristics *(B)*. For site locations see Fig. S3.1. Abbreviations: EPS, Expressed Population Signal; TRW, tree-ring width; Rbar, mean interseries correlation.

(A) Sites				(B) Chronologies						
ID	**Latitude**	**Longitude**	**Elevation (m)**	**Time span**	**EPS > 0.85 since**	**No. trees**	**No. cores**	**TRW±SD (mm)**	**Rbar±SD**	**Reference**
				CENTRAL SIBERIA						
Larix gmelinii (Lg)										
1	72°30'N	102°25'E	60	1924–2011	N/A	14	14	0.44±0.13	0.493± 0.164	Kirdyanov *et al.**
2	72°27'N	101°45'E	70	1624–1990	1705	12	24	0.38±0.13	0.659±0.079	Schweingruber, Briffa (1996)
3	72°27'N	101°54'E	10	1708–2010	1910	14	14	0.42±0.17	0.607±0.082	Kirdyanov *et al.**
4	71°20'N	93°50'E	60	1569–1990	1645	21	42	0.45±0.21	0.662±0.084	Schweingruber, Briffa (1996)
5	70°36'N	104°15'E	130	1563–1990	1645	19	33	0.37±0.13	0.591±0.105	Schweingruber, Briffa (1996)
6	70°36'N	104°15'E	290	1611–2006	1820	11	15	0.65±0.23	0.538±0.121	Esper *et al.* (2010b)
7	70°36'N	104°15'E	130	1855–1990	1910	9	18	0.17±0.05	0.414±0.143	Schweingruber, Briffa (1996)
8	70°31'N	89°30'E	50	1657–1990	1710	19	38	0.55±0.25	0.647±0.082	Schweingruber, Briffa (1996)
9	70°30'N	93°10'E	360	1689–2002	1740	19	34	0.37±0.11	0.690±0.077	Kirdyanov *et al.* (2012)
10	70°30'N	93°10'E	164	1684–2003	1740	13	13	0.37±0.09	0.577±0.083	Kirdyanov *et al.* (2012)
11	64°32'N	100°14'E	204	1747–2005	1800	22	22	0.37±0.13	0.343±0.090	Sidorova *et al.* (2009)
12	64°22'N	92°05'E	80	1670–1992	1755	11	11	0.33±0.05	0.466±0.069	Panyushkina *et al.* (1996)
13	64°19'N	100°14'E	160	1817–2008	1870	21	21	0.41±0.07	0.502±0.076	Kirdyanov *et al.**
14	64°19'N	100°15'E	150	1814–2007	1870	16	16	0.53±0.15	0.350±0.092	Knorre *et al.**
15	64°17'N	93°22'E	120	1612–1992	1670	15	15	0.34±0.08	0.519±0.067	Panyushkina *et al.* (1996)
16	64°09'N	95°27'E	110	1617–1992	1670	12	12	0.41±0.14	0.512±0.075	Panyushkina *et al.* (1996)
17	64°08'N	100°52'E	150	1694–2009	1775	15	15	0.82±0.34	0.346±0.136	Knorre *et al.**
18	63°52'N	96°00'E	110	1679–1992	1755	11	12	0.42±0.08	0.417±0.122	Panyushkina *et al.* (1996)
19	63°44'N	97°55'E	190	1611–1992	1720	12	13	0.46±0.16	0.452±0.093	Panyushkina *et al.* (1996)

(A) Sites				(B) Chronologies						
ID	**Latitude**	**Longitude**	**Elevation (m)**	**Time span**	**EPS > 0.85 since**	**No. trees**	**No. cores**	**TRW±SD (mm)**	**Rbar±SD**	**Reference**
Larix sibirica (Ls)										
1	69°07'N	84°30'E	80	1624–1990	1680	16	29	0.41±0.13	0.661±0.067	Schweingruber, Briffa (1996)
2	68°05'N	86°45'E	33	1638–1998	1690	28	52	0.53±0.13	0.610±0.122	Knorre *et al.* (2006)
3	68°05'N	86°44'E	21	1723–1998	1780	23	35	0.49±0.22	0.518±0.144	Knorre *et al.* (2006)
4	67°58'N	88°55'E	160	1574–1990	1630	11	20	0.58±0.16	0.666±0.065	Schweingruber, Briffa (1996)
5	65°58'N	88°46'E	70	1506–1992	1635	9	10	0.33±0.08	0.539±0.067	Vaganov *et al.* (1996)
6	65°41'N	89°37'E	120	1657–1998	N/A	N/A	N/A	N/A	N/A	Knorre *et al.* (2006)
7	61°54'N	92°44'E	72	1747–1994	1800	10	12	0.62±0.13	0.543±0.096	Kirdyanov (1999)
8	61°52'N	94°40'E	220	1629–1994	1705	11	12	0.74±0.24	0.529±0.059	Kirdyanov (1999)
9	61°51'N	94°19'E	130	1770–1994	1830	12	25	0.51±0.17	0.432±0.122	Kirdyanov (1999)
10	61°51'N	93°24'E	100	1781–1994	1840	19	21	0.80±0.15	0.499±0.118	Kirdyanov (1999)
11	61°49'N	93°43'E	200	1662–1994	1745	14	27	0.55±0.22	0.448±0.124	Kirdyanov (1999)
12	61°46'N	97°29'E	220	1706–1994	1760	10	11	0.40±0.06	0.483±0.078	Kirdyanov (1999)
13	61°33'N	96°56'E	220	1726–1994	1805	10	11	0.80±0.16	0.382±0.085	Kirdyanov (1999)
Picea obovata (Po)										
1	69°35'N	90°30'E	60	1640–1990	1750	20	35	0.50±0.25	0.462±0.143	Schweingruber, Briffa (1996)
2	68°05'N	86°44'E	21	1676–1998	1730	29	46	0.25±0.07	0.433±0.095	Knorre *et al.* (2006)
3	68°05'N	86°45'E	33	1632–1998	1690	29	51	0.41±0.13	0.497±0.122	Knorre *et al.* (2006)
4	67°58'N	88°55'E	160	1661–1990	1720	13	25	0.37±0.16	0.524±0.088	Schweingruber, Briffa (1996)
5	64°21'N	100°25'E	590	1734–2009	1865	17	17	0.42±0.15	0.404±0.096	Shishov *et al.* (2016)
6	64°08'N	100°52'E	150	1855–2009	1910	8	8	1.04±0.22	0.434±0.074	Knorre *et al.**
7	62°21'N	92°03'E	50	1727–1994	1780	14	31	0.50±0.15	0.448±0.112	Kirdyanov (1999)
8	61°59'N	91°31'E	52	1707–1994	1785	13	31	0.62±0.28	0.406±0.135	Kirdyanov (1999)
9	61°56'N	95°09'E	175	1728–1994	1830	12	26	0.96±0.26	0.281±0.164	Kirdyanov (1999)
10	61°54'N	92°44'E	72	1674–1994	1805	12	27	0.68±0.21	0.375±0.112	Kirdyanov (1999)
11	61°51'N	94°19'E	90	1740–1994	1800	14	29	0.34±0.12	0.422±0.110	Kirdyanov (1999)
12	61°49'N	93°43'E	120	1804–1994	1860	10	23	0.84±0.34	0.353±0.123	Kirdyanov (1999)
13	61°42'N	90°25'E	46	1775–1994	1855	13	25	0.81±0.22	0.329±0.154	Kirdyanov (1999)

(A) Sites				(B) Chronologies						
ID	**Latitude**	**Longitude**	**Elevation (m)**	**Time span**	**EPS > 0.85 since**	**No. trees**	**No. cores**	**TRW±SD (mm)**	**Rbar±SD**	**Reference**
					SPAIN					
Abies alba (Aa)										
1	42°55'N	0°47'W	1400	1749–1999	1800	14	28	0.15±1.83	0.404±0.096	Macias *et al.* (2006)
2	42°41'N	1°20'E	1470	1878–1999	1903	15	30	0.11±2.99	0.341±0.150	Macias *et al.* (2006)
3	42°38'N	1°04'E	1750	1767–1999	1790	18	35	0.15±0.89	0.462±0.126	Macias *et al.* (2006)
4	42°34'N	0°23'E	1780	1667–2000	1795	12	24	0.14±2.69	0.352±0.148	Camarero *et al.* (2011)
5	42°31'N	0°32'W	1650	1889–2000	1905	14	28	0.16±2.67	0.525±0.101	Macias *et al.* (2006)
6	42°24'N	2°17'E	1750	1777–1999	1880	15	30	0.17±2.05	0.355±0.121	Macias *et al.* (2006)
7	42°18'N	0°12'W	1500	1893–1999	1905	15	30	0.16±2.99	0.554±0.116	Macias *et al.* (2006)
8	42°19'N	1°49'E	1680	1852–1999	1869	15	31	0.16±1.85	0.425±0.164	Macias *et al.* (2006)
9	42°12'N	1°13'E	1583	1804–1999	1845	17	40	0.16±1.58	0.330±0.130	Macias *et al.* (2006)
10	41°47'N	2°26'E	1550	1587–2010	1640	26	50	0.24±1.23	0.340±0.125	Macias *et al.* (2006, revised)
Pinus nigra (Pn)										
1	42°32'N	0°09'E	700	1819–1999	1860	15	30	1.32±0.36	0.480±0.110	Andreu *et al.* (2007)
2	42°13'N	1°23'E	1200	1867–1999	1890	15	30	1.53±0.31	0.595±0.192	Gutiérrez *et al.**
3	41°16'N	1°00'E	850	1928–1999	1950	15	30	2.18±0.38	0.380±0.157	Gutiérrez *et al.**
4	40°36'N	1°46'W	1450	1655–1998	1750	58	118	1.17±0.32	0.319±0.110	Génova, Martínez-Morillas (2002)
5	40°35'N	0°04'E	1000	1642–2004	1770	25	81	0.91±0.41	0.375±0.138	Fulé *et al.* (2008)
6	40°18'N	0°40'W	1605	1810–2006	1840	14	34	1.09±0.30	0.546±0.095	Camarero *et al.**
7	40°14'N	1°15'W	1450	1485–1988	1570	9	17	0.71±0.10	0.381±0.088	Génova *et al.* (1993)
8	40°13'N	1°55'W	1450	1365–1995	1550	17	31	0.44±0.10	0.277±0.071	Génova, Fernández Canclo (1998/1999)
9	40°11'N	1°56'W	1250	1688–1988	1730	6	12	1.14±0.35	0.412±0.078	Génova *et al.* (1993)
10	40°00'N	0°51'W	1445	1664–2006	1710	14	28	0.98±0.29	0.589±0.105	Camarero *et al.**
11	39°54'N	1°46'W	970	1896–1999	1920	16	31	1.47±0.49	0.425±0.145	Gutiérrez *et al.**
12	38°08'N	2°09'W	1500	1878–1999	1880	15	30	1.27±0.40	0.423±0.129	Gutiérrez *et al.**
13	37°54'N	2°52'W	1435	1816–2010	1940	6	11	1.45±0.55	0.272±0.259	Linares, Tíscar (2010, revised)
14	37°49'N	2°58'W	1819	1596–2010	1940	13	15	0.74±0.21	0.106±0.174	Linares, Tíscar (2010, revised)

(A) Sites				(B) Chronologies						
ID	**Latitude**	**Longitude**	**Elevation (m)**	**Time span**	**EPS > 0.85 since**	**No. trees**	**No. cores**	**TRW±SD (mm)**	**Rbar±SD**	**Reference**
15	37°43'N	3°28'W	1820	1645–2010	1890	19	32	1.08±0.36	0.170±0.128	Linares, Tíscar (2010, revised)
16	37°39'N	2°05'W	1793	1541–2009	1850	9	13	1.14±0.37	0.354±0.138	Camarero *et al.* (2013)
17	37°15'N	2°30'W	1850	1653–1999	1840	15	30	1.92±0.86	0.389±0.200	Andreu *et al.* (2007)
18	37°05'N	3°28'W	1750	1879–1999	1895	13	26	1.93±0.60	0.448±0.120	Gutiérrez *et al.**
Pinus sylvestris (Ps)										
1	43°04'N	5°15'W	1650	1511–2002	1545	15	32	0.78±0.20	0.352±0.096	Andreu *et al.* (2007)
2	42°55'N	0°48'W	1400	1740–1999	1775	15	30	1.51±0.54	0.308±0.127	Gutiérrez *et al.**
3	42°49'N	3°06'W	850	1918–1999	1930	15	30	2.06±0.32	0.363±0.112	Gutiérrez *et al.**
4	42°36'N	1°06'E	1450	1772–1999	1790	15	30	1.05±0.46	0.420±0.123	Gutiérrez *et al.**
5	42°33'N	0°54'E	1888	1747–1995	1780	17	36	1.28±0.58	0.387±0.127	Andreu *et al.* (2007)
6	42°28'N	0°29'E	1540	1786–1999	1820	16	32	1.80±0.58	0.413±0.119	Andreu *et al.* (2007)
7	42°20'N	1°40'E	1585	1921–1999	1945	18	36	2.11±0.57	0.722±0.073	Gutiérrez *et al.**
8	42°19'N	0°26'W	1450	1830–1999	1855	16	32	1.74±0.63	0.413±0.128	Andreu *et al.* (2007)
9	41°58'N	2°49'W	1750	1612–1999	1785	16	32	1.45±0.50	0.329±0.112	Andreu *et al.* (2007)
10	41°20'N	1°01'E	950	1861–1999	1875	11	22	1.54±0.43	0.457±0.135	Andreu *et al.* (2007)
11	40°50'N	4°02'W	1864	1818–2011	1830	35	81	1.27±0.24	0.317±0.102	Génova (2000), extended with Touchan *et al.* (2013)
12	40°48'N	0°21'E	1250	1797–2000	1815	15	30	1.09±0.31	0.353±0.115	Andreu *et al.* (2007)
13	40°44'N	4°06'W	1500	1763–1991	1890	9	18	1.64±0.26	0.360±0.082	Génova (2000)
14	40°25'N	1°43'W	1860	1791–2006	1815	20	40	0.95±0.29	0.327±0.115	Camarero *et al.**
15	40°21'N	5°06'W	1550	1805–2011	1830	30	65	2.22±0.66	0.296±0.122	Génova*
16	40°20'N	0°43'W	1510	1835–2006	1865	15	29	1.43±0.37	0.460±0.112	Camarero *et al.**
17	40°03'N	0°59'W	1865	1774–2006	1810	16	32	1.63±0.46	0.510±0.122	Camarero *et al.**
18	37°23'N	2°52'W	2050	1584–2002	1615	19	62	1.15±0.37	0.460±0.116	Gutiérrez *et al.**
19	37°12'N	3°10'W	1966	1828–2009	1890	18	23	0.23±0.09	0.345±0.155	Sánchez-Salguero *et al.* (2015)
20	37°04'N	3°27'W	2000	1875–1999	1895	15	30	2.61±0.61	0.547±0.142	Gutiérrez *et al.**

*Data available from authors

Table S3.2. Description of the variance-covariance (VCOV) structures used for modelling synchrony patterns for the study period (1890–2009) according to the assignment of chronologies to pre-defined groups.

	VCOV structures and interpretation	Covariance structure	Variances	Covariances	Correlations	Residual variance
S_1	Homogeneity of year variances and covariances across groups	Compound symmetry	Homogeneous	Homogeneous	Homogeneous*	Homoscedastic / Heteroscedastic
S_2	Different variances but equal year correlation between all group pairs[2]	Heterogeneous compound symmetry	Heterogeneous	Heterogeneous	Homogeneous†	Homoscedastic / Heteroscedastic
S_3	One multiplicative term that approximates the full VCOV structure as in S_4	Factor analytic	Heterogeneous	Heterogeneous	Heterogeneous	Homoscedastic / Heteroscedastic
S_4	Full model (different variances and covariances). All causes of year × group interaction are allowed	Unstructured	Heterogeneous	Heterogeneous	Heterogeneous	Homoscedastic / Heteroscedastic
S_5	Narrow evaluation. Lack of common signal between groups	Banded main diagonal	Heterogeneous	Zero	Zero	Homoscedastic / Heteroscedastic
S_6	Null model. Broad evaluation ignoring groups	None	Single	–	–	Homoscedastic

*if homoscedastic residual variance; † if null residual variance

Table S3.3. Selection of variance-covariance (VCOV) structures for modelling synchrony patterns for the study period (1890–2009). Chronologies are grouped according to membership to (1) a particular region (central Siberia or Spain, left column) or (2) a particular species within a given region (central and right columns). The table lists the best VCOV model for each time period as suggested by Akaike and Bayesian information criteria. Nr refers to the number of VCOV parameters for the model of choice.

	Model of choice		Model of choice		Model of choice	
Period	***Region***	**Nr**	***Central Siberia (by species)***	**Nr**	***Spain (by species)***	**Nr**
1890–1919	Narrow evaluation	4	Unstructured	9	Compound symmetry	5
1895–1924	"	4	Factor-analytic	7	"	5
1900–1929	"	4	Unstructured	9	"	5
1905–1934	"	4	"	9	"	5
1910–1939	"	4	"	9	"	5
1915–1944	"	4	"	9	"	5
1920–1949	"	4	"	9	"	5
1925–1954	"	4	"	9	Factor-analytic	7
1930–1959	"	4	Factor-analytic	7	"	7
1935–1964	"	4	"	7	"	7
1940–1969	"	4	"	7	"	7
1945–1974	"	4	"	7	"	7
1950–1979	"	4	"	7	Heter. compound symmetry	7
1955–1984	"	4	"	7	"	7
1960–1989	"	4	"	7	"	7
1965–1994	"	4	"	7	"	7
1970–1999	"	4	"	7	"	7
1975–2004	"	4	Compound symmetry	5	"	7
1980–2009	"	4	"	5	"	7

Supplementary figures

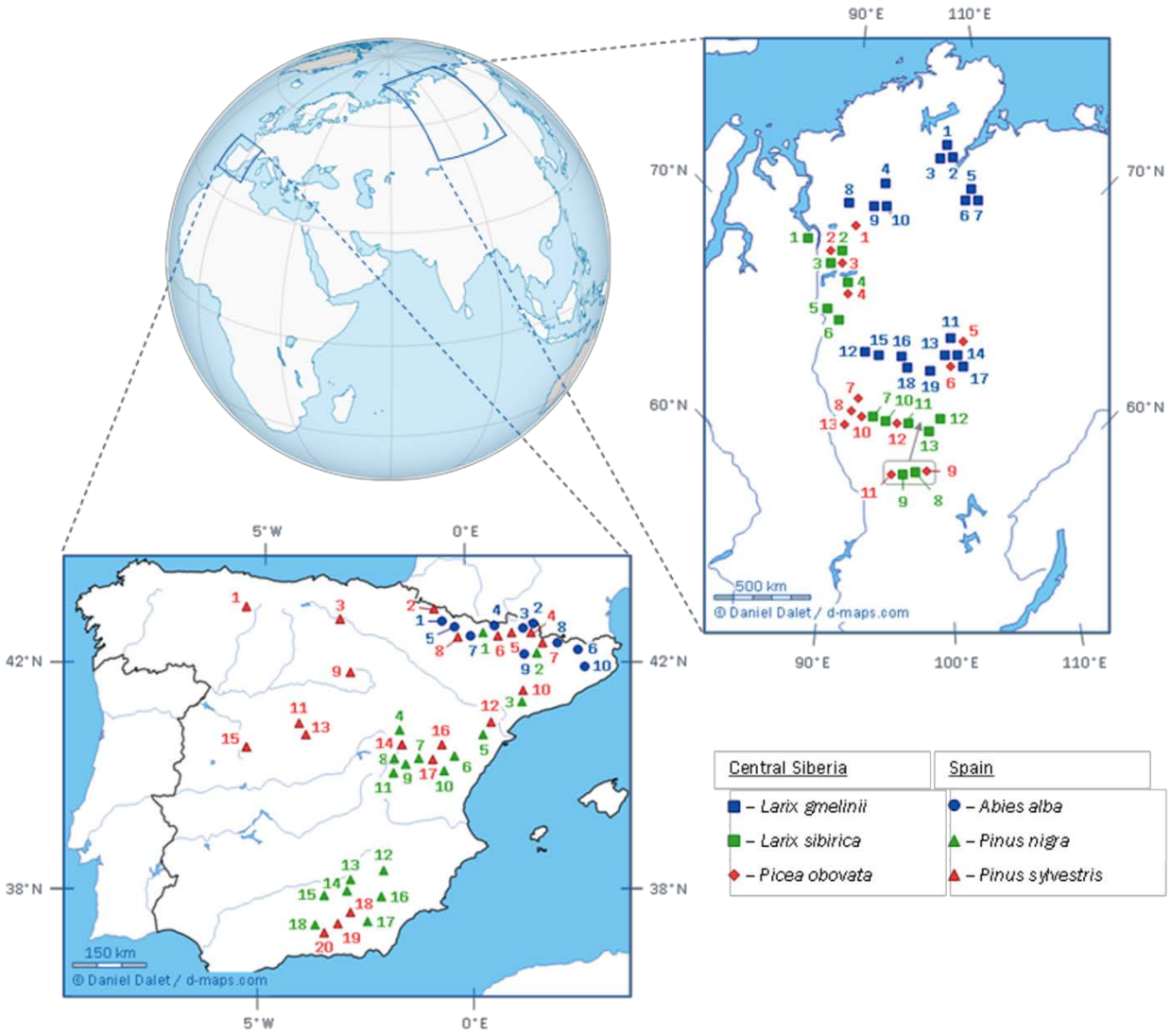

Figure S3.1. Site locations in central Siberia (Russia) and Spain. Genus symbols are as follows: circle, *Abies*; square, *Larix*; diamond, *Picea*; triangle, *Pinus*. See Table S3.1 for specific details on study sites and tree-ring width chronologies.

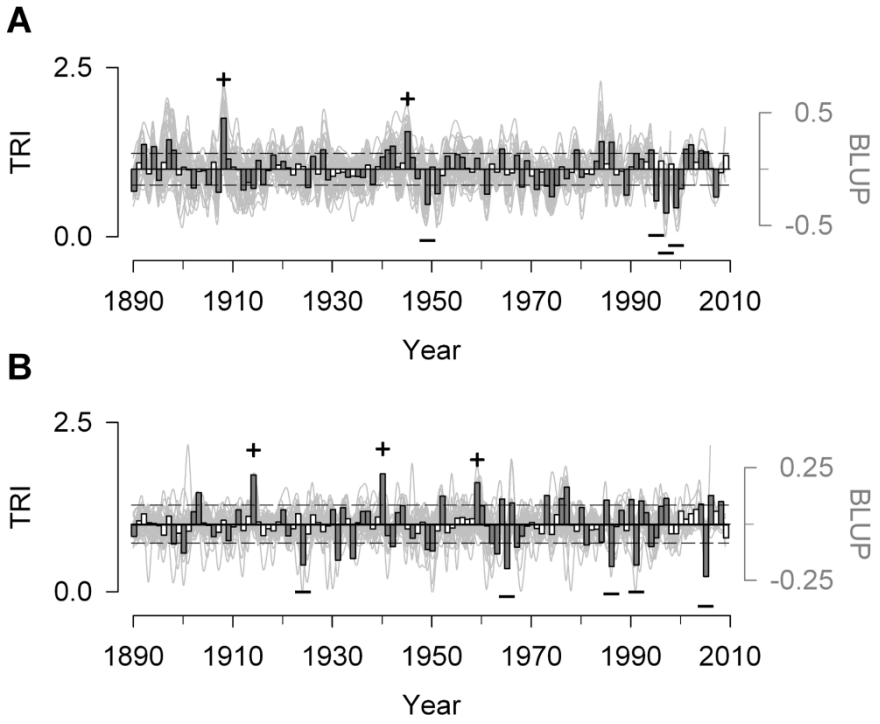

Figure S3.2. Regional master tree-ring chronologies for central Siberia *(A)* and Spain **(*B*)**. Variability of tree-ring width indices (TRI) for each site chronology (grey lines) and of regional master chronologies (bars) are presented over the period 1890–2009. The regional master chronologies were derived as best linear unbiased predictors (BLUPs) of tree-ring indices estimated from the best variance-covariance model for the study period (i.e., narrow evaluation model) using a regional classification as grouping criterion (see Table S3.3). Filled bars denote significant BLUPs according to Student-*t* testing of null BLUP effects ($P < 0.05$). Horizontal dashed lines indicate ±1SD. *Plus* and *minus* signs indicate years of extreme positive (+1.96SD) and negative (–1.96SD) growth estimates, respectively.

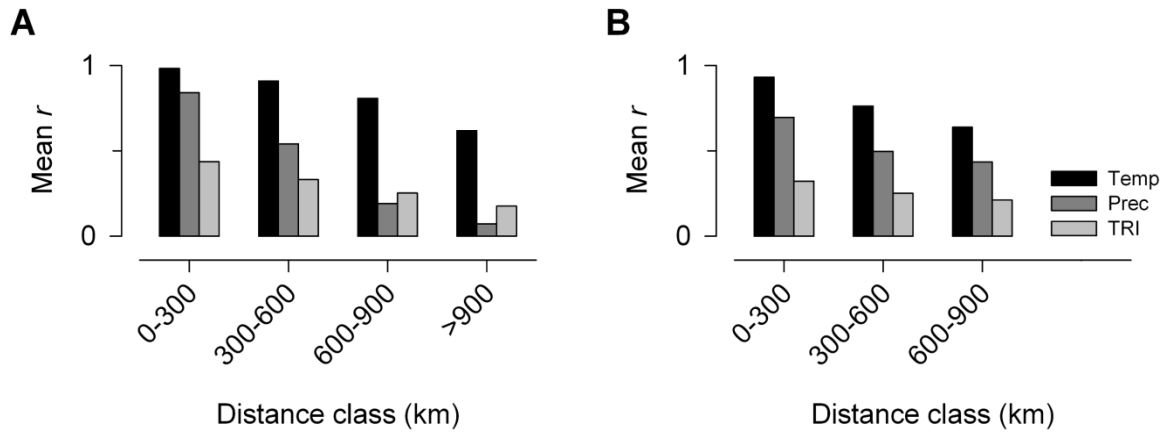

Figure S3.3. Spatial structure (modified correlograms) of synchrony in climate and forest growth for central Siberia **(*A*)** and Spain **(*B*)**. The spatial autocorrelation in mean annual temperature (Temp), annual precipitation (Prec) and tree-ring width indices (TRI) was obtained from pairwise correlations (*r* values) between all sites (chronologies) within each region for the common period 1930–2009. The correlations were divided into four distance classes (0 to 300 km, 300 to 600 km, 600 to 900 km, and >900 km). Mean *r* values and their statistical significance (*P*) within each distance class were estimated from 1,000 randomizations. Significant correlation coefficients ($P < 0.05$) are indicated by filled bars.

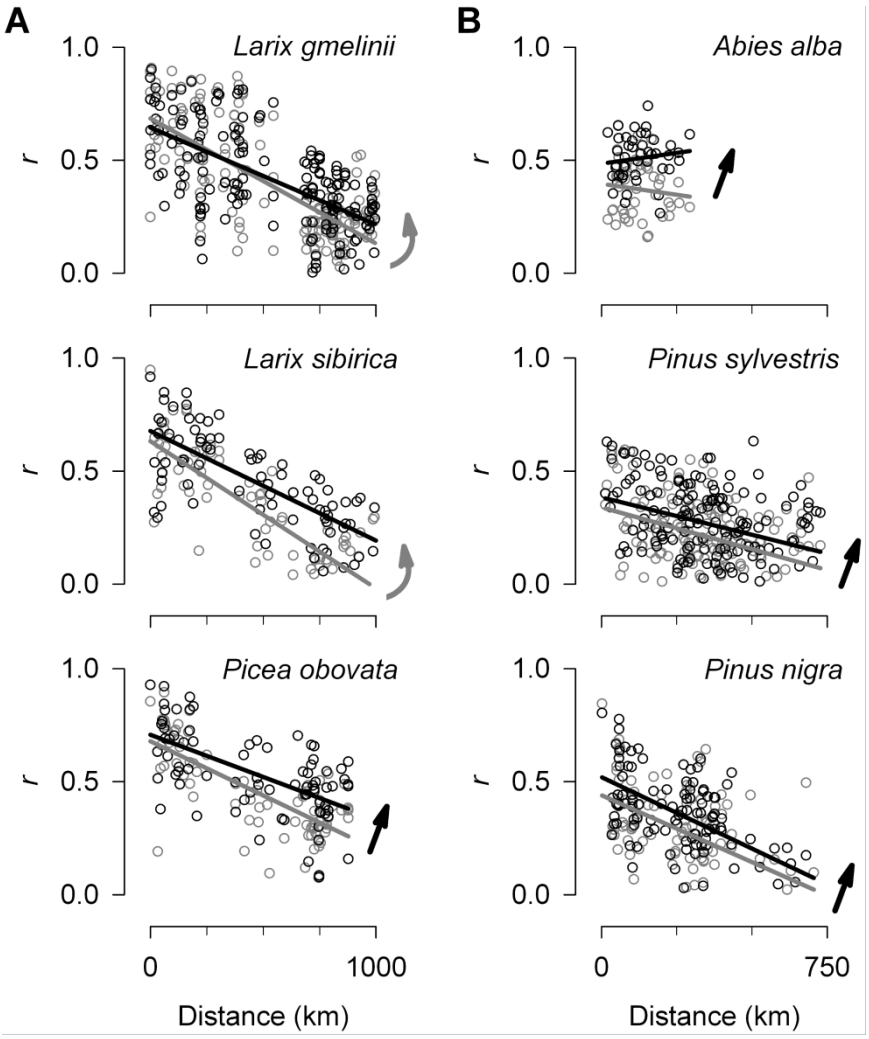

Figure S3.4. Synchrony patterns as a function of distance at the species level in central Siberia **(*A*)** and Spain **(*B*)**. The patterns are characterized as linear regressions of correlation coefficients (*r* values) for pairs of chronologies (*y*-axes) on their corresponding distance (*x*-axes) from1890 to 1949 (grey line) and from 1950 to 2009 (black line). Significant differences in slopes ($P < 0.05$; grey arrows) are found for deciduous conifers in Siberia (*Larix* spp.), whereas significant differences in mean $\hat{a}_C$ values ($P < 0.05$; black arrows) are found for evergreen conifers (*Abies*, *Pinus* and *Picea* spp).

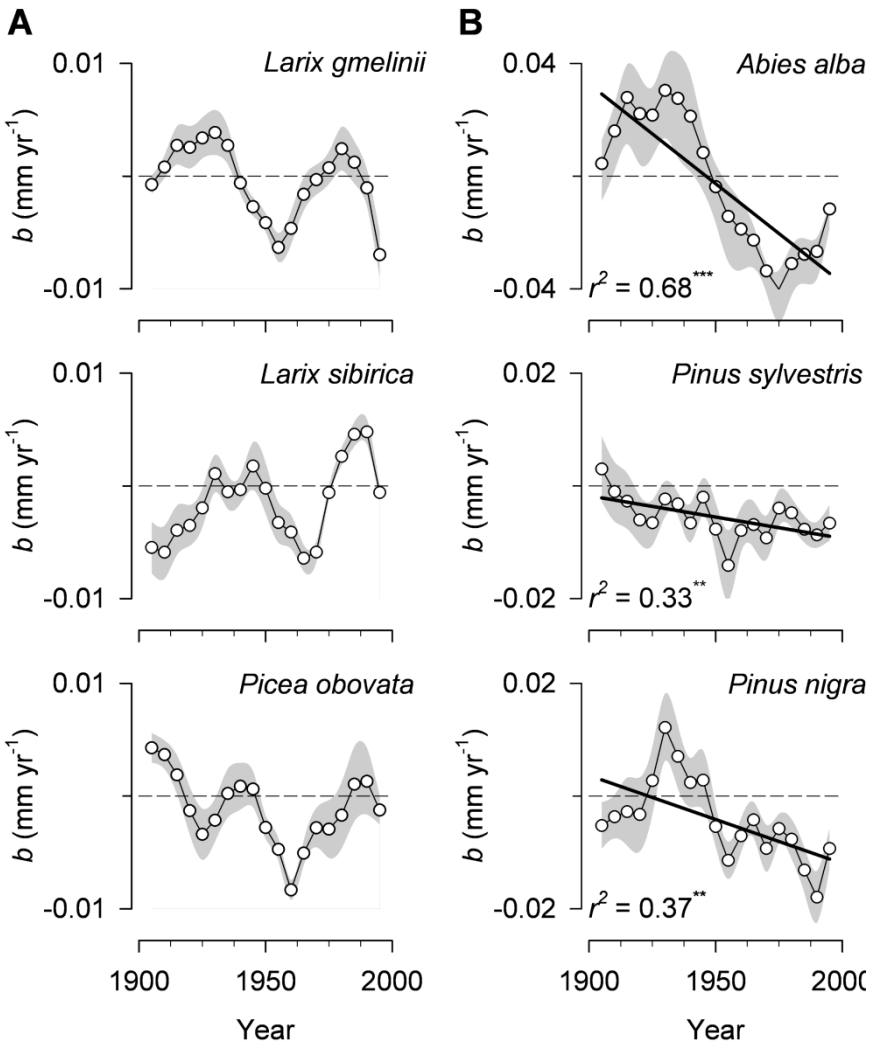

Figure S3.5. Changes in radial growth over time at the species level. Temporal trends in the slope (*b*) of absolute ring-width values are calculated for successive 30-year periods lagged by five years in central Siberia **(*A*)** and Spain **(*B*)**. The estimated rate of growth changes for each period is based on raw (i.e., non-standardised) tree-ring width data as the mean slope value of every chronology of the same species. Standard errors are shown as shaded areas. Significant linear regressions are indicated with black lines. Displayed years in the *x*-axes correspond to the middle year of 30-year moving intervals. Note the change of scale in the *y*-axes between regions and species.

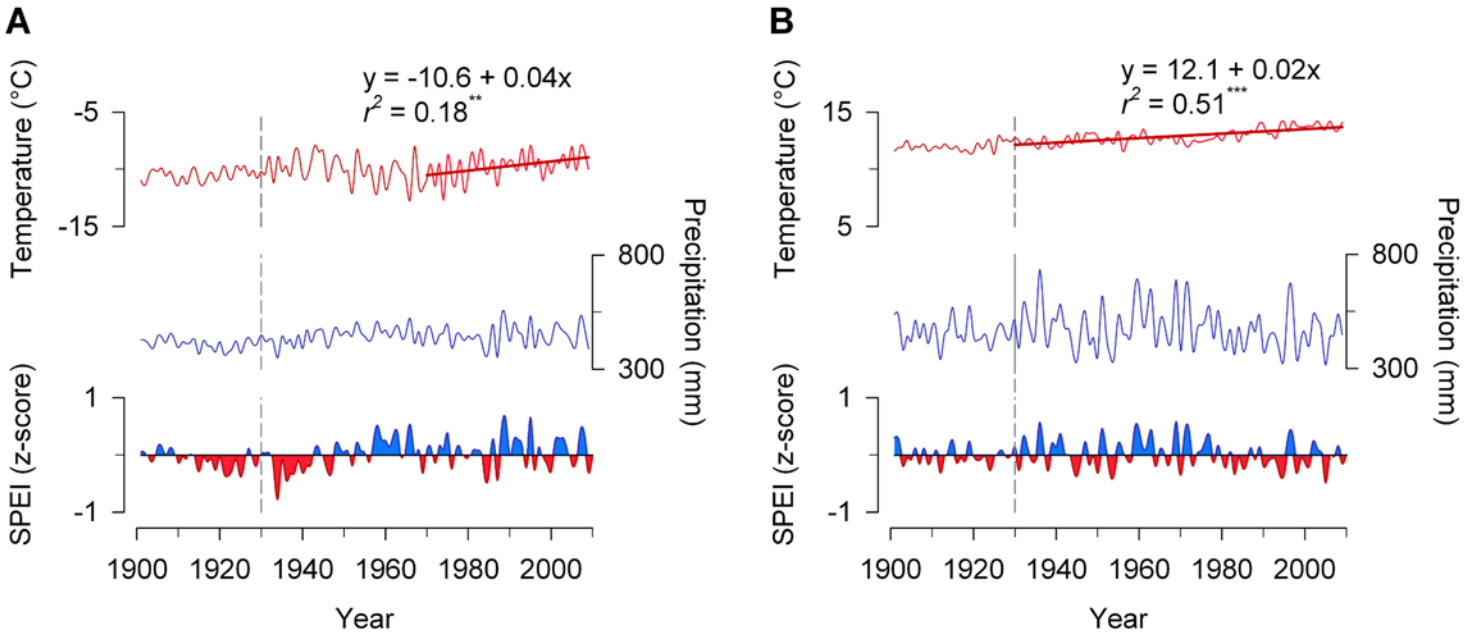

Figure S3.6. Regional climate trends for central Siberia (*A*) and Spain (*B*). From top to bottom, mean temperature, precipitation and SPEI (Standardised Precipitation-Evapotranspiration Index) are obtained as average values of the gridded CRU TS3.10 data set with spatial resolution (0.5° × 0.5°) for each region. The vertical dashed lines indicate the starting year with reliable regional climate records. Significant linear trends ($P < 0.05$) of mean temperature are shown for relevant periods (1970–2009 in Siberia, 1930–2009 in Spain).

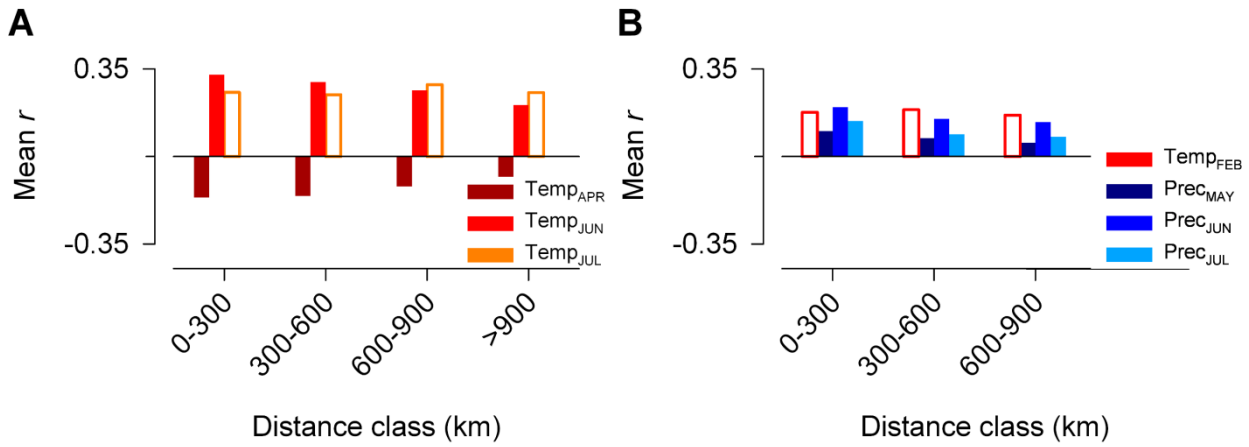

Figure S3.7. Spatial structure of significant growth-climate relationships for central Siberia **(*A*)** and Spain **(*B*)**. Mean spatial cross-correlations between relevant monthly climate factors for growth (see Fig. 3.3) and tree-ring width indices (TRI) were calculated as pairwise correlations (*r* values) between TRI and the corresponding climate factor for all sites within each region for the common period 1930–2009. The cross-correlations were divided into four distance classes (0 to 300 km, 300 to 600 km, 600 to 900 km, and >900 km). Mean cross-correlation *r* values and their statistical significance (*P*) within each distance class were estimated from 1,000 randomizations. Significant correlation coefficients ($P < 0.05$) are indicated by filled bars.

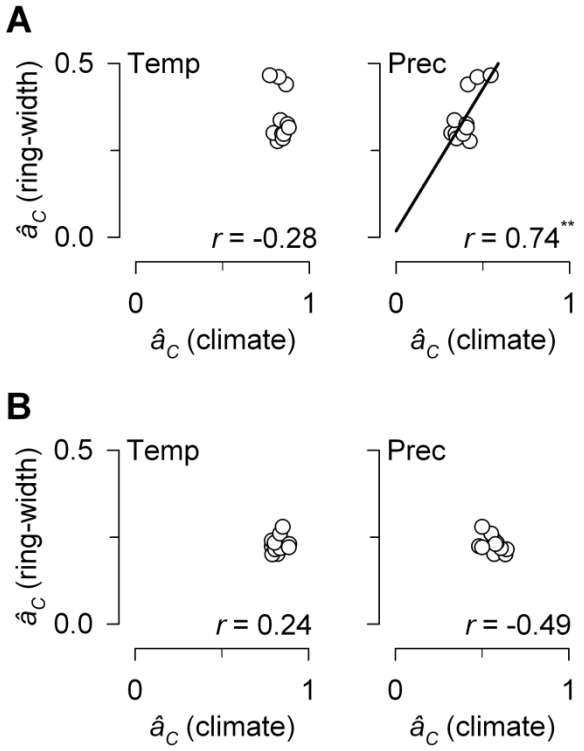

Figure S3.8. Relationships between temporal changes in spatial synchrony in climate factors and forest growth for central Siberia **(*A*)** and Spain **(*B*)**. The spatial synchrony ($\hat{a}_C$) is estimated for mean annual temperature (Temp), annual precipitation (Prec) and indexed ring-width chronologies for successive 30-year periods lagged by five years. Note that only precipitation in Siberia is significantly correlated to $\hat{a}_C$ of growth ($^{**}P < 0.01$).

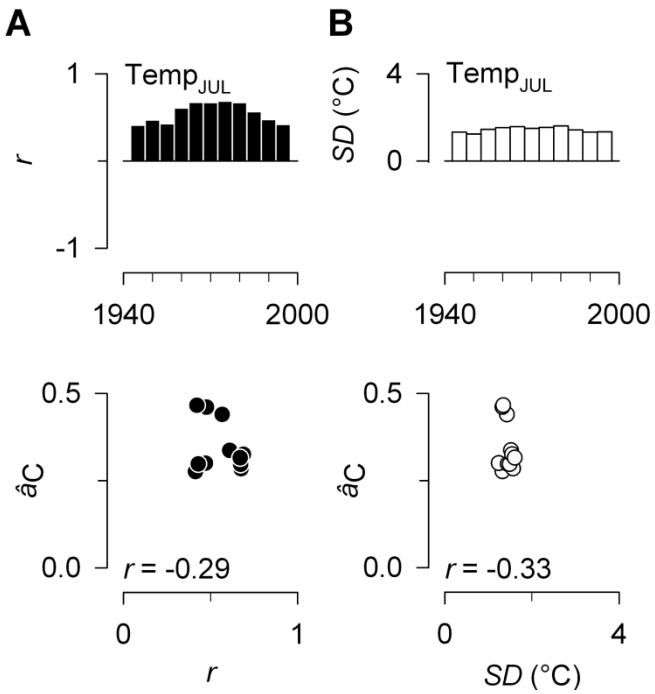

Figure S3.9. Climate factors underlying synchrony changes in central Siberia (1930-2009). Moving correlation analyses (*r* values) between the regional chronology and ***(A)*** July mean temperature (Temp) and **(*B*)** standard deviates (SD) of July mean temperatures are displayed in bar diagrams for successive 30-year periods lagged by five years (*upper panel*). Significant correlations are indicated by filled bars in (*A*) ($P < 0.05$). Relationships between synchrony estimates ($\hat{a}_C$) and *r* values of the relationship between BLUP-derived tree-ring indices and mean temperature or SD of mean temperature for July are presented in scatterplots (*lower panel*). The filled circles correspond to the periods with significant growth-climate relationships as indicated by moving correlation analyses in the upper panels. Only months showing a significant association with BLUP-derived tree-ring indices over the study period (Fig. 3.3) are examined; significant climate factors related to synchrony patterns are displayed in Fig. 3.4. Displayed years in the *x*-axes correspond to the middle year of 30-year moving intervals.

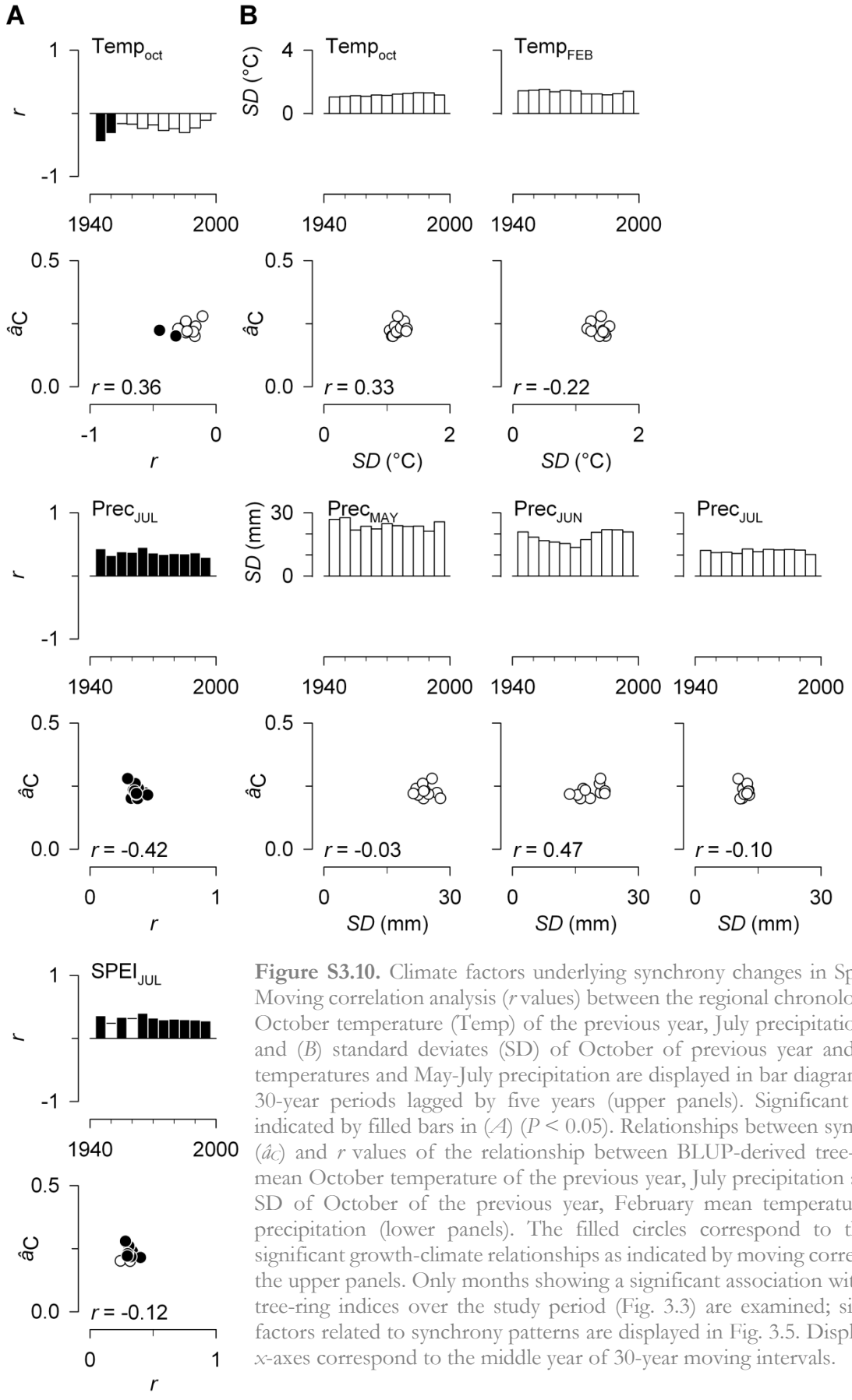

Figure S3.10. Climate factors underlying synchrony changes in Spain (1930-2009). Moving correlation analysis (*r* values) between the regional chronology and (*A*) mean October temperature (Temp) of the previous year, July precipitation and July SPEI and (*B*) standard deviates (SD) of October of previous year and February mean temperatures and May-July precipitation are displayed in bar diagrams for successive 30-year periods lagged by five years (upper panels). Significant correlations are indicated by filled bars in (*A*) ($P < 0.05$). Relationships between synchrony estimates ($\hat{a}_C$) and *r* values of the relationship between BLUP-derived tree-ring indices and mean October temperature of the previous year, July precipitation and July SPEI or SD of October of the previous year, February mean temperature and May-July precipitation (lower panels). The filled circles correspond to the periods with significant growth-climate relationships as indicated by moving correlation analyses in the upper panels. Only months showing a significant association with BLUP-derived tree-ring indices over the study period (Fig. 3.3) are examined; significant climate factors related to synchrony patterns are displayed in Fig. 3.5. Displayed years in the *x*-axes correspond to the middle year of 30-year moving intervals.

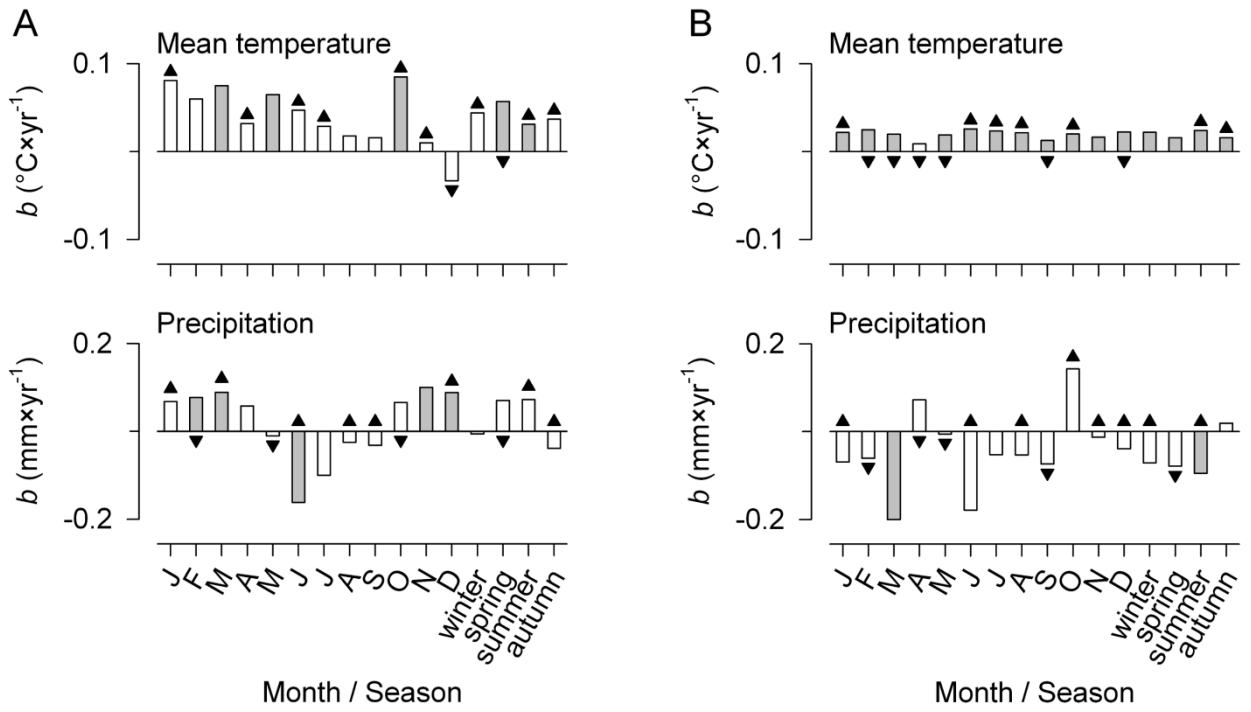

Figure S3.11. Summary of regional temporal trends in monthly and seasonal climatic data for central Siberia **(*A*)** and Spain **(*B*)**. Mean temperature and precipitation are obtained as average values of the gridded CRU TS3.10 data set with spatial resolution (0.5° × 0.5°) for each region. Bars represent the slopes of linear regressions of climate factors as a function of time estimated for relevant periods (1970–2009 in Siberia, 1930–2009 in Spain in accordance with Fig. 3.6). Filled bars indicate significant linear trends over time ($P < 0.05$). Triangles identify months with significant linear trends in climate variability (standard deviates of climate factors) estimated for the period 1930–2009 (upward triangles denote positive trends, downward triangles negative trends).

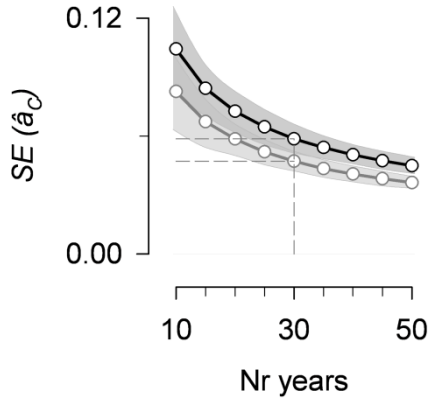

Figure S3.12. Precision of synchrony ($\hat{a}_C$) values (standard error of the mean, SE) as a function of considered number of years for central Siberia (black line) and Spain (grey line). The shaded areas indicate standard deviations of SE values estimated for every interval across the study period (1890–2009). The dashed lines indicate the inflection points of the curves and denote a balance between number of years in each time period and precision of synchrony estimates.

CHAPTER 4

Increasing drought effects on five European pines modulate $\Delta^{13}C$-growth coupling along a Mediterranean altitudinal gradient

Submitted to *Functional Ecology* (May 2016)

Increasing drought effects on five European pines modulate $\Delta^{13}C$-growth coupling along a Mediterranean altitudinal gradient

Shestakova TA, Camarero JJ, Ferrio JP, Knorre AA, Gutiérrez E, Voltas J

Submitted to *Functional Ecology* (May 2016)

Abstract

Climate warming increases the risk of regional forest vulnerability, especially in drought-constrained ecosystems. However, we still lack knowledge on the ecophysiological responses of coexisting tree species and their ability to cope with the ongoing temperature rise. This work investigated spatiotemporal patterns of climate sensitivity in five pines (*Pinus halepensis*, *P. nigra*, *P. pinaster*, *P. sylvestris* and *P. uncinata*) along an altitudinal gradient of *ca.* 1,000 m (1,090–2,010 m a.s.l.) in the eastern Iberian Peninsula. This gradient offers an exceptional opportunity to test for climate change impacts on Mediterranean forests as the most widely distributed European pines coexist at different elevations. We used long-term tree ring-width (TRW) records to assess changes in the temporal coherence of radial growth over three elevation belts (spatial synchrony). In combination with carbon isotope discrimination ($\Delta^{13}C$), we also examined the extent to which radial growth is adjusted to leaf-level gas exchange processes under varying degrees of water stress along the gradient. Finally, we studied shifts in climate sensitivity for both traits (TRW and $\Delta^{13}C$) in response to an amplified regional drought stress. We found that increasing drought stress in the region prompted more synchronous growth between low- and mid-elevation sites and more consistent physiological reactions across species, as tree growth at mid elevations became progressively more dependent on leaf-level gas exchange processes (inferred from $\Delta^{13}C$), hence resembling low-elevation stands. In contrast, high-elevation pinewoods showed a recent and sudden uncoupling between ring-width and $\Delta^{13}C$ likely triggered by a winter drought event. Growth-climate analyses highlighted the major role of the elevation-induced thermal gradient in growth responsiveness to climate. However, coherent shifts in vegetative activity towards more favourable periods (spring) were found along the gradient. Thus, our results indicate that warming-induced drought stress is spreading upwards in altitude in Mediterranean pinewoods because of an intensified climate influence on leaf-level ecophysiological processes controlling tree growth and overriding taxonomic imprints and local drivers. However, the high-elevation belt exhibited a diverging reaction to warming, which highlights the complexities of drought effects on Mediterranean forests.

Introduction

Understanding climate influences on forest ecosystems is crucial in a global warming context, especially in vulnerable areas such as the Mediterranean Basin (IPCC 2013). In this region, the increase in frequency and duration of drought and heat stress has caused widespread tree growth decline, reducing productivity and inducing forest die-off both at dry (e.g., Sarris *et al.* 2007) and mesic sites (e.g., Jump *et al.* 2006). Recent studies indicate that such forest responses to warming produce more coherent temporal growth patterns over large areas (i.e., spatial synchrony; Shestakova *et al.* 2016), which could be symptomatic of increasing risk of regional forest deterioration (Dorman *et al.* 2015).

In lowland Mediterranean ecosystems, forest growth is primarily constrained by water availability (e.g., del Castillo *et al.* 2015). In Mediterranean mountain forests, however, trees are subjected to varying degrees of water stress depending on their position along altitudinal gradients and the modulation exerted by topography-controlled variation in temperature and soil moisture (Bunn *et al.* 2005). This leads to distinct growth-climate associations depending on whether drought or low temperature is the predominant factor controlling tree performance (Sánchez-Salguero *et al.* 2015). Thus, unravelling growth responses to climate along altitudinal gradients may provide valuable clues on how forests will respond to future climate.

A key assumption in dendrochronology is that growth-climate relationships are stable over time so that temporal patterns in radial growth reliably reflect site climate variation (Hughes *et al.* 2009). However, this assumption has been challenged based on how trees are reacting to warming (e.g., DeSoto *et al.* 2012). For instance, higher temperatures alter seasonal growth patterns by increasing drought and heat stress and rising evapotranspiration. This effect has modified growth-climate associations as observed for Iberian pinewoods (Andreu *et al.* 2007).

While most studies rely on radial growth to assess climate change effects on long-term tree performance, additional information on physiological responses can be gained through the analysis of stable isotopes in tree rings (McCarroll & Loader 2004). Particularly, the ratio of the heavy to light carbon isotopes ($^{13}C/^{12}C$) depends on factors affecting CO_2 uptake, being mainly controlled by photosynthetic rate (A) and stomatal conductance (g_s), as expressed in the ratio A/g_s (intrinsic water-use efficiency; Farquhar *et al.* 1989). Changes in gas exchange are recorded in annual rings through carbon isotope discrimination ($\Delta^{13}C$), which gives insight into how trees respond to drought stress (e.g., Saurer *et al.* 2014; Shestakova *et al.* 2014). The combined analysis of ring-width and $\Delta^{13}C$ may improve our understanding of forest growth dynamics underlying biogeographical interactions by providing information on spatial response patterns to climate instability (Voelker *et al.* 2014).

Despite the available wealth in dendroecological archives, we still lack knowledge on the response of coexisting species to ongoing climate change (Lindner *et al.* 2010). However, there are indications for regionally coherent multispecies responses to climate, as imprinted in

tree rings (e.g., Wettstein *et al.* 2011; Shestakova *et al.* 2016). This is especially true for regions where growth is mainly constrained by few climate factors as for circum-Mediterranean forests, which are affected by water shortage (Galván *et al.* 2015). Here, we analyse the response patterns to climate of five widely distributed European pines (*Pinus halepensis*, *P. nigra*, *P. pinaster*, *P. sylvestris* and *P. uncinata*) along an altitudinal gradient of *ca.* 1,000 m in the Gúdar range (eastern Spain). This small area (*ca.* 250 km^2) offers a unique opportunity to test for global change effects on Mediterranean forests as most Iberian pines coexist at different elevations. Besides, *P. sylvestris* and *P. uncinata* are near and at its southernmost distribution limit in Europe, respectively. We hypothesize that increased regional drought stress is homogenizing climate responses in trees, superimposing on species-specific and local drivers of performance, hence resulting in more synchronous growth across species and elevations. Through the combined analysis of ring-width and $\Delta^{13}C$ variability, we also address the extent to which radial growth depends on leaf-level gas exchange processes along this altitudinal gradient and how this dependence is changing as climate becomes warmer and drier.

Materials & methods

Study area and field sampling

The study was performed in natural mixed-pine forest stands located in Gúdar, Iberian System, eastern Spain (Fig. 4.1). The area is characterized by a continental Mediterranean climate with two precipitation maxima in spring and autumn. Mean annual precipitation is 636 mm (summer precipitation ≈ 100 mm) and mean annual temperature is +8.3°C, with January being the coldest (+0.9°C) and July the warmest month (+17.9°C), respectively (period 1950–2011, European high-resolution climate dataset, E-OBS; Haylock *et al.* 2008). However, climate conditions vary with altitude, ranging from relatively warm, drought-prone environments at low elevations to cold and humid sites upwards (*SI Appendix*, Fig. S4.1). Soils are mainly basic, and clayey or loamy textured.

Sampling sites spread along an altitudinal gradient ranging from 1,090 m up to 2,020 m a.s.l. (highest point in the Gúdar range). The estimated range of variation between low- and high-elevation sites was 5.6°C (4.9–10.5°C) for mean annual temperature and 439 mm (465–904 mm) for annual precipitation (*SI Appendix*, section 1). Although regional forests have been exposed to intensive land-use and management practices (e.g., logging, grazing) before the mid-twentieth century, the study sites did not show visible human or natural disturbances (e.g., stumps, fire scars). Altogether, five co-occurring pine species dominating different elevation belts were sampled: two Eurosiberian species (*P. sylvestris* L. and *P. uncinata* Ram.) and three Mediterranean species (*P. halepensis* Mill., *P. nigra* Arn. subsp. *salzmannii* (Dunal) Franco, and *P. pinaster* Ait.) (Fig. 4.1, Table 4.1). *P. halepensis* and *P. pinaster* are only present at low elevations (up to 1,200 m a.s.l.), and are, thus, subjected to prolonged summer drought. In contrast, *P. sylvestris* and *P. uncinata* are found above 1,500 m and 1,800 m a.s.l., respectively,

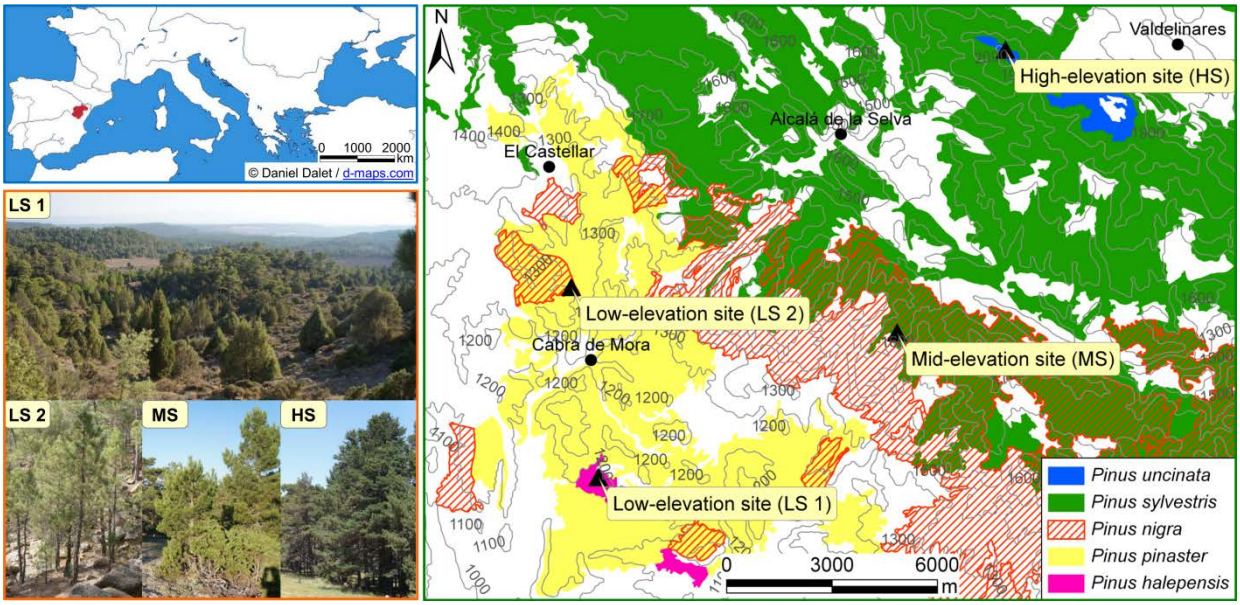

Figure 4.1. Location of the study area (top left) and topography and distribution of pine stands in the Gúdar mountain range (right). Photographs (centre left, down left) show the stand conditions at each sampling site.

in cold environments with a relatively short, dry summer. In turn, *P. nigra* is distributed in sub-Mediterranean transitional areas (1,100–1,600 m a.s.l.), forming mixed stands with *P. pinaster* and *P. sylvestris* at low and mid elevations, respectively.

Field work was done in summer 2012 following stratified sampling according to the distribution range of each species (Fig. 4.1). Altogether, four pine stands corresponding to the three altitudinal belts (low ≈ 1,100 m a.s.l., mid = 1,615 m a.s.l. and high = 2,020 m a.s.l.) were sampled with the following species representation: *P. halepensis* (low-elevation site 1), *P. pinaster* and *P. nigra* (low-elevation site 2), *P. nigra* and *P. sylvestris* (mid-elevation site), and *P. sylvestris* and *P. uncinata* (high-elevation site) (for details see Table 4.1). Twenty mature, dominant and healthy trees were randomly selected per site and species and their size was measured (diameter at breast height and total height). Two cores were extracted at 1.30 m from cross-slope sides of the trunk whenever possible using a 5-mm diameter increment borer. These samples were complemented with data compiled from a previous study (Camarero *et al.* 2015) in which the same forest stands were sampled in summer 2006 following the same sampling protocol. A total of 518 increment cores from 259 living pines were collected along the gradient. Both cores collected in 2006, together with one core collected in 2012, were used for ring dating, while the second core sampled in 2012 was kept intact for isotope analysis.

Table 4.1. Geographical and topographic characteristics of the sampling sites.

Latitude (N)	Longitude (W)	Elevation (m)	Aspect	Geological substrate	Sampled species	Other woody species*
High-elevation site (HS)						
40º23'30"	0º39'50"	2020	N-NE	Limestones	*P. sylvestris, P. uncinata*	*Jc, Js, Ra*
Mid-elevation site (MS)						
40º19'19"	0º42'08"	1615	SE	Limestones	*P. nigra, P. sylvestris*	*Jc, Jt, Bv, Qi, Ao*
Low-elevation sites (LS)						
(1) 40º17'17"	0º48'03"	1095	S-SW	Limestones	*P. halepensis*	*Pp, Gs, Jp, Qi*
(2) 40º19'45"	0º48'26"	1090	E	Sandstones	*P. nigra, P. pinaster*	*Qf, Qi, Jo, Jp*

*Species' codes: *Ao*, *Amelanchier ovalis*; *Bv*, *Berberis vulgaris*; *Gs*, *Genista scorpius*; *Jc*, *Juniperus communis*; *Jo*, *J. oxycedrus*; *Jp*, *J. phoenicea*; *Js*, *J. sabina*; *Jt*, *J. thurifera*; *Pp*, *Pinus pinaster*; *Qf*, *Quercus faginea*; *Qi*, *Q. ilex*; Ra, *Rhamnus alpina.*

Sample preparation and ring-width measurements

For tree-ring dating, samples were oven-dried at 60°C for 48 h and sanded until tree rings were clearly visible under a binocular microscope. Tree rings were visually cross-dated and measured with precision of 0.001 mm using a Lintab system (Fig. S4.2a). Cross-dating was verified with the COFECHA program (Holmes 1983). A few tree-ring series (<5%) could not be properly cross-dated and were discarded. Tree-ring series were then used to build residual tree ring-width (TRW) chronologies for each site and species (*SI Appendix*, Fig. S4.2b). The study period was 1903–2011 (period with *EPS* > 0.85, except for *P. halepensis*) (Table 4.2; *SI Appendix*, section 2).

Carbon isotope analysis

The five best cross-dated trees per site and species sampled in 2012 were selected for isotope measurements. Tree rings were split with annual resolution for the period 1950–2011, which was considered a reliable common time span for all tree-ring chronologies (i.e., excluding at least the first 30 years to avoid juvenile effects on carbon isotopes; Table 4.2). Rings corresponding to the same year were pooled into a single sample before analysis. Every ten years (1951, 1961, etc.), tree rings were analysed individually to estimate between-tree variability in isotope signal. The resulting samples were homogenized to a fine powder with a ball mill (Retsch MM301, Haan, Germany). Then, 0.30–0.40 mg of dry wood material was weighed into tin foil capsules and combusted to CO_2 using a Flash EA-1112 elemental analyser interfaced with a Finnigan MAT Delta isotope ratio mass spectrometer (Thermo Fisher Scientific Inc., MA, USA). Stable isotope ratios were expressed as per mil deviations

Table 4.2. Structural and dendrochronological characteristics of the sampled sites. Abbreviations: DBH, diameter at breast height (1.30 m); *EPS*, Expressed Population Signal; TRW, tree-ring width; $\Delta^{13}C$, carbon isotope discrimination; *Rbar*, mean interseries correlation. The variability of mean values is expressed as standard error (± SE). *EPS* and *Rbar* values for $\Delta^{13}C$ chronologies are calculated using a limited number of years (seven) in which individual tree rings were analysed.

									TRW (1950–2011)		$\Delta^{13}C$ (1950–2011)		
Tree species	**Code**	**Basal area (m^2 ha^{-1})**	**DBH (cm)**	**Height (m)**	**No. trees (cores)**	**Age (years)**	**Time span**	**EPS > 0.85 since**	**Mean (mm)**	***Rbar***	**EPS**	**Mean (‰)**	***Rbar***
High-elevation site (HS)													
P. sylvestris	Ps_{HS}	36.6	43.6 ± 2.0	9.3 ± 0.5	51 (71)	116 ± 10	1609–2011	1866	1.12 ± 0.09	0.41	0.82	17.31 ± 0.22	0.48
P. uncinata	Pu_{HS}	36.6	39.8 ± 1.7	10.4 ± 0.3	40 (51)	100 ± 5	1758–2011	1903	1.31 ± 0.09	0.45	0.74	17.30 ± 0.21	0.36
Mid-elevation site (MS)													
P. nigra	Pn_{MS}	38.0	46.6 ± 2.7	9.9 ± 0.5	30 (39)	131 ± 5	1815–2011	1861	0.77 ± 0.05	0.58	0.82	17.23 ± 0.20	0.47
P. sylvestris	Ps_{MS}	38.0	41.0 ± 2.0	10.5 ± 1.0	31 (40)	114 ± 8	1770–2011	1880	1.11 ± 0.12	0.53	0.81	16.44 ± 0.24	0.45
Low-elevation sites (LS)													
P. nigra	Pn_{LS}	28.0	35.6 ± 1.4	10.0 ± 0.4	37 (54)	112 ± 6	1796–2011	1868	0.93 ± 0.13	0.60	0.81	17.25 ± 0.24	0.46
P. pinaster	Pp_{LS}	28.0	38.8 ± 2.7	10.1 ± 0.5	33 (49)	89 ± 3	1887–2011	1902	1.09 ± 0.14	0.67	0.75	16.97 ± 0.25	0.37
P. halepensis	Ph_{LS}	8.2	40.0 ± 2.7	8.6 ± 0.8	32 (48)	75 ± 3	1894–2011	1915	1.68 ± 0.09	0.67	0.94	16.85 ± 0.34	0.76

using the δ notation relative to Vienna Pee Dee Belemnite (VPDB). The accuracy of the analyses (SD of working standards) was 0.06‰.

To account for changes in $\delta^{13}C$ of atmospheric CO_2 ($\delta^{13}C_{air}$), we calculated carbon isotope discrimination ($\Delta^{13}C$) from $\delta^{13}C_{air}$ and wood $\delta^{13}C$ ($\delta^{13}C$) (Fig. S4.3a) following Farquhar *et al.* (1989):

$$\Delta^{13}C = \frac{\delta^{13}C_{air} - \delta^{13}C}{1 + \delta^{13}C} \quad (4.1)$$

The $\delta^{13}C_{air}$ values applied to wood samples varied between −8.28‰ and −6.94‰ for the period 1950–2011 following Ferrio *et al.* (2005) (http://web.udl.es/usuaris/x3845331/AIRCO2_LOESS.xls).

Residual $\Delta^{13}C$ chronologies were obtained following the same procedure used for TRW (Fig. S4.3b). *Rbar* and *EPS* statistics (*SI Appendix*, section 2) were used to estimate the internal coherence of each chronology using the subset of years (n = 7) in which individual $\Delta^{13}C$ records were available (Table 4.2). Both TRW and $\Delta^{13}C$ chronologies were used as input for statistical analyses.

Meteorological data

Monthly mean temperature and precipitation were used to assess relationships with TRW and $\Delta^{13}C$. As long-term instrumental records are scarce in the region, estimates of climate variables were obtained from the nearest 0.25°-grid point (40°23'N, 0°38'W) of the European high-resolution climate dataset (E-OBS; Haylock *et al.* 2008).

Statistical analysis

Long-term trends in TRW patterns

The quantification of common TRW patterns among chronologies over the whole study period (i.e., common signal strength or synchrony, $\hat{a}_C$) and of changes in the coherence of these patterns over time (i.e., changes in synchrony) were investigated through (*i*) principal component analysis and (*ii*) variance-covariance (VCOV) modelling following Shestakova *et al.* (2014). For details see *SI Appendix*, section 3*A*.

Relationships between tree-ring width and Δ13C

A bivariate random linear model was used to take into account simultaneously the information available on TRW and $\Delta^{13}C$. This allowed for a straightforward estimation of the degree of temporal association between the traits. Briefly, the correlation of year effects (r_Y) between traits 1 and 2 can be expressed as:

$$r_Y = \frac{\sigma_{Y_{12}}}{\sqrt{\sigma^2_{Y_1} \times \sigma^2_{Y_2}}} \quad (4.2)$$

where $\sigma_{Y_{12}}$ is the common variability of year effects underlying traits 1 and 2 (covariance), and $\sigma^2_{Y_1}$ and $\sigma^2_{Y_2}$ stand for the variance component of year effects for traits 1 and 2 respectively. Following (2), we calculated the correlation of year effects between TRW and $\Delta^{13}C$ chronologies (and their standard errors) for each altitudinal belt. These relationships were calculated for 25-year periods lagged by one year starting in 1950. For further details see *SI Appendix*, section 3*B*.

Development of altitudinal master chronologies

A master chronology corresponding to each altitudinal belt was obtained using either TRW or $\Delta^{13}C$ chronologies by *best linear unbiased prediction* (BLUP) of year effects (Shestakova *et al.* 2016). BLUP increases accuracy relative to ordinary least squares methods (i.e., standard Analysis of Variance) and maximizes, under certain rather general assumptions, the correlation between true and predicted values (e.g., for TRW or $\Delta^{13}C$) associated to the random (year) effect (Piepho & Möhring 2005). BLUP estimates were derived for the period 1950–2011 using Eq. (4.1) of *SI Appendix*, section 3*A* and were subsequently used as input for climate analysis.

Relationships of tree-ring traits with climate

Pearson correlations were calculated for the period 1950–2011 to quantify climate-trait relationships. Temporal stability of these associations was assessed through moving correlation analysis for 25-year segments lagged by one year. Moreover, we checked for the presence of overlapping climatic information present in both TRW and $\Delta^{13}C$ chronologies through partial correlation analysis. Climate relationships were analysed from previous October to September of the year of tree-ring formation.

Results

Regional climate trends

There was a consistent upward trend in mean annual temperature since 1970 (absolute increase of +1.8°C for the last four decades; Fig. S4.4a) that affected especially the growing season period (absolute warming in spring and summer of +2.8°C and +2.6°C after 1970, respectively) (Fig. S4.4b). Changes in precipitation were less clear-cut, with non-significant linear trends but high interannual variability (Fig. S4.4). The period 1950–1979 was relatively wet (mean annual precipitation = 681 mm) and was followed by three drier decades (mean =

596 mm). The associations between monthly temperature and precipitation (not shown) were negative and significant from March to October, reinforcing the recent increase in warming-induced drought severity during the growing season.

Characteristics of radial growth and $\Delta^{13}C$ along the altitudinal gradient

The sampled trees originated from open pinewoods made up of individuals of similar size, with low-elevation sites (LS) showing the lowest basal area (Table 4.2). The altitudinal decrease in temporal coherence of TRW patterns (*Rbar* statistic) (Table 4.2) points to progressively less limiting climatic factors for growth (e.g., reduced drought stress) upwards in the gradient. There was no clear pattern of $\Delta^{13}C$ changes with altitude (Table 4.2). However, significant differences ($P \leq 0.05$) were found between *P. sylvestris* stands (suggesting less water deficit at high elevation, HS, than at mid elevation, MS) and also between co-occurring pines at MS (suggesting less water deficit for *P. nigra* compared with *P. sylvestris*).

The correlations between pairs of chronologies for TRW ranged from nearly zero to 0.87 (Table S4.1), indicating a diversity of growth patterns. Naturally, neighbouring chronologies correlated better than distant ones. In contrast, the association between pairs of $\Delta^{13}C$ chronologies was always significant, but again higher between neighbouring chronologies (Table S4.1). The relationship between TRW and $\Delta^{13}C$ showed a clear altitudinal trend, decreasing with increasingly humid and cold conditions (Table S4.1). This trend was also noticeable at the intra-specific level (i.e., for *P. nigra* and *P. sylvestris*).

Tree-ring width patterns

Groups of chronologies with similar TRW patterns were defined through principal component analysis (Fig. 4.2a). The loadings of the first (PC1) and second (PC2) principal components accounted for 59.7% and 23.6% of the total variance, respectively. All chronologies had positive PC1 loadings, suggesting a common climate signal along the gradient. However, high-elevation *P. sylvestris* and *P. uncinata* chronologies had positive PC2 loadings, while low-elevation *P. halepensis*, *P. nigra* and *P. pinaster* chronologies had negative PC2 loadings. In turn, mid-elevation *P. nigra* and *P. sylvestris* chronologies had nearly zero PC2 loadings. This result confirms the existence of three different growth patterns concomitant to the altitudinal position of each site.

A comparison of tree growth patterns among chronologies evidenced regional synchrony at both within- ($\hat{a}_{Cw}$) and between-group ($\hat{a}_{Cb}$) levels. The highest synchrony involved *P. sylvestris* and *P. uncinata* at HS ($\hat{a}_{Cw} = 0.90 \pm 0.01$; mean ± SE), followed by *P. nigra* and *P. sylvestris* at MS (0.80 ± 0.02) and *P. halepensis*, *P. nigra* and *P. pinaster* at LS (0.68 ± 0.03). As for synchrony among pairs of altitudinal belts, $\hat{a}_{Cb}$ decreased with increasing altitudinal difference between stands: synchrony was similar between neighbouring belts ($\hat{a}_{Cb} = 0.50 \pm 0.03$ and 0.41 ± 0.03 for LS/MS and MS/HS, respectively), whereas it was relatively weak

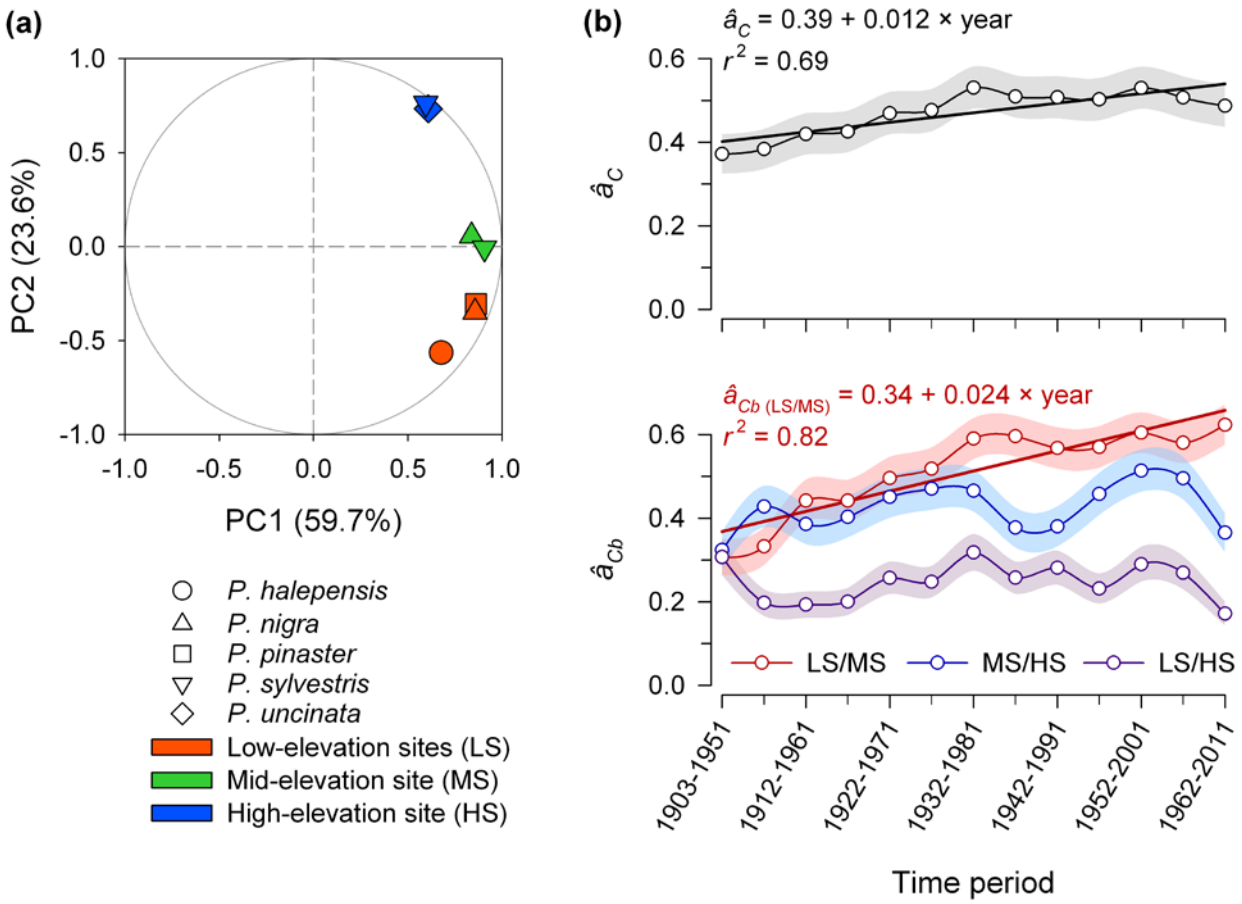

Figure 4.2. Principal component analysis **(a)** and synchrony patterns **(b)** along the altitudinal gradient. All calculations are based on residual tree-ring width (TRW) chronologies. The plot of the first and second principal components (PC1 and PC2) shows the loadings of each chronology for the common period 1950–2011. Temporal trends in spatial synchrony are estimated for 50-year periods lagged by five years for all chronologies ($\hat{a}_C$) (Eq. [S4.3] of *SI Appendix*, section 3*A*) and for pairs of chronologies belonging to different altitudinal belts ($\hat{a}_{Cb}$) (Eq. [S4.4], idem). Significant linear trends of $\hat{a}_C$ and $\hat{a}_{Cb}$ values over time are depicted as straight lines ($P \leq 0.05$). Shaded areas indicate standard errors.

between altitudinal extremes (0.22 ± 0.02 for LS/HS). There was strong growth synchrony among the complete set of chronologies ($\hat{a}_C$ = 0.46 ± 0.03), similar to that observed among trees within a stand ($\bar{R}bar$ = 0.56 ± 0.04), suggesting that regional growth is strongly influenced by climate.

Temporal trends in regional growth synchrony

The regional synchrony ($\hat{a}_C$) showed a steady increase over the period 1903–2011 (b = 0.012 year^{-1}; $P < 0.001$) (Fig. 4.2b, upper panel), ranging from 0.37 ± 0.05 (1903–1951 period)

to 0.53 ± 0.05 (1952–2001 period). However, the temporal evolution of synchrony between pairs of elevation belts ($\hat{a}_{Cb}$) was inconsistent (Fig. 4.2b, lower panel). LS and MS showed a significant increase in common TRW signals (b = 0.024 year^{-1}; $P < 0.001$), rising two-fold from 0.31 ± 0.04 (1903–1951 period) to 0.62 ± 0.05 (1962–2011 period). Conversely, synchrony changes between LS and HS or between MS and HS showed no clear temporal trend. These patterns were unaffected by the rigidity of splines used for chronology building (Fig. S4.5).

Temporal trends in TRW vs. ⊿^{13}C relationships

We found a strong, although geographically-structured, correlation of year effects between TRW and $\Delta^{13}C$ over the period 1950–2011, with the highest value observed at LS (r_Y = 0.83 ± 0.06; ± SE), followed by MS (r_Y = 0.59 ± 0.12) and HS (r_Y = 0.42 ± 0.12). These relationships, however, diverged at MS and HS at the turn of this century (Fig. 4.3). On the one hand, the association strengthened at MS, reaching similar values to those found at the lowest altitudinal belt; conversely, it became non-significant at HS. These changing patterns (increasing at MS, decreasing at HS) differed from the consistently strong association between TRW and $\Delta^{13}C$ found at LS, which fluctuated within a narrow range over the study period (r_Y > 0.70) (Fig. S4.6).

Climate drivers of TRW and ⊿^{13}C

The relationships between either TRW or $\Delta^{13}C$ and climate were geographically structured along the gradient. Growth responses to climate were similar at LS and MS,

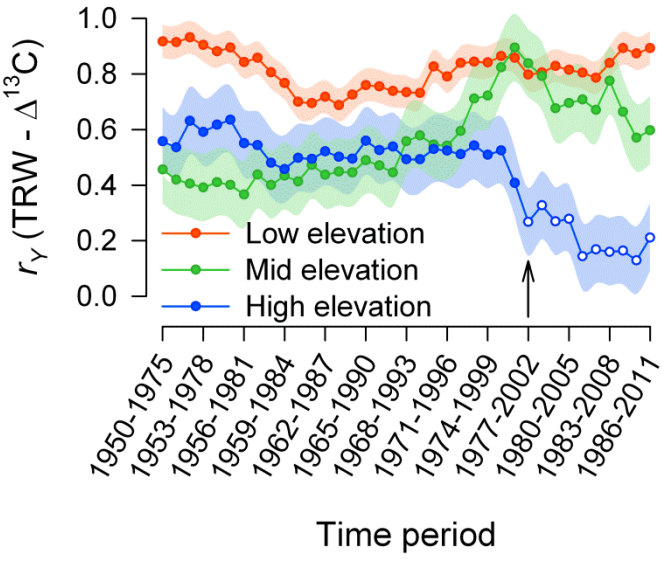

Figure 4.3. Temporal trends in intra-site associations between tree-ring width (TRW) and $\Delta^{13}C$ signals along the altitudinal gradient. The correlations of year effects (r_Y) are estimated using residual TRW and $\Delta^{13}C$ chronologies for 25-year periods lagged by one year following Eq. (4.2) of Materials & methods. The standard error of r_Y is used to determine the confidence intervals around a true correlation of zero (±2SE). Significant correlations (correlation coefficients falling outside of this range) are depicted as filled dots. The arrow indicates the first period embracing the winter-drought die-off episode observed in winter 2001–2002.

although there was higher tree sensitivity at low elevations (Fig. 4.4a). Particularly, TRW was enhanced by previous winter (December), spring and summer precipitation. We also found significant relationships with February (positive) and summer temperature (negative). At LS, TRW also correlated positively with February precipitation and negatively with May temperature. At HS, TRW was associated with previous October (negatively) and current August precipitation (positively), and also with April temperature (positively).

For Δ13C, there were positive and mostly significant relationships with precipitation along the gradient throughout the year (with the exception of previous autumn) (Fig. 4.4b). The highest correlations were found in spring at LS and MS and in summer at HS. In contrast, the temperature signal in Δ13C was weak, with significant (negative) associations from May to September (at LS and MS) and from June to September (at HS).

Temporal trends of TRW and Δ13C associations with climate

The associations between either TRW or Δ13C and climate were unstable along the gradient over the period 1950–2011. At LS and MS, we detected an increase in TRW sensitivity to both summer temperature (negative) and spring precipitation (positive) (Fig. 4.5). Particularly, we found a significant negative correlation between TRW and July temperature

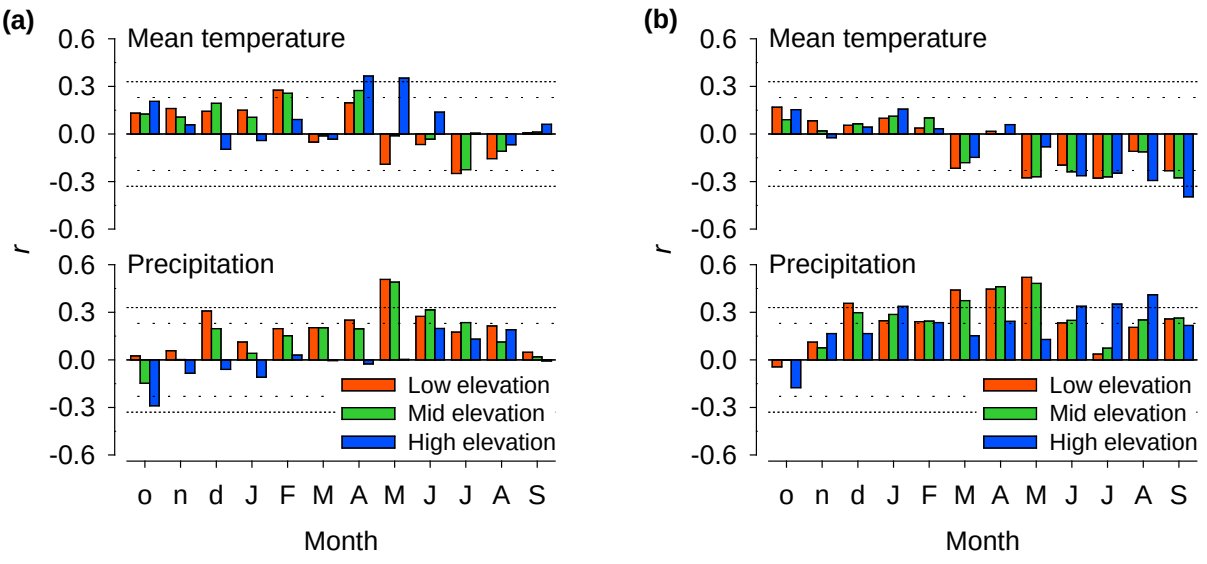

Figure 4.4. Altitudinal changes in ring-width and Δ13C responses to climate. Tree-ring width **(a)** and Δ13C **(b)** relationships with climate are based on Pearson correlations between the master chronology corresponding to each altitudinal belt and monthly mean temperature and precipitation for the period 1950–2011. The horizontal lines indicate the threshold for significance (dashed line, $P \leq 0.05$; dotted line, $P \leq 0.01$). Lowercase and uppercase letters in the *x*-axes correspond to months of the years before and during tree-ring formation, respectively.

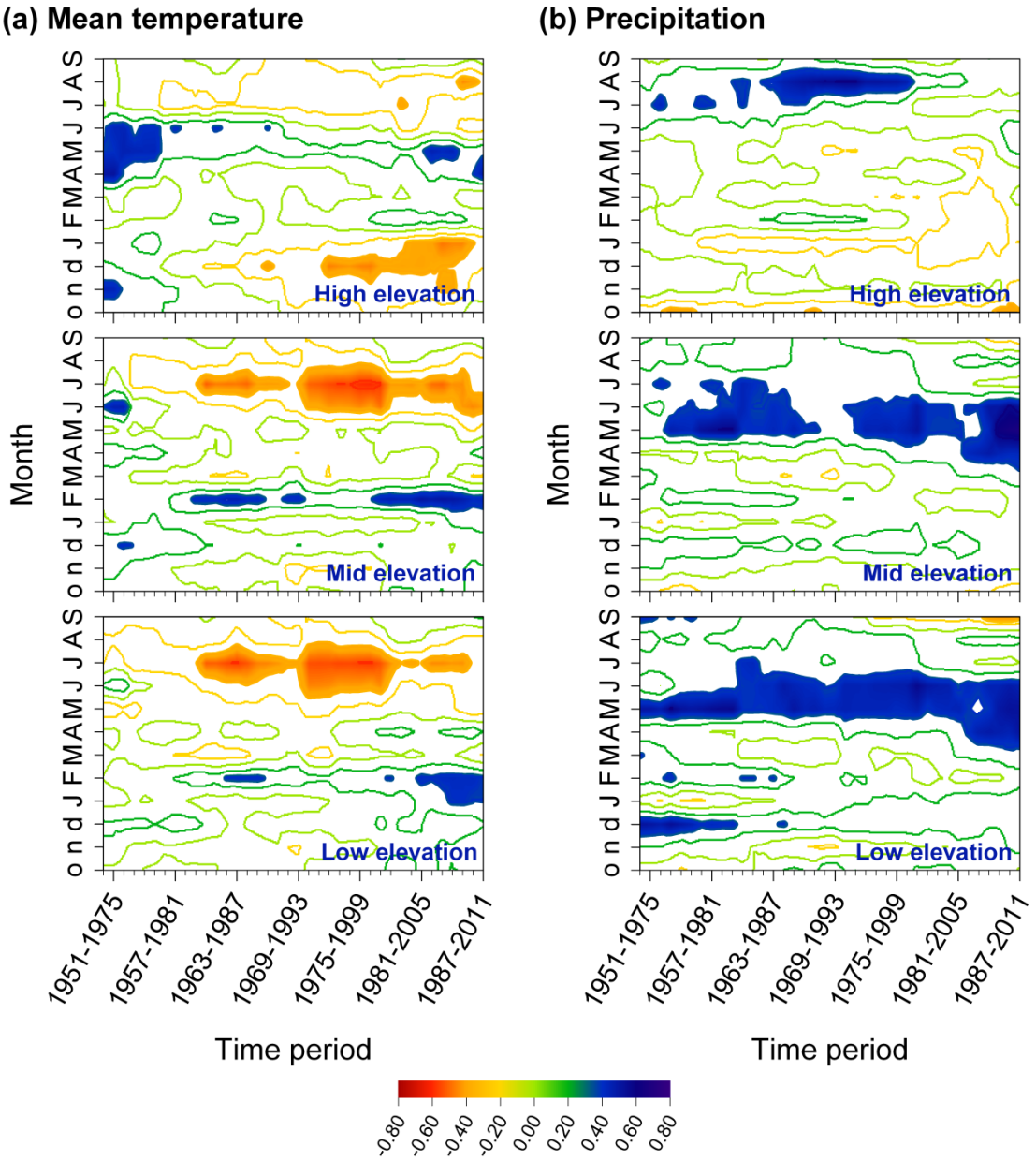

Figure 4.5. Moving correlations between the master ring-width chronology of each altitudinal belt and monthly mean temperature **(a)** and precipitation **(b)** (1950–2011). The threshold for significance ($P \leq 0.05$) is $r = \pm 0.37$ ($n = 25$). Non-filled areas denote non-significant correlations. Lowercase and uppercase letters in the *y*-axes correspond to months of the years before and during tree-ring formation, respectively.

since the 1980s, which later expanded to June. Likewise, there was a positive association with temperature in February since the 1980s, which extended to January at the turn of the century at LS. Finally, a positive correlation between TRW and May precipitationwas present over the

study period at LS and MS, which extended to April and June since the 2000s and 1980s, respectively.

At HS, the initial positive correlation with May-June temperature shifted to April in recent decades. A negative correlation with previous December temperature was detected in the 1990s, which extended to January in the 2000s. We also found a temporal shift in the association between TRW and summer precipitation at HS, with significant correlations in July-August from 1950 to 2000 and no signal onwards.

$\Delta^{13}C$ was more related to precipitation than to temperature along the gradient (Fig. 4.6). For LS and MS, positive correlations were found with precipitation in spring, September (until the 1990s) and previous December (shifting to January in the 2000s). Conversely, HS showed a positive correlation with precipitation in July-August (shifting to June from 2000 onwards), February (until 1980) and January (in the 2000s). For temperature, $\Delta^{13}C$ sensitivity to late spring-early summer was unstable at LS and MS, with significant negative correlations in May (1950 to 1980) and June-July (1980 to 2000). A negative correlation with March temperature was relevant until the late 1980s. At HS, we found a shifted (negative) response of $\Delta^{13}C$ to temperature over time, with significant correlations in August-September (1950 to 1990), July (1970 to 1990) and June (from 2000 onwards).

The tight association between TRW and $\Delta^{13}C$ (decreasing upwards along the gradient) suggested the existence of overlapping environmental information in these traits. To check for such redundancy we evaluated the relationships between TRW and climate after controlling for the effect of $\Delta^{13}C$ through partial correlation (Fig. S4.7). Mainly winter and early summer temperature signals were preserved in TRW records, but only at HS: December-January (negative, from the 1990s) and April-June (positive, until the 1980s). Also, a negative association between TRW and precipitation in March-April was preserved at LS (until the 1990s).

Discussion

Regional coherence of TRW patterns

The high regional tree growth synchrony (similar to that observed in trees co-occurring within a stand) points to the existence of common climatic factors driving growth across species along the altitudinal gradient. This suggests that environmental factors override taxonomic imprints in Mediterranean conifer forests constrained by climatic stressors. Besides, the steady increase in synchrony, peaking at the turn of the twenty-first century, indicates that the influence of environmental conditions on tree performance strengthens as climate warms and dries, hence prevailing over local forest drivers (e.g., topography, nutrient availability, competition). Although enhanced warming-induced growth synchrony has also been reported in Mediterranean forests at regional (Andreu *et al.* 2007; Natalini *et al.* 2015) and sub-continental scales (Shestakova *et al.* 2016), the observed

synchrony patterns among elevation belts provide further evidence for an increasingly large impact of warming on water-limited forests. Gradually, low- and mid-elevation trees grew more synchronously over the twentieth century, suggesting that drought-induced growth limitation is spreading upwards in Mediterranean mountains (Galván *et al.* 2015).

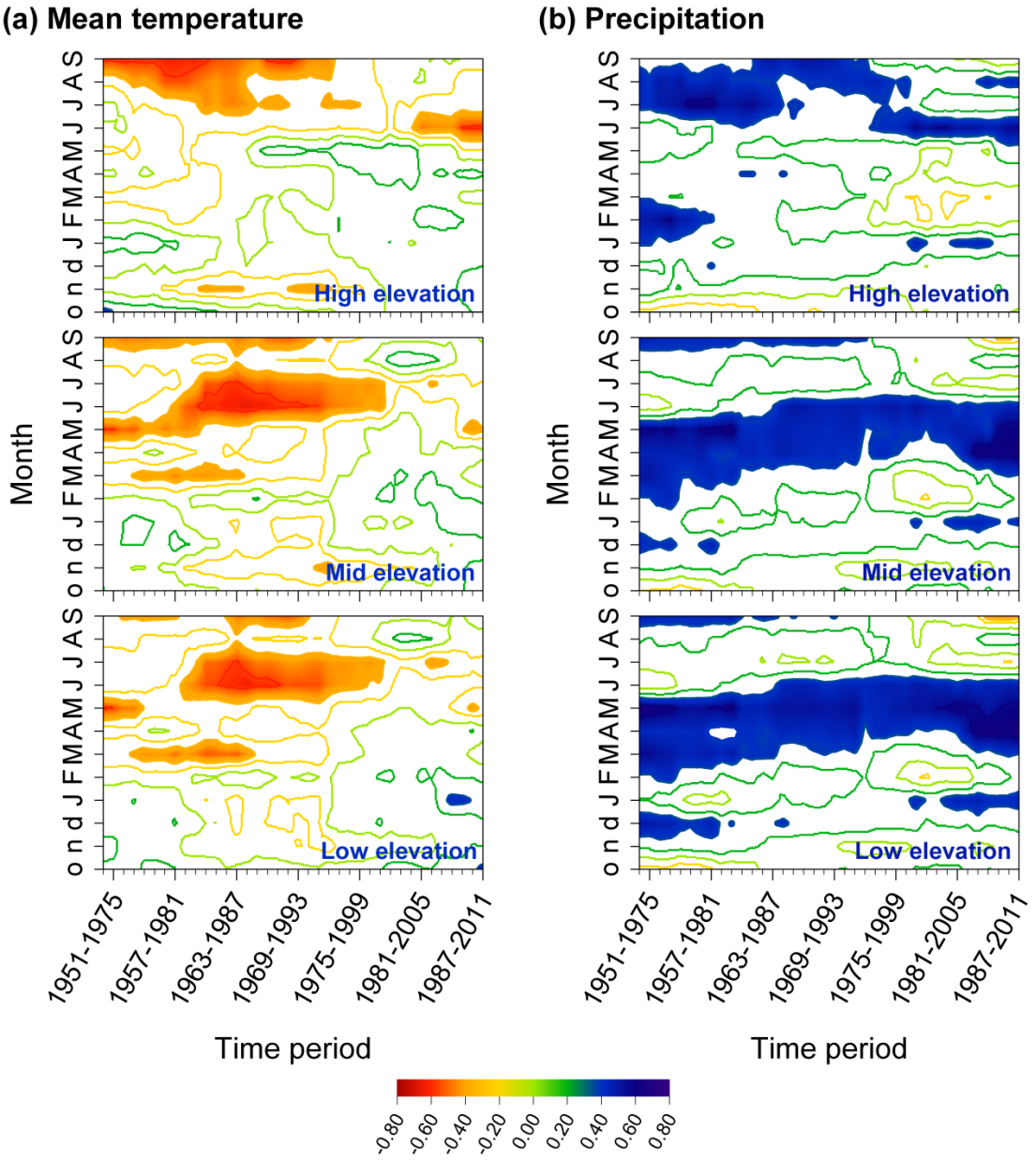

Figure 4.6. Moving correlations between the master $\Delta^{13}C$ chronology of each altitudinal belt and monthly mean temperature **(a)** and precipitation **(b)** (1950–2011). The threshold for significance ($P \leq 0.05$) is $r = \pm 0.37$ ($n = 25$). Non-filled areas denote non-significant correlations. Lowercase and uppercase letters in the *y*-axes correspond to months of the years before and during tree-ring formation, respectively.

Temporal changes in $\Delta^{13}C$–growth relationships depend on the altitudinal belt

We found a stronger association between $\Delta^{13}C$ records compared with TRW along the gradient, suggesting that carbon isotopes are better tracers of regional climate signals than radial growth (McCarroll & Loader 2004; Andreu *et al.* 2008). The temporal agreement between TRW and $\Delta^{13}C$ increased at MS from the 1980s onwards, reaching values comparable to those at LS. Such increasing agreement suggests that drought is becoming the main climatic stressor at the transitional area between low- and high-elevation forests, progressively limiting growth through a tighter stomatal control in mixed stands of Mediterranean (*P. nigra*) and Eurosiberian (*P. sylvestris*) pines. A recent strengthening of the common signal shared by TRW and $\Delta^{13}C$ has also been documented for *P. sylvestris* in Finland (Hilasvuori *et al.* 2009), which was attributed to an intensification of the common forcing (i.e., summer temperatures) driven by current warming.

Conversely, the recent and sudden weakening of common TRW and $\Delta^{13}C$ signals in high-elevation forests is intriguing and indicates an uncoupling between radial growth and leaf-level gas exchange processes first observed for the period of 1977–2002 (*cf.* Fig. 4.3). This phenomenon was likely triggered by a winter drought event that produced a massive regional die-off episode affecting ~14,000 ha of *P. sylvestris* at above 1,600 m a.s.l. in 2001–2002 (Voltas *et al.* 2013). Peguero-Pina *et al.* (2011) attributed this episode to the combination of (*i*) low soil temperatures limiting water uptake, (*ii*) high vulnerability to drought-induced embolism owing to the presence of repeated freeze-thaw cycles, and (*iii*) high winter radiation levels increasing transpiration. In fact, the difference between the average maximum October temperature and the average minimum December temperature in 2001 was 25.7°C, which exceeded by 8.6°C the average difference for the period 1950–2011 (E-OBS; Haylock *et al.* 2008). Although we sampled trees without visual symptoms of defoliation ten years after the die-off episode occurred, a long-lasting physiological impairment, as observed in terms of reduced hydraulic conductivity and low stem water potential (Peguero-Pina *et al.* 2011), may underlie the recent TRW–$\Delta^{13}C$ uncoupling at high elevations. Indeed, the reduced cavitation resistance of these populations and/or the uncoupling of regulatory mechanisms of water-carbon economy in senescing needles may have influenced water relations from 2002 onwards, decreasing $\Delta^{13}C$ (especially in *P. sylvestris*, as already observed for asymptomatic individuals; Voltas *et al.* 2013) but without clearly reducing secondary growth (*cf.* Figs S2a and S3a). In fact, Voltas *et al.* (2013) reported that carbon reserves were not depleted in severely defoliated trees, hence sustaining the possibility of a rapid recovery of canopy functions following needle shedding.

The extent of distinct growth and $\Delta^{13}C$ responses to climate

In mountain ecosystems, climatic conditions and forest productivity are strongly influenced by elevation (Kienast *et al.* 1987). However, we have identified drought occurring

during the growing season as main factor limiting tree performance across the altitudinal gradient, which we postulate as responsible for the strong regional growth synchrony. Yet it should be noted that growth responses to drought were not exactly coincident across altitudinal belts. We observed altitude-dependent climate–growth relationships, highlighting the major role of the elevation-induced thermal gradient in growth responsiveness to climate. Topographic and soil characteristics might have further exacerbated such differences, since low- and mid-elevation forests were located in rocky slopes or on shallow soils, whereas the high-elevation site was found in a plateau with deeper soils.

Our findings indicate that drought stress starts earlier in the growing season at low and mid elevations (i.e., driest sites). At the high-elevation belt, tree growth is only sensitive to late summer drought. These results agree with other studies indicating that pine growth is mainly controlled by winter-spring precipitation in lowland Mediterranean forests (e.g., Pasho *et al.* 2011), being mostly influenced by summer water availability at high elevations (e.g., Andreu *et al.* 2007). In Mediterranean forests, growth conditions generally improve with elevation which lowers summer temperatures and demand. Furthermore, prolonged snowmelt may also help to mitigate drought stress. Radial growth was also differentially influenced by off-season climate conditions. Particularly, enhanced growth after a humid winter-early spring highlights the importance of soil water recharge prior to cambial activity in lowland forests (Pasho *et al.* 2011). Also, the positive growth responses to February (at low and mid elevations) and April temperature (at high elevation) might indicate earlier cambium resumption (Deslauriers *et al.* 2008).

Trees growing at high elevation were the most $\Delta^{13}C$-responsive to summer precipitation, as previously reported in Spain (Andreu *et al.* 2008) and in the French Alps (Gagen *et al.* 2006). Conversely, $\Delta^{13}C$ was positively related to spring and early autumn precipitation at low and mid elevations (del Castillo *et al.* 2015). Indeed, cambial activity is almost ceased in sub-Mediterranean pinewoods during summer due to water shortage (Voltas *et al.* 2013), suggesting that growth is often more limited by turgor than by carbon supply (Woodruff & Meinzer 2011). $\Delta^{13}C$ was also sensitive to high summer temperatures through increased evapotranspiration rates, hence decreasing $\Delta^{13}C$ provided the soil does not completely dry out (Saurer *et al.* 2008). Besides, $\Delta^{13}C$ was positively associated with winter precipitation. Cold season precipitation often falls as snow in Gúdar, determining the soil moisture status early in the vegetative period. This condition may cause a lag between the period imprinted on $\Delta^{13}C$ and the actual growing season (Holzkämper *et al.* 2008). Indeed, the climate analysis reveals a delay in growth responses to precipitation compared to $\Delta^{13}C$, suggesting that the latter may be more sensitive to changes in moisture conditions (Hartl-Meier *et al.* 2014).

Interpreting temporal changes of growth and $\Delta^{13}C$ responses to warming

Our results suggest that the conspicuous warming trend and a decrease in precipitation from the 1970s onwards are producing the following effects on sub-Mediterranean (i.e., low and mid elevations) pinewoods: (*i*) a shift of the temperature-sensitive growth period towards earlier months (February), which points to an advanced cambial growth onset; (*ii*) an increasingly negative dependence of growth on peak summer temperatures; and (*iii*) an increasing reliance of tree performance on early spring precipitation. At high elevations, low summer temperatures do not constrain growth, hence challenging the assumption that productivity is temperature-limited in Mediterranean high-mountain ecosystems (Galván *et al.* 2015). However, growth is becoming negatively influenced by warm winters (*cf.* Fig. 4.5), which may indicate a greater cavitation risk during freeze-thaw episodes linked to winter-drought events (Peguero-Pina *et al.* 2011). Altogether, our findings agree with previous work on Mediterranean pines describing a shift in growth responses to climate during the second half of the twentieth century (e.g., Andreu *et al.* 2007). They also suggest that the productivity of Mediterranean mountain forests is becoming more limited by increased severity and duration of drought episodes (Martínez-Vilalta *et al.* 2008). This effect has been recently postulated as a major cause for widespread growth decline in regional pinewoods (Camarero *et al.* 2015), with the exception of *P. halepensis*, which may be favoured by increasing winter temperatures (de Luis *et al.* 2013).

The intensified $\Delta^{13}C$ response to early spring precipitation (a high precipitation period in the western Mediterranean) can be a consequence of more recurrent and prolonged drought episodes early in the season. Interestingly, the recent absence of $\Delta^{13}C$ sensitivity to September precipitation points to a decreasing imprint of latewood on whole-ring $\Delta^{13}C$. At high elevation, the recent shift in $\Delta^{13}C$-sensitivity from July-August to June precipitation suggests an earlier impact of drought stress that could slow down cambial activity in peak summer, as observed in high-elevation or high-latitude forests (Reynolds-Henne *et al.* 2007; Hilasvuori *et al.* 2009). Our results expand this observation to low-elevation Mediterranean forests subjected to high temperatures and prolonged summer drought, indicating coherent, although altitude-dependent, regional shifts in vegetative activity towards more favourable periods (spring) in seasonally dry climates.

The only relevant climate signals imprinted in TRW after removing $\Delta^{13}C$-related information were found at high elevation. Particularly, the significance of warm winters for radial growth over the last two decades reinforces the increasing role of xylem embolism in winters experiencing huge temperature fluctuations (Peguero-Pina *et al.* 2011). This finding, however, deserves further attention in relation to its potential future impact on tree performance, which here appears restricted to Eurosiberian pines. With this exception, most significant correlations between TRW and climate disappeared in the 1990s after controlling for $\Delta^{13}C$, which indicates an intensified climate effect on physiological processes underlying regional tree growth.

In conclusion, Iberian pines are becoming increasingly vulnerable to drought during the growing season as reflected by (*i*) enhanced spatial synchrony in radial growth owing to more coherent temporal responses between low- and mid-elevation sites, (*ii*) shifting growth sensitivity to climate towards earlier months in the season, and (*iii*) an increasing dependence of radial growth on $\Delta^{13}C$ for the mid-elevation belt, hence resembling low-elevation stands. Notably, climatic influences on regional tree growth could mainly be explained by gas exchange processes as reflected in wood $\Delta^{13}C$. However, the high-elevation belt exhibited a diverging reaction to warming, showing a sudden uncoupling between leaf-level physiology and growth most likely triggered by a recent winter-drought event. Altogether, our findings underline the complexities of warming-induced drought effects on Mediterranean forest ecosystems. Drier conditions may induce a tighter stomatal control of water losses to prevent hydraulic failure, producing a negative effect on pines along the altitudinal gradient owing to the more positive carbon balance required for drought recovery. Hence, there may be a positive feedback between warming-induced hydraulic dysfunction and indirect depletion of reserves causing major threats to Mediterranean mountain pines.

SUPPORTING INFORMATION (SI Appendix)

Supplementary text

1. Supplementary details on climate analysis

Meteorological data and climate gradients

In general, climate estimates obtained from the European high-resolution climate dataset (E-OBS; Haylock *et al.* 2008) can be considered of reasonable quality (Herrera *et al.* 2010). Here we compared the E-OBS series with local records from the closest weather station (Teruel, 40°21'N, 1°07'W, 900 m a.s.l.; Fig. S4). The correlations between gridded and station data were high ($r = 0.92$, $P < 0.001$ and $r = 0.78$, $P < 0.001$, for mean annual temperature and precipitation, respectively, during the common period 1986-2011), suggesting that the E-OBS dataset are representative of regional climate.

Further, to estimate the range of climatic variation between altitudinal extremes, we applied lapse rate adjustments to the E-OBS dataset as follows (Gandullo 1994): for temperature, decrease in 0.6°C per 100 m; for precipitation, 8% increment per 100 m, except for July and August, when precipitation is unrelated to altitude (Fig. S1).

2. Supplementary details on dendrochronological methods

Development of tree-ring width chronologies

In order to build residual ring-width chronologies for each site and species, the individual series were first standardised using a cubic-smoothing spline curve of 100 years with a 50%-frequency response cut-off. This procedure minimizes the influence of biological trends (e.g., tree age and size) and disturbance effects (e.g., due to forest management) on radial growth, hence preserving high-frequency variability potentially related to climate. Thus, standardisation converted ring-width measurements into dimensionless indices with mean value of 1. This standardisation procedure was complemented with a sensitivity analysis to assess the influence of detrending spline rigidity on the ring-width indices as some sampled trees were relatively young (i.e., <150 years). This means that a spline curve of 100 years could remove less of the variation owing to stand dynamics from the young growth stages compared to older growth stages, hence affecting synchrony estimates as presented in Fig. 2b of main document. To this end, we tested for the effect of cubic smoothing splines of different lengths (50 years, 30 years, and 15 years) on growth synchrony trends (see section 3 of this Appendix).

Next, autoregressive models were applied to remove the first-order temporal autocorrelation in the detrended series and generate residual or pre-whitened indices. Finally, a biweight robust mean was computed to produce residual chronologies for each site and

species and for every cubic smoothing spline tested. Results of the default method (spline of length = 100 years) are shown in Fig. S2b. These procedures were done using the ARSTAN program (Cook & Krusic 2005). The reliability of ring-width chronologies for capturing the hypothetical population signal was checked against the expressed population signal (*EPS*) criterion with a threshold value of 0.85 (Wigley *et al.* 1984). Interseries correlation (*Rbar*) statistics were used to estimate the internal coherence of each chronology (Wigley *et al.* 1984). These parameters are shown in Table 2 of main document.

3. Supplementary details on statistical analysis

A: Long-term trends in tree-ring width patterns

To investigate spatial synchrony patterns in indexed chronologies, we used variance-covariance (VCOV) modelling. First, we calculated the degree to which the complete set of residual ring-width chronologies (i = 1 to 7) contained a common temporal signal. Briefly, suppose that W_{ij} is the jth year of ring-width W_i. The estimators can be defined in terms of the following random linear model (random variables are shown underlined in this paper):

$$\underline{W}_{ij} = \underline{Y}_j + \underline{e}_{ij} \quad \text{(S4.1)}$$

where Y_j is a random time effect of the jth year and e_{ij} is a random deviation of the ith chronology in the jth year. Here, we assume that the year effects behave as if they came from a normal distribution with mean zero and variance σ_Y^2. The reproducibility of observations by the set of I chronologies can be estimated as (Shestakova *et al.* 2014):

$$\hat{a}_C = \frac{\sigma_Y^2}{\sigma_Y^2 + \sigma_e^2} \quad \text{(S4.2)}$$

We will refer to $\hat{a}_C$ as the mean interchronology correlation or growth synchrony among chronologies.

Next, the seven chronologies were grouped into potentially homogeneous subsets aimed at investigating synchrony patterns along the altitudinal gradient. Groups of chronologies with similar growth patterns were defined through principal component analysis (PCA) for the common period 1950–2011 (Fig. 2a of main document). To analyse temporal patterns in synchrony within and between groups with distinct growth signals, corresponding to the three altitudinal belts (r = 1 to 3; for details see Results section), the following variance-covariance (VCOV) structure underlying model (1) was employed (Shestakova *et al.* 2014):

$\text{cov}(\underline{Y}_{jr};\underline{Y}_{jr^*}) = \sigma^2_{Y_r}$, when $r = r^*$,

otherwise $\text{cov}(\underline{Y}_{jr};\underline{Y}_{jr^*}) = \sigma^2_{Y_{rr^*}}$

This structure allows each group to have its own year variance and each pair of groups its own year covariance. The mean correlation (synchrony) estimated between all possible pairs of chronologies as in (2) may be split into (*i*) a mean correlation between pairs of chronologies within every group *r* ($\hat{a}_{Cw}$) and (*ii*) a mean correlation between pairs of chronologies belonging to groups *r* and *r** ($\hat{a}_{Cb}$), as follows (Shestakova *et al.* 2014):

$$\hat{a}_{Cw} = \frac{\sigma^2_{Y_r}}{\sigma^2_{Y_r} + \sigma^2_e} \tag{S4.3}$$

$$\hat{a}_{Cb} = \frac{\sigma^2_{Y_{rr^*}}}{\sqrt{(\sigma^2_{Y_r} + \sigma^2_e) \times (\sigma^2_{Y_{r^*}} + \sigma^2_e)}} \tag{S4.4}$$

In turn, the residual variance σ^2_e may vary among groups, hence producing a heteroscedastic variant of the group-based model.

These models (general and group-based heteroscedastic) were tested for 50-year segments lagged by five years for the period 1903–2011. To this end, we used indexed chronologies obtained from different cubic smoothing splines (length = 100 years, 50 years, 30 years and 15 years), hence obtaining separate synchrony trends testing for the influence of detrending spline rigidity. The results for the default method (spline of length = 100 years) are shown in Fig. 2b of main document. The sensitivity analysis illustrating the effect of different splines in growth synchrony trends over time is shown in Fig. S5.

B: Relationships between radial growth and $\Delta^{13}C$

Frequently, two or more features (ring-width, stable isotopes, wood density, etc.) are simultaneously measured on tree rings aimed at understanding changes in tree performance over time. As these features are a consequence of a number of common plant processes (carbon uptake and storage, water use, etc.) they may contain partially overlapping information. To quantify the association between traits, the Pearson product-moment correlation coefficient applied to the time series of *J* years can be used. This approach is valid for observations obtained annually either in the same tree or in the same chronology (i.e., a composite of individual trees). However, there may be an interest to estimate the overall association between traits for a number of trees (or chronologies) simultaneously. A possible approach consists in calculating the Pearson correlation for pairs of observations across years and trees (or chronologies). If so, this correlation contains three different causes of association: temporal (due to year effects), spatial (due to mean differences among trees

[chronologies]) and residual (quantifying the specificity of temporal variability at the tree [chronology] level). The temporal association (or correlation of year effects) represents how similarly two traits covariate across years, while the residual association quantifies how consistent the interaction between time and tree (chronology) effects is across traits. It must be noted that the spatial association is usually obscured in dendrochronology as time-series (trees or chronologies) are usually detrended or indexed prior to the calculation of Pearson correlations, meaning that they take essentially the same mean value.

In this context, the single trait random model (1) can be extended in order to take into account simultaneously the information available on different features, thus resulting in a multiple trait analysis (White & Hodge 1989). This allows for a straightforward estimation of the degree of temporal association between pairs of traits. Similarly to the calculation of a Pearson correlation (or the covariance between traits divided by the product of their standard deviations), the temporal and residual associations (i.e., correlations) can be estimated by the partition of the general covariance between traits across years and trees (chronologies) in its year and residual components. In this way, the correlation of year effects (r_Y) can be expressed as (Gilmour *et al.* 2002):

$$r_Y = \frac{\sigma_{Y_{12}}}{\sqrt{\sigma^2_{Y_1} \times \sigma^2_{Y_2}}} \qquad \text{(S4.5)}$$

where $\sigma_{Y_{12}}$ is the common variability of year effects underlying traits 1 and 2 (covariance), $\sigma^2_{Y_1}$ stands for the variance component estimate of year effects for trait 1 and $\sigma^2_{Y_2}$ stands for the variance component estimate of year effects for trait 2.

The statistical analyses were performed with SAS/STAT (ver. 9.4, SAS Inc., Cary, NC, USA). We used the MIXED procedure for random modelling and estimation of variance components through restricted maximum likelihood (REML). The covariance structure for groups was specified using the RANDOM statement and the autoregressive structure was fitted using the REPEATED statement. Heterogeneity of residual variances across groups was implemented with the GROUP option of the REPEATED statement.

Supplementary table

Table S1. Pearson correlation coefficients between tree-ring traits (tree-ring width and $\Delta^{13}C$) for the period 1950–2011. Values above the main diagonal are correlations between pairs of residual chronologies for tree-ring width (TRW); values below the main diagonal are correlations between pairs of residual chronologies for $\Delta^{13}C$. Values in the main diagonal (in bold) are correlations between TRW and $\Delta^{13}C$ chronologies of the same site and species. Non-significant correlation coefficients are indicated in italics. Chronology codes are as in Table 2 of main document.

TRW / $\Delta^{13}C$	*Ps*$_{HS}$	*Pu*$_{HS}$	*Pn*$_{MS}$	*Ps*$_{MS}$	*Pn*$_{LS}$	*Pp*$_{LS}$	*Ph*$_{LS}$
Ps$_{HS}$	**0.18**	0.76	0.37	0.38	0.30	0.30	0.39
Pu$_{HS}$	0.91	**0.43**	0.35	0.48	0.30	0.35	0.41
Pn$_{MS}$	0.47	0.48	**0.28**	0.82	0.63	0.63	0.44
Ps$_{MS}$	0.48	0.49	0.61	**0.46**	0.57	0.64	0.50
Pn$_{LS}$	0.28	0.27	0.58	0.74	**0.48**	0.87	0.59
Pp$_{LS}$	0.31	0.31	0.60	0.72	0.70	**0.67**	0.71
Ph$_{LS}$	*0.00*	*0.08*	0.50	0.53	0.71	0.69	**0.71**

Supplementary figures

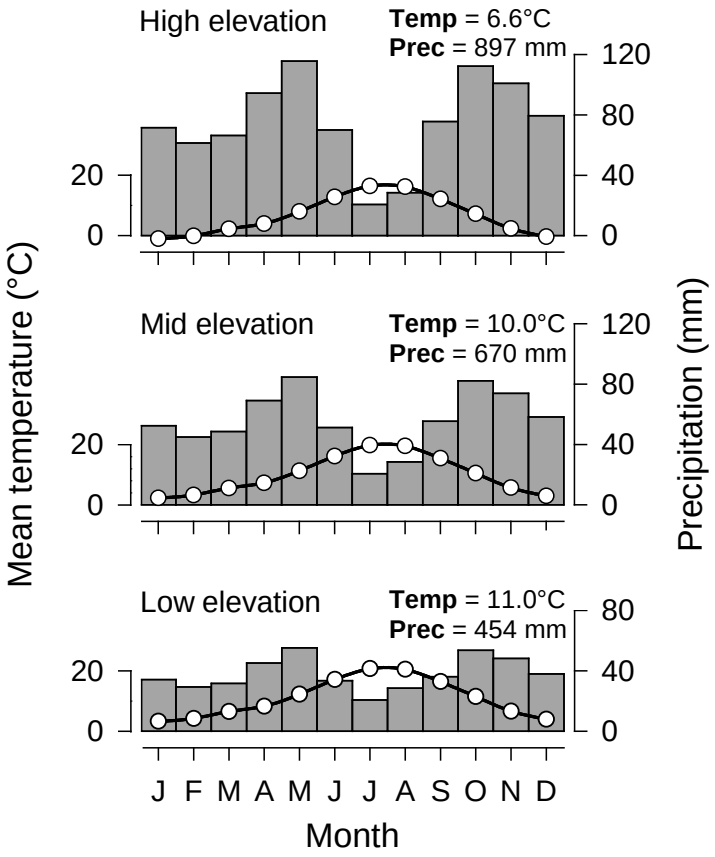

Figure S1. Climate diagrams corresponding to low- (LS), mid- (MS) and high-elevation (HS) sites. The primary *y*-axis indicates monthly mean temperature (lines) and the secondary *y*-axis monthly precipitation (bars). Average monthly values of climate factors were estimated based on the European high-resolution climate dataset (E-OBS) for the period 1980–2011. The mean annual temperature and total annual precipitation are given for each elevation belt.

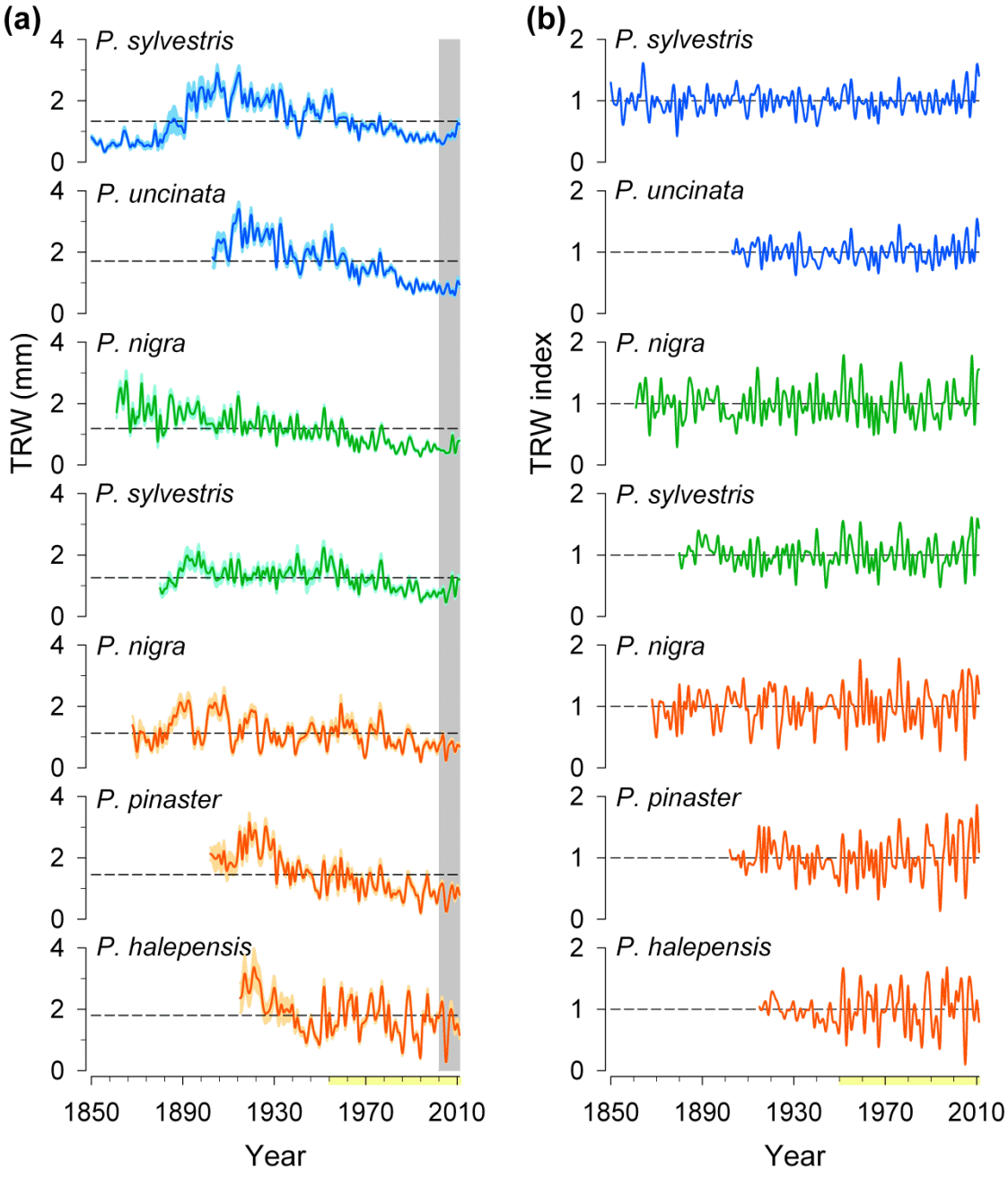

Figure S2. Raw (non-standardized) **(a)** and residual (spline of length = 100 years) **(b)** tree-ring width (TRW) chronologies for every site-species combination with five series cut-off. Red lines refer to low-elevation sites (LS), green lines to the mid-elevation site (MS) and blue lines to the high-elevation site (HS). Shaded areas denote standard errors. Dotted lines indicate sections of residual ring-width chronologies with Expressed Population Signal (EPS) lower than 0.85 (values of *EPS* higher than 0.85 are usually regarded as representing well-replicated chronologies). The dashed lines indicate mean values of each chronology (absolute ring-width, left panels; ring-width index, right panels). The gray area highlights the post-2001 period. The yellow area in the *x*-axis corresponds to years with available $\Delta^{13}C$ records.

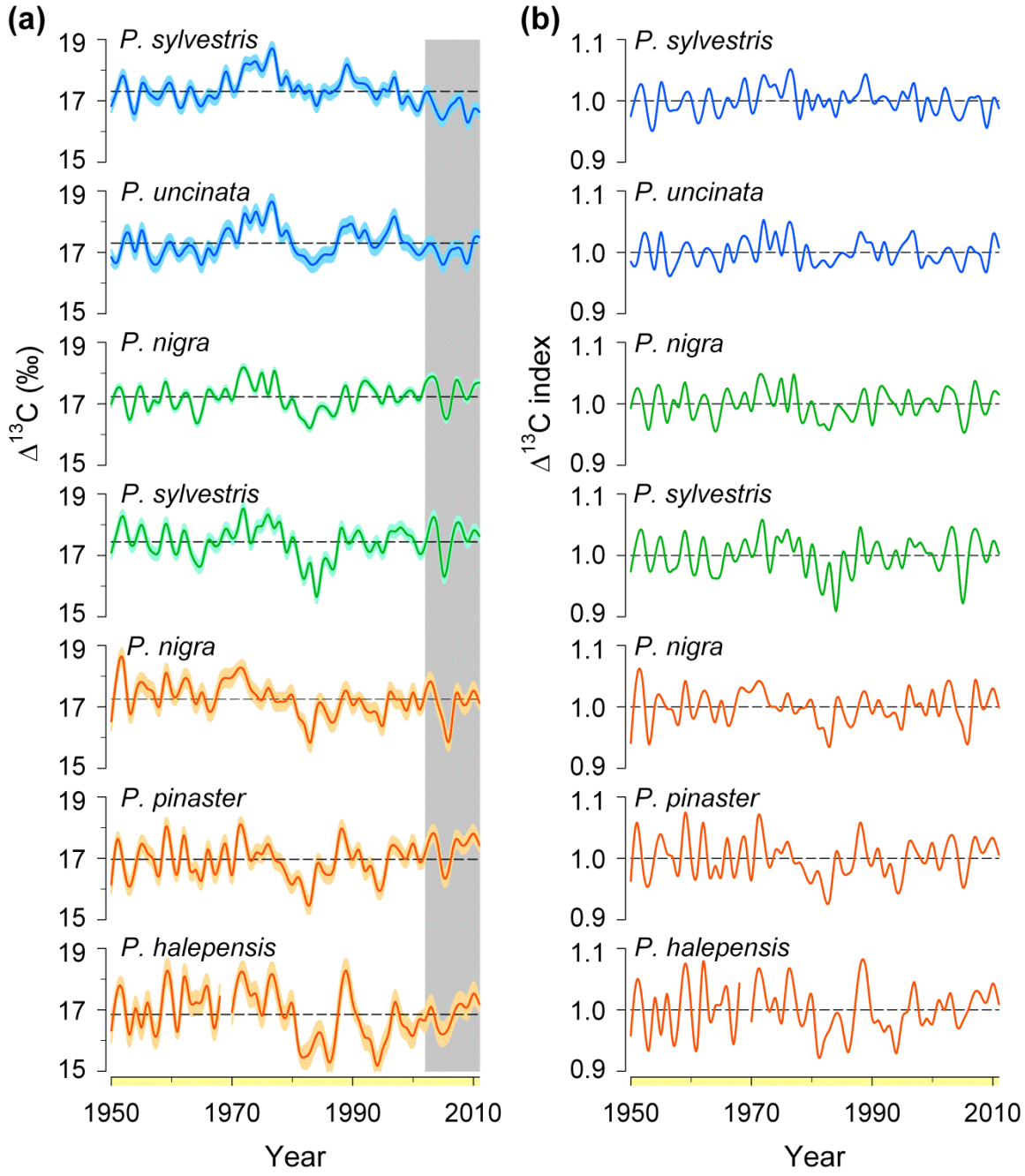

Figure S3. Raw (non-standardised) **(a)** and residual **(b)** carbon isotope discrimination ($\Delta^{13}C$) chronologies for every site-species combination for the period 1950–2011. Red lines refer to low-elevation sites (LS), green lines to the mid-elevation site (MS) and blue lines to the high-elevation site (HS). Shaded areas denote standard errors. The dashed lines indicate mean values of each chronology (original $\Delta^{13}C$, left panels; $\Delta^{13}C$ index, right panels). The gray area highlights the post-2001 period.

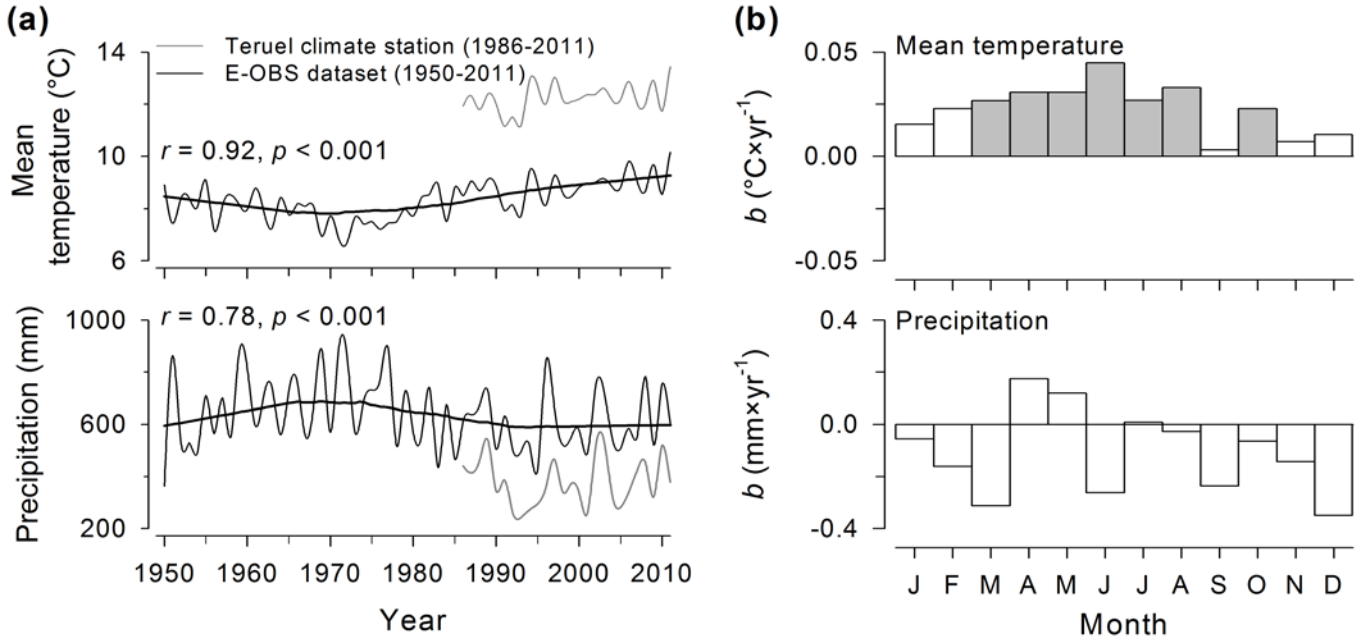

Figure S4. Regional temporal trends in climate data for the study area (period 1950–2011). (a) Annual and (b) monthly long-term changes in mean temperature (top) and total precipitation (bottom) obtained from European high-resolution climate dataset (E-OBS). Annual trends in E-OBS records (black lines) are smoothed by LOESS fitting (span = 0.5). For comparison, data from Teruel meteorological station (grey lines) are also included in (a). Bars represent slopes of linear regressions of monthly climate factors as a function of time. Filled bars indicate significant ($P \leq 0.05$) linear trends over time.

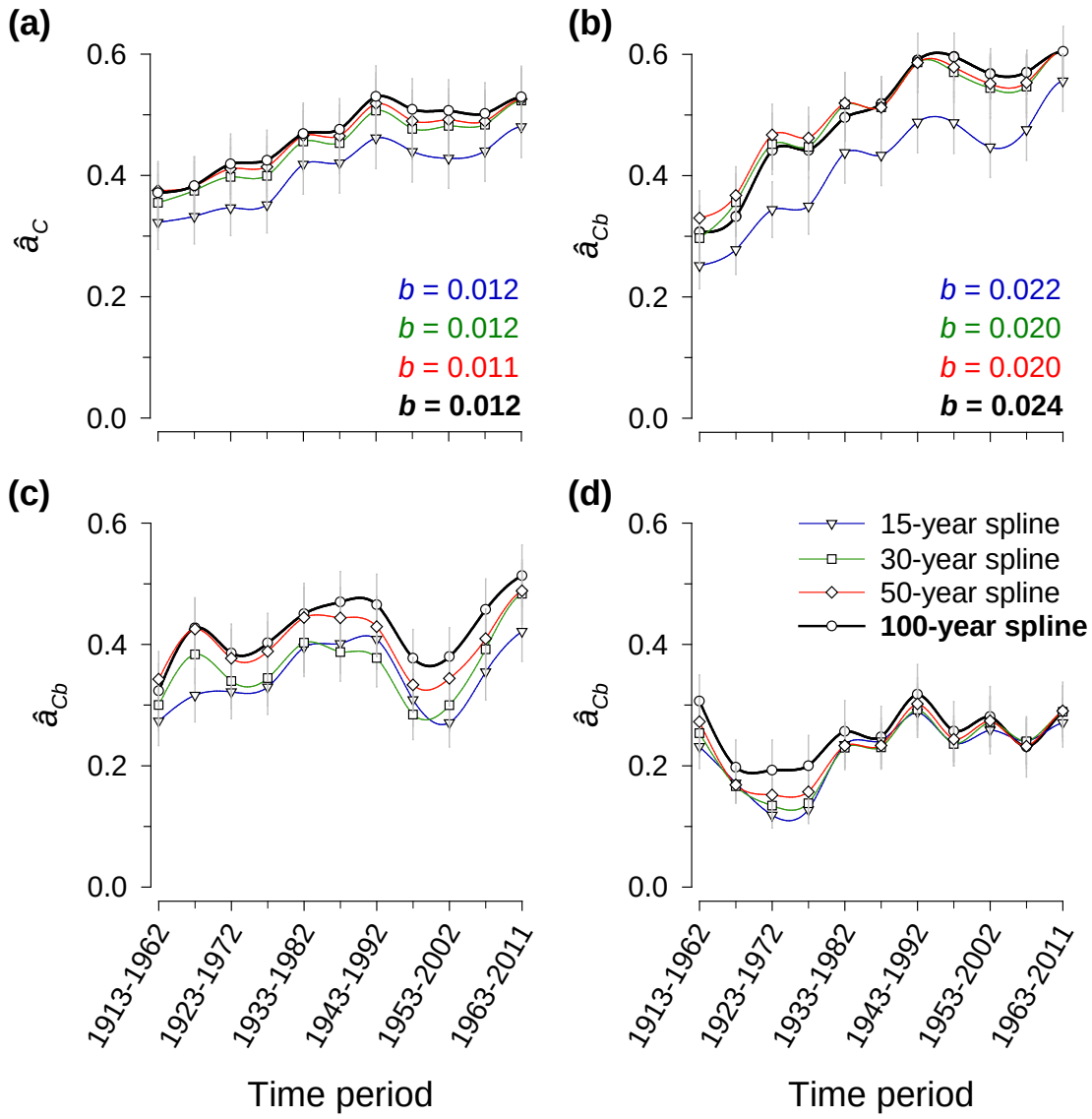

Figure S5. Temporal trends in spatial synchrony along the altitudinal gradient estimated for 50-year periods lagged by five years. Trends are shown for all chronologies together ($\hat{a}_C$) (Eq. [S4.3] in section 3*A* of this Appendix) **(a)**, and also for pairs of chronologies belonging to different altitudinal belts ($\hat{a}_{Cb}$) (Eq. [S4.4], idem) as follows: low-elevation *vs.* mid-elevation chronologies **(b)**, mid-elevation *vs.* high-elevation **(c)**, and low-elevation *vs.* high-elevation **(d)**. Thick black lines depict trends obtained after spline detrending with length = 100 years, red lines with length = 50 years, green lines with length = 30 years and blue lines with length = 15 years. Significant linear trends of $\hat{a}_C$ and $\hat{a}_{Cb}$ values are identified with their corresponding slope estimate.

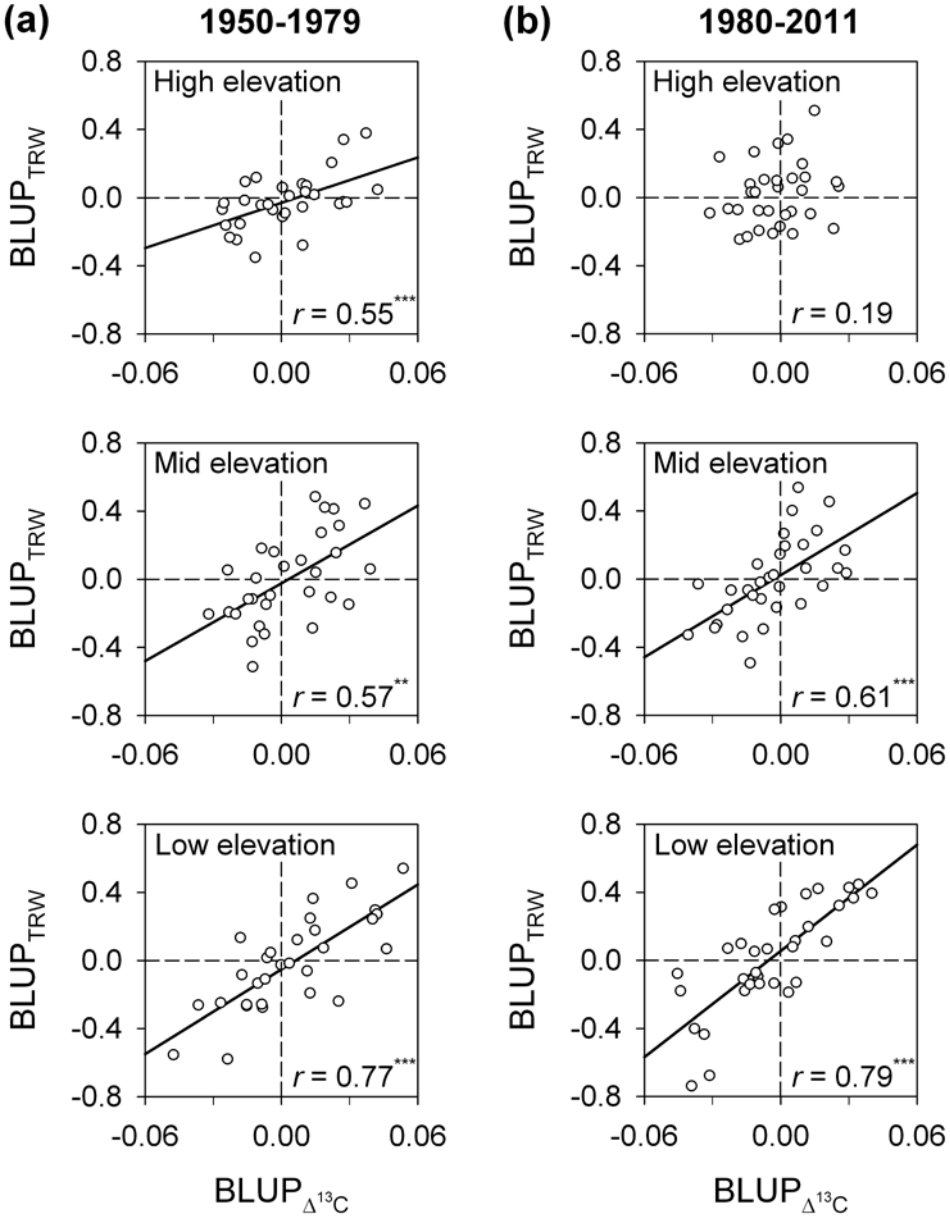

Figure S6. Relationships between tree-ring width (TRW) and carbon isotope discrimination ($\Delta^{13}C$) along the altitudinal gradient. The correlations are estimated using best linear unbiased predictors (BLUPs) of year effects ($\Delta^{13}C$, *x*-axis; TRW, *y*-axis) for two consecutive periods: **(a)** 1950–1979 and **(b)** 1980–2011. Significant linear associations are depicted as black lines ($^{**}P < 0.01$; $^{***}P < 0.001$).

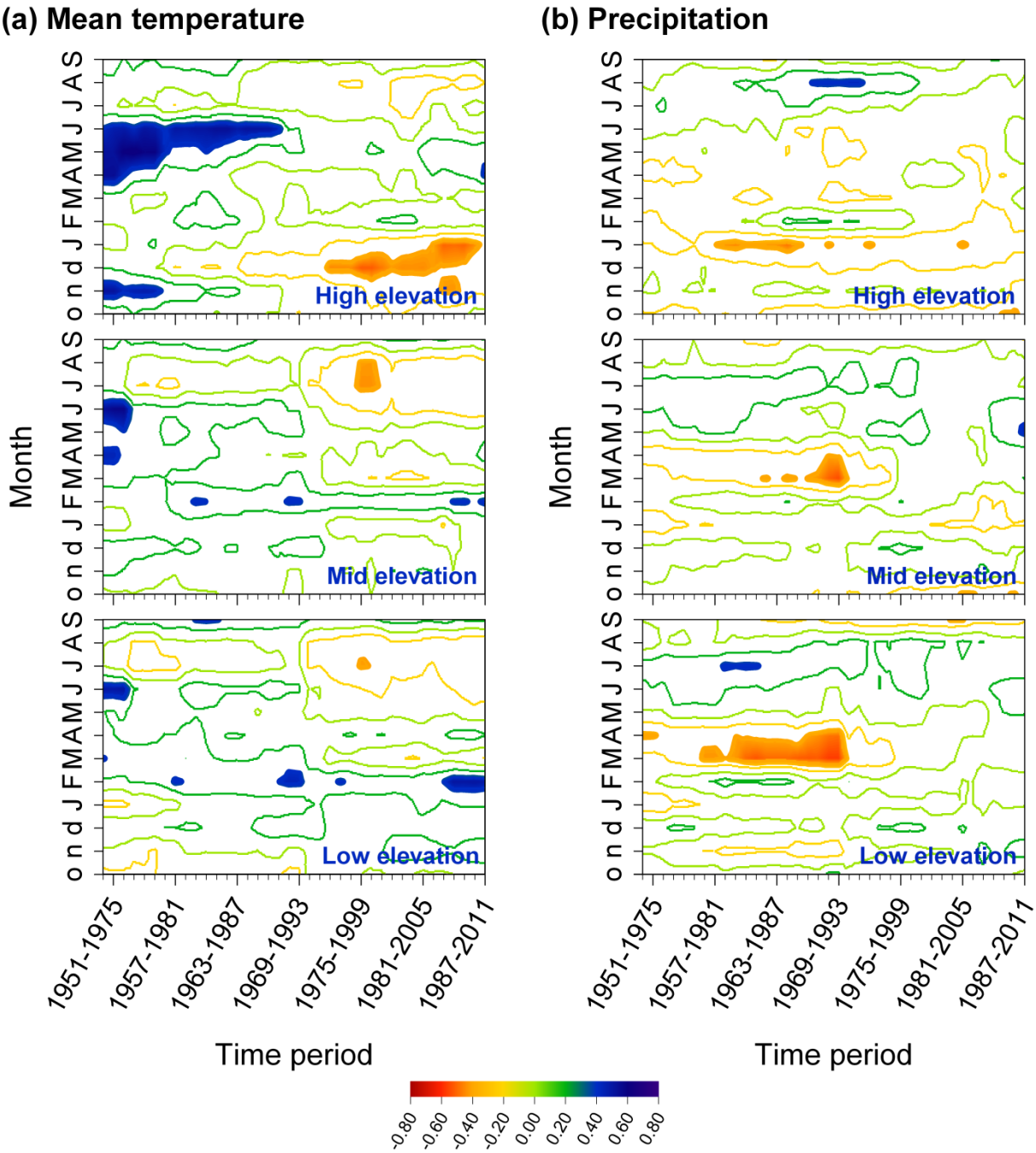

Figure S7. Moving correlations (after controlling for the effect of carbon isotope discrimination ($\Delta^{13}C$) through partial correlation analysis) between ring-width chronologies and monthly mean temperature **(a)** and precipitation **(b)** for each altitudinal belt (period 1950–2011). The threshold for significance ($P \leq 0.05$) is $r = \pm 0.41$ ($n = 25$; *d.f.* = 22). Non-filled areas denote non-significant correlations. Lowercase and uppercase letters in the *y*-axes correspond to months of the years before and during tree-ring formation, respectively.

CHAPTER 5

Physiological drivers of twentieth-century forest growth in Europe

Manuscript in preparation

Physiological drivers of twentieth-century forest growth in Europe

Shestakova TA, Voltas J, Saurer M, Gutiérrez E, *et al.*

Manuscript in preparation

Abstract

Improving our understanding of the spatiotemporal diversity in tree performance must provide insights on the environmental responses of forests and their function as future carbon holders. This research priority can be tackled through the analysis of functional traits including stable isotopes, which are applied to track the balance between carbon uptake and water losses at leaf level. Here we attempt at characterizing the physiological drivers (inferred through carbon isotope discrimination, $\Delta^{13}C$, and oxygen isotope composition, $\delta^{18}O$) of forest tree productivity across Europe using a network of 23 tree-ring sites (1900–2003). We hypothesize that the temporal coherence in ring-width records is geographically structured (i.e., spatially synchronized) following a latitudinal gradient, and this structure is related to the relative significance of gas exchange processes (photosynthesis, stomatal conductance) as potential drivers of productivity. We found significant spatial autocorrelations for ring-width, $\delta^{13}C$ and $\delta^{18}O$ spreading over sites separated up to 1,000 km. However, growth synchrony was not uniform continent-wide, increasing along a latitudinal gradient ($r = 0.77$; $P < 0.01$) concurrent with a northward trend of decreasing temperatures and reduced evapotranspiration. Also, there were geographically-structured relationships between ring-width and either $\Delta^{13}C$ (decreasing northwards; $r = –0.90$; $P < 0.001$) and $\delta^{18}O$ (increasing northwards; $r = 0.62$; $P < 0.05$). These results point to limited CO_2 diffusion impairing carbon uptake as main mechanism controlling the temporal coherence of forest growth signals at latitudes below 50°N in Europe. Synchrony increased during the period 1951–2003 across most Europe, except Fennoscandia. This fact, together with a tighter relationship between ring-width and $\Delta^{13}C$ in the same period, suggest increasing drought effects on growth patterns in southern and central European forests. The evidence for substantial, latitudinal variation in tree growth dependencies on leaf-level physiology will be valuable to forecast the extent by which future forests may progressively shift from temperature- to moisture-sensitive growth continent-wide.

Introduction

Forests are the greatest carbon sinks of terrestrial ecosystems, but their current and future importance as net carbon holders can be extremely variable around the globe (Whitehead 2011). Factors such as tree age, forest structure and management, nutrient availability and natural disturbances are influential in determining the carbon budget of a forested area. During the last century, however, the impacts of climate change and increased atmospheric CO_2 on tree functioning are determining the fate of natural forests as contributors to the carbon sink of the biosphere (Norby *et al.* 2005).

Understanding the physiological mechanisms underlying variations in forest productivity as related to global change effects is a key research priority. Most efforts are usually circumscribed to local ecosystems, with one or few representative tree species and their interactions being examined at small scales (e.g., Granda *et al.* 2014). This experimental focus stems from the customary methodological difficulties associated to a thorough ecophysiological characterization of trees, but it is weighed down by site-dependent effects and limited representativeness of environmental conditions. More exhaustive information about the ecophysiological drivers and associated patterns of tree functioning across large geographic scales is urgently needed so as to anticipate the effects of environmental instability on productivity globally (Chown *et al.* 2004). Through the analysis of meaningful functional traits (Violle *et al.* 2014), advancing the understanding of spatiotemporal diversity in tree performance should provide more comprehensive insights on environmental responses of forests and their function as carbon holders or, ultimately, releasers in the next decades (Peñuelas *et al.* 2011; Anderegg *et al.* 2016).

The assortment of factors, mechanisms and processes influencing tree growth is extremely variable and depend on tree characteristics and ontogenetic stage (Gibert *et al.* 2016). Despite such inherent complexity, regionally coherent multispecies tree growth responses (e.g., as imprinted in tree rings) have been successfully linked to global change effects on forest ecosystems (e.g., Allen *et al.* 2010; Wettstein *et al.* 2011; Williams *et al.* 2013; Shestakova *et al.* 2016). Dendroecological studies rely on the presence of common signals archived in tree populations, which are often derived from whole-ring width series reflecting variability in environmental factors (Fritts 2001). Alternatively, stable isotopes are effective proxies of ecophysiological traits for assessing plant carbon and water relations at different spatiotemporal scales (Werner *et al.* 2012). The carbon ($\delta^{13}C$) and oxygen ($\delta^{18}O$) isotopic compositions measured in tree rings differ from classical dendrochronological traits such as ring-width in which they reflect more faithfully and directly the complex array of tree physiological responses to environmental conditions (McCarroll & Loader 2004; Treydte *et al.* 2007; Gessler *et al.* 2014). Indeed, the interannual variation in $\delta^{13}C$ and $\delta^{18}O$ can be evaluated and related retrospectively to leaf-level physiological processes (e.g., Sidorova *et al.* 2009; Andreu-Hayles *et al.* 2011; Shestakova *et al.* 2014). This is especially relevant in temperate forest trees thriving under near-optimal conditions, where tree growth patterns may not be

informative of climate variability but stable isotopes have been shown to respond coherently to environmental variables (Hartl-Meier *et al.* 2014). Indeed, much complementary information can be gained by analysing $\delta^{13}C$ and $\delta^{18}O$ in addition to ring widths (Cernusak & English 2015), as this information appears especially well suited to providing evidence on how forest trees are likely to respond to climate stress (McDowell *et al.* 2010; Levanič *et al.* 2011).

The dual-isotope approach is commonly applied in tree rings to track the balance between carbon uptake and water losses (e.g., Altieri *et al.* 2015; Moreno-Gutiérrez *et al.* 2015). On one hand, $\delta^{13}C$ depends on factors affecting CO_2 assimilation, being mainly controlled by photosynthetic rate (A) and stomatal conductance (g_s), as expressed in the ratio A/g_s (intrinsic water-use efficiency; Farquhar *et al.* 1989). On the other hand, $\delta^{18}O$ is mainly influenced by source water isotopic composition (i.e., precipitation modulated by residence time in soil and associated evaporation effects) and leaf water enrichment due to transpiration at the stomata (Treydte *et al.* 2014). Both isotope types are therefore linked via effects at the leaf level, mediated through changes in stomatal conductance caused by varying soil moisture and atmospheric evapotranspirative demand. As $\delta^{18}O$ is not influenced by photosynthetic processes, combining $\delta^{13}C$ and $\delta^{18}O$ allows distinguishing between stomatal and photosynthetic effects on tree performance, which may ultimately determine changes in productivity (Barbour *et al.* 2002; Ripullone *et al.* 2009; Barnard *et al.* 2012).

This study attempts at characterizing the functional drivers (as inferred through $\delta^{13}C$ and $\delta^{18}O$) of forest tree productivity across Europe and northern Africa (from *ca.* 33°N to 69°N) using an *ad-hoc* tree-ring network. Indeed, latitudinal gradients are extremely relevant to the analysis of large-scale patterns in trait variability and their relationships with ecosystem functioning (Violle *et al.* 2014). We hypothesise that (*i*) the temporal coherence in radial growth patterns is geographically structured following a latitudinal gradient continent-wide, with higher coherence (i.e., more synchronous growth) found in temperature-limited, high-latitude forests; (*ii*) the patterns of spatial synchrony are linked to the relative significance, modulated by climate, of carbon assimilation or stomatal control as potential drivers of tree productivity, and (*iii*) a tighter control of water losses impacting on tree growth is spreading latitudinally northward as a consequence of climate change, hence increasing the spatial coherence in growth patterns across Europe. To this end, 23 chronologies from old trees comprising conifers (*Cedrus*, *Pinus*) and hardwoods (*Quercus*) are used spanning the twentieth century. By informing on spatial responses to environmental changes, we expect that the joint analysis of ring-width and stable isotopes will be of value to understand patterns of tree growth and physiology underlying biogeographical interactions in Europe.

Materials & methods

Tree-ring network and data processing

We used a tree-ring dataset from the pan-European network ISONET (European Union, EVK2-2001-00237), which is made up of 23 sampling sites ranging from Mediterranean to Boreal latitudes (*SI Appendix*, Table S5.1). This network provides a comprehensive coverage of the natural biogeographic conditions found across Europe and also northern Africa (Morocco). Sites were selected consisting of old-growth forests (mean age = 453 ± 174 years [SD]) of coniferous or broad-leaved species from the two main genera of forest trees in Europe (*Pinus* and *Quercus*) plus *Cedrus atlantica* (Morocco) in semiarid (Mediterranean basin), temperate oceanic (western Europe), cool-summer continental (central Europe) and subarctic (Fennoscandia) climates. The most sampled trees were temperate (*Quercus robur*, *Q. petraea*) and Euro-Siberian (*Pinus sylvestris*, *P. uncinata*) taxa, with sites distributed across most of their climatic ranges, including both interior (e.g., 'Dra' in Germany, 'Ren' in France) and peripheral (e.g., 'Ina' in Finland, 'Lil' in Spain) populations. Sampled stands spread along broad latitudinal (from 32°58'N to 68°56'N) and altitudinal (from 5 to 2,200 m a.s.l.) gradients, with high-altitude sites concentrated in southern Europe and Morocco. Conifers were the dominant species in cold boreal and dry Mediterranean zones (i.e., high latitude or altitude sites), whereas oaks were mainly found in humid western and central European lowlands. The distance between pairs of sites varied from about 50 km up to 4,500 km.

Increment cores were collected from numerous dominant trees (mean = 41; median = 25) at each site (*SI Appendix*, Table S5.2), and tree-ring width (TRW) series were prepared and cross-dated following standard dendrochronological procedures (Cook & Kairiukstis 1990). Tree-ring width was measured under a binocular microscope to a precision of ±0.01 mm. Visual cross-dating and ring-width measurements were validated using the program COFECHA (Holmes 1983). Temporal trends in absolute tree growth were estimated for the period 1900–2003 through the slope (*b*) of the linear regression of raw TRW records on time. We considered that these trends were age-independent as it is customarily assumed for old-growth forest stands (>200 years old). Individual series were then subjected to detrending with the Friedman supersmoother spline (Friedman 1984) and posterior autoregressive modelling. This procedure aims at eliminating biological growth trends and potential disturbance effects and generates stationary (mean = 1) series of dimensionless indices that preserve a common variance encompassing interannual time scales (i.e., high-frequency variability potentially related to climate). Finally, site chronologies were obtained by averaging the index values of the series using a bi-weight robust mean (Cook & Kairiukstis 1990). These procedures were performed using the program ARSTAN (Cook & Krusic 2005). The expressed population signal (*EPS*) with a threshold value of 0.85 was used to evaluate the adequacy of the sample size for capturing the hypothetical population signal at

the stand level (Wigley *et al.* 1984). As a result, all chronologies were found to be well replicated, showing a reliable TRW signal for the study period 1900–2003 (*SI Appendix*, Table S5.2).

At least two accurately dated intact cores from four or more trees per site were selected for subsequent isotope analyses (McCarroll & Loader 2004). Annual tree rings from each core were split under a microscope on a glass plate using a razor-blade. In general, the whole ring was analyzed for conifers, whereas only latewood was used for oaks to avoid carry-over effects from previous year reserves on earlywood production (Helle & Schleser 2004). At most sites, rings corresponding to the same year were pooled and milled to provide enough material for isotope analysis. To remove extractives and lignin from wood samples, *a*-cellulose extraction was applied following standard protocols (Boettger *et al.* 2007). Carbon was extracted from samples as CO_2 using conventional combustion methods and oxygen was converted to CO by pyrolysis prior to mass spectrometer analysis. Isotope ratios were expressed as per mil deviations using the δ notation relative to Vienna Pee Dee Belemnite (VPDB; for carbon) and Vienna Standard Mean Ocean Water (VSMOW; for oxygen) standards. Overall accuracy of the analyses (SD of working standards) was 0.06‰ ($\delta^{13}C$) and 0.25‰ ($\delta^{18}O$).

To account for changes in $\delta^{13}C$ of atmospheric CO_2 ($\delta^{13}C_{air}$) due to fossil fuel emissions (Keeling 1979), carbon isotope discrimination in wood samples ($\Delta^{13}C$) was estimated from $\delta^{13}C_{air}$ and *a*-cellulose $\delta^{13}C$ in plant material ($\delta^{13}C$), as described by Farquhar & Richards (1984):

$$\Delta^{13}C = \frac{\delta^{13}C_{air} - \delta^{13}C}{1 + \delta^{13}C} \quad (5.1)$$

$\delta^{13}C_{air}$ was inferred by interpolating a range of data from Antarctic ice-core records, together with modern data from two Antarctic stations (Halley Bay and Palmer Station) of the CU-INSTAAR/NOAA-CMDL network for atmospheric CO_2 measurements, as described in Ferrio *et al.* (2005). According to these records, the $\delta^{13}C_{air}$ value applied to extant α-cellulose samples varied between −8.09 and −6.64‰ for the period 1900–2003.

Residual isotope chronologies ($\Delta^{13}C$ and $\delta^{18}O$) were obtained following the same procedure applied to ring-width records. Both residual ring-width and isotope chronologies were used as input for statistical analyses. The time span covered by the study was the whole twentieth century (1900–2003), that is, the period when the impact of climate change on tree performance becomes noticeable (e.g., Pretzsch *et al.* 2014; Shestakova *et al.* 2016).

Analysis of spatial variability in tree growth

First, principal component analyses (PCA) was used to summarize temporal (annual) growth patterns across the network of 23 chronologies. PCA was performed on the

correlation matrix for the time span common to all TRW chronologies (1900–1998). Next, the temporal coherence in growth patterns across chronologies was characterized to determine how distant the common variability in ring-width patterns (i.e., spatial synchrony) extended over Europe. To this end, simple correlation coefficients (*r*) between all pairs of chronologies, calculated over the period 1900–2003 on a yearly basis, were regressed on the geographic distance for site pairs using a negative exponential function. Moreover, the modified correlogram technique (Koenig & Knops 1998) was employed to characterize the spatial autocorrelation in the network by testing for significant correlations among chronologies located at 500 km distance classes. Chronologies located farther than 2,500 km apart were combined into a single class in order to ensure similar number of pairwise comparisons at each distance class. Hence, six classes were defined ranging from 0–500 to >2,500 km. Besides, we also investigated the temporal stability of spatial patterns for the two halves of the study period separately (1900–1950 and 1951–2003). To carry out spatial analyses we used the non-centered correlogram function (correlog.nc) implemented in the package 'ncf' ver. 1.1-5 (R software, ver. 3.2.2, R Foundation for Statistical Computing, Vienna, Austria).

The outcome of the spatial analysis was used to group chronologies into homogeneous subsets so as to characterize growth patterns along environmental (geographic, climatic) gradients. To this end, the following two criteria were applied: (*i*) at any given subset the maximum distance among chronologies should fall within the range of significant spatial signals as inferred from spatial autocorrelations; (*ii*) the minimum group size should be restricted to four sites to ensure reliability of statistical inference (see below). Due to the relatively sparse spatial coverage of sampling sites, we allowed an individual site to be assigned simultaneously to more than one group following criterion (*i*). As a result, a total of 14 groups were obtained.

Modeling of spatio-temporal patterns in tree performance

Temporal coherence of ring-width signals among chronologies

The investigation of common ring-width fluctuations among chronologies (i.e., common signal strength) was performed through random modeling as described in Shestakova *et al.* (2014). First, we calculated the degree to which the complete set of chronologies ($i = 1$ to 23) contained a common temporal signal over the study period (1900–2003). Let W_{ij} stand for ring-width W of the ith chronology in the jth year. Then the estimators can be defined in terms of the following random model (random variables are shown underlined):

$$\underline{W}_{ij} = \underline{Y}_j + \underline{e}_{ij} \qquad (5.2)$$

where Y_j is a random effect of the jth year and e_{ij} is a random deviation of the ith chronology

in the *j*th year. Here, we assume that the year effects behave as if they came from a normal distribution with mean zero and variance σ_Y^2. The reproducibility of observations by the set of *I* chronologies can be estimated as (Shestakova *et al.* 2014):

$$\hat{a} = \frac{\sigma_Y^2}{\sigma_Y^2 + \sigma_e^2} \tag{5.3}$$

Hereafter we will refer to $\hat{a}$ as the intra-class correlation or spatial synchrony for the set of *I* chronologies.

Next, the 23 chronologies were grouped into 14 homogeneous subsets as described in the previous section. Spatial synchrony estimates at the group level were also obtained by applying Eq. 5.3. Each group consisted of a number of neighboring forest stands (≥4) sharing some degree of growth variability. Four was the minimum amount of chronologies that ensured convergence in the iteration process, hence providing a model solution to Eq. 5.2. This approach was tested for the entire study period (1900–2003) and for two consecutive, non-overlapping periods: 1900–1950 and 1951–2003. Based on these results, we also found appropriate to investigate the general patterns of spatial synchrony for functional groups (conifers or oaks) or subregions (north or central-south-west) independently.

Relationships between radial growth and stable isotopes

The associations between pairs of traits (TRW, $\Delta^{13}C$, $\delta^{18}O$) at the group level were investigated through bivariate analyses applied to the time series (chronologies) of *J* years (White & Hodge 1989). Following Shestakova *et al.* (submitted), the single trait mixed model (3) was extended to take into account simultaneously the information available on a pair of traits (TRW and $\Delta^{13}C$; TRW and $\delta^{18}O$; $\Delta^{13}C$ and $\delta^{18}O$). The temporal (year) component of a general (simple) correlation between traits, which also includes residual cross-product effects as detailed in Shestakova *et al.* (submitted), was estimated by the partition of the general covariance (i.e., across years and chronologies) in its year and residual components. Broadly speaking, this approach measures (through a correlation coefficient) the extent by which TRW variability common to a set of chronologies is associated to variability in isotope records that is also common to the same set of chronologies. In other words, we propose to quantify the relevance of a physiological trait ($\Delta^{13}C$, $\delta^{18}O$) as driver of regional forest growth by estimating how much of the temporally coherent variability in TRW across chronologies is attributable to a concurrent change in temporally coherent variability in isotopic records. We claim that this novel quantification is very pertinent for characterizing the variable role of a putative physiological driver of tree growth across large geographical areas, since it allows characterizing external forcing influences on tree performance separately from local effects and species-specific responses in a straightforward manner. Therefore, inferences on physiological drivers of tree growth continent-wide were based on this approach.

In particular, the correlation of year effects (r_Y) was calculated as:

$$r_Y = \frac{\sigma_{Y_{12}}}{\sqrt{\sigma^2_{Y_1} \times \sigma^2_{Y_2}}} \quad (5.4)$$

where $\sigma_{Y_{12}}$ is the common variability of year effects underlying traits 1 and 2 (covariance), $\sigma^2_{Y_1}$ stands for the variance component estimate of year effects for trait 1 and $\sigma^2_{Y_2}$ stands for the variance component estimate of year effects for trait 2. We estimated the covariance component matrix between pairs of traits from the bivariate analysis for the entire period (1900–2003) and, also, for the two halves of the study period (1900–1950 and 1951–2003).

The statistical analyses were performed with SAS/STAT (ver. 9.4, SAS Inc., Cary, NC, USA). We used the MIXED procedure for variance-covariance modeling and estimation of variance components through restricted maximum likelihood (REML). The covariance structure was specified using the RANDOM statement.

Meteorological data

Monthly mean temperature, total precipitation and potential evapotranspiration were used to assess relationships with radial growth. Meteorological variables (mean temperature and total precipitation) were obtained from the nearest grid point to each sampling site of the high-resolution climate network (Climatic Research Unit, CRU TS 3.21; Harris *et al.* 2014). The CRU dataset provides climate series available on a 0.5°×0.5° grid-box basis interpolated from meteorological stations across the globe and extends back to 1901. Potential evapotranspiration was estimated using the Hargreaves method (Hargreaves & Samani 1982).

To assess site-specific growth and physiological responses to climate, simple correlations between TRW, $\Delta^{13}C$ or $\delta^{18}O$ chronologies and climate were computed over the period 1901–2003. To assess temporal stability of trait relationships with climate, correlation analyses were also conducted for the two halves of the study period (1900–1950 and 1951–2003). Climate relationships were analyzed from the previous October to September of the year of tree-ring formation.

Interpretation of biogeographical patterns of tree performance

To understand and summarize spatial patterns of tree growth and its ecophysiological drivers across environmental gradients, changes in growth synchrony ($\hat{d}$) and in the relationships between radial growth and stable isotopes (r_Y) were characterized at the group level and evaluated as a function of biophysical variables. To this end, we used geographic (latitude, longitude and altitude) and climate (mean annual temperature [MAT], mean annual precipitation [MAP] and potential evapotranspiration [PET]) records averaged across sites for any particular group. It should be noted, however, that geographical and climatic records

in the network correlated quite strongly among themselves: MAT decreased linearly with increasing latitude ($r = –0.84$; $P < 0.001$) and longitude (or distance inland from the Atlantic Sea) ($r = –0.58$; $P < 0.01$); MAT also increased with increasing elevation, as high altitude sites were located in southern Europe and Morocco ($r = 0.40$; $P < 0.05$). Similarly, PET was negatively related to latitude ($r = –0.88$; $P < 0.001$) and longitude ($r = –0.59$; $P < 0.01$), and positively to elevation ($r = 0.62$; $P < 0.01$). Conversely, MAP did not show significant relationships with geographical features. Simple correlation coefficients (r) were used to investigate the relationships between $\hat{a}$ or r_Y values and their underlying environmental factors. Also, the stability of these relationships over time was assessed through correlation analysis for both halves of the study period independently (1900–1950 and 1951–2003).

Results

General features of tree-ring chronologies

The ring-width chronologies were of good quality for the period 1900–2003 (*EPS* > 0.85), with *Rbar* values ranging from 0.21 (*Pinus sylvestris* in Switzerland) to 0.51 (*Cedrus atlantica* in Morocco) (*SI Appendix*, Table S5.2). *Rbar* values were similar for hardwoods and conifers (mean = 0.39 *vs.* 0.36, respectively; two-tailed Student *t*-test, $P > 0.05$), indicating a comparable internal coherency of chronologies for both functional groups. MAT ranged from –1.2 to 15.1°C among sites. January was the coldest month (mean temperatures ranging from –14.1 to 7.6°C) and July the warmest month (mean temperatures ranging from 12.6 to 24.0°C). MAP was highly variable and ranged from 432 to 1,880 mm among sites. Water deficit (i.e., evapotranspiration exceeding precipitation) occurred for periods of up to seven months (from March until October), depending on site, with summer drought (June to August) being a common feature at most sites (*SI Appendix*, Table S5.1).

In general, hardwoods had greater radial growth than conifers (average mean ring-width of the raw chronologies = 1.38 mm *vs.* 0.72 mm, respectively; two-tailed *t*-test, $P < 0.001$). Also, temperate forests from central Europe, situated at the core of most species' distribution areas (~ 45°–55°N), had greater radial growth (mean = 1.12 mm) and growth fluctuations (±0.028 mm; average of ring-width standard deviation [SD] of the raw chronologies) than geographically peripheral populations (0.79 mm and ±0.017 mm, for average growth and fluctuations, respectively; one tailed *t*-tests, $P < 0.05$) (*SI Appendix*, Table S5.2). At the site level, four and nine chronologies showed significant positive and negative trends in absolute radial growth (slope b, $P < 0.05$) for the period 1900–2003, respectively, while no significant trend was detected for the remaining ten chronologies (*SI Appendix*, Table S5.2). However, growth trends were not statistically different between functional groups (mean = –0.0017 mm year^{-1} *vs.* –0.0013 mm year^{-1} for conifers and hardwoods, respectively; two-tailed Student *t*-test, $P > 0.05$). There were geographical gradients neither in

the distribution of mean ring-width values of the raw chronologies nor in temporal trends of radial growth across the study area (*SI Appendix*, Table S5.3).

Hardwoods consistently showed higher $\Delta^{13}C$ mean values than conifers (18.4‰ *vs.* 16.8‰, respectively; two-tailed *t*-test, $P < 0.01$) and also higher $\Delta^{13}C$ fluctuations (SD = ±0.07‰ *vs.* ±0.05‰, respectively; two-tailed *t*-test, $P < 0.05$). On the other hand, $\delta^{18}O$ mean and SD values did not vary significantly between functional groups (*SI Appendix*, Table S5.2). There were significant latitudinal gradients in stable isotope signals, with a positive relationship between mean chronology $\Delta^{13}C$ and latitude ($r = 0.72$; $P < 0.001$) and a negative relationship between mean chronology $\delta^{18}O$ and latitude ($r = –0.82$; $P < 0.001$) (*SI Appendix*, Table S5.3). The mean isotopic records were also associated with longitude and altitude, although the relationships were weaker than those with latitude (*SI Appendix*, Table S5.3). Overall, hot and dry sites had lower $\Delta^{13}C$ and higher $\delta^{18}O$ values compared to cool and moist sites (*SI Appendix*, Table S5.3). In both cases, thermal variables (MAT and PET) explained a sizeable fraction of variation in isotope signals ($r = 0.46–0.81$), whereas MAP was unrelated to site differences in mean isotope values. The observed spatial patterns in $\Delta^{13}C$ and $\delta^{18}O$ were primarily due to conifers, which spanned across larger geographical area as compared to broad-leaved species (*SI Appendix*, Table S5.3). The relationship between mean $\Delta^{13}C$ and $\delta^{18}O$ was significant across Europe ($r = –0.80$; $P < 0.001$), but not the association between mean ring-width and $\Delta^{13}C$.

Spatial consistency in tree-ring signals

The Principal Component Analysis performed on TRW chronologies detected five principal components (PCs) accounting for 48.0% of total variance for the period 1900–1998. The first PC, which explained 13.2% of variance, had positive loadings for all chronologies, except for the Moroccan site with the only *Cedrus atlantica* stand (*SI Appendix*, Fig. S5.1). The highest PC1 loadings corresponded to western and central European chronologies, indicating larger similarities in growth as compared to peripheral chronologies, located farther away from each other. The second PC, which explained 10.1% of variance, was also related to geographic position: positive PC2 loadings corresponded to southwestern chronologies, while northeastern chronologies had negative loadings (*SI Appendix*, Fig. S5.1). The remaining three PCs accounted for 9.1, 8.4 and 7.2% of variance, respectively, and showed mixed spatial signals indicating species-specific differences and/or the influence of local conditions on tree growth.

Next, the correlations between pairs of chronologies were examined. Naturally, such correlations decreased gradually with increasing distance among sites (Fig. 5.1a); this effect accounted for 27% of variability in inter-site correlation coefficients ($P < 0.001$). The highest correlations were found between *Quercus* stands from central Europe and between *Pinus*

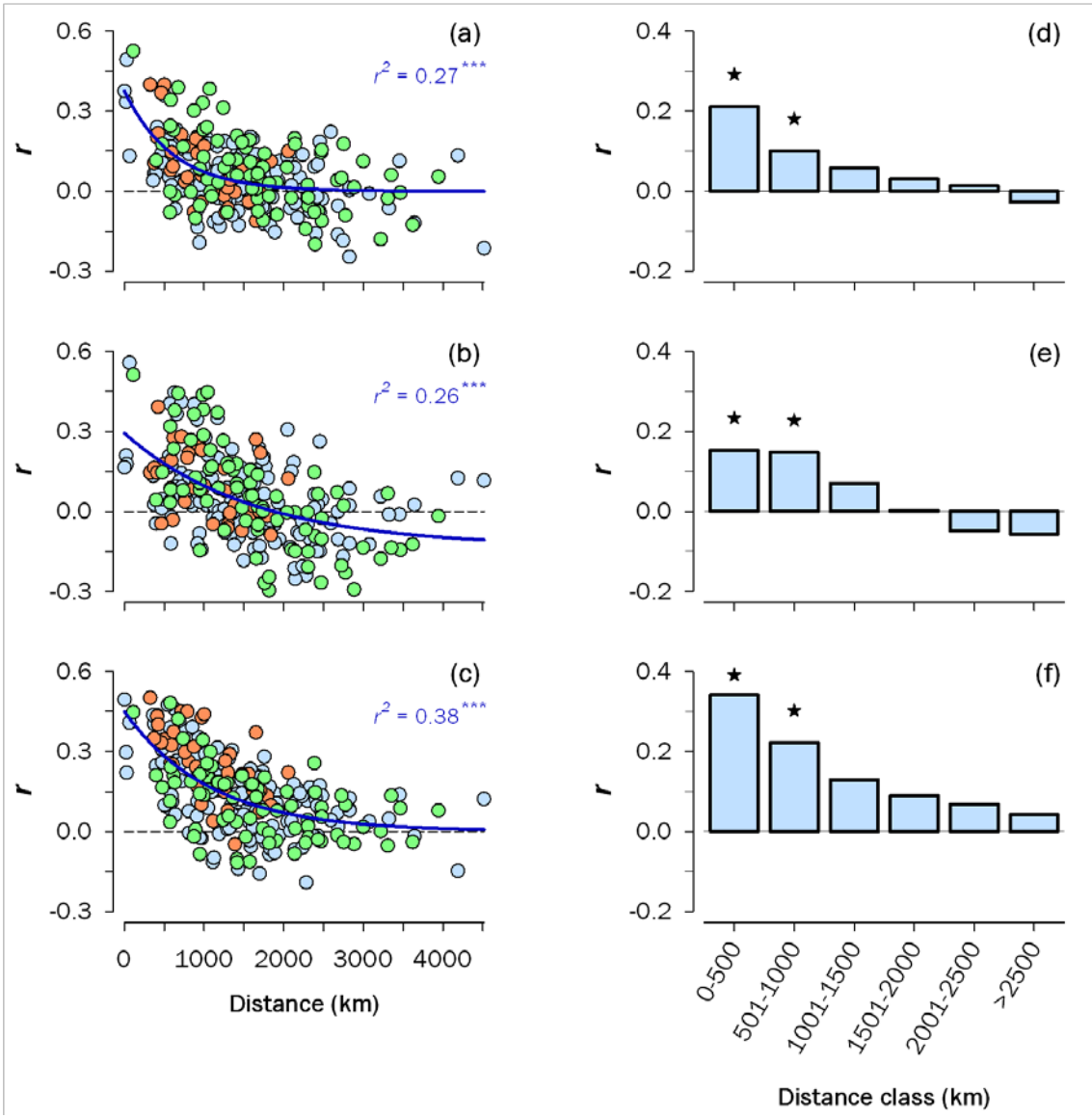

Figure 5.1. Spatial patterns of tree performance across Europe for the period 1900–2003: **(a, d)** tree-ring width, **(b, e)** $\Delta^{13}C$, **(c, f)** $\delta^{18}O$. *(Left panels)* Pairwise correlations of tree-ring chronologies as a function of geographical distance. The patterns are summarized by regressing the correlation coefficients (*r* values) involving pairs of chronologies (*y*-axis) on their corresponding distance (*x*-axis) by using a negative exponential function ($y = a + be^{-cx}$). Note that $a = 0$ in panels (a) and (c). Different dot colors indicate pairwise correlations within and between functional groups: conifers (green), oaks (orange), and blue (mixed conifer–oak). *(Right panels)* Spatial structure of tree growth patterns across European forests. The spatial autocorrelation in the tree-ring network was characterized for six consecutive distance classes (listed on the *x*-axis). Mean *r* values and their statistical significance (*P*) within each distance class were estimated from 1,000 randomizations. Significant correlation coefficients ($P < 0.05$) are indicated by asterisks.

stands from northeastern Europe ($r \geq 0.30$). Significant spatial autocorrelations spread over distances up to 1,000 km, with a mean correlation of 0.21 and 0.10 for sites within distance ranges of 0–500 and 501–1,000 km, respectively (Fig. 5.1d).

Spatial associations were also investigated for stable isotope chronologies. We found spatial autocorrelation patterns similar to those observed for ring-width, with distance between chronology pairs accounting for 26 and 38% of variability in inter-site correlation coefficients for $\Delta^{13}C$ and $\delta^{18}O$, respectively ($P < 0.001$; Fig. 5.1b,c). Significant spatial autocorrelations in both isotopes also spread over distances up to 1,000 km, with generally higher values for $\delta^{18}O$ than for $\Delta^{13}C$ (Fig. 5.1e,f).

Geographic patterns in growth synchrony

The selected 14 groups were comprised of four to seven chronologies sharing temporal growth patterns, with the largest groups corresponding to central Europe (i.e., area with higher density of sampling sites) (Fig. 5.2). Growth synchrony ($\hat{a}$) varied considerably among groups, ranging from 0.04 ± 0.006 to 0.27 ± 0.028 (mean ± SE) for the period 1900–2003 (Fig. 5.2). $\hat{a}$ values were independent of the average distance between sites at the group level, with groups showing the lowest and highest $\hat{a}$ having average inter-site distances of 785 ± 118 km and 821 ± 94 km (mean ± SE), respectively. Also, the number of chronologies at the group level did not influence $\hat{a}$ values (results not shown).

Differences in growth synchrony among groups were related to their spatial distribution across Europe. Specifically, $\hat{a}$ correlated positively with group mean latitude ($r = 0.77$, $P < 0.01$) (Fig. 5.3a), followed by elevation ($r = –0.68$, $P < 0.01$) and longitude ($r = 0.53$, $P = 0.06$) (*SI Appendix*, Fig. S5.2a,b). It should be noted, however, that geographic coordinates were not independent at the group level: latitude was positively related to longitude ($r = 0.78$, $P < 0.01$) and negatively to elevation ($r = –0.77$, $P < 0.01$), and longitude and elevation were also negatively associated ($r = –0.55$, $P < 0.05$). To check for consistency in such geographical gradients we explored an independent, larger dataset of ring-width chronologies obtained from the International Tree-Ring Data Bank (ITRDB; Grissino-Mayer & Fritts 1997) and made up of the same species present in ISONET ($n = 80$; 52 *Pinus* chronologies and 28 *Quercus* chronologies). We also detected strong latitudinal and longitudinal gradients in $\hat{a}$ (*SI Appendix*, section 1 and Fig. S5.3). This led us to discard the possibility that the geographical trends in $\hat{a}$ could be sensitive to the characteristics of the tree-ring network used.

Next, chronologies were classified into independent groups according to taxonomic (conifers *vs.* hardwoods) or geographic (north *vs.* central-south-west) criteria. We found that $\hat{a}$ value in hardwoods was over 2.5-fold higher than that of coniferous (Fig. 5.3b), which could be attributed, at least partly, to a lower average distance among oak chronologies as compared to the more widely distributed conifer species (897 ± 76 km and 1,497 ± 100 km, respectively;

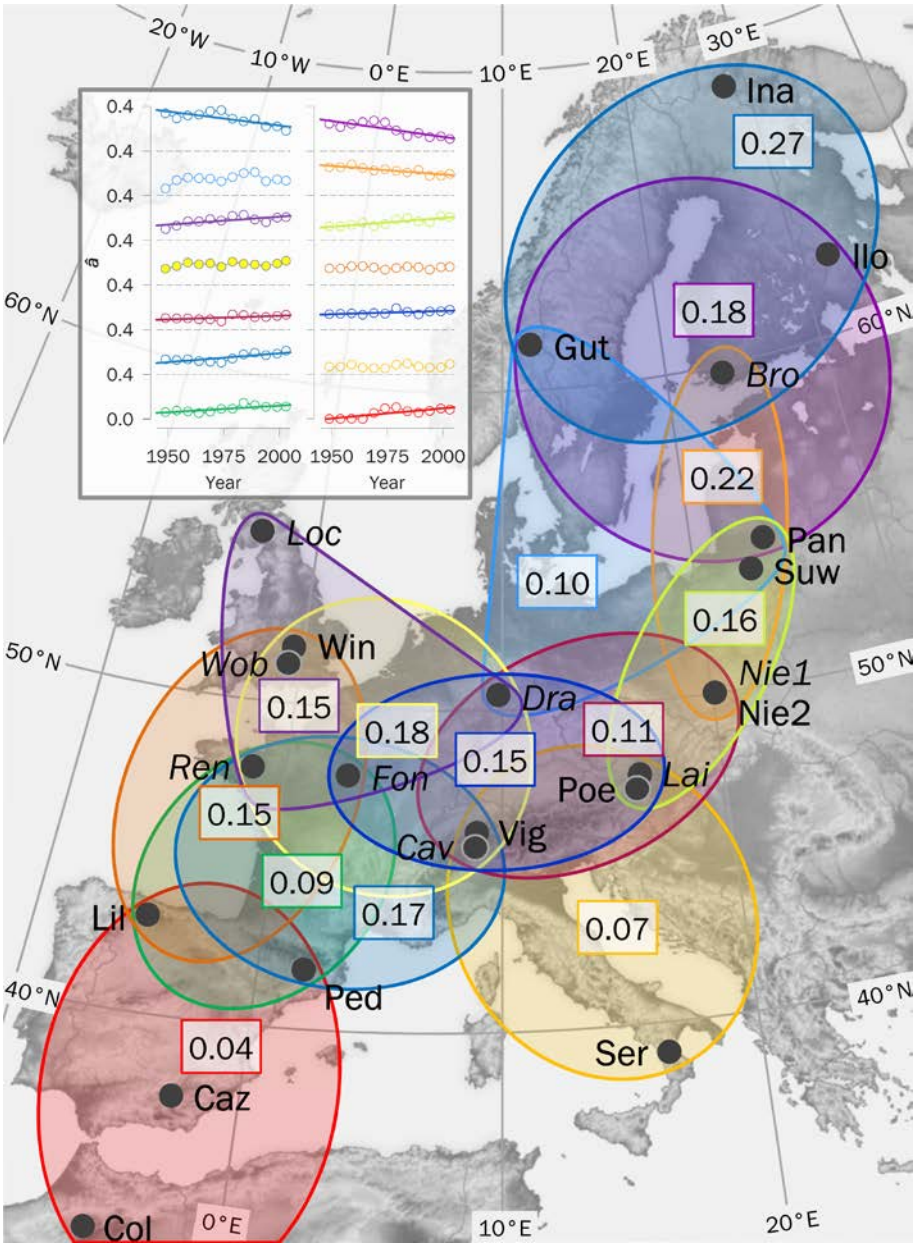

Figure 5.2. Geographical distribution of study sites, definition of site groups and synchrony in radial growth at the group level. Each dot identifies a chronology (n = 23) according to the codes shown in *SI Appendix*, Table S5.1 (conifer codes are shown all-uppercase; oak codes are additionally shown in italics). Each colored circle identifies a group of chronologies that are separated in pairs <1,000 km (see Fig. 5.1d for the distance threshold where significant radial growth patterns are shared among chronologies) with its corresponding growth synchrony ($\hat{a}$) shown in a rectangle. At least four neighbouring sites form a group (total number of groups, n = 14). $\hat{a}$ values are estimated using residual ring-width chronologies for the period 1900–2003. (*Inset*) Temporal trends in growth synchrony at the group level calculated for successive 50-year periods lagged by five years. Different colors identify individual group as defined in above. Only significant linear trends ($P < 0.05$) are shown. Groups sorted latitudinally, from north (top) to south (bottom). Values on the x-axes correspond to the last years of 50-year moving intervals.

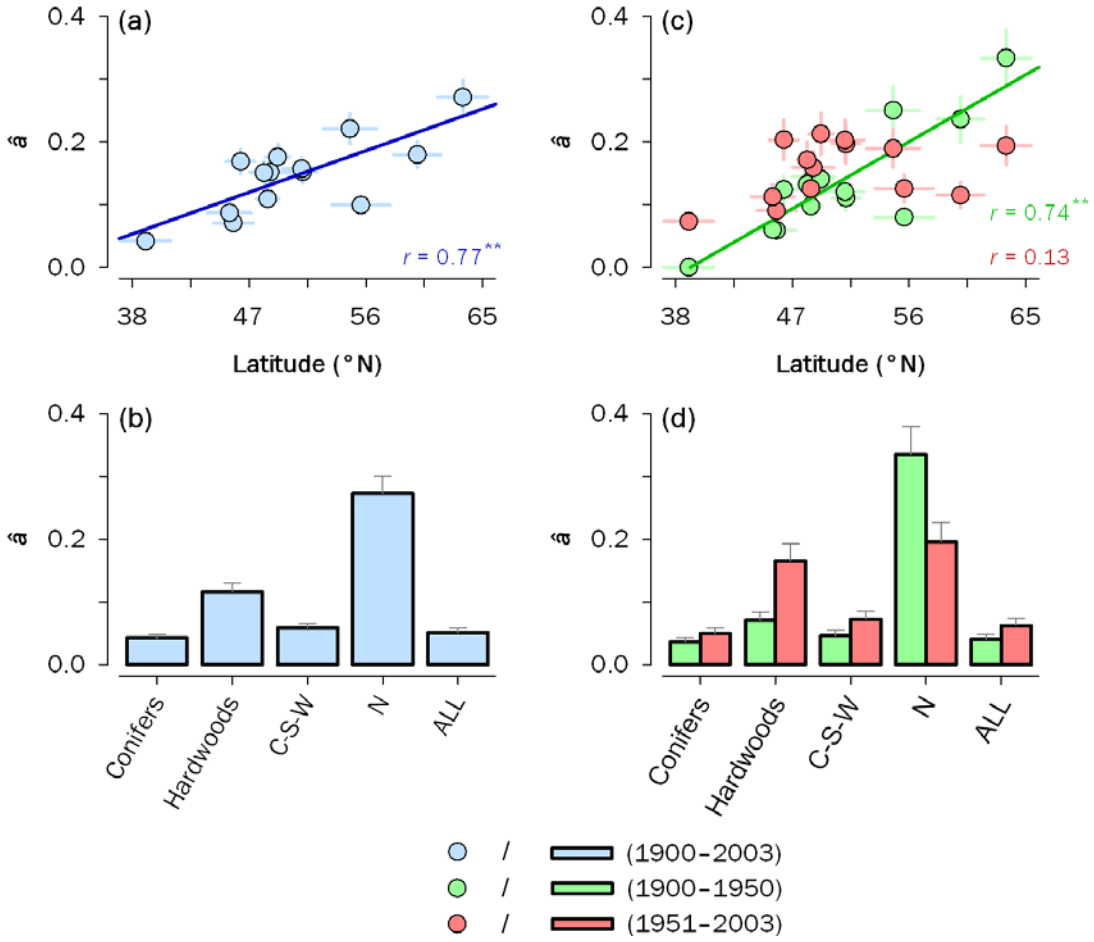

Figure 5.3. Growth synchrony patterns across Europe. *(Upper panel)* Geographical patterns of growth synchrony (*â*) at the group level for the entire period 1900–2003 **(a)** and change in *â* for two consecutive periods (1900–1950 and 1951–2003) **(c)** as a function of latitude. The patterns are characterized as linear regressions of spatial synchrony for each group (*y*-axis) on its corresponding latitude (*x*-axis). Significant linear trends along the latitudinal gradient are depicted as thick lines ($^{*}P < 0.05$; $^{***}P < 0.001$). *(Lower panel)* Patterns of growth synchrony according to functional group (Conifers or Hardwoods), subregion (Central-South-West [C-S-W] or North [N]) and also for the entire set of chronologies (ALL), estimated for the entire period 1900–2003 **(b)** and for two consecutive periods (1900–1950 and 1951–2003) **(d)**. All calculations are based on residual ring-width chronologies. Error bars denote standard errors.

mean ± SE). On average, northern chronologies showed a *ca.* 4.5-fold higher spatial synchrony than their counterparts from the rest of Europe plus Morocco (Fig. 5.3b). Although the mean distance among pairs of chronologies was lower in northern Europe than in central-southern-western Europe, the aforementioned latitudinal trend in *â* suggests that such differences in spatial synchrony across Europe constitute a salient property of forest ecosystems continent-wide. Such remarkable synchrony gradient continent-wide could be

related to the fact that the main climatic drivers of tree growth changed quite consistently along the network, being mainly dependent on latitude. Indeed, the best climatic predictor of annual growth in Fennoscandia was summer temperature, with productivity peaking in years with warmer summers (*SI Appendix*, Fig. S5.5a). In contrast, fluctuations in radial growth were best captured by drought-related indicators at central and southern latitudes, with productivity often decreasing during dry and/or hot summer years (*SI Appendix*, Fig. S5.5a,b). Here we often observed positive growth responses to high winter temperatures, suggesting a varying degree of co-limitation by cold winters and dry summers. More clear-cut, common climate signals were present in isotope records, especially associated to summer temperatures (negatively with $\Delta^{13}C$, positively with $\delta^{18}O$) and summer precipitation (positively with $\Delta^{13}C$, negatively with $\delta^{18}O$) (*SI Appendix*, Fig. S5.5c–f). Notably, climate variables underlay most geographic variation in $\hat{a}$ among groups (Fig. 5.4). We found strong negative relationships between $\hat{a}$ and both MAT ($r = -0.84$, $P < 0.001$) and PET ($r = -0.88$, $P < 0.001$), which is consistent with a gradual decrease in temperature with increasing latitude, whereas the correlation with MAP was weak (Fig. 5.4a–c).

We then examined if synchrony patterns across European forests changed between both halves of the twentieth century. At the group level, $\hat{a}$ often increased after 1950 compared with the preceding period, especially at low and mid latitudes (Fig. 5.2 inset; Fig. 5.3c). However, three groups from northern Europe exhibited a marked decrease in $\hat{a}$ after 1950 (Fig. 5.2 inset; Fig. 5.3c). On the other hand, less coherent changes in $\hat{a}$ across climatic gradients (MAT, PET) were observed in the second half of the twentieth century (Fig. 5.4d–f). Such opposite changes in growth synchrony between northern and central-southern-western Europe along the twentieth century weakened the association between $\hat{a}$ and biogeographic factors, resulting in more comparable, but less geographically and climatically dependent $\hat{a}$ values across the continent in the second half of the century (Figs. 5.3, 4 and *SI Appendix*, Fig. S5.2). These results agreed with the observed temporal changes in regional synchrony patterns (i.e., increase in central-southern-western Europe and decrease in northern Europe) (Fig. 5.3d) and with the increase of common variance gathered by the PC1, from 14.9% to 24.1% for the first and second half of the twentieth century, respectively. Moreover, when northern chronologies were excluded from the analysis, the spatial autocorrelation in growth fluctuations after 1950 spread over distances up to 1,000 km, with significant autocorrelations reaching smaller distances before 1950 (up to 500 km) (*SI Appendix*, Fig. S5.4). At the taxonomic level, both functional groups exhibited enhanced growth synchrony in the latter period, especially for hardwoods (Fig. 5.3d).

Tree growth patterns as related to isotopic signals

The amount of common information imprinted in both record types (ring-width and stable isotopes) was also investigated at the group level. We found very different, geographically-

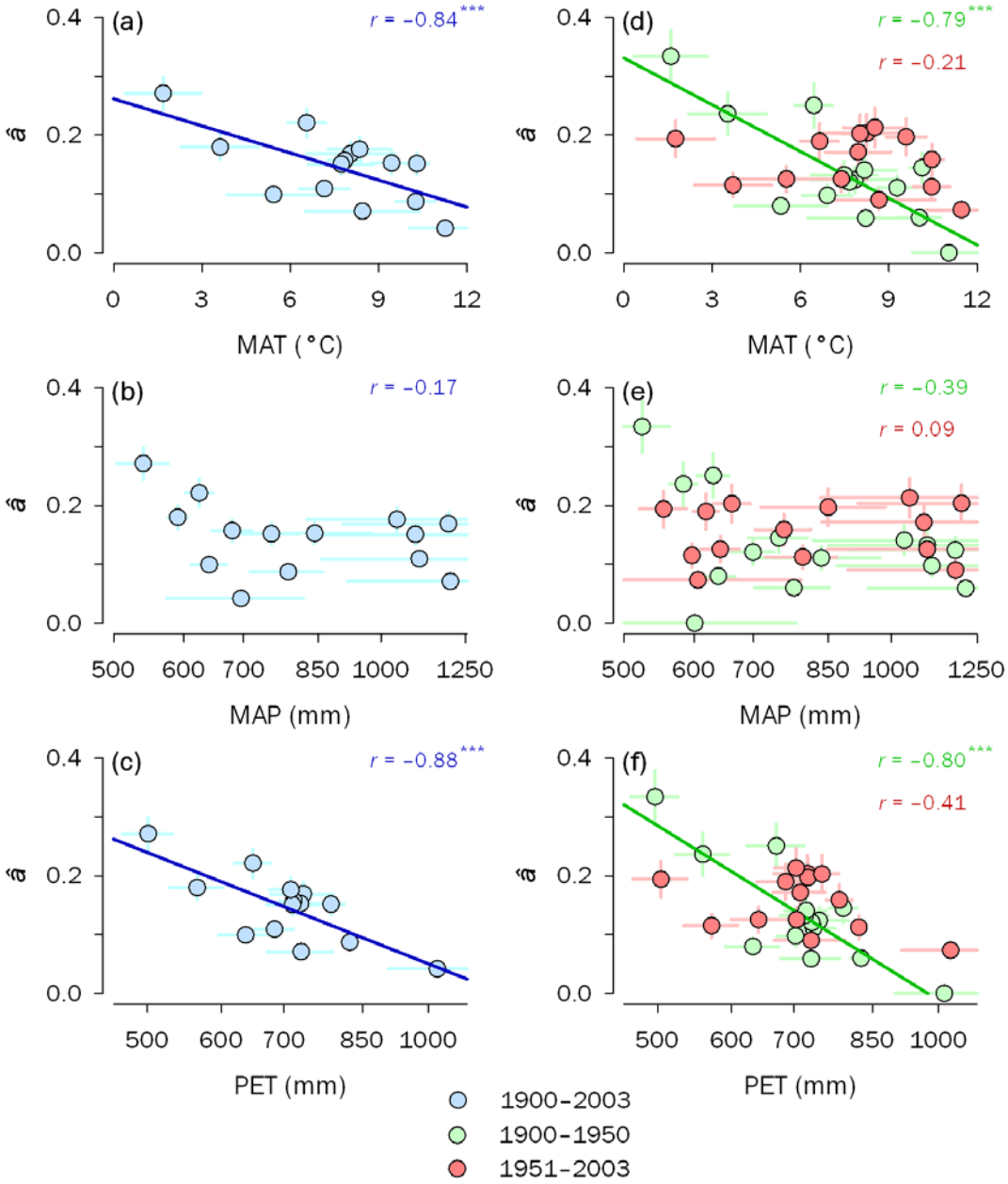

Figure 5.4. Growth synchrony patterns along climatic gradients at the group level. Synchrony patterns (*â*) for the entire period 1900–2003 *(left panel)* and change in *â* for two consecutive periods (1900–1950 and 1951–2003; *right panel*) as a function of **(a, d)** mean annual temperature (MAT); **(b, e)** total annual precipitation (MAP); (**c, f)** annual potential evapotranspiration (PET). The patterns are characterized as linear regressions of spatial synchrony for each group (*y*-axis) on its corresponding mean climate variable (*x*-axis). Significant linear trends along the climatic gradients are depicted as thick lines ($^{*}P < 0.05$; $^{***}P < 0.001$). Error bars denote standard errors.

structured relationships between ring-width and either $\Delta^{13}C$ or $\delta^{18}O$ strongly positive at low latitudes (<45°N), while it reversed at high latitudes (>55°N), hence following a clear

latitudinal gradient (r = –0.90, P < 0.001). Similarly, we detected a latitudinal trend in the relationship TRW *vs.* $\delta^{18}O$, with more negative associations found at low latitudes (r = 0.62, P < 0.05; Fig. 5.5b). On the other hand, the longitudinal pattern of the relationships between TRW and isotope records was weaker (negative for $\Delta^{13}C$, positive for $\delta^{18}O$), whereas it was non-significant for elevation (*SI Appendix*, Figs. S5.6 and S5.7). The relationships between TRW and stable isotopes were also related to both MAT and PET at the group level, but no significant associations were found with MAP (Fig. 5.6). The climate gradients in the relationships between TRW and stable isotopes were always stronger for $\Delta^{13}C$ than for $\delta^{18}O$. On the contrary, the relationships between $\Delta^{13}C$ and $\delta^{18}O$ calculated at the group level were systematically negative, but unrelated to geographical gradients (*SI Appendix*, Fig. S5.8). It is interesting to stress that these clear biogeographical structures were very much obscured if using site-level simple correlations instead of group-level correlations of year effects (*SI Appendix*, Fig. S5.9).

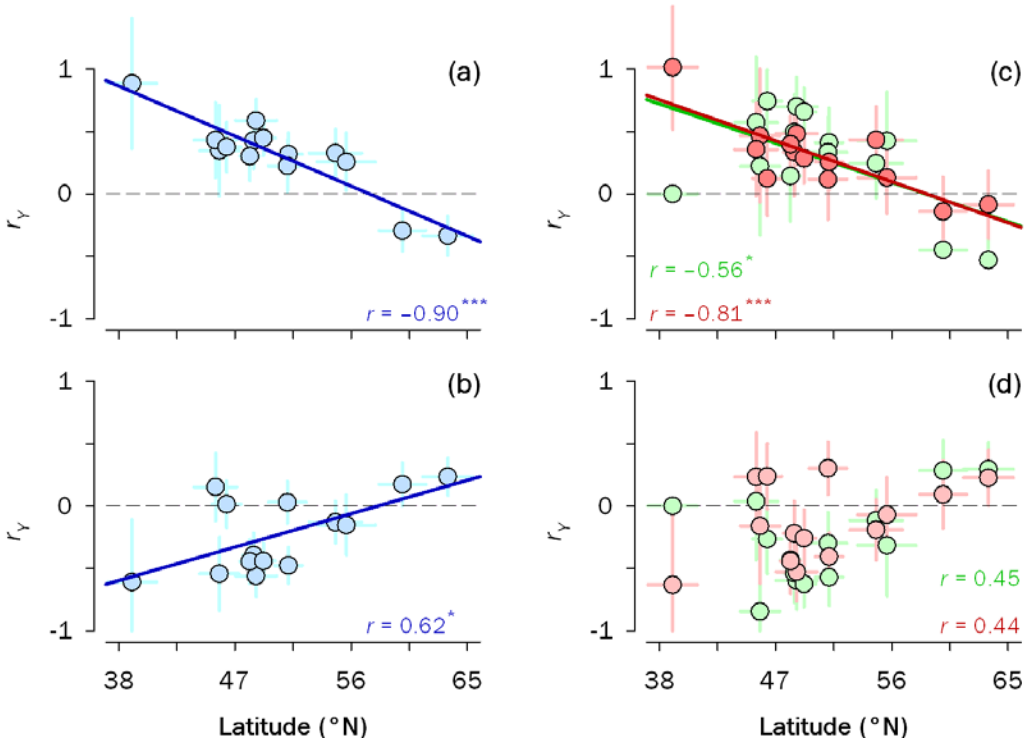

Figure 5.5. Geographical patterns of the relationship between ring-width and isotope chronologies across Europe for **(a, c)** $\Delta^{13}C$ and **(b, d)** $\delta^{18}O$. The correlations of year effects (r_Y) at the group level are estimated using residual ring-width and isotope chronologies for the entire period 1900–2003 *(left panels)* and for two periods separately (1900–1950 and 1951–2003; *right panels*). The patterns are characterized as linear regressions of mean bivariate correlations for each group (y-axis) on its corresponding latitude (x-axis). Significant linear trends along the latitudinal gradient are depicted as thick lines ($^{*}P < 0.05$; $^{***}P < 0.001$). Error bars denote standard errors.

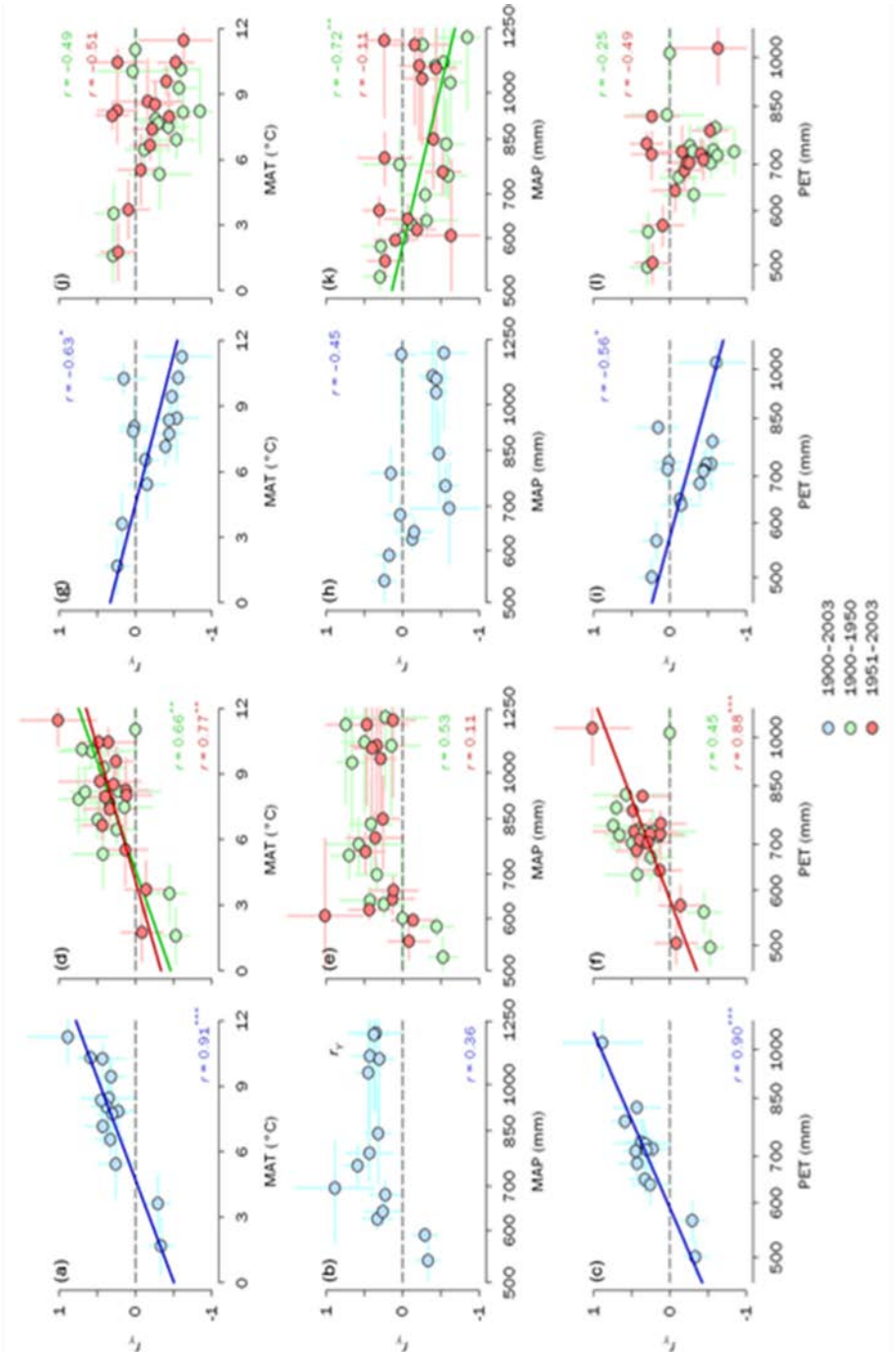

Figure 5.6. Patterns of the relationship between ring-width and stable isotope chronologies along climatic gradients across Europe. The correlations of year effects (r_Y) at the group level are estimated using residual ring-width and **(a–f)** $\Delta^{13}C$ or **(g–l)** $\delta^{18}O$ chronologies for the entire period 1900–2003 *(first and third panels)* and for two periods separately (1900–1950 and 1951–2003; *second and fourth panels*). The patterns are characterized as linear regressions of bivariate correlations for each group (*y*-axis) on its corresponding mean climate variable (x-axis) as follows: *(upper panel)* mean annual temperature (MAT); *(middle panel)* total annual precipitation (MAP); *(lower panel)* annual potential evapotranspiration (PET). Significant linear trends along the climatic gradients are depicted as thick lines ($^{*}P < 0.05$; $^{**}P < 0.01$; $^{***}P < 0.001$). Error bars denote standard errors.

Finally, we evaluated the associations between ring-width and stable isotopes across Europe for each half of the twentieth century independently. The latitudinal signal of the relationship TRW *vs.* $\Delta^{13}C$ was tighter in the second than in the first half of the century (Fig. 5.5c). In turn, this relationship was more dependent on climate factors (MAT and PET) after 1950 (Fig. 5.6d, f); on the contrary, the relationship with MAP vanished in the same period (Fig. 5.6e). As for the relationship TRW *vs.* $\delta^{18}O$, we could not detect clear geographic nor climatic trends for both periods (Figs. 5.5d, 5.6j–l and *SI Appendix*, Fig. S5.7c,d) with the exception of MAP, which showed more negative associations in areas with higher precipitation prior to 1950 (Fig. 5.6k). Notably, correlations between isotopes and climate on a site basis increased consistently in early summer (June) and decreased in September from1950 onwards; conversely, TRW-climate associations became essentially unaltered (*SI Appendix*, Fig. S5.10).

Discussion

This study provides new evidence for substantial, geographically-structured variation in forest tree growth dependencies on leaf-level physiology across Europe and northern Africa. Specifically, our results link tree-ring $\Delta^{13}C$ and $\delta^{18}O$ records to radial growth dynamics of old trees at a continental scale. We report more consistent changes in ring-width *vs.* $\Delta^{13}C$ relationships across biogeographical gradients compared to ring-width *vs.* $\delta^{18}O$, suggesting that $\Delta^{13}C$ is a better indicator of tree performance over continental areas as it integrates simultaneously information on plant carbon and water economies.

The expectation that productivity must be higher in optimal habitats than at the edges of specie's range of distribution was confirmed by differences in site mean radial growth. This observation provided the appropriate frame for evaluating changes in tree growth dependence on physiological performance continent-wide. Since no clear geographical structure in growth changes (stimulation, decline) was found along the twentieth century across Europe, we can argue that the combined effect of climate change and increase in atmospheric CO_2 is eliciting intricate responses in terms of tree productivity and, therefore, forest contribution to Europe's carbon budget, as reported elsewhere (e.g., Jump *et al.* 2006; Lévesque *et al.* 2014; Pretzsch *et al.* 2014).

Despite the existence of taxonomic imprints (e.g., conifers *vs.* oaks; Ferrio *et al.* 2003) and potentially different signals stored in whole-ring and latewood (e.g., Kress *et al.* 2009), stable isotopes records showed strong latitudinal gradients across Europe and northern Africa: indeed, a consistent increment in $\Delta^{13}C$ northwards was accompanied by a clear $\delta^{18}O$ increase southwards which, altogether, translated into a negative association between both isotopes across sites. Although changes in $\delta^{18}O$ could be partly related to varying source water signals, this result pointed to the existence of a latitudinal gradient in water availability (i.e., variation in $\Delta^{13}C$) controlling tree performance across Europe through varying stomatal

regulation of water losses (i.e., variation in $\delta^{18}O$) (Scheidegger *et al.* 2000), as reported at smaller geographical scales (e.g., Shestakova *et al.* 2014).

The extent by which the temporal coherence in radial growth patterns continent-wide was modulated by leaf-level physiological processes (as assessed through stable isotopes) warrants detailed examination. Matching previous observations at subcontinental scales in Eurasia (Shestakova *et al.* 2016), common ring-width signals spread over stands separated up to 1,000 km apart. This realization emphasizes that, along with species-specific properties and local site conditions, climate exerts an important influence determining tree growth across continental areas (Wettstein *et al.* 2011; Babst *et al.* 2013), as no other environmental driver is likely to act on the same range in time and space (Fritts 2001).

Climatic controls of tree-ring signals in European forests

Growth responses to climate continent-wide were largely confirmatory, with temperature-sensitive growth at northern latitudes, precipitation-sensitive growth at central-southern latitudes and mixed signals in temperate and high-elevation European forests (e.g., Babst *et al.* 2013; Sánchez-Salguero *et al.* 2015). Interestingly, site selection in this network was not performed to emphasize climate-growth relationships, but rather to provide a representative coverage of biophysical conditions present across European forests, including taxonomical diversity (Cernusak & English 2015).

The extent of common climate signals present in both isotopes indicated a tight stomatal control of water losses and, indirectly, photosynthesis in summer across Europe (Cullen *et al.* 2008). The fact that such correlations became stronger in June during 1950–2003 points to an advanced onset of drought impacting on tree performance continent-wide, although this effect did not modify ring-width *vs.* climate associations in summer. In fact, aboveground growth is only one of the many possible fates of assimilates and secondary growth is usually regarded as of low priority in carbon allocation strategies for trees (e.g., Sala *et al.* 2012); thus, our results indicate that drought is impacting on leaf-level tree physiology across Europe but without obvious consequences for growth, as current evidence suggests that trees are sink- rather than source-limited (Körner 2003; Zhao & Zeng 2014). Details on the nature and magnitude of such climate signals have been extensively reported by Treydte *et al.* (2007).

Interpreting ring-width patterns across biogeographical gradients

Our study demonstrates that a pronounced geographical organization of spatial synchrony (*â*) in tree growth is present across Europe. The most conspicuous pattern of changes in *â* was detected along a north-south gradient, with increasing *â* values concurrent with a northward thermal gradient of decreasing temperature and reduced evapotranspiration. This agreed with our hypothesis of higher temporal coherence (i.e., more

synchronous growth) in temperature-limited, high-latitude forests that owes to the greater spatial homogeneity of temperature effects on tree growth in northern Europe (Düthorn *et al.* 2016a) compared with the more complex drought patterns in central and southern Europe (Leal *et al.* 2008; Friedrichs *et al.* 2009; Sánchez-Salguero *et al.* 2015). Besides, southern Europe is characterized by a high topographical variability which further tangles climate signals among neighbouring stands (Martín-Benito *et al.* 2010; Herguido *et al.* 2016). In this context, the negative association between $\hat{a}$ and elevation seems counterintuitive, but it must be noted that elevation and latitude were negatively correlated (principally reflecting the elevational decrease in treeline) and, additionally, latitude bore a stronger temperature signal than elevation.

Notably and with the exception of Fennoscandia, $\hat{a}$ increased in most cases during the second half of the twentieth century weakening the latitudinal gradient. This outcome suggests increased climatic forcing in central and southern Europe enhancing synchrony, irrespective of species and local site conditions, and is in line with previous findings on high-frequency adjustments of ring-width patterns in response to an amplified climatic control of growth in temperate and semiarid regions (Tardif *et al.* 2003; Andreu *et al.* 2007; Latte *et al.* 2015; Natalini *et al.* 2015; Shestakova *et al.* 2016). In contrast, higher temperatures in Fennoscandia seemed to progressively favor tree growth in subarctic forests (Mathisen & Hoofgard 2011; Düthorn *et al.* 2016b) and, thus, decrease climatic constraints on tree performance, leading to more asynchronous growth (but see Shestakova *et al.* 2016). Altogether, this contributed to a relaxation of the aforementioned biogeographical synchrony patterns for the period 1950–2003, which we interpret as an unambiguous signal of increasing climate warming effects on forest growth dynamics spreading northwards across Europe.

Leaf-level physiology underlie spatial patterns of forest growth in Europe

The physiological drivers of growth synchrony, assessed through tree-ring stable isotopes, could be identified by random modeling (see Materials & Methods) of the temporal signal presented simultaneously in ring-width and either $\Delta^{13}C$ or $\delta^{18}O$ at the group level. In this way, we obtained associations free of unwanted local effects (e.g., due to differential management, competition, soil depth and fertility, etc.) for the purpose of characterizing trends in correlation strength and direction between tree-ring record types across Europe. This approach sets a new methodological basis for in-depth investigations of physiological, morphological or phenological effects underlying geographically-structured temporal growth signals.

The positive relationships between ring-width and $\Delta^{13}C$ at low and mid latitudes suggests that a varying degree of CO_2 diffusion impairing leaf carbon uptake is the main mechanism controlling the temporal coherence of tree growth signals up to *ca.* 50°–55°N in Europe (*cf.* Fig. 5.5a). This finding is corroborated by negative associations between ring-width and $\delta^{18}O$ predominant at latitudes below 50°N (*cf.* Fig. 5.5b), which points to the

presence of stomatal limitations to photosynthesis in cool-summer continental and semiarid climates. It can therefore be concluded that leaf-level physiology and variability in tree growth are jointly constrained by moisture stress (driven by high temperatures and evapotranspiration) at about half the study area (including e.g., France, Austria and part of Poland) during the twentieth century. Conversely, the negative relationships between ring-width and $\Delta^{13}C$ at high latitudes (i.e., Fennoscandia), coupled with weak ring-width *vs.* $\delta^{18}O$ associations, indicate that photosynthesis became constrained by low temperatures likely via low irradiance and cloudy conditions (Dorado-Liñán *et al.* 2016) as factors linking temperature and carbon isotope fractionation (e.g., Voelker *et al.* 2014). Arguably, these results must be weighed against the limited spatial representativeness of the sampling network, but they allow delineating broad geographical trends that have been so far difficult to ascertain continent-wide partly due to the unsystematic and still sparse nature of the data collection (Saurer *et al.* 2014). Besides, these trends agree with previous studies performed across more restricted areas showing strong positive ring-width *vs.* $\Delta^{13}C$ site correlations for trees growing in water-limited conditions, but weak correlations at wetter and colder regions (e.g., Kirdyanov *et al.* 2008; Leavitt *et al.* 2010; Maseyk *et al.* 2011; Voelker *et al.* 2014; del Castillo *et al.* 2015).

Strengthening of $\Delta^{13}C$–growth relationships in response to climate change

The geographical structure in tree growth dependencies on leaf-level physiology became clearer during the second half of the twentieth century. Together with the observed increase in growth synchrony at most sites, this result suggests an intensified climate control of physiological processes underlying tree growth in Europe. It must be noted, however, that the main changes in correlation between ring-width and $\Delta^{13}C$ involved the two northernmost groups and, particularly, the southernmost group (*cf.* Fig. 5.5c). In the former case, the previous negative ring-width dependence on $\Delta^{13}C$ vanished after 1950, which suggests that an earlier photosynthetic limitation of growth driven by low temperatures essentially disappeared in recent decades, most likely as a direct consequence of climate warming.

For the southernmost group the correlation jumped from zero to nearly one after 1950. This result warrants clarification. Prior to 1950, growth synchrony among the four chronologies composing this group was inexistent, hence rendering a null signal shared by ring-width and $\Delta^{13}C$ for this particular group. After 1950, the growth signal was low but relevant, and this signal was essentially related to $\Delta^{13}C$ fluctuations, hence the highly positive correlation (albeit poorly estimated, i.e., with high SE). Although such correlation implies a tight stomatal control as emerging driver of common radial growth in high-mountain forests of the Iberian Peninsula and Morocco, the limited number of chronologies and the sudden change in tree performance between both halves of the century may question such interpretation. Interestingly, a recent study carried out in mountain forests of the eastern Iberian Peninsula allows downscaling our observations to a more restricted geographical area

(Shestakova *et al.* submitted). The authors reported that tree growth at about 1,600 m a.s.l. is becoming progressively more dependent on leaf-level gas exchange processes (inferred from $\Delta^{13}C$), hence resembling low elevation stands (about 1,100 m a.s.l.) in the last three decades. Although more data supporting this evidence at a regional scale are still needed, the results by Shestakova *et al.* (submitted) reinforce our observations. Unfortunately, studies reporting on long-term shifts in radial growth as related to switches of the primary environmental limitations to photosynthetic carbon gain are scarce to date (e.g., Voelker *et al.* 2014).

Concluding remarks

Leaf-level physiology and secondary growth are ultimately linked via carbon allocation strategies in trees, with carbon availability being considered seldom limiting for tree growth (e.g., Palacio *et al.* 2014). However, common signals imprinted in ring-width and stable isotopes are often reported in the literature, either along geographical gradients (i.e., concurrent changes in phenotypic plasticity; del Castillo *et al.* 2015), over time (i.e., temporal covariation; Voelker *et al.* 2014; this work) or at the intraspecific level (i.e., genetic correlation; Fardusi *et al.* 2016). This evidence is supportive of (direct or indirect) effects of carbon uptake processes on growth. Indeed, a number of alternative physiological processes related to above-ground growth may (co)vary with photosynthetic mechanisms, for example a critical turgor disrupting cell growth or the appearance of hydraulic constraints under drought (Sperry 2000), or the impairment of meristematic growth under low temperatures (Rossi *et al.* 2008). Eventually, these processes would need to be carefully assessed against stable isotope signals.

Together with climatic changes over the last century, the increasing carbon dioxide concentration in the atmosphere might have also played a role in the observed shifts in spatial synchrony in tree growth and the tighter associations between $\Delta^{13}C$ and ring-width. CO_2 fertilization has boosted water-use efficiency of European forests in the twentieth-century (Saurer *et al.* 2014), which overall concurs with a moderate control of gas exchange towards a constant ratio of intercellular to atmospheric CO_2 concentrations (Frank *et al.* 2015). However, these increments are not spatially uniform and, notably, the strongest increase has been reported in response to summer drought for temperate forests in central Europe (Saurer *et al.* 2014), an area in which we also observe the largest increase in spatial synchrony for the period 1951–2003. Both findings definitely point to an increasing impact of water stress spreading northwards across European forests.

SUPPORTING INFORMATION (SI Appendix)

Supplementary text

1. Evaluation of geographical trends in growth synchrony across Europe

The analyses of growth synchrony and its geographical trends across Europe were conducted based on the delineation of homogeneous groups of chronologies with regard temporal growth patterns, as described in the main text. We also allowed a particular chronology to be ascribed simultaneously to more than one group, resulting in non-independent groups. This decision stemmed from the well-known interrelation of climate processes at large spatiotemporal scales (Koenig 2002), which should affect forest growth dynamics without breaks in continuity. To guarantee the scope of our inferences, however, we checked for consistency in the reported geographical gradients. For this purpose, we explored an independent, larger dataset of ring-width chronologies available from the International Tree-Ring Data Bank (ITRDB; Grissino-Mayer & Fritts 1997). The selection criteria were: (*i*) geographic coverage: European continent; (*ii*) time span: at least 1900–1998 (i.e., common time period for ISONET chronologies); and (*iii*) taxonomic criterion: membership to the same species used in ISONET network. In total, 103 chronologies met these requirements. Then we checked for the spatial distribution of the chronologies across the continent and picked those that might be stratified into potential groups with sufficient amount of chronologies ($n \geq 4$) given the pre-requisite of 1,000 km maximum distance between sites. Residual ring-width chronologies were built for each site following the same procedure as described in Materials & methods. Therefore, 80 chronologies arranged into 8 groups (Fig. S5.3a) were used for subsequent statistical analysis of growth synchrony ($\hat{a}$) and assessment of geographical patterns in $\hat{a}$.

Supplementary tables

Table S5.1. Geographical features and climatic characteristics of the sampling sites. Sites are sorted latitudinally, from north (top) to south (bottom). Climate parameters are calculated over the period 1901–2003. Abbreviations: MAT, mean annual temperature; MAP, mean annual precipitation; PET, potential evapotranspiration.

No	Country	Site name	Code[1]	Latitude (°N)	Longitude (°E)	Elevation (m)	MAT (°C)	MAP (mm)	PET (mm)	PET > MAP
1	Finland	Kessi, Inari	Ina*	68.93	28.42	150	–1.2	432	414	Apr-Aug
2	Finland	Sivakkovaara, Ilomantsi	Ilo*	62.98	31.27	200	2.2	573	515	Apr-Aug
3	Norway	Gutuli	Gut*	62.00	12.18	800	0.7	586	512	Apr-Aug
4	Finland	Bromarv	Bro*	60.00	23.08	5	4.9	568	562	Apr-Aug
5	UK	Lochwood	Loc	55.27	–3.43	175	7.4	1517	589	Jun
6	Lithuania	Panemunes Silas	Pan	54.88	23.97	45	6.6	634	672	Apr-Sep
7	Poland	Suwalki	Suw	54.10	22.93	160	6.7	619	686	Apr-Sep
8	UK	Woburn Abbey	Wob	51.98	–0.59	50	9.5	709	724	Apr-Sep
9	Germany	Dransfeld	Dra	51.50	9.78	320	7.7	723	677	Apr-Sep
10	UK	Windsor	Win	51.41	–0.59	10	9.5	763	738	Apr-Sep
11	Poland	Niepolomice, Gibiel	Nie1	50.12	20.38	190	8.0	676	674	Apr-Aug
12	Poland	Niepolomice, Gibiel	Nie2	50.12	20.38	190	8.0	676	674	Apr-Aug
13	France	Fontainebleau	Fon	48.38	2.67	100	11.5	608	861	Mar-Sep
14	France	Rennes	Ren	48.25	–1.70	100	11.1	733	786	Apr-Sep
15	Austria	Lainzer Tiergarte	Lai	48.18	16.20	300	9.6	654	792	Mar-Sep
16	Austria	Poellau	Poe	47.95	16.06	500	8.3	815	762	Apr-Aug
17	Switzerland	Vigera	Vig	46.50	8.77	1400	4.6	1880	599	non
18	Switzerland	Cavergno	Cav	46.35	8.60	900	4.6	1880	600	non
19	Spain	Pinar de Lillo	Lil	43.07	–5.25	1600	10.0	950	823	May-Sep
20	Spain	Massis de Pedraforca	Ped	42.23	1.70	2100	8.5	855	825	Jun-Aug
21	Italy	Serra di Crispo	Ser	39.93	16.20	1900	15.1	757	900	Apr-Sep
22	Spain	Sierra de Cazorla	Caz	37.80	–2.95	1816	13.4	450	1172	Mar-Oct
23	Morocco	Col du Zad	Col	32.97	–5.07	2200	13.2	527	1271	Mar-Oct

[1]Chronologies marked with an asterisk are from Fennoscandia (northern subregion of the study)

Table S5.2. Dendrochronological characteristics of the sampled sites. Mean values are calculated over the period 1900–2003. Abbreviations: *EPS*, Expressed Population Signal; *Rbar*, mean interseries correlation; TRW, tree-ring width; $\Delta^{13}C$, carbon isotope discrimination; $\delta^{18}O$, oxygen isotope composition. The variability of mean values is expressed as standard error (± SD).

No	Code	Species	No. trees/cores	Time span	EPS > 0.85 since	Rbar±SD	TRW±SD (mm)	Growth trend, *b* (mm year^{-1})[1]	$\Delta^{13}C$±SD (‰)	$\delta^{18}O$±SD (‰)
1	Ina	*Pinus sylvestris*	15/32	1508–2003	1570	0.44±0.10	0.52±0.01	–0.001	18.46±0.04	26.34±0.07
2	Ilo	*Pinus sylvestris*	28/39	1580–2003	1610	0.33±0.07	0.29±0.004	0.000	17.81±0.04	27.07±0.08
3	Gut	*Pinus sylvestris*	45/89	1449–2004	1510	0.45±0.10	0.50±0.01	0.000	17.39±0.05	27.64±0.09
4	Bro	*Quercus robur*	7/19	1822–2004	1850	0.44±0.13	1.84±0.06	–0.011*	18.90±0.07	25.64±0.09
5	Loc	*Quercus robur*	28/38	1706–2003	1750	0.29±0.14	1.16±0.02	0.003*	19.30±0.06	27.83±0.05
6	Pan	*Pinus sylvestris*	30/61	1487–2003	1590	0.28±0.11	0.79±0.02	–0.003*	16.93±0.05	28.68±0.09
7	Suw	*Pinus sylvestris*	76/76	1600–2004	1620	0.31±0.14	1.02±0.03	–0.005*	17.10±0.08	28.47±0.08
8	Wob	*Quercus robur*	20/30	1613–2003	1640	0.445±0.11	1.37±0.02	0.001	17.37±0.09	29.08±0.06
9	Dra	*Quercus petraea*	16/45	1770–2002	1800	0.49±0.11	1.42±0.05	–0.009*	17.53±0.07	28.67±0.07
10	Win	*Pinus sylvestris*	16/21	1763–2003	1790	0.28±0.12	1.22±0.03	–0.003*	16.90±0.06	30.36±0.06
11	Nie1	*Quercus robur*	35/39	1768–2003	1810	0.37±0.11	1.88±0.04	0.003*	19.83±0.09	27.76±0.11
12	Nie2	*Pinus sylvestris*	72/78	1622–2003	1650	0.25±0.15	1.01±0.03	–0.005*	17.36±0.10	29.25±0.11
13	Fon	*Quercus petraea*	30/60	1306–2000	1530	0.31±0.13	0.87±0.03	0.007*	17.85±0.07	31.27±0.06
14	Ren	*Quercus robur*	11/30	1751–1998	1860	0.43±0.16	1.63±0.05	–0.009*	18.89±0.05	30.23±0.08
15	Lai	*Quercus petraea*	55/81	1462–2003	1510	0.39±0.17	1.18±0.02	0.000	18.86±0.07	27.51±0.09
16	Poe	*Pinus nigra*	326/588	1319–2002	1500	0.37±0.11	0.62±0.02	–0.003*	18.32±0.06	27.01±0.13
17	Vig	*Pinus sylvestris*	15/46	1622–2002	1710	0.21±0.12	0.47±0.01	0.001	17.16±0.05	30.78±0.10
18	Cav	*Quercus petraea*	25/55	1562–2002	1610	0.34±0.13	1.11±0.02	0.003*	17.32±0.06	29.21±0.07
19	Lil	*Pinus sylvestris*	15/32	1511–2002	1560	0.35±0.10	0.47±0.01	–0.001	16.22±0.05	30.86±0.08
20	Ped	*Pinus uncinata*	23/56	1269–2003	1510	0.33±0.09	1.00±0.01	0.000	15.91±0.05	30.83±0.08
21	Ser	*Pinus leucodermis*	15/41	1464–2003	1490	0.48±0.08	0.52±0.01	–0.002*	16.29±0.03	29.98±0.08
22	Caz	*Pinus nigra*	33/68	1125–2002	1190	0.47±0.10	0.47±0.01	0.000	15.03±0.04	33.59±0.10
23	Col	*Cedrus atlantica*	10/40	1560–2000	1590	0.51±0.09	1.12±0.03	–0.001	14.50±0.04	32.71±0.06

[1]Chronologies marked with an asterisk show significant ($P < 0.05$) change in absolute growth for the period 1900–2003

Table S5.3. Biogeographic trends in absolute radial growth, linear change in absolute radial growth and stable isotopes: simple correlation coefficients, *r*, and probabilities (in parentheses) between mean chronology values for tree-ring width (TRW), temporal trend in slope (*b*) of TRW changes, $\Delta^{13}C$ or $\delta^{18}O$ and geographic and climatic variables for 23 site chronologies distributed across Europe and northern Africa calculated over the period 1900–2003. For correlations involving both conifers and hardwoods, the partial correlation coefficient after controlling for the effect of functional type is presented. Bold values denote significant relationships ($P < 0.05$).

	Geographical gradients			*Climatic gradients*		
	Latitude (°N)	**Longitude (°E)**	**Elevation (m)**	**MAT (°C)**	**MAP (mm)**	**PET (mm)**
TRW (mm)						
Conifers	–0.27 (*0.37*)	–0.27 (*0.37*)	–0.08 (*0.81*)	0.37 (*0.21*)	–0.14 (*0.66*)	0.28 (*0.36*)
Hardwoods	0.45 (*0.16*)	0.52 (*0.10*)	–0.36 (*0.23*)	–0.25 (*0.35*)	–0.40 (*0.20*)	–0.37 (*0.23*)
All	–0.10 (*0.66*)	0.01 (*0.96*)	–0.12 (*0.59*)	0.19 (*0.39*)	–0.24 (*0.29*)	0.15 (*0.49*)
TRW trend, b (mm yr^{-1})						
Conifers	–0.21 (*0.49*)	0.26 (*0.40*)	0.03 (*0.95*)	–0.03 (*0.95*)	–0.30 (*0.31*)	0.51 (*0.07*)
Hardwoods	0.20 (*0.41*)	0.36 (*0.24*)	0.26 (*0.34*)	–0.47 (*0.14*)	–0.24 (*0.36*)	0.28 (*0.32*)
All	0.01 (*0.70*)	0.30 (*0.18*)	0.08 (*0.52*)	–0.14 (*0.38*)	–0.21 (*0.25*)	0.19 (*0.29*)
⊿^{13}C (‰)						
Conifers	**0.83 (*<0.001*)**	**0.76 (*0.002*)**	**–0.78 (*0.001*)**	**–0.80 (*<0.001*)**	0.05 (*0.89*)	**–0.89 (*<0.001*)**
Hardwoods	0.30 (*0.30*)	0.32 (*0.28*)	–0.40 (*0.20*)	0.03 (*0.63*)	–0.20 (*0.42*)	–0.14 (*0.49*)
All	**0.72 (*<0.001*)**	**0.64 (*0.001*)**	**–0.69 (*<0.001*)**	**–0.53 (*0.012*)**	0.05 (*0.83*)	**–0.66 (*<0.001*)**
$\delta^{18}O$ (‰)						
Conifers	**–0.83 (*<0.001*)**	**–0.81 (*<0.001*)**	**0.68 (*0.008*)**	**0.77 (*0.001*)**	0.20 (*0.52*)	**0.85 (*<0.001*)**
Hardwoods	**–0.71 (*0.02*)**	**–0.68 (*<0.03*)**	0.12 (*0.51*)	**0.65 (*0.04*)**	0.06 (*0.59*)	**0.69 (*0.03*)**
All	**–0.81 (*<0.001*)**	**–0.80 (*<0.001*)**	**0.63 (*0.002*)**	**0.68 (*<0.001*)**	0.09 (*0.69*)	**0.75 (*<0.001*)**

Supplementary figures

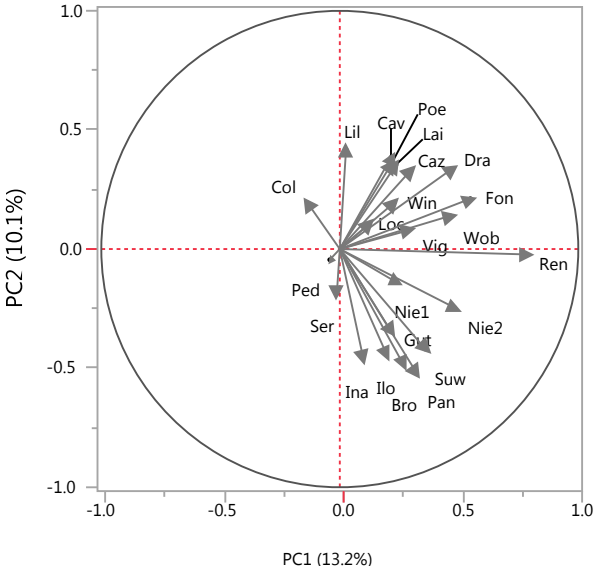

Figure S5.1. Principal component analysis performed on 23 residual ring-width chronologies distributed across Europe and northern Africa for the common period 1900–1998. The biplot shows the loadings of the first and second principal components (PC1 and PC2) for each chronology. Codes are as in Table S5.1.

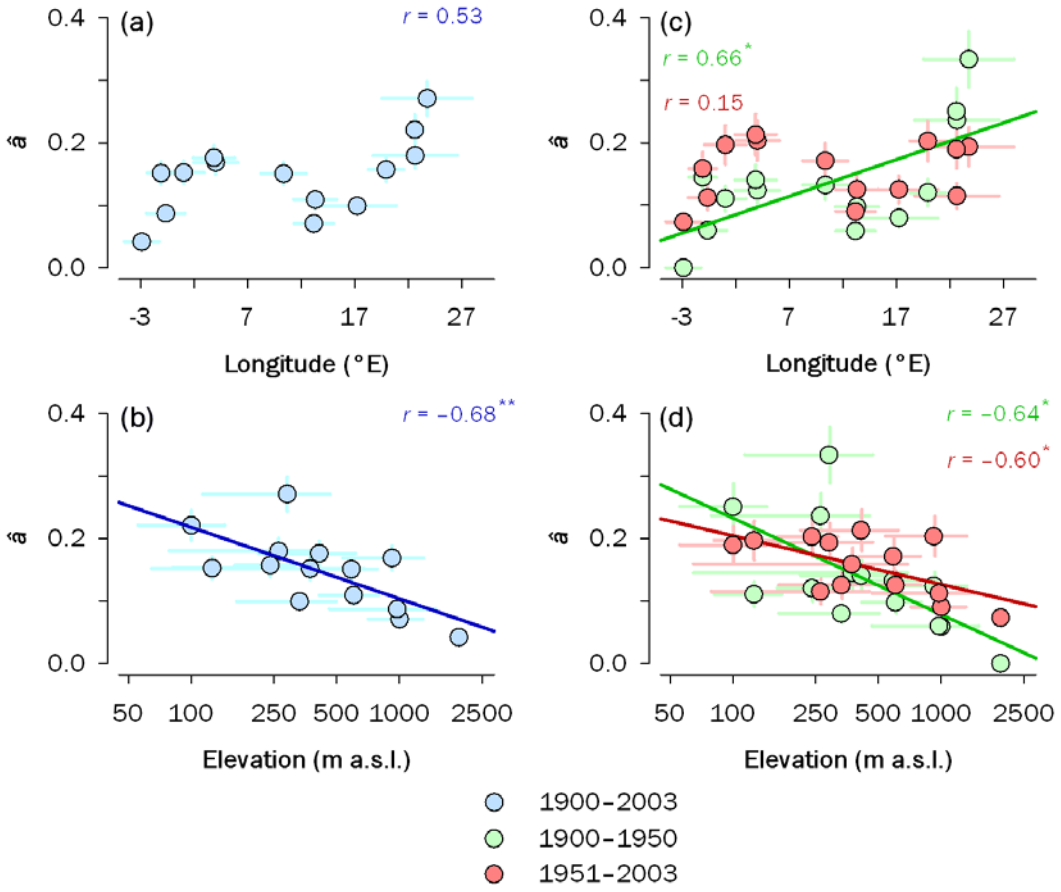

Figure S5.2. Geographical patterns of growth synchrony (*â*) at the group level for the entire period 1900–2003 **(a, b)** and change in *â* for two consecutive periods (1900–1950 and 1951–2003; **c, d**). The patterns are characterized as linear regressions of spatial synchrony for each group (*y*-axis) on its corresponding *(upper panel)* longitude or *(lower panel)* elevation (*x*-axis). Note that the abscissa in the lower panel has a logarithmic scale. Significant linear trends along the geographical gradients are depicted as thick lines ($^{*}P < 0.05$; $^{**}P < 0.01$). All calculations are based on residual ring-width chronologies. Error bars denote standard errors.

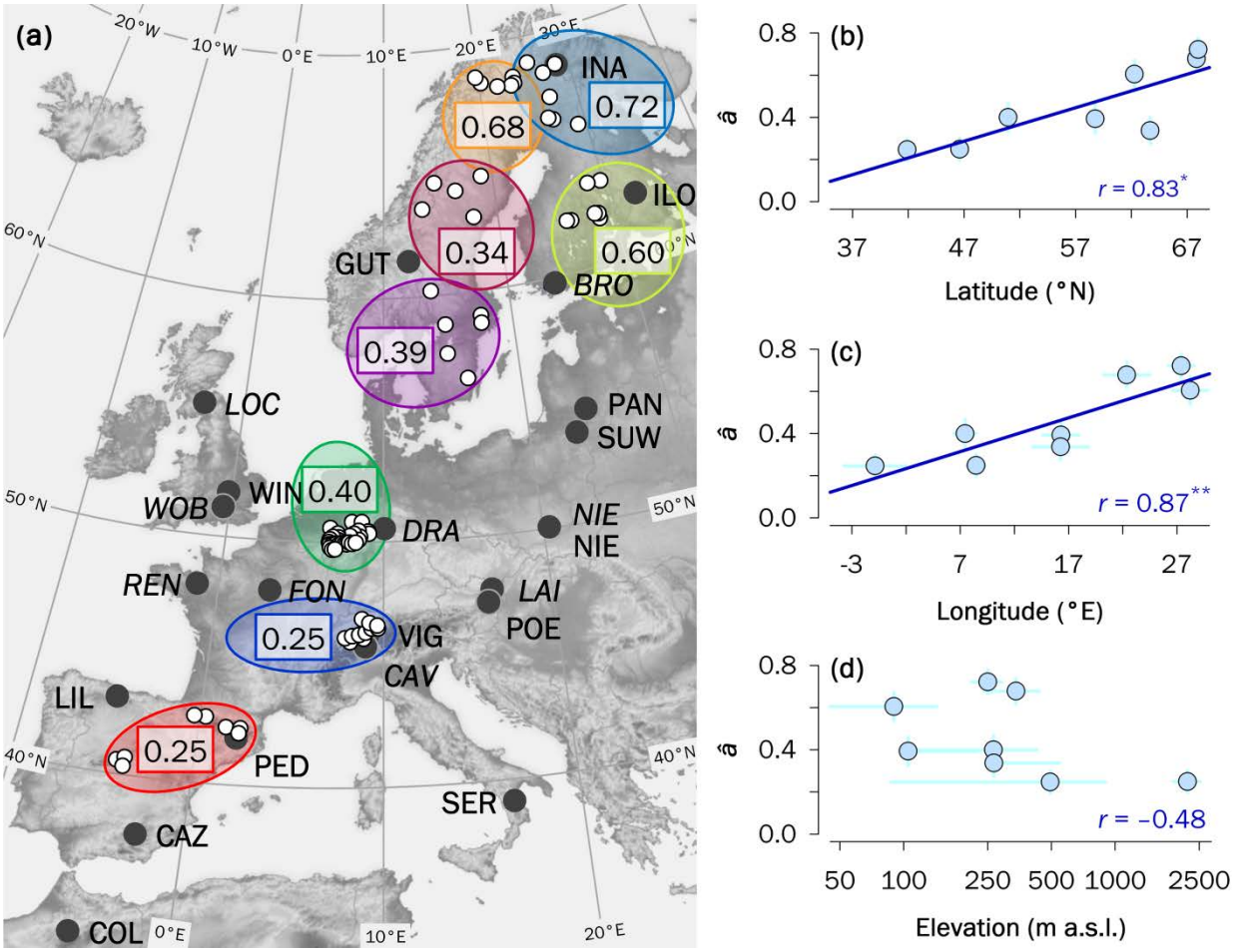

Figure S5.3. Geographical patterns of growth synchrony (*â*) at the group level for ITRDB (International Tree-Ring Data Bank) dataset for the period 1900–2003. **(a)** Geographical distribution of sampling sites for two independent datasets: pan-European network ISONET (black dots) and ITRDB (white dots). Colored circles identify groups of neighboring chronologies from ITRDB (n = 8) for subsequent spatial synchrony analysis. Numbers indicate *â* values at group level estimated for the period 1900–2003. The patterns of *â* are characterized as linear regressions of spatial synchrony for each group (y-axis) on its corresponding **(b)** latitude, **(c)** longitude or **(d)** elevation (x-axis). Note that the abscissa in (d) has a logarithmic scale. Significant linear trends along the geographical gradients are depicted as thick lines ($^{*}P < 0.05$; $^{**}P < 0.01$). All calculations are based on residual ring-width chronologies. Error bars denote standard errors.

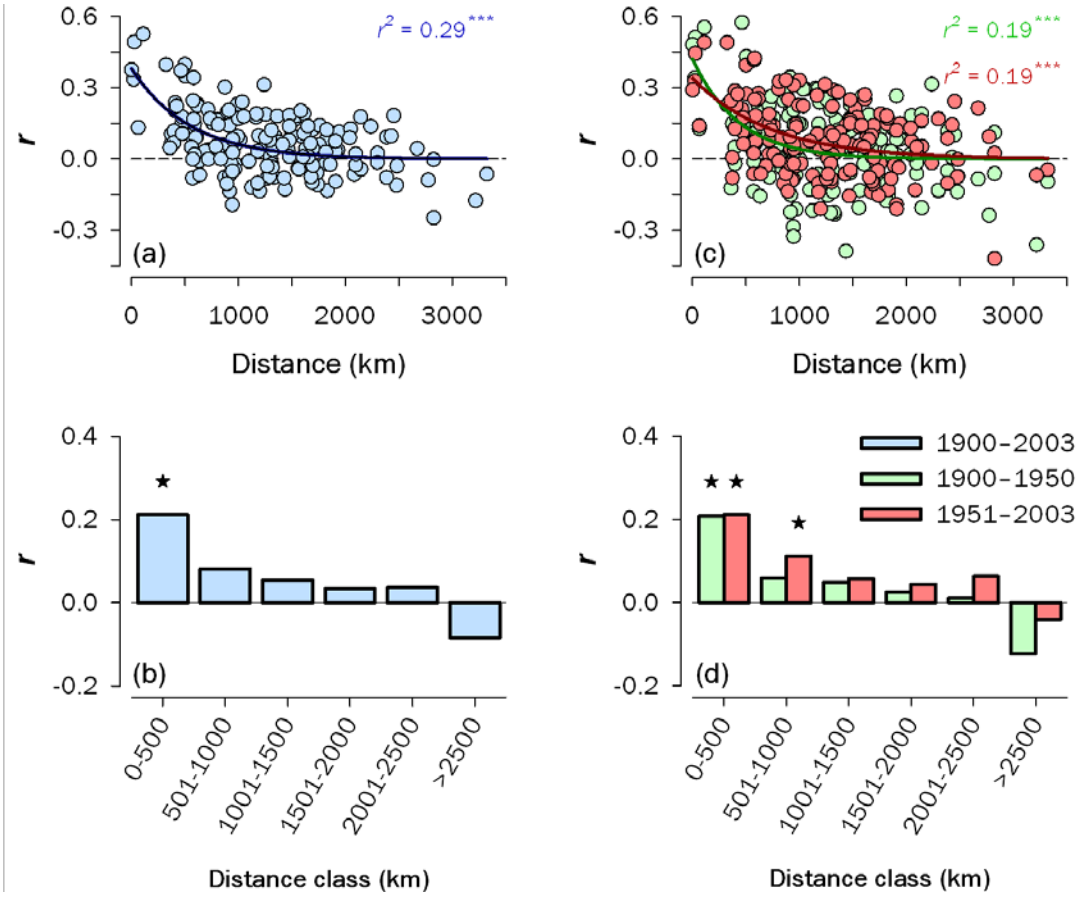

Figure S5.4. Spatial patterns of forest growth across Central and Southern Europe for the entire period 1900–2003 *(left panel)* and change in *á* for two consecutive periods (1900–1950 and 1951–2003; *right panel*). **(a, c)** Pairwise correlations of tree-ring width chronologies as a function of geographical distance. The patterns are summarized by regressing the correlation coefficients (*r* values) involving pairs of chronologies (*y*-axis) on their corresponding distance (*x*-axis). Significant differences in mean *á* values (p_a = 0.024) are found between the two halves of the twentieth century. **(b, d)** Spatial structure (modified correlograms) of radial growth among sites. The spatial autocorrelation in the ring-width network was characterized for six consecutive distance classes (listed on the *x*-axis). Mean *r* values and their statistical significance (*P*) within each distance class were estimated from 1,000 randomizations. Significant correlation coefficients ($P < 0.05$) are indicated by asterisks.

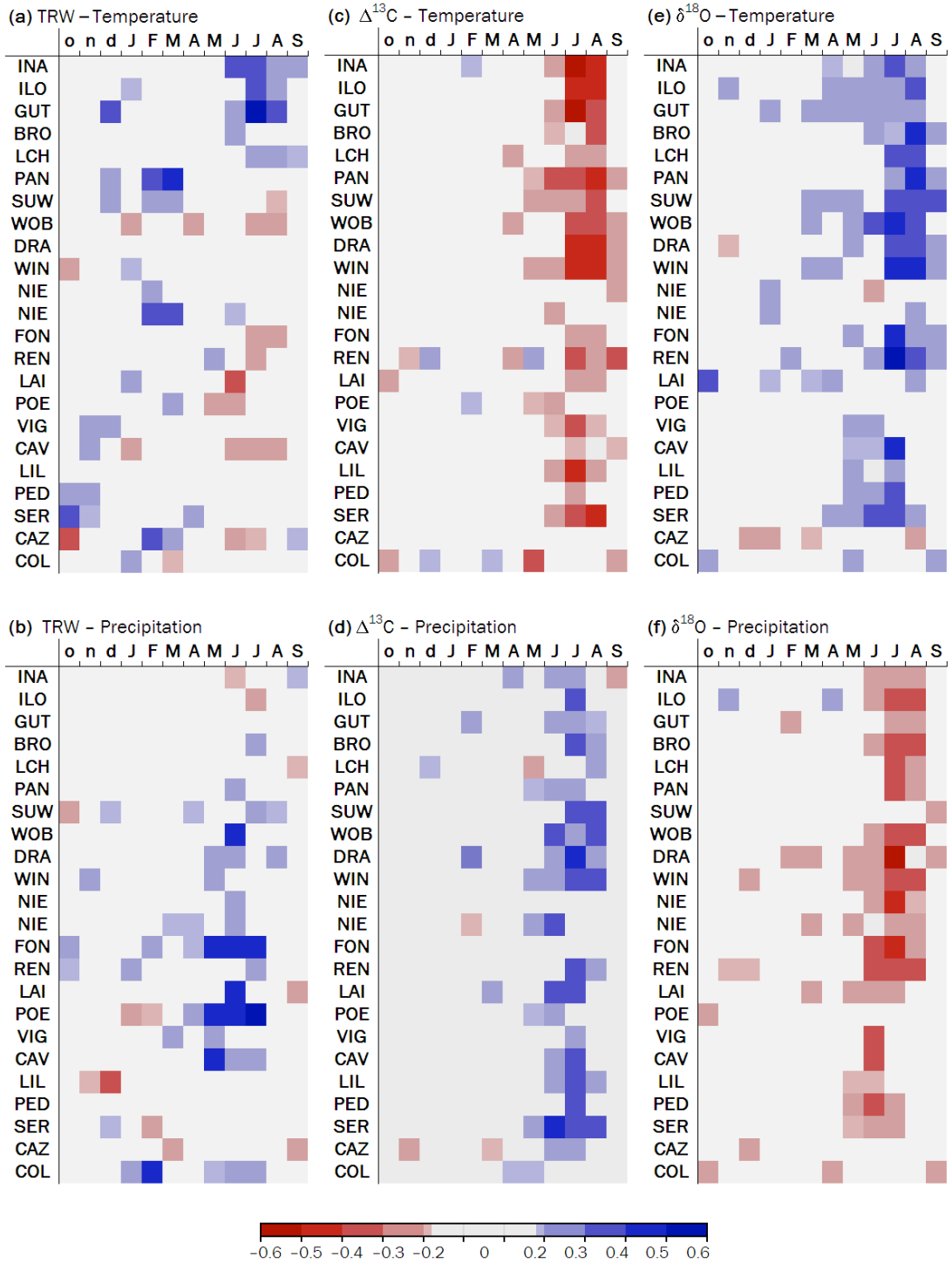

Figure S5.5. Climate relationships at the site level for **(a, b)** tree-ring width, **(c, d)** $\Delta^{13}C$, **(e, f)** $\delta^{18}O$ for the period 1900–2003. Tree responses to climate are based on simple correlations between tree-ring traits and monthly mean temperature *(upper panel)* and precipitation *(lower panel)*. Red and blue colors denote negative and positive relationships, respectively. Only significant correlations ($P < 0.05$) are shown. Sites are sorted latitudinally, from north (top) to south (bottom). Lowercase and uppercase letters correspond to month of the years before and during tree-ring formation, respectively.

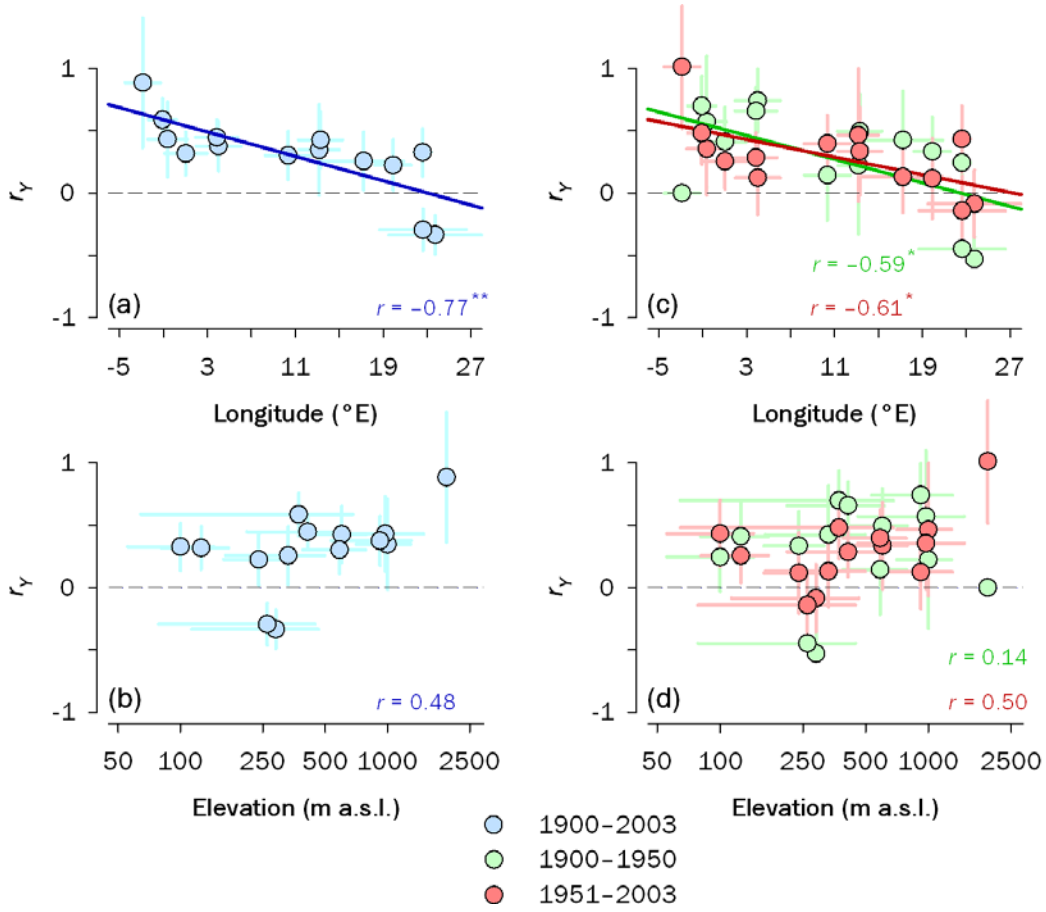

Figure S5.6. Geographical patterns of the relationship between ring-width and $\Delta^{13}C$ chronologies across Europe. The correlations of year effects (r_Y) at the group level are estimated using residual ring-width and isotope chronologies for the entire period 1900–2003 (*left panel*) and for two periods separately (1900–1950 and 1951–2003; *right panel*). The patterns are characterized as linear regressions of mean bivariate correlations for each group (*y*-axis) on its corresponding (**a, c**) longitude and (**b, d**) elevation (*x*-axis). Significant linear trends along the geographical gradients are depicted as thick lines ($^{*}P < 0.05$; $^{**}P < 0.01$). Error bars denote standard errors.

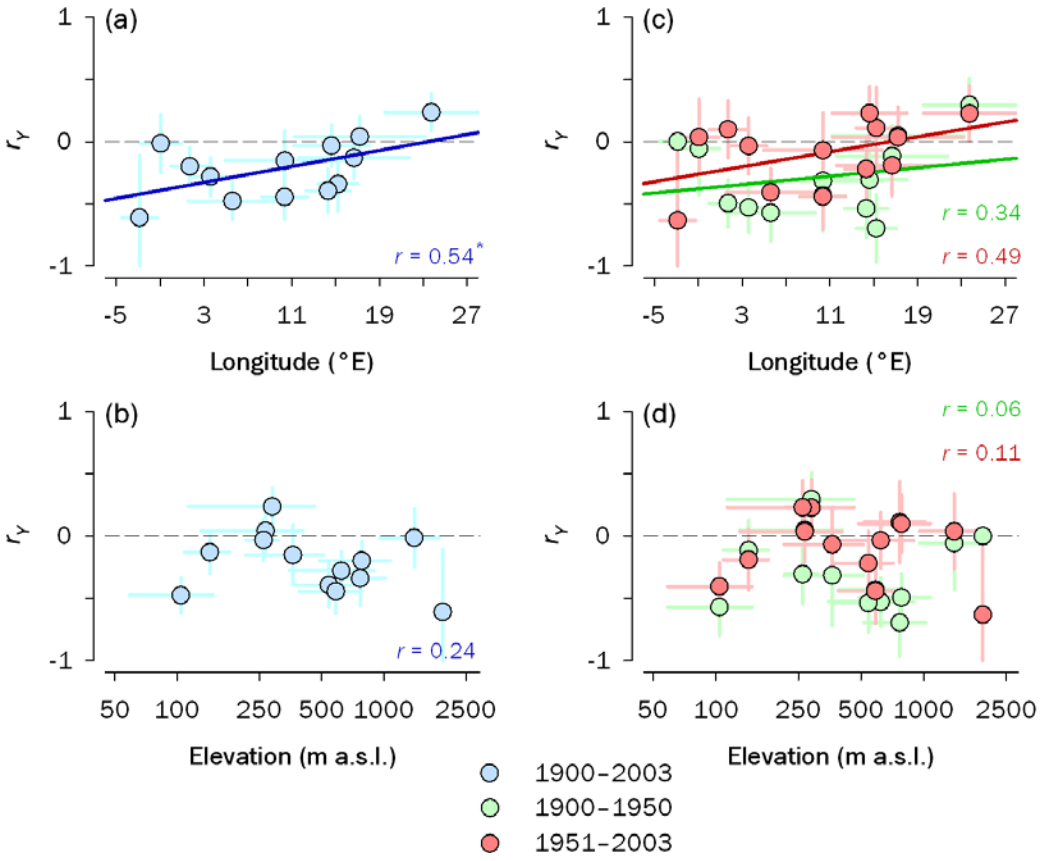

Figure S5.7. Geographical patterns of the relationship between ring-width and $\delta^{18}O$ chronologies across Europe. The correlations of year effects (r_Y) at the group level are estimated using residual ring-width and isotope chronologies for the entire period 1900–2003 (*left panel*) and for two periods separately (1900–1950 and 1951–2003; *right panel*). The patterns are characterized as linear regressions of mean bivariate correlations for each group (*y*-axis) on its corresponding longitude (**a, c**) longitude and (**b, d**) elevation (*x*-axis). Significant linear trends along the geographical gradients are depicted as thick lines ($^*P < 0.05$). Error bars denote standard errors.

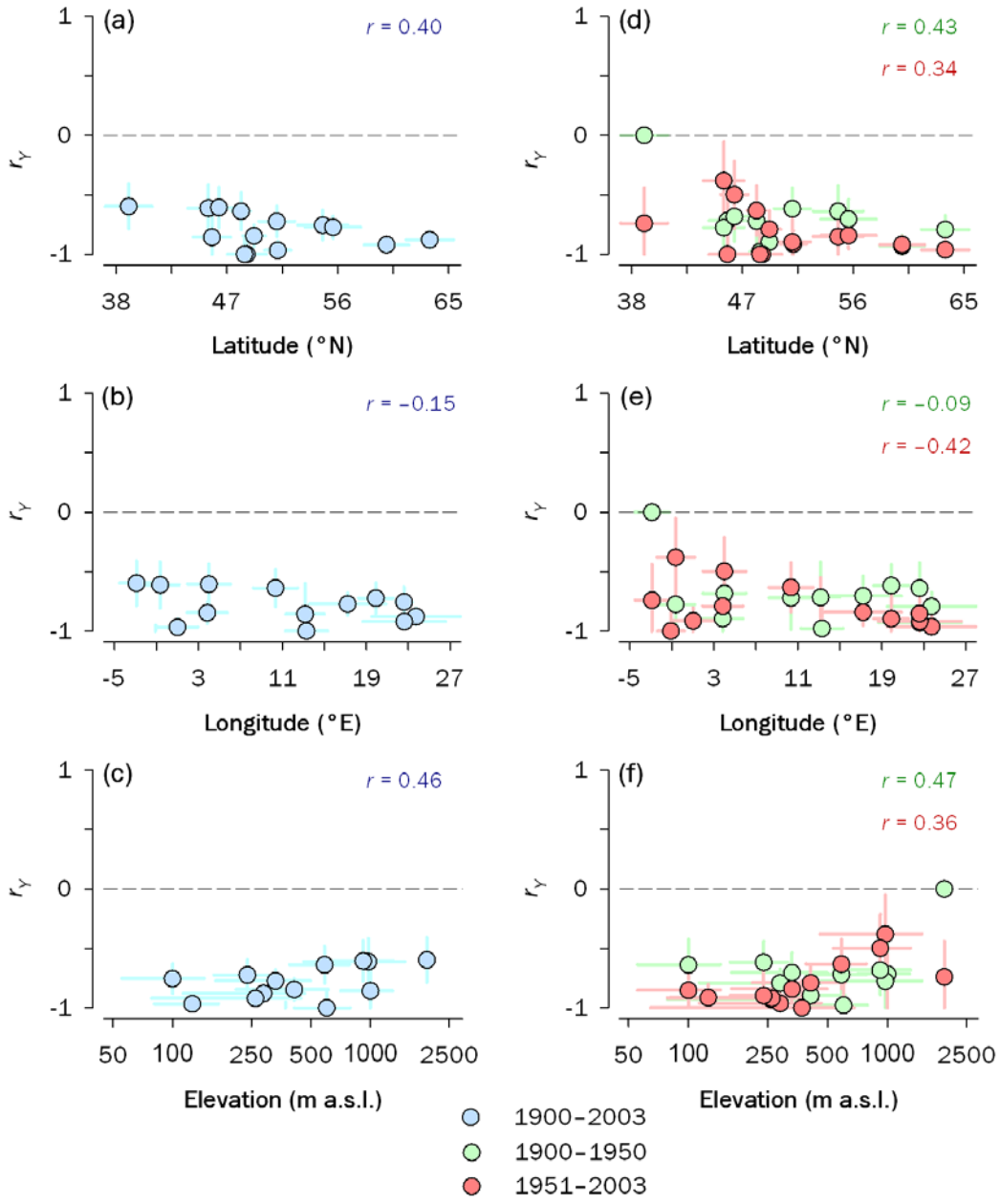

Figure S5.8. Geographical patterns of the relationship between $\Delta^{13}C$ and $\delta^{18}O$ chronologies across Europe. The correlations of year effects (r_Y) at the group level are estimated using residual isotope chronologies for the entire period 1900–2003 *(left panel)* and for two periods separately (1900–1950 and 1951–2003; *right panel*). The patterns are characterized as linear regressions of mean bivariate correlations for each group (*y*-axis) on its corresponding latitude **(a, d)**, longitude (**b, e**) longitude and (**c, f**) elevation (*x*-axis). No significant linear trends along the geographical gradients are detected. Error bars denote standard errors.

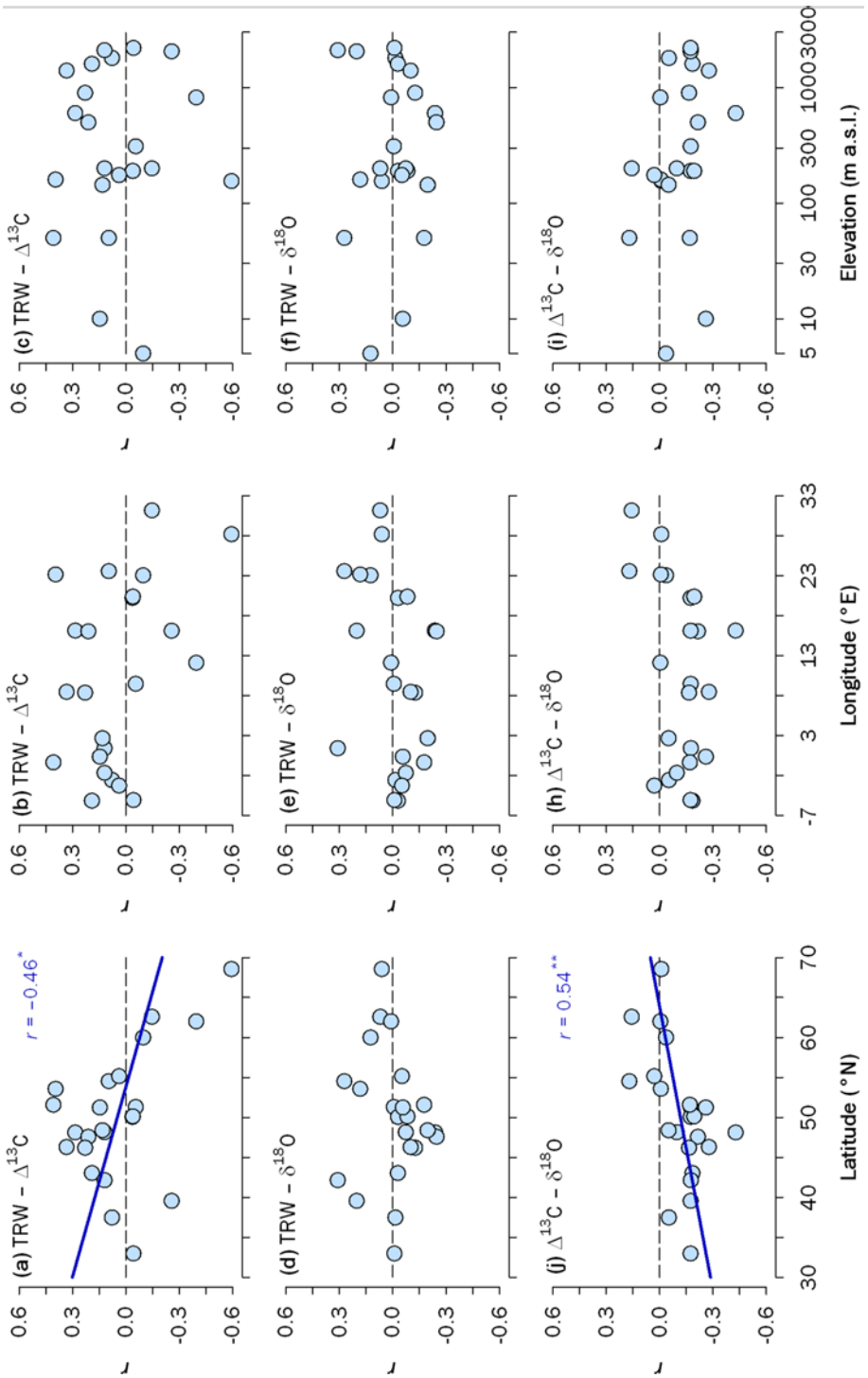

Figure S5.9. Patterns of relationships between tree-ring traits along geographical gradients across Europe. The panels depict simple correlations between pairs of traits at the site level estimated using residual ring-width and $\Delta^{13}C$ **(a–c)**, ring-width and $\delta^{18}O$ **(d–f)** or $\Delta^{13}C$ and $\delta^{18}O$ **(j–i)** chronologies for the period 1900–2003. The patterns are characterized as linear regressions of correlations (*r* values) for each site (*y*-axis) on its corresponding latitude *(left panels)*, longitude *(middle panels)* and elevation *(right panels)* (*x*-axis). Significant linear trends along the geographical gradients are depicted as thick lines ($^{*}P < 0.05$; $^{**}P < 0.01$). Error bars denote standard errors.

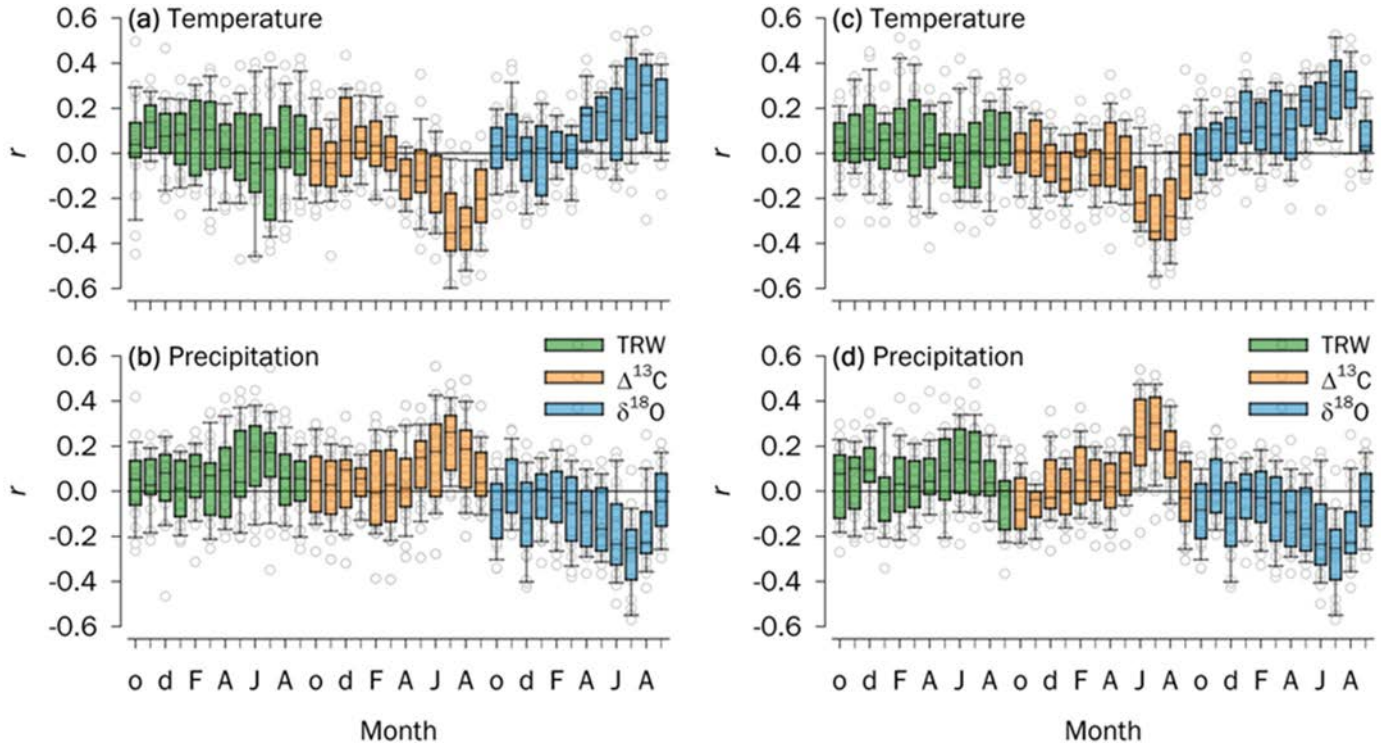

Figure S5.10. Box-plot summary of site-level climate *vs.* tree-ring traits relationships for two subsequent periods: 1900–1950 (**a, b**) and 1951–2003 (**c, d**). Tree responses to climate are based on simple correlations between tree-ring width (green bars), $\Delta^{13}C$ (orange bars) and $\delta^{18}O$ (blue bars) and monthly mean temperature *(upper panels)* and precipitation *(lower panels)*. Gray dots indicate climate response at the site level. Lowercase and uppercase letters correspond to month of the years before and during tree-ring formation, respectively.

CHAPTER 6

General Discussion & Conclusions

General Discussion

Modeling spatiotemporal structure of tree-ring traits

The rising interest in the spatial and temporal dependences of forest processes on climate has resulted in an explosion of tree-ring networks worldwide which comprise ring-width measurements (e.g., Cook *et al.* 2004; Andreu *et al.* 2007; Babst *et al.* 2013; Seim *et al.* 2015), densitometric data (e.g., Schweingruber *et al.* 1993; Vaganov *et al.* 1999; Briffa *et al.* 2002; Büntgen *et al.* 2006) and carbon and oxygen stable isotopes (e.g., Treydte *et al.* 2007; Gagen *et al.* 2008; Leavitt *et al.* 2010; Saurer *et al.* 2012). The conventional approach to investigate the magnitude of common information shared by tree-ring records relies on the application of classical analysis of variance (ANOVA) principles (Wigley *et al.* 1984; Fritts 2001). However, in case of temporal series when multiple measurements are available repeatedly over time (i.e., longitudinal data or repeated measures), the standard ANOVA is not necessarily the best choice since the assumption of data independence may not hold true. Furthermore, as it is usually the case in dendrochronology, the available temporal series may overlap partially because trees of different ages are used to build a chronology or, alternatively, chronologies of different length may be subjected to joint examination. It seems therefore sensible to consider more flexible approaches for interpreting the complex structures embedded in tree-ring datasets which are expected to exist in natural populations. For this aim, a full-fledged mixed modeling framework was presented in this thesis that provides a statistically rigorous tool for investigating patterns of annually resolved tree-ring signals at multiple spatiotemporal scales.

A mixed model applied to dendro-sciences typically consists of both fixed-effects parameters (i.e., series or chronologies, groups of series or chronologies) and random-effects parameters (i.e., years and their interactions with fixed effects). Maximum likelihood (ML) approaches are most common for fitting mixed models as they maximize the 'agreement' of the selected model with the observed data. Nowadays it has become customary to use a special type of maximum likelihood that is directed at optimizing the likelihood for the observations after 'correction' for fixed effects. This type of likelihood is called restricted maximum likelihood (REML), restricted in the sense that only the likelihood for the random part of the model is maximized (Verbeke & Molenberghs 2000). When fitting these parameters, dendroecologists may be more interested in the variance components associated with random coefficients than in the prediction of the random parameters themselves, as variance components allow for a straightforward estimation of the signal strength shared between series or chronologies (Chapter 2). The fixed parameters are estimated once variance components are obtained.

We have proposed to assess fixed-effects coefficients through selection of meaningful dependent factors (e.g., based on taxonomic or geographic criteria for grouping temporal

series into hypothetically homogeneous subsets). This is useful for two reasons: first, if not modelled, these effects may bias estimates of the model; and secondly, understanding the species- or site-specific responses to environmental influence is an important part of most dendroecological studies. Often, however, the temporal series are detrended or indexed, meaning that fixed factors can be actually saved from modeling (but not their interactions with the random year effect). In fact, we reckon that variance component estimation lies at the heart of mixed modeling techniques when applied to dendroecology, as proper variance-covariance structures can be used to account for complex spatial and temporal associations simultaneously.

Mixed models are flexible to handle variable, albeit non-trivial, amounts of unbalanced data, although unbalanceness will obviously reduce estimate precision. Indeed, the problem of missing data is a neglected topic in the field of ecology (Nakagawa & Freckleton 2008). A usual way to deal with unbalanced datasets is to delete missing observations and work with complete cases, despite such complete case analyses may often lead to reduced statistical power. Fortunately, mixed models are capable of dealing with partially overlapping chronologies, yielding valid inferences of common signal patterns for large areas in which tree-ring data are available but covering different time periods.

Multivariate methods such as principal component analysis or cluster analysis are often used to allow for the identification of homogeneous subsets of chronologies (e.g., Andreu *et al.* 2007; Seim *et al.* 2015). An important drawback of these methods is that they cannot test for possible processes underlying patterns of signal strength in a straightforward manner. Furthermore, most dendrochronological studies assume a homoscedastic error distribution, i.e., normally distributed residuals with mean zero and constant variance. We have shown that deviations from this assumption can be easily embedded in a mixed model setting, which allows for flexible modeling of different group and error covariance structures. Therefore, the assumption of homogeneity of variances can be relaxed (McCulloch & Searle 2001). This may be of interest in dendrochronology as time series of tree-ring traits are used that can show weak stationarity (i.e., constant mean but not variance). Modeling the spatiotemporal correlation structure of observations increases the precision of model parameter estimates (Brown & Prescott 1999), as manifested by decreased standard errors and reduced bias.

The main task in parameterizing mixed models is to develop a parsimonious but well-fitted correlation structure of the observations. This is executed by fitting models with alternative variance-covariance matrices. Here we proposed an efficient and statistically sound approach to obtain parameter estimates and their standard errors in dendro-sciences which is grounded on the application of different evaluation criteria for model selection. Particularly, models are fit by REML and the best fit is chosen based on minimizing Akaike information criterion (AIC) and Bayesian information criterion (BIC), goodness-of-fit statistics commonly used in model selection (Verbeke & Molenberghs 2000). For practical

purposes in dendroecological studies, it might be useful to consider the implications of changes in the estimated parameters along with changes of the assumed correlation structures. This could be achieved by evaluating and comparing different variance-covariance structures for modeling and analyzing truncated longitudinal data using simulation techniques.

Unscrambling the complexities of tree-ring signals at multiple spatiotemporal scales

At the core of dendrochronology lies the fundamental principle of a common signal shared by tree rings across time and space (Fritts 2001). Climate is generally accepted as the major driver of tree performance (Hughes *et al.* 2009), which results in common variability of tree-ring traits that often spreads over large geographical areas (Briffa *et al.* 2002; Wettstein *et al.* 2011; Babst *et al.* 2013). However, differential physiological responses among species and/or across environmental gradients challenge inferences on emergent ecological properties and processes in broad dendrochronological networks (e.g., Galván *et al.* 2014). Unscrambling the complexities of tree-ring signals offers a tremendous opportunity for an enhanced understanding of the environmental drivers of forest performance across multiple spatiotemporal scales, which become especially important in the global change context.

Dendrochronological techniques are traditionally used to analyze climate–growth relationships based on interannual ring-width fluctuations. In recent decades this approach has been extended to the analysis of stable isotopes in wood or wood constituents, which provides valuable information on tree physiology (McCarroll & Loader 2004; Gessler *et al.* 2014). Previous studies have already reported that isotope variations captured by trees strongly depend on ecological site conditions (e.g., Barbour *et al.* 2001). Thus, it is difficult to generalize stand-level findings on tree-ring isotopes to large regions, because the spatial and temporal variability of tree responses to environmental cues remains poorly characterized (Saurer *et al.* 2004).

The results presented in Chapter 2 revealed that ecophysiological responses of Mediterranean oak forests are spatially structured along an aridity gradient as inferred from carbon ($\Delta^{13}C$) and oxygen ($\delta^{18}O$) stable isotopes. We also found that spatial signals recorded by tree-ring isotopes were essentially similar among deciduous oak species (*Q. faginea*, *Q. humilis* and *Q. petraea*). Hartl-Meier *et al.* (2014) have similarly reported coherent imprints of tree-ring isotopes across different species (*Fagus sylvatica* L., *Larix decidua* Mill. and *Picea abies* [L.] Karst.) from a temperate forest in the Austrian pre-Alps. Conversely, we observed substantial differences between two functional groups co-occurring in mixed Mediterranean forests (deciduous *vs.* evergreen oaks). These dissimilarities suggest different sensitivities of deciduous oak species and evergreen *Q. ilex* to climate factors owing to differences in

physiological properties, phenology, leaf characteristics and varying rooting depths (Ferrio *et al.* 2003; Marshall & Monserud 2006; Tsuji *et al.* 2006; Leavitt *et al.* 2010).

We also detected a stronger coherence in $\delta^{18}O$ variation between trees across sites compared with $\Delta^{13}C$ for either deciduous or evergreen oaks. Similarly, a higher common signal for neighbouring (<1,000 km) forest stands was found for oxygen isotopes across a pan-European tree-ring network (Chapter 5). These results were attributed to different C and O substrate sources and fractionation processes driving carbon and oxygen isotope signals in tree rings (Gessler *et al.* 2014). Although there are still important gaps in our understanding of isotopic variation in tree rings (Gessler *et al.* 2014), our results indicate that both carbon and oxygen stable isotopes are largely determined by water availability in Mediterranean climates, thus partially simplifying the interpretation of signals stored in wood. In dry environments, $\Delta^{13}C$ is mainly controlled by stomatal conductance, a functional trait that may be subject to sizeable species-specific variation (Farquhar *et al.* 1989; Ferrio *et al.* 2003; Gessler *et al.* 2009). Although leaf-level signals of $\delta^{18}O$ are also responsive to stomatal conductance, they seem largely modulated by variations in relative humidity and source water, that is, site-specific variation (Gessler *et al.* 2013; Treydte *et al.* 2014).

Interestingly, our results showed that the ecophysiological drivers of tree growth may not necessarily coincide at the spatial (e.g., inter-site variability) and temporal (e.g., inter-annual fluctuations) levels. In spite of significant (negative) year-to-year correlations between both isotopes, the annually-resolved $\delta^{18}O$ chronologies showed much less similarities to each other compared with $\Delta^{13}C$. As mentioned above, carbon and oxygen stable isotopes are partially linked through variation in stomatal conductance. However, the larger sensitivity of $\delta^{18}O$ to environmental variation may override the presence of coordinated isotopic signals in tree rings (Saurer *et al.* 2003; Roden & Farquhar 2012). Saurer *et al.* (2008) have similarly shown more robust signals for $\Delta^{13}C$ than for $\delta^{18}O$ across temperate sites from Switzerland. Altogether, these results pointed to the existence of more complex drivers of temporal $\delta^{18}O$ signals in Mediterranean oaks compared to $\Delta^{13}C$.

When scaled up to a much larger area, these temporal patterns coincided with the results reported in Chapter 5. We showed that, in addition to the presence of significant (negative) interannual correlations between both isotopes at site level, temporal signals in stable isotopes were geographically structured across the European continent, irrespective of potential taxonomical differences among species. The temporal associations between both stable isotopes and tree-ring width (TRW) values also followed a geographic structure, although they were stronger for $\Delta^{13}C$ compared to $\delta^{18}O$. Particularly, the strength of the relationship TRW *vs.* $\Delta^{13}C$ was strongly positive at low latitudes, while it reversed at high latitudes, hence following a clear latitudinal gradient that switched from drought-constrained growth (i.e., stomatal control) to cold-limited growth (i.e., photosynthetic limitation). Similar results were reported in Chapter 4, where we found a strong positive association among ring-width and carbon isotopes, which declined with elevation (i.e., along a hot/dry –

cool/moist gradient). On the other hand, although we detected a latitudinal (positive) trend in the relationship TRW *vs.* $\delta^{18}O$, significant (negative) associations were only found at low latitudes, where seasonal stomatal control seems to dominate tree growth, thus having stronger imprints on both isotopes.

Tree-ring width integrates the prevailing environmental conditions during the growing season and, thus, reflects changes in the physical environment in a straightforward manner. Consequently, it can be argued that the spatial patterns of tree growth are strongly driven by the spatial coherence of those external factors controlling tree growth. Indeed, we found that the amount of temporal coherence in growth among stands (spatial synchrony, *â*) largely depends on the dominating climate factor controlling tree performance in a region. Boreal forests (e.g., central Siberia, Fennoscandia) showed high *â* values quite similar to the mean synchrony between co-occurring trees within a stand (*Rbar*), while they dropped significantly towards lower latitudes (e.g, Iberian Peninsula) ($P < 0.05$, paired *t*-test; Fig. 6.1a). We attributed this difference in common growth variability to the degree of spatial coherence of the main climatic drivers of regional tree growth (temperature in high latitudes *vs.* precipitation in mid latitudes, respectively) (Wettstein *et al.* 2011). Although *â* values reported in Chapter 3 were slightly higher than those in Chapter 5, these results could be explained by a greater spatial saturation of sampling sites in the former study and, thus, lower distances among pairs of chronologies.

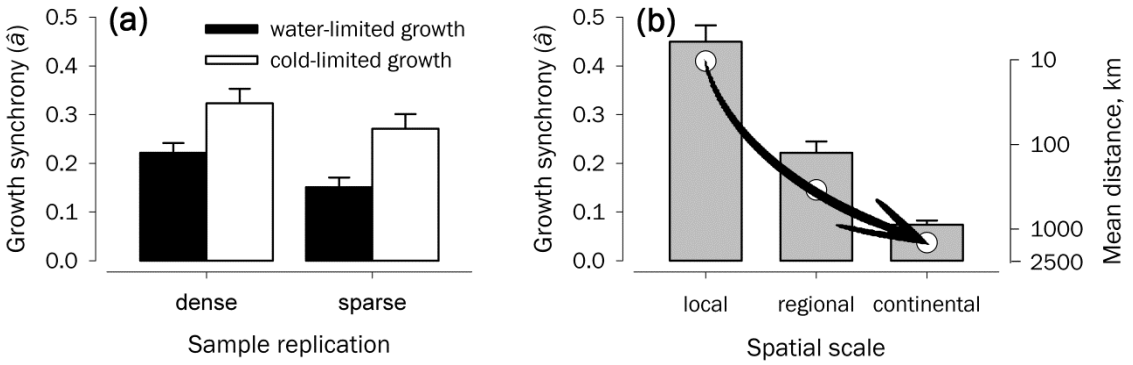

Figure 6.1. Spatial patterns of growth synchrony over the twentieth century depending on (a) sample replication and (b) spatial scale. **(a)** Regional patterns of growth coherence estimated based on dense ($n \geq 45$ chronologies; Chapter 3) or sparse ($n = 4$ chronologies; Chapter 5) tree-ring networks for Iberian Peninsula (water-limited growth; black bars) and central Siberia or Fennoscandia (cold-limited growth; white bars). **(b)** The degree of common variability in tree growth (bars) estimated at local (the Gúdar range, eastern Spain; Chapter 4), regional (Iberian Peninsula; Chapter 3) and continental (Europe; Chapter 5) scales. Dots denote mean geographical distance among chronologies (on a log scale) at each spatial level. All calculations are based on residual ring-width chronologies for the common period 1900–2003. Error bars denote standard errors.

We also found that the temporal coherence in tree growth is stronger at smaller scales and declines as the distance among sampled sites increases (Fig. 6.1b). These dependencies are expected and indicate that the strength of common climate forcing declines with distance (Koenig 2002). Interestingly, even when examining large geographical scales (e.g., continental) and mixing species from different functional groups (broad-leaved and conifers), a common signal can still be detected (Fig. 6.1b). This reinforces the climatic origin of the shared variability among chronologies as no other factor can vary synchronously in time and space to such extent (Hughes *et al.* 2009). Altogether, our results suggest that a proper spatial and taxonomic coverage aids at enhancing local to continental climate signals derived from tree-ring records. However, it is important to account for the complexities in the spatiotemporal organization of the different proxies. For example, while ring-width and $\Delta^{13}C$ seem to reliably reflect temporal variability, $\delta^{18}O$ signals are preferentially spatially structured. In addition to encouraging stand level studies, a better understanding of spatiotemporal patterns of tree growth along the local–global continuum must become central for examining ecophysiological performance of trees and associated changes in performance in response to climate change.

Climate drivers of tree growth

Tree rings are proxies of climate information that offer insights into life-history growth patterns, allowing long-term climate impacts on trees to be evaluated (Fritts 2001). Furthermore, tree-ring archives are the most widespread source of non-instrumental climate data with high temporal resolution, and provide valuable information on broad patterns of climate variability on a quantitative basis (e.g., D'Arrigo *et al.* 2003; Cook *et al.* 2004; D'Arrigo & Wilson 2006; Treydte *et al.* 2006; Briffa *et al.* 2008; Trouet *et al.* 2009; Büntgen *et al.* 2011; Yang *et al.* 2014). In dendrochronology, stand-level growth responses to environmental factors are often examined through the analysis of a number of tree-ring features (e.g., ring width, wood density, stable isotopes). However, if the goal is to develop a comprehensive understanding of tree ecophysiological responses to climate for large geographic areas, several tree species in a variety of forest types and growth environments need to be characterized in order to capture the desired range of spatial variability (Holman & Peterson 2006). Indeed, heterogeneity in temporal tree patterns at small scales may indicate that trees are preferentially responding to variable local growth conditions (e.g., Kruse *et al.* 2012; Primicia *et al.* 2015). Alternatively, if a significant portion of variability in a particular tree-ring trait is shared among disjunct populations, a common macroclimatic influence is likely to control tree performance over large areas (e.g., Andreu *et al.* 2007). Thus, assessing functional responses to climate at various spatial scales provide different but complementary information about the environmental factors affecting tree growth.

Climate effects on tree growth and performance are known to vary across biogeographical gradients, hence modifying physiological responses to local factors that

influence growth (Babst *et al.* 2013). The results reported in Chapter 2 showed that the spatial patterns of isotope signals in *Quercus* species were structured along a Mediterranean aridity transect. However, we found that Mediterranean deciduous (*Q. faginea*, *Q. humilis* and *Q. petraea*) and evergreen (*Q. ilex*) oaks constitute two clearly differentiated functional groups in terms of their carbon and water economies; conversely, species-specific variation within a functional group was small. Particularly, we observed a strong spatial dependence of the evergreen oak on temperature for both isotopes, while deciduous oaks showed more consistent responses to precipitation. Despite the differences in climate drivers found for co-occurring oak species, both functional groups revealed bimodal responses to climate as revealed by their isotope signals, which correspond to the double climatic stress typical of Mediterranean environments: summer drought and winter cold (Mitrakos 1980; Terradas & Savé 1992; Larcher 2000). For example, *Q. ilex* positively responded to winter ($\Delta^{13}C$) and summer ($\delta^{18}O$) temperatures, suggesting photosynthesis limitation during the cold season and water stress during the warm season. On the other hand, $\delta^{18}O$ variability in deciduous oaks was related to rainfall from autumn through spring, which coincides with precipitation peaks during intermediate seasons (spring and autumn) and atmospheric cooling in winter, a response in agreement with Treydte *et al.* (2014) on how the ^{18}O isotopic signal is integrated in tree rings.

Our results, thus, reflect complex effects of varying air humidity and soil water availability on plant physiology (Dansgaard 1964; Roden *et al.* 2000; McCarroll & Loader 2004). They also suggest a strong reliance of deciduous species on precipitation-derived soil moisture, which may be attributed to their relatively shallow root system as compared to the evergreen *Q. ilex*. In addition, our results pointed to contrasting strategies to cope with summer drought adopted by each functional group. Indeed, deciduous oaks show lower physiological activity than *Q. ilex* during summer (Montserrat-Martí *et al.* 2009). This physiological behaviour indicates a tendency to 'avoid' rather than 'tolerate' summer drought for deciduous species. These ideas were confirmed by climate analysis at the temporal level. Drought-avoiding deciduous oaks (*Q. humilis* and *Q. petraea*) were negatively affected by summer drought (June), as growth and carbon gain are limited to spring and autumn in these species (Montserrat-Martí *et al.* 2009). In contrast, the evergreen oak responded to early spring (March) and autumn (September) conditions, with positive imprints of temperature on $\delta^{18}O$ and precipitation on $\Delta^{13}C$. These results indicate a temporal agreement of isotopic signals in *Q. ilex* with the two peaks of precipitation, accompanied with optimum temperatures for growth, in the western Mediterranean (Gutiérrez *et al.* 2011). Despite striking differences between functional groups, we observed a common negative response to high summer (July) temperatures on $\Delta^{13}C$, suggesting reduced stomatal conductance (i.e., increased water-use efficiency), which is coincident with the hottest period of the growing season. However, the climate influence on carbon and oxygen stable isotopes was more clearly imprinted in the spatial signal recorded along the aridity transect than in the annually

resolved chronologies; this is probably because the latter originated from coastal, mild sites lacking a strong influence of winter cold.

As outlined in Chapter 4, topography strongly determines spatiotemporal variation of tree growth and forest carbon budget in mountainous regions. In particular, elevation plays a decisive role in the balance between soil moisture and temperature and eventually drives the response of forests to environmental conditions (Körner 2007). Many studies have reported that growth-climate relationships vary considerably together with thermal and moisture variation across broad altitudinal gradients (e.g., McKenzie *et al.* 2003; Bunn *et al.* 2005; Büntgen *et al.* 2007). In our study, we found that both ring-width and carbon isotope discrimination ($\Delta^{13}C$) in pines were far more responsive to water availability than to temperature along a Mediterranean elevational gradient. At xeric sites (i.e., lowest elevational limit of the studied gradient), we showed that Mediterranean pines are mainly responsive to spring and, to a lesser degree, autumn climate conditions; conversely, mountain pines at mesic sites (*ca.* 2,000 m elevation) were most sensitive to summer conditions. Indeed, the analysis showed that cambial resumption at high altitudes was delayed compared with lower elevations (April *vs.* February), thus shifting soil drying out in time. Despite differences in climate responses along the gradient, we detected the presence of a summer drought signal as common feature explaining growth patterns across the gradient. The negative effect of high temperatures was registered in both TRW (July to August) and $\Delta^{13}C$ (May to September). Remarkably, interspecific differences in climate responses were blurred by site differences along the gradient (Villalba *et al.* 1994).

At a larger scale, summer drought was the main climate driver of tree growth in the Iberian Peninsula (Chapter 3). Although our tree-ring network consisted of high-elevation stands, we detected strong positive associations between growth and either precipitation or the SPEI drought index (May to July) as common feature across chronologies. This reinforces our previous results suggesting that growth of Mediterranean forests is primarily water-limited (Andreu *et al.* 2007). Similarly, we found a regionally coherent response of boreal forests to June–July temperatures in central Siberia (Vaganov *et al.* 1999; Knorre *et al.* 2006). In addition to summer, we also observed consistent imprints of early season temperature on growth in both regions. Particularly, tree growth correlated with early spring (April) temperature in Siberia (negatively) and with late winter (February) temperature in Spain (positively). Such contrasting regional responses to temperature in the early growing season may be a consequence of varying physiological processes underlying the mechanisms of dormancy breaking as discussed in detail in Chapter 3. It is worth noting that the main climate variables related to growth are regionally consistent across taxa, despite species-specific ecological features (*Abies*, *Larix*, *Picea*, *Pinus*).

At the continental scale our results support general knowledge on climate drivers of growth, which points to temperature limitation at northern latitudes and drought stress at southern latitudes of Europe, with miscellaneous climate signals present in the temperate

zone. In contrast, stable isotopes responded more uniformly to summer conditions across the network. Particularly, we found strong temporal associations between $\Delta^{13}C$ and June–August temperature (negative) and precipitation (positive). The inverse relationships were found for $\delta^{18}O$ (positive with temperature, negative with precipitation). These Europe-wide relationships were first reported by Treydte *et al.* (2007) and are consistent with expectations from theory.

For oxygen, the positive correlation with temperature reflects the influence of the isotope signal of precipitation in tree rings, as precipitation is known to be strongly determined by temperature (Dansgaard 1964). Precipitation may also have a direct influence on $\delta^{18}O$ in tree rings via the effect on leaf water enrichment because wet climatic conditions (high precipitation) are associated with increased relative humidity, which in turn results in lower leaf water enrichment (hence the observed negative correlation) (Edwards & Fritz 1986; Roden & Ehleringer 1999). Altogether, there is no doubt that there is usually a combined signal of temperature and precipitation in oxygen isotope ratios, which may accordingly lead to a high correlation with drought indices (Treydte *et al.* 2007). Regarding the relationship between climate and carbon isotopes, drought conditions (i.e., high temperature/low precipitation) are known to result in lower stomatal conductance and lower isotope discrimination in tree rings (Farquhar *et al.* 1982; Leavitt & Long 1989; Saurer *et al.* 1995). However, the investigated sites were scattered across a wide latitudinal gradient with varying degree of water stress and, therefore, the observed $\Delta^{13}C$ changes in tree rings only reflected a stomatal signal, but also fluctuations in assimilation rates in subarctic regions where low temperatures limit growth.

Effects and future implications of climate warming on tree growth

Tree rings are a direct measure of stem growth, which represents the principal above-ground carbon accumulation pool. Because tree growth is sensitive to changes in the physical environment, tree-ring proxies are valuable tools to track population responses to moving climate optima in time and space (Pease *et al.* 1989; Polechová *et al.* 2009). These responses will play a crucial role in determining future carbon dynamics in forest ecosystems. Although huge research efforts have been made over the last decades to understand the impact of climate change on forest ecosystems, many uncertainties still remain (IPCC 2007). The importance of tree sensitivity to climate in modulating spatiotemporal growth variability and in shaping communities affected by forest die-off episodes has, however, been reported worldwide (Ciais *et al.* 2005; Allen *et al.* 2010, 2015; Anderegg *et al.* 2013; Williams *et al.* 2013), including regions that are not typically considered to be drought-limited (Barber *et al.* 2000; Wilmking *et al.* 2005; Silva *et al.* 2010). Thus, our approach offers a systematic way to assess subtle changes in temporal growth patterns according to the shifting magnitude of shared variability among adjacent or disjunct populations (spatial synchrony, *â*) and, hence, it

ultimately evaluates forest vulnerability in the face of rapid climate change at multiple spatiotemporal scales.

In our studies, we found two major responses of forest trees to temperature warming, namely an advancement of early season responsiveness and a clear change in ecophysiological performance. Many studies have documented shifts in the timing of life cycle events (i.e., phenology) across the year in response to warming, especially at the beginning of the growing season (e.g., Parmesan & Yohe 2003; Menzel *et al.* 2006; Reyes-Fox *et al.* 2014). From a simplistic perspective, advancement in spring events may be thought to enhance tree growth due to earlier initiation of cambial reactivation and, thus, extended growth period (Parmesan & Yohe 2003). However, there is emerging evidence that different physiological processes induced by warming along the course of the year may cancel out this positive impact, causing non-response or even delay in spring phases (Cook *et al.* 2012).

Indeed, the timing of cambial reactivation plays an important role in determining the amount of wood synthesized and the environmental adaptiveness of trees. The results reported in Chapter 3 indicated that temperatures from late winter to early spring affected the physiological processes that are involved in the initiation of cambial cell division and xylem differentiation in trees from both Boreal and Mediterranean forests. Similar results have been reported for several regions, including cold, northern biomes and Mediterranean areas (e.g., Badeck *et al.* 2004; Aerts *et al.* 2006; Gordo & Sanz 2009). However, these advances in early season phenology led to contrasting growth responses in these two contrasting regions. Particularly, warmer springs were negatively related to tree growth in central Siberia, which might be associated with increasing risk of frost damage to the cambium (Begum *et al.* 2013). In contrast, early cambial reactivation triggered by warm winters increased carbon uptake and enhanced wood formation in Mediterranean environments (Bigelow *et al.* 2014).

On the other hand, the relaxation of cold limitation of growth during summer was observed at high latitudes, while an increase in drought stress negatively impacted on growth in mid latitudes. Moreover, we observed temporal shifts in climate sensitivity of growth from summer months towards earlier in the season in the Iberian Peninsula (Chapter 3 and Chapter 4), which suggests reduced cambial activity in peak summer (Voltas *et al.* 2013) in response to warming-induced drought. As the result of these distinct responses to different time periods, we found steady growth rates in Siberia over the last century, but a gradual growth decline in Spain (Chapter 3). Similarly, Bernal *et al.* (2011) reported that increased drought stress advanced the onset of growth in spring, but led to reductions in annual growth in Mediterranean shrubs.

As mentioned above, growth was tightly controlled by leave-level gas exchange processes in drought-prone environments (Leavitt *et al.* 2010). We observed that the coherence between ring-width and $\Delta^{13}C$ signals increased throughout the second half of the 20th century in the Iberian Peninsula (Chapter 4). Notably, this effect became more pronounced at a larger geographic scale over the whole continent, especially in Central and

Southern Europe (Chapter 5), which suggests increasing drought stress and, thus, enhanced climatic control of tree performance over vast areas (Saurer *et al.* 2014). Owing to an intensified influence of climate on leaf-level ecophysiological processes controlling tree growth, our result suggests that warming-induced drought stress is spreading upwards along altitudinal transects in water-limited Mediterranean forests and northwards along latitudinal gradients in temperate European forests. This effect overrides taxonomic imprints and local forest drivers of tree performance (e.g., topography, nutrient availability, tree competition).

Altogether, we demonstrated that the observed responses (i.e., shifts in spring phenology and tree physiology) are producing substantial changes in tree performance and, in turn, triggering more synchronous growth patterns from small to large scales (Fig. 6.2). This effect was attributed to an amplified climatic control of tree growth through vast geographical areas due to increasing heat and drought stresses over the growing season which, in turn, exert negative impacts on forest productivity (Ciais *et al.* 2005; Allen *et al.* 2010, 2015; Anderegg *et al.* 2013; Williams *et al.* 2013). Remarkably, enhanced spatial synchrony was observed among co-occurring species and populations growing under common climate influences, which may imply increasing vulnerability of forests across wide range of environmental gradients. A natural threshold for such increase is logically imposed by the degree of synchronous growth between co-occurring trees within a stand (*Rbar* statistic *sensu* Wigley *et al.* [1984]), as observed in the studied region (Fig. 6.2). If so, our results provide evidence that small-scale growth synchrony is currently approaching its maximum theoretical level in water-limited environments. If warming continues, we might expect strong decline in growth vigor and, eventually, mass extinction events across forest populations.

Outlook for further research: where to go from here?

Over the past few decades, numerous studies have addressed the effects of climate change on terrestrial ecosystems. Despite these efforts, the response of forest ecosystems to

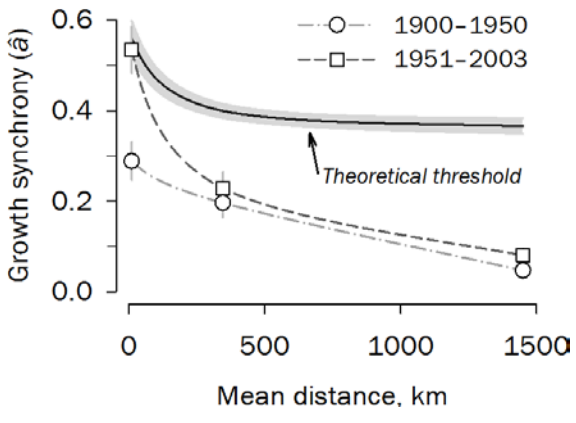

Figure 6.2. Temporal trends in spatial synchrony over the twentieth century at multiple spatial scales. Spatial synchrony (*â*) is estimated at local, regional and continental scales (see Fig. 6.1 for details) using residual ring-width chronologies for two consecutive, non-overlapping periods (1900–1950 and 1951–2003). Solid line indicates hypothesized *â* maxima over the period 1900–2003 as inferred from mean synchrony between co-occurring trees within a stand (*Rbar* statistic). Error bars and shaded area denote standard errors.

environmental variability and extremes remains uncertain. Using dendroecological techniques, significant progress has been made to improve our knowledge in tree growth variability in response to climate at different spatial scales, ranging from local(e.g., Tardif *et al.* 2003; Carrer & Urbinati 2006), regional (e.g., Andreu *et al.* 2007; Natalini *et al.* 2015) and continental (e.g., Babst *et al.* 2012). This work has further contributed to our understanding of the complex patterns of tree-ring signals across multiple spatiotemporal scales and how these patterns are modified by recent climate warming. Yet, many questions remain unanswered, even to the light of recent advances.

Despite tree-ring traits have been widely employed to characterize growth dynamics in response to environmental conditions, recent research has suggested that commonly applied sampling designs may introduce considerable biases in quantifying growth responses to climate variation and extremes (e.g., Cherubini *et al.* 1998; Brienen *et al.* 2012; Bowman *et al.* 2013). Although dendrochronologists generally aim to obtain a good representation of the population variability, field sampling is often biased towards dominant, large and healthy trees (Bowman *et al.* 2013). Thus, the appropriateness of such sampling schemes to accurately represent population responses to environmental variation is increasingly questioned (Cherubini *et al.* 1998; Brienen *et al.* 2012). A stratified sampling scheme, including trees of different age, size and social status in future dendrochronological studies, would allow separating class-specific variability from a population-wide response which, in turn, would improve our ability for detecting climatic and ecological processes underlying complex spatiotemporal patterns embedded in tree rings (Voelker 2011).

As a rule, dendrochronologists seek trees that demonstrate sensitive growth responses, as these contain more climatic information and are more likely to cross-date (Fritts 2001). The choice of sampling sites, guided by this distinction, often leads to another important caveat in most tree-ring datasets which are increasingly being used to assess forest ecology, tree population dynamics and growth response to environmental instability. Being particularly susceptible to climate, trees growing in marginal conditions such as altitudinal or latitudinal limits may largely mislead our conclusions on forest vulnerability to climate change effects (Cernusak & English 2015). Moreover, the most extensively sampled regions in the world consist of coniferous species due to their high tolerance to harsh environmental conditions and accurate cross-dating. Indeed, enhanced warming-induced growth synchrony has been reported mainly for conifer forests growing under Mediterranean climate (Tardif *et al.* 2003; Andreu *et al.* 2007; Dolanc *et al.* 2013; Natalini *et al.* 2015; but see Latte *et al.* 2015). However, our work evidences that this pattern is not tied to a certain species or region (Wettstein *et al.* 2011), and further research including temperate regions and new sets of tree species are urgently needed to allow evaluating general patterns of growth synchrony and their drivers. Thus, there is a necessity for more exhaustive studies across species and regions, especially in areas located at the interior of the climatic space over which temperate forest species are distributed.

Regional- to continental-scale syntheses of climate change impacts on forest populations are essential for understanding long-term spatiotemporal variability in tree growth and for properly assessing ecosystem risks on short- and long-term timescales. However, comprehensive dendroecological investigations based on annual stem growth could be challenged by miscellaneous environmental signals recorded in ring-width chronologies. Meanwhile, tree-ring stable isotopes have been shown to be less dependent on local site conditions compared with growth and, therefore, studies into isotope variations can provide additional information on the physiological responses of trees (McCarroll & Loader 2004; Gessler *et al.* 2014). Furthermore, we showed here that simultaneous analysis of both ring-width and isotope signals hold the potential of broadening and enhancing our understanding of the complex biogeographical interactions underlying spatial patterns of tree growth dynamics, especially in a climate change context. Although multi-proxy datasets are relatively new in dendroecology, this approach enables more detailed knowledge about the physiological processes underlying climate-induced growth changes of different tree species, and their varying capabilities to cope with enhanced climate stress, which is required for the estimation of future forest vulnerability to climate change. Emerging multi-proxy archives are, thus, a powerful way of testing climate change impacts on tree performance and it should be undertaken more widely in the future research.

The mixed model framework proposed in this Thesis is a powerful tool to investigate spatiotemporal patterns of tree-ring signals. However it is of linear type, which allows detecting only simplified structures in natural populations. Thus, we cannot overlook that linear methods might not detect potential non-linear relationships often found in nature. Indeed, we observed non-linear relationships between tree growth rates and latitude (see Chapter 5). Similar non-linear associations have also been documented between radial growth and altitude (Paulsen *et al.* 2000; Coomes & Allen 2007; Voelker 2011). Altogether, they suggest that growth responses to climate are not necessarily linear in their parameters, as most physiological and developmental processes behave essentially in a non-linear manner in relation to the environment. This calls for either polynomial expansions or intrinsically non-linear approaches, with the latter being in principle most preferable. Owing to the flexibility of mixed models, our approach could be extended to non-linear relationships. Nevertheless, it cannot be denied that these models require a considerable amount of statistical expertise for successful application.

General Conclusions

Forest tree growth and ecophysiological performance are geographically structured across environmental gradients, providing valuable information to assess spatiotemporal patterns of tree responses to climate variability along the local–global continuum. Besides, mixed modelling allows a flexible fitting of general statistical structures to tree-ring chronologies and aids at delivering valid inferences on physiological drivers of tree growth at multiple scales, opening new avenues for unscrambling the complexities of tree-ring signals in dendroecology.

At local scale

The high spatial synchrony in ring-width patterns in Mediterranean pinewoods points to the existence of common climatic factors controlling tree growth across species along altitudinal gradients. Enhanced synchrony in radial growth during the twentieth century is driven by more synchronous temporal responses among Mediterranean forests spreading upwards in elevation, owing to increased drought stress as indicated by shifting growth sensitivity to climate towards earlier months in the season.

Climatic influences on tree growth in Mediterranean pine forests could mainly be explained by leaf-level physiological processes as reflected in wood $\Delta^{13}C$. Warming-induced drought effects induce a tighter stomatal control of water losses to prevent desiccation and/or hydraulic failure which, in turn, override taxonomic imprints and local drivers of tree growth progressively and towards higher elevations in mountain areas.

The use of stable isotope records ($\Delta^{13}C$ and $\delta^{18}O$) improves our understanding of complex spatiotemporal patterns of tree performance in Mediterranean forest ecosystems. Large differences between deciduous and evergreen *Quercus* species in the organization of their temporal and spatial isotope signals highlight contrasting strategies in response to drought in terms of their carbon and water economies, despite co-existence along broad aridity gradients. Climate factors impact differentially on isotope records of these two functional groups at both taxonomic and geographical levels, most likely through contrasting interspecific physiological adaptations and phenotypic plasticity linked to phenology and wood growth dynamics.

At regional scale

The spatial variability of tree growth at regional (subcontinental) scales is driven by regional climate factors superimposing over taxonomic imprints and local site conditions. Warming-induced heat and drought effects increase spatial synchrony within contrasting (boreal and Mediterranean) Eurasian biomes, ultimately leading to unprecedented temporal

coherence in ring-width records at the turn of this century. Enhanced synchrony is becoming a widespread, although regionally dependent, phenomenon related to warmer springs and increased temperature variability in high latitudes and to warmer winters and drier growing seasons in mid-latitudes.

At continental scale

The temporal coherence in ring-width records is geographically structured across Europe following a latitudinal gradient owing to the relative significance of leaf-level physiological processes (i.e., photosynthesis or stomatal conductance) as drivers of forest productivity. The extent of spatial synchrony among forests increases from south to north switching from primarily water-limited to cold-constrained tree growth and reflecting greater spatial homogeneity of regional temperature signals compared with more complex rainfall patterns.

Leaf-level physiology and secondary growth are ultimately linked via carbon allocation strategies in trees. The geographically-structured relationships between ring-width and either $\Delta^{13}C$ (decreasing northwards) or $\delta^{18}O$ (increasing northwards) follow a latitudinal gradient concurrent with a northward trend of decreasing temperatures and reduced atmospheric evapotranspirative demand.

The increase in growth synchrony together with a tighter relationship between ring-width and $\Delta^{13}C$ in the second half of the twentieth century compared with the first half suggest increasing drought effects on growth patterns in southern and central Europe. Both findings point to an increasing impact of global warming, related to higher atmospheric moisture demand and hotter drought spells, spreading northwards across European forests.

Finally, the nature of these studies, as the ones carried out in this PhD thesis, demonstrates that broad-scale climatic variation influence ecophysiological traits in ways that have previously gone unrecognized, which can help to understand the ecological implications of ecosystem functioning and make better predictions to the ongoing global warming.

REFERENCES

References

Aerts R, Cornelissen JHC, Dorrepaal E (**2006**) Plant performance in a warmer world: general responses of plants from cold, northern biomes and the importance of winter and spring events. *Plant Ecol* **182**:65–77.

Aguilera M, Espinar C, Ferrio JP, Pérez G, Voltas J (**2009**) A map of autumn precipitation for the third millennium BP in the Eastern Iberian Peninsula from charcoal carbon isotopes. *J Geochem Explor* **102**:157–165.

Aguilera M, Ferrio JP, Araus JL, Tarrús J, Voltas J (**2011**) Climate at the onset of western Mediterranean agriculture expansion: evidence from stable isotopes of sub-fossil oak tree rings in Spain. *Palaeogeogr Palaeoclimatol Palaeoecol* **299**:541–551.

Allen CD, Macalady AK, Chenchouni H, *et al.* (**2010**) A global overview of drought and heat-induced tree mortality reveals emerging climate change risks for forests. *For Ecol Manage* **259**:660–684.

Allen CD, Breshears DD, McDowell NG (**2015**) On underestimation of global vulnerability to tree mortality and forest die-off from hotter drought in the Anthropocene. *Ecosphere* **6**:129.

Altieri S, Mereu S, Cherubini P, *et al.* (**2015**) Tree-ring carbon and oxygen isotopes indicate different water use strategies in three Mediterranean shrubs at Capo Caccia (Sardinia, Italy). *Trees* **29**:1593–1603.

Altman J, Hédl R, Szabó P, *et al.* (**2013**) Tree-rings mirror management legacy: dramatic response of standard oaks to past coppicing in Central Europe. *PLoS One* **8**:e55770.

Amritkar RE, **Rangarajan G** (**2006**) Spatially synchronous extinction of species under external forcing. *Phys Rev Lett* **96**:258102.

Anderegg WRL, Kane JM, Anderegg LDL (**2013**) Consequences of widespread tree mortality triggered by drought and temperature stress. *Nat Clim Chang* **3**:30–36.

Anderegg WRL, Klein T, Barlett M, *et al.* (**2016**) Meta-analysis reveals that hydraulic traits explain cross-species patterns of drought-induced tree mortality across the globe. *Proc Natl Acad Sci USA* **113**:5024–5029.

Andreu L, Gutiérrez E, Macias M, Ribas M, Bosch O, Camarero JJ (**2007**) Climate increases regional tree-growth variability in Iberian pine forests. *Glob Chang Biol* **13**:804–815.

Andreu L, Planells O, Gutiérrez E, Helle G, Schleser GH (**2008**) Climatic significance of tree-ring width and $\delta^{13}C$ in a Spanish pine forest network. *Tellus B* **60**:771–781.

Andreu-Hayles L, Gutiérrez E, Muntan E, Helle G, Anchukaitis KJ, Schleser GH (**2011**) Long tree-ring chronologies reveal 20th century increases in water-use efficiency but no enhancement of tree growth at five Iberian pine forests. *Glob Chang Biol* **17**:2095–2112.

Arend M, Kuster T, Günthardt-Goerg MS, Dobbertin M (**2011**) Provenance-specific growth responses to drought and air warming in three European oak species (*Quercus robur*, *Q. petraea* and *Q. pubescens*). *Tree Physiol* **31**:287–297.

Babst F, Carrer M, Urbinati C, Neuwirth B, Frank DC (**2012**) 500 years of regional forest growth variability and links to climatic extreme events in Europe. *Environ Res Lett* **7**:1–11.

Babst F, Poulter B, Trouet V, *et al.* (**2013**) Site- and species-specific responses of forest growth to climate across the European continent. *Glob Ecol Biogeogr* **22**:706–717.

Babst F, Alexander MR, Szejner P, *et al.* (**2014**) A tree-ring perspective on the terrestrial carbon cycle. *Oecologia* **176**:307–322.

Badeck FW, Bondeau A, Bottcher K, *et al.* (**2004**) Responses of spring phenology to climate change. *New Phytol* **162**:295–309.

Barber V, Juday G.P, Finney B (**2000**) Reduced growth of Alaska white spruce in the twentieth century from temperature-induced drought stress. *Nature* **405**:668–672.

Barbero M, Loisel R, Quézel P (**1992**) Biogeography, ecology and history of Mediterranean *Quercus ilex* ecosystems. *Vegetatio* **99–100**:19–34.

Barbour MM, Andrews TJ, Farquhar GD (**2001**) Correlations between oxygen isotope ratios of wood constituents of *Quercus* and *Pinus* samples from around the world. *Aust J Plant Physiol* **28**:335–348.

Barbour MM, Walcroft AS, Farquhar GD (**2002**) Seasonal variation in $\delta^{13}C$ and $\delta^{18}O$ of cellulose from growth rings of *Pinus radiata*. *Plant Cell Environ* **25**:1483–1499.

Barnard HR, Brooks JR, Bond BJ (**2012**) Applying the dual-isotope conceptual model to interpret physiological trends under controlled conditions. *Tree Physiol* **32**:1183–1198.

Barnard RL, Salmon Y, Kodama N, *et al.* (**2007**) Evaporative enrichment and time lags between $\delta^{18}O$ of leaf water and organic pools in a pine stand. *Plant Cell Environ* **30**:539–550.

Barnett AG, Koper N, Dobson AJ, Schmiegelow F, Manseau M (**2010**) Using information criteria to select the correct variance–covariance structure for longitudinal data in ecology. *Methods Ecol Evol* **1**:15–24.

Battipaglia G, De Micco V, Brand WA, *et al.* (**2010**) Variations of vessel diameter and delta ^{13}C in false rings of *Arbutus unedo* L. reflect different environmental conditions. *New Phytol* **188**:1099–1112.

Begum S, Nakaba S, Yamagishi Y, Oribe Y, Funada R (**2013**) Regulation of cambial activity in relation to environmental conditions: understanding the role of temperature in wood formation of trees. *Physiol Plantarum* **147**:46–54.

Bernal M, Estiarte M, Penuelas J (**2011**) Drought advances spring growth phenology of the Mediterranean shrub Erica multiflora. *Plant Biol (Stuttg)* **13**:252–257.

Bigelow SW, Papaik MJ, Caum C, North MP (**2014**) Faster growth in warmer winters for large trees in a Mediterranean-climate ecosystem. *Clim Change* **123**:215–224.

Bjørnstad ON, Ims RA, Lambin X (**1999**) Spatial population dynamics: analyzing patterns and processes of population synchrony. *Trends Ecol Evol* **14**:427–431.

Boettger T, Haupt M, Knöller K, *et al.* (**2007**) Wood cellulose preparation methods and mass spectrometric analyses of $\delta^{13}C$, $\delta^{18}O$, and nonexchangeable $\delta^{2}H$ values in cellulose, sugar, and starch: an interlaboratory comparison. *Anal Chem* **79**:4603–4612.

Bonan GB (**2008**) Forests and climate change: forcings, feedbacks, and the climate benefits of forests. *Science* **320**:1444–1449.

Bowman DMJS, Brienen RJW, Gloor E, Phillips OL, Prior LD (**2013**) Detecting trends in tree growth: not so simple. *Trends Plant Sci* **18**:11–17.

Brienen RJW, Gloor E, Zuidema PA (**2012**) Detecting evidence for CO_2 fertilization from tree ring studies: the potential role of sampling biases. *Global Biogeochem Cycles* **26**:GB1025.

Briffa KR, **Jones PD** (**1990**) Basic chronology statistics and assessment. In: Cook ER, Kairiukstis LA (eds) *Methods of dendrochronology: applications in the environmental sciences*. Kluwer Acad Publ, Dordrecht, pp 137–152.

Briffa KR, Osborn TJ, Schweingruber F, Jones PD, Shiyatov SG, Vaganov EA (**2002**) Tree-ring width and density data around the Northern Hemisphere: Part 1, local and regional climate signals. *Holocene* **12**:737–757.

Briffa KR, Shishov VV, Melvin TM, *et al.* (**2008**) Trends in recent temperature and radial tree growth spanning 2000 years across northwest Eurasia. *Philos Trans R Soc Lond B Biol Sci* **363**: 2271–2284.

Brown H, **Prescott R** (**1999**) *Applied mixed models in medicine*. Wiley, Chichester.

Bunn AG, Waggoner LA, Graumlich LJ (**2005**) Topographic mediation of growth in high elevation foxtail pine (*Pinus balfouriana* Grev. et Balf.) forests in the Sierra Nevada, USA. *Glob Ecol Biogeogr* **14**:103–114.

Büntgen U, Frank DC, Nievergelt D, Esper J (**2006**) Summer temperature variations in the European Alps, AD 755–2004. *J Clim* **19**:5606–5623.

Büntgen U, Frank DC, Kaczka RJ, Verstege A, Zwijacz-Kozica T, Esper J (**2007**) Growth responses to climate in a multi-species tree-ring network in the Western Carpathian Tatra Mountains, Poland and Slovakia. *Tree Physiol* **27**:689–702.

Büntgen U, Frank DC, Liebhold A, *et al.* (**2009**) Three centuries of insect outbreaks across the European Alps. *New Phytol* **182**:929–941.

Büntgen U, Tegel W, Nicolussi K, *et al.* (**2011**) 2500 years of European climate variability and human susceptibility. *Science* **331**:578–582.

Burnham KP, **Anderson DR** (**2002**) *Model selection and multimodel inference: a practical information–theoretic approach*. Springer, New York.

Camarero JJ, Bigler C, Linares JC, Gil-Pelegrín E (**2011**) Synergistic effects of past historical logging and drought on the decline of Pyrenean silver fir forests. *For Ecol Manage* **262**:759–769.

Camarero JJ, Manzanedo RD, Sánchez-Salguero R, Navarro-Cerrillo RM (**2013**) Growth response to climate and drought change along an aridity gradient in the southernmost *Pinus nigra* relict forests. *Ann For Sci* **70**:769–780.

Camarero JJ, Gazol A, Tardif JC, Conciatori F (**2015**) Attributing forest responses to global-change drivers: limited evidence of a CO_2-fertilization effect in Iberian pine growth. *J Biogeogr* **42**:2220–2233.

Carrer M (**2011**) Individualistic and time-varying tree-ring growth to climate sensitivity. *PLoS One* **6**:e22813.

Carrer M, **Urbinati C** (**2006**) Long-term change in the sensitivity of tree-ring growth to climate forcing in *Larix decidua*. *New Phytol* **170**:861–871.

Cernusak LA, **English NB** (**2015**) Beyond tree-ring widths: stable isotopes sharpen the focus of climate response of temperate forest trees. *Tree Physiol* **35**:1–3.

Cernusak LA, Farquhar GD, Pate JS (**2005**) Environmental and physiological controls over oxygen and carbon isotope composition of Tasmanian blue gum, *Eucalyptus globulus*. *Tree Physiol* **25**:129–146.

Cernusak LA, Wong SC, Farquhar GD (**2003**) Oxygen isotope composition of phloem sap in relation to leaf water in *Ricinus communis*. *Funct Plant Biol* **30**:1059–1070.

Cherubini P, Dobbertin M, Innes JL (**1998**) Potential sampling bias in long-term forest growth trends reconstructed from tree rings: a case study from the Italian Alps. *For Ecol Manage* **109**:103–118.

Cherubini P, Gartner BL, Tognetti R, Bräker OU, Schoch W, Innes JL (**2003**) Identification, measurement and interpretation of tree rings in woody species from Mediterranean climates. *Biol Rev* **78**:119–148.

Chown SL, Gaston KJ, Robinson D (**2004**) Macrophysiology: large-scale patterns in physiological traits and their ecological implications. *Funct Ecol* **18**:159–167.

Christopoulou A, Fulé PZ, Andriopoulos P, Sarris D, Arianoutsou M (**2013**) Dendrochronology-based fire history of *Pinus nigraforests* in Mount Taygetos, Southern Greece. *For Ecol Manage* **293**:132–139.

Ciais P, Reichstein M, Viovy N, *et al.* (**2005**) Europe-wide reduction in primary productivity caused by the heat and drought in 2003. *Nature* **437**:529–533.

Clark NE, Blasing TJ, Fritts HC (**1975**) Influence of interannual climatic fluctuations on biological systems. *Nature* **256**:302–305.

Cook BI, Wolkovich EM, Parmesan C (**2012**) Divergent responses to spring and winter warming drive community level flowering trends. *Proc Natl Acad Sci USA* **109**:9000–9005.

Cook ER, **Kairiukstis LA** (**1990**) *Methods of dendrochronology: applications in the environmental sciences*. Kluwer Acad Publ, Dordrecht.

Cook ER, **Krusic PJ** (**2005**) *Program ARSTAN: A treering standardization program based on detrending and autoregressive time series modeling, with interactive graphics*. Columbia Univ, Palisades, NY.

Cook ER, Woodhouse CA, Eakin CM, Meko DM, Stahle DW (**2004**) Long-term aridity changes in the western United States. *Science* **306**:1015–1018.

Coomes DA, **Allen RB** (**2007**) Effects of size, competition and altitude on tree growth. *J Ecol* **95**:1084–1097.

Corcuera L, Camarero JJ, Gil-Pelegrín E (**2002**) Functional groups in *Quercus* species derived from the analysis of pressure–volume curves. *Trees* **16**:465–472.

Craig H, **Gordon LI** (**1965**) Deuterium and oxygen-18 variations in the ocean and the marine atmospheres. In: Tongoirgi E (ed) *Proc Stable Isotopes in Oceanographic Studies and Paleotemperatures*. Lischi & Figli, Pisa, pp 9–130.

Cullen LE, Adams MA, Anderson MJ, Grierson PF (**2008**) Analyses of $\delta^{13}C$ and $\delta^{18}O$ in tree rings of *Callitris columellaris* provide evidence of a change in stomatal control of photosynthesis in response to regional changes in climate. *Tree Physiol* **28**:1525–1533.

Cuntz M, Ogee J, Farquhar GD, Peylin P, Cernusak LA (**2007**) Modelling advection and diffusion of water isotopologues in leaves. *Plant Cell Environ* **30**:892–909.

Damesin C, Rambal S, Joffre R (**1997**) Between-tree variations in leaf $\delta^{13}C$ of *Quercus pubescens* and *Quercus ilex* among Mediterranean habitats with different water availability. *Oecologia* **111**:26–35.

Damesin C, Rambal S, Joffre R (**1998**) Co-occurrence of trees with different leaf habit: a functional approach on Mediterranean oaks. *Acta Oecol* **19**:195–204.

Dansgaard W (**1964**) Stable isotopes in precipitation. *Tellus B* **16**:436–468.

D'Arrigo R, **Wilson R** (**2006**) On the Asian expression of the PDO. *Int J Climatol* **26**:1607–1617.

D'Arrigo R, Cook ER, Mann ME, GC Jacoby (**2003**) Tree-ring reconstructions of temperature and sea-level pressure variability associated with the warm-season Arctic Oscillation since AD 1650. *Geophys Res Lett* **30**:1549.

D'Arrigo R, Wilson R, Liepert B, Cherubini P (**2008**) On the 'Divergence Problem' in Northern Forests: a review of the tree-ring evidence and possible causes. *Glob Planet Change* **60**:289–305.

David TS, Henriques MO, Kurz-Besson C, *et al.* (**2007**) Water-use strategies in two co-occurring Mediterranean evergreen oaks: surviving the summer drought. *Tree Physiol* **27**:793–803.

Dawson TE, **Ehleringer JR** (**1991**) Streamside trees that do not use stream water. *Nature* **350**:335–337.

de Luis M, Cufar K, Di Filippo A, *et al.* (**2013**) Plasticity in dendroclimatic response across the distribution range of Aleppo Pine (*Pinus halepensis*). *PLoS One* **8**:e83550.

De Micco V, Aronne G, Baas P (**2008**) Wood anatomy and hydraulic architecture of stems and twigs of some Mediterranean trees and shrubs along a mesic–xeric gradient. *Trees* **22**:643–655.

del Castillo J, Aguilera M, Voltas J, Ferrio JP (**2013**) Isoscapes of tree-ring carbon-13 perform like meteorological networks in predicting regional precipitation patterns. *J Geophys Res Biogeosci* **118**:352–360.

del Castillo J, Voltas J, Ferrio JP (**2015**) Carbon isotope discrimination, radial growth, and NDVI share spatiotemporal responses to precipitation in Aleppo pine. *Trees* **29**:223–233.

Demidenko E (**2004**) *Mixed models: theory and applications*. Wiley, New York.

Deslauriers A, Rossi S, Anfodillo T, Saracino A (**2008**) Cambial phenology, wood formation and temperature thresholds in two contrasting years at high altitude in southern Italy. *Tree Physiol* **28**:863–871.

DeSoto L, Camarero JJ, Olano JM, Rozas V (**2012**) Geographically structured and temporally unstable growth responses of *Juniperus thurifera* to recent climate variability in the Iberian Peninsula. *Eur J For Res* **131**:905–917.

Dlugokencky E, **Tans P** (**2016**) Trends in atmospheric carbon dioxide, NOAA/ESRL. http://www.esrl.noaa.gov/gmd/ccgg/trends/ (29 August 2016, date last accessed).

Dolanc CR, Westfall RD, Safford HD, Thorne JH, Schwartza MW (**2013**) Growth–climate relationships for six subalpine tree species in a Mediterranean climate. *Can J For Res* **43**:1114–1126.

Dongmann G, Nürnberg HW, Förstel H, Wagener K (**1974**) On the enrichment of $H_2{}^{18}O$ in the leaves of transpiring plants. *Radiat Environ Biophys* **11**:41–52.

Dorado-Liñán I, Sanchez-Lorenzo A, Gutiérrez E, *et al.* (**2016**) Changes in surface solar radiation in Northeastern Spain over the past six centuries recorded by tree-ring $\delta^{13}C$. *Clim Dynam* **47**:937–950.

Dorman M, Svoray T, Perevolotsky A, Moshe Y, Sarris D (**2015**) What determines tree mortality in dry environments? A multi-perspective approach. *Ecol Appl* **25**:1054–1071.

Düthorn E, Hartl-Meier C, Kirchhefer A, *et al.* (**2016a**) Identification of macro-scale groups among 17 site chronologies from Fennoscandia. *TRACE* **14**:32–37.

Düthorn E, Schneider L, Günther B, Gläser S, Esper J (**2016b**) Ecological and climatological signals in tree-ring width and density chronologies along a latitudinal boreal transect. *Scand J For Res* (Doi: 10.1080/02827581.2016.1181201).

Earn DJD, Levin SA, Rohani P (**2000**) Coherence and conservation. *Science* **290**:1360–1364.

Edwards TWD, **Fritz P** (**1986**) Assessing meteoric water composition and relative humidity from ^{18}O and ^{2}H in wood cellulose: paleoclimatic implications for southern Ontario, Canada. *Appl Geochem* **1**:715–723.

Ehleringer JR, **Dawson TE** (**1992**) Water uptake by plants: perspectives from stable isotope composition. *Plant Cell Environ* **15**:1073–1082.

Ehleringer JR, **Rundel PW** (**1989**) Stable isotopes: history, units and instrumentation. In: Rundel PW, Ehleringer JR, Nagy KA (eds) *Stable isotopes in ecological research*. Springer, New York, pp 1–15.

Epron D, **Dreyer E** (**1990**) Stomatal and non stomatal limitation of photosynthesis by leaf water deficits in three oak species: a comparison of gas-exchange and chlorophyll a fluorescence data. *Ann Sci For* **47**:435–450.

Esper J, Frank DC, Battipaglia G, *et al.* (**2010a**) Low-frequency noise in $\delta^{13}C$ and $\delta^{18}O$ tree-ring data: a case study of *Pinus uncinata* in the Spanish Pyearenees. *Global Biogeochem Cycles* **24**:GB4018.

Esper J, Frank DC, Büntgen U, Verstege A, Hantemirov RM, Kirdyanov AV (**2010b**) Trends and uncertainties in Siberian indicators of 20th century warming. *Glob Chang Biol* **16**:386–398.

Fardusi MS, Ferrio JP, Comas C, Voltas J, Resco de Dios V, Serrano L (**2016**) Intra-specific association between carbon isotope composition and productivity in woody plants: a meta-analysis. *Plant Sci* (Doi: 10.1016/j.plantsci.2016.04.005).

Farquhar GD, **Lloyd J** (**1993**) Carbon and oxygen isotope effects in the exchange of carbon dioxide between terrestrial plants and the atmosphere. In Ehleringer JR, Hall AE, Farquhar GD (eds) *Stable isotopes and plant carbon–water relations*. Acad Press, San Diego, pp 47–70.

Farquhar GD, **Richards RA** (**1984**) Isotopic composition of plant carbon correlates with water-use efficiency of wheat genotypes. *Aust J Plant Physiol* **11**:539–552.

Farquhar GD, O'Leary MH, Berry JA (**1982**) On the relationship between carbon isotope discrimination and the inter-cellular carbon dioxide concentration in leaves. *Aust J Plant Physiol* **9**:121–137.

Farquhar GD, Ehleringer JR, Hubick KT (**1989**) Carbon isotope discrimination and photosynthesis. *Annu Rev Plant Physiol Plant Mol Biol* **40**:503–537.

Farquhar GD, Barbour MM, Henry BK (**1998**) Interpretation of oxygen isotope composition of leaf material. In: Griffiths H (ed) *Stable isotopes—integration of biological, ecological and geochemical processes*. BIOS Sci Publ, Oxford, pp 27–74.

Ferrio JP, **Voltas J** (**2005**) Carbon and oxygen isotope ratios in wood constituents of *Pinus halepensis* as indicators of precipitation, temperature and vapour pressure deficit. *Tellus* B **57**:164–173.

Ferrio JP, Florit A, Vega A, Serrano L, Voltas J (**2003**) $\Delta^{13}C$ and tree-ring width reflect different drought responses in *Quercus ilex* and *Pinus halepensis*. *Oecologia* **137**:512–518.

Ferrio JP, Araus JL, Buxó R, Voltas J, Bort J (**2005**) Water management practices and climate in ancient agriculture: inferences from the stable isotope composition of archaeobotanical remains. *Veg Hist Archaeobot* **14**:510–517.

Fischer EM, **Knutti R** (**2015**) Anthropogenic contribution to global occurrence of heavy-precipitation and high-temperature extremes. *Nat Clim Chang* **5**:560–564.

Fonti P, Cherubini P, Rigling A, Weber P, Biging G (**2006**) Tree rings show competition dynamics in abandoned Castanea sativa coppices after land-use changes. *J Veg Sci* **17**:103–112.

Frank DC, Poulter B, Saurer M, *et al.* (**2015**) Water-use efficiency and transpiration across European forests during the Anthropocene. *Nat Clim Chang* **5**:579–584.

Friedman JH (**1984**) *A Variable Span Smoother*. Stanford Univ, Stanford, CA.

Friedrichs DA, Trouet V, Büntgen U, *et al.* (**2009**) Species- specific climate sensitivity of tree growth in Central-West Germany. *Trees* **23**:729–739.

Fritts HC (**1965**) Tree-ring evidence for climatic changes in western North America. *Mon Weather Rev* **93**:421–443.

Fritts HC (**1971**) Dendroclimatology and dendroecology. *Quaternary Res* **1**:419–449.

Fritts HC (**2001**) *Tree rings and climate*. Blackburn Press, Caldwell, NJ.

Fritts HC, **Swetnam TW** (**1989**). Dendroecology: a tool for evaluating variations in past and present forest environments. *Adv Ecol Res* **19**:111–188.

Fulé PZ, Ribas M, Gutiérrez E, Vallejo R, Kaye MW (**2008**) Forest structure and fire history in an old *Pinus nigra* forest, eastern Spain. *For Ecol Manage* **255**:1234–1242.

Gagen M, McCarroll D, Edouard JL (**2004**) Latewood width, maximum density, and stable carbon isotope ratios of pine as climate indicators in a dry subalpine environment, French Alps. *Arct Antarct Alp Res* **36**:166–171.

Gagen M, McCarroll D, Edouard JL (**2006**) Combining tree ring width, density and stable carbon isotope series to enhance the climate signal in tree rings: an example from the French Alps. *Clim Change* **78**:363–379.

Gagen M, McCarroll D, Robertson I, Loader NJ, Jalkanen R (**2008**) Do tree-ring $\delta^{13}C$ series from *Pinus sylvestris* in northern Fennoscandia contain long-term non-climatic trends? *Chem Geol* **252**:42–51.

Galván JD, Camarero JJ, Ginzler C, Buntgen U (**2014**) Spatial diversity of recent trends in Mediterranean tree growth. *Environ Res Lett* **9**:084001.

Galván JD, Büntgen U, Ginzler C, *et al.* (**2015**) Drought-induced weakening of growth-temperature associations in high-elevation Iberian pines. *Glob Planet Change* **124**:95–106.

Gandullo JM (**1994**) *Climatología y ciencia del suelo*. Fundación Conde del Valle de Salazar, Madrid.

Gazol A, Camarero JJ, Gutiérrez E, *et al.* (**2015**) Distinct effects of climate warming on populations of silver fir (*Abies alba*) across Europe. *J Biogeogr* **42**:1150–1162.

Génova M (**2000**) Anillos de crecimiento y años característicos en el Sistema Central (España) durante los últimos cuatrocientos años. *Bol R Soc Esp Hist Nat* **96**:33–42.

Génova M, **Fernández Canclo A** (**1998/1999**) Tree rings and climate of *Pinus nigra* subsp. *salzmannii* in Central Spain. *Dendrochronologia* **16–17**:75–86.

Génova M, **Martínez-Morillas D** (**2002**). Estudio dendroecológico de *Pinus nigra* en Checa (Guadalajara). *Ecología* **16**:83–95.

Génova M, Fernández Canclo A, Creus J (**1993**) Diez series medias de anillos de crecimiento en los sistemas Carpetano e Ibérico. *Invest Agrar-Sist Recur For* **2**:151–172.

Gessler A, Peuke AD, Keitel C, Farquhar GD (**2007**) Oxygen isotope enrichment of organic matter in *Ricinus communis* during the diel course and as affected by assimilate transport. *New Phytol* **174**:600–613.

Gessler A, Brandes E, Buchmann N, Helle G, Rennenberg H, Barnard RL (**2009**) Tracing carbon and oxygen isotope signals from newly assimilated sugars in the leaves to the tree-ring archive. *Plant Cell Environ* **32**:780–795.

Gessler A, Brandes E, Keitel C, *et al.* (**2013**) The oxygen isotope enrichment of leaf-exported assimilates—does it always reflect lamina leaf water enrichment? *New Phytol* **200**:144–157.

Gessler A, Ferrio JP, Hommel R, Treydte K, Werner R, Monson R (**2014**) Stable isotopes in tree rings: toward a mechanistic understanding of fractionation and mixing processes from the leaves to the wood. *Tree Physiol* **34**:796–818.

Gibert A, Gray EF, Westoby M, Wright IJ, Falster DS (**2016**) On the link between functional traits and growth rate: meta-analysis shows effects change with plant size, as predicted. *J Ecol* **104**:1488–1503.

Gilmour AR, Gogel BJ, Gullis BR, Welham SJ, Thompson R (**2002**) *ASReml user guide release 1.0*. VSN Int, Hemel Hempstead.

Gordo O, **Sanz JJ** (**2009**) Long-term temporal changes of plant phenology in the Western Mediterranean. *Glob Chang Biol* **15**:1930–1948.

Granda E, Rossatto DR, Camarero JJ, Voltas J, Valladares F (**2014**) Growth and carbon isotopes of Mediterranean trees reveal contrasting responses to increased carbon dioxide and drought. *Oecologia* **174**:307–317.

Grenfell BT, Wilson K, Finkenstädt BF, *et al.* (**1998**) Noise and determinism in synchronized sheep dynamics. *Nature* **394**:674–677.

Grenfell BT, Finkenstädt BF, Wilson K, Coulson TN, Crawley MJ (**2000**) Reply: Nonlinearity and the Moran effect. *Nature* **406**:847.

Grissino-Mayer HD, **Fritts HC** (**1997**) The International Tree-Ring Data Bank: an enhanced global database serving the global scientific community. *Holocene* **7**:235–228.

Gunderson CA, **Wullschleger SD** (**1994**) Photosynthetic acclimation in trees to rising atmospheric CO_2: A broader perspective. *Photosynth Res* **39**:369–388.

Gutiérrez E, Campelo F, Camarero JJ, *et al.* (**2011**) Climate controls act at different scales on the seasonal pattern of *Quercus ilex* L. stem radial increments in NE Spain. *Trees* **25**:637–646.

Hampe A, **Petit RJ** (**2005**) Conserving biodiversity under climate change: the rear edge matters. *Ecol Lett* **8**:461–467.

Hargreaves GH, **Samani ZA** (**1982**). Estimating potential evapotranspiration. *J Irr Drain Div* **108**:225–230.

Harris I, Jones PD, Osborn TJ, Lister DH (**2014**) Updated high-resolution grids of monthly climatic observations—the CRU TS3.10 Dataset. *Int J Climatol* **34**:623–642.

Hartl-Meier C, Zang C, Büntgen U, *et al.* (**2014**) Uniform climate sensitivity in tree-ring stable isotopes across species and sites in a mid-latitude temperate forest. *Tree Physiol* **35**:4–15.

Haydon DT, **Steen H** (**1997**) The effects of large- and small-scale random events on the synchrony of metapopulation dynamics: a theoretical analysis. *Proc R Soc Lond B Bio* **264**:1375–1381.

Hayes JM (**1983**) Practice and principles of isotopic measurements in organic geochemistry. In: Meinschein WG (ed) *Organic geochemistry of contemporaneous and ancient sediments*. SEPM, Bloomington, IN, pp 5–31.

Haylock MR, Hofstra N, Klein Tank AMG, Klok EJ, Jones PD, New M (**2008**) A European daily high-resolution gridded dataset of surface temperature and precipitation. *J Geophys Res Atmos* **113**:D20119.

Heide OM (**1993**) Day length and thermal time responses of bud burst during dormancy release in some northern deciduous trees. *Physiol Plantarum* **88**:531–540.

Heino M, Kaitala V, Ranta E, Lindström J (**1997**) Synchronous dynamics and rates of extinction in spatially structured populations. *Proc R Soc Lond B Bio* **264**:481–486.

Helle G, **Schleser GH** (**2004**) Beyond CO_2-fixation by Rubisco—an interpretation of $^{13}C/^{12}C$ variations in tree rings from novel intra-seasonal studies on broad-leaf trees. *Plant Cell Environ* **27**:367–380.

Hemming DL, Switsur VR, Waterhouse JS, Heaton THE, Carter AHC (**1998**) Climate variation and the stable carbon isotope composition of tree-ring cellulose: an intercomparison of *Quercus robur*, *Fagus sylvatica* and *Pinus silvestris*. *Tellus B* **50**:25–33.

Henderson CR (**1984**) *Applications of linear models in animal breeding* .Univ Guelph Press, Guelph.

Herguido E, Granda E, Benavides R, García-Cervigón AI, Camarero JJ, Valladares F (**2016**) Contrasting growth and mortality responses to climate warming of two pine species in a continental Mediterranean ecosystem. *Forest Ecol Manage* **363**:149–158.

Herrera S, Fita L, Fernández J, Gutiérrez J (**2010**) Evaluation of the mean and extreme precipitation regimes from the ENSEMBLES regional climate multimodel simulations over Spain. *J Geophys Res Atmos* **115**:D21117.

Hietz P, Turner BL, Wanek W, Richter A, Nock CA, Wright SJ (**2011**) Long-term change in the nitrogen cycle of tropical forests. *Science* **334**:664–666.

Hilasvuori E, Berninger F, Sonninen E, Tuomenvirta H, Jungner H (**2009**) Stability of climate signal in carbon and oxygen isotope records and ring width from Scots pine (*Pinus sylvestris* L.) in Finland. *J Quat Sci* **24**:469−480

Holman ML, **Peterson DL** (**2006**) Spatial and temporal variability in forest growth in the Olympic Mountains, Washington: sensitivity to climatic variability. *Can J For Res* **36**:92–104.

Holmes RL (**1983**) Computer-assisted quality control in tree-ring dating and measurement. *Tree Ring Res* **43**:69–78.

Holzkämper S, Kuhry P, Kultti S, Gunnarson B, Sonninen E (**2008**) Stable isotopes in tree rings as proxies for winter precipitation changes in the Russian Arctic over the past 150 years. *Geochronometria* **32**:37–46.

Hughes MK, Kelly PM, Pilcher JR, La Marche JrVC. (**2009**) *Climate from tree rings*. Cambridge Univ Press, Cambridge.

IPCC (**2007**) *Climate change 2007: The physical science basis. Contribution of Working Group I to the Fourth Assessment Report of the Intergovernmental Panel on Climate Change*. Cambridge Univ Press, Cambridge.

IPCC (**2013**) *Climate change 2013: The physical science basis. Contribution of Working Group I to the Fifth Assessment Report of the Intergovernmental Panel on Climate Change*. Cambridge Univ Press, Cambridge.

Jennrich RI, **Schluchter MD** (**1986**) Unbalanced repeated-measures models with structured covariance matrices. *Biometrics* **42**:805–820.

Jones PD, Osborn TJ, Briffa KR (**1997**) Estimating sampling errors in large-scale temperature averages. *J Clim* **10**:2548–2568.

Juárez-López FJ, Escuder A, Mediavilla S (**2008**) Ontogenetic changes in stomatal and biochemical limitations to photosynthesis of two co-occurring Mediterranean oaks differing in leaf life span. *Tree Physiol* **28**:367–374.

Jump AS, Hunt JM, Peñuelas J (**2006**) Rapid climate change-related growth decline at the southern range edge of *Fagus sylvatica*. *Glob Chang Biol* **12**:2163–2174.

Keeling CD (**1979**) The Suess effect: ^{13}Carbon–^{14}Carbon interrelations. *Environ Int* **2**:229–300.

Keeling CD, Mook WG, Tans PP (**1979**) Recent trends in the $^{13}C/^{12}C$ ratio of atmospheric carbon dioxide. *Nature* **277**:121–123.

Keenan TF, Hollinger DY, Bohrer G, *et al.* (**2013**) Increase in forest water-use efficiency as atmospheric carbon dioxide concentrations rise. *Nature* **499**:324–327.

Kendall BE, Briggs CJ, Murdoch WW, *et al.* (**1999**) Why do populations cycle? A synthesis of statistical and mechanistic modeling approaches. *Ecology* **80**:1789–1805.

Kienast F, Schweingruber FH, Braker OU, Schar E (**1987**) Tree-ring studies on conifers along ecological gradients and potential of single-year analyses. *Can J For Res* **17**:683–696.

Kirdyanov AV (**1999**) *Comparative analysis of growth and structure of conifer tree rings from the forest tundra, the northern and middle taiga zones of Central Siberia* (PhD Thesis). Institute of Forest SB RAS, Krasnoyarsk.

Kirdyanov AV, Treydte K, Nikolaev A, Helle G, Schleser GH (**2008**) Climate signals in tree-ring width, density and $\delta^{13}C$ from larches in Eastern Siberia (Russia). *Chem Geol* **252**:31–41.

Kirdyanov AV, Hagedorn F, Knorre AA, *et al.* (**2012**) 20th century tree-line advance and vegetation changes along an altitudinal transect in the Putorana Mountains, northern Siberia. *Boreas* **41**:56–67.

Kish L (**1965**) Sampling organizations and groups of unequal sizes. *Am Sociol Rev* **30**:564–572.

Klein T, Shpringer I, Fikler B, Elbaz G, Cohen S, Yakir D (**2013**) Relationships between stomatal regulation, water-use, and water-use efficiency of two coexisting key Mediterranean tree species. *For Ecol Manage* **302**:34–42.

Kneeshaw DD, **Bergeron Y** (**1998**) Canopy gap characteristics and tree replacement in the southeastern boreal forest. *Ecology* **79**:783–794.

Knorre AA, Kirdyanov AV, Vaganov EA (**2006**) Climatically induced interannual variability in aboveground production in forest-tundra and northern taiga of central Siberia. *Oecologia* **147**:86–95.

Koenig WD (**1999**) Spatial autocorrelation of ecological phenomena. *Trends Ecol Evol* **14**:22–26.

Koenig WD (**2002**) Global patterns of environmental synchrony and the Moran effect. *Ecography* **25**:283–288.

Koenig WD, **Knops JMH** (**1998**) Testing for spatial autocorrelation in ecological studies. *Ecography* **21**:423–429.

Körner C (**2003**) Carbon limitation in trees. *J Ecol* **91**:4–17.

Körner C (**2007**) The use of 'altitude' in ecological research. *Trends Ecol Evol* **22**:569–574.

Kostinski A, **Anderson A** (**2014**) Spatial patterns of record-setting temperatures. *J Environ Stat* **6**:1–13.

Kozlowski TT, Kramer PJ, Pallardy SG (**1991**) *The physiological ecology of woody plants*. Acad Press, San Diego.

Kräuchi N (**1993**) Potential impacts of a climate change on forest ecosystems. *Eur J Forest Pathol* **23**:28–50.

Kress A, Young GHF, Saurer M, Loader NJ, Siegwolf RTW, McCarroll D (**2009**) Stable isotope coherence in the earlywood and latewood of tree-line conifers. *Chem Geol* **268**:52–57.

Kruse J, Hopmans P, Rennenberg H, Adams M (**2012**) Modern tools to tackle traditional concerns: Evaluation of site productivity and *Pinus radiata* management via $\delta^{13}C$- and $\delta^{18}O$-analysis of tree-rings. *For Ecol Manage* **285**:227–238.

Lapointe-Garant MP, Huang JG, Gea-Izquierdo G, Raulier F, Bernier P, Berninger F (**2010**) Use of tree rings to study the effect of climate change on trembling aspen in Québec. *Glob Chang Biol* **16**:2039–2051.

Larcher W (**2000**) Temperature stress and survival ability of Mediterranean sclerophyllous plants. *Plant Biosyst* **134**:279–295.

Latte N, Lebourgeois F, Claessens H (**2015**) Increased tree-growth synchronization of beech (*Fagus sylvatica* L.) in response to climate change in northwestern Europe. *Dendrochronologia* **33**:69–77.

Leal S, Eamus D, Grabner M, Wimmer R, Cherubini P (**2008**) Tree rings of *Pinus nigra* from the Vienna basin region (Austria) show evidence of change in climatic sensitivity in the late 20th century. *Can J For Res* **38**:744–759.

Leaney F, Osmond C, Allison G, Ziegler H (**1985**) Hydrogen-isotope composition of leaf water in C_3 and C_4 plants: its relationship to the hydrogen-isotope composition of dry matter. *Planta* **164**:215–220.

Leavitt SW, **Danzer SR** (**1993**) Method for batch processing small wood samples to holocellulose for stable-carbon isotope analysis. *Anal Chem* **65**:87–88.

Leavitt SW, **Long A** (**1989**) Drought indicated in carbon-13/carbon-12 ratios of southwestern tree rings. *Water Res Bull* **25**:341–347.

Leavitt SW, Chase TN, Rajagopalan B, Lee E, Lawrence PJ, Woodhouse CA (**2007**) Southwestern US drought maps from pinyon tree-ring carbon isotopes. *Eos Trans AGU* **88**:39–40.

Leavitt SW, Treydte K, Yu L (**2010**) Environment in time and space: opportunities from tree-ring isotope networks. In: West JB, Bowen GJ, Dawson TE, Tu KP (eds) *Isoscapes: understanding movement, pattern, and process on earth through isotope mapping*. Springer, Dordrecht, pp 113–135.

Levanič T, Čater M, McDowell NG (**2011**) Associations between growth, wood anatomy, carbon isotope discrimination and mortality in a *Quercus robur* forest. *Tree Physiol* **31**:298–308.

Lévesque M, Rigling A, Bugmann H, Weber P, Brang P (**2014**) Growth response of five co-occurring conifers to drought across a wide climatic gradient in Central Europe. *Agric For Meteorol* **197**:1–12.

Lewis SL, **Maslin MA** (**2015**) Defining the Anthropocene. *Nature* **519**:171–180.

Li Q, Nakatsuka T, Kawamura K, Liu Y, Song H (**2011**) Regional hydroclimate and precipitation $\delta^{18}O$ revealed in tree-ring cellulose $\delta^{18}O$ from different tree species in semi-arid Northern China. *Chem Geol* **282**:19–28.

Liebhold A, Koenig WD, Bjørnstad ON (**2004**) Spatial synchrony in population dynamics. *Annu Rev Ecol Evol Syst* **35**:467–490.

Liepert B (**2002**). Observed reductions of surface solar radiation at sites in the United States and worldwide from 1961 to 1990. *Geophys Res Lett* **29**:1421.

Linares JC, Camarero JJ, Carreira JA (**2010**) Competition modulates the adaptation capacity of forests to climatic stress: insights from recent growth decline and death in relict stands of the Mediterranean fir *Abies pinsapo*. *J Ecol* **98**:592–603.

Linares JC, **Tíscar PA** (**2010**) Climate change impacts and vulnerability of the southern populations of *Pinus nigra* subsp. *salzmannii*. *Tree Physiol* **30**:795–806.

Linares JC, **Tiscar PA** (**2011**) Buffered climate change effects in a Mediterranean pine species: range limit implications from a tree-ring study. *Oecologia* **167**:847–859.

Lindner M, Maroschek M, Netherer S, *et al.* (**2010**) Climate change impacts, adaptive capacity, and vulnerability of European forest ecosystems. *For Ecol Manage* **259**:698–709.

Linkosalo T (**1999**) Regularities and patterns in the spring phenology of some boreal trees. *Silva Fenn* **33**:237–245.

Liphschitz N, **Lev-Yadun S** (**1986**) Cambial activity of evergreen and seasonal dimorphics around the Mediterranean. *IAWA Bull* **7**:145–153.

Little RJA, **Rubin DB** (**2002**) *Statistical analysis with missing data*. Wiley, New York.

Litton CM, Raich JW, Ryan MG (**2007**) Carbon allocation in forest ecosystems. *Glob Chang Biol* **13**:2089–2109.

Livingston NJ, Whitehead D, Kelliher FM, *et al.* (**1998**) Nitrogen allocation and carbon isotope fractionation in relation to intercepted radiation and position in a young *Pinus radiata* D. Don tree. *Plant Cell Environ* **21**:795–803.

Lloyd AH, **Bunn AG** (**2007**) Responses of the circumpolar boreal forest to 20th century climate variability. *Environ Res Lett* **2**:045013.

Loader NJ, Robertson I, Barker AC, Switsur VR, Waterhouse JS (**1997**) An improved technique for the batch processing of small wholewood samples to α-cellulose. *Chem Geol* **136**:313–317.

Loader NJ, Santillo PM, Woodman-Ralph JP, *et al.* (**2008**) Multiple stable isotopes from oak trees in southwestern Scotland and the potential for stable isotope dendroclimatology in maritime climatic regions. *Chem Geol* **252**:62–71.

Loidi J, **Herrera M** (**1990**) The *Quercus pubescens* and *Quercus faginea* forests in the Basque Country (Spain): distribution and typology in relation to climatic factors. *Vegetatio* **90**:81–92.

Lorimer CG (**1985**) Methodological considerations in the analysis of forest disturbance history. *Can J For Res* **15**:200–213.

Macias M, Andreu L, Bosch O, Camarero JJ, Gutiérrez E (**2006**) Increasing aridity is enhancing silver fir (*Abies alba* Mill.) water stress in its south-western distribution limit. *Clim Change* **79**:289–313.

Marshall JD, **Monserud RA** (**2006**) Co-occurring species differ in tree-ring $\delta^{18}O$ trends. *Tree Physiol* **2**:1055–1066.

Martín-Benito D, del Río M, Cañellas I (**2010**) Black pine (*Pinus nigra* Arn.) growth divergence along a latitudinal gradient in Western Mediterranean mountains. *Ann For Sci* **67**:401.

Martínez-Vilalta J, López BC, Adell N, Badiella L, Ninyerola M (**2008**) Twentieth century increase of Scots pine radial growth in NE Spain shows strong climate interactions. *Glob Chang Biol* **14**:2868–2881.

Maseyk K, Hemming D, Angert A, Leavitt SW, Yakir D (**2011**) Increase in water-use efficiency and underlying processes in pine forests across a precipitation gradient in the dry Mediterranean region over the past 30 years. *Oecologia* **167**:573–585.

Mathisen IE, **Hofgaard A** (**2011**) Recent height and diameter growth variation in Scots pine (*Pinus sylvestris* L.) along the Arctic margin: the importance of growing season versus non-growing season climate factors. *Plant Ecol Divers* **4**:1–11.

McCarroll D, **Loader NJ** (**2004**) Stable isotopes in tree rings. *Quat Sci Rev* **23**:771–801.

McCarroll D, **Pawellek F** (**1998**) Stable carbon isotope ratios of latewood cellulose in *Pinus sylvestris* from northern Finland: variability and signal-strength. *Holocene* **8**:675–684.

McCarroll D, **Pawellek F** (**2001**) Stable carbon isotope ratios of *Pinus sylvestris* from northern Finland and the potential for extracting a climate signal from long Fennoscandian chronologies. *Holocene* **11**:517–526.

McCulloch CE, **Searle SR** (**2001**) *Generalized, linear and mixed models*. Wiley, New York.

McDowell N, Allen CD, Marshall L (**2010**) Growth, carbon-isotope discrimination, and drought-associated mortality across a *Pinus ponderosa* elevational transect. *Glob Chang Biol* **16**:399–415.

McKenzie D, Peterson DW, Peterson DL, Thornton PE (**2003**) Climatic and biophysical controls on conifer species distributions in mountain forests of Washington State, USA. *J Biogeogr* **30**:1093–1108.

McKinney CR, McCrea JM, Epstein S, Allen HA, Urey HC (**1950**) Improvements in mass spectrometers for the measurement of small differences in isotope abundance ratios. *Rev Sci Instrum* **21**:724–730.

McMahon SM, Parker GG, Miller DR (**2010**) Evidence for a recent increase in forest growth. *Proc Natl Acad Sci USA* **107**:3611–3615.

Mediavilla S, **Escudero A** (**2010**) Differences in biomass allocation patterns between saplings of two co-occurring Mediterranean oaks as reflecting different strategies in the use of light and water. *Eur J For Res* **129**:697–706.

Menzel A, Sparks T, Estrella N, *et al.* (**2006**) European phenological response to climate change matches the warming pattern. *Glob Chang Biol* **12**:1969–1976.

Mitrakos K (**1980**) A theory for Mediterranean plant life. *Acta Oecol Oecol Plant* **15**:245–252.

Montserrat-Martí G, Camarero JJ, Palacio S, *et al.* (**2009**) Summer-drought constrains the phenology and growth of two coexisting Mediterranean oaks with contrasting leaf habit: implications for their persistence and reproduction. *Trees* **23**:787–799.

Moran PAP (**1953**) The statistical analysis of the Canadian lynx cycle. II. Synchronization and meteorology. *Aust J Zool* **1**:291–298.

Moreno-Gutiérrez C, Dawson TE, Nicolás E, Querejeta JI (**2012**) Isotopes reveal contrasting water use strategies among coexisting plant species in a Mediterranean ecosystem. *New Phytol* **196**:489–496.

Moreno-Gutiérrez C, Battipaglia G, Cherubini P, Delgado Huertas A, Querejeta JI (**2015**) Pine afforestation decreases the long-term performance of understorey shrubs in a semi-arid Mediterranean ecosystem: a stable isotope approach. *Funct Ecol* **29**:15–25.

Nabuurs GJ, Lindner M, Verkerk PJ, *et al.* (**2013**) First signs of carbon sink saturation in European forest biomass. *Nat Clim Chang* **3**:792–796.

Nakagawa S, **Freckleton R** (**2008**) Missing inaction: the dangers of ignoring missing data. *Trends Ecol Evol* **23**:592–596.

Natalini F, Correia AC, Vázquez-Piqué J, Alejano R (**2015**) Tree rings reflect growth adjustments and enhanced synchrony among sites in Iberian stone pine (*Pinus pinea* L.) under climate change. *Ann For Sci* **72**:1023–1033.

Ninyerola M, Pons X, Roure JM (**2005**) *Atlas climático digital de la Península Ibérica. Metodología y aplicaciones en bioclimatología y geobotánica*. Univ Autónoma de Barcelona, Bellaterra.

Norby RJ, DeLucia EH, Gielen B, *et al.* (**2005**) Forest response to elevated CO_2 is conserved across a broad range of productivity. *Proc Natl Acad Sci USA* **102**:18052–18056.

Oden NL, **Sokal RR** (**1986**) Directional autocorrelation: an extension of spatial correlograms to two dimensions. *Syst Zool* **35**:608–617.

Offermann C, Ferrio JP, Holst J, *et al.* (**2011**) The long way down—are carbon and oxygen isotope signals in the tree ring uncoupled from canopy physiological processes? *Tree Physiol* **31**:1088–1102.

Olivier JGJ, Janssens-Maenhout G, Muntean M, Peters JAHW (**2013**) *Trends in global CO_2 emissions: 2013 Report*. PBL Netherlands Environ Assessment Agency, The Hague.

Oquist G, **Huner NP** (**2003**) Photosynthesis of overwintering evergreen plants. *Ann Rev Plant Biol* **54**:329–355.

Palacio S, Hoch G, Sala A, Körner C, Millard P (**2014**) Does carbon storage limit tree growth? *New Phytol* **201**:1096–1100.

Pan Y, Birdsey RA, Fang J, *et al.* (**2011**) A large and persistent carbon sink in the world's forests. *Science* **333**:988–993.

Panyushkina IP, Vaganov EA, Shishov VV (**1996**) Spatial-temporal variation of radial tree growth in relation to climate in the north of middle Siberia. *Dendrochronologia* **14**:115–126.

Parmesan C, **Yohe G** (**2003**) A globally coherent fingerprint of climate change impacts across natural systems. *Nature* **421**:37–42.

Pasho E, Camarero JJ, de Luis M, Vicente-Serrano SM (**2011**) Impacts of drought at different time scales on forest growth across a wide climatic gradient in north-eastern Spain. *Agric For Meteorol* **151**:1800–1811.

Paulsen J, Weber UB, Körner C (**2000**) Tree growth near treeline: abrupt or gradual reduction with altitude? *Arct Antarct Alp Res* **32**:14–20.

Pease CP, Lande R, Bull JJ (**1989**) A model of population growth, dispersal and evolution in a changing environment. *Ecology* **70**:1657–1664.

Peguero-Pina JJ, Alquézar-Alquézar JM, Mayr S, Cochard H, Gil-Pelegrín E (**2011**) Embolism induced by winter drought may be critical for the survival of *Pinus sylvestris* L. near its southern distribution limit. *Ann For Sci* **68**:565–574.

Pena-Angulo D, Cortesi N, Brunetti M, González-Hidalgo JC (**2015**) Spatial variability of maximum and minimum monthly temperature in Spain during 1981–2010 evaluated by correlation decay distance (CDD). *Theor Appl Climatol* **122**:35–45.

Peñuelas J, Canadell JG, Ogaya R (**2011**) Increased water-use efficiency during the 20th century did not translate into enhanced tree growth. *Glob Ecol Biogeogr* **20**:597–608.

Piepho HP, Büchse A, Richter C (**2004**) A mixed modelling approach for randomized experiments with repeated measures. *J Agron Crop Sci* **190**:230–247.

Piepho HP, **Möhring J** (**2005**) Best linear unbiased prediction of cultivar effects for subdivided target regions. *Crop Sci* **45**:1151–1159.

Polechová J, Barton N, Marion G (**2009**) Species' range: adaptation in space and time. *Am Nat* **174**:E186–E204.

Potapov P, Yaroshenko A, Turubanova S, *et al.* (**2008**) Mapping the world's intact forest landscapes by remote sensing. *Ecol Soc* **13**:51.

Pretzsch H, Biber P, Schütze G, Uhl E, Rötzer T (**2014**) Forest stand growth dynamics in Central Europe have accelerated since 1870. *Nat Commun* **5**:4967.

Primicia I, Camarero JJ, Janda P, *et al.* (**2015**) Age, competition, disturbance and elevation effects on tree and stand growth response of primary *Picea abies* forest to climate. *For Ecol Manage* **354**:77–86.

Radoglou K (**1996**) Environmental control of CO_2 assimilation rates and stomatal conductance in five oak species growing under field conditions in Greece. *Ann Sci For* **53**:269–278.

Raffalli-Delerce G, Masson-Delmotte V, Dupouey JL, Stievenard M, Breda N, Moisselin JM (**2004**) Reconstruction of summer droughts using tree-ring cellulose isotopes: a calibration study with living oaks from Brittany (western France). *Tellus B* **56**:160–174.

Raftery AE (**1996**) Approximate Bayes factors and accounting for model uncertainty in generalised linear models. *Biometrika* **83**:251–266.

Ranta E, Kaitala V, Lundberg P (**1997**) The spatial dimension in population fluctuations. *Science* **278**:1621–1623.

Reyes-Fox M, Steltzer H, Trlica MJ, *et al.* (**2014**) Elevated CO_2 further lengthens growing season under warming conditions. *Nature* **510**:259–262.

Reynolds-Henne CE, Siegwolf RTW, Treydte K, Esper J, Henne S, Saurer M (**2007**) Temporal stability of climate-isotope relationships in tree rings of oak and pine (Ticino, Switzerland). *Global Biogeochem Cycles* **21**:GB4009.

Richards MB, **Lamont BB** (**1996**) Post-fire mortality and water relations of three congeneric shrub species under extreme water stress—a trade-off with fecundity? *Oecologia* **107**:53–60.

Richardson AD, Williams M, Hollinger DY, *et al.* (**2010**) Estimating parameters of a forest ecosystem C model with measurements of stocks and fluxes as joint constrains. *Oecologia* **164**:25–40.

Ripullone F, Guerrieri MR, Saurer M, *et al.* (**2009**) Testing a dual isotope model to track carbon and water gas exchanges in a Mediterranean forest. *iForest* **2**:59–66.

Rivas-Martínez S (**1982**) Etages bioclimatiques, secteurs chorologiques et séries de végétation de l'Espagne méditerranéenne. *Ecol Mediterr* **8**:275–288.

Roden JS, **Ehleringer JR** (**1999**) Hydrogen and oxygen isotope ratios of tree-ring cellulose for riparian trees grown long-term under hydroponically controlled environments. *Oecologia* **121**:467–477.

Roden JS, **Farquhar GD** (**2012**) A controlled test of the dual-isotope approach for the interpretation of stable carbon and oxygen isotope ratio variation in tree rings. *Tree Physiol* **32**:490–503.

Roden JS, Lin G, Ehleringer JR (**2000**) A mechanistic model for interpretation of hydrogen and oxygen isotope ratios in tree-ring cellulose. *Geochim Cosmochim Acta* **64**:21–35.

Rodó X, Baert E, Comín FA (**1997**) Variations in seasonal rainfall in Southern Europe during the present century: relationships with the North Atlantic Oscillation and the El Niño-Southern Oscillation. *Clim Dynam* **13**:275–284.

Rossi S, Deslauriers A, Gricar J, *et al.* (**2008**) Critical temperatures for xylogenesis in conifers of cold climates. *Glob Ecol Biogeogr* **17**:696–707.

Rossi S, Girard MJ, Morin H (**2014**) Lengthening of the duration of xylogenesis engenders disproportionate increases in xylem production. *Glob Chang Biol* **20**:2261–2271.

Royama T (**1981**) Fundamental concepts and methodology for the analysis of animal population dynamics, with special reference to univoltine species. *Ecol Monogr* **51**:473–493.

Rozanski K, Araguás-Araguás L, Gonfiantini R (**1992**) Relation between long-term trends of oxygen-18 isotope composition of precipitation and climate. *Science* **258**:981–985.

Ruokolainen L, **Fowler MS** (**2008**) Community extinction patterns in colored environments. *Proc R Soc Lond B Bio* **275**:1775–1783.

Sala A, Woodruff DR, Meinzer FC (**2012**) Carbon dynamics in trees: feast or famine? *Tree Physiol* **32**:765–775.

Sánchez de Dios R, Benito-Garzón M, Sainz-Ollero H (**2009**) Present and future extension of the Iberian submediterranean territories as determined from the distribution of marcescent oaks. *Plant Ecol* **204**:189–205.

Sánchez-Salguero R, Camarero JJ, Hevia A, *et al.* (**2015**) What drives growth of Scots pine in continental Mediterranean climates: Drought, low temperatures or both? *Agric For Meteorol* **206**:151–162.

Sarris D, Christodoulakis D, Körner C (**2007**) Recent decline in precipitation and tree growth in the eastern Mediterranean. *Glob Chang Biol* **13**:1187–1200.

Sarris D, Siegwolf RTW, Körner C (**2013**) Inter- and intra-annual stable carbon and oxygen isotope signals in response to drought in Mediterranean pines. *Agric For Meteorol* **168**:59–68.

Saurer M, Siegenthaler U, Schweingruber F (**1995**) The climate–carbon isotope relationship in tree rings and the significance of site conditions. *Tellus B* **47**:320–330.

Saurer M, Cherubini P, Bonani G, Siegwolf RTW (**2003**) Tracing carbon uptake from a natural CO_2 spring into tree rings: an isotope approach. *Tree Physiol* **23**:997–1004.

Saurer M, Siegwolf RTW, Schweingruber FH (**2004**) Carbon isotope discrimination indicates improving water-use efficiency of trees in northern Eurasia over the last 100 years. *Glob Chang Biol* **10**:2109–2120.

Saurer M, Cherubini P, Reynolds-Henne CE, Treydte K, Anderson WT, Siegwolf RTW (**2008**) An investigation of the common signal in tree-ring stable isotope chronologies at temperate sites. *J Geophys Res Biogeosci* **113**: G04035.

Saurer M, Kress A, Leuenberger M, Rinne KT, Treydte K, Siegwolf RTW (**2012**) Influence of atmospheric circulation patterns on the oxygen isotope ratio of tree rings in the Alpine region. *J Geophys Res Atmos* **117**:D05118.

Saurer M, Spahni R, Frank DC, *et al.* (**2014**) Spatial variability and temporal trends in water-use efficiency of European forest. *Glob Chang Biol* **20**:332–336.

Scheidegger Y, Saurer M, Bahn M, Siegwolf RTW (**2000**) Linking stable oxygen and carbon isotopes with stomatal conductance and photosynthetic capacity: a conceptual model. *Oecologia* **125**:350–357.

Schweingruber F, Briffa KR, Nogler P (**1993**) A tree-ring densitometric transect from Alaska to Labrador. *Int J Biometeorol* **37**:151–169.

Searle SR, Casella G, McCulloch CE (**2006**) *Variance components*. Wiley, New York.

Seim A, Treydte K, Trouet V, *et al.* (**2015**) Climate sensitivity of Mediterranean pine growth reveals distinct east–west dipole. *Int J Climatol* **35**:2503–2513.

Shestakova TA, Aguilera M, Ferrio JP, Gutiérrez E, Voltas J (**2014**) Unravelling spatiotemporal tree-ring signals in Mediterranean oaks: a variance–covariance modelling approach of carbon and oxygen isotope ratios. *Tree Physiol* **34**:819–838.

Shestakova TA, Gutiérrez E, Kirdyanov AV, *et al.* (**2016**) Forests synchronize their growth in contrasting Eurasian regions in response to climate warming. *Proc Natl Acad Sci USA* **113**:662–667.

Shestakova TA, Camarero JJ, Ferrio JP, Knorre AA, Gutiérrez E, Voltas J (**submitted**) Increasing drought effects on five European pines modulate Δ^{13}C-growth coupling along a Mediterranean altitudinal gradient.

Shishov VV, Tychkov II, Popkova MI, Ilyin VA, Bryukhanova MV, Kirdyanov AV (**2016**) VS-oscilloscope: a new tool to parameterize tree radial growth based on climate conditions. *Dendrochronologia* **39**:42–50.

Sidorova OV, Siegwolf RTW, Saurer M, *et al.* (**2009**) Do centennial tree- ring and stable isotope trends of *Larix gmelinii* (Rupr.) Rupr. indicate increasing water shortage in the Siberian north? *Oecologia* **161**:825–835.

Silva LCR, Anand M, Leithead MD (**2010**) Recent widespread tree growth decline despite increasing atmospheric CO_2. *PLoS One* **5**:e11543.

Sperry JS (**2000**) Hydraulic constraints on plant gas exchange. *Agric For Meteorol* **104**:13–23.

Steffen W, Persson Å, Deutsch L, *et al.* (**2011**) The Anthropocene: from global change to planetary stewardship. *Ambio* **40**:739–761.

Sternberg L (**2009**) Oxygen stable isotope ratios of tree-ring cellulose: the next phase of understanding. *New Phytol* **181**:553–562.

Sternberg L, **DeNiro MJ** (**1983**) Bio-geochemical implications of the isotopic equilibrium fractionation factor between oxygen atoms of acetone and water. *Geochim Cosmochim Acta* **47**:2271–2274.

Sternberg L, Pinzon MC, Anderson WT, Jahren AH (**2006**) Variation in oxygen isotope fractionation during cellulose synthesis: intramolecular and biosynthetic effects. *Plant Cell Environ* **29**:1881–1889.

Stine AR, **Huybers P** (**2014**) Arctic tree rings as recorders of variations in light availability. *Nat Commun* **5**:3836.

Tardif J, Camarero JJ, Ribas M, Gutiérrez E (**2003**) Spatiotemporal variability in tree growth in the Central Pyrenees: climatic and site influences. *Ecol Monogr* **73**:241–257.

Tchebakova NM, Monserud RA, Nazimova DI (**1994**) A Siberian vegetation model based on climatic parameters. *Can J For Res* **24**:1597–1607.

Terradas J, **Savé R** (**1992**) The influence of summer and winter stress and water relationships on the distribution of *Quercus ilex* L. *Vegetatio* **99–100**:137–145.

Thomas RQ, Canham CD, Weathers KC, Goodale CL (**2010**) Increased tree carbon storage in response to nitrogen deposition in the US. *Nat Geosci* **3**:13–17.

Tognetti R, Longobucco A, Raschi A (**1998**) Vulnerability of xylem to embolism in relation to plant hydraulic resistance in *Quercus pubescens* and *Quercus ilex* co-occurring in a Mediterranean coppice stand in central Italy. *New Phytol* **139**:437–447.

Touchan R, Meko DM, Ballesteros-Cánovas JA, *et al.* (**2013**). Dendrochronology course in Valsaín Forest, Segovia, Spain. *Tree Ring Res* **69**:93–100.

Treydte K, Schleser GH, Helle G, Frank DC, Winiger M, Haug GH, Esper J (**2006**) The twentieth century was the wettest period in northern Pakistan over the past millennium. *Nature* **440**:1179–1182.

Treydte K, Frank DC, Esper J, *et al.* (**2007**) Signal strength and climate calibration of a European tree-ring isotope network. *Geophys Res Lett* **34**:L24302.

Treydte K, Boda S, Graf Pannatier E, *et al.* (**2014**) Seasonal transfer of oxygen isotopes from precipitation and soil to the tree ring: source water versus needle water enrichment. *New Phytol* **202**:772–783.

Trouet V, Esper J, Graham NE, Baker A, Scourse JD, Frank DC (**2009**) Persistent positive North Atlantic oscillation mode dominated the Medieval Climate Anomaly. *Science* **324**:78–80.

Tsuji H, Nakatsuka T, Takagi K (**2006**) $\delta^{18}O$ of tree-ring cellulose in two species (spruce and oak) as proxies of precipitation amount and relative humidity in northern Japan. *Chem Geol* **231**:67–76.

Turchin P (**1990**) Rarity of density dependence or population regulation with lags? *Nature* **344**:660–663.

Vaganov EA, Naurazhaev MM, Schweingruber FH, Briffa KR, Moell M (**1996**) An 840-year tree-ring width chronology for Taimir as an indicator of summer temperature changes. *Dendrochronologia* **14**:193–205.

Vaganov EA, Hughes MK, Kirdyanov AV, Schweingruber FH, Silkin PP (**1999**) Influence of snowfall and melt timing on tree growth in subarctic Eurasia. *Nature* **400**:149–151.

Verbeke G, **Molenberghs G** (**2000**) *Linear mixed models for longitudinal data*. Springer, New York.

Vicente-Serrano SM, Beguería S, López-Moreno JI (**2010**) A multi-scalar drought index sensitive to global warming: the Standardized Precipitation Evapotranspiration Index—SPEI. *J Clim* **23**:1696–1718.

Vila B, Vennetier M, Ripert C, *et al.* (**2008**) Has global change induced opposite trends in radial growth of *Pinus sylvestris* and *Pinus halepensis* at their bioclimatic limit? The example of the Sainte-Baume forest (south-east France). *Ann For Sci* **65**:709.

Villalba R, Veblen TT, Ogden J (**1994**) Climatic influences on the growth of subalpine trees in the Colorado Front Range. *Ecology* **75**:1450–1462.

Violle C, Reich PB, Pacala SW, Enquist BJ, Kattge J (**2014**) The emergence and promise of functional biogeography. *Proc Natl Acad Sci USA* **111**:13690–13696.

Visscher PM (**1998**) On the sampling variance of intraclass correlations and genetic correlations. *Genetics* **149**:1605–1614.

Voelker SL (**2011**) Age-dependent changes in environmental influences on tree growth and their implications for forest responses to climate change. In: Meinzer FC, Dawson TE, Lachenbruch B (eds) *Size- and age-related changes in tree structure and function*, Springer, Dordrecht, pp 455–479.

Voelker SL, Meinzer FC, Lachenbruch B, Brooks JR, Guyette RP (**2014**) Drivers of radial growth and carbon isotope discrimination of bur oak (*Quercus macrocarpa* Michx.) across continental gradients in precipitation, vapour pressure deficit and irradiance. *Plant Cell Environ* **37**:766–779.

Voltas J, Camarero JJ, Carulla D, Aguilera M, Ortiz A, Ferrio JP (**2013**) A retrospective, dual-isotope approach reveals individual predispositions to winter-drought induced tree dieback in the southernmost distribution limit of Scots pine. *Plant Cell Environ* **36**:1435–1448.

Walker CD, Leaney FW, Dighton JC, Allison GB (**1989**) The influence of transpiration on the equilibration of leaf water with atmospheric water vapour. *Plant Cell Environ* **12**:221–234.

Walther GR, Post E, Convey P, *et al.* (**2002**) Ecological responses to recent climate change. *Nature* **416**:389–395.

Warren CR, McGrath JF, Adams MA (**2001**) Water availability and carbon isotope discrimination in conifers. *Oecologia* **127**:476–486.

Way DA, **Oren R** (**2010**) Differential responses to changes in growth temperature between trees from different functional groups and biomes: a review and synthesis of data. *Tree Physiol* **30**:669–688.

Werner C, Schnyder H, Cuntz M, *et al.* (**2012**) Progress and challenges in using stable isotopes to trace plant carbon and water relations across scales. *Biogeosciences* **9**:3083–3111.

Wettstein JJ, Littell JS, Wallace JM, Gedalof Z (**2011**) Coherent region-, species-, and frequency-dependent local climate signals in Northern Hemisphere tree-ring widths. *J Clim* **24**:5998–6012.

White TL, **Hodge GR** (**1989**) *Predicting breeding values with applications in forest tree improvement*. Kluwer Acad Publ, Dordrecht.

Whitehead D (**2011**) Forests as carbon sinks—benefits and consequences. *Tree Physiol* **31**:893–902.

Wigley TML, Briffa KR, Jones PD (**1984**) On the average value of correlated time series, with applications in dendroclimatology and hydrometerology. *J Clim Appl Meteorol* **23**:201–213.

Williams AP, Allen CD, Macalady AK, *et al.* (**2013**) Temperature as a potent driver of regional forest drought stress and tree mortality. *Nat Clim Chang* **3**:292–297.

Wilmking M, D'Arrigo R, Jacoby GC, Juday GP (**2005**) Increased temperature sensitivity and divergent growth trends in circumpolar boreal forest. *Geophys Res Lett* **32**:L15715.

Wolfinger RD (**1996**) Heterogeneous variance-covariance structures for repeated measures. *J Agric Biol Environ Stat* **1**:205–230.

Woodruff DR, **Meinzer FC** (**2011**) Size-dependent changes in biophysical control of tree growth: the role of turgor. In: Meinzer FC, Dawson TE, Lachenbruch B (eds) *Size- and age-related changes in tree structure and function*, Springer, Dordrecht, pp 363–384.

Yakir D, **DeNiro MJ** (**1990**) Oxygen and hydrogen isotope fractionation during cellulose metabolism in *Lemna gibba* L. *Plant Physiol* **93**:325–332.

Yakir D, **Israeli Y** (**1995**) Reduced solar irradiance effects on net primary productivity (NPP) and the $\delta^{13}C$ and $\delta^{18}O$ values in plantations of *Musa* sp., *Musaceae*. *Geochim Cosmochim Acta* **59**:2149–2151.

Yang B, Qin C, Wang J, *et al.* (**2014**) A 3,500-year tree-ring record of annual precipitation on the northeastern Tibetan Plateau. *Proc Natl Acad Sci USA* **111**:2903–2908.

Zhao F, **Zeng N** (**2014**) Continued increase in atmospheric CO_2 seasonal amplitude in the 21st century projected by the CMIP5 Earth system models. *Earth Syst Dynam* **5**:423–439.

Zhao M, **Running SW** (**2010**) Drought-induced reduction in global terrestrial net primary production from 2000 through 2009. *Science* **329**:940–943.

PUBLICATIONS

Tree Physiology 34, 819–838
doi:10.1093/treephys/tpu037

Research paper

Unravelling spatiotemporal tree-ring signals in Mediterranean oaks: a variance–covariance modelling approach of carbon and oxygen isotope ratios

Tatiana A. Shestakova[1], Mònica Aguilera[2], Juan Pedro Ferrio[2], Emilia Gutiérrez[1] and Jordi Voltas[2,3]

[1]Department of Ecology, University of Barcelona, Avda Diagonal 645, E-08028 Barcelona, Spain; [2]Department of Crop and Forest Sciences—AGROTECNIO Center, University of Lleida, Avda Rovira Roure 191, E-25198 Lleida, Spain; [3]Corresponding author (jvoltas@pvcf.udl.cat)

Received February 4, 2014; accepted April 9, 2014; published online May 28, 2014; handling Editor Annikki Mäkelä

Identifying how physiological responses are structured across environmental gradients is critical to understanding in what manner ecological factors determine tree performance. Here, we investigated the spatiotemporal patterns of signal strength of carbon isotope discrimination ($\Delta^{13}C$) and oxygen isotope composition ($\delta^{18}O$) for three deciduous oaks (*Quercus faginea* (Lam.), *Q. humilis* Mill. and *Q. petraea* (Matt.) Liebl.) and one evergreen oak (*Q. ilex* L.) co-occurring in Mediterranean forests along an aridity gradient. We hypothesized that contrasting strategies in response to drought would lead to differential climate sensitivities between functional groups. Such differential sensitivities could result in a contrasting imprint on stable isotopes, depending on whether the spatial or temporal organization of tree-ring signals was analysed. To test these hypotheses, we proposed a mixed modelling framework to group isotopic records into potentially homogeneous subsets according to taxonomic or geographical criteria. To this end, carbon and oxygen isotopes were modelled through different variance–covariance structures for the variability among years (at the temporal level) or sites (at the spatial level). Signal-strength parameters were estimated from the outcome of selected models. We found striking differences between deciduous and evergreen oaks in the organization of their temporal and spatial signals. Therefore, the relationships with climate were examined independently for each functional group. While *Q. ilex* exhibited a large spatial dependence of isotopic signals on the temperature regime, deciduous oaks showed a greater dependence on precipitation, confirming their higher susceptibility to drought. Such contrasting responses to drought among oak types were also observed at the temporal level (interannual variability), with stronger associations with growing-season water availability in deciduous oaks. Thus, our results indicate that Mediterranean deciduous and evergreen oaks constitute two clearly differentiated functional groups in terms of their carbon and water economies, despite co-existing in a wide range of environments. In contrast, deciduous oaks form a rather homogeneous group in terms of climate sensitivity.

Keywords: dendroecology, Iberian Peninsula, mixed models, *Quercus*, summer drought, tree-ring networks, water availability.

Introduction

Oak species occurring in the Mediterranean are adapted to varying degrees to a double climatic stress, drought in summer and cold in winter (Mitrakos 1980, Terradas and Savé 1992, Larcher 2000). Representatives of three contrasting phytoclimatic categories (Mediterranean, transitional nemoro-Mediterranean and nemoral) are found in this region that, according to features of their leaf and water relationships, form different functional groups (Corcuera et al. 2002).

The Mediterranean evergreen *Quercus ilex* L. is characteristic of the landscapes dominant in vast areas of the western

Mediterranean basin (Barbero et al. 1992). It grows often in co-existence with winter deciduous oaks in a wide range of climates and soils: from Mediterranean-continental environments, together with *Quercus faginea* (Lam.) (Mediavilla and Escudero 2010), to the sub-Mediterranean stages, where it can form mixed forests with *Quercus humilis* Mill. (syn. *Quercus pubescens* Willd.) and *Quercus petraea* (Matt.) Liebl. (Sánchez de Dios et al. 2009). The nemoro-Mediterranean *Q. faginea* is a relatively drought-tolerant species widely distributed in the Iberian Peninsula and North Africa, preferentially on basic soils (Loidi and Herrera 1990, Mediavilla and Escudero 2010). The nemoro-Mediterranean *Q. humilis* and the nemoral Eurosiberian *Q. petraea* are mainly found throughout eastern and central Europe, reaching their south-western range limit in the north of the Iberian Peninsula. However, *Q. petraea* is rather sensitive to water shortage, while *Q. humilis* may grow under drier conditions, being often found in sub-Mediterranean environments (see, e.g., Epron and Dreyer 1990, Arend et al. 2011). These three deciduous oaks partially overlap along a gradient of increasing humidity in north-eastern Spain, with *Q. faginea* inhabiting the driest, continental areas, followed successively by *Q. humilis* and *Q. petraea*, which occupy the wettest zones. In turn, they co-exist with *Q. ilex* along the entire humidity gradient.

Mediterranean deciduous and evergreen oaks differ considerably in ecophysiological properties, which determine their ability to cope with climatic stressors and, ultimately, define their distribution ranges and ecological fitness (Sánchez de Dios et al. 2009). Evergreen oaks usually show, among other properties, an extended vegetative period (Damesin et al. 1997), sclerophylly (Richards and Lamont 1996), higher turgor pressure (Corcuera et al. 2002), lower hydraulic conductance (Tognetti et al. 1998), higher stomatal limitation to photosynthesis (Juárez-López et al. 2008) and lower susceptibility to photoinhibition (Epron and Dreyer 1990) compared with deciduous oaks, which favour *Q. ilex* in dry years. Besides, deciduous oaks also differ in several features related to water and carbon economies, which help to explain their different distribution. For instance, the nemoral *Q. petraea* tends to maintain turgor pressure at the expense of more water losses than the nemoro-Mediterranean *Q. faginea* and *Q. humilis*, hence performing worse under drought (Corcuera et al. 2002).

The dendrochronological archive of carbon and oxygen stable isotopes simultaneously tracks the balance between assimilation rate and stomatal conductance (or intrinsic water-use efficiency; Farquhar and Richards 1984). In turn, it provides indirectly environmental information relevant to plant functioning with varying temporal resolution. The rising interest in the spatial and temporal dependence of climate processes has resulted in an explosion of tree-ring isotope networks worldwide (Treydte et al. 2007, Gagen et al. 2008, Leavitt et al. 2010, Saurer et al. 2012). Although it is not yet well understood to what degree carbon or oxygen isotope signals of tree rings vary under different climate conditions, there are indications that combining records from different species and sites may enhance the potential of isotope studies for inferring environmental drivers of tree performance (Saurer et al. 2008, Li et al. 2011). On the other hand, this potential is likely to be counterbalanced, to a variable extent, by differences in ecophysiological properties among species. For example, contrasting physiological responses between co-existing oaks in the Mediterranean region (e.g., Tognetti et al. 1998, Corcuera et al. 2002) may cause a differential reaction to environmental conditions that could imprint on the stable isotope signal of tree rings. When facing this issue, the problem of disentangling the spatial and temporal patterns of tree-ring signals needs to be confronted. Indeed, the environmental drivers of changes in stable isotopes may not necessarily coincide at the temporal (e.g., interannual fluctuations) and spatial (e.g., intersite variability) levels. Very few studies have attempted to address this question (e.g., Treydte et al. 2007).

The conventional approach of investigating the magnitude of common information shared by tree-ring records relies on the application of classical analysis of variance (ANOVA) principles (Fritts 1976, Wigley et al. 1984). For this purpose, a two-stage hierarchical scheme of analysis is commonly used in which several trees are first sampled at the stand level. Then, the trees are averaged into an annually resolved chronology, with a set of chronologies for a particular region being subsequently analysed (e.g., Hemming et al. 1998, Saurer et al. 2008). However, the underlying statistical model is of the mixed type because it may include several effects representing different random sources of variation, e.g., those associated with measurements repeated in time (Jennrich and Schluchter 1986). Quite surprisingly, the use of mixed models in dendrochronology does not seem to have reached the level it warrants (but see, e.g., Martínez-Vilalta et al. 2008, Lapointe-Garant et al. 2010, Linares and Tiscar 2011). The primary reasons may be twofold: first, they are computationally demanding, being beyond reach until recently; second, the presentation of the methodology in specialized manuals is often biased towards the theoretical side, which makes mixed models challenging for a wide audience.

Often, it may be of interest to stratify a set of chronologies into potentially more homogeneous subsets (e.g., McCarroll and Pawellek 2001). By applying different grouping criteria, stratification may allow unveiling of factors responsible for enhanced common signal strength (or temporal coherence) among chronologies. These factors may be related to the taxonomic affiliation of chronologies or to their assignment to particular sites or regions, among others. The adopted grouping strategy may be readily embedded in a mixed-model framework, where time is a random factor and chronologies (and their grouping) are fixed. A variant of this approach arises if

emphasis is placed on the spatial interpretation of the signal strength stored in a set of trees (e.g., for variability between sites across years) rather than at the temporal (e.g., for variability between years) level (or spatial coherence).

At the temporal level, the interest lies in interpreting common temporal information stored in tree-ring chronologies; at the spatial level, the aim is the exploration of the spatial variability in tree-ring signals (e.g., Leavitt et al. 2007, del Castillo et al. 2013). In this last case, it may be more informative to group individual tree records (e.g., pooled rings representing a number of years) according to taxonomic criteria in a similar way than to group chronologies. A fundamental advantage of mixed modelling is that all available data are used when assigning chronologies (at the temporal level) or tree records (at the spatial level) to groups, thus allowing for the quantification of common signals at the intra- and intergroup classes.

This study aimed at interpreting the variability and common signal strength of stable carbon and oxygen isotope ratios in tree rings for deciduous and evergreen *Quercus* species co-occurring in mixed Mediterranean forests. Here, we hypothesized that contrasting strategies in response to drought in Mediterranean evergreen (*Q. ilex*), nemoro-Mediterranean deciduous (*Q. faginea* and *Q. humilis*) and nemoral deciduous (*Q. petraea*) oaks would lead to a differential sensitivity to changes in water availability, and that this could be tracked by means of carbon and oxygen isotope analysis in tree rings. In turn, such differential sensitivity could imprint on stable isotopes in a contrasting manner, depending on whether the spatial or temporal organization of tree-ring signals was analysed.

To test these hypotheses, we compared the responses of these species using a tree-ring isotope network consisting of 24 sites (21 new and three already published) scattered across an aridity gradient in the north-eastern Iberian Peninsula covering an area of ~25,000 km^2. For some sites, annually resolved chronologies for stable isotopes were available, which allowed investigation of how temporal signals were structured according to taxonomic or geographical criteria for grouping chronologies and which climate drivers were involved in the observed responses. Alternatively, sites where the evergreen *Q. ilex* co-existed with deciduous oaks were investigated to identify potentially contrasting spatial signals between functional types and their driving climate factors across an aridity gradient in the Mediterranean. To this end, we proposed a new conceptual framework by which the patterns of tree-ring signals were investigated through mixed modelling.

Materials and methods

Study area and sampling strategy

The study was conducted in natural mixed-oak (*Quercus* spp.) forest stands located in the north-eastern Iberian Peninsula, western Mediterranean basin, between latitudes 41°11′N and 42°25′N and longitudes 0°39′E and 2°45′E (Figure 1). Different combinations of one deciduous (either *Q. faginea*, *Q. humilis* or *Q. petraea*) and one evergreen (*Q. ilex*) oak species were present at each site, except for three sites (named Banyoles) in which either a single species or two deciduous co-occurring species were available (Table 1).

The study area is characterized by a complex topography and the interaction of African subtropical, North Atlantic and

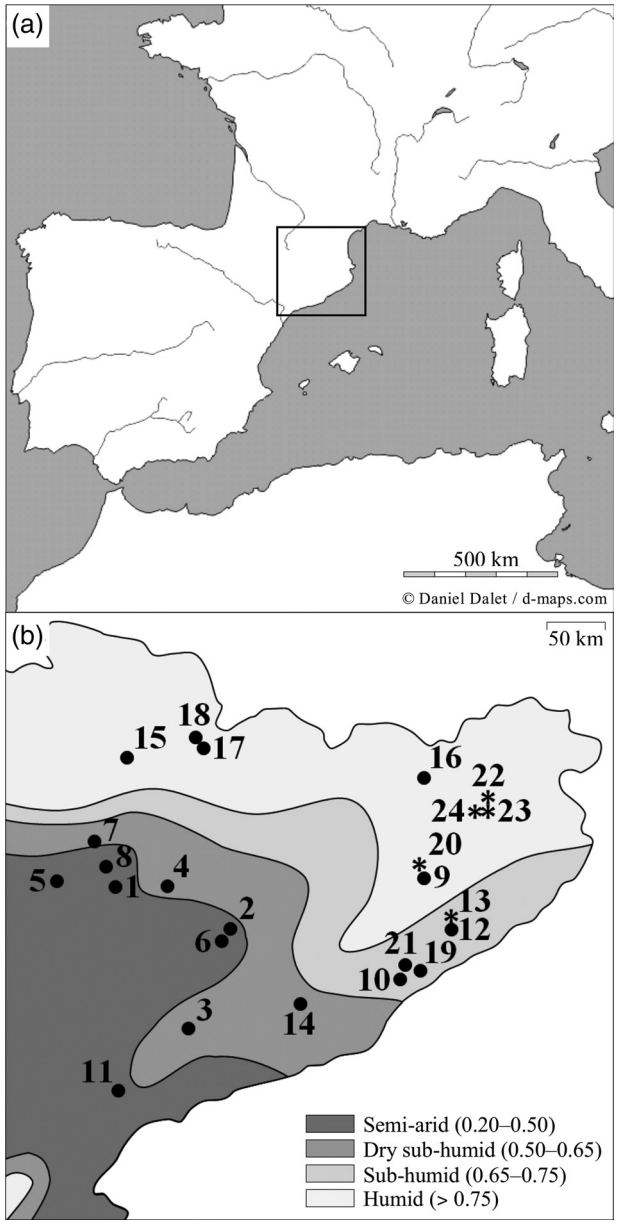

Figure 1. Study area (a) and geographical distribution of sampling sites (b). For reference, a contour map of the main bioclimatic regions in the studied area according to the UNESCO aridity index (total precipitation/Penman–Monteith evapotranspirative demand) is presented. Site numbering is according to Table 1. Asterisks identify sampling sites with availability of annually resolved chronologies for analysis at the temporal level.

Table 1. Main biogeographical variables and carbon ($\Delta^{13}C$) and oxygen ($\delta^{18}O$) stable isotopes (means ± SD) of sampling sites.

Id	Site	Species combination	Latitude	Longitude	Altitude (m a.s.l.)	T (°C)	P (mm)	$\Delta^{13}C$ (‰)		$\delta^{18}O$ (‰)	
								Species 1	Species 2	Species 1	Species 2
1	Alos de Balaguer	*Q. ilex*/*Q. faginea*	41°54′N	0°56′E	429	13.2	622	17.75 ± 0.57	17.85 ± 1.13	33.09 ± 0.50	32.11 ± 0.17
2	Calonge de Segarra	*Q. ilex*/*Q. faginea*	41°44′N	1°28′E	680	12.2	537	17.39 ± 0.57	16.21 ± 1.31	32.56 ± 0.98	31.56 ± 0.88
3	Figuerola del Camp	*Q. ilex*/*Q. faginea*	41°23′N	1°15′E	628	12.8	645	17.14 ± 0.83	18.15 ± 1.15	31.82 ± 0.28	31.64 ± 0.40
4	Oliola	*Q. ilex*/*Q. faginea*	41°54′N	1°11′E	407	13.2	498	16.23 ± 0.74	16.46 ± 0.50	33.26 ± 0.58	32.23 ± 0.41
5	Os de Balaguer	*Q. ilex*/*Q. faginea*	41°56′N	0°39′E	668	12.0	669	17.36 ± 0.53	16.32 ± 0.68	32.43 ± 0.30	31.67 ± 0.36
6	Pujalt	*Q. ilex*/*Q. faginea*	41°42′N	1°26′E	696	12.2	544	15.90 ± 0.89	16.52 ± 0.61	32.70 ± 1.10	32.00 ± 0.92
7	Sant Esteve de la Sarga	*Q. ilex*/*Q. faginea*	42°04′N	0°50′E	745	11.4	505	17.50 ± 0.51	16.99 ± 0.47	33.57 ± 0.30	32.04 ± 0.56
8	Camarasa	*Q. ilex*/*Q. humilis*	41°59′N	0°53′E	737	11.6	558	17.41 ± 0.66	16.70 ± 0.60	32.73 ± 0.88	31.52 ± 0.37
9	Espinelves	*Q. ilex*/*Q. humilis*	41°52′N	2°25′E	793	11.3	816	16.87 ± 0.83	17.38 ± 0.69	31.42 ± 0.25	31.14 ± 0.52
10	Montornès del Vallès	*Q. ilex*/*Q. humilis*	41°32′N	2°17′E	296	14.3	634	16.22 ± 0.73	16.99 ± 0.51	32.07 ± 0.55	31.33 ± 0.50
11	Pradell de la Teixeta	*Q. ilex*/*Q. humilis*	41°10′N	0°54′E	527	13.0	568	17.39 ± 0.95	18.09 ± 0.83	31.61 ± 0.07	31.12 ± 0.87
12	Sant Celoni I	*Q. ilex*/*Q. humilis*	41°42′N	2°32′E	252	14.2	717	16.71 ± 0.58	17.33 ± 1.16	32.27 ± 0.28	32.29 ± 0.24
13	Sant Celoni II[1]	*Q. ilex*/*Q. humilis*	41°43′N	2°32′E	128	15.2	825	17.51 ± 0.47	17.81 ± 0.77	32.42 ± 0.60	32.13 ± 0.50
14	Sant Sadurní d'Anoia	*Q. ilex*/*Q. humilis*	41°27′N	1°47′E	147	15.6	564	15.95 ± 1.29	17.34 ± 0.99	33.46 ± 0.70	32.74 ± 0.24
15	Baix Pallars	*Q. ilex*/*Q. petraea*	42°22′N	1°01′E	1140	9.3	998	17.45 ± 0.65	17.01 ± 0.72	32.66 ± 0.75	32.03 ± 0.63
16	La Vall de Bianya	*Q. ilex*/*Q. petraea*	42°14′N	2°27′E	436	13.0	928	17.31 ± 0.75	17.68 ± 0.82	31.47 ± 0.25	31.38 ± 0.49
17	Montferrer i Castellbò I	*Q. ilex*/*Q. petraea*	42°24′N	1°22′E	1254	8.6	737	17.37 ± 0.43	16.43 ± 0.57	32.67 ± 0.71	31.4 ± 0.12
18	Montferrer i Castellbò II	*Q. ilex*/*Q. petraea*	42°25′N	1°22′E	1300	8.4	799	16.91 ± 0.50	16.58 ± 0.61	32.45 ± 0.48	31.79 ± 0.24
19	Òrrius	*Q. ilex*/*Q. petraea*	41°33′N	2°21′E	371	13.8	718	17.51 ± 0.70	17.79 ± 0.86	32.28 ± 0.21	31.52 ± 0.67
20	Sant Sadurní d'Osormort[1]	*Q. ilex*/*Q. petraea*	41°55′N	2°24′E	626	12.1	787	16.77 ± 0.63	17.74 ± 0.69	32.36 ± 0.44	31.57 ± 0.50
21	Vilanova del Vallès	*Q. ilex*/*Q. petraea*	41°33′N	2°18′E	108	15.2	639	17.22 ± 0.77	17.78 ± 1.17	32.92 ± 0.33	32.77 ± 0.68
22	Banyoles (low altitude)[2]	*Q. humilis*/*Q. petraea*	42°09′N	2°45′E	231	14.0	877	17.32 ± 0.65	17.95 ± 0.54	31.84 ± 0.70	30.87 ± 1.81
23	Banyoles (medium altitude)[2]	*Q. humilis*/*Q. petraea*	42°06′N	2°43′E	310	13.5	937	18.26 ± 0.43	18.44 ± 1.06	27.64 ± 0.84	29.43 ± 1.78
24	Banyoles (high altitude)[2]	*Q. humilis*/–	42°06′N	2°42′E	423	13.1	966	18.11 ± 0.56	–	26.61 ± 0.75	–

[1]Sites used for analysis at the temporal and spatial levels.
[2]Sites used only for analysis at the temporal level.
a.s.l., above sea level; T, temperature; P, precipitation.

Mediterranean climate systems (Rodó et al. 1997), with cold wet winters and a period of summer drought that occurs every year. The mean annual precipitation varies from 498 to 998 mm among the study sites (Table 1), with summer (June to August) precipitation ranging from 102 to 316 mm. The average annual temperature ranges from 8.4 to 15.6 °C (Table 1), with an average minimum temperature of −0.1 °C in January for the coldest site and an average maximum temperature of 28.5 °C in July for the warmest site (Digital Climatic Atlas of the Iberian Peninsula, available at http://www.opengis.uab.es/wms/iberia/mms/index.htm; Ninyerola et al. 2005).

Wood cores of *Q. faginea*, *Q. humilis*, *Q. ilex* and *Q. petraea* were collected using a 5-mm-diameter increment borer in 2009. As a sampling strategy, a representative set of 21 sites encompassing the natural biogeographical range of conditions where deciduous and evergreen Mediterranean oaks co-occur in mature forest stands in the region were identified based on information of the Ecological Forest Inventory of Catalonia. These ranged from humid, relatively mild territories near the Mediterranean coastal strip having a nemoro-Mediterranean vegetation to contact areas between the Mediterranean and Eurosiberian regions, with recurrent presence of winter frosts and characterized by sub-Mediterranean taxa (Rivas-Martínez 1982).

For each of the three deciduous species (*Q. faginea*, *Q. humilis* and *Q. petraea*), seven sites were chosen in which the deciduous oak was found co-occurring with the evergreen holm oak (*Q. ilex*; Table 1). Mean values of altitude, temperature and precipitation for the sampling sites of each deciduous species in combination with *Q. ilex* were 608 m above sea level (a.s.l.), 12.4 °C and 574 mm for *Q. faginea*, 411 m a.s.l., 13.6 °C and 669 mm for *Q. humilis*, and 748 m a.s.l., 11.5 °C and 801 mm for *Q. petraea*. The selection preserved the original range of variation in thermal and precipitation regimes for each species, while avoiding a strong dependence between both bioclimatic indicators for the complete set of sites (correlation between mean annual precipitation and average annual temperature, $r = 0.36$; $P = 0.11$). In this way, we aimed at reducing potential confounding effects in the interpretation of climate-driven variability in the studied traits.

For each species combination, five nearest-neighbour pairs of mature, dominant and healthy trees of a similar size (one deciduous and one evergreen), growing within a radius of 4 m and far from water sources other than precipitation (e.g., springs, gullies, ravines, etc.), were selected at each site. As a result, 35 trees of each deciduous oak (*Q. faginea*, *Q. humilis* and *Q. petraea*) and 105 *Q. ilex* trees were sampled in May–July 2009 (diameters at breast height of 22.0 ± 3.5, 22.6 ± 6.2, 21.0 ± 3.8 and 21.4 ± 4.7 cm, respectively; mean ± standard deviation (SD)). Two cores were taken from the south side of each tree. One core was used for tree-ring dating and the other for subsequent isotope analyses. This sampling scheme was employed to identify potentially contrasting spatial signals in stable isotopes between deciduous and evergreen oaks. The exploration of spatial patterns in stable isotopes was investigated using 20-year pooled tree-ring samples spanning the period 1989–2008 (see the next sections).

In addition, the temporal variability in stable isotopes was explored through annually resolved chronologies in three selected sites representing every species combination (one of the deciduous oak species co-occurring with the evergreen *Q. ilex*), from which additional cores of five trees per species were taken in April 2010. These sites were representative of the average precipitation and temperature conditions in which the above-mentioned tree species combinations were found along the ecological transect. They were complemented by data compiled from a previous study (Aguilera et al. 2011) in which co-occurring *Q. humilis* and *Q. petraea* trees were sampled near Banyoles lake, NE Spain (42°07′N, 2°45′E) in May 2006. In this study, three sites were chosen following an altitudinal gradient, and the criteria for tree selection and the sampling protocol were the same as specified above. However, for the highest elevation site (423 m a.s.l.), only *Q. humilis* individuals were available, while at the medium (310 m a.s.l.) and low (231 m a.s.l.) elevation sites, only two and four trees of *Q. petraea*, respectively, were found having the required features. As a result, a total of 15 trees of *Q. humilis* and six trees of *Q. petraea*, with mean diameters at breast height of 19.8 ± 2.9 and 19.1 ± 2.9 cm, respectively, were sampled. Altogether, a set of 24 sampling sites were used to investigate the spatiotemporal patterns of variability in stable isotopes, with the following representation of species (Table 1): *Q. faginea* (seven sites), *Q. humilis* (10 sites), *Q. ilex* (21 sites) and *Q. petraea* (nine sites).

Sample preparation and tree-ring dating All samples were oven-dried at 60 °C for 48 h and one core per tree was sanded with sandpapers of progressively finer grain until tree rings were clearly visible. The remaining core of every tree was kept intact for isotope analyses. Tree rings were visually cross-dated using a binocular microscope coupled to a PC with the image processing program ImageJ (ImageJ v. 1.42, available at http://rsb.info.nih.gov/ij). The COFECHA program (Holmes 1983) was used to evaluate the visual cross-dating for samples requiring annual resolution (originating from three selected sites of the biogeographical transect, in addition to those reported in Aguilera et al. 2011). Each individual tree-ring width series showed a decreasing growth trend, which was removed by fitting a straight line and keeping the residuals obtained by the difference of this linear fit. The residuals were subjected to autoregressive modelling to remove the first-order autocorrelation. Annually resolved isotope chronologies were produced by pooling dated growth rings from about five trees prior to the isotopic analyses.

A prerequisite for pooling was availability of tree-ring series reflecting consistent ring-width variation common to all trees.

For this purpose, the quality of the average chronology for every site–species combination was examined by calculating the mean interseries correlation ($\hat{a}$), the signal-to-noise ratio (SNR) and the expressed population signal (EPS) statistics according to Wigley et al. (1984). Three site–species chronologies (Oliola, for both *Q. faginea* and *Q. ilex*, and Sant Sadurní d'Osormort, for *Q. ilex*) had low values of $\hat{a}$, SNR and EPS, indicating a poor cross-dating for ring width. This could be due either to the influence of local factors such as micro-topography and competition (bearing in mind the limited amount of sampled trees) or to difficulties in the identification of rings in diffuse-porous species such as *Q. ilex* (Cherubini et al. 2003). These chronologies were therefore excluded from the analysis of isotope patterns at the temporal level. Finally, a total of eight chronologies were used (four chronologies of *Q. humilis*, three of *Q. petraea* and one of *Q. ilex*), which had the following average quality: $\hat{a} = 0.49 \pm 0.02$, SNR = 4.89 ± 0.20, EPS = 0.83 ± 0.03 (mean ± SD; $n = 5$ trees per chronology).

Stable isotope analyses A core fragment containing rings that spanned the period 1989–2008 (20 years) was selected for every tree sampled in 2009. The 20-year wood fragments were split from the original cores using a scalpel. They were used to characterize the spatial pattern of isotope signals along the biogeographical gradient. In addition, eight annually resolved isotope chronologies (see the previous section) were available for a period of 20 years (1986–2005 for the series reported in Aguilera et al. 2011; 1989–2008 for the series obtained in this study). Every 20-year wood fragment corresponding to a particular tree, site and species or, alternatively, every set of rings of the same year from about five trees were purified to α-cellulose with a modification of the method of Leavitt and Danzer (1993) for the removal of extractives and lignin, as detailed in Ferrio and Voltas (2005). Sodium hydroxide was used to obtain α-cellulose (Loader et al. 1997), which was homogenized to a fine powder with a ball mixer mill (Retsch MM301, Haan, Germany).

For carbon isotope analysis, 0.30–0.40 mg of dry α-cellulose was weighed into tin foil capsules and combusted using a Flash EA-1112 elemental analyser (Thermo Fisher Scientific Inc., MA, USA) interfaced with a Finnigan MAT Delta C isotope ratio mass spectrometer (Thermo Fisher Scientific Inc.). For oxygen isotope analysis, 0.30–0.40 mg of dry α-cellulose was weighed into silver foil capsules and combusted using a Carlo Erba 1108 elemental analyser (Carlo Erba Instruments Ltd., Milan, Italy) interfaced with a Finnigan Deltaplus XP isotope ratio mass spectrometer (Thermo Fisher Scientific Inc.). Isotope ratios were expressed as per mil deviations using the δ notation relative to Vienna Pee Dee Belemnite standard (for carbon) and Vienna Standard Mean Ocean Water (for oxygen) standards. The accuracy of the analyses (SD of working standards) was 0.06‰ ($\delta^{13}C$) and 0.25‰ ($\delta^{18}O$).

To account for changes in $\delta^{13}C$ of atmospheric CO_2 ($\delta^{13}C_{air}$), we calculated carbon isotope discrimination in cellulose ($\Delta^{13}C$) from $\delta^{13}C_{air}$ and α-cellulose $\delta^{13}C$ ($\delta^{13}C$), as described by Farquhar and Richards (1984):

$$\Delta^{13}C = \frac{\delta^{13}C_{air} - \delta^{13}C}{1 + \delta^{13}C}. \quad (1)$$

$\delta^{13}C_{air}$ was inferred by interpolating a range of data from Antarctic ice-core records, together with modern data from two Antarctic stations (Halley Bay and Palmer Station) of the CU-INSTAAR/NOAA-CMDL network for atmospheric CO_2 measurements, as first described in Ferrio et al. (2005); smoothed $\delta^{13}C_{atm}$ curve from 16,100 BCE to 2010, available at http://web.udl.es/usuaris/x3845331/AIRCO2_LOESS.xls. According to these records, the $\delta^{13}C_{air}$ value applied to extant α-cellulose samples varied between –8.21 and –7.60‰.

The isotope chronologies (either $\Delta^{13}C$ or $\delta^{18}O$) exhibiting a linear trend over time were detrended by fitting a straight line and keeping the residuals of these linear fits as input for mixed modelling. There were three chronologies for $\Delta^{13}C$ (the two chronologies from Sant Celoni II, with negative trends, and one chronology of *Q. petraea* from Banyoles of medium altitude, with a positive trend) and two for $\delta^{18}O$ (one chronology of *Q. petraea* from Banyoles of low altitude, with a positive trend, and one chronology of *Q. petraea* from Banyoles of medium altitude, with a negative trend). For the rest of the chronologies, which did not show significant trends over time, each individual record was corrected by subtracting from the average value of its corresponding chronology in order to also obtain residual chronologies for mixed modelling. Therefore, mixed modelling focused on the analysis of interannual variability in isotopic signals.

Strategy for grouping isotopic records at spatial and temporal levels We checked several grouping structures. At the temporal level, two different grouping strategies were tested: (i) a taxonomy-based strategy, by which chronologies from the same species were considered as a single group; and (ii) a site-based strategy, by which chronologies from the same site, irrespective of the species, were considered as a single group. In the first case, two groups were formed: *Q. humilis* (consisting of four chronologies) and *Q. petraea* (consisting of three chronologies). In the second, three groups emerged corresponding to three different sites: (i) Banyoles of low elevation (including *Q. humilis* and *Q. petraea*); (ii) Banyoles of medium elevation (including *Q. humilis* and *Q. petraea*); and (iii) Sant Celoni (including *Q. humilis* and *Q. ilex*). It is important to stress that each grouping strategy involved a particular set of chronologies, although five chronologies were used in both analyses.

At the spatial level, 10 oaks from each of the 21 available sites (and represented by their 20-year isotope averages) were classified into two groups, deciduous and evergreen.

This meant that oaks from the three deciduous species formed a single group across the biogeographical transect that was tested for coherence of its isotope signals against the group formed by the evergreen oaks (*Q. ilex*).

Meteorological data Estimates of monthly mean temperatures (minimum, mean and maximum) and total precipitation for each site were obtained from the Digital Climatic Atlas of the Iberian Peninsula (Ninyerola et al. 2005), which provides averages for the period 1950–99 with a spatial resolution of 200 m. These records were used to infer the climatic sensitivity of isotopic signals across the biogeographical transect (i.e., at the spatial level). Annual meteorological records (monthly averages for minimum, mean and maximum temperature, and total monthly precipitation) covering the studied period were supplied by the Spanish National Meteorological Agency for the five sites in which annually resolved tree-ring chronologies were available. They were used to ascertain the relationships of tree-ring isotopes with climate at the temporal level. The records originated from the nearest meteorological station to each sampling point, located <15 km from the study sites. Wherever the altitude of the sampling site differed from that of the meteorological station, we applied the following correction (Gandullo 1994): for temperature, a decrease of 0.6 °C per 100 m; for precipitation, an 8% increment per 100 m, except for July and August, when precipitation is mostly convective and not related to altitude. Climate records and isotope data were compared using simple correlations at both spatial and temporal levels.

Statistical analysis

In dendroclimatology and dendroecology, time series of tree-ring features are averaged to produce 'chronologies' that reflect variability common to all trees at a particular site (Wigley et al. 1984). A particular set of chronologies ($i = 1, N$) can thereafter be analysed together to characterize the strength of their common signal. Suppose that W_{ij} is the jth observation (i.e., year) of a parameter W_i, and that each W_i reflects some controlling process by a particular tree-ring feature (i.e., carbon or oxygen stable isotope ratios) that may be obscured by noise that depends on both i and j. The estimators can be defined in terms of the following random model (random variables are shown underlined in this paper):

$$\underline{W}_{ij} = \underline{Y}_j + \underline{e}_{ij}, \tag{2}$$

where $\underline{Y}_j$ is a random time effect of the jth year and $\underline{e}_{ij}$ is a random deviation of the ith chronology in the jth year. Here, we assume that the year effects behave as if they came from a normal distribution with mean zero and variance σ^2_Y. This means that observations made in the same year have a covariance, and so they are not independent. To quantify how strongly the chronologies ($i = 1, N$) are correlated, let us now consider the values that two chronologies, i and i^*, can attain for a particular year, j. The covariance between observations is

$$\begin{aligned}\operatorname{cov}\left(\underline{W}_{ij},\underline{W}_{i^*j}\right) &= \operatorname{cov}\left(\underline{Y}_j + \underline{e}_{ij},\underline{Y}_j + \underline{e}_{i^*j}\right) = \operatorname{cov}\left(\underline{Y}_j,\underline{Y}_j\right) \\ &+ \operatorname{cov}\left(\underline{e}_{ij},\underline{e}_{i^*j}\right) = \operatorname{Var}\left(\underline{Y}\right) = \sigma^2_Y.\end{aligned} \tag{3}$$

Here, a typical, but not obligatory, assumption in mixed modelling is to take the random effects belonging to different random terms, in our case $\underline{Y}_j$ and $\underline{e}_{ij}$, as independent of each other (Demidenko 2004). This assumption may not necessarily hold for longitudinal data, and can be avoided by allowing for correlation of random effects in Eq. (3). However, the consequences of incorporating such correlation, disregarding parsimony, would need a detailed examination.

Likewise, the variance of chronology i is

$$\operatorname{Var}\left(\underline{W}_i\right) = \operatorname{Var}\left(\underline{Y} + \underline{e}_i\right) = \operatorname{Var}\left(\underline{Y}\right) + \operatorname{Var}\left(\underline{e}_i\right) = \sigma^2_Y + \sigma^2_e. \tag{4}$$

The intraclass correlation (or reproducibility of observations by chronologies i and i^*) then becomes

$$\rho\left(\underline{W}_i,\underline{W}_{i^*}\right) = \frac{\operatorname{cov}\left(\underline{W}_i,\underline{W}_{i^*}\right)}{\sqrt{\operatorname{Var}\left(\underline{W}_i\right) \times \operatorname{Var}\left(\underline{W}_{i^*}\right)}} = \frac{\sigma^2_Y}{\sigma^2_Y + \sigma^2_e}. \tag{5}$$

If the whole set of N chronologies is analysed together, this parameter becomes the average correlation over all possible pairs of chronologies, excluding the N pairs $i = i^*$ for which $r_{ii^*} = 1$. This correlation is closely related to the mean interseries correlation parameter defined at the intrasite level, $\hat{a}$, which is widely used in dendroclimatology and dendroecology (Wigley et al. 1984). We will refer to it as the mean interchronology correlation, $\hat{a}_C$. It estimates the strength of the common signal underlying the set of N chronologies. Unlike the classical ANOVA approach, mixed modelling is capable of dealing with partially overlapping chronologies, so unbalancedness is not a concern here if we consider the missing-data pattern as being completely random (see Little and Rubin 2002 for details).

A natural variant of the model (Eq. (2)) arises if a set of trees ($i = 1, N$) is used across a number of sites to characterize the strength of tree-ring signals at the spatial level (signals are represented here by 20-year pooled isotopic values). In this case, $\underline{W}_{ij}$ is the observation corresponding to the jth site of a parameter $\underline{W}_i$, but now the ith tree is nested to the jth site from where it originates. The model remains the same as in Eq. (2), but now $\underline{Y}_j$ represents a random site effect of the jth site, and $\underline{e}_{ij}$ is a random deviation of the ith tree of the jth site. We assume that the site effects behave as if they came from a normal distribution with mean zero and variance σ^2_S, so the intraclass correlation (Eq. (5)) still holds true by replacing σ^2_Y with σ^2_S.

Such an alternative intraclass correlation will be referred to as spatial signal strength, $\hat{a}_S$. In this case, it estimates the strength of the common signal underlying a set of *N* trees that vary from site to site.

Mixed modelling for grouping chronologies (analysis of temporal variability) In order to search for contributing causes of enhanced common variance for isotope signals among chronologies, these were grouped considering the two above-mentioned criteria: (i) taxonomy (with two groups, *Q. humilis* and *Q. petraea*); and (ii) species co-occurrence (with three groups corresponding to each one of three sites). If a random sample of chronologies is used for trait testing in each group, the resulting data may be regarded as a random stratified sample, with strata corresponding to groups. According to the theory of survey sampling (Kish 1965), stratification is beneficial (i.e., it improves the accuracy of parameter estimates), provided there is heterogeneity between groups as defined by the factor(s) under evaluation.

Now the estimators can be defined in terms of the following mixed model:

$$\underline{W}_{ijr} = \mu_r + \underline{Y}_{jr} + \underline{e}_{ijr}, \quad (6)$$

where μ_r is the expected value in the *r*th group (if the chronologies are detrended or indexed, as in this study, this term vanishes but can be saved for further analysis), $\underline{Y}_{jr}$ is a random time effect of the *j*th year in the *r*th group and $\underline{e}_{ijr}$ is a random deviation of the *i*th chronology in the *j*th year within the *r*th group. The random deviation can be further partitioned as

$$\underline{e}_{ijr} = \underline{p}_{i(r)} + \underline{f}_{ij(r)}, \quad (7)$$

where $\underline{p}_{i(r)}$ is a random effect of the *i*th chronology nested within the *r*th group and $\underline{f}_{ij(r)}$ is a year-specific deviation. Both effects appearing in $\underline{e}_{ijr}$ are assumed to be independent homoscedastic normal deviates with zero means; in particular, if the chronologies are detrended or indexed then the term $\underline{p}_{i(r)}$ has null variability (i.e., all chronologies share the same mean value).

In turn, the year effect may be further partitioned as:

$$\underline{Y}_{jr} = \underline{Y}_j + \underline{(YR)}_{jr}, \quad (8)$$

where $\underline{Y}_j$ is a main effect for the *j*th year and $\underline{(YR)}_{jr}$ is the *jr*th year × group interaction, assuming that $\underline{Y}_j$ and $\underline{(YR)}_{jr}$ are independent homoscedastic normal deviates. This model corresponds to the standard ANOVA partition accommodating between- and within-group variability and has the so-called compound symmetry variance–covariance (VCOV) structure (Model M_1) for the variability among years:

M_1: compound symmetry

$$\mathrm{cov}(\underline{Y}_{jr};\underline{Y}_{jr*}) = \begin{cases} \sigma^2_{Y+YR} & \text{when } r = r^* \\ \sigma^2_Y & \text{otherwise} \end{cases}$$

Under the compound symmetry model, year variances are the same in each group, with $\sigma^2_{Y+YR} = \sigma^2_Y + \sigma^2_{YR}$, and year covariances (and correlations) are the same for each pair of groups. While this assumption may be adequate in some circumstances, a range of alternative assumptions can be covered by other VCOV structures. In some cases, there may be heterogeneity of year variance between groups although the property of constant correlation (ρ) across all pairs of groups may still hold true (Model M_2), provided there is null residual variance associated with the values of $\underline{f}_{ij(r)}$ in Eq. (7):

M_2: heterogeneous compound symmetry

$$\mathrm{cov}(\underline{Y}_{jr};\underline{Y}_{jr*}) = \begin{cases} \sigma^2_{Y_r} & \text{when } r = r^* \\ \sigma_{Y_r} \times \sigma_{Y_{r*}} \times \rho & \text{otherwise} \end{cases}$$

Alternatively, we may assign each group its own year variance and each pair of groups its own year covariance (Model M_3):

M_3: unstructured (full model)

$$\mathrm{cov}(\underline{Y}_{jr};\underline{Y}_{jr*}) = \begin{cases} \sigma^2_{Y_r} & \text{when } r = r^* \\ \sigma^2_{Y_{r*}} & \text{otherwise} \end{cases}$$

Under the unstructured model, all causes of year × group interaction (i.e., year heterogeneity across groups and deviations from equal year correlations between groups) are allowed.

Two simple variants of M_1 can act as a baseline against which to compare the more refined modelling alternatives shown before:

M_4: banded main diagonal (narrow evaluation)

$$\mathrm{cov}(\underline{Y}_{jr};\underline{Y}_{jr*}) = \begin{cases} \sigma^2_{YR} & \text{when } r = r^* \\ 0 & \text{otherwise} \end{cases}$$

Model M_4 constrains the covariance (and correlation) between groups to zero, thus testing for a lack of common signal between chronologies belonging to different groups.

M_5: null model (broad evaluation)

$$\mathrm{cov}(\underline{Y}_{jr};\underline{Y}_{jr*}) = \sigma^2_Y, \text{ when } r = r^* \text{ or } r \neq r^*,$$

Under the null model M_5, we simply ignore the existence of groups so year variance and covariances have the same value. This model is useful for testing the adequacy of grouping chronologies into different classes as for Models M_1–M_4.

Alternative VCOV structures can also be fitted, but here we stuck to the aforementioned models as the number of groups tested in this work was quite limited (two to three), and thus

additional extensions of the standard ANOVA partition (Eq. (8)) were deemed unnecessary. In turn, Models M_1–M_5 can be enhanced in two ways: (i) by allowing the residual variance associated with $f_{ij(r)}$ to vary among groups; and (ii) by assuming a steady decay in correlation with increasing time between observations (i.e., accounting for non-independence of random deviates $f_{ij(r)}$ of Eq. (7)). The former represents a heteroscedastic variant of Models M_1–M_4 (Model M_5 has no definition of groups). Homogeneity of residual variance is a main assumption of standard ANOVA, and conclusions on year × group interactions may not be appropriate if this assumption is not fulfilled. For the latter, we used an autoregressive model of order 1, with one extra correlation parameter in addition to the residual variance associated with $f_{ij(r)}$ in Eq. (7). The correlation between records from a particular chronology i in years j and j^* is $\rho^{|j-j^*|}$ as $|\rho| < 1$. The heteroscedastic variants of Models M_1–M_4 were also tested for independent autoregressive structures at the group level, in association with the random deviates $f_{ij(r)}$ in Eq. (7). A detailed list of the different models is given in Table 2.

Mixed modelling for grouping trees (analysis of spatial variability) At the site level, we grouped trees into two classes (evergreen and deciduous), extending this classification to a number of J sites. Similar to the previous case of chronology grouping, we aimed at searching for contributing causes of enhanced common variance, but focusing on the organization of spatial rather than temporal isotope signals. Equations (5) and (7) are equally valid after replacing the year effect by a site effect j, and the chronology effect by a tree effect i. In turn, model residuals (as for Eq. (7)) appear from the deviation of the ith tree within the rjth group × site interaction. The heteroscedastic variants of Models M_1–M_4 were also tested at the spatial level.

Model selection In mixed modelling, it is important to choose a random structure that combines sufficient flexibility with parsimony in the number of VCOV parameters. The adequacy of different VCOV models can be compared by computing the restricted log-likelihood for each model and deriving criteria such as Akaike's information criterion (AIC) and the Bayesian information criterion (BIC). Both involve a penalty for the number of parameters in the VCOV structure, which favours parsimonious models, but BIC generally penalizes a large number of parameters more strongly than does AIC (however, Barnett et al. (2010) have demonstrated that AIC may over-penalize the covariance parameters for complex structures). Both statistics are in the smaller-is-better form. We considered models with substantial support to be those in which the difference of either AIC or BIC between models was <2 (Raftery 1996, Burnham and Anderson 2002). This difference corresponds to the information loss experienced when using an alternative model instead of the best-fit model for inference (Burnham and Anderson 2002).

Estimation of signal-strength parameters The intraclass correlation defined in Eq. (5) quantifies the degree to which the values of N chronologies (or trees) contain a common temporal (or spatial) signal. Models M_1–M_4 allow for the estimation of intraclass correlations either at the intragroup or intergroup level. The underlying idea is to split the mean correlation estimated between all possible pairs of chronologies (trees) drawn from the whole dataset as in Eq. (5) into: (i) a mean correlation between pairs of chronologies (trees) for every group; and (ii) a mean correlation between pairs of chronologies (trees) for pairs of groups. For the more general M_3 (unstructured) model, the correlation of pairs of chronologies (trees) i and i^* belonging to group r becomes

Table 2. Description of the models used for interpreting temporal and spatial patterns in isotope records according to the assignment of chronologies (for analysis at the temporal level) or trees within a site (for analysis at the spatial level) to pre-defined groups.

Model and interpretation	Covariance structure	Variances	Covariances	Correlations	Residual variance[1]
M_1 Homogeneity of year (temporal) or site (spatial) variances and covariances across groups	Compound symmetry	Homogeneous	Homogeneous	Homogeneous[2]	Homoscedastic/ heteroscedastic
M_2 Different variances but equal year (temporal) or site (spatial) correlation between all group pairs[3]	Heterogeneous compound symmetry	Heterogeneous	Heterogeneous	Homogeneous[3]	Homoscedastic/ heteroscedastic
M_3 Full model (different variances and covariances). All causes of year × group (temporal) or site × group (spatial) interaction are allowed	Unstructured	Heterogeneous	Heterogeneous	Heterogeneous	Homoscedastic/ heteroscedastic
M_4 Lack of common signal between groups	Banded main diagonal	Heterogeneous	Zero	Zero	Homoscedastic/ heteroscedastic
M_5 Null model. Broad evaluation ignoring groups	None	Single	–	–	Homoscedastic

[1]Autoregressive structures at the group level were also tested, accounting for non-independence of temporal (year) random deviates.
[2]If homoscedastic residual variance.
[3]If null residual variance.

$$\rho\left(\underline{W}_i,\underline{W}_{i^*}\right)=\frac{\operatorname{cov}\left(\underline{W}_i,\underline{W}_{i^*}\right)}{\sqrt{\operatorname{Var}\left(\underline{W}_i\right)\times\operatorname{Var}\left(\underline{W}_{i^*}\right)}}=\frac{\sigma^2_{Y_r}}{\sigma^2_{Y_r}+\sigma^2_e}. \quad (9)$$

Conversely, the correlation of pairs of chronologies (trees) i and i^* belonging to groups r and r^* is

$$\rho\left(\underline{W}_i,\underline{W}_{i^*}\right)=\frac{\operatorname{cov}\left(\underline{W}_i,\underline{W}_{i^*}\right)}{\sqrt{\operatorname{Var}\left(\underline{W}_i\right)\times\operatorname{Var}\left(\underline{W}_{i^*}\right)}}=\frac{\sigma^2_{Y_{rr^*}}}{\sqrt{\left(\sigma^2_{Y_r}+\sigma^2_e\right)\times\left(\sigma^2_{Y_{r^*}}+\sigma^2_e\right)}}. \quad (10)$$

Similar to Eq. (5), if the whole set of N chronologies (trees) is analysed together, these parameters become mean correlations over all possible pairs of chronologies ($\hat{a}_C$) or trees ($\hat{a}_S$) at the intragroup or intergroup level, respectively. Alternative mean correlation expressions for Models M_1, M_2 or M_4 can be obtained by applying their corresponding variance–covariance structures to Eq. (5). Note that the mean correlation estimates for M_5 (broad evaluation model) correspond to that defined by Eq. (5). The EPS, which quantifies how well a chronology based on a finite number of trees represents the hypothetical perfect or true chronology, can be generalized from these estimates at either the temporal or spatial level following Wigley et al. (1984):

$$\mathrm{EPS}\approx\frac{N\hat{a}}{1+(N-1)\times\hat{a}}, \quad (11)$$

where N is the number of chronologies (trees) and $\hat{a}$ is the mean correlation at the temporal ($\hat{a}_C$) or spatial ($\hat{a}_S$) level.

All analyses were performed with the MIXED procedure of SAS/STAT (ver. 9.3, SAS, Inc., Cary, NC, USA) using restricted maximum likelihood (REML) for estimation of variance components. The covariance structure for groups was specified using the RANDOM statement and the autoregressive structure was fitted using the REPEATED statement. Heterogeneity of residual variances across groups was implemented with the GROUP option of the REPEATED statement.

Results

Sources of variability in stable isotopes

$\Delta^{13}C$ in *Q. ilex* varied among sites from 16.2 to 18.2‰ (Table 1). For the deciduous oaks co-occurring with *Q. ilex*, $\Delta^{13}C$ ranged from 15.9 to 17.8‰ in *Q. faginea*, from 16.0 to 17.5% in *Q. humilis*, and from 16.8 to 17.5‰ in *Q. petraea* (Table 1). $\delta^{18}O$ in *Q. ilex* varied among sites from 31.1 to 32.8‰ (Table 1). For the deciduous oaks, $\delta^{18}O$ ranged from 31.8 to 33.6‰ in *Q. faginea*, from 31.4 to 33.5‰ in *Q. humilis*, and from 31.5 to 32.9‰ in *Q. petraea* (Table 1). For *Q. humilis* and *Q. petraea*, the range of variability in both isotopes increased considerably after the Banyoles sites (used only for analysis at the temporal level) were included in the dataset (Sites 22, 23 and 24, Table 1; Figure 2). The mean $\Delta^{13}C$ site values for deciduous and evergreen oak combinations were 17.0 and 17.1‰ for *Q. ilex* and *Q. faginea*, 17.4 and 16.9‰ for *Q. ilex* and *Q. humilis*, and 17.3 and 17.3‰ for *Q. ilex* and *Q. petraea*, respectively. The mean $\delta^{18}O$ values were 31.9 and 32.8‰ for *Q. ilex* and *Q. faginea*, 31.8 and 32.3‰ for *Q. ilex* and *Q. humilis*, and 31.8 and 32.4‰ for *Q. ilex* and *Q. petraea*, respectively. Differences between species were significant for $\Delta^{13}C$ (but only for the *Q. ilex*–*Q. humilis* combination) and for $\delta^{18}O$ (for all combinations).

Relationships between $\Delta^{13}C$ and $\delta^{18}O$ were not significant regardless of the species only if sites where evergreen and deciduous oaks co-occurred were considered. However, they became significant (negative) for *Q. humilis* and *Q. petraea* after including Banyoles (Sites 22, 23 and 24; Figure 2). For chronologies, the association between both isotopes was usually significant (negative), except for *Q. humilis* in Banyoles (a low-altitude site) and for *Q. ilex* in Sant Celoni (results not shown).

Model selection at the temporal level (grouping of chronologies)

The $\Delta^{13}C$ and $\delta^{18}O$ residuals that appeared after linear detrending of chronologies or, otherwise, simply differencing from the mean are displayed in Figure 3. The common signal of the eight chronologies seemed much larger for $\Delta^{13}C$ than for $\delta^{18}O$. This visual assessment was checked against mixed

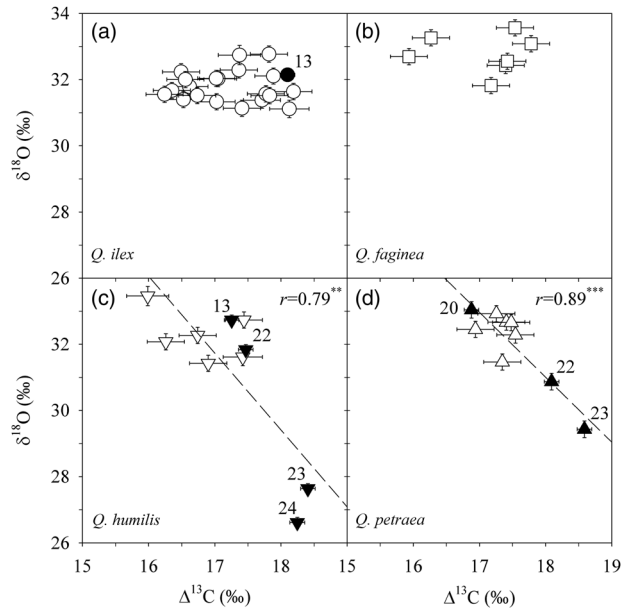

Figure 2. Relationships between carbon isotope discrimination ($\Delta^{13}C$) and oxygen isotope composition ($\delta^{18}O$) at the site level for (a) *Q. ilex*, (b) *Q. faginea*, (c) *Q. humilis* and (d) *Q. petraea*. Error bars indicate standard errors. Filled symbols identify sites with annually resolved chronologies for the analysis of temporal trends in both isotopes. Site numbering is according to Table 1.

modelling results by using the above-mentioned grouping strategies: taxonomy- and site-based. Table 3 shows the log-likelihood statistics for various VCOV structures. The AIC and BIC criteria applied to $\Delta^{13}C$ pointed to the inadequacy of complex VCOV models to describe properly a taxonomy-based grouping of chronologies (with groups *Q. humilis* and *Q. petraea*). In fact, the null model M_5, which simply ignores the presence of groups, obtained better support (i.e., smaller AIC and BIC values), suggesting that common temporal patterns in $\Delta^{13}C$ were independent of taxonomic affiliation of deciduous oaks. Conversely, the M_1 (compound symmetry) model with heteroscedastic error variances was clearly favoured for $\delta^{18}O$. In this case, the $\delta^{18}O$ signal across years was species dependent, since the magnitude of residual variation (random deviations $f_{ij(r)}$ in Eq. (7)) was distinct for each species. A correction for serial autocorrelation was unnecessary for both isotopes.

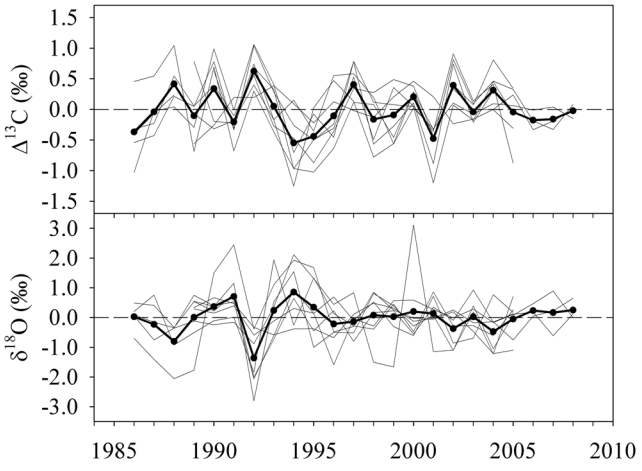

Figure 3. Isotope values indexed (residuals) by linear detrending or by subtracting from the mean of each chronology (above: $\Delta^{13}C$; below: $\delta^{18}O$). Eight chronologies were available: four for *Q. humilis*, three for *Q. petraea* and one for *Q. ilex*. The black line represents the mean chronology.

The alternative, site-based classification of chronologies yielded different results for $\Delta^{13}C$ (Table 3). Here, the M_2 (heterogeneous compound symmetry) model provided the best fit, together with the heteroscedastic M_2 model. We favoured parsimony in the number of VCOV parameters; thus, M_2 was the model of choice. For $\delta^{18}O$, the M_1 heteroscedastic model was again the selected model, being slightly favoured over the M_2 heteroscedastic model (Table 3). The preferred models for both isotopes benefited in this case from site-specific serial autocorrelation corrections, as suggested by decreases in AIC and BIC (results not shown).

Model selection at the spatial level (grouping of trees)

Oaks were grouped into two groups at the site level (deciduous and evergreen). This classification was extended to the total available number of sites (21). As three deciduous species were available, we checked for possible differences in their mean isotopic values (consisting of 20-year pooled tree rings) that could eventually inflate the common signal of trees for this group along the aridity transect. There were no significant differences between species for $\Delta^{13}C$ or $\delta^{18}O$, hence avoiding a correction for shifts in mean isotopic values. Table 4 shows the log-likelihood statistics for VCOV

Table 3. Model comparison for oak chronologies according to AIC and BIC. The model of choice for each grouping and isotope is shown in bold.

Model	$\Delta^{13}C$			$\delta^{18}O$		
	Parameters	AIC	BIC	Parameters	AIC	BIC
		(*smaller is better*)			(*smaller is better*)	
Species grouping						
M_1	3	164.8	168.2	3	362.1	365.5
M_1 (heteroscedastic)	4	166.7	171.3	**4**	**342.9**	**346.3**
M_3	4	164.0	168.6	4	358.2	362.8
M_3 (heteroscedastic)	5	166.0	171.7	5	346.1	351.8
M_4	3	177.6	181.0	3	361.7	365.1
M_4 (heteroscedastic)	4	179.6	184.1	4	349.6	354.2
M_5	**2**	**162.9**	**165.2**	2	360.6	362.8
Site grouping						
M_1	3	138.5	141.9	3	306.9	309.2
M_1 (heteroscedastic)	5	136.1	141.8	**5**	**285.9**	**291.6**
M_2	**5**	**119.5**	**124.0**	5	307.3	312.9
M_2 (heteroscedastic)	7	118.7	125.5	7	286.8	293.6
M_3	7	122.9	129.7	7	305.6	312.4
M_3 (heteroscedastic)	9	123.5	133.7	9	288.9	299.1
M_4	4	135.5	138.9	4	306.0	309.4
M_4 (heteroscedastic)	6	136.0	142.8	6	289.3	296.1
M_5	2	138.2	140.4	2	306.9	309.2

models. The AIC and BIC criteria applied to $\Delta^{13}C$ pointed to M_1 (compound symmetry) as the best explanatory model for differences in signal strength between groups. Although other models seemed also satisfactory (particularly the heteroscedastic M_1), we favoured parsimony in the number of VCOV parameters. In turn, M_4 (banded main diagonal) was the selected model for $\delta^{18}O$, being slightly favoured over M_3 (unstructured; Table 4). This model suggested a lack of relationship (i.e., lack of covariance) between $\delta^{18}O$ signals stored in deciduous and evergreen oaks.

Outcome of mixed models

Restricted maximum likelihood estimates of variance/covariance components under the selected models are given in Table 5. The analysis of temporal signals indicated that a taxonomy-based grouping was inadequate for identifying contrasting changes in $\Delta^{13}C$ of *Q. humilis* and *Q. petraea* over years. Thus, year and residual variances common to all chronologies were estimated (null model M_5). These estimates produced a mean interchronology correlation ($\hat{a}_C$) of 0.44 and an EPS of 0.85. In the case of $\delta^{18}O$, the compound symmetry (M_1) model with heteroscedastic residuals gave a threefold higher residual variance for *Q. petraea* than for *Q. humilis*. Accordingly, *Q. humilis* had substantially higher $\hat{a}_C$ and EPS values than *Q. petraea*, although these values were lower than those for $\Delta^{13}C$. The intergroup mean correlation, $\hat{a}_C$, was higher than the intragroup estimate for *Q. petraea*, which pointed to a weak signal shared by the chronologies of this species.

A site-based grouping of chronologies identified the M_2 (heterogeneous compound symmetry) model, with different

Table 4. Model comparison for spatial records based on taxonomic grouping according to AIC and BIC. The model of choice for each grouping and isotope is shown in bold.

Model	$\Delta^{13}C$			$\delta^{18}O$		
	Parameters	AIC	BIC	Parameters	AIC	BIC
		(*smaller is better*)			(*smaller is better*)	
M_1	**3**	**521.6**	**524.8**	3	423.2	425.4
M_1 (heteroscedastic)	4	520.7	524.9	4	422.9	427.0
M_3	4	523.1	527.2	4	420.9	425.0
M_3 (heteroscedastic)	5	522.5	527.8	5	422.6	427.8
M_4	3	522.6	525.8	**3**	**420.7**	**423.9**
M_4 (heteroscedastic)	4	522.1	526.3	4	422.5	426.7
M_5	2	524.9	526.9	2	454.4	456.5

Table 5. Outcome of mixed-model analyses, including variance/covariance parameters, first-order autocorrelation AC(1) (for annually resolved chronologies) and related statistics: mean interseries correlation ($\hat{a}_C$) or spatial signal strength ($\hat{a}_S$), number of series (Nr) and EPS.

Chronologies	$\Delta^{13}C$						$\delta^{18}O$					
	Variance/ covariance	Residual variance	AC(1)	$\hat{a}_C/\hat{a}_S$	Nr[1]	EPS	Variance/ covariance	Residual variance	AC(1)	$\hat{a}_C/\hat{a}_S$	Nr[1]	EPS
Species grouping												
Q. humilis	0.107	0.136	–	0.439	7 (7)	0.85	0.150	0.323	–	0.317	4 (12)	0.65
Q. petraea							0.150	1.063	–	0.124	3 (>20)	0.30
Q. humilis/*Q. petraea*							0.150			0.198		
Site grouping												
Banyoles, medium altitude (BM)	0.133	0.105	0.308	0.559	2 (5)	0.72	0.092	0.923	–0.211	0.091	2 (>20)	0.17
Banyoles, low altitude (BL)	0.190	0.105	0.308	0.644	2 (4)	0.78	0.092	0.810	0.161	0.102	2 (>20)	0.19
Sant Celoni II (SC)	0.002	0.105	0.308	0.018	2 (>20)	0.04	0.092	0.138	0.213	0.401	2 (9)	0.57
BM/BL	0.159			0.600			0.048			0.050		
BM/SC	0.016			0.100			0.048			0.100		
BL/SC	0.019			0.108			0.048			0.106		
Spatial records												
Quercus spp. (deciduous)	0.215	0.595	–	0.266	5 (16)	0.64	0.191	0.307	–	0.384	5 (9)	0.76
Q. ilex	0.215	0.595	–	0.266	5 (16)	0.64	0.494	0.307	–	0.617	5 (5)	0.89
Quercus spp./*Q. ilex*	0.091			0.112			0			0		

[1]Number of series required to reach EPS ≥ 0.85 is given in parentheses.

variances for each group, as the model of choice for $\Delta^{13}C$. The largest common variance corresponded to the group of chronologies originating from the low-altitude Banyoles site; hence, it provided the highest $\hat{a}_C$ and EPS values (Table 5). Also, the medium-altitude Banyoles site had relatively high $\hat{a}_C$ and EPS values. Chronologies of these sites corresponded to deciduous *Q. humilis* and *Q. petraea* and, in fact, the combined $\hat{a}_C$ of both sites was also very high (0.60), indicating a strong coherence associated with geographical proximity. On the other hand, the synchronicity between chronologies in Sant Celoni II was very weak, in clear disagreement with the Banyoles results. In Sant Celoni II, evergreen (*Q. ilex*) and deciduous (*Q. humilis*) oaks were represented, and genetic differences producing contrasting $\Delta^{13}C$ values could be involved. For $\delta^{18}O$, the compound symmetry (M_1) model with heteroscedastic residuals provided very contrasting residual variances (low for Sant Celoni II, high for Banyoles sites). They translated into very different $\hat{a}_C$ and EPS values, with a relatively high synchronicity between chronologies of Sant Celoni II, an opposite trend to that observed for $\Delta^{13}C$. Overall, signal-strength parameters ($\hat{a}_C$ and EPS) were higher for $\Delta^{13}C$ than for $\delta^{18}O$, regardless of the grouping structure used for estimating VCOV parameters.

The analysis of spatial signals provided REML estimates of variance/covariance parameters, as shown in Table 4. For $\Delta^{13}C$, the compound symmetry M_1 model pointed to a similar signal strength of deciduous and evergreen oaks across sites. However, the site variance was low compared with the residual variance and, therefore, $\hat{a}_S$ values were <0.3. According to dendrochronology standards, about 16 trees per site would be necessary to achieve an EPS of good quality (i.e., ≥0.85), although this parameter should be interpreted flexibly in the context of typifying spatial signals. In any case, the common signal strength between deciduous and evergreen oaks was much weaker ($\hat{a}_S = 0.112$). For $\delta^{18}O$, the narrow evaluation (M_4) model pointed to the lack of a common spatial signal between deciduous and evergreen oaks. Evergreen and deciduous oaks therefore bore totally unrelated information. However, the spatial signal ($\hat{a}_S$) in $\delta^{18}O$ for a given species was higher than that for $\Delta^{13}C$ (particularly for *Q. ilex*), which provided EPS values close to or higher than 0.85.

Relationships with climate

The outcome of the selected VCOV structures provided a guideline for investigating the influence of climate factors on isotope ratios. For $\Delta^{13}C$, the deciduous oak chronologies shared a strong signal that was unrelated to that of *Q. ilex*. Accordingly, the relationships of stable isotopes with climate were assessed separately for these two groups, which showed distinct monthly sensitivities to climate (Figure 4). In particular, maximum temperatures in July were significantly related (negatively) to $\Delta^{13}C$ in deciduous oaks, while a significant negative relationship between $\Delta^{13}C$ and minimum temperatures of November of the previous year was detected for *Q. ilex*. There were also positive relationships between $\Delta^{13}C$ and either June precipitation (for deciduous oaks) or September precipitation (for *Q. ilex*), and negative relationships between $\Delta^{13}C$ and precipitation of both November of the previous year and August (for *Q. ilex*).

For $\delta^{18}O$, the signal shared by *Q. petraea* chronologies was negligible, while Sant Celoni chronologies (*Q. ilex* and *Q. humilis*) on one hand, and *Q. humilis* chronologies from Banyoles sites on the other hand, had relatively high common signals. Based on these results, relationships with climate were assessed separately for the latter two groups only (Figure 4). For Sant Celoni, $\delta^{18}O$ was related (positively) to September temperatures, whereas there was a strong negative relationship between $\delta^{18}O$ and June precipitation for Banyoles.

At the spatial level, mixed modelling reported contrasting patterns of geographical variation for both $\Delta^{13}C$ and $\delta^{18}O$ between evergreen (*Q. ilex*) and deciduous oaks along the aridity transect. Therefore, relationships with temperature and precipitation were obtained independently for each taxonomic group (Figure 5). For $\Delta^{13}C$, *Q. ilex* showed a strong spatial temperature signal, since temperature–$\Delta^{13}C$ associations were positive and mostly significant throughout the year (with the exception of maximum temperature during spring and summer). Also, *Q. ilex* showed positive relationships between $\Delta^{13}C$ and both March and September–October precipitation. Conversely, deciduous oaks were spatially sensitive only to precipitation, with positive relationships with $\Delta^{13}C$ in spring (April–May). For $\delta^{18}O$, *Q. ilex* also showed a strong spatial signal of temperature (especially with maximum temperature), with positive relationships for most of the year (except for winter). Conversely, the deciduous oaks showed a positive (significant) relationship with maximum temperature only for July. *Quercus ilex* also displayed a negative spatial relationship between $\delta^{18}O$ and May precipitation, whereas the deciduous oaks were overall more sensitive to precipitation, with negative relationships with $\delta^{18}O$ in autumn, winter and early spring.

Discussion

Mixed models unravel the complexities of tree-ring signals in stable isotopes

The interpretation of complex temporal patterns in tree-ring records has traditionally relied on the application of the 'mean correlation technique' (Wigley et al. 1984, Briffa and Jones 1990), which uses the mean correlation calculated between all possible pairs of chronologies drawn from a group to quantify their common signal. In turn, between-group signals can be obtained by calculating the mean correlation derived from all possible between-group pairs of chronologies. Examples involving dendro-isotope data can be found in McCarroll and Pawellek (1998), Saurer et al. (2008) and Esper et al. (2010).

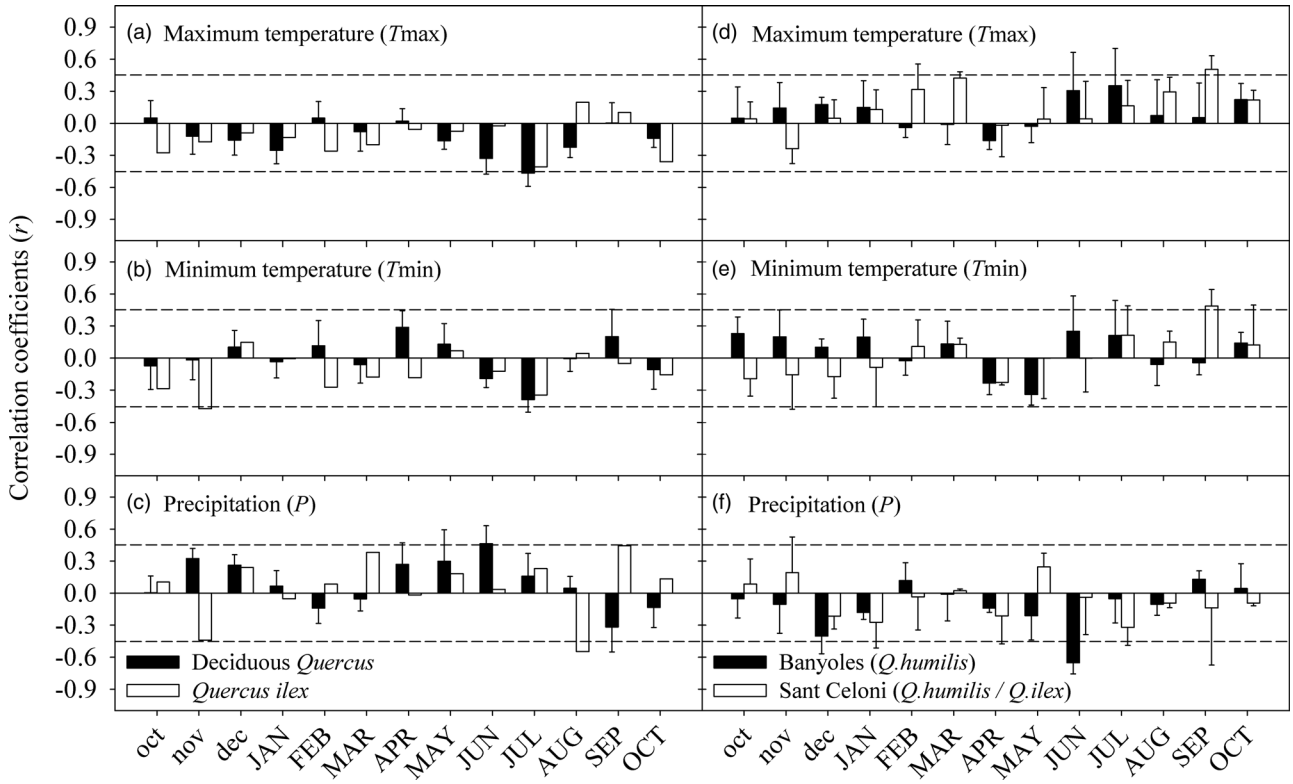

Figure 4. Mean (±SD) correlation coefficients calculated between carbon ($\Delta^{13}C$) (a–c) and oxygen ($\delta^{18}O$) stable isotope chronologies (d–f) and monthly climate variables (maximum and minimum temperature, precipitation). The horizontal lines indicate the threshold for correlations significant at $P \leq 0.05$ ($n = 20$ years). Lower case indicates months of the year prior to tree growth; upper case indicates current-year months. For $\Delta^{13}C$, the number of chronologies involved in the correlation analysis was seven (for deciduous oaks) and one (for *Q. ilex*). For $\delta^{18}O$, the number of chronologies involved in the analysis was three (for *Q. humilis* at Banyoles sites) and two (for *Q. humilis* and *Q. ilex* at the Sant Celoni II site).

Overall, this scheme is roughly equivalent to our unstructured mixed model (M_3) for the variability among years, but other less complex settings may describe the relationships between chronologies more plausibly. In fact, in mixed modelling the model of choice depends on the particular structure and statistical properties of the dataset. This approach of analysing coherence in tree-ring networks can be regarded as complementary to multivariate methods such as principal component or cluster analysis, which allow for the identification of homogeneous subsets of chronologies (Treydte et al. 2007) but without testing on possible processes underlying patterns of signal strength. Conversely, the REML analysis, grounded on the mixed-model theory, allows estimating common signals in tree-ring records by testing for different group and error covariance structures required for characterizing the correlations in the dataset. Another major advantage over multivariate techniques is that mixed modelling is capable of dealing with unbalanced datasets (e.g., partially overlapping chronologies) in a straightforward manner.

Mixed modelling of temporal tree-ring patterns pointed to the suitability of the simple compound symmetry structure (M_1) for explaining variability in $\delta^{18}O$, but only after allowing for heterogeneity of residual variances, either at the species or site level. Conversely, alternative models fitted $\Delta^{13}C$ chronologies better: a heterogeneous compound symmetry structure (M_2) for site-based grouping and the simplest broad evaluation structure (M_5) identified for taxonomy-based grouping. Such an array of selected models highlights the need to understand the complexities in the data in testing and characterizing the nature of common signals shared by a set of chronologies.

The flexibility of mixed models proved equally useful for the investigation of spatial signals stored in tree-ring isotopes. Traditionally, these signals have been considered to be essentially independent among species (Ferrio et al. 2003, Leavitt et al. 2010). Here, the model for independence of $\delta^{18}O$ signals between evergreen and deciduous oaks (M_4) was slightly favoured over alternative variance–covariance structures. This was not the case for $\Delta^{13}C$ records, which showed a common (albeit low) spatial signal shared by both groups, as suggested by the preferred compound symmetry (M_1) model. This contrasting choice of models was somewhat anticipated by the lack of spatial associations observed between $\Delta^{13}C$ and $\delta^{18}O$ at the species level (if the more humid Banyoles sites, where *Q. ilex* was absent, were excluded from the correlation analysis; cf. Figure 2), suggesting that the physiological drivers of carbon and oxygen isotopes did not coincide along the aridity transect.

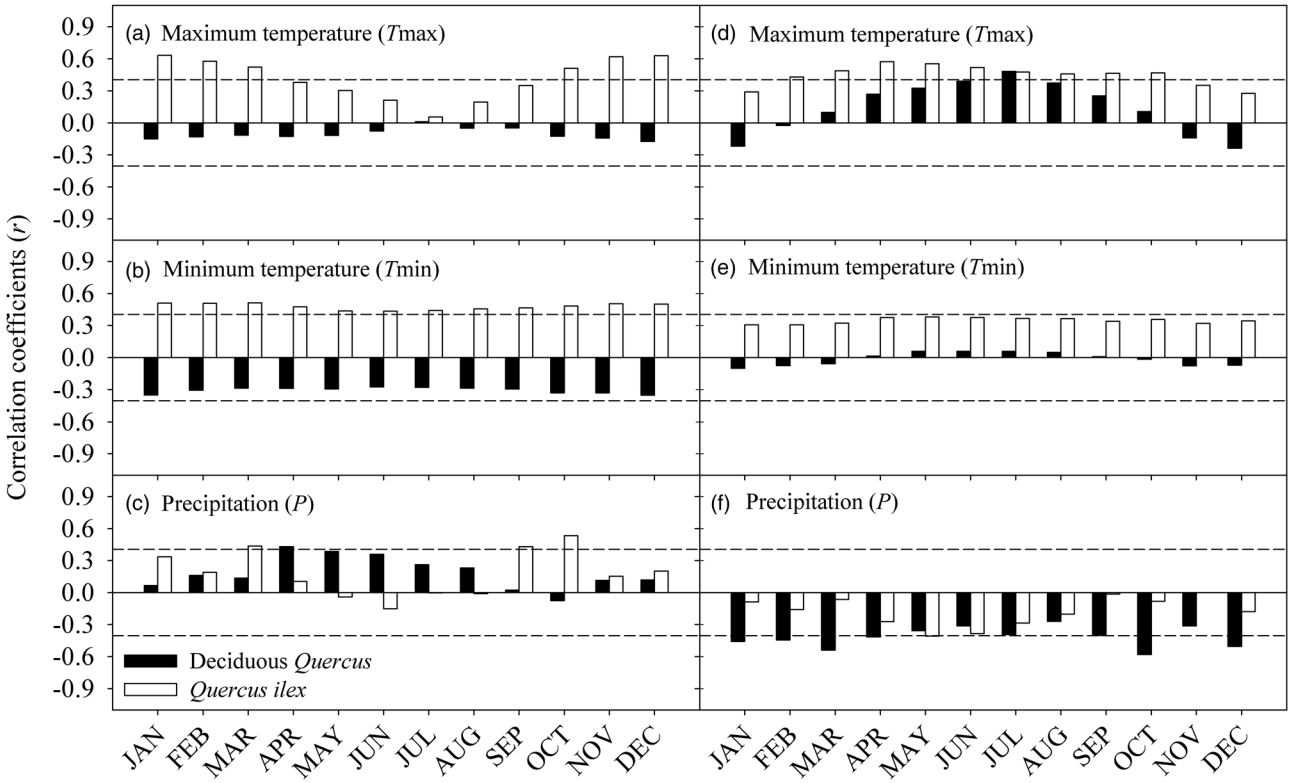

Figure 5. Correlation coefficients calculated between carbon ($\Delta^{13}C$) (a–c) and oxygen ($\delta^{18}O$) spatial records (d–f) and monthly meteorological parameters (maximum and minimum temperature, precipitation). The horizontal lines indicate the threshold for correlations significant at $P \leq 0.05$ ($n = 21$ sites for both deciduous *Quercus* and *Q. ilex*).

Structure and strength of spatiotemporal isotope signals in Mediterranean oaks

The high temporal $\Delta^{13}C$ signal strength for deciduous oaks (the nemoro-Mediterranean *Q. humilis* and the nemoral *Q. petraea*) was the consequence of a strong interannual coherence between chronologies, irrespective of taxonomy or site. In other words, the correlation between chronologies of co-occurring deciduous oaks was similar to the intersite correlation for chronologies of the same or different species. Thus, the combination of chronologies across sites gave EPS values of acceptable statistical quality (0.85; $n = 7$). Similar results have been reported at temperate (Hemming et al. 1998, Saurer et al. 2008) and high-latitude sites (McCarroll and Pawellek 1998) by combining chronologies from different sets of species. Conversely, the only available *Q. ilex* chronology was unrelated to any other chronology, either from the same site or from other sites. This realization points out that Mediterranean deciduous and evergreen oaks constitute two clearly differentiated functional groups, despite co-existing along a wide range of environments (Damesin et al. 1998, Mediavilla and Escudero 2010).

On the contrary, the annually resolved $\delta^{18}O$ chronologies showed much less similarity to each other compared with that for $\Delta^{13}C$, despite the presence of significant (negative) interannual correlations between both isotopes. Nevertheless, both taxonomic (for *Q. humilis*) and site imprints (for Sant Celoni II; the most xeric site with available chronologies) were detected for $\delta^{18}O$, although EPS values were always lower than for $\Delta^{13}C$. Saurer et al. (2008) also reported more robust signals for $\Delta^{13}C$ than for $\delta^{18}O$ across temperate sites from Switzerland. Carbon and oxygen stable isotopes are partially linked through effects at the leaf level that are mediated through variation in stomatal conductance related to moisture conditions (precipitation and relative humidity; Scheidegger et al. 2000). However, different sources and fractionation processes may override, to varying degrees, the presence of co-ordinated isotopic signals (Saurer et al. 2003, Roden and Farquhar 2012). Altogether, these results point to the existence of more complex drivers of temporal $\delta^{18}O$ signals in Mediterranean oaks compared with $\Delta^{13}C$.

In clear contrast to the aforementioned temporal patterns, the examination of spatial signals through mixed modelling indicated a stronger coherence at the species level (i.e., higher $\hat{a}_S$ and EPS statistics) in $\delta^{18}O$ variation between trees across sites compared with $\Delta^{13}C$. This suggests that temporal and spatial variability in external factors (e.g., climate forcing) have a different impact on tree-ring $\Delta^{13}C$ (with higher temporal coherence) and $\delta^{18}O$ (with higher spatial coherence) in either deciduous or evergreen Mediterranean oaks.

In water-limited environments, $\Delta^{13}C$ in tree rings can be mostly explained by the stomatal regulation of CO_2 fluxes into the leaf, integrating any environmental variable related to stomatal conductance (Warren et al. 2001, Ferrio et al. 2003, Gessler et al. 2009). However, it is also affected by changes in photosynthetic activity derived from irradiance, nutritional stresses or phenology when water becomes non-limiting (Yakir and Israeli 1995, Livingston et al. 1998, Ferrio et al. 2003). On the other hand, the signal of $\delta^{18}O$ in tree rings is primarily defined by leaf-level processes, being responsive to stomatal conductance, but not to photosynthetic activity (Farquhar and Lloyd 1993, Yakir and Israeli 1995). Since $\delta^{18}O$ is not sensitive to photosynthetic activity, it has the potential to discriminate between both sources of variation in $\Delta^{13}C$ (Yakir and Israeli 1995, Scheidegger et al. 2000).

However, this dual-isotope model, which has proved to be useful for interpreting tree-ring records, is not always applicable. On one hand, the leaf-level signal of $\delta^{18}O$ responds to variations in relative humidity in a way that is partly independent of stomatal conductance (Roden and Farquhar 2012). On the other hand, the $\delta^{18}O$ of tree-ring cellulose also reflects variability in source water, to a degree that could be variable during the growing season (Offermann et al. 2011, Sarris et al. 2013). The presence of a source-water signature in the $\delta^{18}O$ of wood could explain the strong site-specific signal found in this study (Radoglou 1996, David et al. 2007, Mediavilla and Escudero 2010), but this geographical imprint can be modulated by interspecific differences in water uptake (see, e.g., Moreno-Gutiérrez et al. 2012), as also suggested by the contrasting $\delta^{18}O$ patterns observed between deciduous and evergreen oaks.

Below-ground niche segregation, as a means of reducing competition for water resources, might facilitate the coexistence of evergreen and deciduous oaks, as has been described in other Mediterranean mixed stands (see, e.g., David et al. 2007, Klein et al. 2013), but this possibility needs further examination. Yet, it is somewhat surprising that the relatively low range of intraspecific variation found in $\delta^{18}O$ across sites (<2‰) led to a more consistent spatial signal (i.e., higher $\hat{a}_S$) for both evergreen and deciduous oaks than that associated with $\Delta^{13}C$. In fact, $\Delta^{13}C$ showed a high intraspecific variation across sites, representing a near 20% divergence among extreme sites in intrinsic water-use efficiency (Farquhar and Richards 1984).

Such a relatively low spatial coherence of tree-ring $\Delta^{13}C$ records at the species level does not seem to preclude the use of spatially explicit models of carbon isotope distribution to infer climatic trends (e.g., Leavitt et al. 2007), provided the assumption of a common climatic signal based on customary thresholds (i.e., SNR, EPS) is relaxed. These models have also involved Mediterranean oaks such as the evergreen *Q. ilex* (Aguilera et al. 2009, del Castillo et al. 2013). Overall, spatiotemporal changes in both isotopes seemed strongly dependent on the particular functional imprints of evergreen and deciduous oaks. This is not as clearly observed in temperate regions, where the coherence of spatiotemporal signals seems fairly species independent (e.g., Hemming et al. 1998, Saurer et al. 2012). Altogether, the outcome of the selected VCOV structures suggested investigating the influence of climate factors on stable isotope ratios separately for evergreen and deciduous oaks.

Climate drivers of temporal variation in stable isotopes

The EPS statistic of $\Delta^{13}C$ of deciduous oaks was in the range of previously reported individual chronologies made up of four to six trees (e.g., 0.80–0.90, Gagen et al. 2004; 0.90, Kirdyanov et al. 2008). This result is noteworthy since it was obtained by combining chronologies of limited length (20 years) from different sites and oak species (*Q. humilis* and *Q. petraea*). It suggests a strong climate signal driving changes in $\Delta^{13}C$. In particular, $\Delta^{13}C$ was positively related to precipitation of early summer (June). It is known that the phenological activity of Mediterranean deciduous oaks during summer is almost ceased compared with that of the evergreen *Q. ilex* (Montserrat-Martí et al. 2009). Thus, a rainy late spring–early summer may entail optimal conditions for secondary growth imprinting on tree-ring $\Delta^{13}C$.

Conversely, high temperatures in July are likely to reduce stomatal conductance, leading to a decrease in $\Delta^{13}C$ and increased water-use efficiency. These relationships with climate elements determining water availability agree with the effect of water status on $\Delta^{13}C$ reported for other species in drought-prone environments (Damesin et al. 1997, Warren et al. 2001, Ferrio et al. 2003, Battipaglia et al. 2010). Also, these associations with both precipitation and temperature are in line with the negative correlation between $\delta^{18}O$ and precipitation observed in June, in agreement with earlier works reporting similar relationships for deciduous oaks (Raffalli-Delerce et al. 2004, Loader et al. 2008).

In the present study, the low relative humidity of summer (typical of the Mediterranean climate), linked to low precipitation and high temperatures, would cause an increase in leaf water enrichment, which is not only reflected in $\delta^{18}O$, but also in $\Delta^{13}C$ (Roden et al. 2000, McCarroll and Loader 2004). Altogether, our results confirm the existence of shared temporal responses to climate in two deciduous oaks, *Q. humilis* and *Q. petraea*, which can be found under relatively humid sub-Mediterranean conditions.

On the other hand, climate variables imprinting on $\Delta^{13}C$ for *Q. ilex* were basically unrelated to those for deciduous oaks, with the exception of July temperatures. March precipitation and September precipitation, especially, were associated with high $\Delta^{13}C$. This result indicates a temporal agreement of $\Delta^{13}C$ signals with the bimodal pattern of secondary growth in *Q. ilex*

(Gutiérrez et al. 2011) and the two peaks of precipitation (early spring and early summer) in the western Mediterranean, which supports the dependence of *Q. ilex*, a deep-rooted species with very effective water uptake, on the seasonal recharge of groundwater reservoirs (Ferrio et al. 2003, Aguilera et al. 2009, Klein et al. 2013). In this regard, the imprint of March and September temperatures on $\delta^{18}O$ through leaf water enrichment processes also highlights such a pattern of wood deposition in this species.

The negative association between $\Delta^{13}C$ and August precipitation could be explained by the early restitution of secondary growth in wet but still warm late summers (Gutiérrez et al. 2011), which could imprint wood with low $\Delta^{13}C$ values. Finally, negative associations with precipitation and minimum temperature of November of the previous year might suggest mobilization of carbohydrate reserves synthesized in autumns with very favourable (warm and wet) conditions for tree functioning, one of the most active periods for evergreen oaks (Mediavilla and Escudero 2010, Klein et al. 2013). Indeed, low $\Delta^{13}C$ of current-year wood has been associated with mobilization of previous-year starch reserves (Kozlowski et al. 1991), which are relatively more ^{13}C-enriched than freshly produced assimilates for wood production (Helle and Schleser 2004).

Climate drivers of spatial variation in stable isotopes

The evergreen *Q. ilex* showed a strong spatial dependence on temperature for both isotopes that was linked to the double climate stress typical of Mediterranean environments (summer drought and winter cold). Limitations exerted by low temperatures on the effective vegetative period at cold (i.e., continental) sites are reflected in low $\Delta^{13}C$ values, since trees are obliged to concentrate their photosynthetic activity in warmer and more drought-prone months. Besides, high temperatures associated with high evaporative demand and water stress, especially in spring–summer, are reflected in high $\delta^{18}O$ records. Such a temperature imprint on carbon and oxygen stable isotopes is more clearly observed in the spatial signal recorded along the aridity transect than in the annually resolved chronologies, probably because the latter originate from coastal, mild sites lacking a strong influence of winter cold.

On the other hand, spatial associations with precipitation (basically for $\Delta^{13}C$) were restricted to months of groundwater recharge (autumn and late winter), which again is consistent with the assumption that *Q. ilex* relies mostly on groundwater to thrive in drought-prone environments (Ferrio et al. 2003, Aguilera et al. 2009, Klein et al. 2013). In addition to using groundwater during summer, the strong response to autumn–winter precipitation could be due to the fact that *Q. ilex* can be particularly active during this period, taking advantage of increased water availability, as long as temperatures are still warm (Radoglou 1996, Mediavilla and Escudero 2010, Klein et al. 2013).

Climate drivers of variability in stable isotopes for deciduous oaks were different: they showed more consistent responses to precipitation, not only across the aridity transect, but also at the temporal (interannual) scale (see above). For $\Delta^{13}C$, there was a lagged response to early-season precipitation in deciduous oaks compared with *Q. ilex*, hence reflecting phenological differences in the onset of cambium activity (Liphschitz and Lev-Yadun 1986). For $\delta^{18}O$, a strong negative effect of the amount of soil recharge (autumn and winter) was observed along the transect. This might be associated with partly different strategies of water uptake between deciduous and evergreen oaks, pointing to a stronger reliance on groundwater in deciduous species, since they have fewer alternative mechanisms to cope with drought (Damesin et al. 1998, David et al. 2007). Whereas for deciduous oaks autumn conditions mainly have an indirect effect (through groundwater recharge) on the signature of wood formed in the following year, in the case of evergreen oaks the extension of radial growth over autumn–winter (Gutiérrez et al. 2011) also causes a (direct) response to climate drivers during this period.

Conclusions

This paper provides new information on the ecophysiological performance of Mediterranean oaks using spatiotemporal isotope signals stored in tree rings. Through mixed modelling, we unveiled large differences between deciduous and evergreen *Quercus* species in the organization of their temporal and spatial isotope signals. Climate factors impacted differentially on isotope records at both taxonomic and geographical levels, most likely through contrasting interspecific physiological adaptations and phenotypic plasticity linked to phenology and wood growth (Cherubini et al. 2003, De Micco et al. 2008, Montserrat-Martí et al. 2009).

On one hand, the evergreen *Q. ilex* exhibited a clear spatial dependence of isotopic signals on the temperature regime, likely related to the effective length of its vegetative period in autumn–winter and the incidence of drought in summer. On the other hand, the water and carbon economies of deciduous oaks (*Q. faginea*, *Q. humilis* and *Q. petraea*) showed a more marked dependence on precipitation along the aridity transect, confirming their higher susceptibility to drought in the western Mediterranean. Such contrasting responses to drought among deciduous and evergreen oaks were also observed at an interannual scale, with stronger associations with growing-season water availability in deciduous oaks than in the evergreen *Q. ilex*. The latter, in contrast, was found to rely mainly on the seasonal recharge of groundwater reservoirs. Conversely, the nemoro-Mediterranean *Q. humilis* and the nemoral *Q. petraea* deciduous oaks, co-occurring under relatively humid sub-Mediterranean conditions, shared common temporal responses to climate, showing a similar sensitivity to changes in water availability.

Acknowledgments

The authors acknowledge M. Lucà and P. Sopeña for field and technical assistance.

Conflict of interest

None declared.

Funding

This work was funded by the Spanish projects PALEOISOTREE (CGL2009-13079-C02-01) and RESILFOR (AGL 2012-40039-C02-02). T.A.S. is supported by an ERANET-Mundus fellowship. J.P.F. is supported by the Ramón y Cajal programme (RYC-2008-02050, MCINN, Spain).

References

Aguilera M, Espinar C, Ferrio JP, Pérez G, Voltas J (2009) A map of autumn precipitation for the third millennium BP in the Eastern Iberian Peninsula from charcoal carbon isotopes. J Geochem Explor 102:157–165.

Aguilera M, Ferrio JP, Araus JL, Tarrús J, Voltas J (2011) Climate at the onset of western Mediterranean agriculture expansion: evidence from stable isotopes of sub-fossil oak tree rings in Spain. Palaeogeogr Palaeoclimatol Palaeoecol 299:541–551.

Arend M, Kuster T, Günthardt-Goerg MS, Dobbertin M (2011) Provenance-specific growth responses to drought and air warming in three European oak species (*Quercus robur*, *Q. petraea* and *Q. pubescens*). Tree Physiol 31:287–297.

Barbero M, Loisel R, Quézel P (1992) Biogeography, ecology and history of Mediterranean *Quercus ilex* ecosystems. Vegetatio 99–100:19–34.

Barnett AG, Koper N, Dobson AJ, Schmiegelow F, Manseau M (2010) Using information criteria to select the correct variance–covariance structure for longitudinal data in ecology. Methods Ecol Evol 1: 15–24.

Battipaglia G, De Micco V, Brand WA, Linke P, Aronne G, Saurer M, Cherubini P (2010) Variations of vessel diameter and delta ^{13}C in false rings of *Arbutus unedo* L. reflect different environmental conditions. New Phytol 188:1099–1112.

Briffa KR, Jones PD (1990) Basic chronology statistics and assessment. In: Cook ER, Kairiukstis LA (eds) Methods of dendrochronology: applications in the environmental sciences. Kluwer Academic Publisher, Dordrecht, pp 137–152.

Burnham KP, Anderson DR (eds) (2002) Model selection and multimodel inference: a practical information-theoretic approach. Springer, New York.

Cherubini P, Gartner BL, Tognetti R, Bräker OU, Schoch W, Innes JL (2003) Identification, measurement and interpretation of tree rings in woody species from Mediterranean climates. Biol Rev 78:119–148.

Corcuera L, Camarero JJ, Gil-Pelegrín E (2002) Functional groups in *Quercus* species derived from the analysis of pressure–volume curves. Trees 16:465–472.

Damesin C, Rambal S, Joffre R (1997) Between-tree variations in leaf $\delta^{13}C$ of *Quercus pubescens* and *Quercus ilex* among Mediterranean habitats with different water availability. Oecologia 111:26–35.

Damesin C, Rambal S, Joffre R (1998) Co-occurrence of trees with different leaf habit: a functional approach on Mediterranean oaks. Acta Oecol 19:195–204.

David TS, Henriques MO, Kurz-Besson C et al. (2007) Water-use strategies in two co-occurring Mediterranean evergreen oaks: surviving the summer drought. Tree Physiol 27:793–803.

De Micco V, Aronne G, Baas P (2008) Wood anatomy and hydraulic architecture of stems and twigs of some Mediterranean trees and shrubs along a mesic-xeric gradient. Trees 22:643–655.

del Castillo J, Aguilera M, Voltas J, Ferrio JP (2013) Isoscapes of tree-ring carbon-13 perform like meteorological networks in predicting regional precipitation patterns. J Geophys Res 118:352–360.

Demidenko E (2004) Mixed models: theory and applications. John Wiley & Sons, New York.

Epron D, Dreyer E (1990) Stomatal and non-stomatal limitation of photosynthesis by leaf water deficits in 3 oak species—a comparison of gas-exchange and chlorophyll a fluorescence data. Ann Sci For 47:435–450.

Esper J, Frank DC, Battipaglia G, Büntgen U, Holert C, Treydte K, Siegwolf R, Saurer M (2010) Low-frequency noise in $\delta^{13}C$ and $\delta^{18}O$ tree-ring data: a case study of *Pinus uncinata* in the Spanish Pyrenees. Glob Biogeochem Cycle 24:GB4018.

Farquhar GD, Lloyd J (1993) Carbon and oxygen isotope effects in the exchange of carbon dioxide between terrestrial plants and the atmosphere. In: Ehleringer JR, Hall AE, Farquhar GD (eds) Stable isotopes and plant carbon–water relations. Academic Press, Inc., San Diego, pp 47–70.

Farquhar GD, Richards RA (1984) Isotopic composition of plant carbon correlates with water-use efficiency of wheat genotypes. Aust J Plant Physiol 11:539–552.

Ferrio JP, Voltas J (2005) Carbon and oxygen isotope ratios in wood constituents of *Pinus halepensis* as indicators of precipitation, temperature and vapour pressure deficit. Tellus B 57:164–173.

Ferrio JP, Florit A, Vega A, Serrano L, Voltas J (2003) $\Delta^{13}C$ and tree-ring width reflect different drought responses in *Quercus ilex* and *Pinus halepensis*. Oecologia 137:512–518.

Ferrio JP, Araus JL, Buxó R, Voltas J, Bort J (2005) Water management practices and climate in ancient agriculture: inferences from the stable isotope composition of archaeobotanical remains. Veget Hist Archaeobot 14:510–517.

Fritts HC (ed) (1976) Tree rings and climate. Academic Press, London.

Gagen M, McCarrol D, Edouard JL (2004) Latewood width, maximum density, and stable carbon isotope ratios of pine as climate indicators in a dry subalpine environment, French Alps. Arct Antarct Alp Res 36:166–171.

Gagen M, McCarroll D, Robertson I, Loader NJ, Jalkanen R (2008) Do tree-ring $\delta^{13}C$ series from *Pinus sylvestris* in northern Fennoscandia contain long-term non-climatic trends? Chem Geol 252:42–51.

Gandullo JM (ed) (1994) Climatología y ciencia del suelo. Fundación Conde del Valle de Salazar, Madrid.

Gessler A, Brandes E, Buchmann N, Helle G, Rennenberg H, Barnard RL (2009) Tracing carbon and oxygen isotope signals from newly assimilated sugars in the leaves to the tree-ring archive. Plant Cell Environ 32:780–795.

Gutiérrez E, Campelo F, Camarero JJ, Ribas M, Muntán E, Nabais C, Freitas H (2011) Climate controls act at different scales on the seasonal pattern of *Quercus ilex* L. stem radial increments in NE Spain. Trees 25:637–646.

Helle G, Schleser GH (2004) Beyond CO_2-fixation by Rubisco: an interpretation of $^{13}C/^{12}C$ variations in tree rings from novel intra-seasonal studies on broad-leaf trees. Plant Cell Environ 27:367–380.

Hemming DL, Switsur VR, Waterhouse JS, Heaton THE, Carter AHC (1998) Climate variation and the stable carbon isotope composition

of tree-ring cellulose: an intercomparison of *Quercus robur*, *Fagus sylvatica* and *Pinus silvestris*. Tellus B 50:25–33.

Holmes RL (1983) Computer-assisted quality control in tree-ring dating and measurement. Tree Ring Bull 43:69–78.

Jennrich RI, Schluchter MD (1986) Unbalanced repeated-measures models with structured covariance matrices. Biometrics 42:805–820.

Juárez-López FJ, Escuder A, Mediavilla S (2008) Ontogenetic changes in stomatal and biochemical limitations to photosynthesis of two co-occurring Mediterranean oaks differing in leaf life span. Tree Physiol 28:367–374.

Kirdyanov AV, Treydte KS, Nikolaev A, Helle G, Schleser GH (2008) Climate signals in tree-ring width, density and $\delta^{13}C$ from larches in Eastern Siberia (Russia). Chem Geol 252:31–41.

Kish L (1965) Sampling organizations and groups of unequal sizes. Am Sociol Rev 30:564–572.

Klein T, Shpringer I, Fikler B, Elbaz G, Cohen S, Yakir D (2013) Relationships between stomatal regulation, water-use, and water-use efficiency of two coexisting key Mediterranean tree species. For Ecol Manag 302:34–42.

Kozlowski TT, Kramer PJ, Pallardy SG (eds) (1991) The physiological ecology of woody plants. Academic Press, San Diego.

Lapointe-Garant MP, Huang JG, Gea-Izquierdo G, Raulier F, Bernier P, Berninger F (2010) Use of tree rings to study the effect of climate change on trembling aspen in Québec. Glob Change Biol 16:2039–2051.

Larcher W (2000) Temperature stress and survival ability of Mediterranean sclerophyllous plants. Plant Biosyst 134:279–295.

Leavitt SW, Danzer SR (1993) Method for batch processing small wood samples to holocellulose for stable-carbon isotope analysis. Anal Chem 65:87–88.

Leavitt SW, Chase TN, Rajagopalan B, Lee E, Lawrence PJ, Woodhouse CA (2007) Southwestern US drought maps from pinyon tree-ring carbon isotopes. Eos Trans AGU 88:39–40.

Leavitt SW, Treydte K, Yu L (2010) Environment in time and space: opportunities from tree-ring isotope networks. In: West JB, Bowen GJ, Dawson TE, Tu KP (eds) Isoscapes: understanding movement, pattern, and process on earth through isotope mapping. Springer, Dordrecht, pp 113–135.

Li Q, Nakatsuka T, Kawamura K, Liu Y, Song H (2011) Regional hydroclimate and precipitation $\delta^{18}O$ revealed in tree-ring cellulose $\delta^{18}O$ from different tree species in semi-arid Northern China. Chem Geol 282:19–28.

Linares JC, Tiscar PA (2011) Buffered climate change effects in a Mediterranean pine species: range limit implications from a tree-ring study. Oecologia 167:847–859.

Liphschitz N, Lev-Yadun S (1986) Cambial activity of evergreen and seasonal dimorphics around the Mediterranean. IAWA Bull 7:145–153.

Little RJA, Rubin DB (eds) (2002) Statistical analysis with missing data. John Wiley & Sons, New York.

Livingston NJ, Whitehead D, Kelliher FM, Wang YP, Grace JC, Walcroft AS, Byers JN, Mcseveny TM, Millard P (1998) Nitrogen allocation and carbon isotope fractionation in relation to intercepted radiation and position in a young *Pinus radiata* D. Don tree. Plant Cell Environ 21:795–803.

Loader NJ, Robertson I, Barker AC, Switsur VR, Waterhouse JS (1997) An improved technique for the batch processing of small whole-wood samples to α-cellulose. Chem Geol 136:313–317.

Loader NJ, Santillo PM, Woodman-Ralph JP et al. (2008) Multiple stable isotopes from oak trees in southwestern Scotland and the potential for stable isotope dendroclimatology in maritime climatic regions. Chem Geol 252:62–71.

Loidi J, Herrera M (1990) The *Quercus pubescens* and *Quercus faginea* forests in the Basque Country (Spain): distribution and typology in relation to climatic factors. Vegetatio 90:81–92.

Martínez-Vilalta J, López BC, Adell N, Badiella L, Ninyerola M (2008) Twentieth century increase of Scots pine radial growth in NE Spain shows strong climate interactions. Glob Change Biol 14:2868–2881.

McCarroll D, Loader NJ (2004) Stable isotopes in tree rings. Quaternary Sci Rev 23:771–801.

McCarroll D, Pawellek F (1998) Stable carbon isotope ratios of late-wood cellulose in *Pinus sylvestris* from northern Finland: variability and signal-strength. Holocene 8:675–684.

McCarroll D, Pawellek F (2001) Stable carbon isotope ratios of *Pinus sylvestris* from northern Finland and the potential for extracting a climate signal from long Fennoscandian chronologies. Holocene 11:517–526.

Mediavilla S, Escudero A (2010) Differences in biomass allocation patterns between saplings of two co-occurring Mediterranean oaks as reflecting different strategies in the use of light and water. Eur J For Res 129:697–706.

Mitrakos K (1980) A theory for Mediterranean plant-life. Acta Oecol Oec Plant 15:245–252.

Montserrat-Martí G, Camarero JJ, Palacio S, Pérez-Rontomé C, Milla R, Albuixech J, Maestro M (2009) Summer-drought constrains the phenology and growth of two coexisting Mediterranean oaks with contrasting leaf habit: implications for their persistence and reproduction. Trees 23:787–799.

Moreno-Gutiérrez C, Dawson TE, Nicolás E, Querejeta JI (2012) Isotopes reveal contrasting water use strategies among coexisting plant species in a Mediterranean ecosystem. New Phytol 196:489–496.

Ninyerola M, Pons X, Roure JM (eds) (2005) Atlas climático digital de la Península Ibérica. Metodología y aplicaciones en bioclimatología y geobotánica. Universitat Autónoma de Barcelona, Bellaterra.

Offermann C, Ferrio JP, Holst J, Grote R, Siegwolf R, Kayler Z, Gessler A (2011) The long way down—are carbon and oxygen isotope signals in the tree ring uncoupled from canopy physiological processes? Tree Physiol 31:1088–1102.

Radoglou K (1996) Environmental control of CO_2 assimilation rates and stomatal conductance in five oak species growing under field conditions in Greece. Ann Sci For 53:269–278.

Raffalli-Delerce G, Masson-Delmotte V, Dupouey JL, Stievenard M, Breda N, Moisselin JM (2004) Reconstruction of summer droughts using tree-ring cellulose isotopes: a calibration study with living oaks from Brittany (western France). Tellus B 56:160–174.

Raftery AE (1996) Approximate Bayes factors and accounting for model uncertainty in generalised linear models. Biometrika 83:251–266.

Richards MB, Lamont BB (1996) Post-fire mortality and water relations of three congeneric shrub species under extreme water stress—a trade-off with fecundity? Oecologia 107:53–60.

Rivas-Martínez S (1982) Etages bioclimatiques, secteurs chorologiques et séries de végétation de l'Espagne méditerranéenne. Ecol Mediterr 8:275–288.

Roden JS, Farquhar GD (2012) A controlled test of the dual-isotope approach for the interpretation of stable carbon and oxygen isotope ratio variation in tree rings. Tree Physiol 32:490–503.

Roden JS, Lin GG, Ehleringer JR (2000) A mechanistic model for interpretation of hydrogen and oxygen isotope ratios in tree-ring cellulose. Geochim Cosmochim Acta 64:21–35.

Rodó X, Baert E, Comin FA (1997) Variations in seasonal rainfall in Southern Europe during the present century: relationships with the North Atlantic oscillation and the El Niño-southern oscillation. Clim Dynam 13:275–284.

Sánchez de Dios R, Benito-Garzón M, Sainz-Ollero H (2009) Present and future extension of the Iberian submediterranean territories as determined from the distribution of marcescent oaks. Plant Ecol 204:189–205.

Sarris D, Siegwolf R, Koerner C (2013) Inter- and intra-annual stable carbon and oxygen isotope signals in response to drought in Mediterranean pines. Agric For Meteorol 168:59–68.

Saurer M, Cherubini P, Bonani G, Siegwolf R (2003) Tracing carbon uptake from a natural CO_2 spring into tree rings: an isotope approach. Tree Physiol 23:997–1004.

Saurer M, Cherubini P, Reynolds-Henne CE, Treydte KS, Anderson WT, Siegwolf RTW (2008) An investigation of the common signal in tree ring stable isotope chronologies at temperate sites. J Geophys Res 113:G04035.

Saurer M, Kress A, Leuenberger M, Rinne KT, Treydte KS, Siegwolf RTW (2012) Influence of atmospheric circulation patterns on the oxygen isotope ratio of tree rings in the Alpine region. J Geophys Res 117:D05118.

Scheidegger Y, Saurer M, Bahn M, Siegwolf R (2000) Linking stable oxygen and carbon isotopes with stomatal conductance and photosynthetic capacity: a conceptual model. Oecologia 125:350–357.

Terradas J, Savé R (1992) The influence of summer and winter stress and water relationships on the distribution of *Quercus ilex* L. Vegetatio 99–100:137–145.

Tognetti R, Longobucco A, Raschi A (1998) Vulnerability of xylem to embolism in relation to plant hydraulic resistance in *Quercus pubescens* and *Quercus ilex* co-occurring in a Mediterranean coppice stand in central Italy. New Phytol 139:437–447.

Treydte K, Frank D, Esper J et al. (2007) Signal strength and climate calibration of a European tree-ring isotope network. Geophys Res Lett 34:L24302.

Warren CR, McGrath JF, Adams MA (2001) Water availability and carbon isotope discrimination in conifers. Oecologia 127:476–486.

Wigley TML, Briffa KR, Jones PD (1984) On the average value of correlated time series with applications in dendroclimatology and hydrometeorology. J Clim Appl Meteor 23:201–213.

Yakir D, Israeli Y (1995) Reduced solar irradiance effects on net primary productivity (NPP) and the $\delta^{13}C$ and $\delta^{18}O$ values in plantations of *Musa* sp., Musaceae. Geochim Cosmochim Acta 59:2149–2151.

Forests synchronize their growth in contrasting Eurasian regions in response to climate warming

Tatiana A. Shestakova[a], Emilia Gutiérrez[a], Alexander V. Kirdyanov[b,c], Jesús Julio Camarero[d], Mar Génova[e], Anastasia A. Knorre[b], Juan Carlos Linares[f], Víctor Resco de Dios[g], Raúl Sánchez-Salguero[f], and Jordi Voltas[g,1]

[a]Department of Ecology, University of Barcelona, E-08028 Barcelona, Spain; [b]Sukachev Institute of Forest, 660036 Krasnoyarsk, Russia; [c]Math Methods and IT Department, Siberian Federal University, 660041 Krasnoyarsk, Russia; [d]Pyrenean Institute of Ecology, E-50059 Zaragoza, Spain; [e]Department of Natural Systems and Resources, Technical University of Madrid, E-28040 Madrid, Spain; [f]Department of Physical, Chemical, and Natural Systems, Pablo de Olavide University, E-41013 Sevilla, Spain; and [g]Department of Crop and Forest Sciences and Agrotecnio Center, University of Lleida, E-25198 Lleida, Spain

Edited by William H. Schlesinger, Cary Institute of Ecosystem Studies, Millbrook, NY, and approved December 9, 2015 (received for review July 25, 2015)

Forests play a key role in the carbon balance of terrestrial ecosystems. One of the main uncertainties in global change predictions lies in how the spatiotemporal dynamics of forest productivity will be affected by climate warming. Here we show an increasing influence of climate on the spatial variability of tree growth during the last 120 y, ultimately leading to unprecedented temporal coherence in ring-width records over wide geographical scales (spatial synchrony). Synchrony in growth patterns across cold-constrained (central Siberia) and drought-constrained (Spain) Eurasian conifer forests have peaked in the early 21st century at subcontinental scales (~1,000 km). Such enhanced synchrony is similar to that observed in trees co-occurring within a stand. In boreal forests, the combined effects of recent warming and increasing intensity of climate extremes are enhancing synchrony through an earlier start of wood formation and a stronger impact of year-to-year fluctuations of growing-season temperatures on growth. In Mediterranean forests, the impact of warming on synchrony is related mainly to an advanced onset of growth and the strengthening of drought-induced growth limitations. Spatial patterns of enhanced synchrony represent early warning signals of climate change impacts on forest ecosystems at subcontinental scales.

tree rings | spatial synchrony | global warming | boreal forests | Mediterranean forests

Understanding how climate change affects forests across multiple spatiotemporal scales is important for anticipating its impacts on terrestrial ecosystems. Increases in atmospheric CO_2 concentration and shifts in phenology (1–3) could favor tree growth by enhancing photosynthesis and extending the effective growing period, respectively (4). Conversely, recent warming could increase respiration rates and, together with increasing heat and drought stresses, exert negative impacts on forest productivity (5, 6). Given the uncertainty as to what extent enhanced carbon uptake could be offset by the detrimental effects of warming on tree performance, the actual consequences of climate change on forest carbon cycling remain under debate. Notably, climate change has a stronger impact on forests constrained by climatic stressors, such as suboptimal temperatures or water shortage (7). As high-resolution repositories of biological responses to the environment, dendrochronological archives can be used to monitor this impact (8).

The concept of spatial synchrony in tree growth refers to the extent of coincident changes in ring-width patterns among geographically disjunct tree populations (9). Climatic restrictions tend to strengthen growth–climate relationships, resulting in enhanced common ring-width signals (i.e., more synchronous tree growth). Thus, regional bioclimatic patterns can be delineated by identifying groups of trees whose growth is synchronously driven by certain climatic constraints (10, 11). Previous synthesis studies have provided evidence for globally coherent multispecies responses to climate change in natural systems, including forests, with a focus on the role of increasingly warmer temperatures (12, 13). Indeed, climate has changed markedly over the last decades, prompting an array of physiological reactions in trees that could strengthen growth–climate relationships, thereby enhancing spatial synchrony. Such tree responses may be linked to global shifts in the timing of plant activity (2), drought stress in mid-latitudes (6, 14), or an uncoupling of air and soil thermal regimes in the early growing season (15) and direct heat stress (16) in high latitudes, among other factors. Changing tree growth patterns associated with enhanced synchrony in response to warming have been reported at small geographical scales (<150 km) (14–18, but see ref. 19); however, an extended examination of synchrony patterns is currently lacking for large (i.e., subcontinental) areas.

To determine whether climate warming and increased variability (1) lead to more synchronous tree growth, we examined changes in spatial synchrony over the last 120 y across subcontinental areas by using a comprehensive network of 93 ring-width chronologies from six different conifer species across two climatically contrasting Eurasian biomes: boreal forests in central Siberia (n = 45 chronologies) and Mediterranean forests in Spain (n = 48 chronologies) (*SI Appendix*, Fig. S1 and Table S1). Central Siberia has a severe continental climate with a prolonged cold season, large intra-annual temperature variations, and moderate precipitation. Spain is dominated by a typical Mediterranean climate, with mild (coast) to cool (inland) wet winters and summer droughts. Thus, temperature exerts the main climatic control over productivity in boreal forests, whereas Mediterranean forests are primarily water-limited (*SI Appendix*, section 1A).

Temporal changes in spatial synchrony (hereinafter, $\hat{a}_C$) are quantified using a novel mixed model framework (20). This methodology has two fundamental advantages for dendroscience (21) over other alternative approaches useful for interpreting population dynamics in ecology (22) or patterns of environmental

Significance

Forests dominate carbon fluxes in terrestrial ecosystems. We demonstrate how an intensified climatic influence on tree growth during the last 120 y has increased spatial synchrony in annual ring-width patterns within contrasting (boreal and Mediterranean) Eurasian biomes and on broad spatial scales. Current trends in tree growth synchrony are related to regional changes in climate factors controlling productivity, overriding local and taxonomic imprints on forest carbon dynamics. Enhanced synchrony is becoming a widespread, although regionally dependent, phenomenon related to warmer springs and increased temperature variability in high latitudes and to warmer winters and drier growing seasons in mid-latitudes.

Author contributions: T.A.S., E.G., and J.V. designed research; T.A.S. and J.V. performed research; E.G., A.V.K., J.J.C., M.G., A.A.K., J.C.L., and R.S.-S. contributed data; T.A.S. and J.V. analyzed data; and T.A.S., E.G., A.V.K., J.J.C., M.G., A.A.K., J.C.L., V.R.d.D., R.S.-S., and J.V. wrote the paper.

The authors declare no conflict of interest.

This article is a PNAS Direct Submission.

[1]To whom correspondence should be addressed. Email: jvoltas@pvcf.udl.cat.

This article contains supporting information online at www.pnas.org/lookup/suppl/doi:10.1073/pnas.1514717113/-/DCSupplemental.

synchrony (23): (*i*) it is capable of dealing with partially overlapping chronologies, yielding valid inferences of spatial synchrony for large areas in which ring-width data are available but covering different time periods, and (*ii*) it is highly flexible to fit general statistical structures for subdivided groups of chronologies, opening new avenues for interpreting complex spatial patterns through geographic or taxonomic stratification of a target region.

We hypothesized that climate warming (1) triggers more synchronous tree growth at subcontinental scales owing to an amplified climatic control of growth, e.g., through higher temperatures in Siberia and decreased water availability in Spain. Our objective was to interpret forest reactions to warming through an alternative approach to model-based assessment or field experimentation. Specifically, this study asked the following questions: (*i*) is spatial synchrony of tree growth increasing across terrestrial biomes and if so, at what pace?; (*ii*) how are synchrony patterns related to intraspecific and interspecific responses to climate warming?; and (*iii*) what are the main climate factors underlying more synchronous forest growth? In ecological theory, it is widely accepted that spatial synchrony influences metapopulation persistence and the likelihood of species extinction (24). As forests are becoming more prone to widespread mortality (25), interpreting long-term synchrony patterns of tree growth may be relevant to identifying broad-scale threshold responses to climate change.

Results and Discussion

Increases in Synchrony and Absolute Growth Trends: Regional Patterns. Synchrony trends show that $\hat{a}_C$ has increased during the period 1890–2009 in both study regions (Fig. 1 *A* and *B*), but at a twofold higher pace in Siberia than in Spain (b = 0.002 y^{-1} vs. 0.001 y^{-1}). Whereas the increasing trend is steady over time for Spain, $\hat{a}_C$ has experienced larger fluctuations for Siberia, with an abrupt rise observed in the last three decades. Overall, $\hat{a}_C$ values were significantly higher after 1950 compared with the first half of the 20th century (P = 0.002 for Siberia and P < 0.001 for Spain, one-tailed Student's t-test), reaching unmatched values after the 1970s in both regions.

Notably, peaks in spatial synchrony were reached in the early 21st century (Fig. 1 *A* and *B*). This finding suggests a progressive influence of external forcing mechanisms impacting tree performance through vast geographical areas and overriding local drivers of growth (e.g., topography, nutrient availability, tree competition, management). Regional forest synchrony is currently reaching values comparable to the mean synchrony between co-occurring trees within a stand (mean ± SE, Spain: $\hat{a}_C$ = 0.28 ± 0.06 [region] vs. 0.40 ± 0.13 [stand]; Siberia: $\hat{a}_C$ = 0.47 ± 0.07 [region] vs. 0.49 ± 0.10 [stand]). The lower mean $\hat{a}_C$ in Spain over the study period (0.21 ± 0.02 vs. 0.32 ± 0.03 in Siberia) contrasts with the lower average distance between stands in Spain compared with Siberia (mean ± SD, 346 ± 195 km vs. 575 ± 331 km) (*SI Appendix*, Fig. S1). In any case, synchrony patterns in Siberia and Spain are statistically independent (*SI Appendix*, Tables S2 and S3), indicating that the increasing synchrony in tree growth is a widespread ecological phenomenon, although regionally dependent. Synchrony estimates could be sensitive to the number of available chronologies, a number that has decreased progressively in the most recent years (*SI Appendix*, Table S1); however, there is a close agreement in $\hat{a}_C$ between the complete set of chronologies and a subset that extends beyond the year 2000 (Siberia, r = 0.90; Spain, r = 0.87; P < 0.001 in both cases). An analysis of anomalously wide or narrow rings (i.e., "pointer years"), originating from extreme external events (26), is in agreement with the absolute peaks in synchrony seen in both regions at the turn of this century (*SI Appendix*, section 2A and Fig. S2).

To further explore how increasing synchrony is related to regional growth patterns, we used raw ring-width records and assessed shifts in growth rates over time. We noted differential paces of tree growth in Siberia and Spain for the period 1890–2009. A clear growth slowdown was seen in Spain (b = –0.00024 mm y^{-2}), but no significant trend appeared in Siberia (Fig. 1 *C* and *D*). Such temporal changes could be affected by variations in the population age/size structure (mean ± SD chronology length, 303 ± 82 y for Siberia and 247 ± 129 y for Spain). To check for age-independent growth declines, we assessed growth dynamics only for old-growth forest stands (>200 y old; n = 43 chronologies for Siberia, n = 30 chronologies for Spain). This approach minimizes the temporary dynamics associated with stand development and succession. We observed a good agreement when comparing the results from this subset with the growth patterns found for the complete dataset (r = 0.99, P < 0.001 for Siberia; r = 0.87, P < 0.001 for Spain; slowdown for Spain, b = –0.00014 mm y^{-2}), indicating that age-dependent declines cannot explain temporal changes in growth. The growth reduction in Mediterranean forests may be caused by increasing water limitations (6), but the lack of a positive growth response to warming in boreal forests is puzzling. Various hypotheses have been proposed to explain this phenomenon (27), but temperature-induced drought or direct heat stress are plausible constraints of forest productivity in high latitudes (16).

Increases in Synchrony and Absolute Growth Trends: Taxonomic Patterns. At the species level, $\hat{a}_C$ values peaked at the turn of this century in most cases (Fig. 2). Overall, species-specific changes in synchrony were in good agreement with regional trends, although *Larix gmelinii* in Siberia and *Pinus sylvestris* in Spain exhibited less obvious (but also significant) increments in $\hat{a}_C$ over the past 120 y. Notably, the spatial synchrony between pairs of species also increased with time (Fig. 2); however, $\hat{a}_C$ values across species pairs tended to be lower than those for individual species, indicating that although interspecific variability in growth responses certainly exists and is important (e.g., deciduous vs. evergreen conifers in Siberia), the

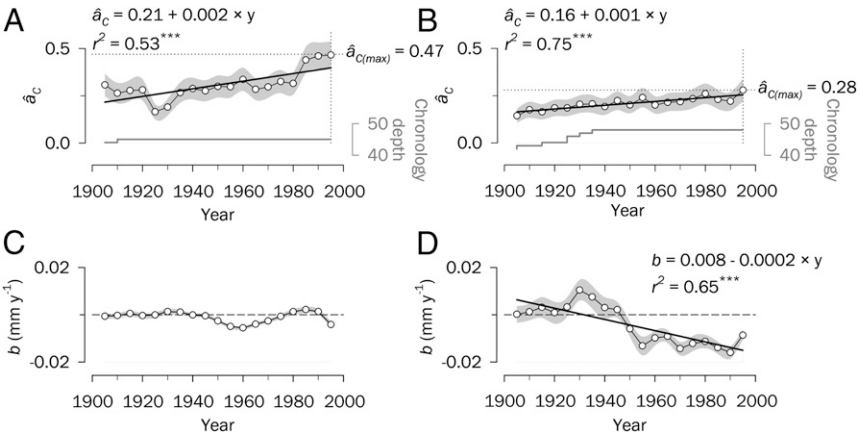

Fig. 1. Synchrony patterns and changes in absolute growth for the period 1890–2009. (*A* and *B*) Spatial synchrony, $\hat{a}_C$, estimated for central Siberia (*A*) and Spain (*B*) using ring-width chronologies for successive 30-y periods lagged by 5 y. The dotted lines indicate $\hat{a}_C$ maxima over the study period. Gray lines represent the number of chronologies with an EPS > 0.85 (i.e., chronology depth). (*C* and *D*) Temporal trends in the slope (b) of growth in central Siberia (*C*) and Spain (*D*) estimated based on raw ring-width data for the same time intervals used for synchrony. The dashed lines indicate no change in growth rate over the study period. Significant linear trends over time are depicted as black lines (***P < 0.001). Shaded areas denote SEs. Values on the x-axes correspond to the middle years of 30-y moving intervals.

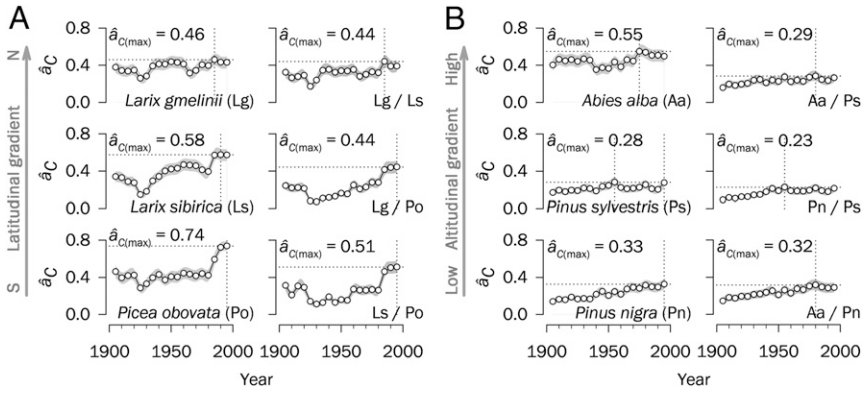

Fig. 2. Temporal trends in spatial synchrony for single and paired species for central Siberia (*A*) and Spain (*B*). Synchrony estimates ($\hat{a}_C$) in single species (first and third columns) and species pairs (second and fourth columns) are calculated based on ring-width chronologies using successive 30-y periods lagged by 5 y. The dotted lines indicate $\hat{a}_C$ maxima over the study period in each case. SEs are shown as shaded areas. Values on the *x*-axes correspond to the middle years of 30-y moving intervals.

strength of these interspecific differences is diminishing with time, resulting in more synchronous tree growth.

Boreal forests in Siberia, limited mainly by low temperatures (15, 16), show high synchrony irrespective of species. In contrast, the primarily water-limited forests in Spain (14, 19) have lower synchrony. It is likely that temperature exerts a greater influence than precipitation on the spatial signals imprinted in tree rings (10), owing to the greater spatial homogeneity of temperature in Siberia compared with the more complex rainfall pattern countrywide in Spain (*SI Appendix*, Fig. S3). In fact, *Abies alba* has the largest $\hat{a}_C$ among the three Spanish species, which could be explained by its limited spatial distribution and narrow niche amplitude at mesic sites in northeastern Spain (mean ± SD distance between stands, 124 ± 68 km) (*SI Appendix*, Fig. S1).

To further test for spatial consistency in synchrony patterns (22), we examined how the correlations between pairs of chronologies vary with distance among forest stands. The spatial synchrony spreads over distances >900 km in Siberia and >600 km in Spain (*SI Appendix*, Fig. S3). More importantly, synchrony was higher in the second half of the 20th century than in the first half for all species and regions at most distances (*SI Appendix*, Fig. S4). The intercept (but not the slope) of the linear relationship between *r* values and distances increased for all evergreen conifers. *Larix* spp. demonstrated significant slope changes, indicating that greater synchrony occurred after 1950 than before 1950 proportionally with distance. Taken together, our results suggest that external forcing factors superimpose on species-specific and local controls, triggering more synchronous tree growth.

We also investigated shifts in absolute growth trends over time at the species level (*SI Appendix*, Fig. S5). We found a growth slowdown for all species in Spain, but a steady growth rate in Siberia. Notably, growth fluctuations in Siberia became more consistent across species after the 1950s (mean correlation of growth trends between pairs of species before 1950, $r = -0.41$; after 1950, $r = 0.53$). A gradual growth decline in Spain, reflecting increasingly limiting conditions over time, and a more systematic pattern of growth changes in Siberia from 1950 onward seems to concur with the rise in synchrony observed at different regional paces (sustained in Spain, abrupt in the last decades in Siberia) over the last 120 y.

Processes Driving Increases in Synchrony. Increases in synchrony are usually attributed to the influence of climate on tree growth, given that no other environmental driver is likely to act on the same range in time and space (8); however, other global drivers also might trigger the observed increase in synchrony through their effect on growth. First, increasing atmospheric CO_2 concentrations can be expected to augment water use efficiency, thereby boosting forest productivity (4). Second, nitrogen deposition could further increase growth through higher rates of carbon sequestration in sites with unfertile or poorly developed soils (28). Third, a decrease in solar radiation caused by anthropogenic aerosol emissions from 1950 (global dimming; ref. 29) may counteract the effect of CO_2 fertilization or rising N deposition, negatively impacting photosynthesis, especially in high latitudes (30). Fourth, changes in stand structure due to rural abandonment, limited forest management, and encroachment usually increase competition for resources and could reduce tree growth (31). A detailed examination of these drivers (*SI Appendix*, section 2B) led us to discard them as major causes of growth synchrony as opposed to climate.

We then examined whether enhanced synchrony is driven by regional climate trends. Although the Earth's surface has experienced conspicuous warming in the last century, the pace of temperature changes differs regionally (1). Interestingly, the steady increase in synchrony among Spanish forests seems in line with the gradual warming observed over the 20th century. In turn, temperatures at high Eurasian latitudes have shown a consistent upward trend since the 1970s, which coincides with the steep increase in synchrony observed in Siberia (*SI Appendix*, Fig. S6).

Our analyses of climatic factors causing changes in growth and of climate drivers underlying $\hat{a}_C$ fluctuations were restricted to data collected after 1930, in concert with the availability of reliable instrumental records (32). Despite species-specific ecological features, the main climate variables related to growth were regionally consistent across taxa (Fig. 3). As expected, we found strong positive associations between growth and June–July temperatures in Siberia (i.e., cold-limited growth) (15, 33) and between May–July precipitation and the Standardized Precipitation Evapotranspiration Index (SPEI) in Spain (i.e., drought-constrained growth) (19). Moreover, growth was correlated with early spring (April) temperatures in Siberia (negatively) and with late winter (February) temperatures in Spain (positively) (Fig. 3). Such contrasting regional responses to temperature in the early growing season may be a consequence of varying physiological processes underlying the mechanisms of dormancy breaking. After chilling requirements are met in winter, cambial reactivation can occur earlier in Siberia under higher April temperatures (34), hastening the onset of xylogenesis (35); however, newly formed tissues can be damaged if followed by severe frosts (33), causing hydraulic dysfunction (i.e., freeze–thaw events) (36). A warm spring also may activate the photosynthetic machinery in crowns that are functionally uncoupled from roots (35), and sudden early-spring temperature drops may impair photosynthesis in boreal evergreen conifers (37). These mechanisms may restrict radial growth in high latitudes (38). In contrast, in Mediterranean environments, early cambial reactivation triggered by warm winters usually increases carbon uptake and enhances wood formation (39).

We characterized the spatial structures of these growth–climate relationships through cross-correlation analyses. The spatial association was significant for most climate factors at sites >900 km apart in Siberia and >600 km apart in Spain (*SI Appendix*, Fig. S7), confirming the existence of consistent subcontinental forest responses to climate (11). This result identifies

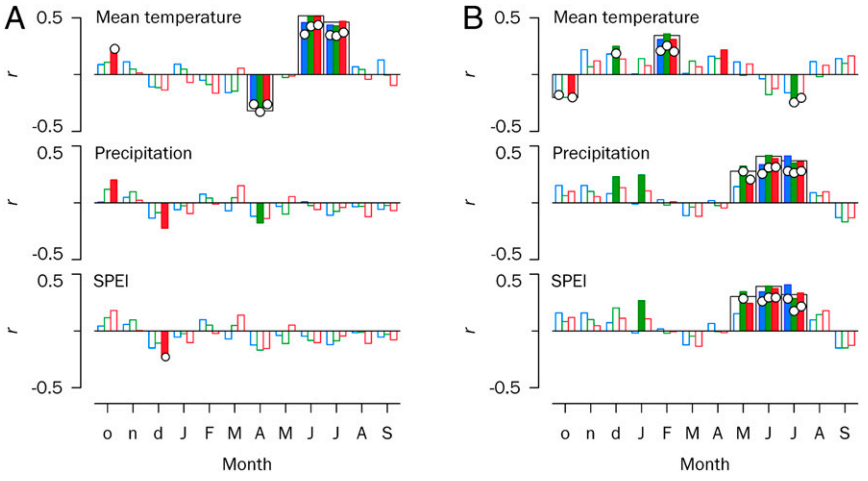

Fig. 3. Growth–climate relationships at the species and regional levels for central Siberia (*A*) and Spain (*B*). Tree growth responses to climate are based on bootstrapped correlations (indicated by bars) and response function partial regression coefficients between tree-ring indices for species or regions and monthly mean temperature, precipitation, and SPEI for 1930–2009. Significant correlation and partial regression coefficients ($P < 0.05$) are indicated by filled bars and white circles, respectively. Species are represented in blue (*Larix gmelinii*, *Abies alba*), green (*Larix sibirica*, *Pinus nigra*), and red (*Picea obovata*, *Pinus sylvestris*). Wide bars denote significant relationships at the regional level. Lowercase and uppercase letters on the *x*-axes correspond to the years before and during tree-ring formation, respectively.

climate as a primary mechanism of synchrony in our tree-ring network, and suggests that increases in forest synchrony could be driven by concomitant increases in regional climate synchrony. We found that this actually was not the case, however (*SI Appendix*, section 2C and Fig. S8).

Alternatively, we evaluated whether enhanced synchrony is related to climate trends and variability. For this purpose, we first assessed regional changes in growth–climate relationships through moving correlations. Most relevant changes span the period from the onset of the growing season through early summer, matching the period of early wood formation. For Siberia, the negative dependence of growth on warmer April temperature increased over time (Fig. 4*A*); for Spain, high February temperatures and high May–June precipitation and SPEI became more important for growth (Fig. 5). In this regard, we found that $\hat{a}_C$ values were significantly associated with the correlation coefficients of the varying relationship between growth and early growing season temperature. Notably, this association was negative for April in Siberia (Fig. 4*A*) and positive for February in Spain (Fig. 5), indicating divergent regional growth dynamics. In both cases, we interpret this result as a sign of earlier cambial reactivation promoting more synchronous growth over time.

Rising temperatures may induce earlier cambial reactivation (40), resulting in both a higher rate of xylem cell production and a longer duration of cambial growth, which in principle should increase ring width (41). This was not the case for Siberia, however, where an earlier onset of cambial activity may be associated with an increased risk of frost damage to the cambium (40). In this region, tree growth has remained limited by low summer temperatures (Fig. 4*A* and *SI Appendix*, Fig. S9), exerting growth desynchronization in June (Fig. 4*A*), but this constraint has decreased after the 1970s because of the positive warming trend (*SI Appendix*, Fig. S6). This effect is counterbalanced by a reinforcement of the negative impact of high April temperatures on growth as a driver of synchrony (Fig. 4*A*). In Spain we also observed a diminishing growth dependence on July precipitation and SPEI (*SI Appendix*, Fig. S10) (19), which suggests reduced cambial activity in summer (36) in response to warming-induced drought (*SI Appendix*, Fig. S11) and a growth shift toward spring (May–June) (Fig. 5), thereby enhancing synchrony.

Synchrony patterns might not be linked exclusively to long-term climate trends, but also to changes in climate extremes over time (26), as suggested by the reported independence of spatial correlations of record-breaking monthly temperature time series from those of the temperatures themselves (42). In general, significant linear trends in climate variability (i.e., standard deviations of monthly climate factors; *SI Appendix*, Fig. S11) were observed for relevant growth periods (Fig. 3). We found that a more synchronous growth pattern in Siberia was related to a larger temperature variability in April and June (Fig. 4*B*), but not in peak summer (July) (*SI Appendix*, Fig. S9). In contrast, climate variability was unrelated to changes in synchrony in Spain (*SI Appendix*, Fig. S10).

Finally, we explored the complementarity of climate trends and variability in explaining regional synchrony through stepwise linear regression (Table 1). Initially, the impact of climate trends on synchrony was considered using the subset of monthly climate factors whose temporal relationships with growth exhibit a significant association with $\hat{a}_C$ values (Figs. 4*A* and 5). These models provide a good explanation of synchrony changes (especially for Spain), identifying recent warming as a significant driver of synchrony across the studied Eurasian forests; however, when climate variability is also considered (Fig. 4*B*), the model fitting is further improved in Siberia, up to r^2 values similar to those for Spain. In fact, climate variability for April and June in Siberia and climate trends for February temperature and June water availability (precipitation and SPEI) in Spain explain 75% of the observed regional synchrony patterns. Unraveling the exact effects of climate warming and extremes on forest synchrony would require both a greater spatial saturation of site chronologies and more detailed instrumental records covering large geographic areas.

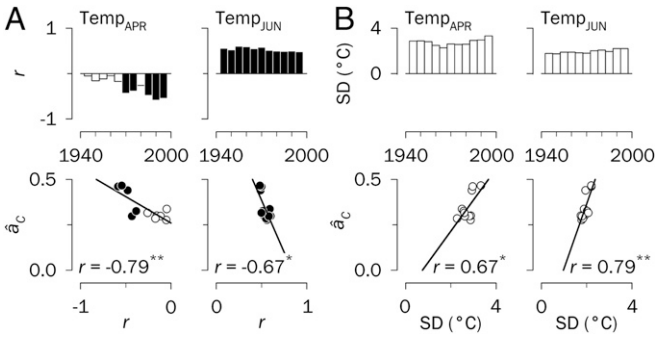

Fig. 4. Climate factors underlying changes in synchrony in central Siberia, 1930–2009. (*Upper*) Moving correlation analyses (*r* values) between regional tree-ring indices and April and June mean temperatures (Temp) (*A*) and standard deviations (SD) of April and June mean temperatures (*B*) displayed in bar diagrams for successive 30-y periods lagged by 5 y. Significant correlations are indicated by filled bars in *A* ($P < 0.05$). (*Lower*) Relationships between synchrony estimates ($\hat{a}_C$) and *r* values (*A*) and SD of climate variables (*B*) presented in scatterplots. Only monthly climate factors significantly correlated with $\hat{a}_C$ are displayed (*$P < 0.05$; **$P < 0.01$). The filled circles correspond to the periods with significant growth–climate relationships, as indicated by the moving correlation analyses. Years displayed on the *x*-axes correspond to the middle years of 30-y moving intervals.

Table 1. Multiple linear stepwise regressions explaining synchrony ($\hat{a}_C$) patterns from changing growth–climate relationships (correlation coefficients; *r*) and climate variability (standard deviations of climate factors; *SD*) over 1930–2009

Synchrony	Initial variable	Initial r^2	Initial MSE	Final stepwise model	Final r^2	Final MSE
Siberia	*Correlation with climate factors* ($r\text{Temp}_{APR}$, $r\text{Temp}_{JUN}$)					
	$r\text{Temp}_{APR}$	0.63**	0.020	$\hat{a}_C = 0.26 - 0.29\ r\text{Temp}_{APR}$	0.63**	0.020
	Correlation with climate factors and variability ($r\text{Temp}_{APR}$, $r\text{Temp}_{JUN}$, $SD\text{Temp}_{APR}$, $SD\text{Temp}_{JUN}$)					
	$SD\text{Temp}_{JUN}$	0.63**	0.020	$\hat{a}_C = -0.47 + 0.28\ SD\text{Temp}_{JUN} + 0.10\ SD\text{Temp}_{APR}$	0.75***	0.013
Spain	*Correlation with climate factors* ($r\text{Temp}_{FEB}$, $r\text{Prec}_{MAY}$, $r\text{Prec}_{JUN}$, $r\text{SPEI}_{MAY}$, $r\text{SPEI}_{JUN}$)					
	$r\text{SPEI}_{JUN}$	0.43*	0.003	$\hat{a}_C = 0.18 + 1.03\ r\text{SPEI}_{JUN} - 0.93\ r\text{Prec}_{JUN} + 0.08\ r\text{Temp}_{FEB}$	0.75***	0.002

Codes for the variables are as in Figs. 4 and 5 (*Upper*) for Siberia and Spain, respectively. MSE, mean squared error.
*$P < 0.05$; **$P < 0.01$; ***$P < 0.001$.

This study illustrates how early signals of climate change impacts on forests can be traced back through the interpretation of synchrony patterns stored in tree rings. Here we demonstrate that climate change is modulating spatial synchrony in forest growth over disparate Eurasian regions, increasing the strength of the common signal shared by trees under warmer conditions to levels comparable to the mean synchrony between co-occurring trees within a stand. Even reporting on different *Pinaceae*, including evergreen and deciduous conifers, our results are consistent across species. The mechanisms behind this pattern require further examination, but they seem to be dependent on the increasing importance of regional-scale climate signals in tree rings overriding local growth drivers. The observed enhanced synchrony may anticipate declines in tree vigor and growth that are critical for the functioning and maintenance of forest ecosystem services under a warmer future climate.

Materials and Methods

Tree-Ring Indices and Absolute Growth Trends. Site chronologies of tree-ring indices were obtained by cross-dating the tree-ring width (TRW) series (*SI Appendix*, section 1B) and posterior detrending and autocorrelation removal with the Friedman supersmoother spline and autoregressive modeling (43). This procedure eliminates the juvenile growth trend and generates stationary (mean = 1) and residual TRW chronologies of dimensionless indices that preserve a common variance encompassing interannual time scales (high-frequency variability potentially related to climate). The adequacy of sample size for capturing the hypothetical population signal was assessed by the expressed population signal (EPS), with a threshold value of 0.85 used to identify the "critical year" at which the site chronology became reliable (44). The study period was 1890–2009, i.e., the period when the impact of climate change on tree performance became noticeable (45). The common time spans across chronologies were 1924–1990 in central Siberia and 1950–1988 in Spain.

Temporal trends in tree growth were characterized by the estimation of growth rate changes using raw TRW records. To this end, the slope of the linear regression of TRW on time was calculated for each chronology for successive 30-y periods lagged by 5 y. The slopes were then averaged for a particular region (or species) and for each period, and a simple linear function was fitted after visual inspection. The slope of this function was interpreted as rate of regional (species) growth change. Comparison of growth rates between regions (species) was performed through ANOVA heterogeneity of slopes.

Mixed Modeling. To investigate spatial synchrony patterns in indexed chronologies, we made extensive use of variance-covariance (VCOV) mixed modeling (20) (*SI Appendix*, section 1C). To this end, chronologies were grouped into potentially homogeneous subsets (20). First, two groups were formed corresponding to each region. Next, chronologies were classified at the regional level into three groups according to membership in a particular species. A number of VCOV models accommodating between- and within-group variability were tested (*SI Appendix*, section 1C) and compared using Akaike and Bayesian information criteria, which favor parsimonious models (46). Then estimates of spatial synchrony (or mean interchronology correlation, $\hat{a}_C$) were derived for chronologies belonging to either the same region (species) or different regions (pairs of species) through the best VCOV model (*SI Appendix*, section 1D and Tables S2 and S3). The parameter $\hat{a}_C$ is related to the mean interseries correlation defined at the intrasite level in dendroscience (44). In both cases, VCOV structures were tested for successive 30-y segments lagged by 5 y. The 30-y duration was established by plotting the SE of $\hat{a}_C$ against segments of varying duration (from 10 to 50 y) for each region. The segment length corresponding to the inflection point of the curves was selected as a balance between number of years and precision achieved (*SI Appendix*, Fig. S12).

Development of Regional and Species Master Chronologies. We estimated TRW indices at the regional and species levels by best linear unbiased prediction (BLUP), thus obtaining regional and species master chronologies underlying the network of site chronologies (*SI Appendix*, section 1E). BLUP estimates were derived from the best VCOV model fitted to the whole study period using either a regional or a species classification as grouping criterion. BLUPs were used as input for climate analysis.

Spatial Patterns in Synchrony. To assess how far the spatial patterns in forest synchrony extend, we calculated the geographical distance between pairs of chronologies, which were used (*i*) to obtain correlograms (47) testing for significant correlations between chronologies located within ranges of 300 km apart (*SI Appendix*, section 1F) and (*ii*) to regress correlations between

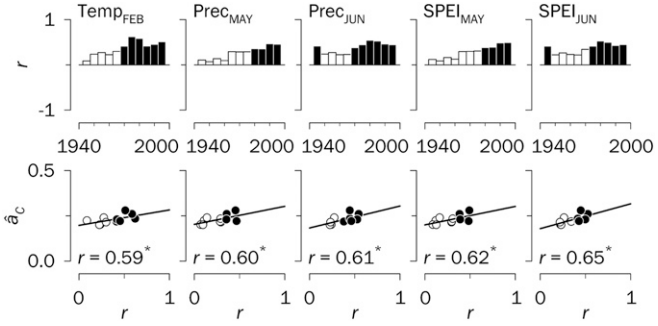

Fig. 5. Climate factors underlying changes in synchrony in Spain, 1930–2009. (*Upper*) Moving correlation analyses (*r* values) between regional tree-ring indices and February mean temperatures (Temp), and May and June precipitation (Prec) and SPEI in May and June displayed in bar diagrams for successive 30-y periods lagged by 5 y. (*Lower*) Relationships between synchrony estimates ($\hat{a}_C$) and *r* values presented in scatterplots. More details are provided in Fig. 4.

pairs of chronologies on distances. The linear regressions were calculated at the species level for the periods 1890–1949 and 1950–2009, and their slopes were tested through ANOVA heterogeneity of slopes. Regression slopes were interpreted as indicators of spatial synchrony.

Relationships with Climate. We quantified the effects of temperature, precipitation, and SPEI (48) on the interannual variability of TRW indices through bootstrapping correlations and response function analyses (8) relating regional and species master chronologies to monthly climatic data (*SI Appendix*, section 1G). We analyzed growth–climate relationships from the previous October to the current September, i.e., the year of tree-ring formation. In addition, we obtained correlograms for temperature and precipitation testing for significant correlations between sites located within 300 km apart (*SI Appendix*, section 1F) (47). We also performed cross-correlation analyses to test for causality of synchrony patterns in relevant climate factors as drivers of forest synchrony over progressively larger distances (*SI Appendix*, section 1F) (47).

We assessed the influence of climate change on regional synchrony through a two-step procedure. First, we performed a moving correlation analysis involving regional chronologies and monthly climate factors for successive 30-y periods lagged by 5 y and then related changes in temporal dependence of growth on climate (i.e., r values of the moving correlation analysis) to variations in $\hat{a}_C$ over time through simple correlations. Second, we examined a possible role of climate variability in explaining changes in synchrony. To this end, we calculated the SD for monthly climate factors of successive 30-y periods lagged by 5 y. We also investigated the relationships between the SD of climate variables and $\hat{a}_C$ through simple correlations. The analyses of both climate trends and variability determining synchrony was restricted to the subset of climate factors showing a significant impact on growth for the entire period 1930–2009, as a prerequisite for identifying climate drivers of $\hat{a}_C$ fluctuations. To determine the predictive ability of climate factors and their variability on the explanation of synchrony patterns, we built linear stepwise models at the regional level using the r values of the moving correlation analysis (step 1) and the SD changes over time (step 2) as independent variables, with a threshold value of $P = 0.15$ as the criterion for the inclusion or removal of variables.

ACKNOWLEDGMENTS. T.A.S. is supported by ERANET-MUNDUS (Euro-Russian Academic Network-Mundus) (European Commission). V.R.d.D. is supported by the Ramón y Cajal Program (Contract RYC-2012-10970). Support for this work was provided by European Union projects ForMAT (Sensitivity of tree growth to climate change and growth modelling from past to future) (Contract ENV4-CT97-0641), ISONET (400 years of annual reconstructions of European climate variability using a high resolution isotopic network) (Contract EV K2-2001-00237), and MILLENNIUM (European climate of the last millennium) (Contract GOCE 017008); the Russian Science Foundation (Project 14-14-00295); the Catalan Government (Project 2014 SGR 1141); Studying Tree Responses to Extreme Events: A Synthesis (STReESS) COST (European Cooperation in Science and Technology) Action FP1106; and Spanish Projects CGL2011-26654 and CGL2013-48843-C2-1-R (Spanish Ministry of Economy and Competitiveness).

1. Intergovernmental Panel on Climate Change (2013) *Climate Change 2013: The Physical Science Basis. Contribution of Working Group I to the Fifth Assessment Report of the Intergovernmental Panel on Climate Change*, eds Stocker TF, et al. (Cambridge Univ Press, Cambridge, UK).
2. Menzel A, et al. (2006) European phenological response to climate change matches the warming pattern. *Glob Change Biol* 12:1969–1976.
3. Reyes-Fox M, et al. (2014) Elevated CO_2 further lengthens growing season under warming conditions. *Nature* 510(7504):259–262.
4. McMahon SM, Parker GG, Miller DR (2010) Evidence for a recent increase in forest growth. *Proc Natl Acad Sci USA* 107(8):3611–3615.
5. Silva LCR, Anand M, Leithead MD (2010) Recent widespread tree growth decline despite increasing atmospheric CO_2. *PLoS One* 5(7):e11543.
6. Williams AP, et al. (2013) Temperature as a potent driver of regional forest drought stress and tree mortality. *Nat Clim Chang* 3:292–297.
7. Hampe A, Petit RJ (2005) Conserving biodiversity under climate change: The rear edge matters. *Ecol Lett* 8(5):461–467.
8. Fritts HC (2001) *Tree Rings and Climate* (Blackburn Press, Caldwell, NJ).
9. Liebhold A, Koenig WD, Bjørnstad ON (2004) Spatial synchrony in population dynamics. *Annu Rev Ecol Evol Syst* 35:467–490.
10. Wettstein JJ, Littell JS, Wallace JM, Gedalof Z (2011) Coherent region-, species-, and frequency-dependent local climate signals in Northern Hemisphere tree-ring widths. *J Climate* 24:5998–6012.
11. Babst F, et al. (2013) Site- and species-specific responses of forest growth to climate across the European continent. *Glob Ecol Biogeogr* 22:706–717.
12. Walther G-R, et al. (2002) Ecological responses to recent climate change. *Nature* 416(6879):389–395.
13. Parmesan C, Yohe G (2003) A globally coherent fingerprint of climate change impacts across natural systems. *Nature* 421(6918):37–42.
14. Macias M, Andreu L, Bosch O, Camarero JJ, Gutiérrez E (2006) Increasing aridity is enhancing silver fir (*Abies alba* Mill.) water stress in its southwestern distribution limit. *Clim Change* 79:289–313.
15. Vaganov EA, Hughes MK, Kirdyanov AV, Schweingruber FH, Silkin PP (1999) Influence of snowfall and melt timing on tree growth in subarctic Eurasia. *Nature* 400:149–151.
16. Lloyd AH, Bunn AG (2007) Responses of the circumpolar boreal forest to 20th century climate variability. *Environ Res Lett* 2:045013.
17. Latte N, Lebourgeois F, Claessens H (2015) Increased tree-growth synchronization of beech (*Fagus sylvatica* L.) in response to climate change in northwestern Europe. *Dendrochronologia* 33:69–77.
18. Tardif J, Camarero JJ, Ribas M, Gutiérrez E (2003) Spatiotemporal variability in tree growth in the central Pyrenees: Climatic and site influences. *Ecol Monogr* 73:241–257.
19. Andreu L, et al. (2007) Climate increases regional tree growth variability in Iberian pine forests. *Glob Change Biol* 13:804–815.
20. Shestakova TA, Aguilera M, Ferrio JP, Gutiérrez E, Voltas J (2014) Unravelling spatiotemporal tree-ring signals in Mediterranean oaks: A variance-covariance modelling approach of carbon and oxygen isotope ratios. *Tree Physiol* 34(8):819–838.
21. Little RJA, Rubin DB (2002) *Statistical Analysis with Missing Data* (Wiley, New York).
22. Koenig WD, Knops JMH (1998) Scale of mast-seeding and tree-ring growth. *Nature* 396:225–226.
23. Jones PD, Osborn TJ, Briffa KR (1997) Estimating sampling errors in large-scale temperature averages. *J Climate* 10:2548–2568.
24. Earn DJD, Levin SA, Rohani P (2000) Coherence and conservation. *Science* 290(5495): 1360–1364.
25. Allen CD, Breshears DD, McDowell NG (2015) On underestimation of global vulnerability to tree mortality and forest die-off from hotter drought in the Anthropocene. *Ecosphere* 6:129.
26. Babst F, Carrer M, Urbinati C, Neuwirth B, Frank D (2012) 500 years of regional forest growth variability and links to climatic extreme events in Europe. *Environ Res Lett* 7:1–11.
27. D'Arrigo R, Wilson R, Liepert B, Cherubini P (2008) On the "divergence problem" in northern forests: A review of the tree ring evidence and possible causes. *Global Planet Change* 60:289–305.
28. Thomas RQ, Canham CD, Weathers KC, Goodale CL (2010) Increased tree carbon storage in response to nitrogen deposition in the US. *Nat Geosci* 3:13–17.
29. Liepert B (2002) Observed reductions of surface solar radiation at sites in the United States and worldwide from 1961 to 1990. *Geophys Res Lett* 29:1421.
30. Stine AR, Huybers P (2014) Arctic tree rings as recorders of variations in light availability. *Nat Commun* 5:3836.
31. Linares JC, Camarero JJ, Carreira JA (2010) Competition modulates the adaptation capacity of forests to climatic stress: Insights from recent growth decline and death in relict stands of the Mediterranean fir *Abies pinsapo*. *J Ecol* 98:592–603.
32. Esper J, et al. (2010) Trends and uncertainties in Siberian indicators of 20th century warming. *Glob Change Biol* 16:386–398.
33. Knorre AA, Kirdyanov AV, Vaganov EA (2006) Climatically induced interannual variability in aboveground production in forest-tundra and northern taiga of central Siberia. *Oecologia* 147(1):86–95.
34. Oquist G, Huner NP (2003) Photosynthesis of overwintering evergreen plants. *Annu Rev Plant Biol* 54:329–355.
35. Linkosalo T (1999) Regularities and patterns in the spring phenology of some boreal trees. *Silva Fenn* 33:237–245.
36. Voltas J, et al. (2013) A retrospective, dual-isotope approach reveals individual predispositions to winter drought-induced tree dieback in the southernmost distribution limit of Scots pine. *Plant Cell Environ* 36(8):1435–1448.
37. Heide OM (1993) Day length and thermal time responses of bud burst during dormancy release in some northern deciduous trees. *Physiol Plant* 88:531–540.
38. Panyushkina IP, Vaganov EA, Shishov VV (1996) Spatial-temporal variation of radial tree growth in relation to climate in the north of middle Siberia. *Dendrochronologia* 14:115–126.
39. Bigelow SW, Papaik MJ, Caum C, North MP (2014) Faster growth in warmer winters for large trees in a Mediterranean-climate ecosystem. *Clim Change* 123:215–224.
40. Begum S, Nakaba S, Yamagishi Y, Oribe Y, Funada R (2013) Regulation of cambial activity in relation to environmental conditions: Understanding the role of temperature in wood formation of trees. *Physiol Plant* 147(1):46–54.
41. Rossi S, Girard MJ, Morin H (2014) Lengthening of the duration of xylogenesis engenders disproportionate increases in xylem production. *Glob Change Biol* 20(7):2261–2271.
42. Kostinski A, Anderson A (2014) Spatial patterns of record-setting temperatures. *J Environ Stat* 6:1–13.
43. Friedman JH (1984) *A Variable Span Smoother* (Stanford University, Stanford, CA), Laboratory for Computational Statistics Technical Report 5.
44. Wigley TML, Briffa KR, Jones PD (1984) On the average value of correlated time series, with applications in dendroclimatology and hydrometerology. *J Clim Appl Meteorol* 23:201–213.
45. Pretzsch H, Biber P, Schütze G, Uhl E, Rötzer T (2014) Forest stand growth dynamics in Central Europe have accelerated since 1870. *Nat Commun* 5:4967.
46. Burnham KP, Anderson DR (2002) *Model Selection and Multi-Model Inference: A Practical Information-Theoretic Approach* (Springer, New York).
47. Koenig WD, Knops JMH (1998) Testing for spatial autocorrelation in ecological studies. *Ecography* 21:423–429.
48. Vicente-Serrano SM, Beguería S, López-Moreno JI (2010) A multi-scalar drought index sensitive to global warming: The Standardized Precipitation Evapotranspiration Index. *J Climate* 23:1696–1718.

SUPPORTING INFORMATION (SI Appendix)

Forests synchronize their growth in contrasting Eurasian regions in response to climate warming

Tatiana A. Shestakova, Emilia Gutiérrez, Alexander V. Kirdyanov, Jesús Julio Camarero, Mar Génova, Anastasia A. Knorre, Juan Carlos Linares, Víctor Resco de Dios, Raúl Sánchez-Salguero, and Jordi Voltas

SUPPLEMENTARY TEXT

1. Materials and Methods

A: Study area

The main environmental factors differentiating central Siberia (Russia) and Spain are temperature and moisture regimes. Central Siberia has a severe continental climate with a prolonged cold season, a large difference between summer and winter temperatures, and a moderate precipitation. Spain is dominated by a typical Mediterranean climate with mild (coast) to cool (inland) wet winters and a summer drought. Tree species occurring in the Mediterranean are adapted to varying degrees to reduced water availability during the growing period (particularly in summer), and tree growth at high latitudes in Eurasia is mainly limited by low temperatures and a very short vegetative period in summer.

The central Siberian region is located in the permafrost zone of the northwestern part of the Central Siberian Plateau (Krasnoyarsk krai, Russia) and extends from the Lower Tunguska River in the south upwards along a latitudinal gradient to the North Siberian Lowland in the north (61°33'–72°30'N, 84°30'–104°15'E) (Fig. S1). It covers an approximate area of 700,000 km^2. The landscape is diverse, with low-altitude plains and high mountain ranges (e.g. the Putorana mountains), and undergoes frequent extreme weather fluctuations. The average annual temperature for the region is –9.9°C, with January being the coldest (–31.1°C) and July the warmest month (+14.0°C) (reference period: 1930 to 2009, CRU TS3.10 dataset; 1). Following a latitudinal gradient, the transition to above-zero mean daily temperatures takes usually place during the second half of May, and to below-zero temperatures from late September through mid-October. The snow cover is formed at this period and lies in the region for about eight months. The mean annual precipitation is 450 mm, with about 40% occurring during summer (June to August) as rain events. The vegetation types can be classified according to three latitudinal subzones that follow a north to south temperature gradient (forest-tundra, northern taiga and middle taiga), with conifers as dominant tree species (2). *Larix gmelinii* is the northernmost conifer species of the region, while *Larix sibirica* and *Picea obovata* can be mainly found in the southern and western parts of the study area. The study sites, as representative of most forest trees growing in the region, range in elevation from 10 to 590 m a.s.l.

Sites located in Spain embrace mainly the southern and northern edges of the Iberian Peninsula, although some additional sites from the Spanish central plateau are also included (37°04'–43°04'N, 5°15'W–2°26'E) (Fig. S1). The study area covers 330,000 km^2 approximately.The region is characterised by a complex topography, ranging from the coastal plains to the slopes of various mountain ranges, and the interaction of

African subtropical, Mediterranean, and North Atlantic climate systems (3). This variety in biogeographical conditions leads to a diverse assortment of forest systems covering a wide range of climates with strong influence of the Mediterranean climate, including semiarid conditions in the south-east, and cooler and more continental and humid conditions in the north. This latitudinal gradient approximately coincides with both increasing precipitation and decreasing temperature gradients (4). The mean annual temperature is +12.9°C, ranging from +5.0°C in January to +22.1°C in July (reference period: 1930 to 2009, CRU TS 3.10 dataset; 1). Mean annual precipitation in the region is about 600 mm, but it varies considerably between the studied sites, from 500 mm to more than 1400 mm. Forests are mainly situated in mountain zones along a pronounced altitudinal gradient (700–2,390 m a.s.l.), ranging from warm sub-Mediterranean conditions in low-elevation sites to cold conditions upwards. The ubiquitous *Pinus nigra* subsp. *salzmannii* (Dunal) Franco and *Pinus sylvestris* L. are distributed across the study area, whereas *Abies alba* Mill. is only present in the north-eastern Iberian Peninsula (Pyrenees). The moisture regime is strongly bimodal, with precipitation concentrated in spring (March to May) and autumn (September to November) and presence of a dry summer (<20% of annual precipitation).

B: Tree-ring network

We compiled a network of 93 annually resolved long-term tree-ring width (TRW) chronologies originating from conifer forests located in central Siberia, Russia (n = 45 sites) and Spain (n = 48 sites). These two Eurasian regions are representative of contrasting conditions in terms of temperature and moisture regimes (*SI Text*, section 1*A*). The chronologies were selected as representative of the range of climatic and biogeographical conditions of each region (Table S1, Fig. S1). In central Siberia, *Larix*

gmelinii (Rupr.) Rupr. and *Larix sibirica* Ledeb. were represented by 19 and 13 chronologies, respectively, and *Picea obovata* Ledeb. by 13 chronologies. In Spain, *Pinus nigra* subsp. *salzmannii* (Dunal) Franco and *Pinus sylvestris* L. were represented by 18 and 20 chronologies, respectively, and *Abies alba* Mill. by 10 chronologies. These chronologies were chosen in accordance with the current species distribution ranges. Each chronology consisted of a time series of annual indices derived from TRW measurements on a number of tree increment cores (Table S1). Core collection, transportation and preprocessing followed standard dendrochronological techniques (5). Altogether, data for a total of 663 trees (1021 radii) in central Siberia and 801 trees (1647 radii) in Spain were used.

C: Mixed modelling

We analysed a particular set of indexed tree-ring chronologies ($I = 1, N$) to characterise the strength of their common signal for ring-width. Let us define W_{ij} as the tree-ring index (TRI) achieved by the jth year of the ith chronology. The estimators can be defined in terms of the following random model (6) (random variables are shown underlined):

$$\underline{W}_{ij} = \underline{Y}_j + \underline{e}_{ij} \qquad [1]$$

where $\underline{Y_j}$ is a random effect of the jth year, and $\underline{e_{ij}}$ is a random deviation of the ith chronology in the jth year. Here we assume that the levels of the factor 'year' come from a random sample of all possible years and, hence, the year effect is defined as random. To quantify the association between a pair of chronologies i and i^*, the intraclass correlation (or reproducibility of TRI observations by chronologies i and i^*) can be calculated as follows (6):

$$\rho(\underline{W}_i, \underline{W}_{i^*}) = \frac{\mathrm{cov}(\underline{W}_i, \underline{W}_{i^*})}{\sqrt{Var(\underline{W}_i) \times Var(\underline{W}_{i^*})}} = \frac{\sigma_Y^2}{\sigma_Y^2 + \sigma_e^2} \quad [2]$$

where σ^2_y refers to the variance of year effects and σ^2_e stands for the residual variance. The parameter ρ becomes the average correlation for TRI over all possible pairs of chronologies provided the whole set of N chronologies is analysed together, but excluding the N pairs $i = i^*$ for which $\rho(\underline{W}_i, \underline{W}_{i^*}) = 1$. It estimates the strength of the common signal for TRI underlying the set of N chronologies. We refer to it as the mean inter-chronology correlation or spatial synchrony, $\hat{a}_C$.

We have grouped the available tree-ring chronologies into subsets representing: (i) different Eurasian regions and (ii) different species within a particular Eurasian region. To this purpose, the following mixed model characterizing synchrony patterns at the between- and within-group levels is used:

$$\underline{W}_{ijr} = \mu_r + \underline{Y}_{jr} + \underline{e}_{ijr} \quad [3]$$

where μ_r is the expected mean value in the rth group (since chronologies are indexed, this term is approximately equal to unity), $\underline{Y_{jr}}$ is a random effect of the jth year in the rth group, and $\underline{e_{ijr}}$ is a random deviation of the ith chronology in the jth year within the rth group.

In turn, the year effect may be further partitioned as:

$$\underline{Y}_{jr} = \underline{Y}_j + \underline{(YR)}_{jr} \quad [4]$$

where $\underline{Y_j}$ is a main effect for the jth year and $\underline{(YR)_{jr}}$ is the jrth year × group interaction, assuming that $\underline{Y_j}$ and $\underline{(YR)_{jr}}$ are independent homoscedastic normal deviates. This model corresponds to the standard analysis of variance (ANOVA) partition accommodating between- and within-group variability, and has the so-called *compound symmetry* variance-covariance (VCOV) structure for variability among years:

$\mathrm{cov}(\underline{Y}_{jr}; \underline{Y}_{jr^*}) = \sigma^2_{Y+YR}$, when $r = r^*$,

$$\text{otherwise}\ \text{cov}(\underline{Y}_{jr};\underline{Y}_{jr^*}) = \sigma_Y^2$$

In the *compound symmetry* structure (S_1) year variances are the same in each group, with $\sigma_{Y+YR}^2 = \sigma_Y^2 + \sigma_{YR}^2$, and year covariances (and correlations) are the same for each pair of groups. However, alternative VCOV structures that cover a range of assumptions may describe the data better in accordance with the properties of the grouped chronologies (which are based here on regional or taxonomic criteria).

In the *heterogeneous compound symmetry* structure (S_2) there may be heterogeneity of year variance between groups, although the property of constant correlation (ρ) across all pairs of groups may still hold true:

$$\text{cov}(\underline{Y}_{jr};\underline{Y}_{jr^*}) = \sigma_{Y_r}^2, \text{ when } r = r^*,$$

$$\text{otherwise}\ \text{cov}(\underline{Y}_{jr};\underline{Y}_{jr^*}) = \sigma_{Y_r} \times \sigma_{Y_{r^*}} \times \rho$$

In the *factor-analytic* structure (S_3) λ_r is a group-specific multiplicative parameter and σ^2_d is a residual variance common to all groups:

$$\text{cov}(\underline{Y}_{jr};\underline{Y}_{jr^*}) = \lambda_r\lambda_{r^*} + \sigma_d^2, \text{ when } r = r^*,$$

$$\text{otherwise}\ \text{cov}(\underline{Y}_{jr};\underline{Y}_{jr^*}) = \lambda_r\lambda_{r^*}$$

This is a simplified, but almost as flexible, variant of the unstructured model (defined below) in which information is gathered from correlated chronologies through (factor-analytic) correlation of year by chronology effects.

In the *unstructured* (or full) structure (S_4) each group has its own year variance and each pair of groups its own year covariance:

$$\text{cov}(\underline{Y}_{jr};\underline{Y}_{jr^*}) = \sigma_{Y_r}^2, \text{ when } r = r^*,$$

$$\text{otherwise}\ \text{cov}(\underline{Y}_{jr};\underline{Y}_{jr^*}) = \sigma_{Y_{rr^*}}^2$$

Two simple variants of the compound symmetry structure act as a baseline against which to compare the more refined modelling alternatives shown before (6).

The *banded main diagonal* (or narrow evaluation) structure (S_5) constrains the covariance (and correlation) between groups to zero, thus testing for a lack of common signal between chronologies belonging to different groups:

$$\text{cov}(\underline{Y}_{jr};\underline{Y}_{jr*}) = \sigma^2_{Y_r}, \text{ when } r = r^*,$$

$$\text{otherwise } \text{cov}(\underline{Y}_{jr};\underline{Y}_{jr*}) = 0$$

In the *null* (or broad evaluation) structure (S_6) the existence of groups is simply ignored so year variance and covariances have the same value:

$$\text{cov}(\underline{Y}_{jr};\underline{Y}_{jr*}) = \sigma^2_{Y}, \text{ when } r = r* \text{ or } r \neq r^*,$$

This last structure is useful for testing the adequacy of grouping chronologies into different classes as for the previous models.

In turn, these structures can be enhanced by allowing the residual variance associated with $\underline{e_{ijr}}$ to vary among groups, hence producing heteroscedastic variants, except for the null model in which no groups are defined. A summary of the properties and interpretation of these structures can be found in Table S2.

The estimation of signal strength parameters for selected structures is grounded on the intra-class correlation expression as defined in equation [2], which quantifies the degree to which the values of N chronologies contain a common temporal signal (i.e. synchrony). The structures defined so far allow estimation of the intra-class correlation either at the intra-group or inter-group levels (except for the null model S_6 in which no groups are defined). Hence the mean correlation estimated between all possible pairs of chronologies drawn from the whole dataset as in equation [2] is split into: (i) a mean correlation between pairs of chronologies for every group; and (ii) a mean correlation between pairs of chronologies for pairs of groups. For the more general unstructured model (S_4), the correlation of pairs of chronologies i and i^* belonging to group r becomes:

$$\rho(\underline{W}_i, \underline{W}_{i^*}) = \frac{\mathrm{cov}(\underline{W}_i, \underline{W}_{i^*})}{\sqrt{Var(\underline{W}_i) \times Var(\underline{W}_{i^*})}} = \frac{\sigma^2_{Y_r}}{\sigma^2_{Y_r} + \sigma^2_e} \quad [5]$$

Besides, the correlation of pairs of chronologies i and i^* belonging to groups r and r^* is:

$$\rho(\underline{W}_i, \underline{W}_{i^*}) = \frac{\mathrm{cov}(\underline{W}_i, \underline{W}_{i^*})}{\sqrt{Var(\underline{W}_i) \times Var(\underline{W}_{i^*})}} = \frac{\sigma^2_{Y_{rr^*}}}{\sqrt{(\sigma^2_{Y_r} + \sigma^2_e) \times (\sigma^2_{Y_{r^*}} + \sigma^2_e)}} \quad [6]$$

If the whole set of N chronologies is analysed together, then these parameters become mean correlations over all possible pairs of chronologies (synchrony, $\hat{a}_C$) at the intra-group or inter-group level, respectively (6, 7). Alternative mean correlation expressions for other models can be obtained by applying their corresponding VCOV structures to equation [3]. The Expressed Population Signal (EPS), which quantifies how well a chronology based on a finite number of trees represents the hypothetical perfect or true chronology, can be generalised from these estimates (7):

$$EPS \approx \frac{N \times \hat{a}_C}{1 + (N-1) \times \hat{a}_C} \quad [7]$$

where N is the number of chronologies at either the intra-group or inter-group levels.

Standard errors for the mean inter-chronology correlation can be estimated as follows (8):

$$SE(\hat{a}_C) \approx \sqrt{\frac{2 \times \hat{a}_C^2 \times (1 - \hat{a}_C)^2}{d.f.}} \quad [8]$$

where *d.f.* are the degrees of freedom from the mean inter-chronology correlation (i.e. number of years).

All analyses were performed with the MIXED procedure of SAS/STAT software (ver. 9.3, SAS Inc., Cary, NC, USA) using restricted maximum likelihood (REML) for estimation of variance components. Further details on the methodological background and on model fitting procedures can be found in (6).

D: Evaluation of changes in synchrony over time

The evolution of changes in $\hat{a}_C$ was studied for successive 30-year segments lagged by five years (Fig. S12). The inter-regional evaluation of $\hat{a}_C$ comprised two groups (Siberia and Spain), whereas the inter-specific evaluation comprised three groups (species) at each region. In the former case, this means that both the heterogeneous compound symmetry and the factor-analytic model provided equivalent results to those of the unstructured model, as the number of parameters to be estimated is three in all cases. It must be taken into account that chronologies do not overlap perfectly until the beginning of the twentieth century and, as expected, the number of series increases over time as younger trees are progressively available for building the site chronologies. Although mixed modelling is capable of dealing with unbalanced datasets (e.g. partially overlapping chronologies) provided the missing-data pattern is considered at random (9), the reliability of every chronology in terms of its temporal signal has to be warranted to some extent. In this regard, we adopted as criterion for the year of inclusion of a chronology in the VCOV analysis the year at which its EPS becomes ≥ 0.85. The regional trends in synchrony (as reported in Fig. 1*A* and *B*) were mostly insensitive to the progressive inclusion of chronologies for two decades in Siberia (with 3 chronologies progressively incorporated) and four decades in Spain (with 10 chronologies progressively incorporated) starting in 1890 (Table S1) (correlation coefficient between $\hat{a}_C$ values for the complete set of chronologies and a subset covering the whole study period: $r = 0.99$, $p < 0.001$ for Siberia; $r = 0.94$, $p < 0.001$ for Spain).

E: Best linear unbiased prediction of tree-ring width indices

The best linear unbiased prediction (BLUP) method was developed for estimation of breeding values in animals and it is currently applied in many areas of research through

mixed modelling (10). However, its application to dendrochronology remains untested to the best of our knowledge.

Best linear unbiased prediction (BLUP) increases accuracy of tree-ring width indices (TRI) relative to ordinary least squares (OLS) methods (i.e. standard ANOVA) and maximizes, under certain rather general assumptions, the correlation between true and predicted TRI values associated to the random year effect (11). For this purpose, the predictors of random year effects (i.e. TRI defined as $\underline{Y_{jr}}$ in equation 3) are shrunken towards zero compared with OLS estimates (12). For a balanced (i.e. perfectly overlapping) network of chronologies, the impact of shrinkage across years is constant and the shrinkage factor equals the synchrony estimate ($\hat{a}_C$) (or reproducibility of year effects by a set of chronologies), as defined in (12). However, for unbalanced datasets (this study) BLUP and OLS are not exactly proportional, with under-represented years having predictors more severely shrunken towards zero.

F: Evaluation of the geographic extent of forest and climate synchrony

To evaluate the geographic extent of forest and climate synchrony, spatial autocorrelation was analyzed using a modified correlogram procedure (14). To this end, tree-ring width indices and climate factors (mean temperature and total precipitation) were used. Site climate series were obtained through bilinear interpolation of the four nearest CRU TS 3.10 grid (0.5° × 0.5°) point values using an inverse distance squared weighting. The resulting series were finally standardized by fitting a straight line and keeping the residuals of these linear fits in order to ensure that results were due to regional processes rather than to long-term trends (e.g., global warming). For statistical analyses, four distance classes were defined depending on geographical distance between sites: <300 km, 300–600 km, 600–900 km, and ≥900 km.

We also evaluated spatial patterns of growth-climate relationships by using cross-correlation analyses (14). These analyses involved tree-ring width indices and monthly climate factors showing a significant impact on growth for the entire period (1930 to 2009). In both cases (autocorrelation and cross-correlation analyses) the mean *r* value and its statistical significance (*p*) within each distance category was estimated from 1000 randomization trials as described in (14). All analyses were performed with the non-centred (cross-)correlogram function (correlog.nc) in the package ncf ver. 1.1-5 in R software (ver. 3.2.2, R Foundation for Statistical Computing, Vienna, Austria).

G: Meteorological data and regional climate time series

Monthly mean temperature, precipitation and the Standardized Precipitation Evapotranspiration Index (SPEI) were used for climate analyses. Estimates of monthly temperature and precipitation were obtained from the high-resolution CRU TS 3.10 dataset (http://badc.nerc.ac.uk/data/cru/) available on a 0.5° × 0.5° grid-box basis (1). The SPEI was obtained from the Global SPEI database (http://sac.csic.es/spei/), which is based on monthly precipitation and potential evapotranspiration available at the CRU TS 3.22 dataset (13). For each climate variable data were averaged over each region as covered by the network of chronologies in order to create monthly-resolved regional climate time series, hence resulting in regional climate trends (Figs. S6 and S11). Regional series were then used to assess the relationships between climate and both TRI and synchrony through correlation and response functions. The significance of function parameters was estimated by drawing 1,000 bootstrapped samples with replacement from the initial data set. All climate analyses were performed with the dcc function in the package bootRes ver. 1.2.3 in R software (ver. 3.2.2, R Foundation for Statistical Computing, Vienna, Austria).

2. Additional analyses

A: Pointer years: regional patterns

Extreme external events originate anomalously wide or narrow rings (i.e. "pointer years"), hence being potent drivers of spatial synchrony. To test for the frequency of regional pointer years we use best linear unbiased predictors (BLUPs) of tree-ring width indices derived from mixed modelling (*SI Text*, section 1*E*). Growth anomalies are tagged as those years having BLUPs deviating > ±1SD from the mean. The threshold of ±1.96SD is also used to highlight extraordinary growth reactions at the regional scale. Overall, we find slightly more years with growth anomalies in Siberia (32%) than in Spain (28%) (Fig. S2). We also detect more extreme growth anomalies after 1950 in both regions. Hence, the frequency of pointer years has increased from 27% (period 1890–1949) to 37% (1950–2009) in Siberia and from 17% to 40% in Spain. In addition, three pointer years with exceptionally low growth (i.e. deviating over –1.96 SD from the average index) are found in both Siberia and Spain after 1985 (Fig. S2). A higher incidence of growth extremes present in the last decades is in agreement with the absolute peaks in synchrony found in both regions at the turn of this century.

B: Attribution analysis: Discarding non-climatic factors as drivers of increased synchrony in forest growth

Two major reasons lead us to reject a CO_2 fertilization effect as the main cause of increased regional synchrony. First, the distinct pace of synchrony changes in Siberia and Spain is barely compatible with the expected uniform effect of atmospheric CO_2 increasing carbon uptake in temperate and boreal biomes (Fig. 1). Second, we did not detect any enhancement of absolute radial growth over time that may underlie the rise in

spatial synchrony observed in both regions. Because of such non-positive growth trends, the effect of N deposition as fundamental driver of synchrony, either alone or in conjunction with the increase in atmospheric CO_2 concentration, can also be discarded. Also N deposition is a phenomenon acting at regional scales that should not lead to more homogeneous forest growth across large areas with contrasting N deposition rates. On the other hand, a potential effect of global dimming in boreal forests limited by incoming radiation cannot be neglected, although the lack of growth suppression observed for Siberia and the small impact of global dimming previously reported for radial growth (unlike for wood density) (15) points to its limited role as trigger of synchrony. Finally, changes in land use and management practices might affect mainly Spanish forests (16), which display marked use legacies, whereas historical anthropogenic disturbances are negligible in Siberia (17). However, the selected Spanish chronologies originate mostly from undisturbed forests composed by old trees, which suggest a reduced influence of stand dynamics on synchrony patterns.

C: Attribution analysis: Discarding the Moran effect as a driver of increased synchrony in forest growth

In order to examine whether the observed increase in regional forest synchrony was driven by more homogeneous climate signals over time (i.e. enhanced 'Moran effect' (18, 19, 20), we obtained temporal changes in synchrony patterns of mean annual temperature and annual precipitation for Siberia and Spain. To this end, we used the CRU TS 3.10 dataset using the interpolation scheme outlined in *SI Text*, section 1*F*, and applied the methodology described for tree-ring width records in *SI Text*, section 1*C*. Environmental synchrony patterns are not significantly related to those of forest growth (Fig. S8), except for growth vs. precipitation in Siberia. However, even in this last case

we interpret that such correlation does not imply causation (that increasing rainfall synchrony leads to increased growth synchrony) because of two reasons: (i) precipitation, unlike temperature, is not consistently related to growth in Siberia (Fig. 3), and (ii) for forest growth to be synchronized by an exogenous factor ('Moran effect'), the spatial autocorrelation in the putative environmental factor (precipitation) must extend, in principle, over greater distances that that of the outcome of the cause (forest growth) (21, 22); however, the spatial autocorrelation of forest growth in Siberia is higher between geographically distant sites (>600 km) as compared with precipitation (Fig. S3). Altogether, both considerations lead us to reject an enhanced Moran effect involving precipitation as driver of increased regional synchrony among boreal forests.

Supplementary References

1. Harris I, Jones PD, Osborn TJ, Lister DH (2014) Updated high-resolution grids of monthly climatic observations – the CRU TS3.10 Dataset. *Int J Climatol* **34**:623–642.

2. Tchebakova NM, Monserud RA, Nazimova DI (1994) A Siberian vegetation model based on climatic parameters. *Can J For Res* **24**:1597–1607.

3. Rodó X, Baert E, Comín FA (1997) Variations in seasonal rainfall in Southern Europe during the present century: relationships with the North Atlantic Oscillation and the El Niño-Southern Oscillation. *Clim Dyn* **13**:275–284.

4. Sánchez-Salguero R, et al. (2015) What drives growth of Scots pine in continental Mediterranean climates: Drought, low temperatures or both? *Agric For Meteorol* **206**:151–162.

5 Cook ER, Kairiukstis LA (1990). *Methods of Dendrochronology: Applications in the Environmental Sciences* (Kluwer Acad Publ, Dordrecht).

6. Shestakova TA, Aguilera M, Ferrio JP, Gutiérrez E, Voltas J (2014) Unravelling spatiotemporal tree-ring signals in Mediterranean oaks: a variance-covariance modelling approach of carbon and oxygen isotope ratios. *Tree Physiol* **34:**819–838.

7. Wigley TML, Briffa KR, Jones PD (1984) On the average value of correlated time series, with applications in dendroclimatology and hydrometerology. *J Clim Appl Meteorol* **23**:201–213.

8. Visscher PM (1998) On the sampling variance of intraclass correlations and genetic correlations. *Genetics* **149**:1605–1614.

9. Little RJA, Rubin DB (2002) *Statistical Analysis with Missing Data* (Wiley, New York).

10. Henderson CR (1984) *Applications of Linear Models in Animal Breeding* (Univ Guelph Press, Guelph).

11. Piepho HP, Möhring J (2005) Best linear unbiased prediction of cultivar effects for subdivided target regions. *Crop Sci* **45**:1151–1159.

12. Searle SR, Casella G, McCulloch CE(2006) *Variance Components* (Wiley, New York).

13. Vicente-Serrano SM, Beguería S, López-Moreno JI (2010) A multi-scalar drought index sensitive to global warming: The Standardized Precipitation Evapotranspiration Index – SPEI. *J Clim* **23**:1696–1718.

14. Koenig WD, Knops JMH (1998) Testing for spatial autocorrelation in ecological studies. *Ecography* **21**:423–429.

15. Stine AR, Huybers P (2014). Arctic tree rings as recorders of variations in light availability. *Nat commun* **5**:3836.

16. Linares JC, Camarero JJ, Carreira JA (2010) Competition modulates the adaptation capacity of forests to climatic stress: insights from recent growth decline and death in relict stands of the Mediterranean fir *Abies pinsapo*. *J Ecol* **98**:592–603.

17. Potapov P, et al. (2008) Mapping the world's intact forest landscapes by remote sensing. *Ecol Soc* **13**:51.

18. Moran PAP (1953) The statistical analysis of the Canadian lynx cycle. II. Synchronization and meteorology. *Aust J Zool* **1**:291–298.

19. Ranta E, Kaitala V, Lundberg P (1997) The spatial dimension in population fluctuations. *Science* **278**:1621–1623.

20. Pena-Angulo D, Cortesi N, Brunetti M, González-Hidalgo JC (2015) Spatial variability of maximum and minimum monthly temperature in Spain during 1981–2010 evaluated by correlation decay distance (CDD). *Theor Appl Climatol* **122**:35–45.

21. Grenfell BT, et al. (1998) Noise and determinism in synchronized sheep dynamics. *Nature* **394**:674–677.

22. Grenfell BT, Finkenstädt BF, Wilson K, Coulson TN, Crawley MJ (2000) *Grenfell* et al. reply: Nonlinearity and the Moran effect. *Nature* **406**:847.

SUPPLEMENTARY FIGURES

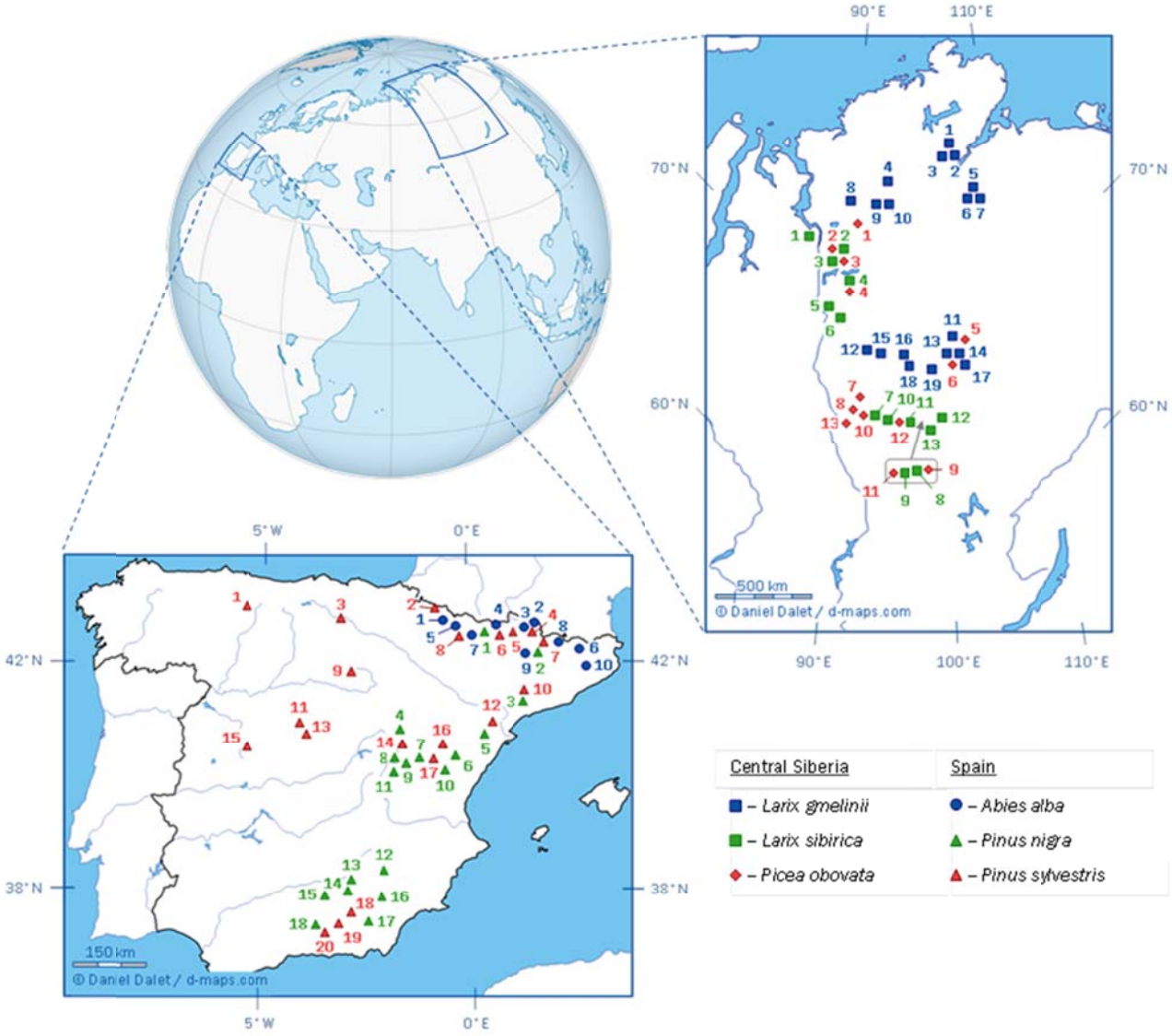

Fig. S1. Site locations in central Siberia (Russia) and Spain. Genus symbols are as follows: circle, *Abies*; square, *Larix*; diamond, *Picea*; triangle, *Pinus*. See Table S1 for specific details on study sites and tree-ring width chronologies.

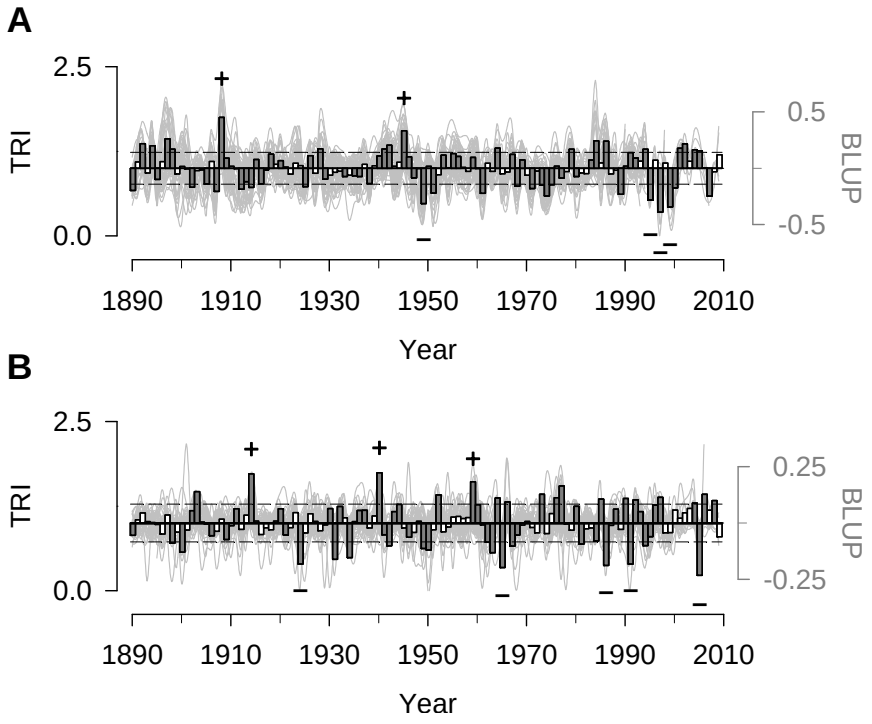

Fig. S2. Regional master tree-ring chronologies for central Siberia (*A*) and Spain (*B*). Variability of tree-ring width indices (TRI) for each site chronology (grey lines) and of regional master chronologies (bars) are presented over the period 1890–2009. The regional master chronologies were derived as best linear unbiased predictors (BLUPs) of tree-ring indices estimated from the best variance-covariance model for the study period (i.e. narrow evaluation model) using a regional classification as grouping criterion (see Table S3). Filled bars denote significant BLUPs according to Student-*t* testing of null BLUP effects ($p < 0.05$). Horizontal dashed lines indicate ±1SD. *Plus* and *minus* signs indicate years of extreme positive (+1.96SD) and negative (–1.96SD) growth estimates, respectively.

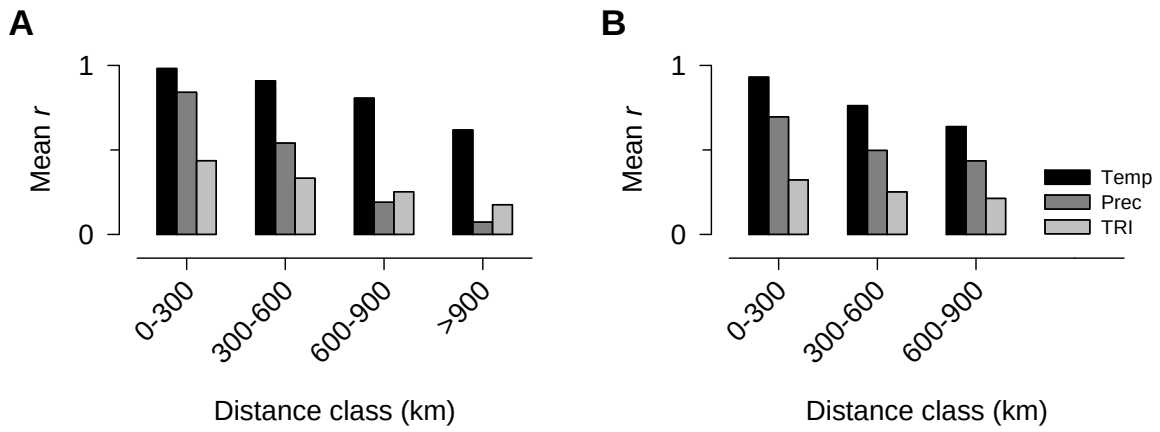

Fig. S3. Spatial structure (modified correlograms) of synchrony in climate and forest growth for central Siberia (*A*) and Spain (*B*). The spatial autocorrelation in mean annual temperature (Temp), annual precipitation (Prec) and tree-ring width indices (TRI) was obtained from pairwise correlations (*r*-values) between all sites (chronologies) within each region for the common period 1930–2009. The correlations were divided into four distance classes (0 to 300 km, 300 to 600 km, 600 to 900 km, and >900 km). Mean *r*-values and their statistical significance (*p*) within each distance class were estimated from 1000 randomizations. Significant correlation coefficients ($p < 0.05$) are indicated by filled bars.

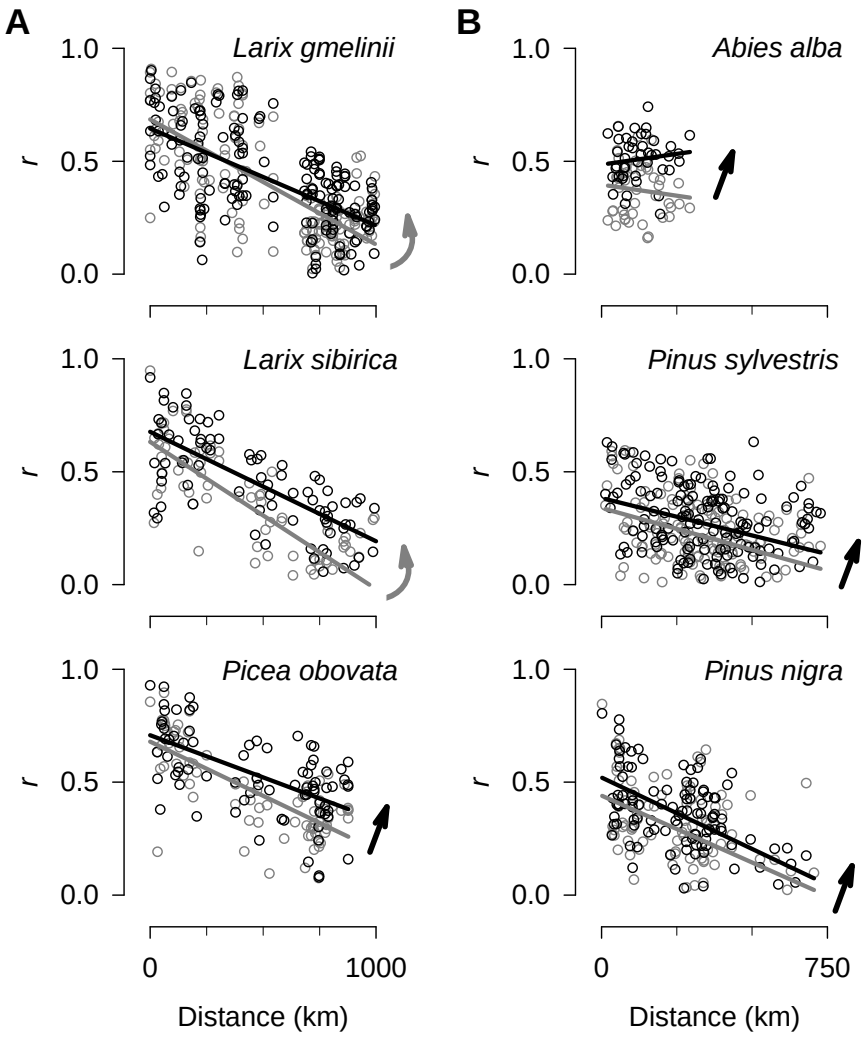

Fig. S4. Synchrony patterns as a function of distance at the species level in central Siberia (*A*) and Spain (*B*). The patterns are characterized as linear regressions of correlation coefficients (*r*-values) for pairs of chronologies (*y*-axes) on their corresponding distance (*x*-axes) from1890 to 1949 (grey line) and from 1950 to 2009 (black line). Significant differences in slopes ($p < 0.05$; grey arrows) are found for deciduous conifers in Siberia (*Larix* spp.), whereas significant differences in mean $\hat{a}_C$ values ($p < 0.05$; black arrows) are found for evergreen conifers (*Abies*, *Pinus* and *Picea* spp).

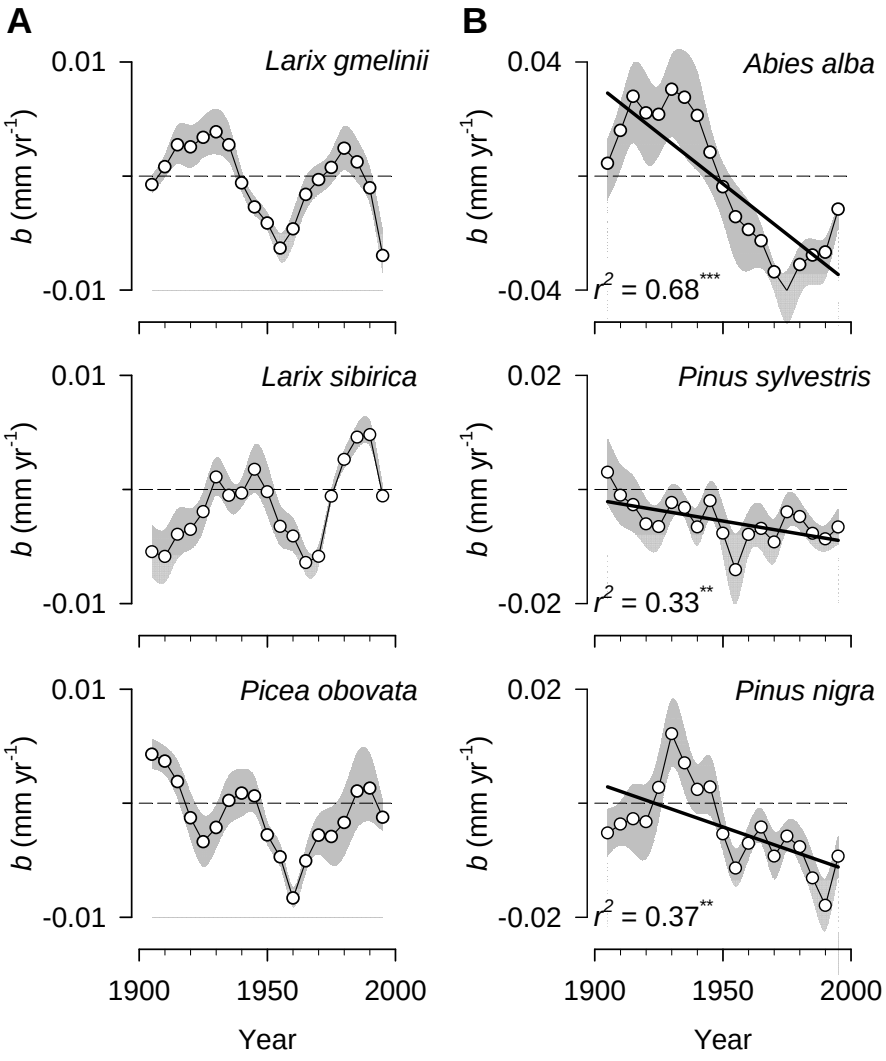

Fig. S5. Changes in radial growth over time at the species level. Temporal trends in the slope (*b*) of absolute ring-width values are calculated for successive 30-year periods lagged by five years in central Siberia (*A*) and Spain (*B*). The estimated rate of growth changes for each period is based on raw (i.e. non-standardised) tree-ring width data as the mean slope value of every chronology of the same species. Standard errors are shown as shaded areas. Significant linear regressions are indicated with black lines. Displayed years in the *x*-axes correspond to the middle year of 30-year moving intervals. Note the change of scale in the *y*-axes between regions and species.

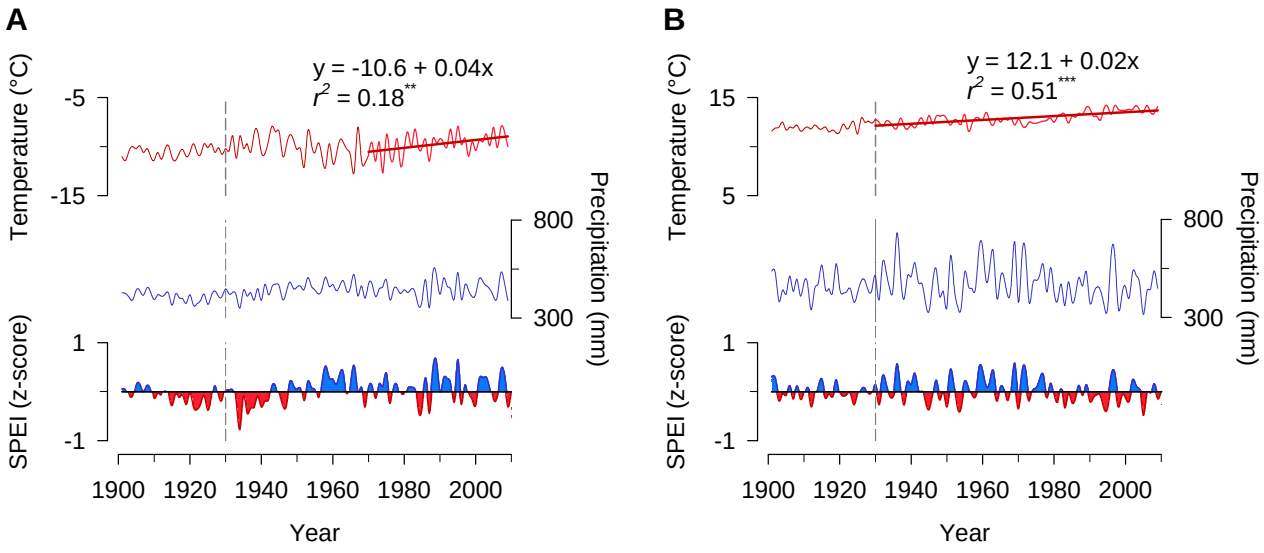

Fig. S6. Regional climate trends for central Siberia (*A*) and Spain (*B*). From top to bottom, mean temperature, precipitation and SPEI (Standardised Precipitation-Evapotranspiration Index) are obtained as average values of the gridded CRU TS3.10 data set with spatial resolution (0.5° × 0.5°) for each region. The vertical dashed lines indicate the starting year with reliable regional climate records. Significant linear trends ($p < 0.05$) of mean temperature are shown for relevant periods (1970–2009 in Siberia, 1930–2009 in Spain).

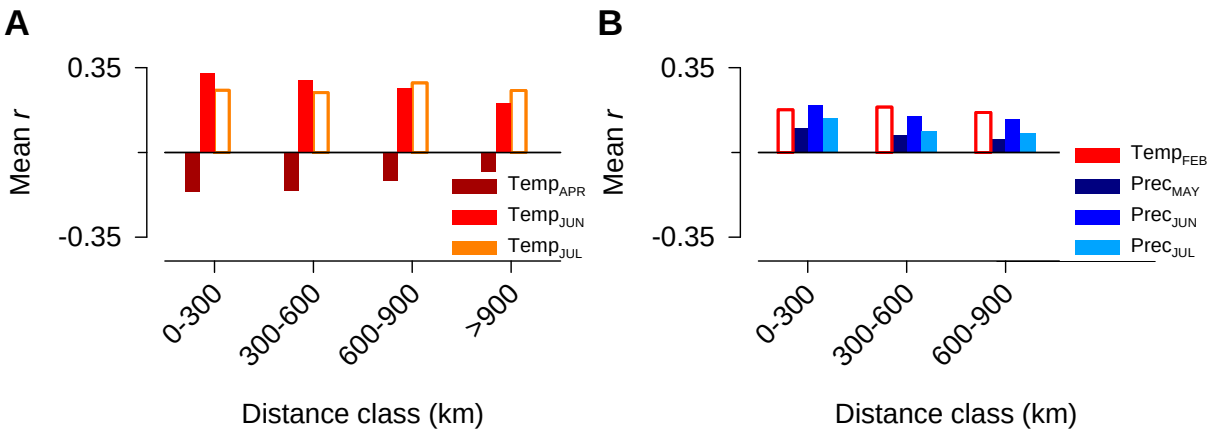

Fig. S7. Spatial structure of significant growth-climate relationships for central Siberia (*A*) and Spain (*B*). Mean spatial cross-correlations between relevant monthly climate factors for growth (see Fig. 3) and tree-ring width indices (TRI) were calculated as pairwise correlations (*r*-values) between TRI and the corresponding climate factor for all sites within each region for the common period 1930–2009. The cross-correlations were divided into four distance classes (0 to 300 km, 300 to 600 km, 600 to 900 km, and >900 km). Mean cross-correlation *r*-values and their statistical significance (*p*) within each distance class were estimated from 1000 randomizations. Significant correlation coefficients ($p < 0.05$) are indicated by filled bars.

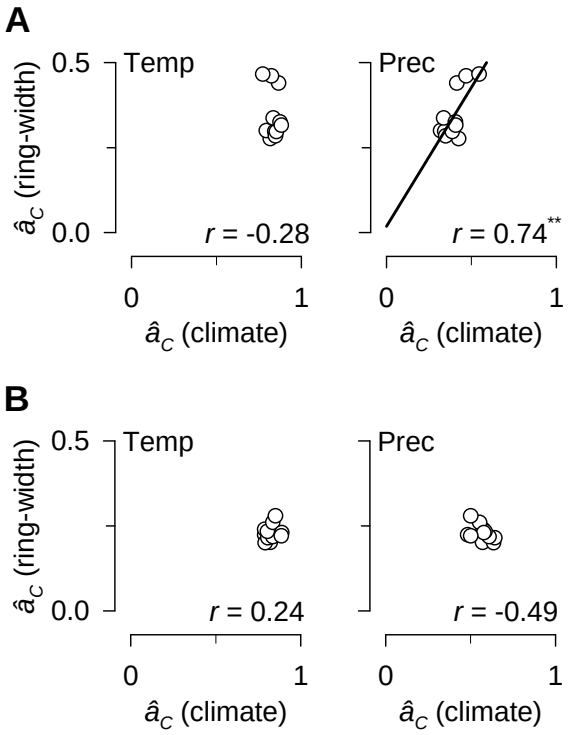

Fig. S8. Relationships between temporal changes in spatial synchrony in climate factors and forest growth for central Siberia (*A*) and Spain (*B*). The spatial synchrony ($\hat{a}_C$) is estimated for mean annual temperature (Temp), annual precipitation (Prec) and indexed ring-width chronologies for successive 30-year periods lagged by five years. Note that only precipitation in Siberia is significantly correlated to $\hat{a}_C$ of growth (**, $p < 0.01$).

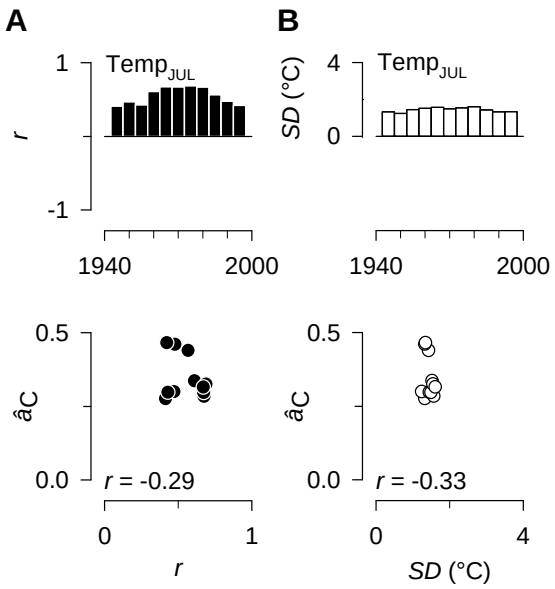

Fig. S9. Climate factors underlying synchrony changes in central Siberia (1930-2009). Moving correlation analyses (*r*-values) between the regional chronology and *(A)* July mean temperature (Temp) and (*B*) standard deviates (SD) of July mean temperatures are displayed in bar diagrams for successive 30-year periods lagged by five years (upper panels). Significant correlations are indicated by filled bars in (*A*) ($p < 0.05$). Relationships between synchrony estimates ($\hat{a}_C$) and *r*-values of the relationship between BLUP-derived tree-ring indices and mean temperature or SD of mean temperature for July are presented in scatter plots (lower panels). The filled circles correspond to the periods with significant growth-climate relationships as indicated by moving correlation analyses in the upper panels. Only months showing a significant association with BLUP-derived tree-ring indices over the study period (Fig. 3) are examined; significant climate factors related to synchrony patterns are displayed in Fig. 4. Displayed years in the *x*-axes correspond to the middle year of 30-year moving intervals.

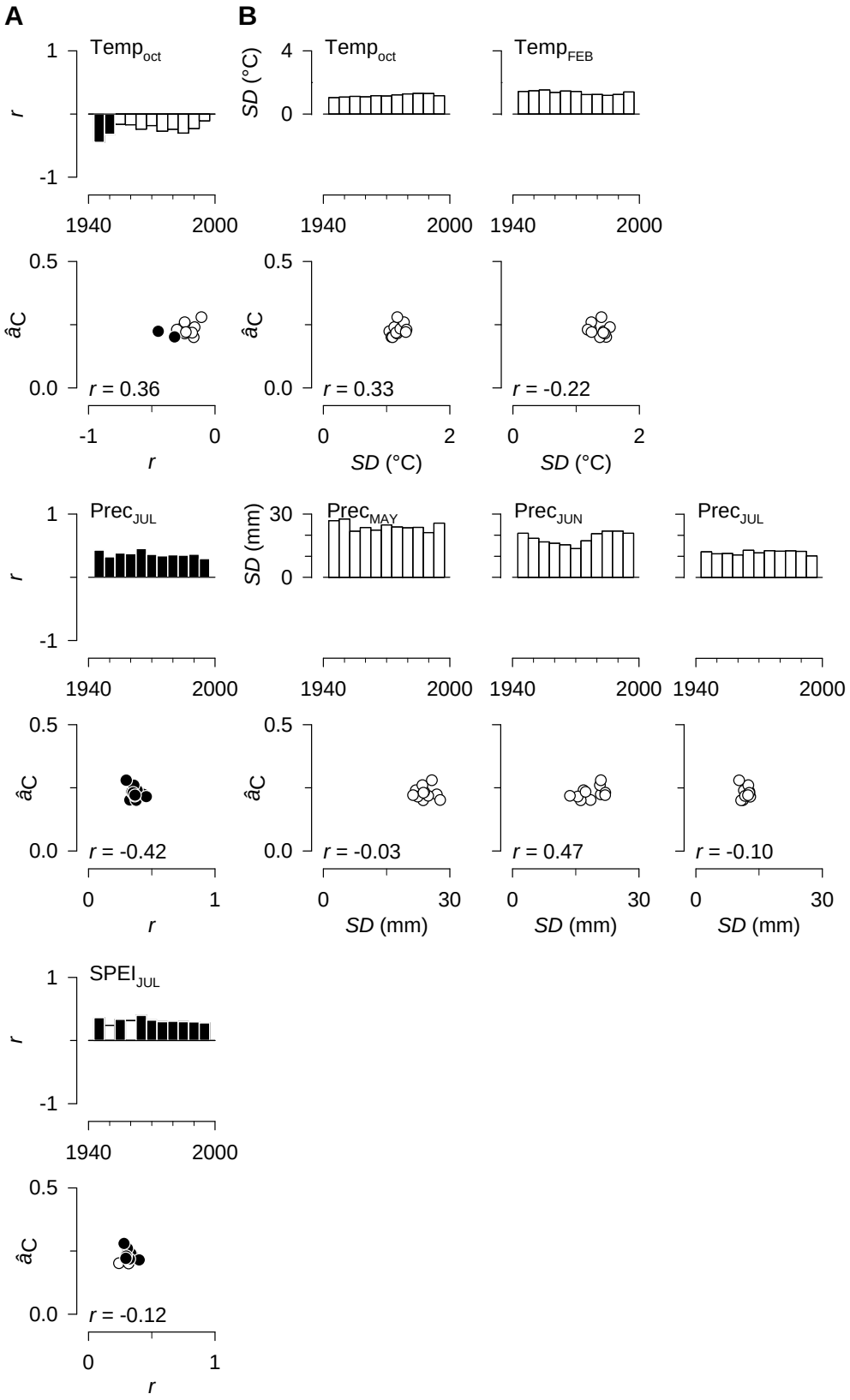

Fig. S10. Climate factors underlying synchrony changes in Spain (1930-2009). Moving correlation analysis (*r*-values) between the regional chronology and (*A*) mean October

temperature (Temp) of the previous year, July precipitation and July SPEI and (*B*) standard deviates (SD) of October of previous year and February mean temperatures and May-July precipitation are displayed in bar diagrams for successive 30-year periods lagged by five years (upper panels). Significant correlations are indicated by filled bars in (*A*) ($p < 0.05$). Relationships between synchrony estimates ($\hat{a}_C$) and *r*-values of the relationship between BLUP-derived tree-ring indices and mean October temperature of the previous year, July precipitation and July SPEI or SD of October of the previous year, February mean temperature and May-July precipitation (lower panels). The filled circles correspond to the periods with significant growth-climate relationships as indicated by moving correlation analyses in the upper panels. Only months showing a significant association with BLUP-derived tree-ring indices over the study period (Fig. 3) are examined; significant climate factors related to synchrony patterns are displayed in Fig. 5. Displayed years in the *x*-axes correspond to the middle year of 30-year moving intervals.

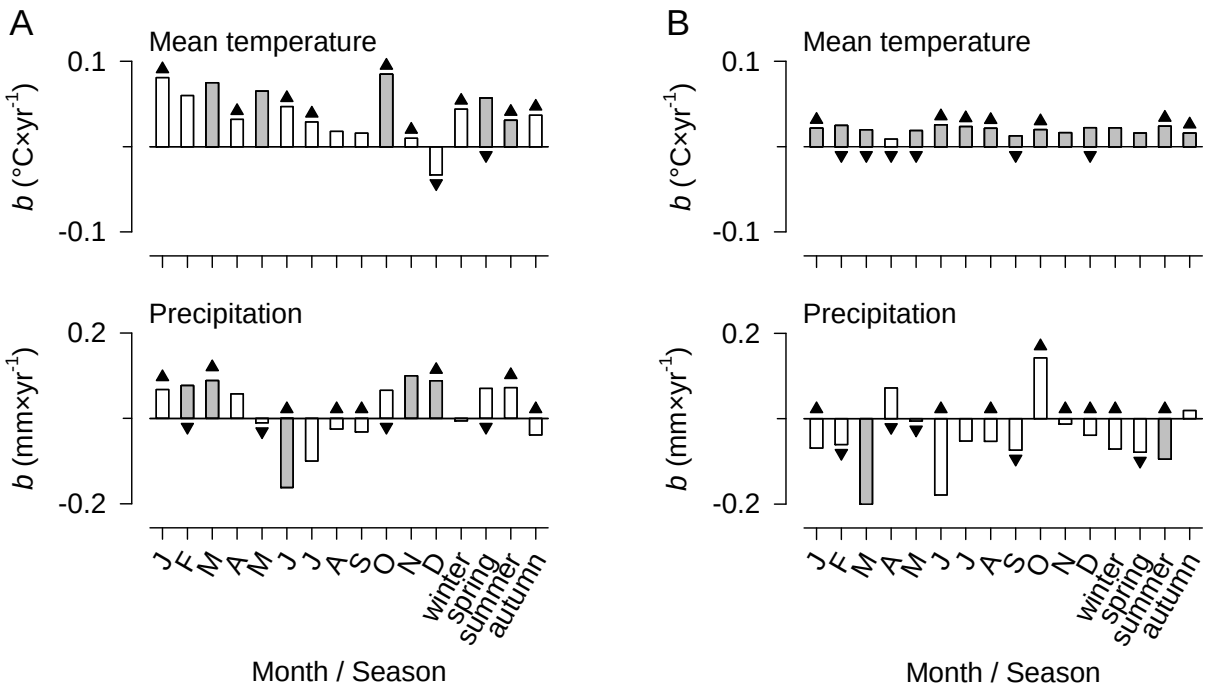

Fig. S11. Summary of regional temporal trends in monthly and seasonal climatic data for central Siberia (*A*) and Spain (*B*). Mean temperature and precipitation are obtained as average values of the gridded CRU TS3.10 data set with spatial resolution (0.5° × 0.5°) for each region. Bars represent the slopes of linear regressions of climate factors as a function of time estimated for relevant periods (1970–2009 in Siberia, 1930–2009 in Spain in accordance with Fig. S6). Filled bars indicate significant linear trends over time ($p < 0.05$). Triangles identify months with significant linear trends in climate variability (standard deviates of climate factors) estimated for the period 1930–2009 (upward triangles denote positive trends, downward triangles negative trends).

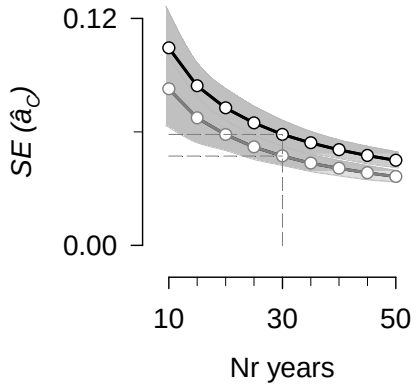

Fig. S12. Precision of synchrony ($\hat{a}_C$) values (standard error of the mean, SE) as a function of considered number of years for central Siberia (black line) and Spain (grey line). The shaded areas indicate standard deviations of SE values estimated for every interval across the study period (1890–2009). The dashed lines indicate the inflection points of the curves and denote a balance between number of years in each time period and precision of synchrony estimates.

SUPPLEMENTARY TABLES

Table S1. Tree-ring sampling sites: geographic features *(A)* and chronology characteristics *(B)*. For site locations see Fig. S1. Abbreviations: EPS, Expressed Population Signal; TRW, tree-ring width; Rbar, mean interseries correlation.

(A) Sites				(B) Chronologies						
ID	**Latitude**	**Longitude**	**Elevation (m)**	**Time span**	**EPS > 0.85 since**	**No. trees**	**No. cores**	**TRW±SD (mm)**	**Rbar±SD**	**Reference**
					CENTRAL SIBERIA					
Larix gmelinii (Lg)										
1	72°30'N	102°25'E	60	1924–2011	N/A	14	14	0.44±0.13	0.493± 0.164	Kirdyanov et al.*
2	72°27'N	101°45'E	70	1624–1990	1705	12	24	0.38±0.13	0.659±0.079	Schweingruber, Briffa (1996)
3	72°27'N	101°54'E	10	1708–2010	1910	14	14	0.42±0.17	0.607±0.082	Kirdyanov et al.*
4	71°20'N	93°50'E	60	1569–1990	1645	21	42	0.45±0.21	0.662±0.084	Schweingruber, Briffa (1996)
5	70°36'N	104°15'E	130	1563–1990	1645	19	33	0.37±0.13	0.591±0.105	Schweingruber, Briffa (1996)
6	70°36'N	104°15'E	290	1611–2006	1820	11	15	0.65±0.23	0.538±0.121	Esper et al. (2010)
7	70°36'N	104°15'E	130	1855–1990	1910	9	18	0.17±0.05	0.414±0.143	Schweingruber, Briffa (1996)
8	70°31'N	89°30'E	50	1657–1990	1710	19	38	0.55±0.25	0.647±0.082	Schweingruber, Briffa (1996)
9	70°30'N	93°10'E	360	1689–2002	1740	19	34	0.37±0.11	0.690±0.077	Kirdyanov et al. (2012)
10	70°30'N	93°10'E	164	1684–2003	1740	13	13	0.37±0.09	0.577±0.083	Kirdyanov et al. (2012)
11	64°32'N	100°14'E	204	1747–2005	1800	22	22	0.37±0.13	0.343±0.090	Sidorova et al. (2009)
12	64°22'N	92°05'E	80	1670–1992	1755	11	11	0.33±0.05	0.466±0.069	Panyushkina et al. (1996)
13	64°19'N	100°14'E	160	1817–2008	1870	21	21	0.41±0.07	0.502±0.076	Kirdyanov et al.*
14	64°19'N	100°15'E	150	1814–2007	1870	16	16	0.53±0.15	0.350±0.092	Knorre et al.*
15	64°17'N	93°22'E	120	1612–1992	1670	15	15	0.34±0.08	0.519±0.067	Panyushkina et al. (1996)
16	64°09'N	95°27'E	110	1617–1992	1670	12	12	0.41±0.14	0.512±0.075	Panyushkina et al. (1996)
17	64°08'N	100°52'E	150	1694–2009	1775	15	15	0.82±0.34	0.346±0.136	Knorre et al.*
18	63°52'N	96°00'E	110	1679–1992	1755	11	12	0.42±0.08	0.417±0.122	Panyushkina et al. (1996)
19	63°44'N	97°55'E	190	1611–1992	1720	12	13	0.46±0.16	0.452±0.093	Panyushkina et al. (1996)

(A) Sites (B) Chronologies

ID	Latitude	Longitude	Elevation (m)	Time span	EPS > 0.85 since	No. trees	No. cores	TRW±SD (mm)	Rbar±SD	Reference
Larix sibirica (Ls)										
1	69°07'N	84°30'E	80	1624–1990	1680	16	29	0.41±0.13	0.661±0.067	Schweingruber, Briffa (1996)
2	68°05'N	86°45'E	33	1638–1998	1690	28	52	0.53±0.13	0.610±0.122	Knorre et al. (2006)
3	68°05'N	86°44'E	21	1723–1998	1780	23	35	0.49±0.22	0.518±0.144	Knorre et al. (2006)
4	67°58'N	88°55'E	160	1574–1990	1630	11	20	0.58±0.16	0.666±0.065	Schweingruber, Briffa (1996)
5	65°58'N	88°46'E	70	1506–1992	1635	9	10	0.33±0.08	0.539±0.067	Vaganov et al. (1996)
6	65°41'N	89°37'E	120	1657–1998	N/A	N/A	N/A	N/A	N/A	Knorre et al. (2006)
7	61°54'N	92°44'E	72	1747–1994	1800	10	12	0.62±0.13	0.543±0.096	Kirdyanov (1999)
8	61°52'N	94°40'E	220	1629–1994	1705	11	12	0.74±0.24	0.529±0.059	Kirdyanov (1999)
9	61°51'N	94°19'E	130	1770–1994	1830	12	25	0.51±0.17	0.432±0.122	Kirdyanov (1999)
10	61°51'N	93°24'E	100	1781–1994	1840	19	21	0.80±0.15	0.499±0.118	Kirdyanov (1999)
11	61°49'N	93°43'E	200	1662–1994	1745	14	27	0.55±0.22	0.448±0.124	Kirdyanov (1999)
12	61°46'N	97°29'E	220	1706–1994	1760	10	11	0.40±0.06	0.483±0.078	Kirdyanov (1999)
13	61°33'N	96°56'E	220	1726–1994	1805	10	11	0.80±0.16	0.382±0.085	Kirdyanov (1999)
Picea obovata (Po)										
1	69°35'N	90°30'E	60	1640–1990	1750	20	35	0.50±0.25	0.462±0.143	Schweingruber, Briffa (1996)
2	68°05'N	86°44'E	21	1676–1998	1730	29	46	0.25±0.07	0.433±0.095	Knorre et al. (2006)
3	68°05'N	86°45'E	33	1632–1998	1690	29	51	0.41±0.13	0.497±0.122	Knorre et al. (2006)
4	67°58'N	88°55'E	160	1661–1990	1720	13	25	0.37±0.16	0.524±0.088	Schweingruber, Briffa (1996)
5	64°21'N	100°25'E	590	1734–2009	1865	17	17	0.42±0.15	0.404±0.096	Shishov et al. (in press)
6	64°08'N	100°52'E	150	1855–2009	1910	8	8	1.04±0.22	0.434±0.074	Knorre et al.*
7	62°21'N	92°03'E	50	1727–1994	1780	14	31	0.50±0.15	0.448±0.112	Kirdyanov (1999)
8	61°59'N	91°31'E	52	1707–1994	1785	13	31	0.62±0.28	0.406±0.135	Kirdyanov (1999)
9	61°56'N	95°09'E	175	1728–1994	1830	12	26	0.96±0.26	0.281±0.164	Kirdyanov (1999)
10	61°54'N	92°44'E	72	1674–1994	1805	12	27	0.68±0.21	0.375±0.112	Kirdyanov (1999)
11	61°51'N	94°19'E	90	1740–1994	1800	14	29	0.34±0.12	0.422±0.110	Kirdyanov (1999)
12	61°49'N	93°43'E	120	1804–1994	1860	10	23	0.84±0.34	0.353±0.123	Kirdyanov (1999)
13	61°42'N	90°25'E	46	1775–1994	1855	13	25	0.81±0.22	0.329±0.154	Kirdyanov (1999)

(A) Sites (B) Chronologies

ID	Latitude	Longitude	Elevation (m)	Time span	EPS > 0.85 since	No. trees	No. cores	TRW±SD (mm)	Rbar±SD	Reference
					SPAIN					
Abies alba (Aa)										
1	42°55'N	0°47'W	1400	1749–1999	1800	14	28	0.15±1.83	0.404±0.096	Macias et al. (2006)
2	42°41'N	1°20'E	1470	1878–1999	1903	15	30	0.11±2.99	0.341±0.150	Macias et al. (2006)
3	42°38'N	1°04'E	1750	1767–1999	1790	18	35	0.15±0.89	0.462±0.126	Macias et al. (2006)
4	42°34'N	0°23'E	1780	1667–2000	1795	12	24	0.14±2.69	0.352±0.148	Camarero et al. (2011)
5	42°31'N	0°32'W	1650	1889–2000	1905	14	28	0.16±2.67	0.525±0.101	Macias et al. (2006)
6	42°24'N	2°17'E	1750	1777–1999	1880	15	30	0.17±2.05	0.355±0.121	Macias et al. (2006)
7	42°18'N	0°12'W	1500	1893–1999	1905	15	30	0.16±2.99	0.554±0.116	Macias et al. (2006)
8	42°19'N	1°49'E	1680	1852–1999	1869	15	31	0.16±1.85	0.425±0.164	Macias et al. (2006)
9	42°12'N	1°13'E	1583	1804–1999	1845	17	40	0.16±1.58	0.330±0.130	Macias et al. (2006)
10	41°47'N	2°26'E	1550	1587–2010	1640	26	50	0.24±1.23	0.340±0.125	Macias et al. (2006, revised)
Pinus nigra (Pn)										
1	42°32'N	0°09'E	700	1819–1999	1860	15	30	1.32±0.36	0.480±0.110	Andreu et al. (2007)
2	42°13'N	1°23'E	1200	1867–1999	1890	15	30	1.53±0.31	0.595±0.192	Gutiérrez et al.*
3	41°16'N	1°00'E	850	1928–1999	1950	15	30	2.18±0.38	0.380±0.157	Gutiérrez et al.*
4	40°36'N	1°46'W	1450	1655–1998	1750	58	118	1.17±0.32	0.319±0.110	Génova, Martínez-Morillas (2002)
5	40°35'N	0°04'E	1000	1642–2004	1770	25	81	0.91±0.41	0.375±0.138	Fulé et al. (2008)
6	40°18'N	0°40'W	1605	1810–2006	1840	14	34	1.09±0.30	0.546±0.095	Camarero et al.*
7	40°14'N	1°15'W	1450	1485–1988	1570	9	17	0.71±0.10	0.381±0.088	Génova Fuster et al. (1993)
8	40°13'N	1°55'W	1450	1365–1995	1550	17	31	0.44±0.10	0.277±0.071	Génova Fuster, Fernández Canclo (1998/1999)
9	40°11'N	1°56'W	1250	1688–1988	1730	6	12	1.14±0.35	0.412±0.078	Génova Fuster et al. (1993)
10	40°00'N	0°51'W	1445	1664–2006	1710	14	28	0.98±0.29	0.589±0.105	Camarero et al.*
11	39°54'N	1°46'W	970	1896–1999	1920	16	31	1.47±0.49	0.425±0.145	Gutiérrez et al.*
12	38°08'N	2°09'W	1500	1878–1999	1880	15	30	1.27±0.40	0.423±0.129	Gutiérrez et al.*
13	37°54'N	2°52'W	1435	1816–2010	1940	6	11	1.45±0.55	0.272±0.259	Linares, Tíscar (2010, revised)
14	37°49'N	2°58'W	1819	1596–2010	1940	13	15	0.74±0.21	0.106±0.174	Linares, Tíscar (2010, revised)

(A) Sites (B) Chronologies

ID	Latitude	Longitude	Elevation (m)	Time span	EPS > 0.85 since	No. trees	No. cores	TRW±SD (mm)	Rbar±SD	Reference
15	37°43'N	3°28'W	1820	1645–2010	1890	19	32	1.08±0.36	0.170±0.128	Linares, Tíscar (2010, revised)
16	37°39'N	2°05'W	1793	1541–2009	1850	9	13	1.14±0.37	0.354±0.138	Camarero et al. (2013)
17	37°15'N	2°30'W	1850	1653–1999	1840	15	30	1.92±0.86	0.389±0.200	Andreu et al. (2007)
18	37°05'N	3°28'W	1750	1879–1999	1895	13	26	1.93±0.60	0.448±0.120	Gutiérrez et al.*
Pinus sylvestris (Ps)										
1	43°04'N	5°15'W	1650	1511–2002	1545	15	32	0.78±0.20	0.352±0.096	Andreu et al. (2007)
2	42°55'N	0°48'W	1400	1740–1999	1775	15	30	1.51±0.54	0.308±0.127	Gutiérrez et al.*
3	42°49'N	3°06'W	850	1918–1999	1930	15	30	2.06±0.32	0.363±0.112	Gutiérrez et al.*
4	42°36'N	1°06'E	1450	1772–1999	1790	15	30	1.05±0.46	0.420±0.123	Gutiérrez et al.*
5	42°33'N	0°54'E	1888	1747–1995	1780	17	36	1.28±0.58	0.387±0.127	Andreu et al. (2007)
6	42°28'N	0°29'E	1540	1786–1999	1820	16	32	1.80±0.58	0.413±0.119	Andreu et al. (2007)
7	42°20'N	1°40'E	1585	1921–1999	1945	18	36	2.11±0.57	0.722±0.073	Gutiérrez et al.*
8	42°19'N	0°26'W	1450	1830–1999	1855	16	32	1.74±0.63	0.413±0.128	Andreu et al. (2007)
9	41°58'N	2°49'W	1750	1612–1999	1785	16	32	1.45±0.50	0.329±0.112	Andreu et al. (2007)
10	41°20'N	1°01'E	950	1861–1999	1875	11	22	1.54±0.43	0.457±0.135	Andreu et al. (2007)
11	40°50'N	4°02'W	1864	1818–2011	1830	35	81	1.27±0.24	0.317±0.102	Génova (2000), extended with Touchan et al. (2013)
12	40°48'N	0°21'E	1250	1797–2000	1815	15	30	1.09±0.31	0.353±0.115	Andreu et al. (2007)
13	40°44'N	4°06'W	1500	1763–1991	1890	9	18	1.64±0.26	0.360±0.082	Génova Fuster (2000)
14	40°25'N	1°43'W	1860	1791–2006	1815	20	40	0.95±0.29	0.327±0.115	Camarero et al.*
15	40°21'N	5°06'W	1550	1805–2011	1830	30	65	2.22±0.66	0.296±0.122	Génova*
16	40°20'N	0°43'W	1510	1835–2006	1865	15	29	1.43±0.37	0.460±0.112	Camarero et al.*
17	40°03'N	0°59'W	1865	1774–2006	1810	16	32	1.63±0.46	0.510±0.122	Camarero et al.*
18	37°23'N	2°52'W	2050	1584–2002	1615	19	62	1.15±0.37	0.460±0.116	Gutiérrez et al.*
19	37°12'N	3°10'W	1966	1828–2009	1890	18	23	0.23±0.09	0.345±0.155	Sánchez-Salguero et al. (2015)
20	37°04'N	3°27'W	2000	1875–1999	1895	15	30	2.61±0.61	0.547±0.142	Gutiérrez et al.*

* Data available from authors

References cited in Table S1 (in alphabetical order):

1. Andreu L, *et al*. (2007) Climate increases regional tree-growth variability in Iberian pine forests. *Glob Change Biol* **13**:804–815.

2. Camarero JJ, Bigler C, Linares JC, Gil-Pelegrín E (2011) Synergistic effects of past historical logging and drought on the decline of Pyrenean silver fir forests. *For Ecol Manage* **262**:759–769.

3. Camarero JJ, Manzanedo RD, Sánchez-Salguero R, Navarro-Cerrillo RM (2013) Growth response to climate and drought change along an aridity gradient in the southernmost *Pinus nigra* relict forests. *Ann For Sci* **70**:769–780.

4. Esper J, *et al*. (2010) Trends and uncertainties in Siberian indicators of 20th century warming. *Glob Change Biol* **16**:386–398.

5. Fulé PZ, Ribas M, Gutiérrez E, Vallejo R, Kaye MW (2008) Forest structure and fire history in an old *Pinus nigra* forest, eastern Spain. *For Ecol Manage* **255**:1234–1242.

6. Génova Fuster M (2000) Tree rings and pointer years in Sistema Central (Spain) for the last four hundred years (in Spanish). *Bol R Soc Esp Hist Nat* **96**:33–42.

7. Génova Fuster M, Fernández Canclo A (1998/1999) Tree rings and climate of *Pinus nigra* subsp. *salzmannii* in Central Spain. *Dendrochronologia* **16–17**:75–86.

8. Génova Fuster MM, Fernández Canclo A, Creus J (1993) Analysis of ten tree-ring chronologies from the Iberian Range (in Spanish). *Invest Agrar, Sist Recur For* **2**:151–172.

9. Génova M, Martínez-Morillas D (2002). Dendroecological study of *Pinus nigra* in Checa (Guadalajara, Spain) (in Spanish). *Ecología* **16**:83–95.

10. Kirdyanov AV (1999) *Comparative analysis of growth and structure of conifer tree rings from the forest tundra, the northern and middle taiga zones of Central Siberia* (in Russian). PhD Thesis (Institute of forest SB RAS, Krasnoyarsk).

11. Kirdyanov AV, *et al*. (2012) 20th century tree-line advance and vegetation changes along an altitudinal transect in the Putorana Mountains, northern Siberia. *Boreas* **41**:56–67.

12. Knorre AA, Kirdyanov AV, Vaganov EA (2006) Climatically induced interannual variability in aboveground production in forest-tundra and northern taiga of central Siberia. *Oecologia* **147**:86–95.

13. Linares JC, Tíscar PA (2010) Climate change impacts and vulnerability of the southern populations of *Pinus nigra* subsp. *salzmannii*. *Tree Physiol* **30**:795–806.

14. Macias M, Andreu L, Bosch O, Camarero JJ, Gutiérrez E (2006) Increasing aridity is enhancing silver fir (*Abies alba* Mill.) water stress in its south-western distribution limit. *Clim Change* **79**:289–313.

15. Panyushkina IP, Vaganov EA, Shishov VV (1996) Spatial-temporal variation of radial tree growth in relation to climate in the north of middle Siberia. *Dendrochronologia* **14**:115–126.

16. Sánchez-Salguero R, *et al*. (2015) What drives growth of Scots pine in continental Mediterranean climates: Drought, low temperatures or both? *Agric For Meteorol* **206**:151–162.

17. Schweingruber FH, Briffa KR (1996) Tree-ring density network and climate reconstruction. *Climatic variations and forcing mechanisms of the last 2000 years*, eds Jones PD, Bradley RS, Jouzel J (Springer, Berlin), *NATO ASI Series* **141**:43–66.

18. Shishov VV, et al. VS-oscilloscope: a new tool to parameterize tree radial growth based on climate conditions. *Dendrochronologia* (in press).

19. Sidorova OV, Siegwolf R, Saurer M, Shashkin AV, Knorre AA, Prokushkin AS, Vaganov EA, Kirdyanov AA (2009) Do centennial tree-ring and stable isotope trends of

Larix gmelinii (Rupr.) Rupr. indicate increasing water shortage in the Siberian north? *Oecologia*, **161**:825–835.

20. Touchan R, *et al*. (2013). Dendrochronology course in Valsaín Forest, Segovia, Spain. *Tree-Ring Res* **69**:93–100.

21. Vaganov EA, Naurazhaev MM, Schweingruber FH, Briffa KR, Moell M (1996) An 840-year tree-ring width chronology for Taimir as an indicator of summer temperature changes. *Dendrochronologia* **14**:193–205.

Table S2. Description of the variance-covariance (VCOV) structures used for modelling synchrony patterns for the study period (1890–2009) according to the assignment of chronologies to pre-defined groups.

	VCOV structures and interpretation	Covariance structure	Variances	Covariances	Correlations	Residual variance
S_1	Homogeneity of year variances and covariances across groups	Compound symmetry	Homogeneous	Homogeneous	Homogeneous*	Homoscedastic / Heteroscedastic
S_2	Different variances but equal year correlation between all group pairs[2]	Heterogeneous compound symmetry	Heterogeneous	Heterogeneous	Homogeneous†	Homoscedastic / Heteroscedastic
S_3	One multiplicative term that approximates the full VCOV structure as in S_4	Factor analytic	Heterogeneous	Heterogeneous	Heterogeneous	Homoscedastic / Heteroscedastic
S_4	Full model (different variances and covariances). All causes of year × group interaction are allowed	Unstructured	Heterogeneous	Heterogeneous	Heterogeneous	Homoscedastic / Heteroscedastic
S_5	Narrow evaluation. Lack of common signal between groups	Banded main diagonal	Heterogeneous	Zero	Zero	Homoscedastic / Heteroscedastic
S_6	Null model. Broad evaluation ignoring groups	None	Single	–	–	Homoscedastic

* if homoscedastic residual variance; † if null residual variance

Table S3. Selection of variance-covariance (VCOV) structures for modelling synchrony patterns for the study period (1890–2009). Chronologies are grouped according to membership to (1) a particular region (central Siberia or Spain, left column) or (2) a particular species within a given region (central and right columns). The table lists the best VCOV model for each time period as suggested by Akaike and Bayesian information criteria. Nr refers to the number of VCOV parameters for the model of choice.

	Model of choice		**Model of choice**		**Model of choice**	
Period	***Region***	**Nr**	***central Siberia (by species)***	**Nr**	***Spain (by species)***	**Nr**
1890–1919	Narrow evaluation	4	Unstructured	9	Compound symmetry	5
1895–1924	"	4	Factor-analytic	7	"	5
1900–1929	"	4	Unstructured	9	"	5
1905–1934	"	4	"	9	"	5
1910–1939	"	4	"	9	"	5
1915–1944	"	4	"	9	"	5
1920–1949	"	4	"	9	"	5
1925–1954	"	4	"	9	Factor-analytic	7
1930–1959	"	4	Factor-analytic	7	"	7
1935–1964	"	4	"	7	"	7
1940–1969	"	4	"	7	"	7
1945–1974	"	4	"	7	"	7
1950–1979	"	4	"	7	Heter. compound symmetry	7
1955–1984	"	4	"	7	"	7
1960–1989	"	4	"	7	"	7
1965–1994	"	4	"	7	"	7
1970–1999	"	4	"	7	"	7
1975–2004	"	4	Compound symmetry	5	"	7
1980–2009	"	4	"	5	"	7